Alan G. Davenport Wind Engineering Group

A STUDY OF WIND EFFECTS FOR

PROSPECT VERONA BRIDGE MAINE, USA

J.P.C. KING / G. KOPP / P.J. VICKERY / M. MIKITIUK / L. KONG

BLWT-SS5-2005 / February 2005

The Boundary Layer Wind Tunnel Laboratory
The University of Western Ontario, Faculty of Engineering Science
London, Ontario, Canada N6A 5B9; Tel: (519) 661-3338; Fax: (519) 661-3339
Internet: www.blwtl.uwo.ca; E-mail: info@blwtl.uwo.ca

TABLE OF CONTENTS

ACKNOWLEDGEMENTS **x**

SUMMARY AND MAIN FINDINGS **xi**

DETAILS OF THE STUDY **1**

1 INTRODUCTION **2**
1.1 General 2
1.2 Scope of Report 2

2 THE MODELING OF THE WIND **8**
2.1 Introduction 8
2.2 Analysis of Surface Wind Data 8
2.3 Monte Carlo Simulation of Hurricane Winds 9
2.4 Design Wind Climate for Bridge Site 9

3 SECTION MODEL STUDY **28**
3.1 General 28
3.2 Dynamic Response Testing 28
3.2.1 General 28
3.2.2 Modeling of Wind 29
3.2.3 Dynamic Bridge Response 29
3.3 Static Response Testing 30

4 EQUIVALENT STATIC LOAD ANALYSIS **43**
4.1 General 43
4.2 Adaptation of Section Model Tests Results 43

5 PROSPECT PYLON PRESSURE STUDY **57**
5.1 Overall Approach 57
5.2 Pylon Pressure Results 58

6 DETERMINATION OF PEDESTRIAN LEVEL WIND **67**
6.1 Overall Approach 67
6.2 Statistical Prediction of Pedestrian Level Winds 67

7 FULL AEROELASTIC MODEL STUDY **76**
7.1 General 76
7.2 Dynamic Similarity 76
7.3 Description of Model Design 77
7.3.1 Pylon 77
7.3.2 Deck 78
7.3.3 Connections and Bearings 78
7.3.4 Cables 78
7.3.5 Construction Enclosure 78
7.4 Instrumentation 78
7.5 Wind Simulation 79
7.6 Wind Speed Measurements 80
7.7 Aeroelastic Model Test Procedure 80
7.8 Response of Completed Bridge and Construction Stage Configurations 81
7.8.1 General 81

7.8.2 Completed Bridge 81
7.8.3 Bridge Under Construction 82
7.9 Pylon Accelerations at Observation Level 83
7.10 Pedestrian Level Wind at Prospect Pylon Entrance 83

REFERENCES **115**

APPENDIX A THE SECTION MODEL APPROACH FOR THE STUDY OF WIND ACTION ON LONG SPAN BRIDGES

APPENDIX B RESULTS OF DYNAMIC SECTION MODEL TESTS

APPENDIX C RESULTS OF STATIC SECTION MODEL TESTS

APPENDIX D FLUTTER INSTABILITY CRITERIA

APPENDIX E DYNAMIC WIND LOAD FORCES ON LONG SPAN BRIDGES USING EQUIVALENT STATIC LOADS

APPENDIX F RESULTS OF PYLON PRESSURE TEST

APPENDIX G RESULTS OF FULL BRIDGE AEROELASTIC TESTS, COMPLETED BRIDGE

APPENDIX H RESULTS OF FULL BRIDGE AEROELASTIC TESTS, CONSTRUCTION STAGE

LIST OF TABLES

TABLE i PREDICTED WIND SPEEDS AT VARIOUS HEIGHTS FOR WINDS OVER LAND xviii

TABLE ii SUMMARY OF STATIC TEST RESULTS AT 0° ANGLE OF ATTACK xix

TABLE iii SUMMARY OF DYNAMIC TEST RESULTS xx

TABLE iv VALUES OF $\overline{W}$, $\tilde{W}_1$ AND $\tilde{W}_2$ FOR A WIND SPEED OF 80 MPH xxi

TABLE v SUMMARY OF THE PREDICTED PEAK DIFFERENTIAL PRESSURES AND SUCTIONS (PSF) xxii

TABLE vi PREDICTED WIND CONDITIONS AT THE TWO LOCATIONS xxiii

TABLE vii COMPARISON OF WIND SPEED RATIOS IN PYLON PRESSURE TEST AND FULL BRIDGE AEROELASTIC TEST FOR THE TWO WIND PROBES MEASURED AT THE PROSPECT PYLON ENTRANCE FOR FIVE WIND ANGLES xxiv

TABLE viii SUMMARY OF FULL BRIDGE AEROELASTIC MODEL TESTS, COMPLETED BRIDGE CONFIGURATION xxv

TABLE ix SUMMARY OF FULL BRIDGE AEROELASTIC MODEL TESTS, DOUBLE CANTILEVERED CONSTRUCTION STAGE xxvi

TABLE 2.1 PREDICTED WIND SPEEDS AT VARIOUS HEIGHTS FOR WINDS OVER LAND 11

TABLE 3.1 SECTION MODEL SCALING PARAMETERS 32

TABLE 3.2 FULL SCALE AND MODEL SCALE PROPERTIES FOR THE BASIC DECK SECTION 33

TABLE 3.3 RESULTS OF DYNAMIC SECTION MODEL TESTS FOR 0° ANGLE OF ATTACK 34

TABLE 3.4 STATIC FORCE COEFFICIENTS, NO SIDEWALK, SMOOTH FLOW 35

TABLE 3.5 STATIC FORCE COEFFICIENTS, NO SIDEWALK, TURBULENT FLOW 36

TABLE 4.1 SUMMARY OF PROTOTYPE PROPERTIES 45

TABLE 4.2 SUMMARY OF MODEL PROPERTIES, NO SIDEWALK 46

TABLE 4.3 SUMMARY OF MODEL PROPERTIES, SIDEWALK UPWIND 47

TABLE 4.4 SUMMARY OF MODEL PROPERTIES, SIDEWALK DOWNWIND 48

TABLE 4.5 SUMMARY OF WIND CHARACTERISTICS 49

TABLE 4.6 VALUES OF $\overline{W}$, $\tilde{W}_1$ AND $\tilde{W}_2$ FOR A WIND SPEED OF 80 MPH 50

TABLE 5.1 SUMMARY OF THE MAXIMUM AND MINIMUM EXTERNAL PRESSURE COEFFICIENTS 59

TABLE 5.2 SUMMARY OF THE MEAN INTERNAL PRESSURE COEFFICIENTS 60

TABLE 5.3 SUMMARY OF THE PREDICTED PEAK DIFFERENTIAL PRESSURES AND SUCTIONS (PSF) 61

TABLE 5.4 SUMMARY OF THE PREDICTED PEAK EXTERNAL PRESSURES AND SUCTIONS (PSF) 62

TABLE 6.1 PREDICTED WIND CONDITIONS AT THE TWO LOCATIONS TESTED 69

TABLE 7.1 AEROELASTIC SCALING PARAMETERS (FROUDE SCALED) 85

TABLE 7.2 PARAMETERS FOR DESIGN OF THE AEROELASTIC MODEL 86

TABLE 7.3 INSTRUMENTATION LOCATIONS, PROSPECT VERONA BRIDGE 87

TABLE 7.4 SUMMARY OF FULL BRIDGE AEROELASTIC MODEL TESTS, COMPLETED BRIDGE CONFIGURATION 88

TABLE 7.5 SUMMARY OF FULL BRIDGE AEROELASTIC MODEL TESTS, CONSTRUCTION STGE 89

TABLE 7.6 SUMMARY OF WIND SPEED (MPH) FOR PYLON ACCELERATIONS WITHIN 20 MILLI-G, AND COMPARISON TO CRITERIA 90

TABLE 7.7 COMPARISON OF WIND SPEED RATIOS IN PYLON PRESSURE TEST AND FULL BRIDGE AEROELASTIC TEST FOR THE TWO WIND PROBES MEASURED AT THE PROSPECT PYLON ENTRANCE FOR FIVE WIND ANGLES 91

LIST OF FIGURES

FIGURE i RELATIVE IMPORTANCE FACTORS FOR VARIOUS WIND DIRECTIONS AND MAXIMUM WIND SPEEDS WITH DIFFERENT RECURRENCE INTERVALS - HURRICANE WINDS AT 10M xxvii

FIGURE ii PREDICTED EXTREME HOURLY-MEAN WIND SPEEDS FOR VARIOUS RETURN PERIODS FOR HURRICANE WINDS AT 10 M (33 FT) xxviii

FIGURE iii SKETCH SHOWING SIGN CONVENTION OF FORCES xxix

FIGURE iv STATIC FORCE COEFFICIENTS (NO SIDEWALK) XXX

FIGURE v DYNAMIC TEST RESULT, TURBULENT FLOW AT 0° ANGLE OF ATTACK, SIDEWALK UPSTREAM WITH MODIFIED FREQUENCIES xxxi

FIGURE vi MODE SHAPES USED IN THE EQUIVALENT STATIC LOAD ANALYSIS – COMPLETED BRIDGE xxxii

FIGURE vii WIND LOAD COMPONENTS FOR THE BRIDGE DECK – COMPLETED BRIDGE CONFIGURATION xxxiii

FIGURE viii MODE SHAPES USED IN THE EQUIVALENT STATIC LOAD ANALYSIS – CONSTRUCTION STAGE xxxiv

FIGURE ix WIND LOAD COMPONENTS FOR THE BRIDGE DECK – CONSTRUCTION STAGE CONFIGURATION xxxv

FIGURE x LOCATIONS OF PRESSURE TAPS AND WIND PROBES xxxvi

FIGURE xi PREDICTED MEAN WIND SPEEDS COMPARED WITH CRITERIA FOR PEDESTRIAN COMFORT AND SAFETY xxxvii

FIGURE xii PYLON ACCELERATIONS AT 30° WIND xxxviii

FIGURE 1.1 LOCATION OF THE PROSPECT VERONA BRIDGE, MAINE 4

FIGURE 1.2 PROTOTYPE DIMENSIONS – MAIN SPAN 5

FIGURE 1.3 PROTOTYPE DIMENSIONS – CROSS SECTION OF DECK 6

FIGURE 1.4 PROTOTYPE DIMENSIONS – BRIDGE PYLONS 7

FIGURE 2.1 LOCATIONS OF THE PROSPECT VERONA BRIDGE AND PRIMARY WEATHER STATIONS AT ROCKLAND, MAINE AND BANGOR, MAINE 12

FIGURE 2.2 ANNUAL PROBABILITY DISTRIBUTION OF SURFACE HOURLY-MEAN WIND SPEED AND WIND DIRECTION – ROCKLAND, MAINE (1977-2003) 13

FIGURE 2.3 SEASONAL PROBABILITY DISTRIBUTION OF SURFACE HOURLY-MEAN WIND SPEED AND WIND DIRECTION – ROCKLAND, MAINE (1977-2003) 14

FIGURE 2.4 ANNUAL PROBABILITY DISTRIBUTION OF SURFACE HOURLY-MEAN WIND SPEED AND WIND DIRECTION – BANGOR, MAINE (1942-2003) 15

FIGURE 2.5 SEASONAL PROBABILITY DISTRIBUTION OF SURFACE HOURLY-MEAN WIND SPEED AND WIND DIRECTION – BANGOR, MAINE (1942-2003) 16

FIGURE 2.6 ANNUAL RELATIVE IMPORTANCE FACTORS FOR VARIOUS WIND DIRECTIONS AND MAXIMUM WIND SPEEDS WITH DIFFERENT RECURRENCE INTERVALS, ROCKLAND, MAINE (1977-2003) 17

FIGURE 2.7 SEASONAL RELATIVE IMPORTANCE FACTORS FOR VARIOUS WIND DIRECTIONS AND MAXIMUM WIND SPEEDS WITH DIFFERENT RECURRENCE INTERVALS, ROCKLAND, MAINE (1977-2003) 18

FIGURE 2.8 ANNUAL RELATIVE IMPORTANCE FACTORS FOR VARIOUS WIND DIRECTIONS AND MAXIMUM WIND SPEEDS WITH DIFFERENT RECURRENCE INTERVALS, BANGOR, MAINE (1942-2003) 19

FIGURE 2.9 SEASONAL RELATIVE IMPORTANCE FACTORS FOR VARIOUS WIND DIRECTIONS AND MAXIMUM WIND SPEEDS WITH DIFFERENT RECURRENCE INTERVALS, BANGOR, MAINE (1942-2003) 20

FIGURE 2.10 PREDICTED EXTREME HOURLY-MEAN SURFACE AND GRADIENT WIND SPEEDS FOR VARIOUS RETURN PERIODS 21

FIGURE 2.11 TROPICAL STORMS PASSING WITHIN A 250 KM RADIUS OF PROSPECT VERONA BRIDGE FOR THE RECORD PERIOD 1851-2002 – ALL STORMS CASE 22

FIGURE 2.12 TROPICAL STORMS PASSING WITHIN A 250 KM RADIUS OF PROSPECT VERONA BRIDGE FOR THE RECORD PERIOD 1851-2002 – STORM SEQUENCES REACHING "HURRICANE" STAGE (V>33M/S) 23

FIGURE 2.13 TROPICAL STORMS PASSING WITHIN A 250 KM RADIUS OF PROSPECT VERONA BRIDGE FOR THE RECORD PERIOD 1851-2002 – STORM SEQUENCES REACHING "TROPICAL STORM" STAGE (V<33M/S) 24

FIGURE 2.14 ANNUAL PROBABILITY DISTRIBUTION OF SURFACE HOURLY-MEAN WIND SPEED AND WIND DIRECTION – HURRICANE WINDS AT 10M - OBTAINED FROM MONTE CARLO SIMULATION OVER 100,000 YEARS (37,150 STORMS) 25

FIGURE 2.15 RELATIVE IMPORTANCE FACTORS FOR VARIOUS WIND DIRECTIONS AND MAXIMUM WIND SPEEDS WITH DIFFERENT RECURRENCE INTERVALS - HURRICANE WINDS AT 10M 26

FIGURE 2.16 PREDICTED EXTREME HOURLY-MEAN WIND SPEEDS FOR VARIOUS RETURN PERIODS FOR HURRICANE WINDS AT 10 M (33 FT) 27

FIGURE 3.1 SECTION MODEL TEST SET-UP 37

FIGURE 3.2 CLOSE-UP VIEWS OF THE SECTION MODEL 38

FIGURE 3.3 MODEL DETAILS 39

FIGURE 3.4 DYNAMIC TEST RESULT, DECK WITHOUT SIDEWALK IN SMOOTH FLOW, 0 DEGREES ANGLE OF ATTACK AND DAMPING OF 0.5% 40

FIGURE 3.5 SKETCH SHOWING SIGN CONVENTION OF FORCES 41

FIGURE 3.6 STATIC FORCE COEFFICIENTS – NO SIDEWALK 42

FIGURE 4.1 DYNAMIC TEST RESULT, TURBULENT FLOW AT 0° ANGLE OF ATTACK, NO SIDEWALK 51

FIGURE 4.2 DISTRIBUTED WIND LOAD COMPONENTS 52

FIGURE 4.3 MODE SHAPE DISTRIBUTION FUNCTIONS FOR COMPLETED BRIDGE (NO SIDEWALK) 53

FIGURE 4.4 MODE SHAPE DISTRIBUTION FUNCTIONS FOR CONSTRUCTION STAGE (NO SIDEWALK) 54

FIGURE 4.5 WIND LOAD COMPONENTS FOR COMPLETED BRIDGE (NO SIDEWALK) 55

FIGURE 4.6 WIND LOAD COMPONENTS FOR CONSTRUCTION STAGE (NO SIDEWALK) 56

FIGURE 5.1 PHOTOGRAPHS OF THE MODEL IN THE WIND TUNNEL SHOWING THE UPSTREAM TERRAIN MODEL (EXPOSURE) USED 63

FIGURE 5.2 CLOSE UP VIEWS OF THE PRESSURE MODEL 64

FIGURE 5.3 VERTICAL PROFILE OF MEAN WIND SPEED AND LONGITUDINAL TURBULENCE INTENSITY MEASURED JUST UPSTREAM OF THE PROXIMITY MODEL. 65

FIGURE 5.4 LOCATIONS OF PRESSURE TAPS AND WIND PROBES 66

FIGURE 6.1 PREDICTED EXTREME HOURLY MEAN SURFACE WIND SPEEDS FOR VARIOUS RETURN PERIODS, WIND CLIMATE DATA AT BANGOR AND ROCKLAND 70

FIGURE 6.2 PREDICTED EXTREME HOURLY MEAN SURFACE WIND SPEEDS FOR VARIOUS RETURN PERIODS, HURRICANE WINDS 71

FIGURE 6.3 LOCATION MAP FOR THE PROSPECT-VERONA BRIDGE AND THE PRIMARY WEATHER STATIONS AT ROCKLAND, MAINE AND BANGOR, MAINE 72

FIGURE 6.4 LOCATIONS OF PRESSURE TAPS AND WIND PROBES 73

FIGURE 6.5 POLAR PLOTS OF SPEED COEFFICIENTS 74

FIGURE 6.6 PREDICTED MEAN WIND SPEEDS COMPARED WITH CRITERIA FOR PEDESTRIAN COMFORT AND SAFETY 75

FIGURE 7.1 PHOTOGRAPHS OF THE AEROELASTIC MODEL IN THE WIND TUNNEL SHOWING THE UPSTREAM TERRAIN MODELS (EXPOSURES) USED 92

FIGURE 7.2 PHOTOGRAPHS OF THE AEROELASTIC MODEL IN THE WIND TUNNEL, WITH AND WITHOUT THE EXISTING BRIDGE 94

FIGURE 7.3 CLOSE-UP VIEWS OF THE AEROELASTIC MODEL, PROXIMITY MODEL AND INSTRUMENTATION 95

FIGURE 7.4 PHOTOGRAPHS OF THE AEROELASTIC MODEL AT DIFFERENT WIND ANGLES 98

FIGURE 7.5 (A) LOCATION OF THE PROPOSED PROSPECT VERONA BRIDGE AND THE SURROUNDING TERRAIN 101

FIGURE 7.5 (B) LOCATION OF EXISTING BRIDGE AND WIND DIRECTIONS TESTED 102

FIGURE 7.6 THE 1:200 SCALE AEROELASTIC MODEL 103

FIGURE 7.7 INSTRUMENTATION LOCATIONS AND SIGN CONVENTION, COMPLETED BRIDGE (CABLES REMOVED IN THIS FIGURE) 107

FIGURE 7.8 WIND PROFILES USED IN THE FULL BRIDGE MODEL TESTS, HURRICANE AND OPEN COUNTRY EXPOSURES 108

FIGURE 7.9 RATIO OF PROBABLE MAXIMUM SPEED AVERAGED OVER T SECONDS TO HOURLY MEAN SPEED 109

FIGURE 7.10 DEFINITION OF WIND SPEEDS FOR VARIOUS AVERAGING TIME 110

FIGURE 7.11 PYLON ACCELERATIONS AT 30° WIND 111

FIGURE 7.12 PYLON ACCELERATIONS AT 90° WIND (PERPENDICULAR TO BRIDGE) 112

FIGURE 7.13 CLOSE-UP VIEWS OF THE WIND PROBE LOCATIONS AT PROSPECT PYLON ENTRANCE AREA 113

FIGURE 7.14 SAMPLE PLOT OF WIND SPEEDS MEASURED IN FULL BRIDGE AEROELASTIC TEST, AT 90 DEGREE WIND 114

ACKNOWLEDGEMENTS

The study of wind effects for the Prospect Verona Bridge, Maine, was initiated by Mr. Jay Rohleder of Figg Bridge Engineers. The assistance and continued co-operation and support of Messrs. Jay Rohleder, Chris Burgess and William Johnson, all of Figg Bridge Engineers are gratefully acknowledged.

Acknowledgment is also made of the contributions by various members of the technical staff of the Laboratory, particularly: Messrs. Gerry Dafoe, Alex Shyluk and Chris Gavin who carried out the experimental phases of the study and Mr. Tomasz Kawa who made some of the illustrations for the report. The CAD drawings for the section and the full bridge aeroelastic models were made by Mr. Kevin Barker and Mr. Albert Whatmough of the University Machine Services. Mr. Kevin Barker and Mr. Albert Whatmough also took the lead in the direction of team members in the fabrication of the section and full aeroelastic models.

SUMMARY AND MAIN FINDINGS

This report on the study of wind action on the Prospect Verona Bridge, Maine, provides information from the section model test, the pylon pressure model test as well as the full bridge aeroelastic model test. The aim of this study was to provide:

1. Wind climate and wind speed information at the project site;
2. Basic aerodynamic information for the deck design;
3. Information on the overall stability of the deck in high wind conditions;
4. Information on the deck behavior with respect to vortex shedding induced oscillation in smooth wind;
5. Definition of the behavior of the deck due to buffeting in turbulent wind;
6. Determination of the static force coefficients in both smooth and turbulent flows for the deck;
7. Determination of the equivalent static wind loads for the bridge deck;
8. Determination of the wind-induced cladding loads at the observation level of the Prospect Pylon;
9. Determination of the pedestrian level winds at the entrance area to the Prospect Pylon;
10. Determination of the response characteristics of the full bridge aeroelastic model to three dimensional turbulent wind over a full range of wind speeds for both the completed bridge and the double cantilevered construction stage;
11. Determination of the response characteristics of the full bridge aeroelastic model in winds with low turbulence conditions to confirm the potential for vortex shedding induced bridge response and flutter instability for both the completed bridge and the double cantilevered construction stage;
12. Investigation of the accelerations at the observation level of the Prospect Pylon and occupant comfort.

The section model was constructed at a geometric scale of 1:70.5 relative to full scale. The model was tested at the inlet to the High-Speed Test Section of the Boundary Layer Wind Tunnel II. The section model test was performed in two phases: i) on a static force balance in which the overall static forces and moment in vertical, lateral and torsional directions were measured at different angles of vertical wind inclination; and ii) with scaled dynamic structural properties of the prototype, to monitor the dynamic response. The section model was tested in smooth flow and grid-generated turbulent wind representative of the natural wind conditions at the project site. The section model test methodology is presented in Appendix A.

A pressure model of the pylon was designed and constructed at a geometric scale of 1:200 and tested on the automatic turntable of the High-Speed Test Section. Detailed measurements were made of wind-induced pressures and suctions on the glass cladding of the Prospect Pylon at the observation level in representatively scaled atmospheric flow conditions. In the test, the upwind terrain was modeled within the 42.6m long wind tunnel test section, which represents approximately 5 miles of upwind fetch. The oncoming flow was conditioned by a set of turbulence generating roughness, including spires, floor roughness and a large scale eddy generating trip. However, the hills immediately around the bridge site were not modeled in this pressure test. Measurements were also made of pedestrian level wind speeds at two locations around the entrance area of the Prospect Pylon, to provide predictions of the wind conditions.

The full bridge aeroelastic model was also constructed at a geometric scale of 1:200 relative to the prototype. The model was tested on the turntable of the Low Speed Test Section of the Boundary Layer Wind Tunnel II, in three dimensional turbulent wind conditions. The long upwind fetch within the wind tunnel allows extended modeling of upwind terrains, thus permits the simulation of wind conditions

representative of those anticipated for the project site. Two upstream terrain conditions were used in the tests; namely, a hurricane profile and an open country exposure. The existing bridge (upwind of the proposed Prospect Verona Bridge for a wind angle of 270°) was also constructed, in order to assess its effect on the proposed bridge. Five different wind angles (0°, 30°, 60°, 90° and 270° relative to the longitudinal axis of the bridge) were examined in the test.

A design probability distribution of surface wind speed and direction was developed for the bridge site on the basis of full scale meteorological records from the weather stations in the area. In addition, a study was carried out to include Monte Carlo computer simulations of tropical storms and to assess their impact on the climate of extreme winds. The methodology and the wind speed results from these analyses are given in Section 2 of this report.

The highlights and main findings of these studies are as follows:

Wind Climate

- The design probability distribution of surface wind speed and direction in the wind climate study was developed on the basis of full scale meteorological records from nearby weather stations at Rockland, Maine and Bangor, Maine.
- Monte Carlo simulations of the tropical storms were carried out and their impact on extreme winds was analyzed.
- The directional characteristics associated with service-level hurricane winds are shown in Figure i for various return periods. Strong winds during hurricane events are likely to come from any wind direction with a preference to the southeast sector.
- Predictions of the hourly mean wind speed for winds over land at various heights, regardless of wind direction, are shown in Figure ii. The predicted hourly mean wind speeds at various heights for wind over land are also presented in Table i.

Static Test of Section Model

- The 1:70.5 scale section model was mounted on the BLWTL Bridge Section Model force balance which is capable of measuring the total forces on the section (*X* and *Z* body forces, as well as the torque). The lift and drag forces were computed from the measured *X* and *Z* body forces. Tests were carried out in both smooth and grid generated turbulent flow conditions for angles of mean vertical inclination between -10° to +10° in increments of 1°. The sign convention for the definition of the force coefficients is given in Figure iii.
- The static tests were performed for the deck section (a) without the sidewalk, (b) with the sidewalk on the upwind side, and (c) with the sidewalk on the downwind side.
- The static aerodynamic force coefficients from the section model tests (without the sidewalk) are summarized in Figure iv for both smooth and turbulent flow conditions without the sidewalk, and are listed in Table ii. The static force coefficients are also tabulated and plotted in Appendix C for all test conditions.
- It was observed that the turbulent flow coefficients are smaller than those obtained in smooth flow, which implies that smaller mean loads in turbulent wind can be expected, except for C_z for angles greater than +3° with the sidewalk upwind and +5° with the sidewalk downwind. Turbulence has the general effect of decreasing the *X*-force (drag) coefficient at all angles of attack. This is believed to be the result of an altered flow reattachment location on the deck, which is affected by the intensity and scale of turbulence. In general, turbulence increases the size of the wake region, decreasing the curveature of the streamlines around the deck, thereby reducing the magnitude of the wind pressure on the deck.
- There are significant differences in the slope of both C_m and C_z at 0°. These slopes are always larger in turbulent flow. The moment coefficient is negative in smooth flow and near zero in turbulent flow at 0°. The lift coefficient is positive and larger in magnitude in turbulent flow.

- The sidewalk has a significant effect on the static coefficients and slopes. However, the *X*-force (drag) coefficient at 0° is not significantly affected and is largest for the no sidewalk case. The C_z and C_m coefficients are also largest for the no sidewalk case at 0°. The slopes of the C_m and C_Z curves are directly proportional to the dynamic load – the steeper the curve, the larger will be the dynamic loading. The slope of the C_m curve at 0° is about the same in all three cases (and near zero) although the slope of C_z is significantly greater with the presence of the sidewalk and, in particular, on the upwind (windward) side. This behavior indicates that although mean loads may be lower with the sidewalk in place, the dynamic loads due to turbulent buffeting will be significantly larger.

Dynamic Test of Section Model

Response to Extreme Wind in Smooth Flow Conditions:

- These tests were conducted to provide: a) lower bound estimates of the response to vortex shedding and b) estimates of the wind speeds associated with any possible flutter instability up to the design wind speed.
- The onset of a "Flutter Instability" was defined as when the character of the response changed from a random type motion to that of a regular, sinusoidal motion, involving either pure torsional or a coupled vertical-torsional vibration. This can be clearly identified through an examination of the "peak factor" which is defined as the ratio of the largest observed reading during the sample period to the Root Mean Square (RMS) of the sample. A random signal has peak factors in the 3-4 range, while a sinusoid has a peak factor of $\sqrt{2}$ or 1.41.

Response to Winds in Expected Site Turbulence Conditions:

- These tests were conducted to provide: a) estimates of the response to turbulent buffeting and b) assessment of the effects of turbulence on any observed vortex shedding induced response found in the smooth flow test.
- Turbulence in the wind tunnel was generated by a grid placed upwind of the model. The grid has a mesh size of 5.5 inches and 24 inches center to center spacing. The vertical, I_w, and longitudinal, I_u, turbulence intensities generated using this grid are about 7.2% and 9.0%, respectively. Turbulence developed using the fixed grid technique is normally lacking sufficient energy in the low frequency - large scale range to match full scale, resulting in an overall lower turbulence intensity than that expected at the site. The energy in the high frequency end of the spectrum, however, is well modelled using this grid, which is critical for the definition of resonant response and the overall behavior of the structure to turbulent wind.
- All dynamic section model tests were performed at relatively low damping ratios with nominal values of 0.5% and 1.0% of critical.

Dynamic Test Results:

- The dynamic section model tests for this study were carried out for three test configurations, viz., (a) without the sidewalk, (b) with the sidewalk on the upwind (windward) side and (c) with the sidewalk on the downwind (leeward) side.
- Results are summarized in Table iii. The test results including the detailed response plots are also given in Appendix B.
- No flutter instability was observed during the tests. The maximum (scaled) mean-hourly wind speed at the deck height was 145 mph, a speed which corresponds to a return period of greater than 10,000 years.

- Vortex-induced responses were observed in the smooth flow tests. Vertical motions were observed with peak amplitudes in the range of 21~22 mph. For 0.5% damping, the maximum amplitudes varied between 0.55 and 0.84 ft. The worst case was observed to be with the sidewalk on the upwind (windward) side. Increased damping significantly mitigated these responses, as did turbulence (which eliminated it entirely). Torsional motions with peak amplitudes were observed to occur between speeds of 78~82 mph; however, these motions were small.

- Response under turbulent flow conditions was characterized by turbulent buffeting. Generally, the dynamic components due to buffeting of the deck in turbulent flow are significantly higher than those observed in smooth flow. The mean components of the response are smaller than those found in the smooth flow tests (consistent with the results from the static tests). The effect of turbulence helps to reduce any vortex shedding peaks and to increase the wind speeds at which flutter occurs.

- A sample plot of the dynamic section model test results is given in Figure v for the basic deck section in smooth flow.

Equivalent Static Loads

- Wind loads were estimated for the deck section with and without the sidewalk for the complete bridge and one construction stage (also without sidewalk). The analysis is based upon the measured response of the section model in turbulent flow, with suitable corrections for discrepancies in the intensity and spectrum of turbulence, the damping and the mode shapes. The design loads were determined from estimates of the dynamic motion in the lowest symmetric and anti-symmetric modes as well as the mean load and is fully described in Appendix E. The distribution of each load component follows the actual mode shapes shown in Figure vi for the complete bridge and Figure viii for the construction stage.

- The equivalent static wind load plots resulting from this analysis at 0 degrees are presented in Figures vii (completed bridge) and ix (construction stage). These wind loads are obtained for an assumed prototype damping of 0.5% of critical for all modes. A mean hourly wind speed of 80 mph at deck height is used as a reference wind speed for the purposes of illustration and the equivalent static loads at this wind speed are reproduced in equation form as shown below. The actual values of $\overline{W}$, $\tilde{W}_1$ and $\tilde{W}_2$ are given in Table iv for both bridge configurations at a wind angle of 0°. The values presented in Table iv are interpolated from the data presented in Figures vii and ix. The equivalent static loads at other wind speeds can be estimated from the plots.

$$W_x(\eta) = \overline{W}_x \alpha(\eta) \pm \gamma_{1x} \tilde{W}_{1x} \alpha_{1x}(\eta) \pm \gamma_{2x} \tilde{W}_{2x} \alpha_{2x}(\eta) \qquad (1)$$

$$W_z(\eta) = \overline{W}_z \alpha(\eta) \pm \gamma_{1z} \tilde{W}_{1z} \alpha_{1z}(\eta) \pm \gamma_{2z} \tilde{W}_{2z} \alpha_{2z}(\eta) \qquad (2)$$

$$W_\theta(\eta) = \overline{W}_\theta \alpha(\eta) \pm \gamma_{1\theta} \tilde{W}_{1\theta} \alpha_{1\theta}(\eta) \pm \gamma_{2\theta} \tilde{W}_{2\theta} \alpha_{2\theta}(\eta) \qquad (3)$$

- In the equations, W_x (lb/ft), W_z (lb/ft) and W_θ (lb-ft/ft) are the desired wind loads per unit length resulting from the application of: $\overline{W}$, the mean, distributed according to $\alpha(\eta)$ (normally with a constant value of 1), $\tilde{W}_1$, the symmetric, according to $\alpha_1(\eta)$ and $\tilde{W}_2$, the asymmetric, according to $\alpha_2(\eta)$. These distribution functions vary according to the mode shapes presented in Figures vi and viii with a maximum value of 1.0.

- To reflect the multitude of combinations with which the fluctuating loads can occur, the load combination factors γ_{1x}, γ_{2x} γ_{1z}, γ_{2z}, $\gamma_{1\theta}$, $\gamma_{2\theta}$ should be used in any combination of the modal terms whose values are taken as follows: $\gamma = \pm 1.0$ if only one modal term is included; ±0.8 for two terms;

±0.7 for three terms and ±0.6 for four or more terms. This applies to all modal terms whether they are in *X, Z* and θ, singly or together.

Pylon Pressure Model Test

- Detailed measurements of the wind-induced external pressures on the glass cladding at the observation level of the Prospect Pylon were performed using the 1:200 scale pressure model in representatively scaled atmospheric flow conditions.
- A total of 30 pressure taps were installed at the observation level of the pressure model, with the numbering and associated location given in Figure x. An additional 4 taps were installed on each face of the sloped pylon top.
- Internal pressure coefficients were determined assuming a nominally sealed condition (uniform leakage) for the portion of the wall at the observation level and were subtracted from the measured external pressure coefficients.
- The resulting differential pressure coefficients were combined with the design probability distributions of wind speed and direction to form predictions of differential pressures and suctions for various return periods. The results are summarized in Table v.
- The largest predicted differential pressure (inward-acting load) and suction (outward-acting load) are 54 and 63 psf respectively. The largest pressure occurs on the south face of the pylon, while the worst suction occurs on the pylon east side near the top corner.
- To use these wind loads in the design of the curtain wall and exterior cladding, the loads must be multiplied by appropriate load factor, which has not been included in the results. In addition, these results do not include any allowance for stack (thermal) effects or the direct effects of mechanical systems used in the pylon.

Pedestrian Level Wind Study

- Figure x also shows the 2 locations at which wind speed measurements were taken at the entrance to the Prospect Pylon.
- Experimental results have been combined with the extratropical wind climate to provide predictions of the wind speeds expected to be exceeded for 5% of the time and those expected to be exceeded once per year. These predictions can be compared directly with acceptance criteria for pedestrian comfort and safety respectively.
- Figure xi, showing the predictions, indicates that these two locations meet the criteria for pedestrian comfort conditions for intended activities (short sitting and leisurely walking). Table vi lists the wind speeds predicted.
- To assure the safety of pedestrians in public areas, accepted criteria recommends that a 34 mph threshold of potentially hazardous wind conditions should not be exceeded more than once per year for all weather areas. At location 2, the predicted wind speed exceeded once per year is about 36 mph, slightly larger than this threshold.
- Since none of the local terrain was modeled in the pressure study, the pedestrian level wind conditions at these two probe locations were also examined in the aeroelastic model test which included a topographic model representing the immediate surroundings of the project site within a radius of 1600ft. Five wind angles were studied in the aeroelastic test at 0°, 30°, 60°, 90° and 270° relative to the longitudinal axis of the bridge, corresponding to true azimuths of 110°, 140°, 170°, 200° and 20° respectively, which were used in the pressure study.
- The wind speeds at Location 1 of the Prospect Pylon entrance are reduced for the five wind angles in the aeroelatic test when compared to the results from the pressure test. The wind conditions at the northeast corner of the pylon are also improved for four of the five wind angles tested. However, the wind speed was increased at the wind angle 30° in the aeroelastic test

(corresponding to a true azimuth of 140°). The wind speed increase is considered to be due to the upwind hills at the Prospect side, which re-direct the wind to an angle critical to the pylon northeast corner.

- Since only five wind angles were tested in the aeroelastic test, it is not appropriate to conclude that the presence of the local terrain improves the wind conditions at the northeast corner of the Prospect Pylon for all wind angles. However, when coupled with acceleration criteria for the pylon discussed below, it is considered likely that the pylon will be closed to public in extreme weather conditions. Figure xi shows that Location 2 satisfies the safety criteria in fair weather conditions.
- Table vii presents the comparison of the wind speed ratio obtained in both the pressure model test and the aeroelastic model test. The wind speed ratio is defined as the ratio of the pedestrian level wind speed over a reference wind speed at the upper level where the effect of ground terrain condition becomes negligible.

Bridge Aeroelastic Model Tests, Completed Bridge

- No flutter instability was observed in any of the tests performed for the completed bridge configuration up to a full scale wind speed of 140 mph ~ 180 mph at deck height.
- No vortex shedding peaks were observed in the tests of 0° wind (wind along the bridge), which includes the wind directions important for pylon cross-wind motion.
- A wide vortex peak between 40 and 80mph was observed in the response of backspan mid-point torsional acceleration at 30° wind in the hurricane exposure. A similar peak was also observed in the same response at 30° wind in the open country exposure. The peak becomes narrower and smaller because of the higher turbulence in the flow.
- There were three peaks observed in the backspan mid-point torsional acceleration at 30mph, 50mph and 90mph at 60° wind. Some of these peaks were also seen in other responses, such as the pylon longitudinal acceleration and the backspan mid-point lift acceleration.
- The smooth flow test results at 90° wind showed very small peaks at various responses, which are not considered to be significant. However, two dominant peaks were observed at about 45mph and 90mph in both the hurricane exposure and the open country exposure. The peak at 45mph was reduced with higher turbulence in the open country exposure, while the peak at 90mph was about the same in the two exposures. It is suspected that the hills which were upwind of the bridge site may have played a significant role in creating these vortex peaks through a funnelling of the wind.
- The effect of the existing bridge upwind of the model at 270° was examined. There was no significant vortex peaks observed in any of the responses with the existing bridge, an indication of the suppression effect of the existing bridge on the various vortex shedding peaks.
- As shown in the plots, buffeting responses in the open country exposure (with a larger turbulence intensity) were found to be slightly higher than the responses in the hurricane profile (which was smoother and less turbulent). The effect of the upstream exposure is small on the deck and pylon responses (i.e. not in proportion to the turbulence intensity of the oncoming flow), which is an indication that the effect of the topography is the primary contributor to turbulent buffeting.
- Tests performed for the completed bridge configuration are summarized in Table viii. All test results, including the detailed response plots, are given in Appendix G for the completed bridge.

Bridge Aeroelastic Model Tests, Construction Stage

- No flutter instability was observed in any of the tests performed for the double cantilevered construction stage configuration up to a full scale wind speed of 100 mph at deck height.
- No vortex shedding peaks were observed in the tests of 0° wind (along the bridge).

- No significant vortex peaks were seen in the tests performed in 30° wind, other than a small peak at about 25mph in the backspan mid-point torque and the pylon longitudinal acceleration. This peak was found to exist with both upstream exposures.

- The smooth flow test in 90° wind indicated two vortex peaks at about 35mph and 45mph in the mainspan lift moment at the face of the pylon. Both peaks were still visible in the test with the hurricane exposure. Though the peak at 35mph was still present in the response in the rougher open country exposure, the peak at 45mph was eliminated. In addition, the peak at 35mph was observed in the 60° wind in both exposures.

- The effect of the presence of the construction enclosures at the cantilever ends was examined for the 90° wind. The vortex peak at about 35mph was somewhat reduced with the construction enclosures. Otherwise, the effect of the presence of construction enclosures on the various deck and pylon responses is small.

- There was no vortex peak observed in any of the responses with the existing bridge at 270° wind.

- Buffeting responses in the open country exposure (with larger turbulence intensity) are generally higher than the responses in the hurricane profile.

- Tests performed for the bridge configuration of double cantilevered construction stage are summarized in Table ix. All test results, including the detailed response plots, are given in Appendix H.

Pylon Accelerations at the Observation level

- The lateral and longitudinal accelerations were measured at top of the observation level of the Prospect Pylon at a full scale height of 435ft. The observed accelerations are compared with a widely used criterion with acceptability of structural motions of 20~25 milli-g.

- It was observed that the worst case comes from wind at 30° to the longitudinal axis of the bridge, in which both the pylon lateral and longitudinal accelerations became larger than 20 milli-g when the mean wind at deck height reached 23 mph. This wind speed corresponds to a 3-second gust wind speed commonly reported by weather services of approximately 34 mph. The damping values were 0.55% for the pylon lateral motion and 0.20% for the pylon longitudinal direction, which was considered low compared to the values that may be present in the full scale concrete pylon. Prototype structural damping that is higher than that used in the test will result in lower acceleration for a given wind speed.

- Figure xii shows the pylon acceleration at different damping values for the 30° wind. In the plots, the direct test values are marked with symbols, and the fitted data are plotted in solid curves (since response is generally proportional to V^2). The fitted curves can be regarded as pure turbulent buffeting response with no vortex shedding peaks. Estimates of the pylon responses for higher damping values were made, which correspond to damping values considered to be more representative of full scale than those used in the tests. A value of 1.0% was used for the lateral response, while both 0.5% and 1.0% were used for the longitudinal response. For reference, the criterion of 20 milli-g is also given in the plots.

- The pylon longitudinal response at 30° wind shows a critical mean hourly wind speed at deck height of over 50 mph with 1.0% damping. However, for the pylon lateral response, the vortex shedding peak between 30 mph and 40 mph can not be reduced below the 20 milli-g by increasing the structural damping to 1.0%. Spectral analysis of the pylon lateral acceleration at these wind speeds does not show a single dominant peak, rather a few peaks with similar magnitudes. The critical wind speed for the pylon lateral acceleration at 1.0% damping is found to be about 28mph.

TABLE i PREDICTED WIND SPEEDS AT VARIOUS HEIGHTS FOR WINDS OVER LAND

Return Period (Years)	Surface Level (10 m)			Upper Level (500 m)		
	Hourly Mean m/s	Hourly Mean mph	3-Sec. Gust mph	Hourly Mean m/s	Hourly Mean mph	3-Sec. Gust mph
50	24.0	54	82	38.5	86	131
100	28.0	63	95	44.1	99	150
500	35.1	79	119	54.4	122	185
1000	37.9	85	129	58.7	131	200

TABLE ii SUMMARY OF STATIC TEST RESULTS AT 0° ANGLE OF ATTACK

Variable	Smooth Flow			Turbulent Flow		
Sidewalk Configuration	**None**	**Upwind**	**Downwind**	**None**	**Upwind**	**Downwind**
X-Force, C_x	0.324	0.312	0.322	0.261	0.249	0.253
Z-Force, C_z	0.484	0.266	0.434	0.161	0.131	0.127
Lift Slope, $dC_z/d\alpha$	0.61	-0.89	0.13	0.85	1.87	1.11
Torque, C_m	0.168	0.110	0.171	0.129	0.082	0.127
Torque Slope, $dC_m/d\alpha$	-0.16	-0.35	-0.18	0.01	-0.02	0.00

TABLE iii SUMMARY OF DYNAMIC TEST RESULTS

Test No.	Label	Flow	Sidewalk	Damping (nominal)	f_v (Hz)	f_t (Hz)	Vmax (mph)	Flutter	Vortex-Induced Vibrations
1	sma101	smooth	none	0.5%	4.476	15.197	145	none observed	Vertical: 21 mph, 0.55 ft Torsional: 81 mph, 0.15^o
2	sma201	turbulent	none	0.5%	4.476	15.197	145	none observed	none observed
3	sha101	smooth	none	1.0%	4.476	15.197	147	none observed	Torsional: 82 mph, 0.16^o
4	smb101	smooth	upstr.	0.5%	4.414	14.816	146	none observed	Vertical: 22 mph, 0.84 ft Torsional: 79 mph, 0.12^o
5	smb201	turbulent	upstr.	0.5%	4.414	14.816	148	none observed	none observed
6	shb101	smooth	upstr.	1.0%	4.414	14.816	145	none observed	Vertical: 21 mph, 0.38 ft Torsional: 78 mph, 0.10^o
7	smc101	smooth	downstr.	0.5%	4.414	14.816	147	none observed	Vertical: 22 mph, 0.58 ft Torsional: 76 mph, 0.16^o
8	smc201	turbulent	downstr.	0.5%	4.414	14.816	148	none observed	none observed

TABLE iv VALUES OF $\overline{W}$, $\tilde{W}_1$ AND $\tilde{W}_2$ FOR A WIND SPEED OF 80 mph

Configuration	**Completed bridge**									**Construction stage**		
Sidewalk	**No sidewalk**			**Sidewalk upwind**			**Sidewalk downwind**			**No sidewalk**		
Load Direction	x	z	θ	x	z	θ	x	z	θ	x	z	θ
$\overline{W}$ (lb/ft for force and lb-ft/ft for torque)	250	150	6560	238	116	4340	242	128	6930	250	190	6710
$\tilde{W}_1$ (lb/ft for force and lb-ft/ft for torque)	404	1670	14800	387	1730	14400	392	1900	14500	593	2510	13900
$\tilde{W}_2$ (lb/ft for force and lb-ft/ft for torque)	161	1180	9030	154	1130	9490	157	1260	9500	177	1530	11400

TABLE v SUMMARY OF THE PREDICTED PEAK DIFFERENTIAL PRESSURES AND SUCTIONS (PSF)

Tap Location No.	Peak Pressures (PSF)	Peak Suctions (PSF)
1	29.1	50.8
2	40.5	62.4
3	35.9	46.3
4	27.7	48.9
5	45.0	51.2
6	39.2	51.6
7	32.1	57.8
8	44.2	53.4
9	39.2	48.9
10	29.1	58.7
11	24.6	54.5
12	31.1	49.9
13	38.7	59.0
14	31.7	50.1
15	40.5	55.2
16	32.9	48.7
17	41.1	55.1
18	42.0	50.3
19	46.7	44.8
20	50.2	49.9
21	48.3	62.1
22	48.7	55.4
23	53.3	48.7
24	49.8	45.6
25	46.0	55.5
26	53.5	51.2
27	49.7	46.6
28	34.0	54.7
29	48.8	63.2
30	46.5	45.2
31	52.3	59.5
32	50.2	48.8
33	52.6	56.0
34	51.1	51.2

TABLE vi PREDICTED WIND CONDITIONS AT THE TWO LOCATIONS

Probe Location No.	Hourly Mean Wind Speeds Exceeded During 5% of the Time Annually (mph)	Hourly Mean Wind Speeds Exceeded Once per year (mph)
1	13.7	32.0
2	16.7	35.7

Notes:

1. The mean wind speed which is exceeded 5% of the time is used to check the comfort level of the location in comparison to accepted comfort criteria.

2. The mean wind speed which is exceeded once per year is used to check the pedestrian safety of the location in comparison to accepted pedestrian safety criteria.

TABLE vii COMPARISON OF WIND SPEED RATIOS IN PYLON PRESSURE TEST AND FULL BRIDGE AEROELASTIC TEST FOR THE TWO WIND PROBES MEASURED AT THE PROSPECT PYLON ENTRANCE FOR FIVE WIND ANGLES

True Azimuth, used in Pressure Test	Corresponding Wind Angles Defined in Aeroelastic Test	Speed Ratio in Pressure Test		Speed Ratio in Aeroelastic Test	
		Probe at Entrance	Probe at Corner	Probe at Entrance	Probe at Corner
degree	degree	V / Vg	V / Vg	V / Vg	V / Vg
20	270 (perpendicular to bridge, with existing bridge upwind)	0.183	0.391	0.124	0.328
110	0 (along bridge)	0.518	0.789	0.293	0.409
140	30	0.151	0.198	0.110	0.514
170	60	0.137	0.198	0.114	0.163
200	90 (perpendicular to bridge)	0.173	0.162	0.163	0.143

TABLE viii SUMMARY OF FULL BRIDGE AEROELASTIC MODEL TESTS, COMPLETED BRIDGE CONFIGURATION

Test File	Test No.	Flow condition	Existing bridge	Wind direction (Test angle)	V_{deck} (mph) Maximum wind speed at deck height
VS9201	1	Hurricane profile	No	Perpendicular to bridge (90°)	158
VS0201	2	Hurricane profile	No	Along the Bridge (0°)	143
VS3201	3	Hurricane profile	No	30° to the bridge	140
VS6201	4	Hurricane profile	No	60° to the bridge	142
VS2201	5	Hurricane profile	Yes	Perpendicular to bridge (270°)	150
VS6301	6	Open Country profile	No	60° to the bridge	163
VS3301	7	Open Country profile	No	30° to the bridge	155
VS0301	8	Open Country profile	No	Along the Bridge (0°)	161
VS9301	9	Open Country profile	No	Perpendicular to bridge (90°)	169
VS2301	10	Open Country profile	Yes	Perpendicular to bridge (270°)	183
VS9101	11	Smooth Flow	No	Perpendicular to bridge (90°)	147

TABLE ix SUMMARY OF FULL BRIDGE AEROELASTIC MODEL TESTS, DOUBLE CANTILEVERED CONSTRUCTION STAGE

Test File	Test No.	Flow condition	Existing bridge	Construction Box at Cantilever Ends	Wind direction (Test angle)	V_{deck} (mph) Maximum wind speed at deck height
VC9201	1	Hurricane profile	No	Yes	Perpendicular to bridge (90°)	103
VC9202	2	Hurricane profile	No	No	Perpendicular to bridge (90°)	103
VC0201	3	Hurricane profile	No	No	Along the Bridge (0°)	99
VC3201	4	Hurricane profile	No	No	30° to the bridge	100
VC6201	5	Hurricane profile	No	No	60° to the bridge	99
VC2201	6	Hurricane profile	Yes	Yes	Perpendicular to bridge (270°)	99
VC6301	7	Open Country profile	No	No	60° to the bridge	101
VC3301	8	Open Country profile	No	No	30° to the bridge	106
VC0301	9	Open Country profile	No	No	Along the Bridge (0°)	111
VC9301	10	Open Country profile	No	No	Perpendicular to bridge (90°)	105
VC2301	11	Open Country profile	Yes	Yes	Perpendicular to bridge (270°)	127
VC9101	12	Smooth Flow	No	No	Perpendicular to bridge (90°)	122

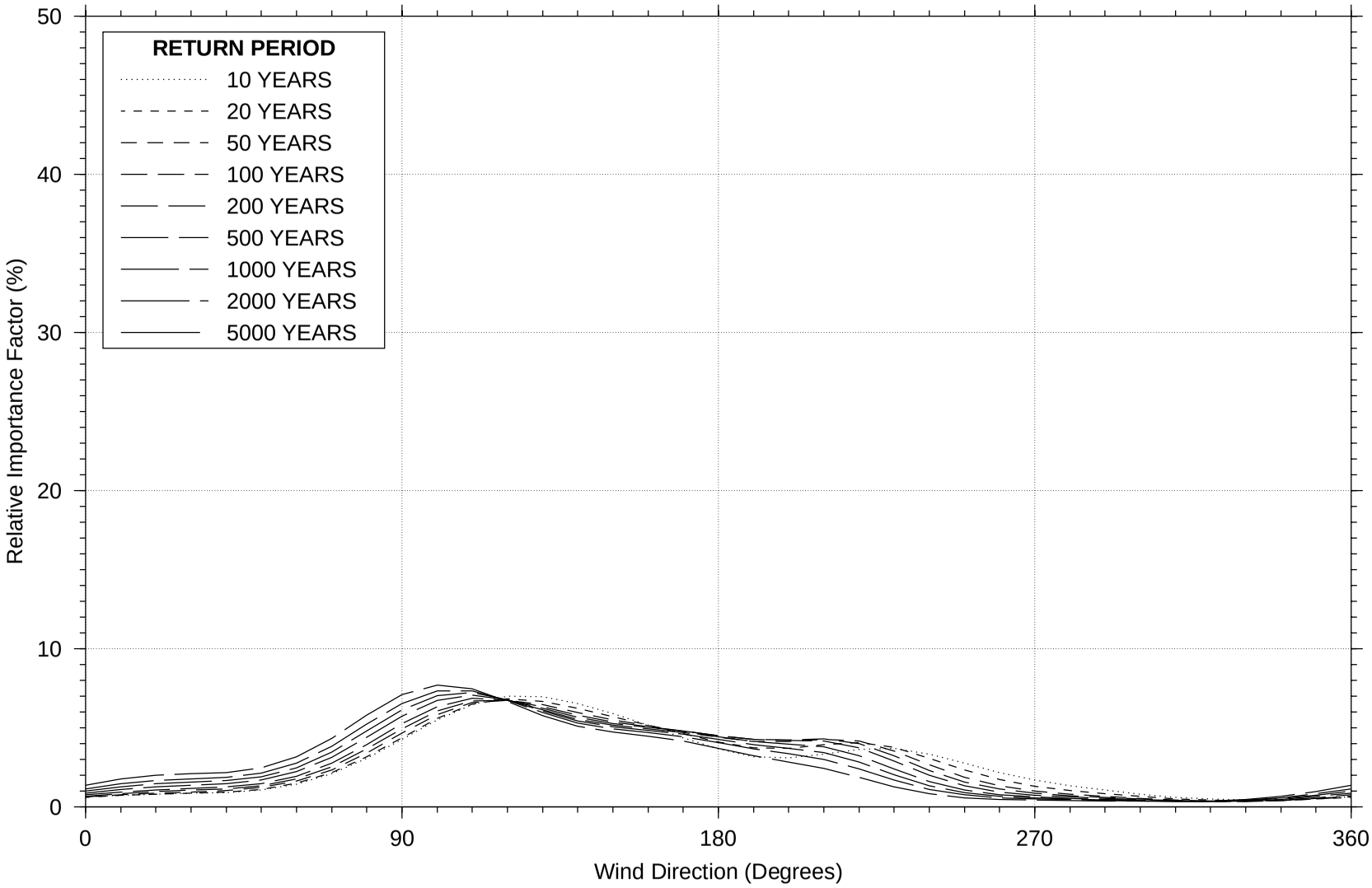

FIGURE i RELATIVE IMPORTANCE FACTORS FOR VARIOUS WIND DIRECTIONS AND MAXIMUM WIND SPEEDS WITH DIFFERENT RECURRENCE INTERVALS - HURRICANE WINDS AT 10m

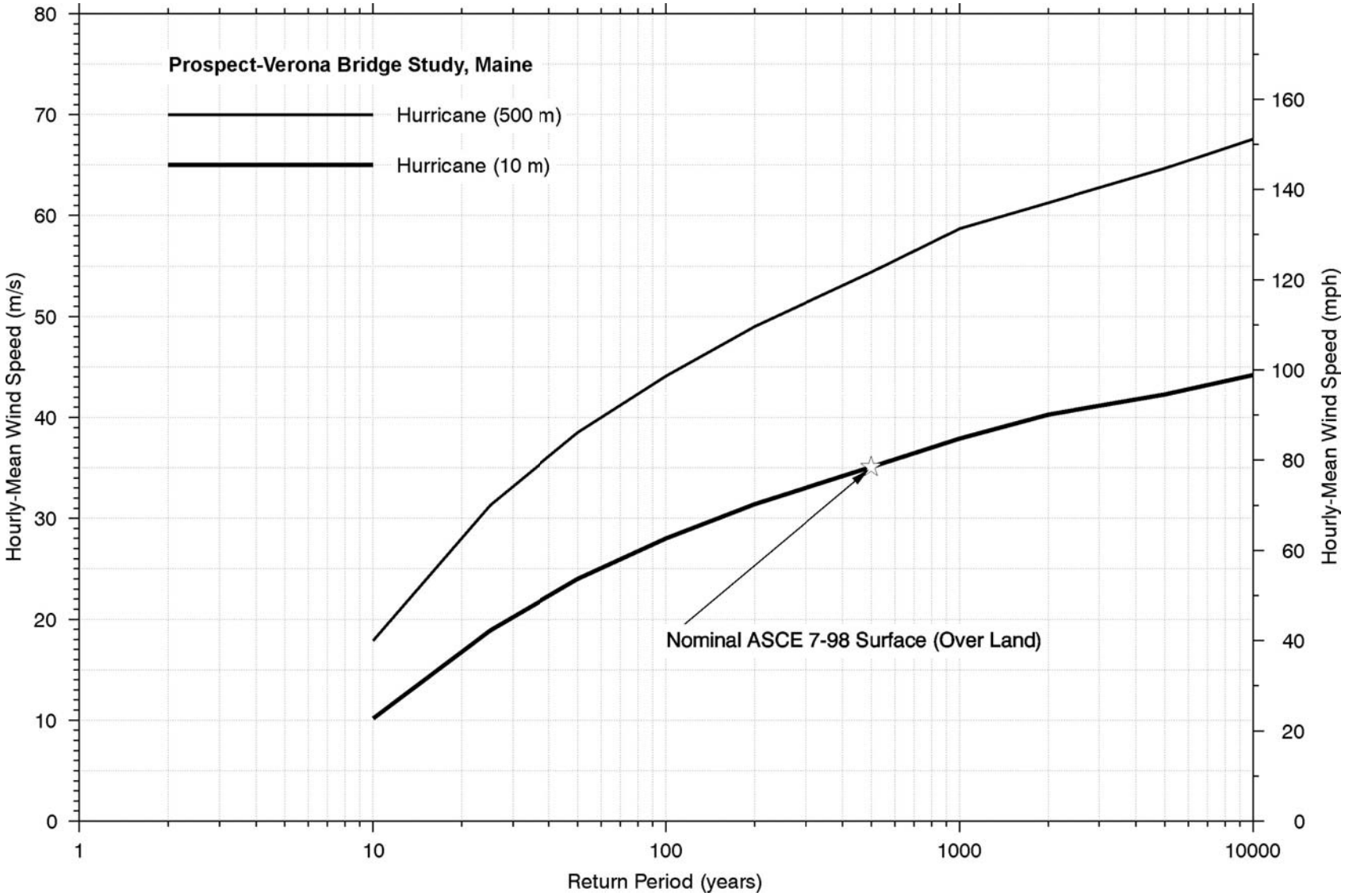

FIGURE ii PREDICTED EXTREME HOURLY-MEAN WIND SPEEDS FOR VARIOUS RETURN PERIODS FOR HURRICANE WINDS AT 10 m (33 ft)

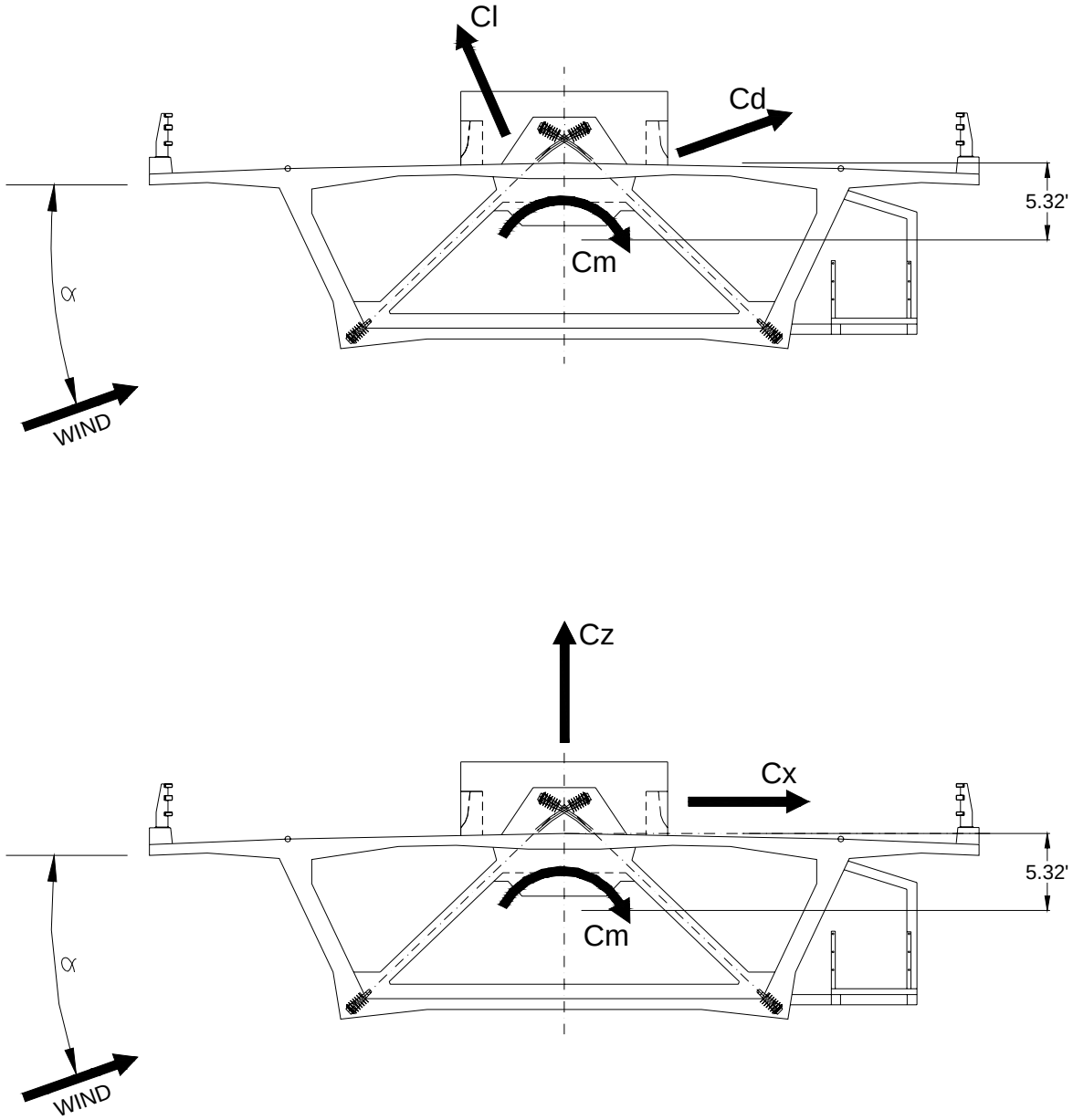

FIGURE iii SKETCH SHOWING SIGN CONVENTION OF FORCES

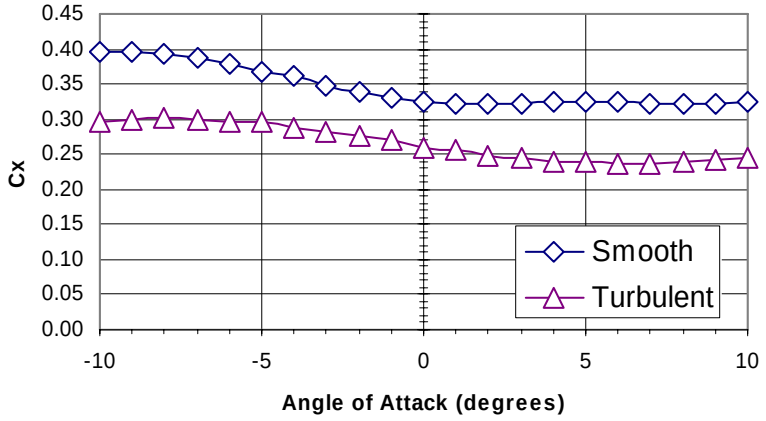

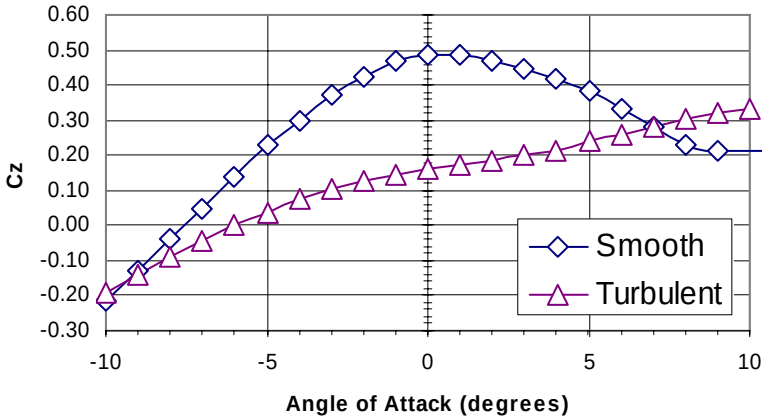

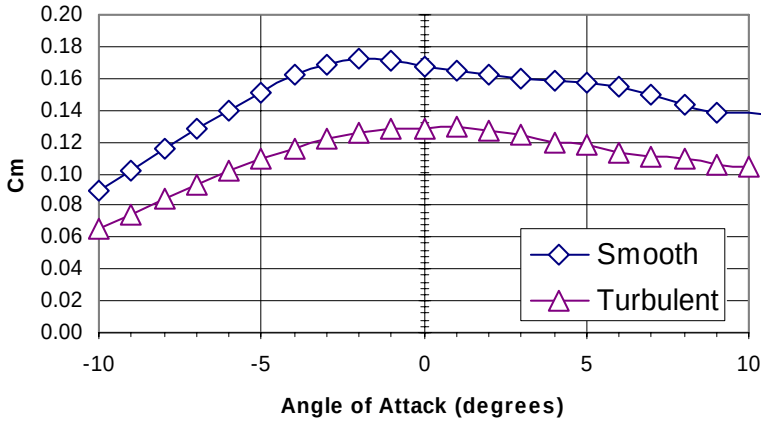

FIGURE iv STATIC FORCE COEFFICIENTS (NO SIDEWALK)

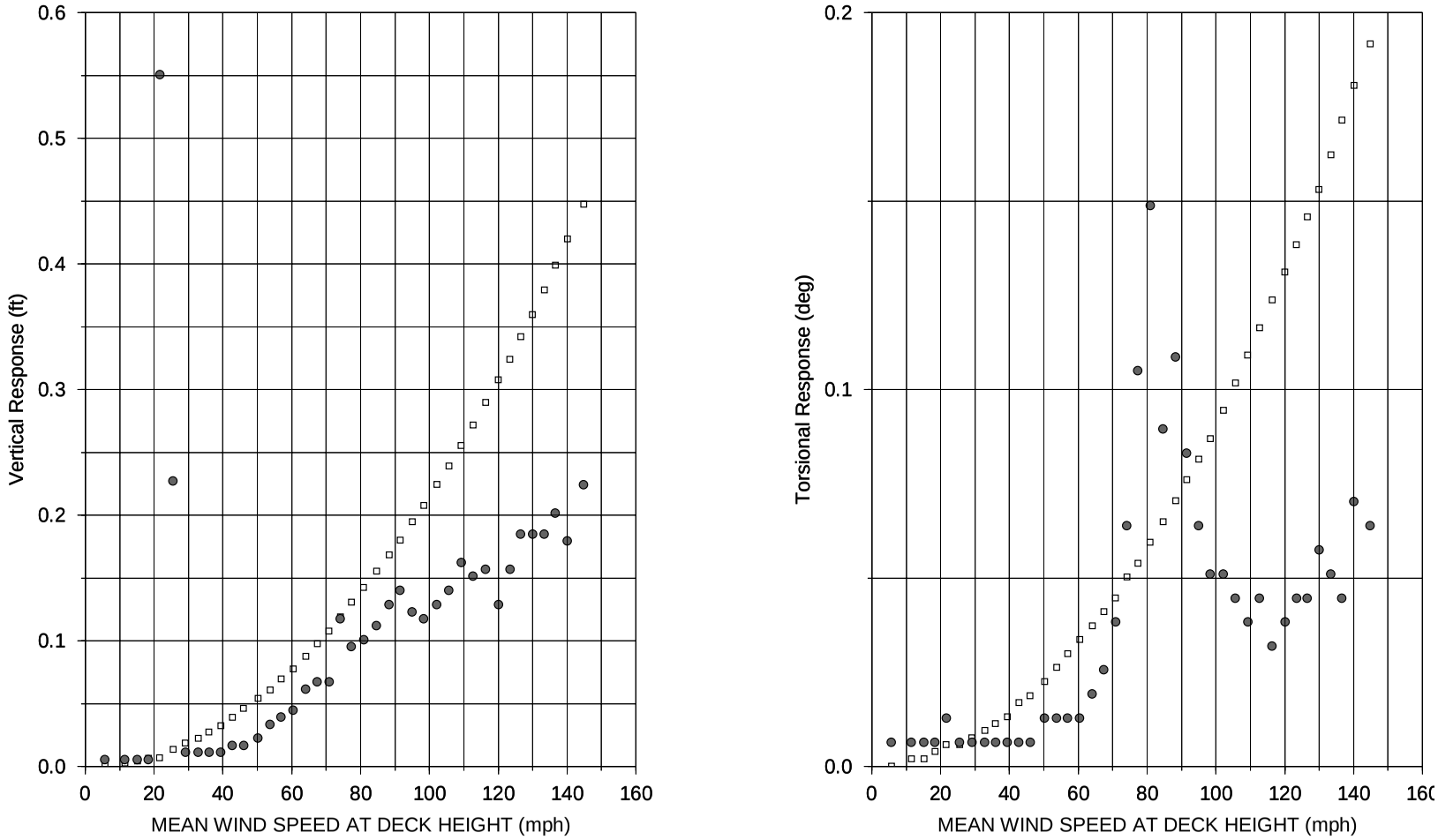

FIGURE v DYNAMIC TEST RESULT, TURBULENT FLOW AT 0° ANGLE OF ATTACK, SIDEWALK UPSTREAM WITH MODIFIED FREQUENCIES

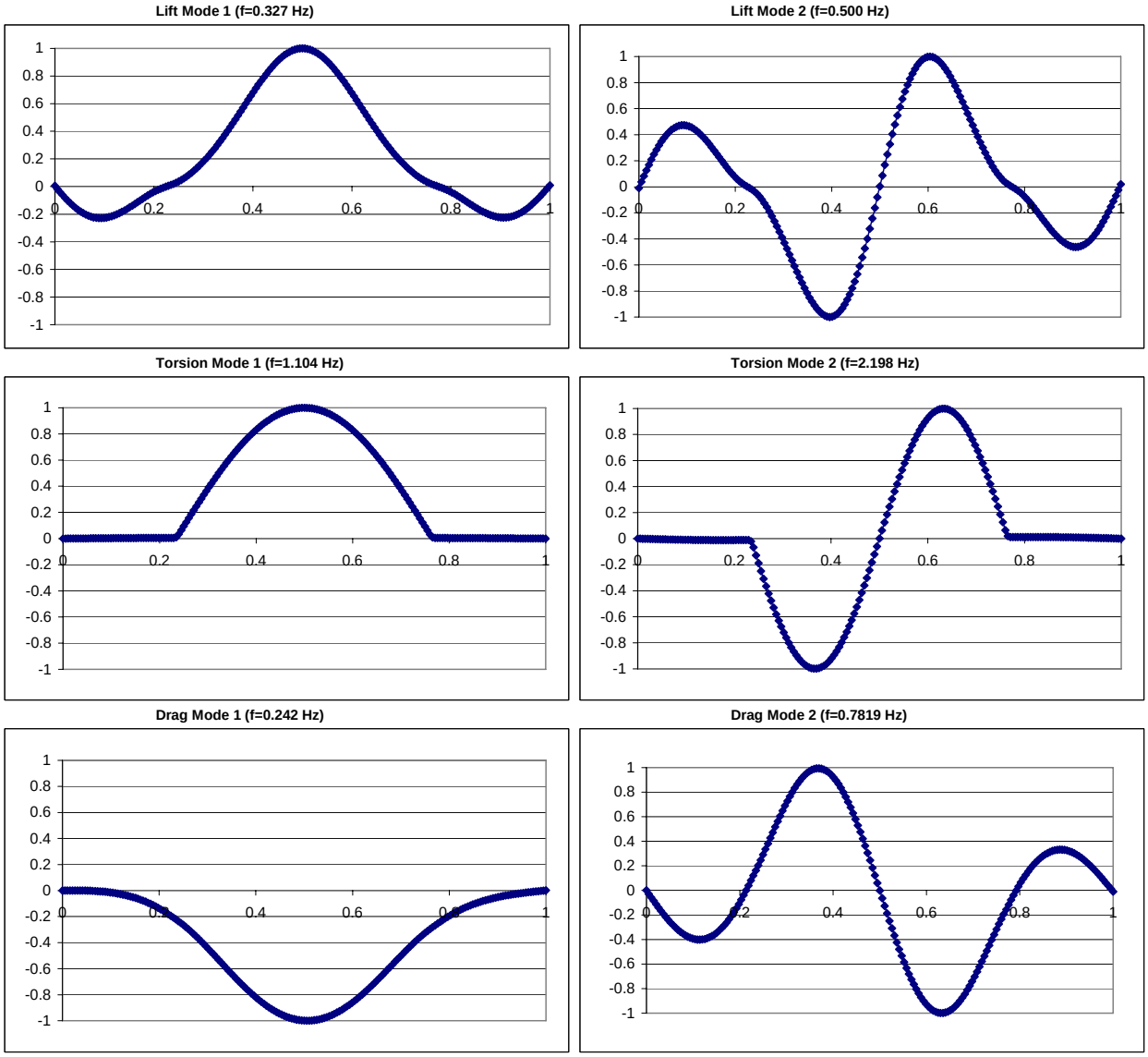

FIGURE vi MODE SHAPES USED IN THE EQUIVALENT STATIC LOAD ANALYSIS – COMPLETED BRIDGE

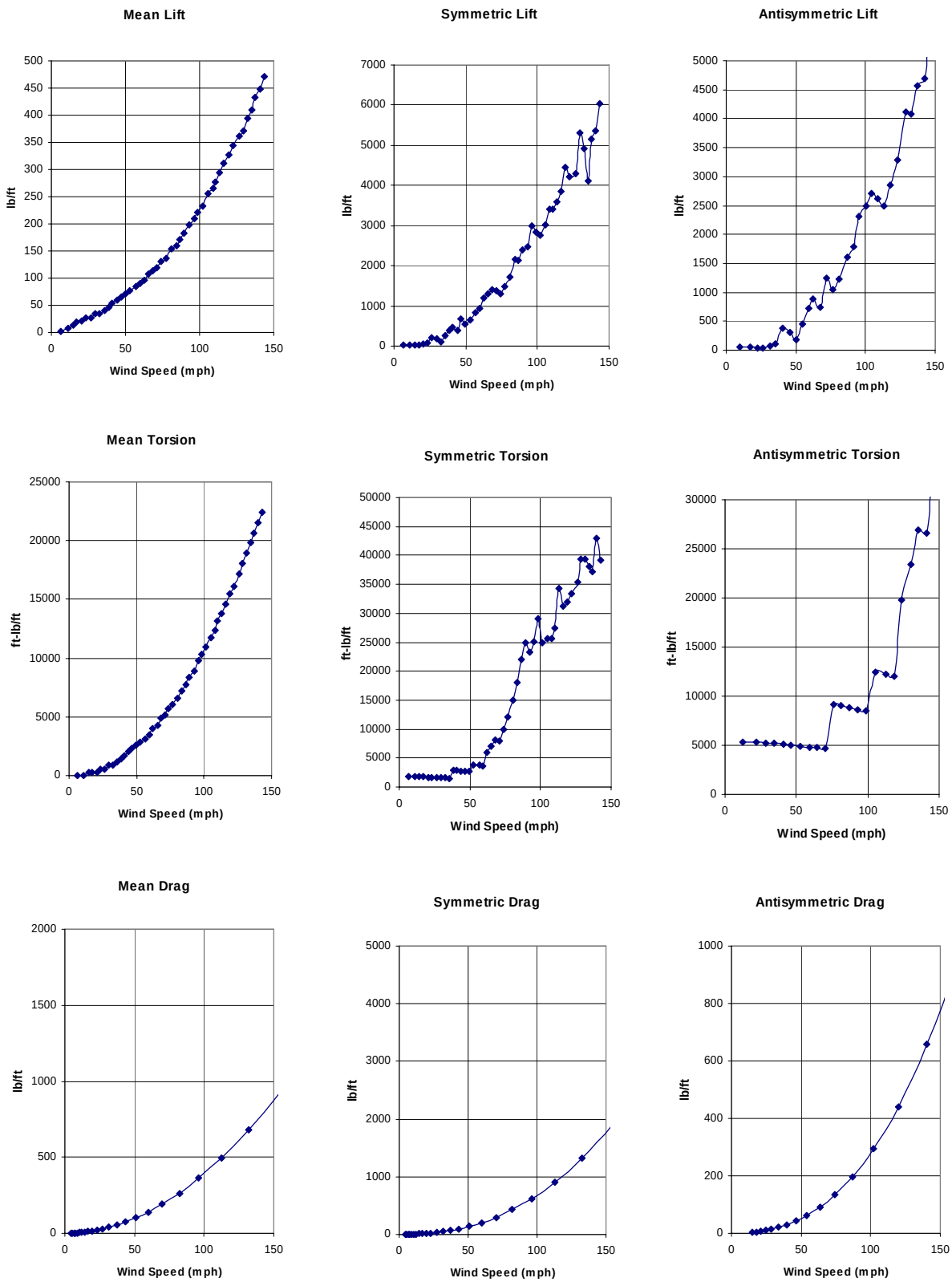

FIGURE vii WIND LOAD COMPONENTS FOR THE BRIDGE DECK – COMPLETED BRIDGE CONFIGURATION

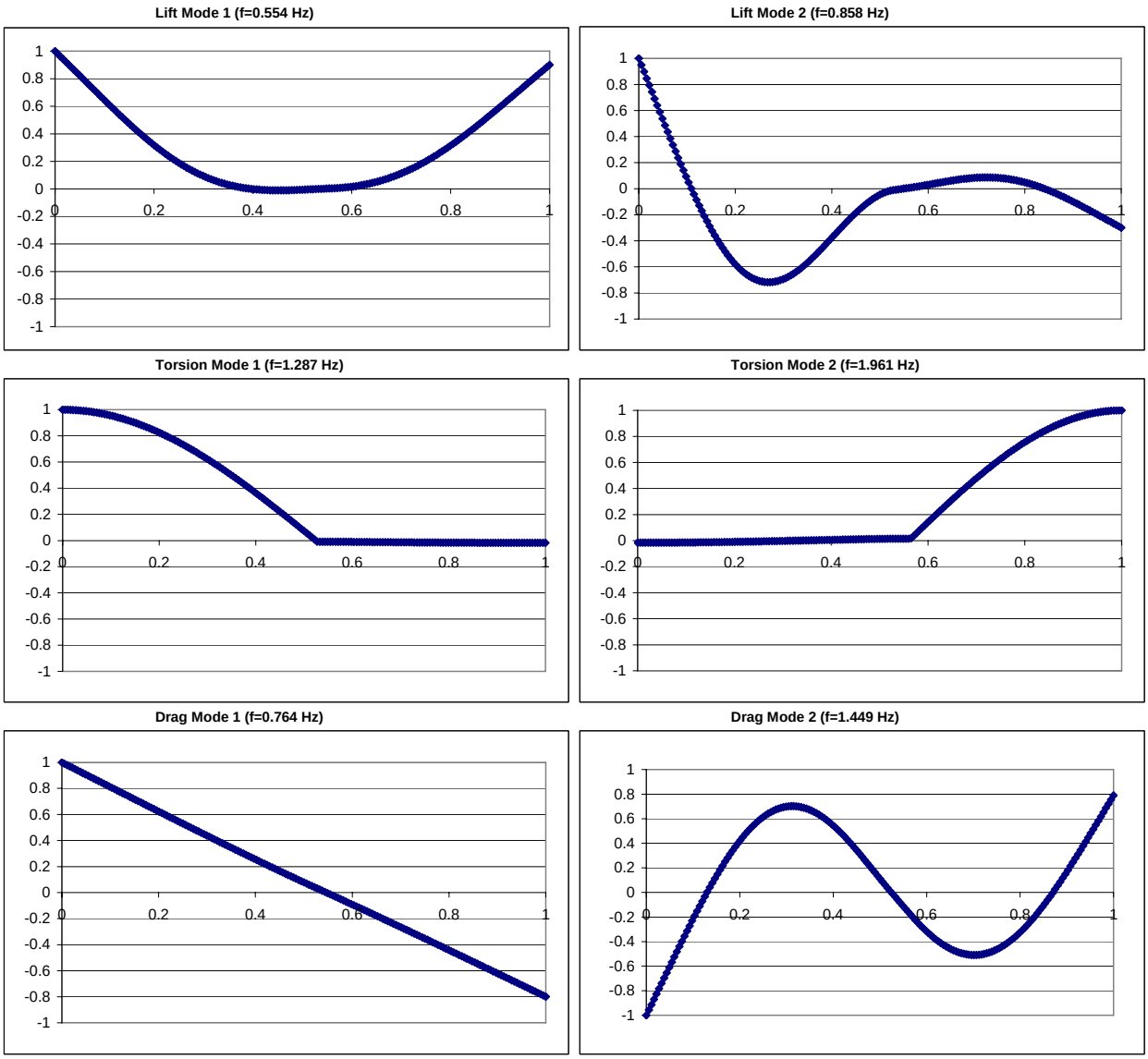

FIGURE viii MODE SHAPES USED IN THE EQUIVALENT STATIC LOAD ANALYSIS – CONSTRUCTION STAGE

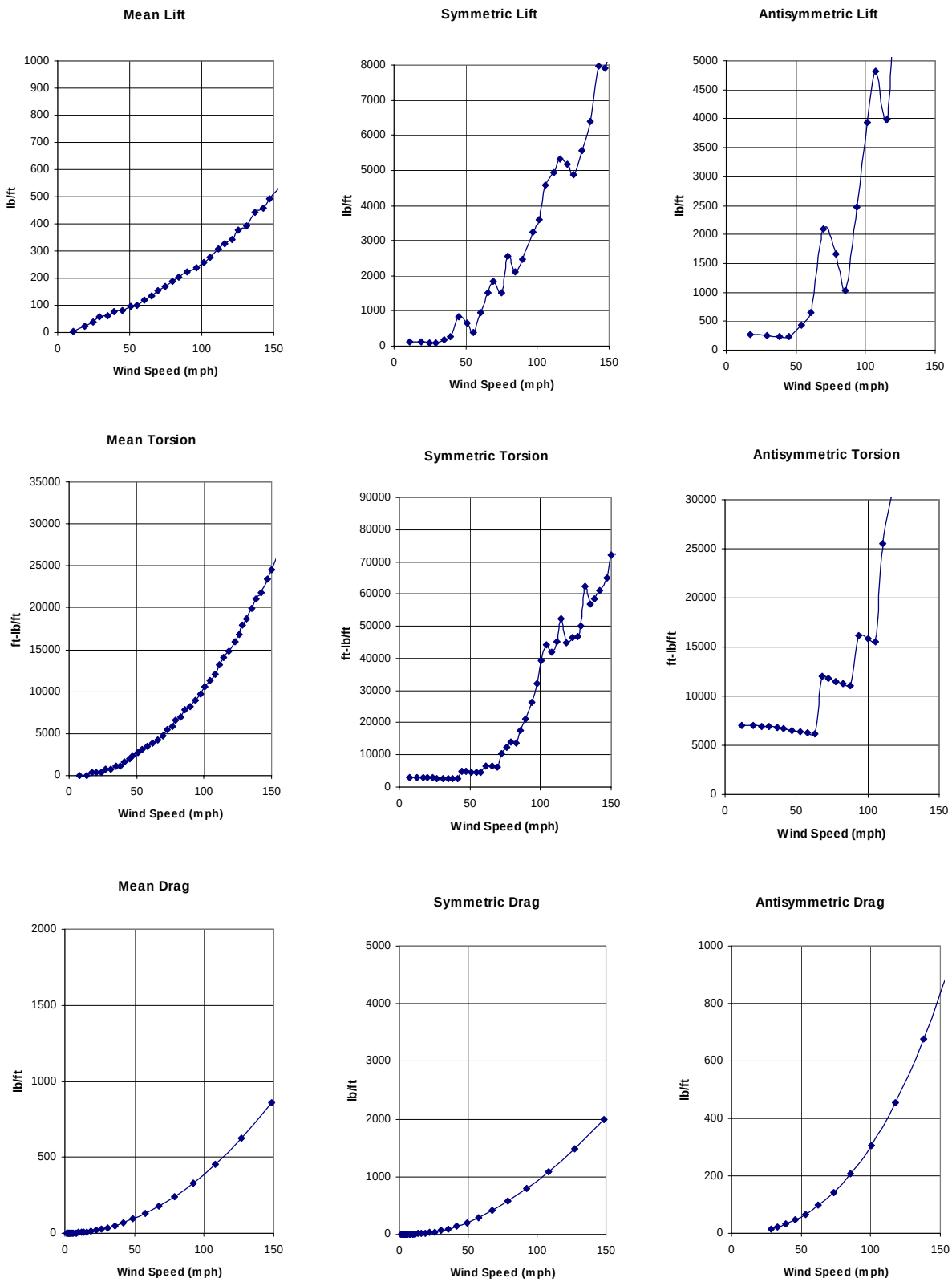

FIGURE ix WIND LOAD COMPONENTS FOR THE BRIDGE DECK – CONSTRUCTION STAGE CONFIGURATION

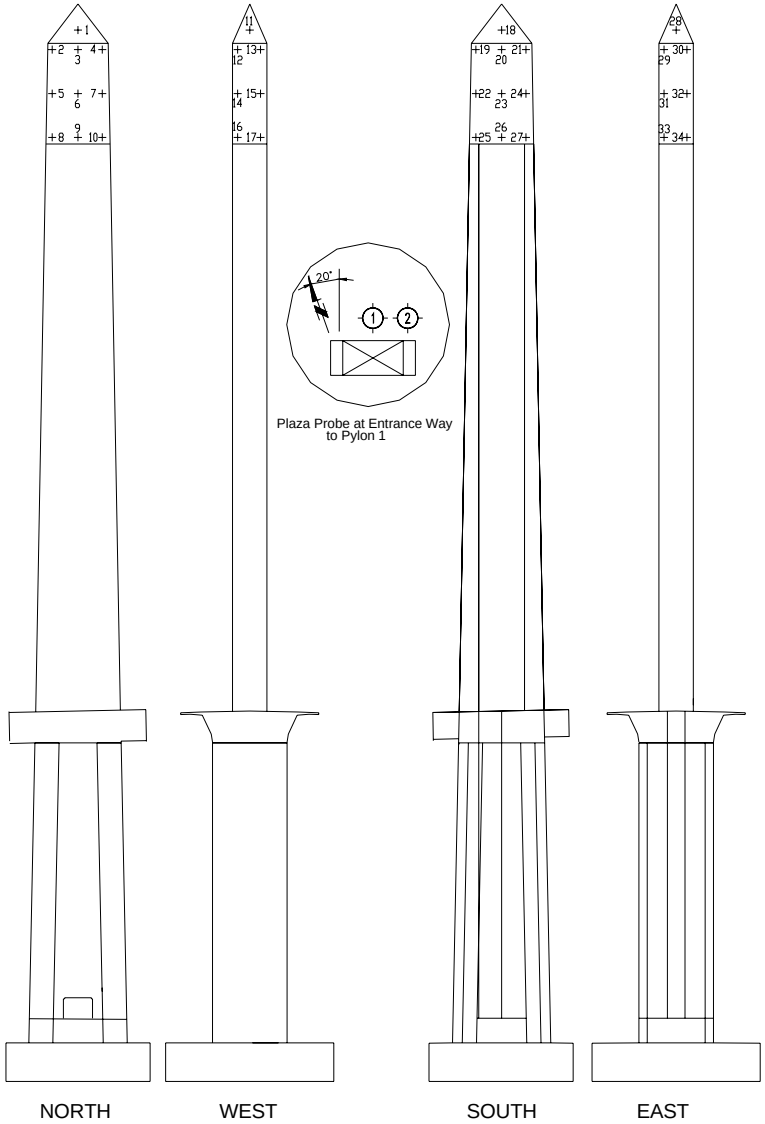

FIGURE x LOCATIONS OF PRESSURE TAPS AND WIND PROBES

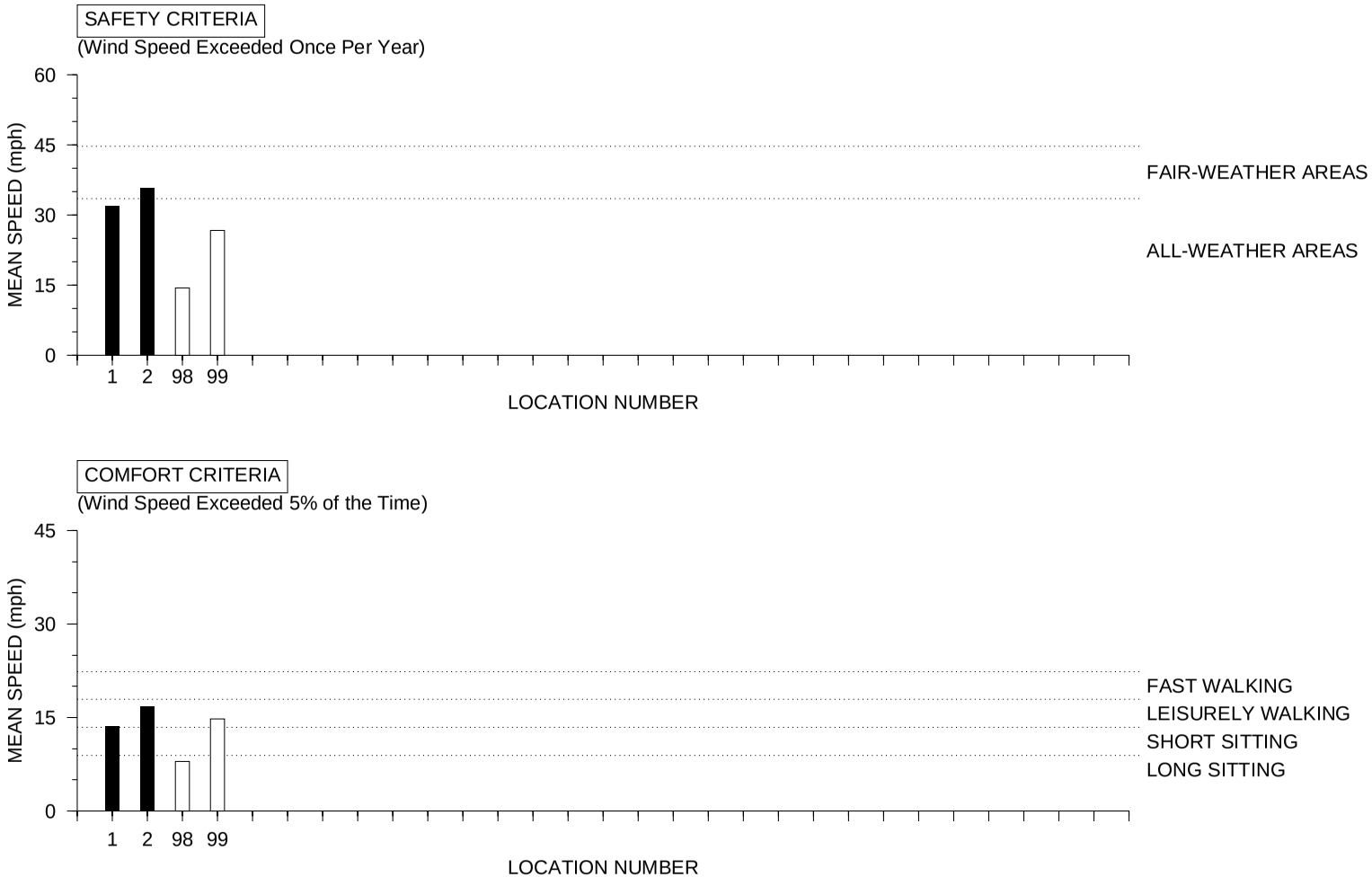

LOCATION 98: TYPICAL SUBURBAN
LOCATION 99: TYPICAL OPEN COUNTRY

File: p025
Dec. 01, 2004

FIGURE xi PREDICTED MEAN WIND SPEEDS COMPARED WITH CRITERIA FOR PEDESTRIAN COMFORT AND SAFETY

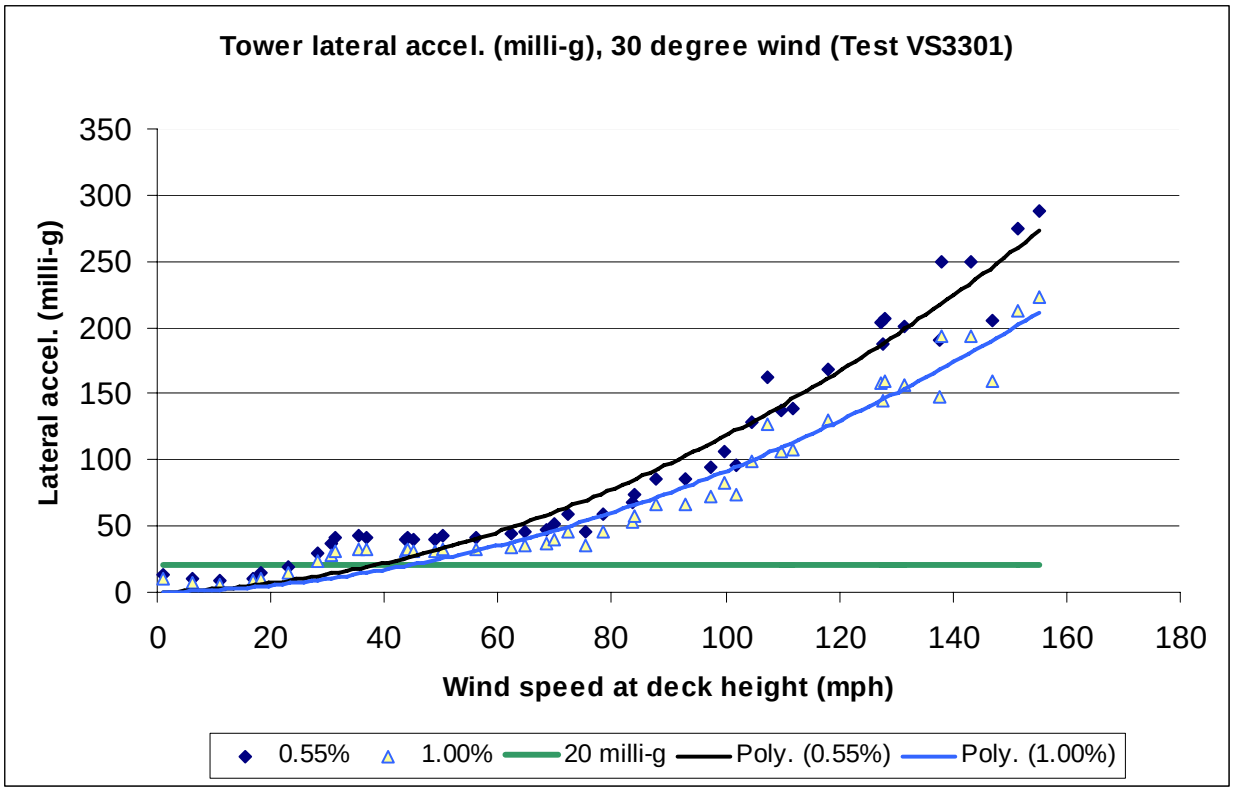

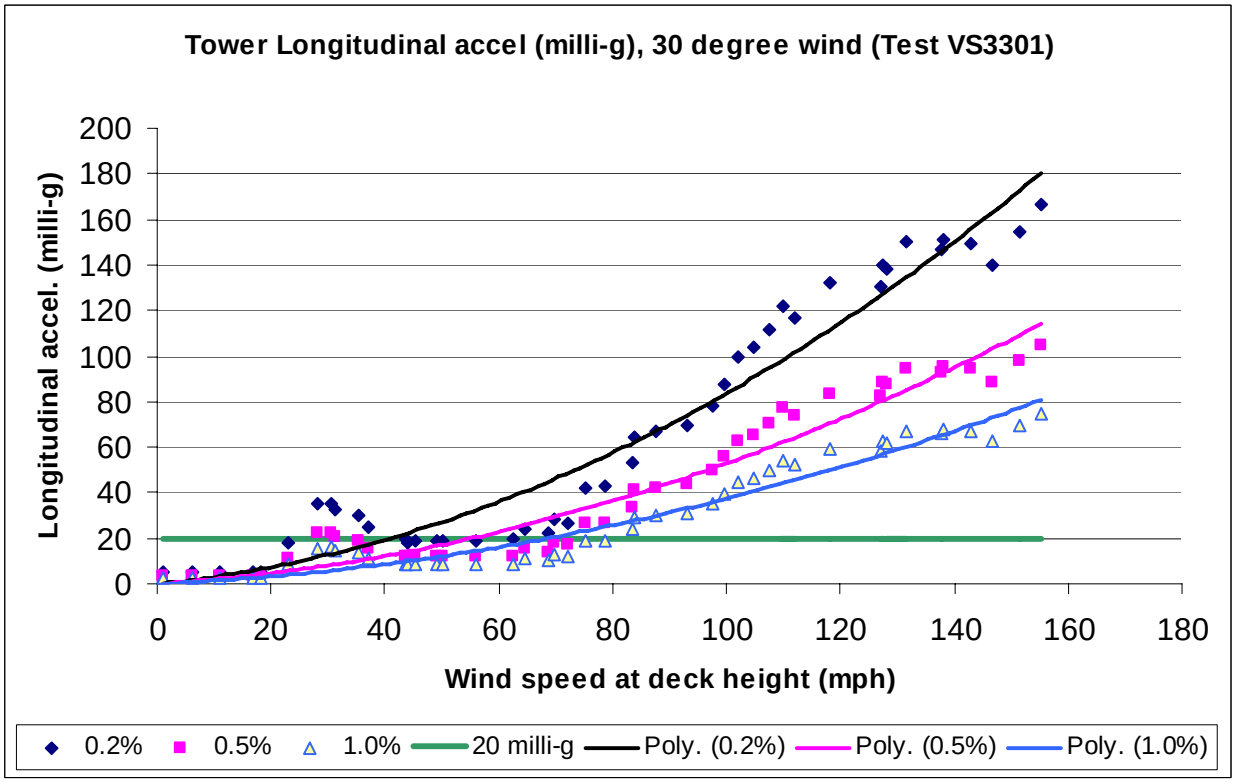

FIGURE xii PYLON ACCELERATIONS AT 30° WIND

DETAILS OF THE STUDY

Project Name: The Prospect Verona Bridge

Project Location: Maine, USA.

Project Descriptions: The proposed Prospect Verona Bridge is planned as a replacement for the Waldo-Hancock Bridge on US Route 1 between the towns of Prospect and Verona, Maine, over the Penobscot River. The proposed cable stay bridge has a single plane of stays from two pylons supporting a cast-in-place concrete deck. The pylons are about 430 ft high and are of rectangular plan with variable dimensions. They are similar in appearance to the Washington Monument. There will be an observation deck at the top of one of the pylons, which will be accessed by elevator at the base of the pylon. The concrete deck is a closed box 57.5 ft wide and 12.8 ft deep at a maximum elevation of 154 ft above the water. The total length of the bridge is 2120 ft with a main span of 1161 ft. There will possibly be a sidewalk built on the bridge at a future date, placed below one of the "wings" of the deck.

Test Dates:
Section Model (Dynamic) – July 2004
Section Model (Static) – July 2004
Pylon Pressure Model – October 2004
Full Aeroelastic Model (Completed Bridge and Construction Stage) – December 2004

Preliminary Reporting:
Section Model (Dynamic) – September 2004
Section Model (Static) – September 2004
Equivalent Static Loads – September 2004
Pylon Cladding Pressure and Pedestrian Level Wind – November 2004
Full Aeroelastic Model (Completed Bridge and Construction Stage) – November to December 2004

Report Scope: The report is organized as follows:

Section 1 – Introduction
Section 2 – The Modeling of the Wind
Section 3 - Section Model Study
Section 4 - Equivalent Static Load Analysis
Section 5 – Pylon Pressure Study
Section 6 – Determination of Pedestrian Level Wind
Section 7 – Full Aeroelastic Model Study

1 INTRODUCTION

1.1 General

This report describes the section model, pylon pressure model and full aeroelastic model studies for the proposed Prospect Verona Bridge in Maine. The proposed bridge is planned as a replacement for the Waldo-Hancock Bridge on US Route 1 between the towns of Prospect and Verona, Maine, over the Penobscot River. The proposed cable stay bridge has a single plane of stays from two pylons supporting a cast-in-place concrete deck. The pylons are about 430 ft high and are of rectangular plan with variable dimensions. There will be an observation deck near the top of the Prospect Pylon, which will be accessed by elevator at the base of the pylon. The concrete deck is a closed box, and is 57.5 ft wide and 12.8 ft deep with a maximum elevation of 154 ft above the water. The total length of the bridge is 2120 ft with a main span of 1161 ft. A suspended sidewalk will possibly be constructed at a future date, placed below one of the “wings” of the deck.

Figure 1.1 shows the location of the bridge, and Figure 1.2 shows the overall outline of the bridge. Dimensions of the deck and pylon are given in Figures 1.3 and 1.4 respectively.

A primary objective of the section model study was to investigate the overall aeroelastic stability in high wind conditions and to define the wind speeds associated with possible flutter instability and vortex shedding induced oscillation. The investigation also was intended to define the dynamic response characteristics of the section to turbulent wind over a full range of wind speed and to provide information for the design of the structure against wind effects. Since the Prospect Pylon includes a multi storey observation area with glass curtain walls, a pressure model study was conducted to obtain the wind cladding loads on this portion of the pylon. The pressure study was also used to provide measurements of the pedestrian level wind speeds at the Prospect Pylon entrance area and to provide predictions of wind speeds expected at the site, which were then compared with acceptance criteria for pedestrian comfort and safety. The bridge aeroelastic model was designed and constructed to determine the response characteristics of the bridge to three-dimensional turbulent flow in wind conditions characteristic of the site winds. Two configurations of the bridge were studied in the aeroelastic model investigation. These included the completed bridge and the double cantilevered construction stage,.

The behavior of the 1:70.5 scale section model was studied in the 3.4m wide by 2.5m high High-Speed Test Section of the Boundary Layer Wind Tunnel II (BLWTII) located at the Boundary Layer Wind Tunnel Laboratory, the University of Western Ontario. Section model tests were conducted at the inlet to the test section in both smooth flow and grid-generated turbulent flow conditions. The 1:200 scale pylon pressure model was studied on the automated turntable in the High-Speed Test Section. The 1:200 scale bridge aeroelastic model was tested on the turntable in the Low Speed Test Section of BLWTII under a hurricane profile corresponding to a roughness length of Z_o=0.03ft and a typical open country exposure corresponding to a roughness length of Z_o=0.1ft. An additional “smooth flow” test was carried out with the bridge model elevated above the boundary layer of the tunnel floor in order to identify any potential vortex shedding induced vibration and flutter instability.

1.2 Scope of Report

A wind climate study was carried out for the Prospect Verona Bridge (see Section 2). The design probability distribution of surface wind speed and direction was developed on the basis of full scale meteorological records from nearby weather stations. Monte Carlo simulations of the tropical storms were also carried out to assess their impact on extreme winds expected to affect the Prospect Verona Bridge.

A rigid section model for the basic deck cross section was designed and constructed at a scale of 1:70.5. The total length of the model was 7ft. The section model was ballasted to the scaled mass and mass moment of inertia of the prototype and mounted on a dynamic test rig. The stiffness of the model support system was adjusted to simulate the scaled frequencies of the prototype in lift and torsion. The model was tested in both smooth and turbulent flow conditions to measure the response of the deck (see Section 3).

Information from the static and dynamic section model tests were used in combination with the computed dynamic mode shapes and frequencies (provided by the engineers) to predict the full scale equivalent static loads for the structure (see Section 4).

A pressure model of the pylon was constructed at a scale of 1:200 and tested on the automated turntable in the High-Speed Test Section. Detailed measurements were made of wind-induced pressures and suctions on the glass cladding portion of the Prospect Pylon at the observation level (see Section 5). In addition, two wind probes were installed at the entrance area to the pylon in the pressure model study to measure the pedestrian level wind speeds (see Section 6).

A full aeroelastic model of the bridge was designed and constructed at a geometric scale of 1:200 relative to the prototype. Two bridge configurations were studied. These included the completed bridge and the double cantilever construction stage. The models were tested for representative site wind conditions (see Section 7). Two typical upstream terrain conditions were used in the tests. These included a hurricane exposure and an open country exposure. Measurements of bridge responses were taken at five different wind azimuths of 0°, 30°, 60°, 90° and 270° relative to the longitudinal axis of the bridge. Tests under 270° wind were conducted with the existing bridge upwind to assess its effect on the proposed Prospect Verona Bridge.

The wind characteristics generated in the wind tunnel are considered to be representative of the wind conditions at the bridge site. In addition, a “smooth flow” test was carried out with the bridge model elevated above the turbulent boundary layer of the tunnel floor (i.e. in “smooth” flow) in order to identify any potential vortex shedding induced vibration and flutter instability.

Presented in this report are results from:

- the meteorological study;
- the static section model tests of the bridge deck (i.e. the static force coefficients);
- the dynamic section model tests of the bridge deck (i.e. the response to vortex shedding and flutter instability in smooth flow, and buffeting responses in turbulent flow);
- the equivalent static load study of the bridge deck;
- the wind cladding load study from the pressure model test of the pylon, which includes predictions of differential pressures and suctions;
- the pedestrian level wind study;
- the bridge aeroelastic model study for the completed bridge and the double cantilever construction stage.

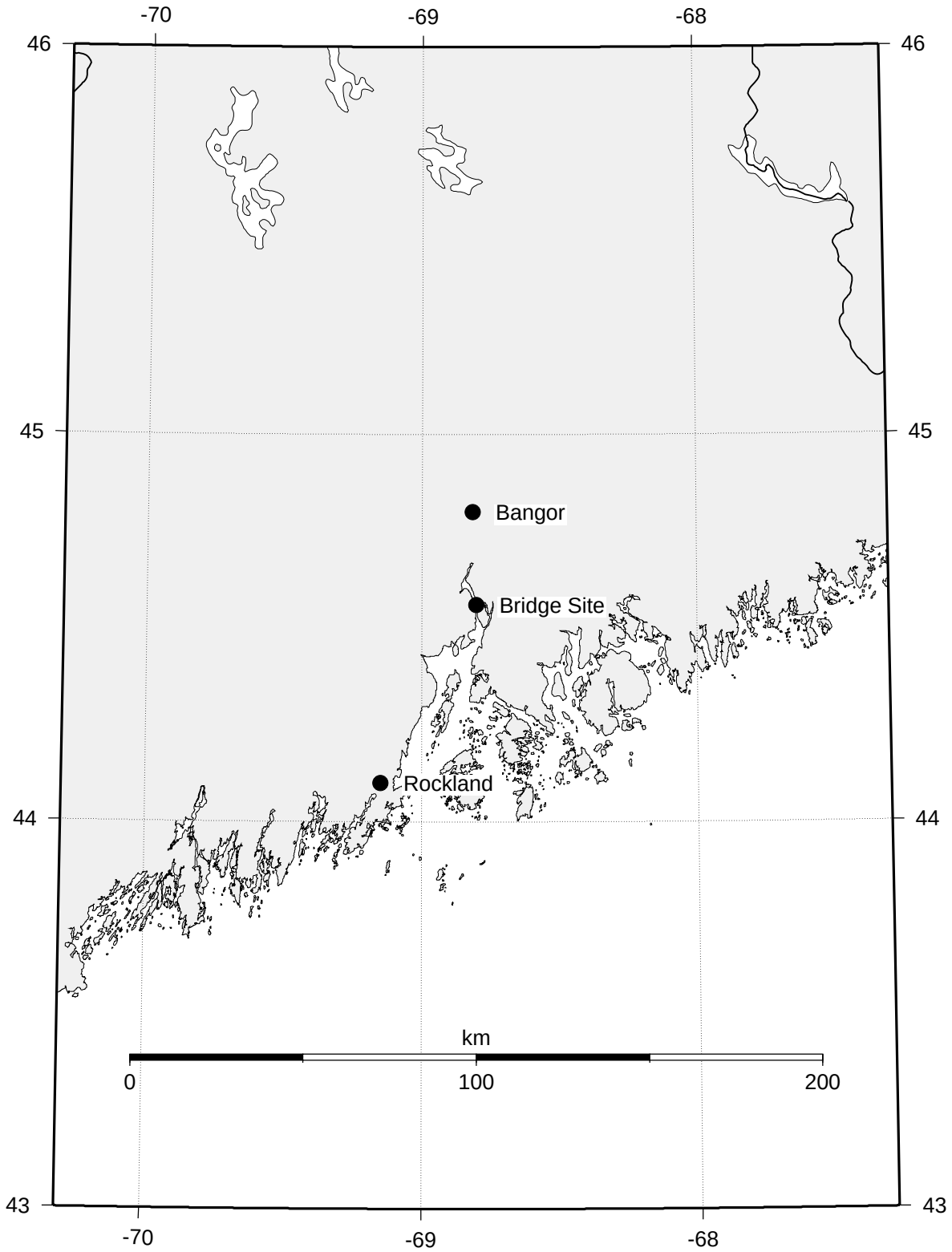

FIGURE 1.1 LOCATION OF THE PROSPECT VERONA BRIDGE, MAINE

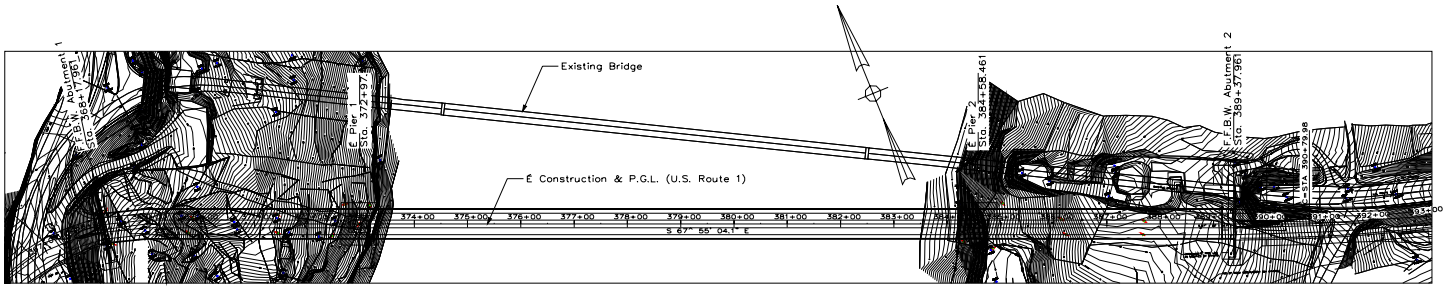

PLAN

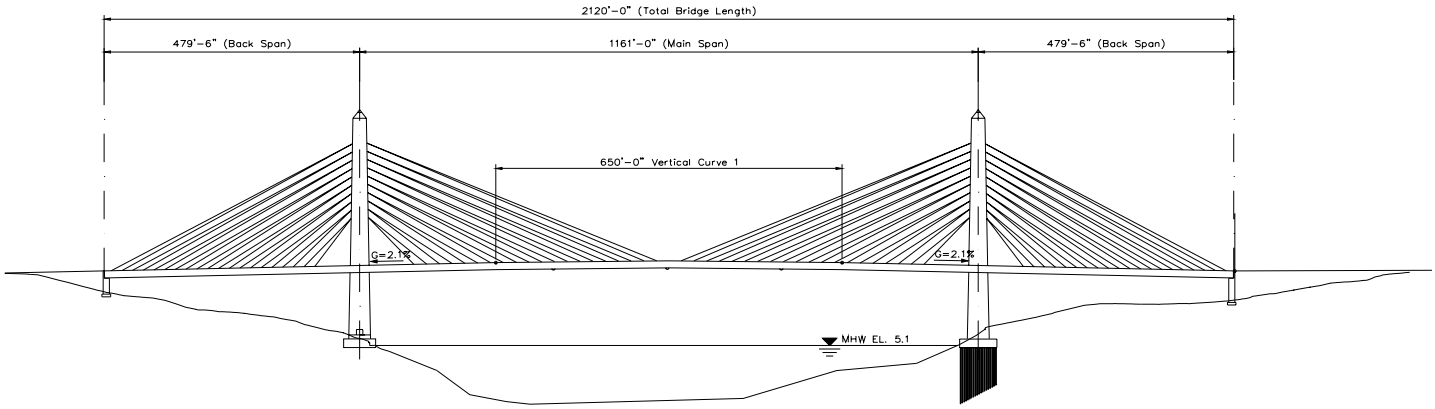

ELEVATION

FIGURE 1.2 PROTOTYPE DIMENSIONS – MAIN SPAN

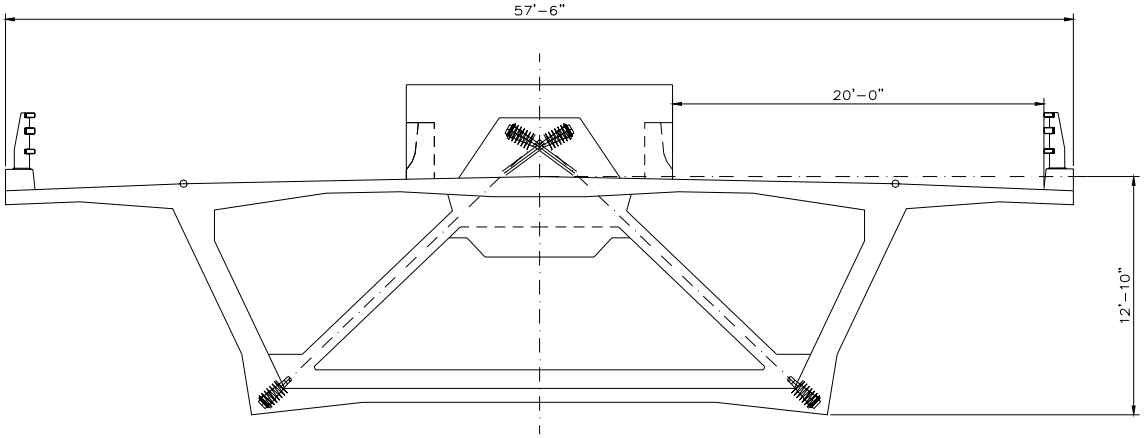

MAIN SPAN SECTION SHOWN

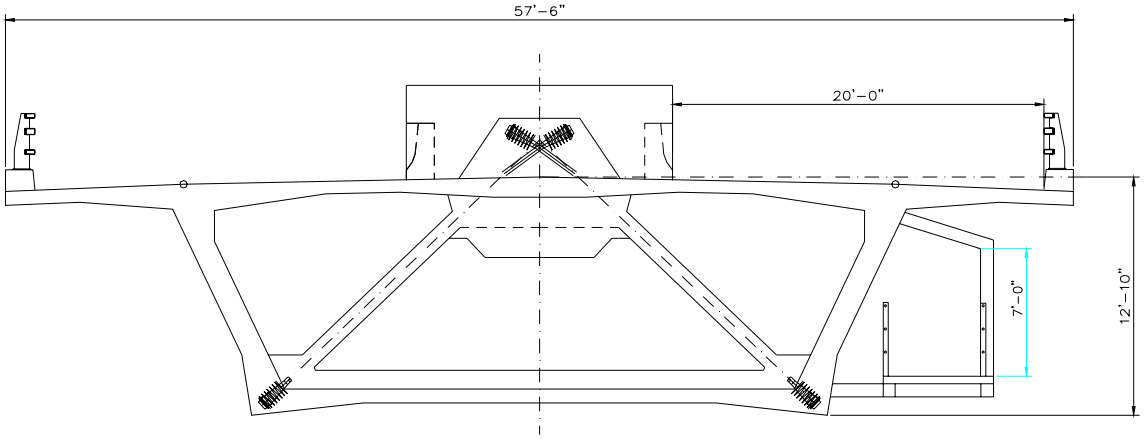

MAIN SPAN SECTION SHOWN
WITH SIDEWALK

FIGURE 1.3 PROTOTYPE DIMENSIONS – CROSS SECTION OF DECK

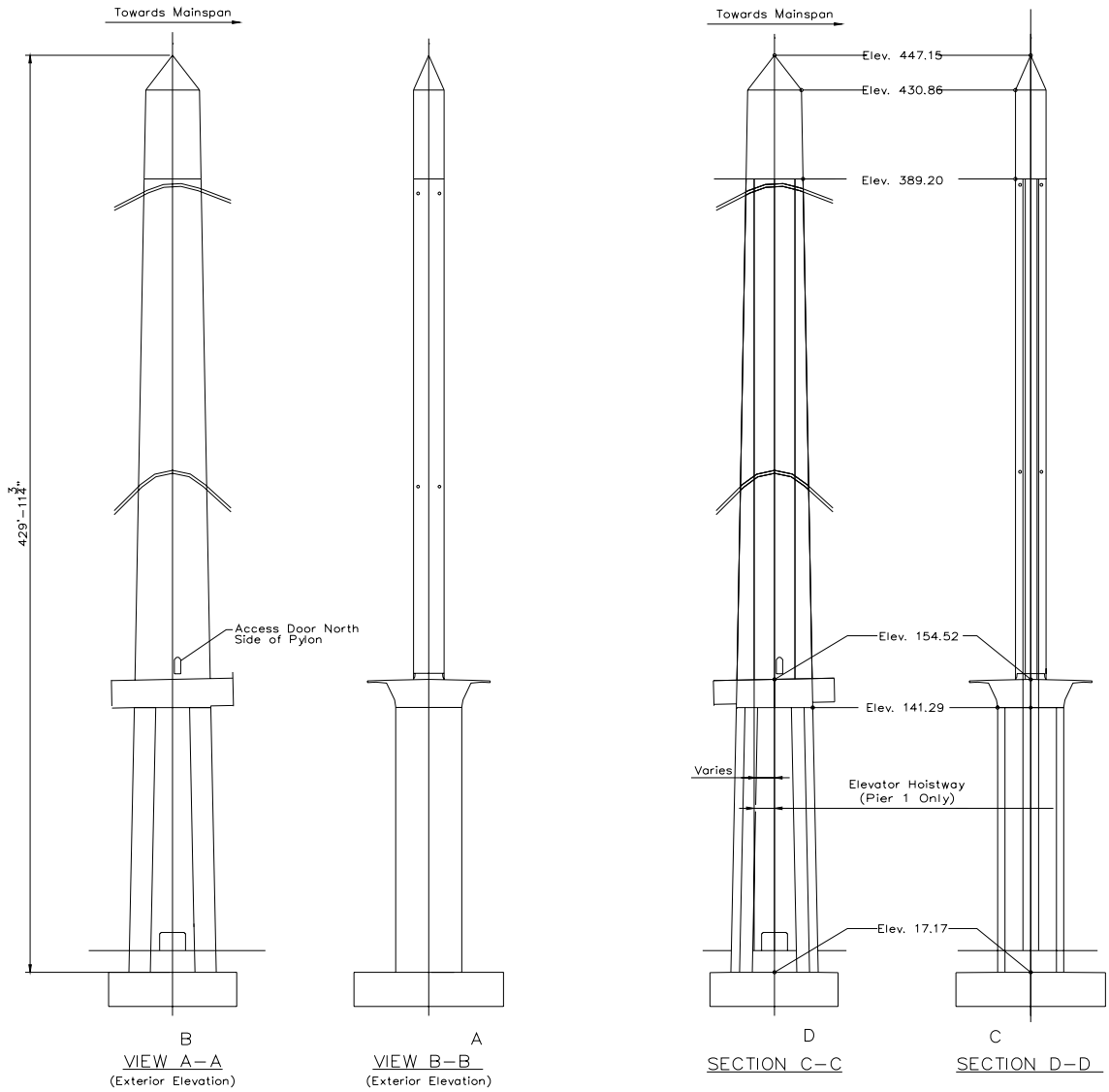

FIGURE 1.4 PROTOTYPE DIMENSIONS – BRIDGE PYLONS

2 THE MODELING OF THE WIND

2.1 Introduction

This section presents the findings of a study carried out to evaluate the statistical wind climate for the Prospect-Verona Bridge. Wind tunnel model studies provide information on wind forces and different measures of the bridge performance during wind events for which the speed and the direction of the approach wind are known. The wind climate provides a statistical prediction of the combinations of wind speed and wind direction which are expected at the bridge site. This information is then used to put the wind tunnel findings into context and to assess the risk of exceeding different levels of the bridge response during its design lifetime and beyond.

A statistical model of the wind climate can be determined from historical records of previously-observed wind speed and wind directions at particular weather stations. The locations of these weather stations should be such that the observed winds can be reliably related to those at the site of interest. Figure 2.1 shows the location of the bridge and the locations of the two principal nearby weather stations. These are weather stations at Rockland, Maine and Bangor, Maine. Surface wind-speed observations are typically made at 10 m above local ground in open-country type exposures at these stations. These sites are usually free of the influence of the local terrain roughness and provide representative measures of wind speed and wind direction for the region.

The study also includes Monte Carlo computer simulations of tropical storms and assesses their impact on extreme winds expected to affect the Prospect-Verona Bridge in the future. The findings of the Monte Carlo simulations show that extreme winds in the Prospect-Verona area are expected to result due to hurricanes rather than extratropical storms. This diminishes the importance of historical records of surface wind data. Typical record lengths of such observations are not long enough to predict future hurricane events; hence the reliance on Monte Carlo simulations to assess hurricane risk. With the importance of surface data diminished, the detailed reconciliation of data at the Rockland and Bangor anemometers becomes less important, except for commonly-occurring winds.

2.2 Analysis of Surface Wind Data

While the directional characteristics directional characteristics of surface data tend to be biased by local topographic differences, they are usually recorded much more frequently (8-24 readings per day) than upper-level measurements and hence offer better statistical estimates. An appropriate average conversion factor, relating mean surface and gradient wind speeds, can usually be estimated for sites with an open exposure (i.e. airports). The bases for such conversion factors are the power law (Reference 1) and established values for the power law exponent and gradient height. Thus, the overall speed predictions arising from surface data are generally better than their directional characteristics.

Surface wind speed and wind direction data for Rockland, Maine and Bangor, Maine were obtained as time histories of wind speed and direction. A location map for the various sites is shown in Figure 2.1. The time histories of wind speed and direction were processed to remove any data associated with known historical tropical storms in the area and then formed into monthly and annual frequency histograms of wind speed versus wind direction. The annual and seasonal frequency histograms were analyzed using the methodology outlined in Reference 1.

The main characteristics of the surface wind climate for Rockland, Maine are summarized in Figures 2.2 and 2.3. Figure 2.2 shows the shows the annual probability distribution of the mean hourly wind speed and wind direction at the surface (10m) level. The radial distance to a probability contour for a particular wind direction indicates the wind speed which is exceeded with that probability level within a sector of 22.5^{o}. The innermost contour indicates the directional variation of common wind speeds (exceeded an average of 1% of the time from each azimuth sector) and is comparable to a conventional wind rose. The shape of the outermost contour indicates the directional preferences of extreme winds. The data presented in Figure 2.2 indicate a directional preference of strong winds at the Rockland site from the northwest quadrant with a secondary lobe from the east.

Seasonal probability distributions are presented in Figure 2.3. Winter season is the combined months of December, January and February. Summer is the least windy period with maximum winds most likely in the spring and winter. The directional characteristics of the wind climate do not change significantly with season.

Similar plots for the Bangor site are shown in Figures 2.4 and 2.5. Bangor also shows a directional preference for strong winds from the northwest sector.

The directional characteristics of the surface wind climates are further illustrated in Figure 2.6 through 2.9. These diagrams shows the relative contribution of particular azimuth sectors to the exceedance of wind speeds associated with different recurrence frequencies. Data here are presented for average occurrence rates ranging from once per week through once per 500 years. Extreme winds are predominant from the northwest sector.

The overall strength of the wind climate can be ascertained from the prediction of the hourly mean wind speed expected for a given return period, regardless of wind direction. The hourly-mean wind speeds predicted for various return periods at these stations, at a 10 m reference height in open-country exposure, are summarized in Figure 2.10.

Also shown in Figure 2.10 is the nominal ASCE 7-98 [4] surface (over-land) hourly-mean wind speed. It is important to note that the current approach of the ASCE 7-98 is to predict 500-year wind speed and to reduce this by the square-root of the load factor to arrive at the “basic” wind speed. The basic wind speed is no longer directly associated with a 50-year return period.

The parent surface wind climate models were extrapolated to gradient height using the ASCE 7-98 Exposure ‘D’ power-law relationship (i.e. a factor of 1.4). Predicted hourly-mean wind speeds for various return periods are shown for this gradient climate model in Figure 2.10.

2.3 Monte Carlo Simulation of Hurricane Winds

Historical wind records at a particular weather station are insufficient to reliably predict extreme wind speeds which may be expected due to future hurricane passages. Typically weather data are available for station records of 20 to 40 years and are unlikely to capture a significant number of hurricane events during the recording life of the station. The approach used to overcome this difficulty is to determine the statistical parameters of tropical storms for the project area and to use a Monte Carlo simulation of hurricane events over a period of 100,000 years so that a statistically-meaningful sample of extreme winds at the project site can be examined. The average annual occurrence rate of these storms in the Prospect-Verona area is approximately 0.17. That is, on average, the area experiences one storm every five to six years. Depending on the storm track and the translation velocity, the duration of each storm passage may be 1 to 2 days. The procedures followed in such Monte Carlo simulations at the BLWTL are described elsewhere [Refs. 1, 2, 3].

Figure 2.11 shows the tracks of all tropical storms which have passed within 250 km of Prospect-Verona within the 1851 to 2002 period. Tropical storms are labelled as hurricanes when the one-minute sustained wind speed at 10 m above the water surface exceeds 64 knots any where within the storm system. The portions of tropical storm tracks with a sustained one-minute wind speed in excess of 64 knots (i.e. hurricane strength) are shown in Figure 2.12. The portions of tropical storms tracks which have reached tropical-storm strength are shown in Figure 2.13. In the northern hemisphere, the maximum wind speeds within a hurricane storm cell are to the right of the track which traces the movement of the eye of the hurricane. From Figure 2.12 it is clear that the majority of past hurricanes have passed to the south and the east of the bridge site and the corresponding maximum winds would have been experienced over water.

2.4 Design Wind Climate for Bridge Site

In addition to selecting a full-scale wind speed which is unaffected by the local terrain, it is also important that this reference value can be related to wind speeds in the wind tunnel model simulation.

This matching of model and full-scale reference speeds is essential in order to permit the transfer of wind-tunnel data to full scale. For this reason, two reference levels for the final design wind climate models were chosen to be surface level (i.e. 33 feet or 10 m above ground level) and upper level (i.e. 1640 feet or 500 m above ground level). The choice of these reference levels is consistent with state-of-the-art wind tunnel modeling techniques and properly relates model and full-scale values.

The variation of wind speed with height (from the surface upwards) has been modeled using a logarithmic profile law, which is valid in the lower ~100m of the boundary layer. The variation of the hourly-mean wind speed with height is given as:

$$U(z) = U_{10} \frac{ln(z / z_0)}{ln(10 / z_0)}$$

where $U(z)$ is the hourly-mean wind speed at height z, U_{10} is the hourly-mean wind speed at a height of 10m above the surface and z_0 is the aerodynamic surface roughness length, which is normally assigned a value of 0.03 m for smooth open terrain (typical of an airport).

The hurricane wind speeds are given for the case of the wind blowing over the land, computed for a roughness parameter, z_0, equal to 0.03 m.

Figure 2.14 shows the probability distribution of wind speeds and directions at surface level (33 ft or 10 m) for the Prospect-Verona area obtained from the Monte Carlo simulation of hurricane passages over a simulation period of 100,000 years. The characteristics of these hurricanes, including the central pressure, the translational speed, the track angle and the distance to the maximum wind speed are described by their statistical properties using the methodology described in Vickery et al [Ref. 3]. Figure 2.11 shows the tracks of all tropical storms that have passed within 250 km of the bridge site during the period 1851 to 2002.

Relative importance factors for the surface-level hurricane wind climate model are shown in Figure 2.15. Strong winds during hurricane events are equally likely to come from any wind direction with a slight preference to the southeast sector. This is consistent with the observation that the majority of hurricane tracks pass to the southeast of the site, thus locating Prospect-Verona on the ‘weaker’ side of the eyewall.

Predictions of the hourly-mean wind speed for winds blowing over land at various heights, regardless of wind direction, are shown in Figure 2.16. Predicted hourly-mean wind speeds at various heights above land are also presented in Table 2.1.

The prediction of extreme winds likely to be seen by the bridge does not rely on a reconciliation of the directional characteristics of the surface non-hurricane wind data. Extreme winds in the Prospect-Verona area are expected to result due to tropical rather than extratropical storms.

TABLE 2.1 PREDICTED WIND SPEEDS AT VARIOUS HEIGHTS FOR WINDS OVER LAND

Return Period (Years)	Surface Level (10 m)			Upper Level (500 m)		
	Hourly Mean m/s	Hourly Mean mph	3-Sec. Gust mph	Hourly Mean m/s	Hourly Mean mph	3-Sec. Gust mph
50	24.0	54	82	38.5	86	131
100	28.0	63	95	44.1	99	150
500	35.1	79	119	54.4	122	185
1000	37.9	85	129	58.7	131	200

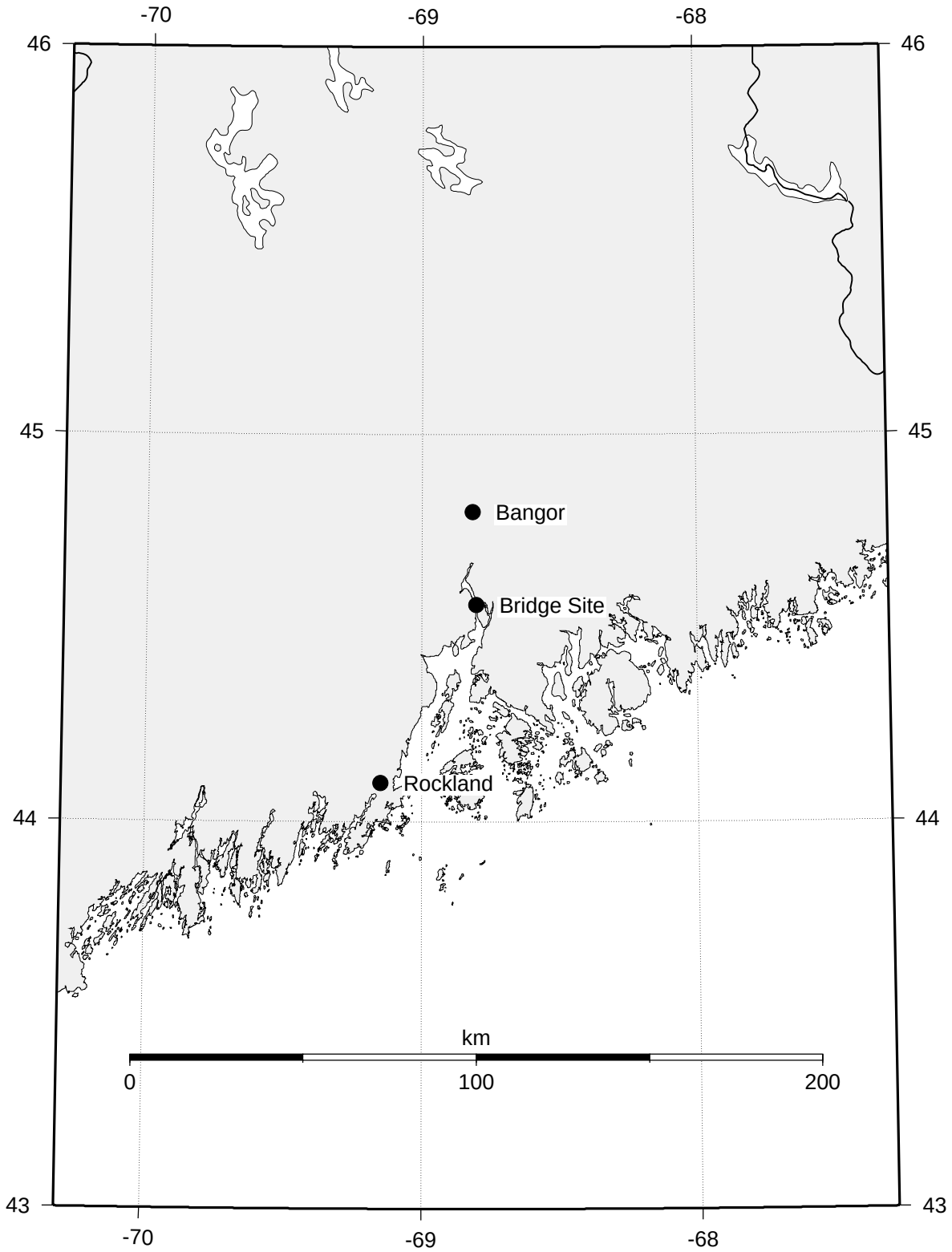

FIGURE 2.1 LOCATIONS OF THE PROSPECT VERONA BRIDGE AND PRIMARY WEATHER STATIONS AT ROCKLAND, MAINE AND BANGOR, MAINE

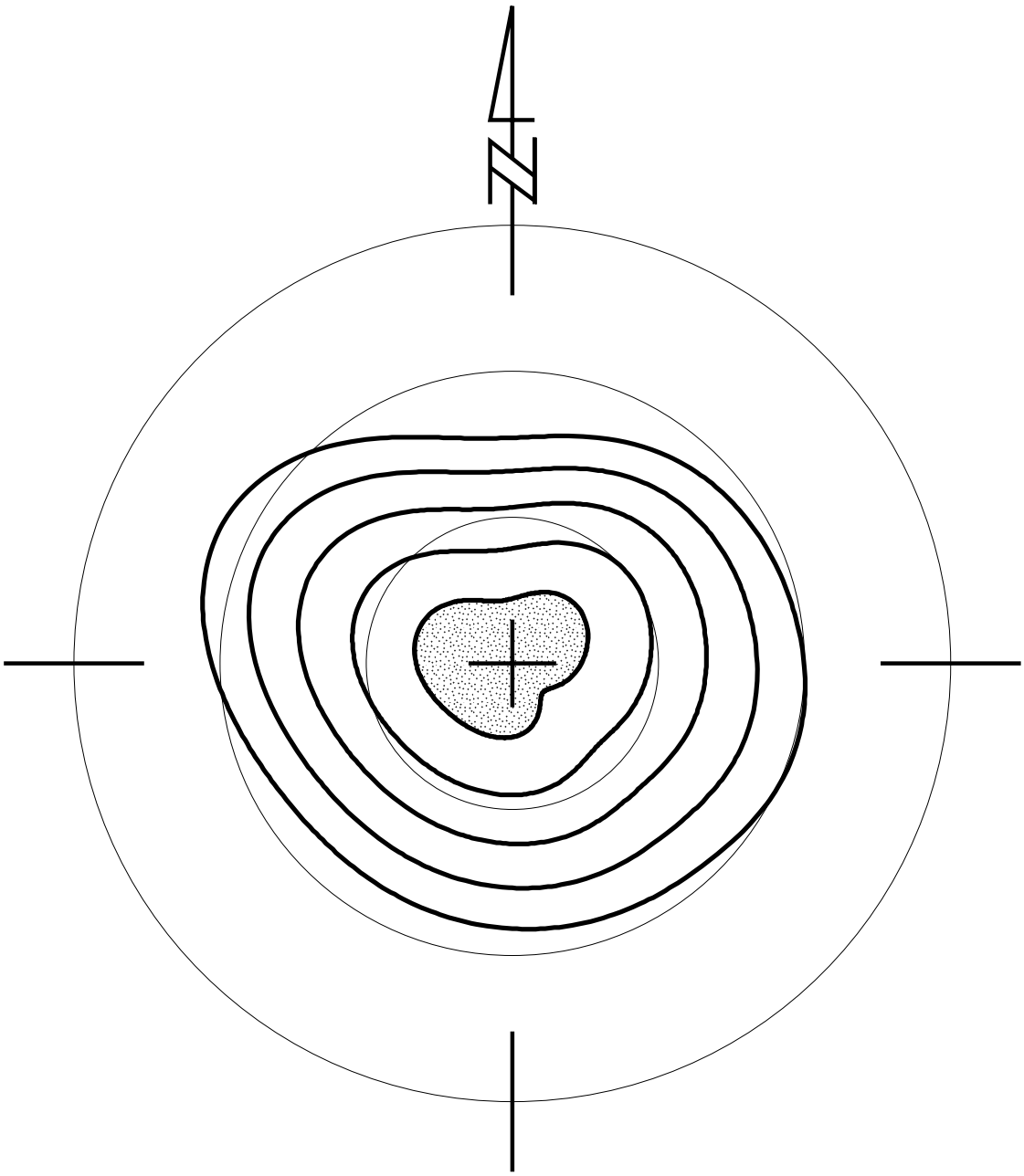

ANNUAL

Radial distances indicate wind speed in m/s

0 10 20

A point along the innermost contour represents the wind speed exceeded on average 1% of the time within a 22.5 degree sector centred on that direction. Other contours represent probability levels of 0.1%, 0.01%, 0.001% and 0.0001%, respectively.

Rockland, Maine

FIGURE 2.2 ANNUAL PROBABILITY DISTRIBUTION OF SURFACE HOURLY-MEAN WIND SPEED AND WIND DIRECTION – ROCKLAND, MAINE (1977-2003)

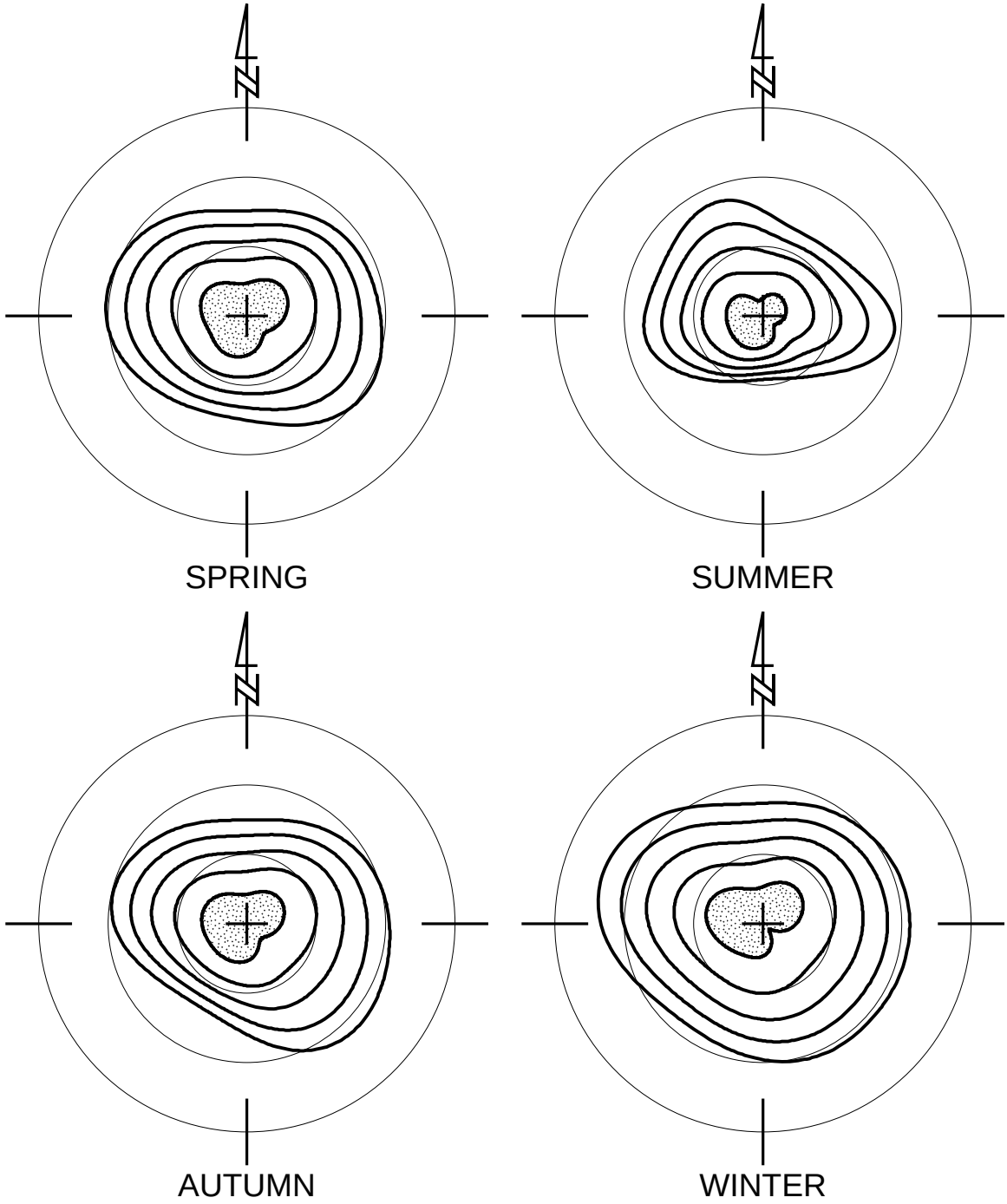

Radial distances indicate wind speed in m/s

0 10 20

A point along the innermost contour represents the wind speed exceeded on average 1% of the time within a 22.5 degree sector centred on that direction. Other contours represent probability levels of 0.1%, 0.01%, 0.001% and 0.0001%, respectively.

Rockland, Maine

FIGURE 2.3 SEASONAL PROBABILITY DISTRIBUTION OF SURFACE HOURLY-MEAN WIND SPEED AND WIND DIRECTION – ROCKLAND, MAINE (1977-2003)

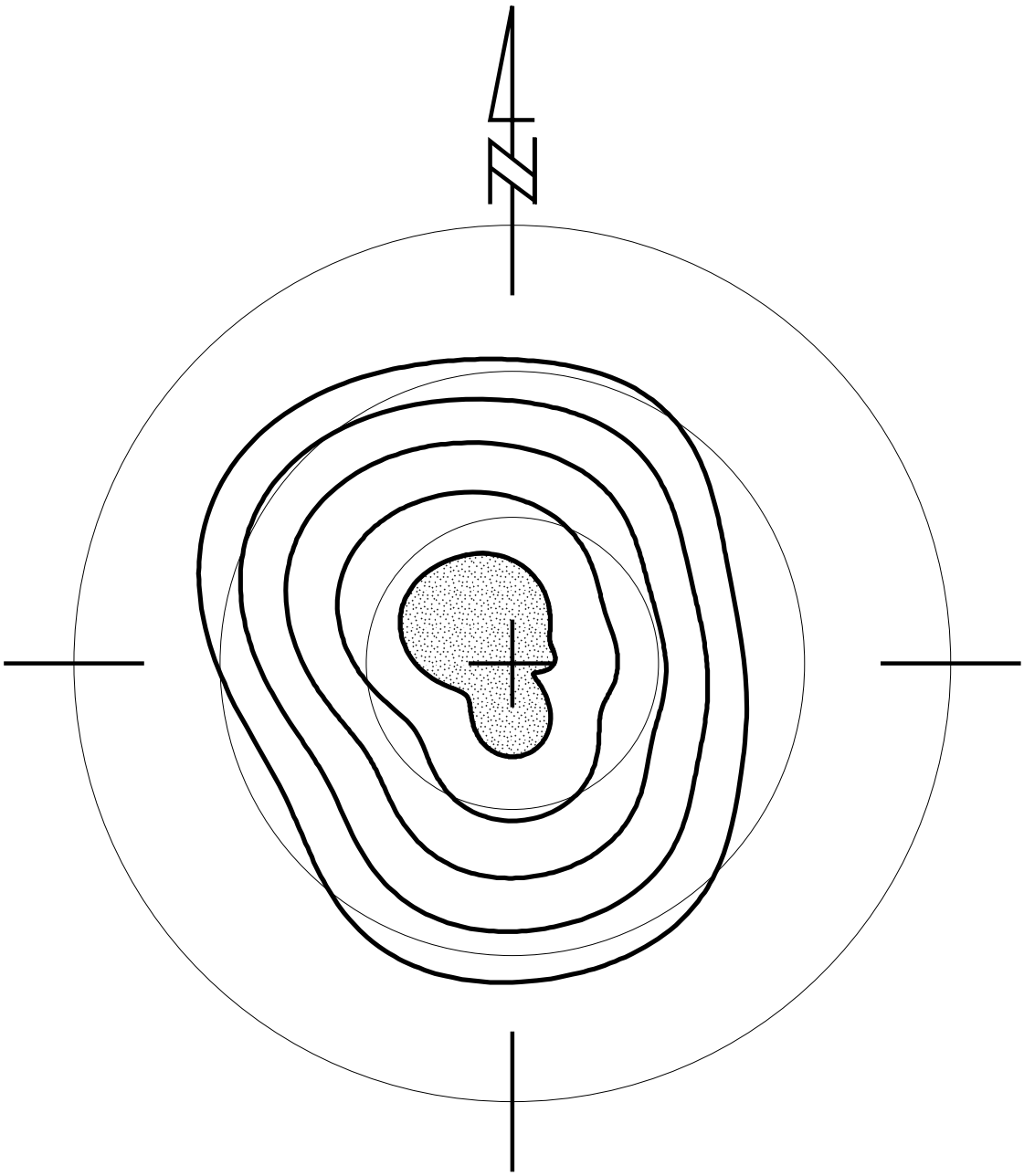

ANNUAL

Radial distances indicate wind speed in m/s

0 10 20

A point along the innermost contour represents the wind speed exceeded on average 1% of the time within a 22.5 degree sector centred on that direction. Other contours represent probability levels of 0.1%, 0.01%, 0.001% and 0.0001%, respectively.

Bangor, Maine

FIGURE 2.4 ANNUAL PROBABILITY DISTRIBUTION OF SURFACE HOURLY-MEAN WIND SPEED AND WIND DIRECTION – BANGOR, MAINE (1942-2003)

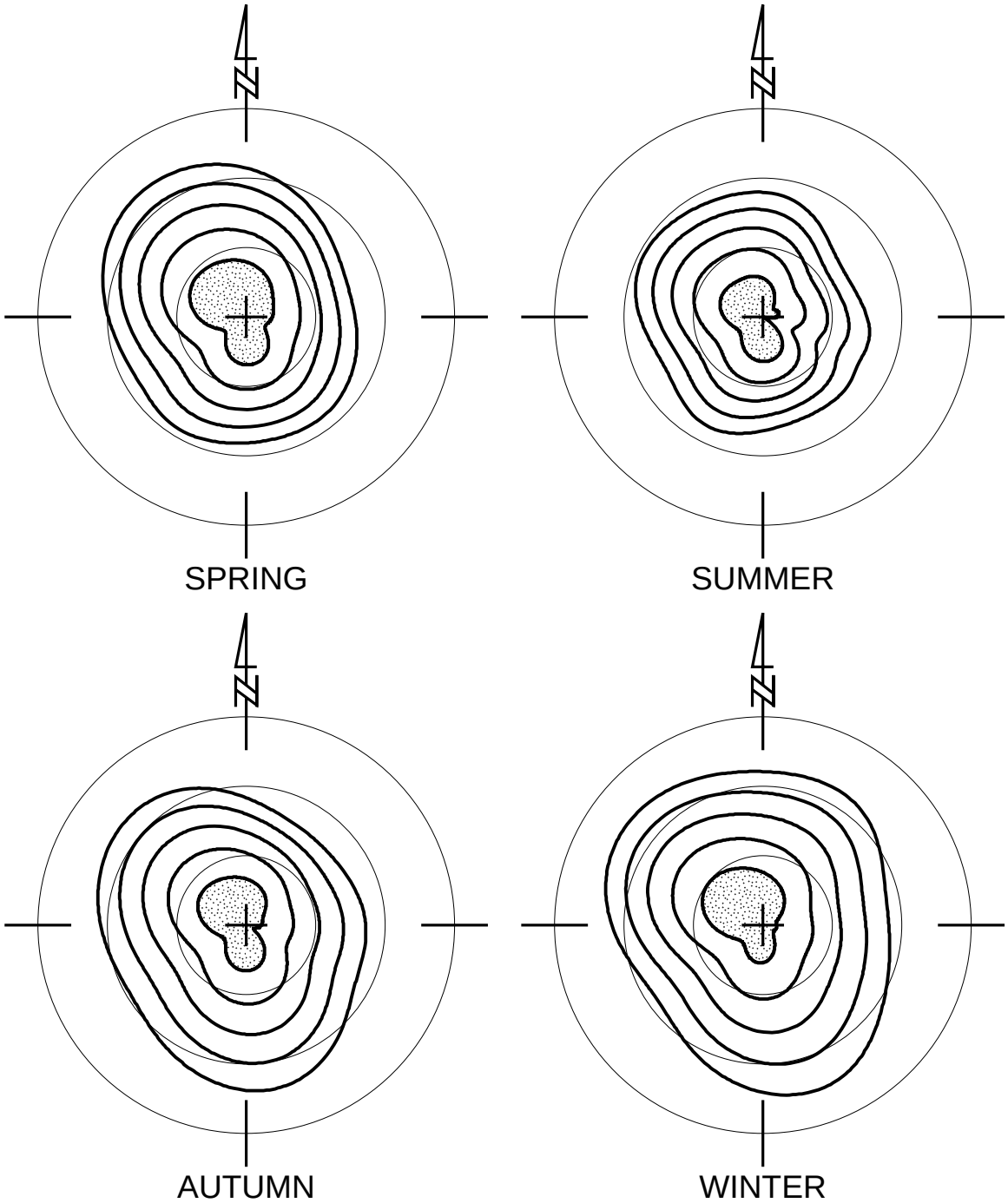

Radial distances indicate wind speed in m/s

0 10 20

A point along the innermost contour represents the wind speed exceeded on average 1% of the time within a 22.5 degree sector centred on that direction. Other contours represent probability levels of 0.1%, 0.01%, 0.001% and 0.0001%, respectively.

Bangor, Maine

FIGURE 2.5 SEASONAL PROBABILITY DISTRIBUTION OF SURFACE HOURLY-MEAN WIND SPEED AND WIND DIRECTION – BANGOR, MAINE (1942-2003)

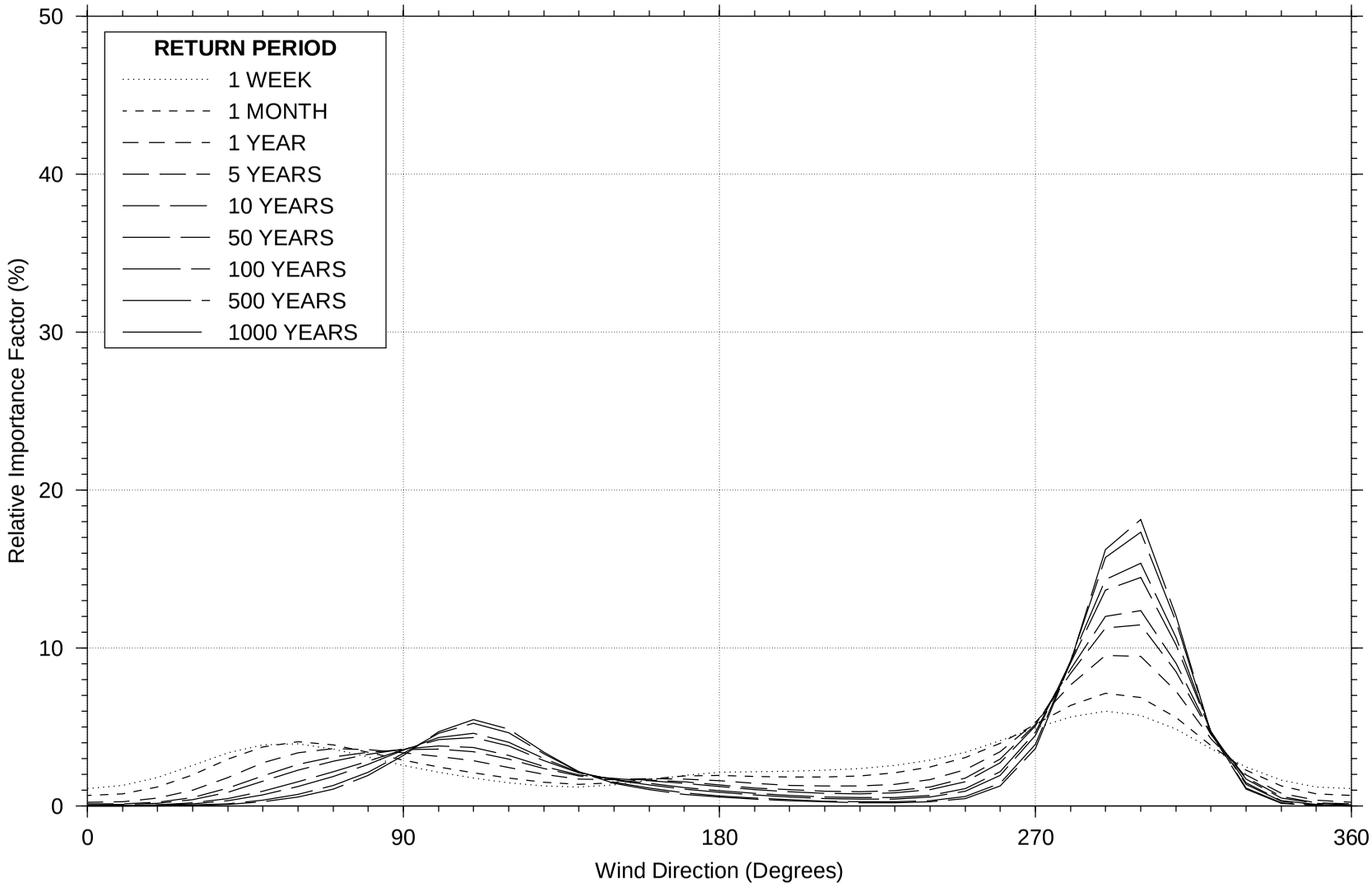

FIGURE 2.6 ANNUAL RELATIVE IMPORTANCE FACTORS FOR VARIOUS WIND DIRECTIONS AND MAXIMUM WIND SPEEDS WITH DIFFERENT RECURRENCE INTERVALS, ROCKLAND, MAINE (1977-2003)

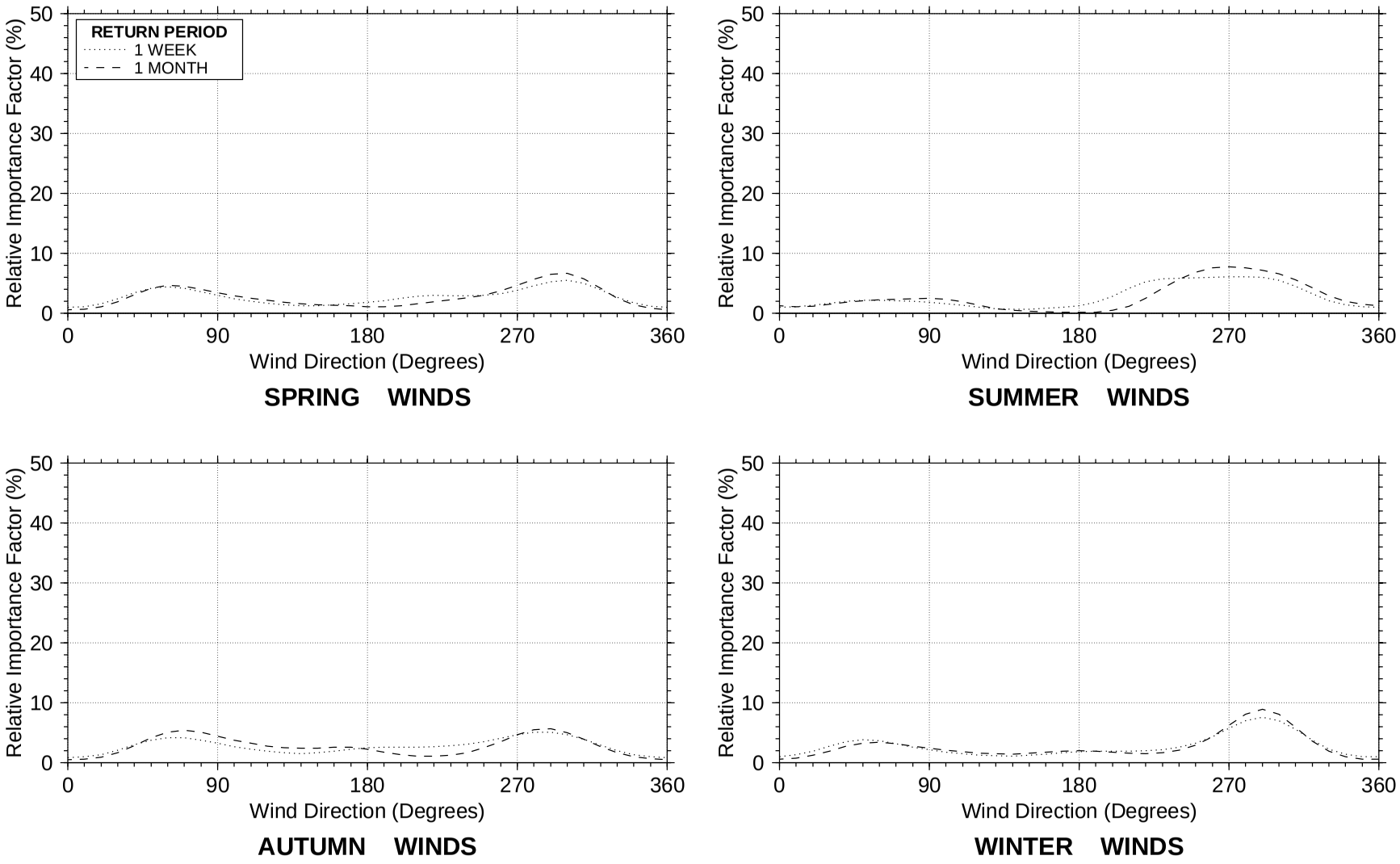

FIGURE 2.7 SEASONAL RELATIVE IMPORTANCE FACTORS FOR VARIOUS WIND DIRECTIONS AND MAXIMUM WIND SPEEDS WITH DIFFERENT RECURRENCE INTERVALS, ROCKLAND, MAINE (1977-2003)

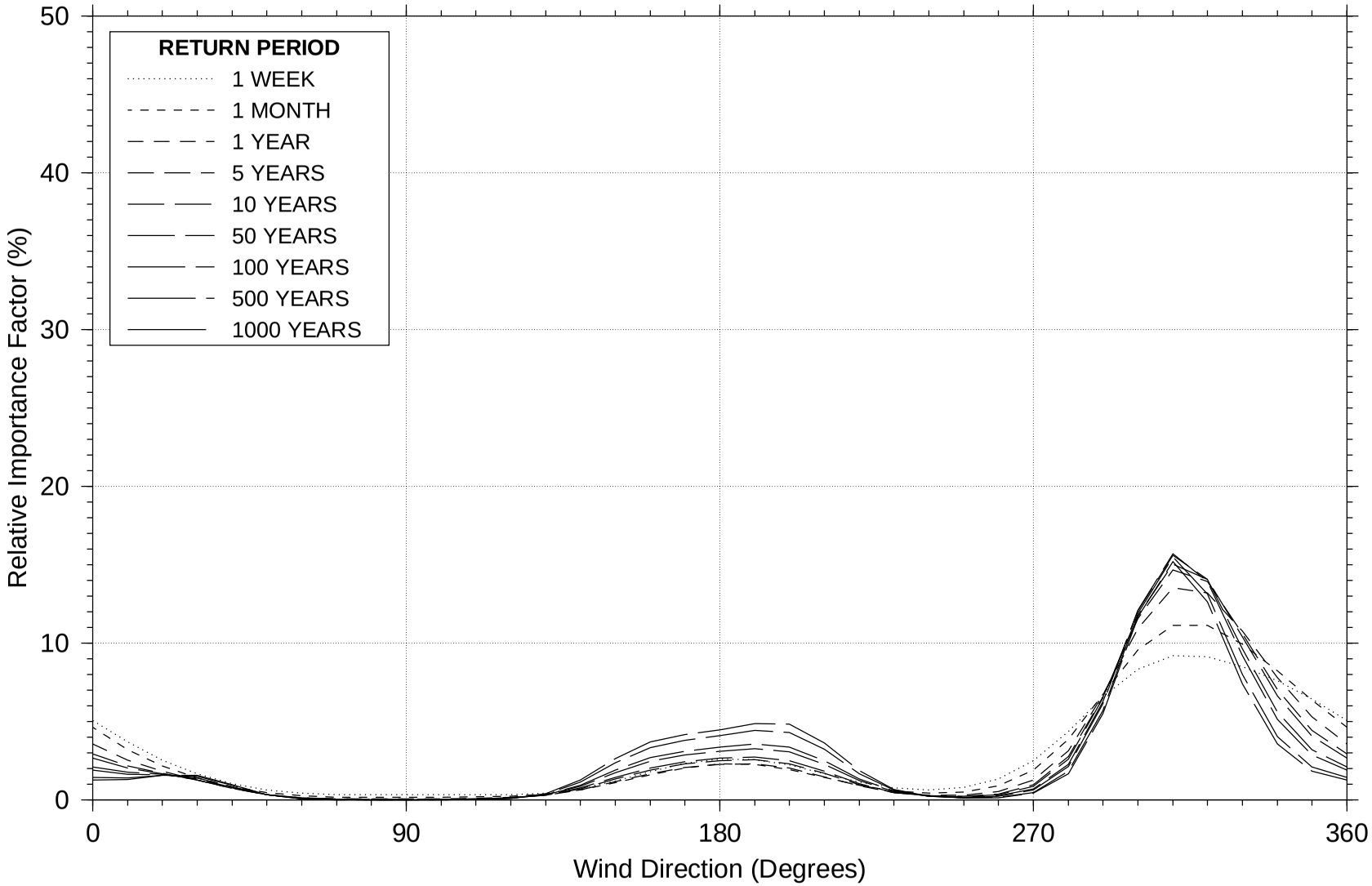

FIGURE 2.8 ANNUAL RELATIVE IMPORTANCE FACTORS FOR VARIOUS WIND DIRECTIONS AND MAXIMUM WIND SPEEDS WITH DIFFERENT RECURRENCE INTERVALS, BANGOR, MAINE (1942-2003)

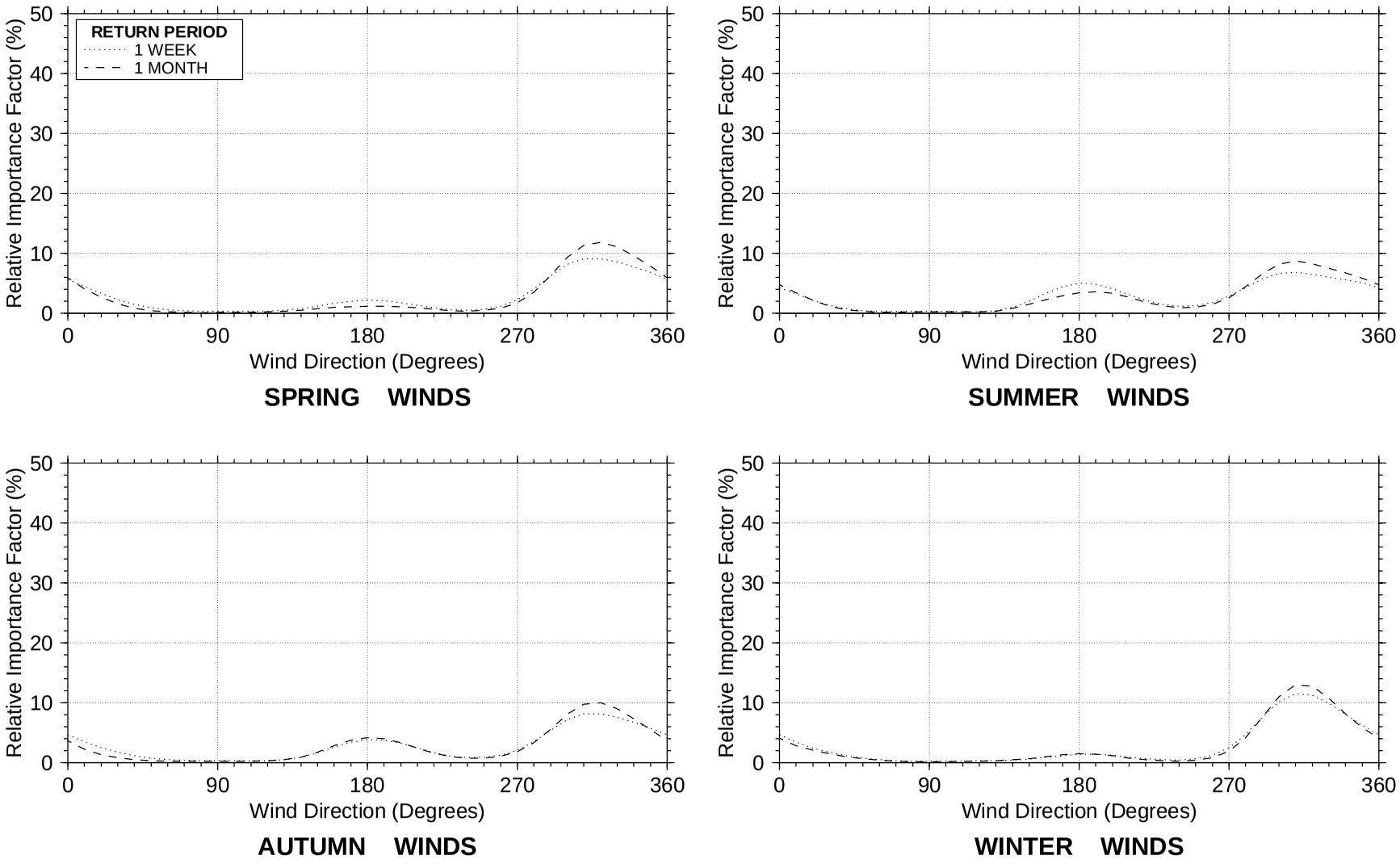

FIGURE 2.9 SEASONAL RELATIVE IMPORTANCE FACTORS FOR VARIOUS WIND DIRECTIONS AND MAXIMUM WIND SPEEDS WITH DIFFERENT RECURRENCE INTERVALS, BANGOR, MAINE (1942-2003)

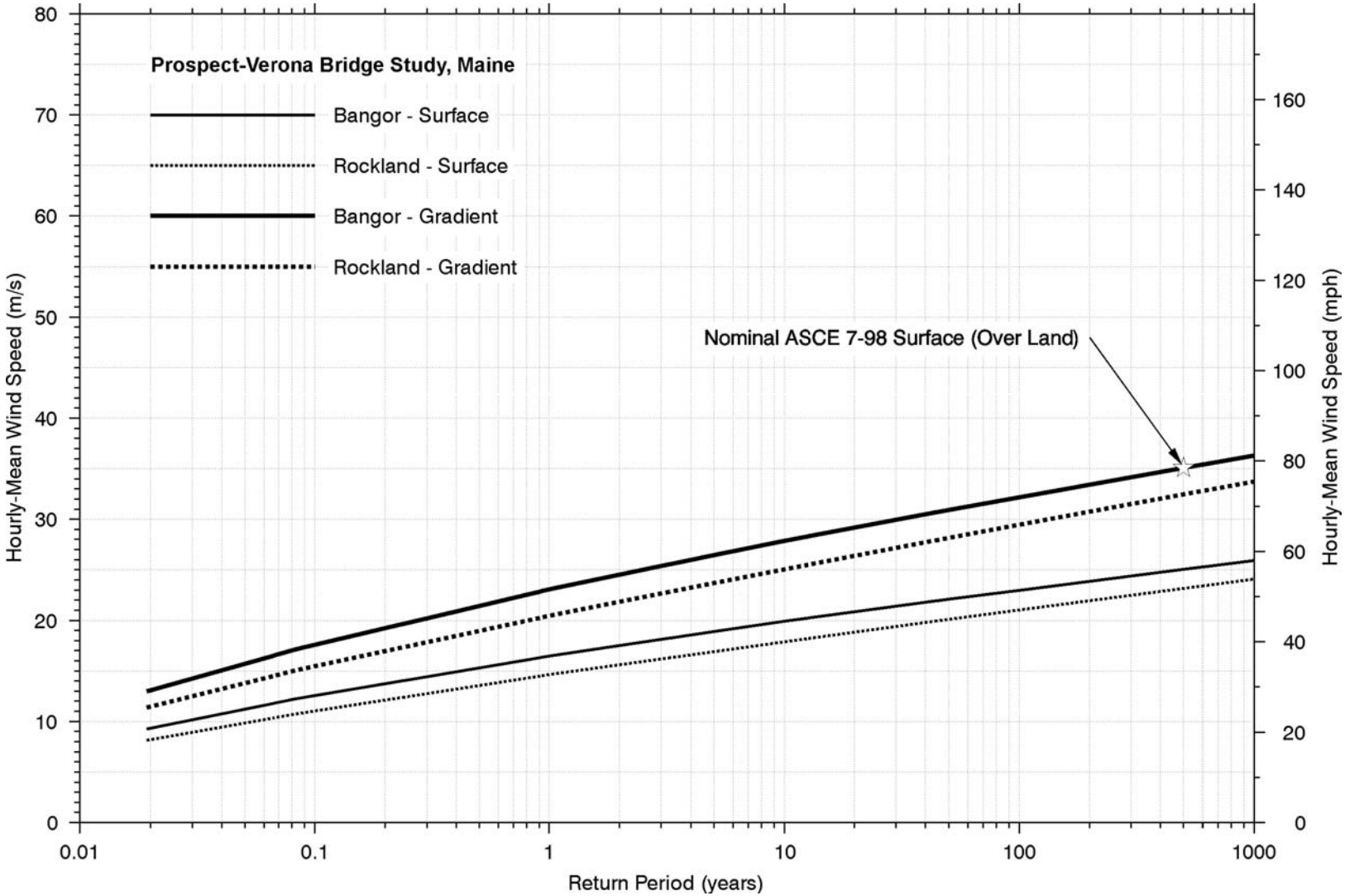

FIGURE 2.10 PREDICTED EXTREME HOURLY-MEAN SURFACE AND GRADIENT WIND SPEEDS FOR VARIOUS RETURN PERIODS

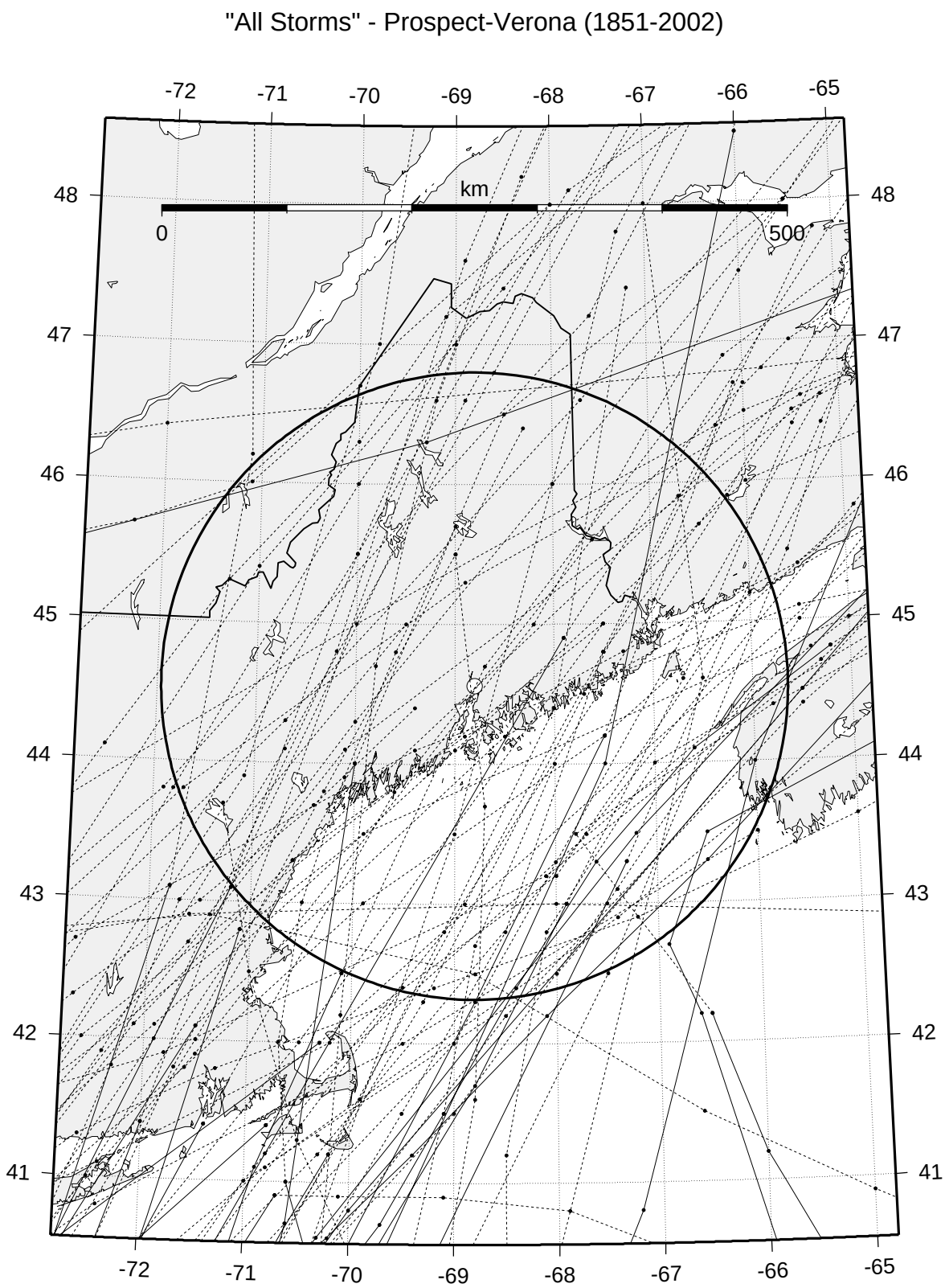

FIGURE 2.11 TROPICAL STORMS PASSING WITHIN A 250 KM RADIUS OF PROSPECT VERONA BRIDGE FOR THE RECORD PERIOD 1851-2002 – ALL STORMS CASE

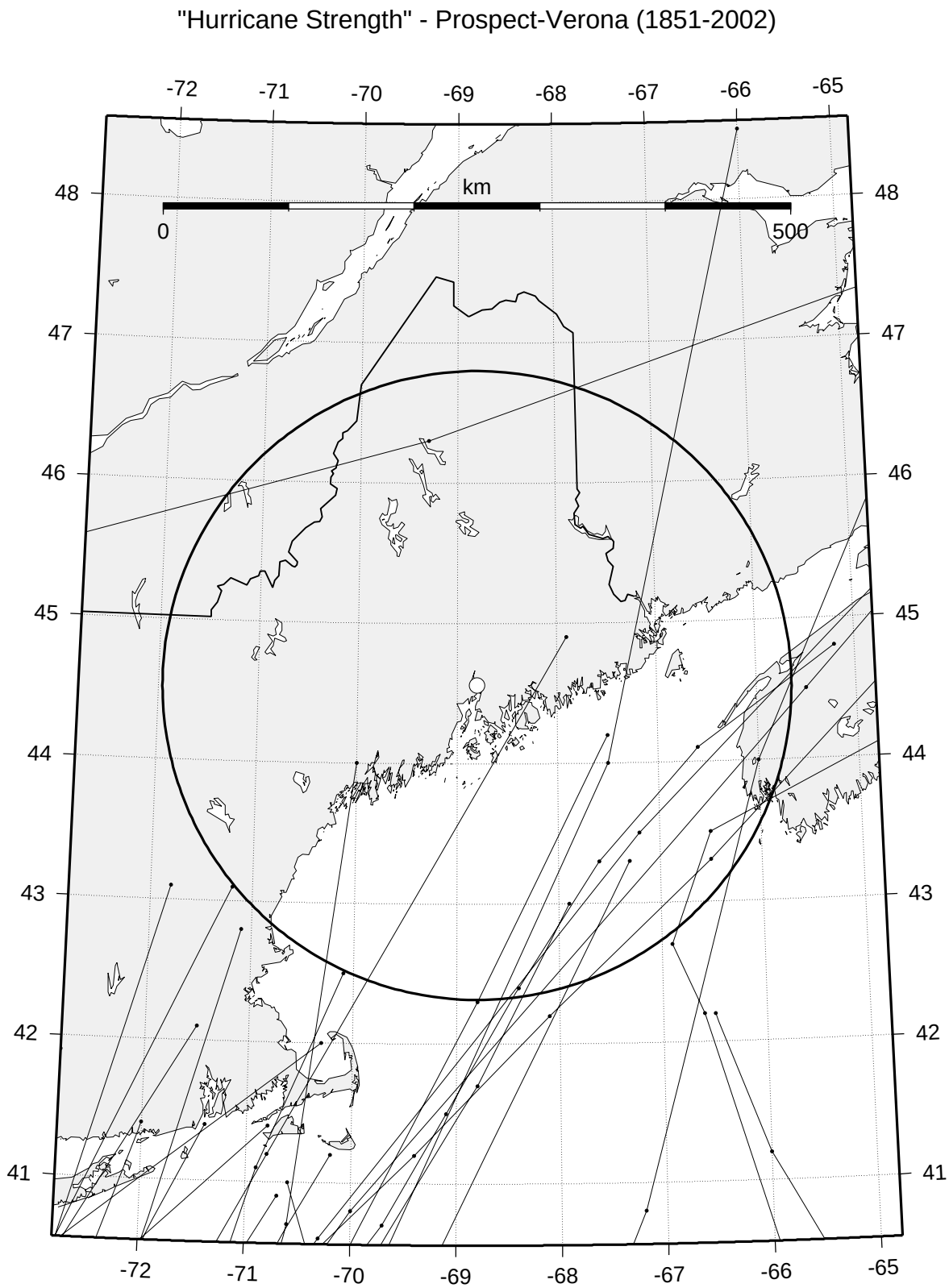

FIGURE 2.12 TROPICAL STORMS PASSING WITHIN A 250 KM RADIUS OF PROSPECT VERONA BRIDGE FOR THE RECORD PERIOD 1851-2002 – STORM SEQUENCES REACHING "HURRICANE" STAGE (V>33m/s)

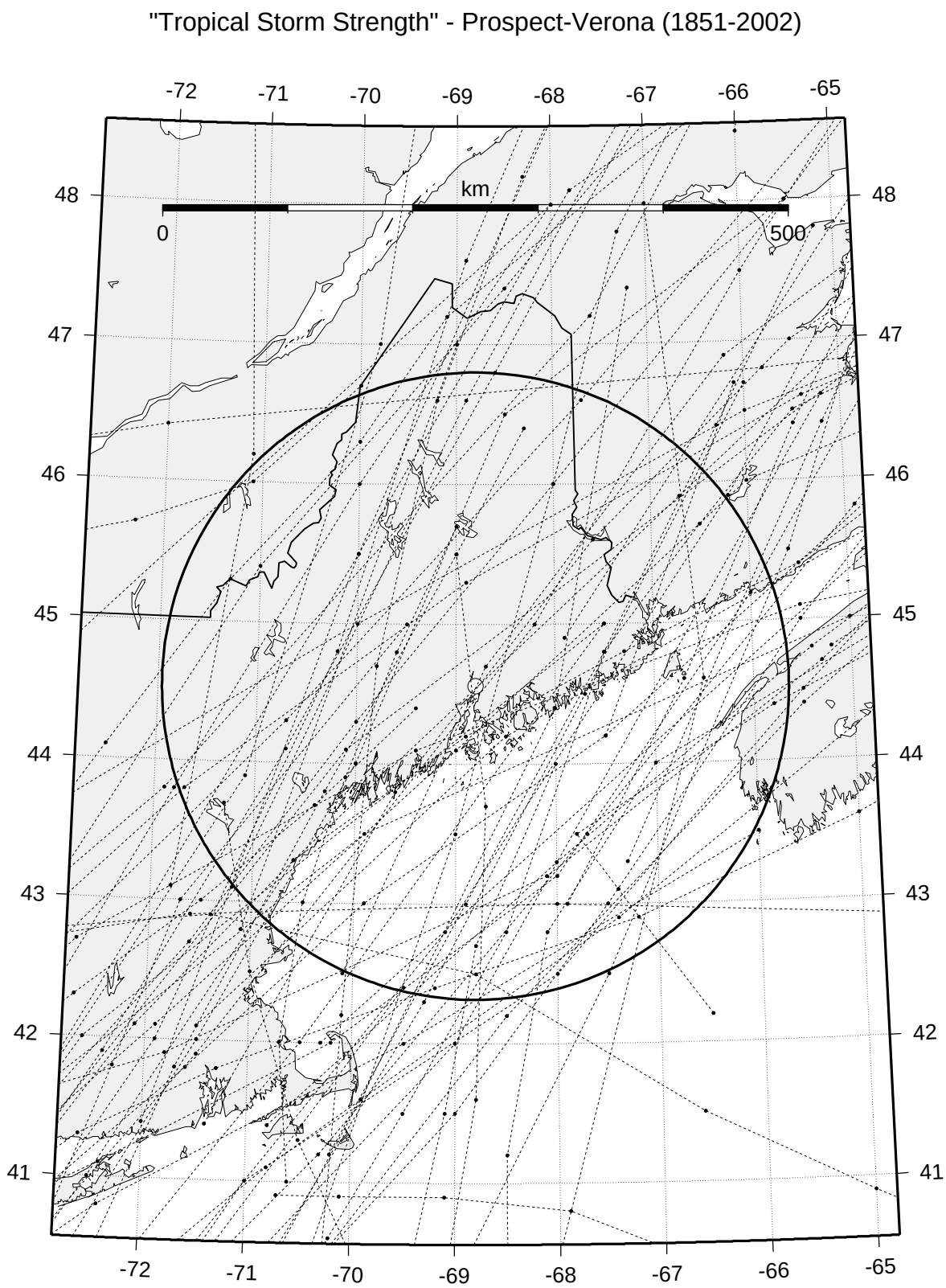

FIGURE 2.13 TROPICAL STORMS PASSING WITHIN A 250 KM RADIUS OF PROSPECT VERONA BRIDGE FOR THE RECORD PERIOD 1851-2002 – STORM SEQUENCES REACHING "TROPICAL STORM" STAGE (V<33m/s)

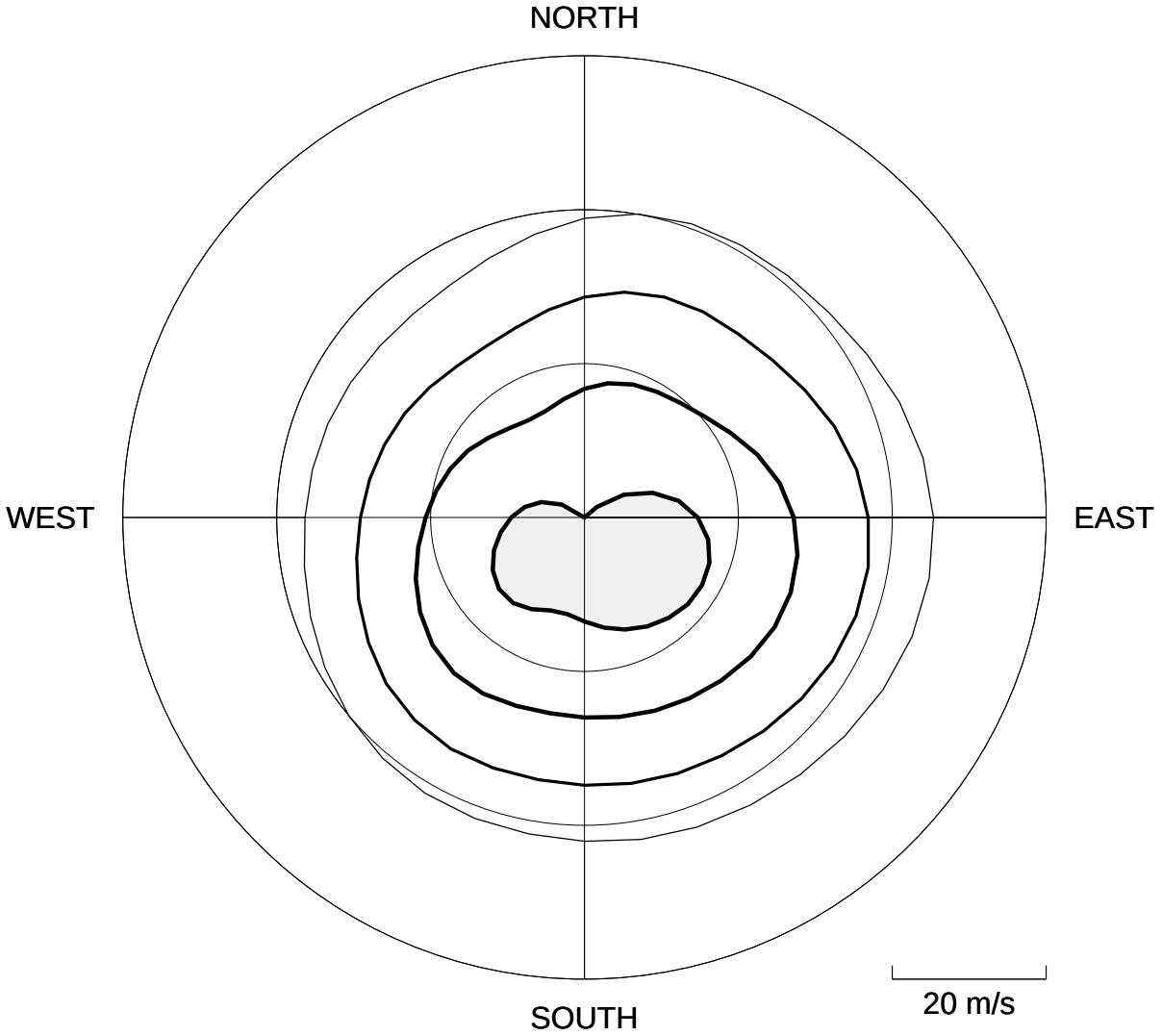

ANNUAL WINDS

A point on the innermost contour represents the wind speed exceeded 1% of the time within a 10 degree sector centred on that direction. Other contours represent probability levels of: 0.1%, 0.01% and 0.001% respectively.

FIGURE 2.14 ANNUAL PROBABILITY DISTRIBUTION OF SURFACE HOURLY-MEAN WIND SPEED AND WIND DIRECTION – HURRICANE WINDS AT 10m - OBTAINED FROM MONTE CARLO SIMULATION OVER 100,000 YEARS (37,150 STORMS)

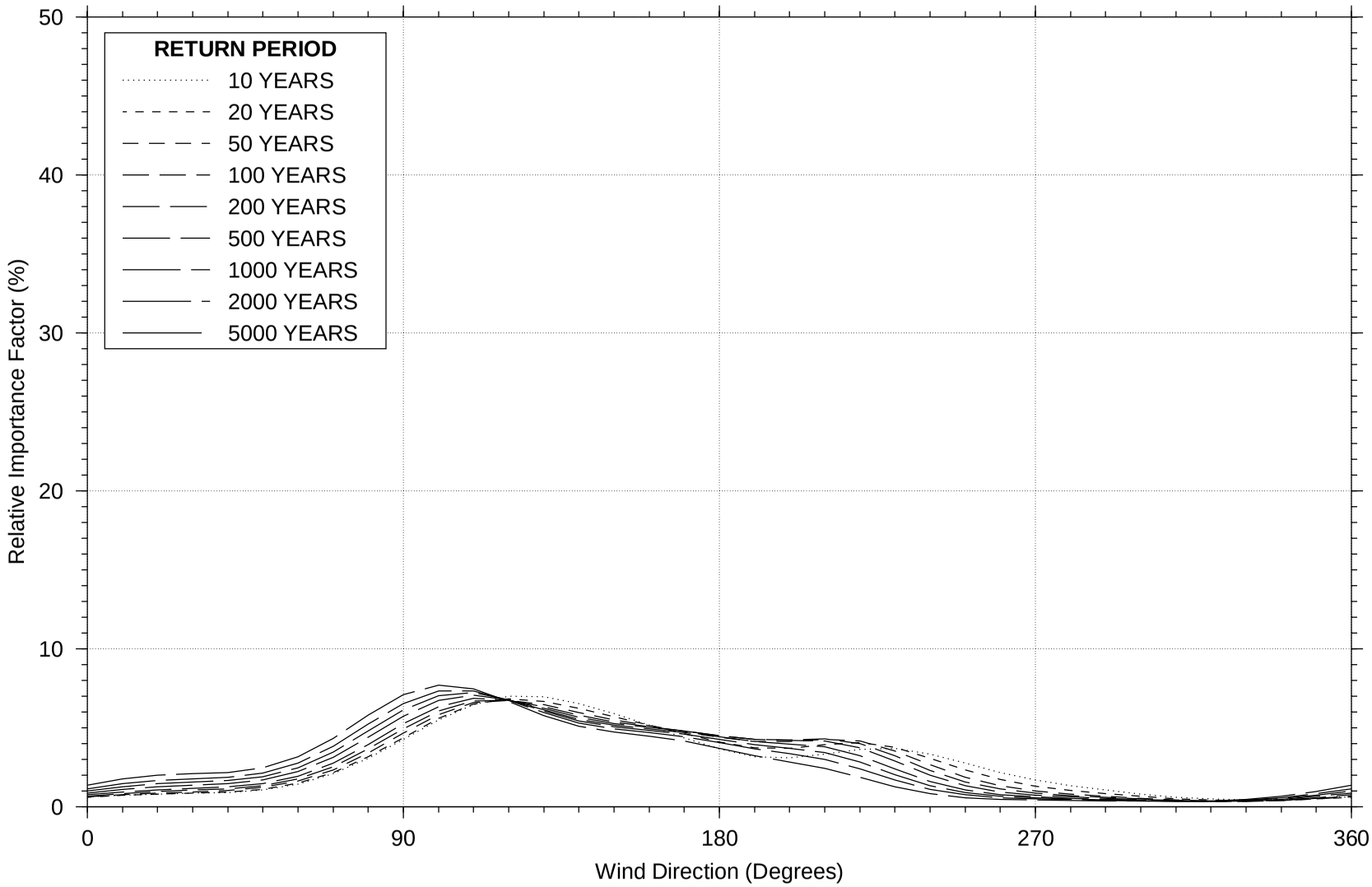

FIGURE 2.15 RELATIVE IMPORTANCE FACTORS FOR VARIOUS WIND DIRECTIONS AND MAXIMUM WIND SPEEDS WITH DIFFERENT RECURRENCE INTERVALS - HURRICANE WINDS AT 10m

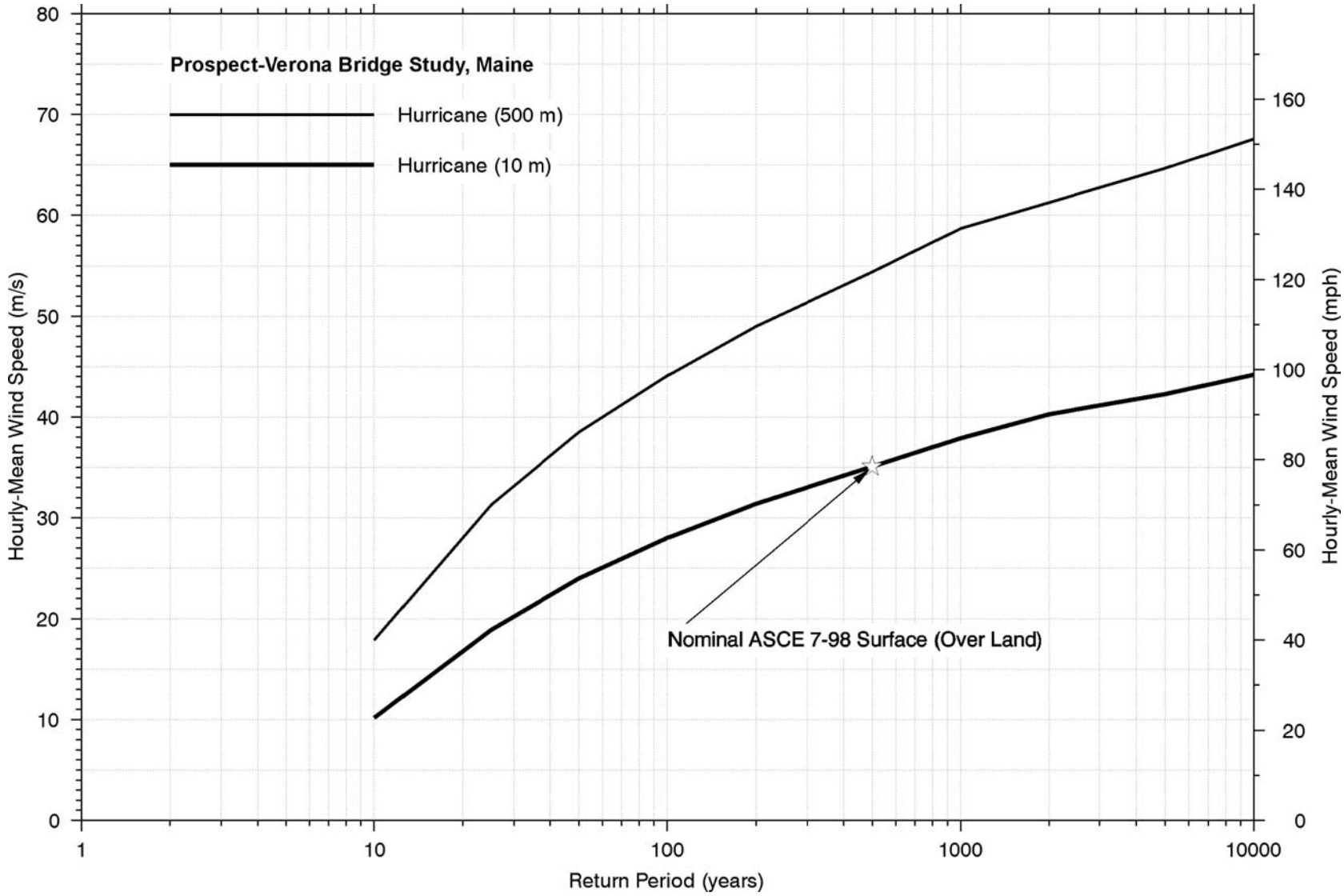

FIGURE 2.16 PREDICTED EXTREME HOURLY-MEAN WIND SPEEDS FOR VARIOUS RETURN PERIODS FOR HURRICANE WINDS

3 SECTION MODEL STUDY

3.1 General

The behavior of the Prospect Verona Bridge was studied using the section model technique. The model was placed in the test rig at the inlet to the High Speed Section of Boundary Layer Wind Tunnel II. Tests of the deck section model were conducted under the both grid-generated turbulence and in uniform flow conditions. The approach taken has been described in Appendix A and outlined in Reference [1]. The method of describing the dynamic wind loads as a series of equivalent static modal loads has been applied to more than 50 bridges since its first use [5, 6, 7] and is applied to the Prospect Verona Bridge in Section 4. The background theory for the Equivalent Static Load (ESL) analysis is outlined in Appendix E.

The 1:70.5 scale, rigid, 7 ft long section model corresponds to a 493.5 ft long section of the full scale bridge deck. A rectangular aluminium tube provided the basic stiffness of the model. To this was fastened an aluminium top plate and machined foam pieces so that the scaled geometric, mass and mass moment of inertia were maintained. The model was designed with a sidewalk which could easily be affixed to or removed from the model as required. The springing system in the section model rig allowed the adjustment of the vertical and torsional stiffnesses in order that the scaled frequencies of the prototype could be simulated.

A typical section model test setup is shown in Figure 3.1. The turbulence generating grid at the inlet of the wind tunnel can be seen in the background. Close-up views of the models tested at different stages are shown in Figure 3.2. Details of the section model construction are given in Figure 3.3.

A summary of the similitude requirements for the design of the basic deck section model is shown in Table 3.1. Further details concerning the design of section models and the approach to testing can be found in Appendix A.

Full scale dynamic properties of the basic deck section were provided by the Engineers and are given in Table 3.2. The fundamental vertical and torsional symmetrical modal frequencies of vibration were selected as the frequencies to be simulated in the section model testing, since these two modes of vibration provide the highest likelihood of a coupled type of flutter instability. During the test, the model was matched to the scaled mass and mass moment of inertia properties of the corresponding deck section. The scaled model properties are also presented in Table 3.2.

In consultation with the Engineers, it was decided that the sidewalk would not alter the stiffness of the deck in a significant way. The sidewalk was correctly scaled for both geometry and mass so no other changes were required to the test set-up to simulate the dynamic behavior of the prototype bridge.

3.2 Dynamic Response Testing

3.2.1 General

The section model was mounted on soft springs permitting the simulation of the vertical and torsional frequencies of vibration. The sprung model was ballasted with additional mass to represent the dynamically scaled mass and mass moment of inertia for the corresponding frequency ratio. Modification to the structural damping of the sprung model was made through the adjustment of the orifice opening in small, pneumatic dashpots. Historically, the development of section model testing was done in aeronautical wind tunnels in smooth, uniform flow and included testing under conditions of inclined mean flow in an attempt to handle the fluctuating component of turbulence. The use of turbulent flow in the test procedure generally makes it unnecessary to consider the effect of wind inclination in dynamic tests. Nominal structural damping ratios of 0.5% and 1.0% of critical were used. Table 3.3 summarizes the test conditions and parameters.

3.2.2 Modeling of Wind

Turbulence in the wind tunnel was generated by a grid placed upwind of the model. The grid has a mesh size of 5.5 inches with 24 inch center to center spacing. The vertical, I_w, and horizontal, I_u, turbulence intensities generated using this grid are about 7.2% and 9.0%, respectively. Turbulence developed using the fixed grid technique is normally lacking sufficient energy in the low frequency - large scale range to match full scale, resulting in an overall lower turbulence intensity than that expected at the site. The energy in the high frequency end of the spectrum, however, is well modelled using this grid, which is critical for the definition of resonant response and the overall behavior of the structure to turbulent wind.

As discussed above, turbulence developed in the wind tunnel using the fixed grid technique has a lower turbulence intensity than full scale. Therefore, a correction using quasi-steady aerodynamics is made when developing Equivalent Static Loads to account for the difference of turbulent energy levels and frequency content. This approach is used in the analysis of Section 4 and described in Appendix E of this report.

3.2.3 Dynamic Bridge Response

The results of the dynamic tests are summarized in Table 3.3. A sample plot for the deck without the sidewalk in smooth flow is given in Figure 3.4. All results from the dynamic section model tests are presented in graphical form in Appendix B. The peak response was formed from the root-mean-square (RMS) response multiplied by a peak factor. Thus, the <u>total</u> response is equal to the mean, <u>plus or minus</u> the peak. In these plots, for the range of wind speeds where the model is stable, the peak shown is formed from the RMS multiplied by a statistically-based peak factor of 3.5. Since the peak factor during instability (i.e. when the motion becomes sinusoidal) decreases to a value approaching $\sqrt{2}$ or 1.41, the use of a constant value of 3.5 for all wind speeds would over-estimate the dynamic response during an instability. Thus, for the range of wind speeds where the model has shown either a large vortex shedding peak or flutter instability, the actual peak factor calculated from the test for the corresponding wind speed was used. Rotations and full scale displacements have been plotted against the full scale mean wind speed at deck height in mph. Full scale displacements were obtained from the measured model displacements and converted using the geometric length scaling of 1:70.5. Rotations need no such scaling. The full scale and model frequencies have been used to determine the conversion factors from model scale velocity to full scale wind speed through the following relationship:

$$V_{\text{full scale}} = V_{\text{model}} \cdot \left(\frac{f_{\text{full scale}}}{f_{\text{model}}} \right) \cdot \left(\frac{1}{\lambda_L} \right)$$

where $(1/\lambda_L) = 70.5$, the geometric scale of the model, and f is the natural frequency of either the vertical or torsional mode of vibration.

In section model testing, the onset of a “Flutter Instability” can be defined as when the character of the response changes from a random type motion to that of a regular, sinusoidal motion, involving either pure torsional or a coupled vertical-torsional vibration. This can be clearly identified through an examination of the “peak factor” which is defined as the ratio of the largest observed reading during the sample period to the Root Mean Square (RMS) of the sample. A random signal has peak factors in the 3-4 range, while a sinusoid has a peak factor of $\sqrt{2}$ or 1.41. A discussion of the peak factor with respect to its use in determining conditions of flutter instability is contained in Appendix D.

Some general comments on the dynamic response results of the section model tests are given below.

- No flutter instability was observed during the tests. The maximum (scaled) mean-hourly wind speed at the deck height was 145 mph, a speed which corresponds to a return period of greater than 10,000 years.

- Vortex-induced responses were observed in the smooth flow tests. Vertical motions were observed with peak amplitudes in the range of 21-22 mph. For 0.5% damping, the maximum amplitudes varied between 0.55 and 0.84 ft. The worst case was observed to be with the sidewalk on the upwind (windward) side. Increased damping significantly mitigated these responses, as did turbulence (which eliminated it entirely). Torsional motions with peak amplitudes were observed to occur between speeds of 78-82 mph; however, these were small.

- Response under turbulent flow conditions was characterized by turbulent buffeting. Generally, the dynamic components due to buffeting of the deck in turbulent flow are significantly higher than those in observed in smooth flow. The mean components of the response are smaller than those found in the smooth flow tests (consistent with the results from the static tests). The effect of turbulence helps to reduce any vortex shedding peaks and to increase the wind speeds at which flutter occurs.

3.3 Static Response Testing

The section model was mounted on the BLWTL Bridge 3-component balance, which is capable of measuring the total forces on the section (X and Z body forces as well as the torque). Tests were performed adjusting the model inclination relative to the mean wind flow. Lift and Drag were calculated from the measured X and Z body force components. The sign convention for the definition of the force coefficients is given in Figure 3.5.

A typical force coefficient is defined as follows:

$$C_{x,z} = \frac{F_{x,z,l,d}}{qB}$$

in which C is an aerodynamic coefficient, F is the mean aerodynamic force per unit span length, $q = \frac{1}{2}\rho V^2$ is the mean wind velocity pressure at deck level, ρ is the density of air (0.00238 slugs/ft³), V is the mean wind velocity at deck level in ft/s, and B is the bridge deck width. The subscripts x,z,l,d refer to the X and Z body force components and lift and drag respectively.

The torque coefficient is defined:

$$C_t = \frac{F_t}{qB^2}$$

Tests were carried out in both smooth flow (I_u= 0.5%) and grid generated turbulent flow (I_u= 9.0%) for angles of mean vertical inclination between -10 to +10 degrees in 1 degree increments. The tests were repeated for two different wind speeds to investigate a potential for Reynolds number effects. Three configurations were tested, namely: without the sidewalk and with the sidewalk on the upwind and downwind sides of the deck.

The static aerodynamic coefficients from both the tests without the sidewalk are summarized in Tables 3.6 and 3.7.respectively. The corresponding curves of force coefficient vs. angle of attack are shown in Figure 3.6. A complete data set of the force coefficients as well as the slopes of the Z and torsional forces (based upon the angle of attack in radians) is given in Appendix C.

The coefficients are normalized by deck width to make comparisons with other structures more meaningful. Should the results be desired on a projected area to the wind basis, as is sometimes the case, the $C_{x,z,l,d}$ coefficients should be multiplied by the ratio of deck width to overall section height (for example, 57.5/12.83=4.48), and for C_t by the square of this value ($(57.5/12.83)^2$=20.1). The center of measurement of the forces was at 5.32 ft from the deck top surface in the middle of the section.

It was observed that the turbulent flow coefficients are smaller than those obtained in smooth flow (except for C_z for angles greater than +3° with the sidewalk upwind and +5° with the sidewalk downwind). Turbulence has the general effect of decreasing the *X*-force (drag) coefficient at all angles of attack. This is believed to be the result of an altered flow reattachment location on the deck, which is affected by the intensity and scale of turbulence.

There are significant differences in the slope of both C_m and C_z at 0°. These slopes are always larger in turbulent flow. The moment coefficient is negative in smooth flow and near zero in turbulent flow at 0°. The lift coefficient is positive and larger in magnitude in turbulent flow.

The sidewalk has a significant effect on the static coefficients and slopes. The X-force (drag) coefficient at 0° is not significantly affected and is worst for the no sidewalk case. The C_z and C_m coefficients are also largest for the no sidewalk case at 0°. The slope of C_m at 0° is about the same in all three cases (and near zero) although the slope of C_z is significantly greater when the sidewalk is present and, in particular, is on the upwind (windward) side. This behavior indicates that although mean loads may be lower with the sidewalk in place, the dynamic loads due to turbulent buffeting will be significantly larger.

TABLE 3.1 SECTION MODEL SCALING PARAMETERS

PARAMETER	SIMILITUDE REQUIREMENT	VALUE
Length*	$\lambda_L = \mathbf{L}_m / \mathbf{L}_p$	0.014
Density	$\lambda\rho = \rho_m / \rho_p$	1.0
Velocity (refer to Table 2.2)	$\lambda_V = \mathbf{V}_m / \mathbf{V}_p = \lambda_L \ \mathbf{f}_m / \mathbf{f}_p$	0.195
Mass per Unit Length	$\lambda_m = \lambda_\rho \lambda_L^2$	2.0E-04
Mass	$\lambda_M = \lambda_\rho \lambda_L^3$	2.9E-06
Mass Moment of Inertia per Unit Length	$\lambda_i = \lambda_m \lambda_L^2$	4.0E-08
Mass Moment of Inertia	$\lambda_I = \lambda_M \lambda_L^2$	5.7E-10
Time	$\lambda_T = \mathbf{T}_m / \mathbf{T}_p = \lambda_L / \lambda_V$	0.073
Damping	$\lambda_\zeta = \zeta_m / \zeta_p$	1.0

* Length Scale 1: 70.5

TABLE 3.2 FULL SCALE AND MODEL SCALE PROPERTIES FOR THE BASIC DECK SECTION

	PROTOTYPE	MODEL
Characteristic Length B	57.5 ft	0.816 ft
Mass*		
lift	25100 lb/ft	5.04 lb/ft
torque	6.101E+06 lb-ft^2/ft	0.244 lb-ft^2/ft
Frequency		
lift	0.3268 Hz	4.48 Hz
torque	1.104 Hz	15.20 Hz
f_t/f_l	3.38	3.40
Stiffness		
lift	3.3 kip/ft/ft	123 lb/ft/ft
torque	159 kip-ft/ft/degree	1.18 lb-ft/ft/degree
Damping (% of critical)		
lift	0.5% ~ 1.0%	0.5% and 0.9%
torque	0.5% ~ 1.0%	0.4% and 1.1%

Velocity Scaling:

Vertical: $$\frac{V_m}{V_p} = \frac{(fB)_m}{(fB)_p} = \frac{4.476}{0.3268}\frac{1}{70.5} = \frac{1}{5.15}$$

Torsional: $$\frac{V_m}{V_p} = \frac{(fB)_m}{(fB)_p} = \frac{15.197}{1.104}\frac{1}{70.5} = \frac{1}{5.12}$$

Average: $$\frac{V_m}{V_p} = \left(\frac{1}{5.15} + \frac{1}{5.12}\right) \bullet 0.5 = \frac{1}{5.14}$$

* Mass of sidewalk was 76 lb/ft in full-scale and 0.15 lb/ft in model scale.

TABLE 3.3 RESULTS OF DYNAMIC SECTION MODEL TESTS FOR 0° ANGLE OF ATTACK

No.	Label	Flow	Sidewalk	Damping (nominal)	f_v (Hz)	f_t (Hz)	Vmax (mph)	Flutter	Vortex-Induced Vibrations
1	sma101	smooth	none	0.5%	4.476	15.197	145	none observed	Vertical: 21 mph, 0.55 ft Torsional: 81 mph, 0.15^{o}
2	sma201	turbulent	none	0.5%	4.476	15.197	145	none observed	none observed
3	sha101	smooth	none	1.0%	4.476	15.197	147	none observed	Torsional: 82 mph, 0.16^{o}
4	smb101	smooth	upstr.	0.5%	4.414	14.816	146	none observed	Vertical: 22 mph, 0.84 ft Torsional: 79 mph, 0.12^{o}
5	smb201	turbulent	upstr.	0.5%	4.414	14.816	148	none observed	none observed
6	shb101	smooth	upstr.	1.0%	4.414	14.816	145	none observed	Vertical: 21 mph, 0.38 ft Torsional: 78 mph, 0.10^{o}
7	smc101	smooth	downstr.	0.5%	4.414	14.816	147	none observed	Vertical: 22 mph, 0.58 ft Torsional: 76 mph, 0.16^{o}
8	smc201	turbulent	downstr.	0.5%	4.414	14.816	148	none observed	none observed

TABLE 3.4 STATIC FORCE COEFFICIENTS, NO SIDEWALK, SMOOTH FLOW

Angle of Attack	Cx	Cz	Cm
-10	0.39455	-0.21665	0.089258
-9	0.396079	-0.13002	0.102209
-8	0.394058	-0.03931	0.115827
-7	0.388132	0.050262	0.128527
-6	0.37932	0.140506	0.139508
-5	0.366372	0.23054	0.150851
-4	0.360798	0.295682	0.16204
-3	0.346472	0.374409	0.168402
-2	0.338713	0.426248	0.172505
-1	0.329796	0.467381	0.17136
0	0.323554	0.483535	0.167679
1	0.322412	0.483305	0.164508
2	0.322356	0.47112	0.161926
3	0.32274	0.448058	0.159904
4	0.324364	0.418435	0.158329
5	0.325596	0.382916	0.15699
6	0.325218	0.333956	0.154164
7	0.322934	0.278366	0.149613
8	0.320972	0.230341	0.143574
9	0.321257	0.210818	0.137885
10	0.324964	0.214826	0.13486

Slope of C_z Curve =	0.61
Slope of C_m Curve =	-0.16
C_z at 0° =	0.484
C_x at 0° =	0.324
C_m at 0° =	0.168

TABLE 3.5 STATIC FORCE COEFFICIENTS, NO SIDEWALK, TURBULENT FLOW

Angle of Attack	Cx	Cz	Cm
-10	0.296552	-0.19145	0.065211
-9	0.299308	-0.14174	0.074398
-8	0.300704	-0.09074	0.084058
-7	0.30018	-0.04479	0.092938
-6	0.29651	0.000299	0.101507
-5	0.294937	0.038811	0.109747
-4	0.288432	0.074414	0.116267
-3	0.281805	0.104511	0.121909
-2	0.275181	0.128083	0.125873
-1	0.269276	0.144769	0.12863
0	0.260501	0.160723	0.128766
1	0.255931	0.175032	0.129085
2	0.248568	0.186701	0.12669
3	0.244568	0.201493	0.12462
4	0.237998	0.213927	0.119437
5	0.238078	0.239384	0.11784
6	0.235189	0.257437	0.113603
7	0.2363	0.279994	0.110892
8	0.239533	0.301592	0.108932
9	0.24192	0.319516	0.106268
10	0.24482	0.334105	0.10417

Slope of C_z Curve =	0.85
Slope of C_m Curve =	0.01
C_z at 0° =	0.161
C_x at 0° =	0.261
C_m at 0° =	0.129

a) TURBULENT FLOW

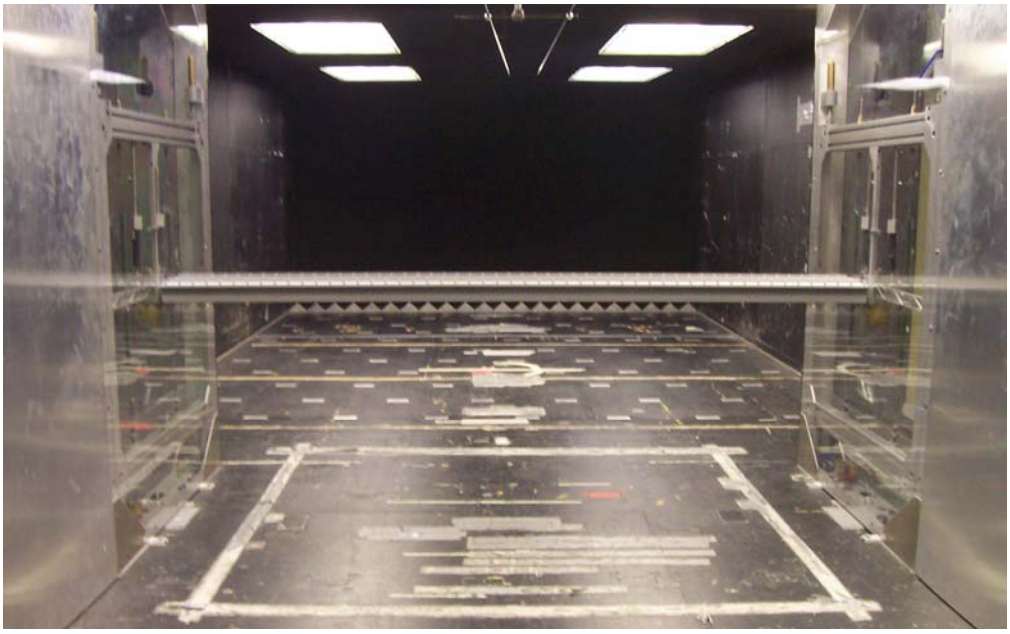

b) SMOOTH FLOW

FIGURE 3.1 SECTION MODEL TEST SET-UP

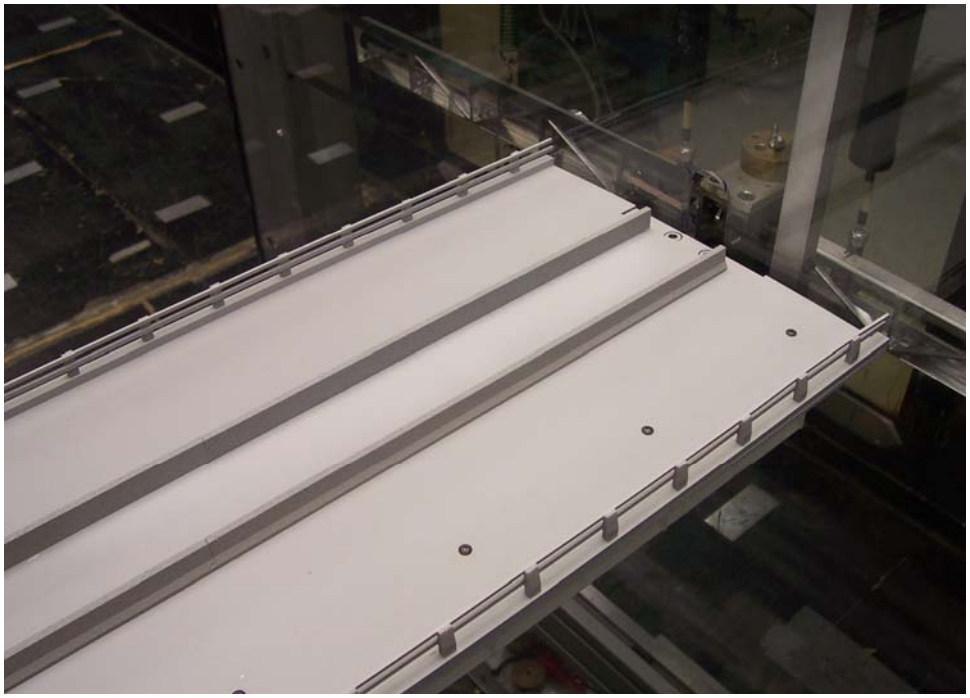

a) UPPER SURFACE OF DECK SECTION

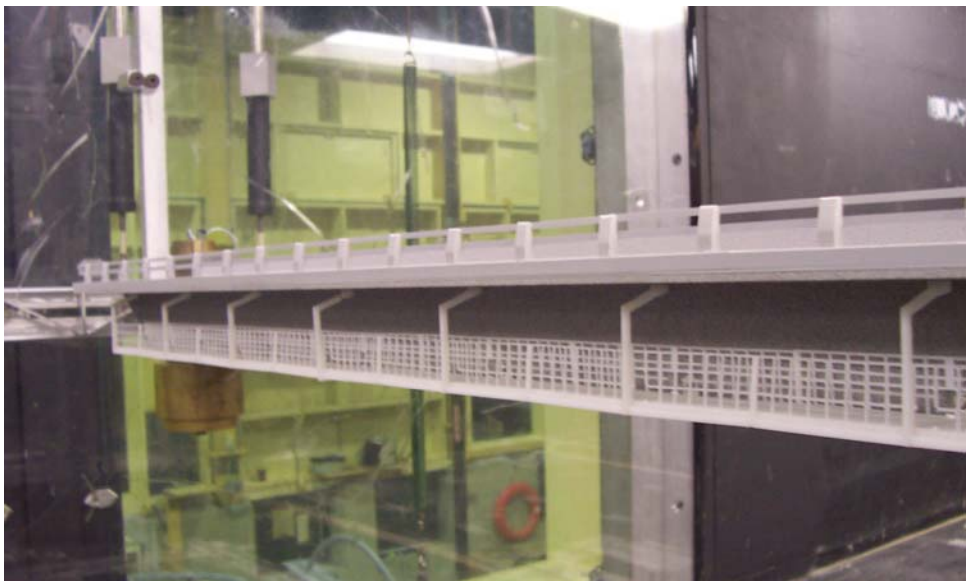

b) UNDERSIDE OF DECK SECTION SHOWING THE SIDEWALK

FIGURE 3.2 CLOSE-UP VIEWS OF THE SECTION MODEL

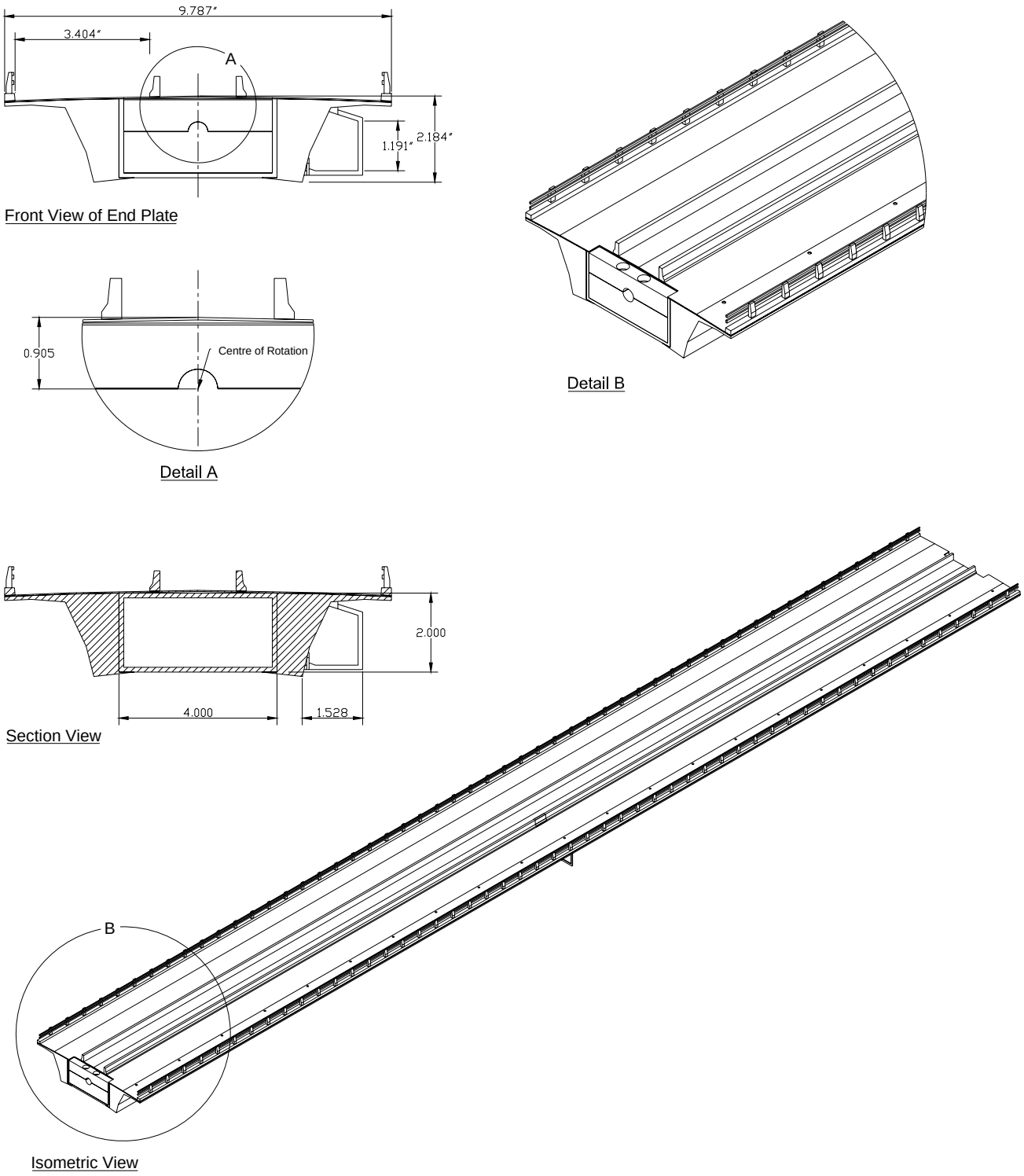

FIGURE 3.3 MODEL DETAILS

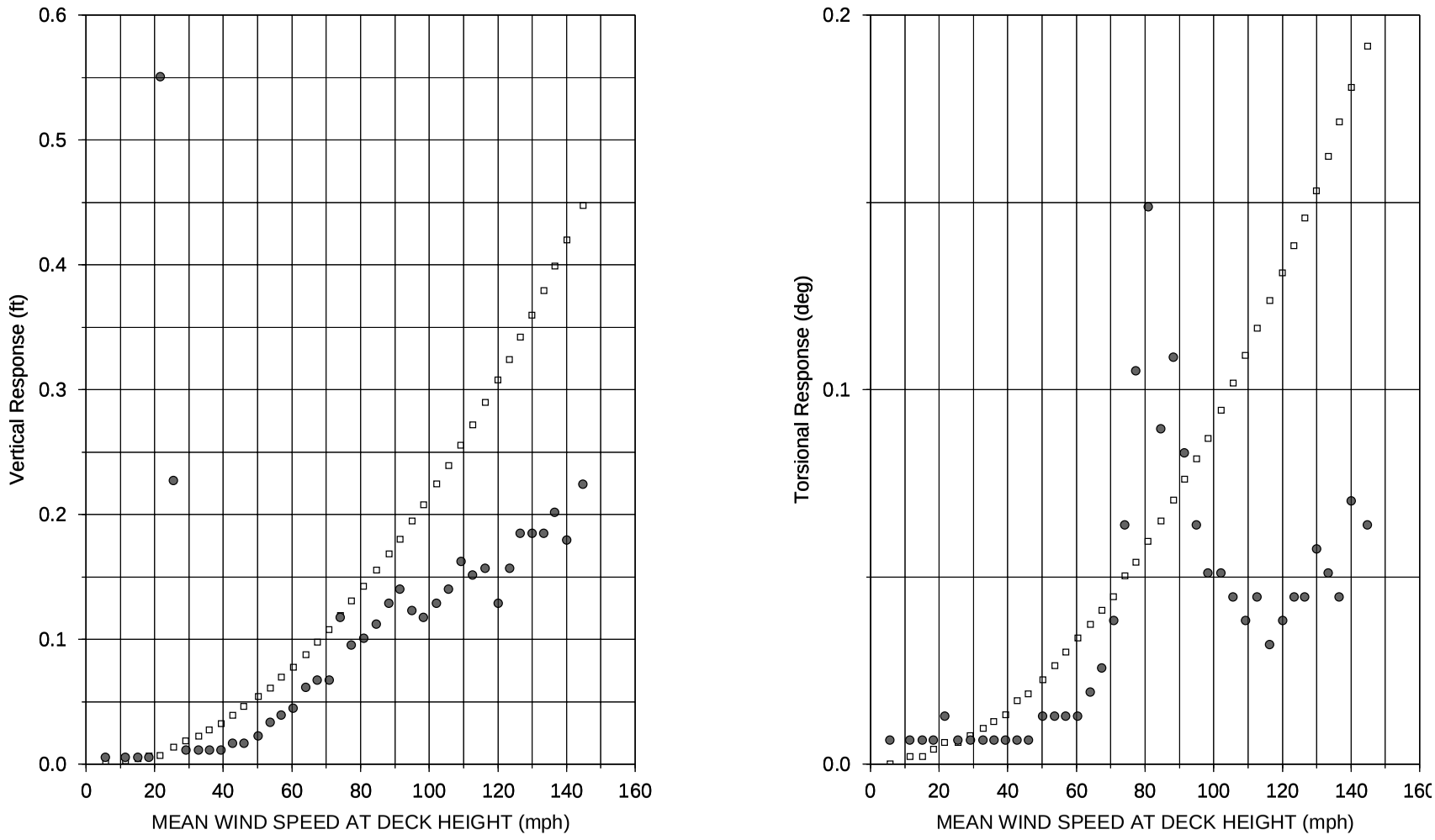

FIGURE 3.4 DYNAMIC TEST RESULT, DECK WITHOUT SIDEWALK IN SMOOTH FLOW, 0 DEGREES ANGLE OF ATTACK AND DAMPING OF 0.5%

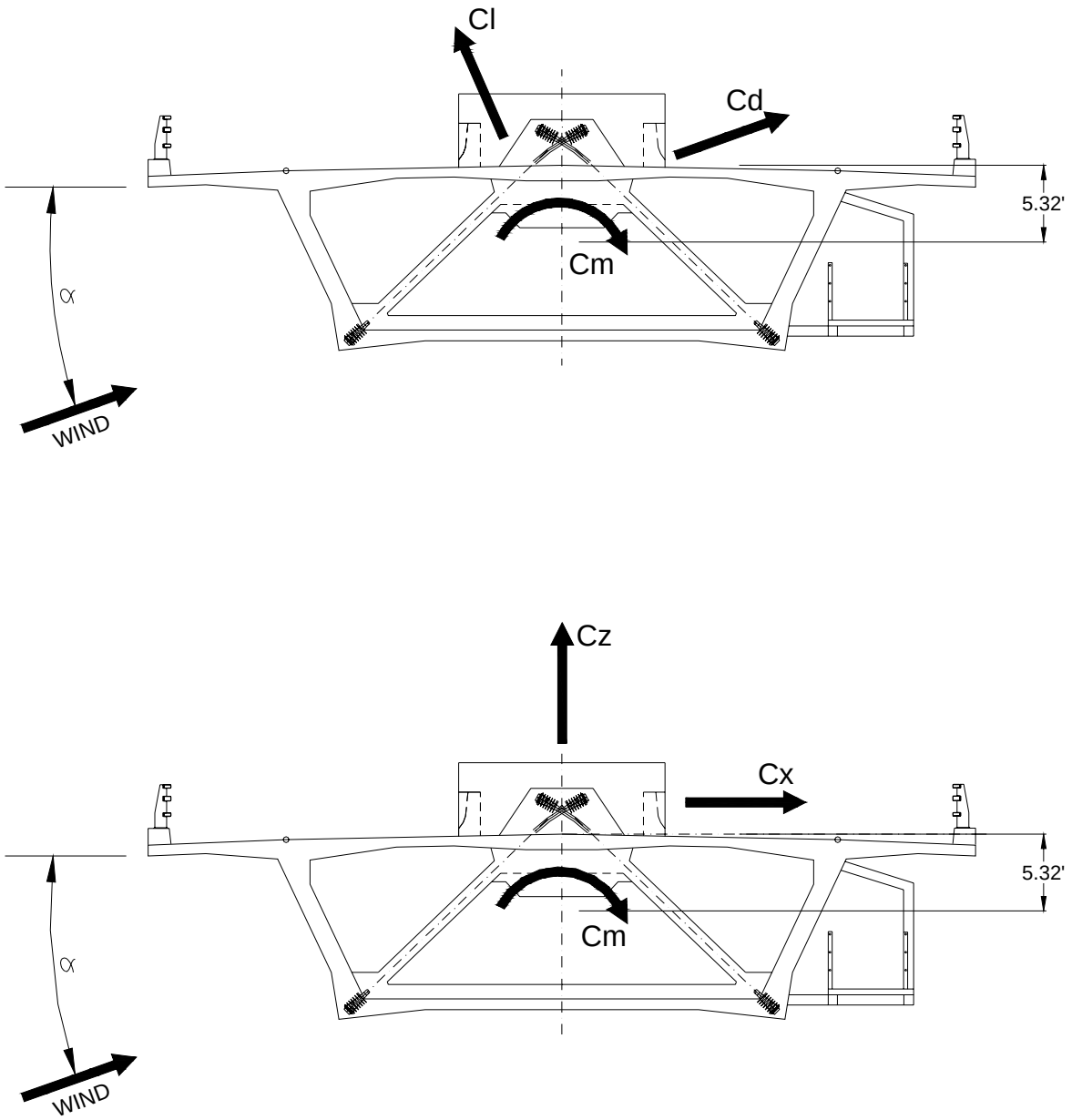

FIGURE 3.5 SKETCH SHOWING SIGN CONVENTION OF FORCES

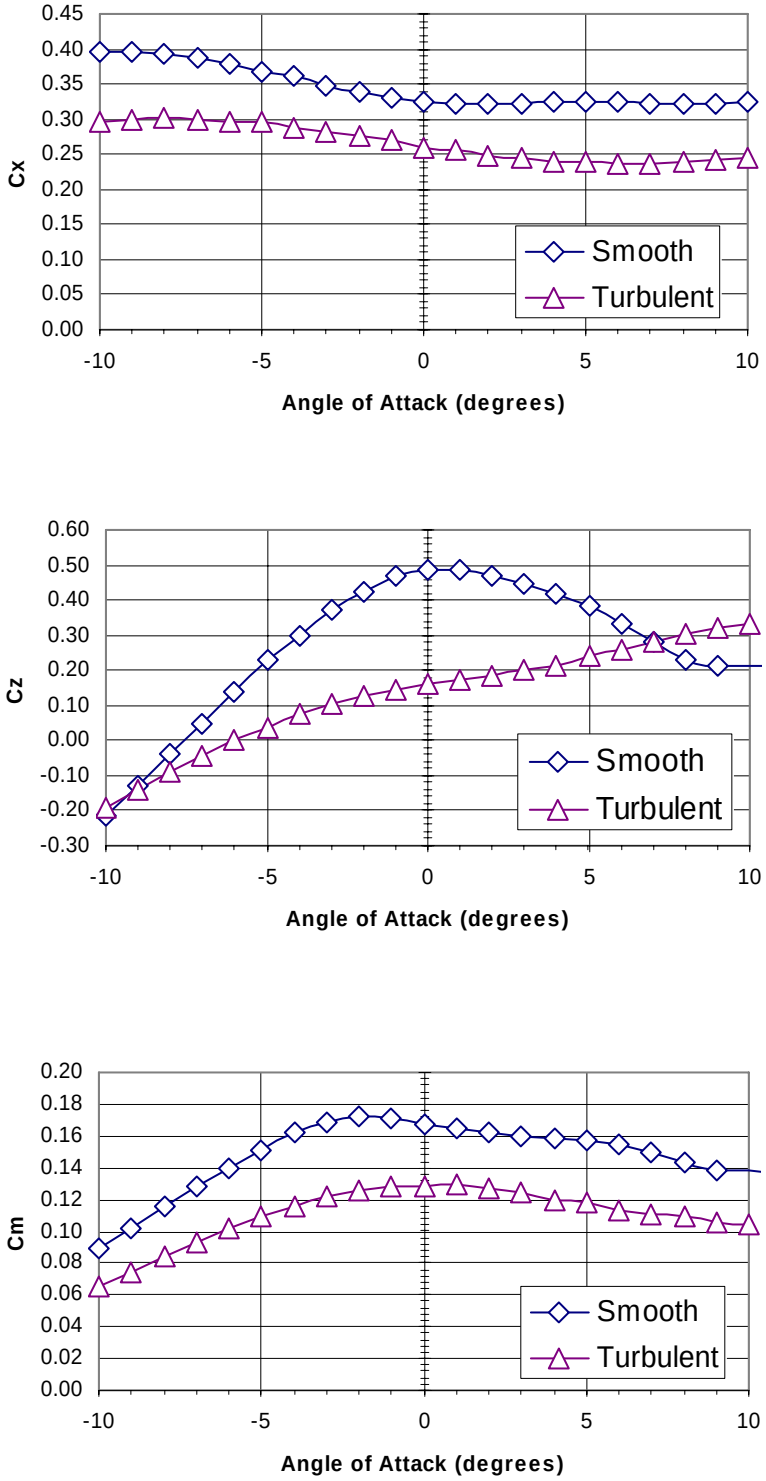

FIGURE 3.6 STATIC FORCE COEFFICIENTS – NO SIDEWALK

4 EQUIVALENT STATIC LOAD ANALYSIS

4.1 General

The definition of wind loads on the Prospect Verona Bridge follows the approach taken by the Laboratory during the study of wind action on the Sunshine Skyway Bridge, in Tampa, Florida, USA [8, 9]. The definition of wind loads on the structure depends upon the measurements of the dynamic response of a model to turbulent wind and the correction of this response for discrepancies in the intensity and spectrum of turbulence, the damping and the Joint Acceptance Function (a measure of the aerodynamic efficiency of the bridge in its response to turbulence). This approach is described in detail in Appendix E and in References [10, 11].

Note that in this analysis, the deck configurations used for the completed bridge include the basic configuration (no sidewalk), the sidewalk on the windward (or upwind) side of the deck and the sidewalk on the leeward (downwind) side. For the construction stage, there is no sidewalk on the deck.

4.2 Adaptation of Section Model Tests Results

The section model responses shown in Figure 4.1 (for basic configuration) in turbulent flow were used as the basis for the derivation of the wind loading for the structure. The prototype modes and frequencies used for the prediction of the full scale deck loading were based upon a dynamic analysis of the structure which was supplied by the Engineers. The dynamic analysis of equivalent static wind loads was performed in two stages; i) with the vertical and torsional degrees of freedom, and ii) with the lateral degree of freedom. The results of these two analyses were merged to produce the approximate modal characteristics for use in the analysis. The fundamental symmetric and asymmetric modes of vibration in lift, torque and drag were used in the determination of the equivalent static wind loads. The prototype and model properties used in the analysis are shown in Tables 4.1 through 4.4.

The turbulence intensities developed in the wind tunnel using grid turbulence is normally lacking sufficient energy in the low frequency - large scale range. While adequate for the definition of resonant response and the overall behavior of the structure to turbulent wind, a slight correction to the loading is made to account for the difference in frequency content. The amplitudes of the spectra of turbulence are matched over the range of reduced frequencies ($f^* = fB/V$) of interest for the deck. The response is adjusted for the deficiency in low frequency turbulence which acts more or less quasi-statically.

The intensities of grid-generated turbulence in the wind tunnel were about 7.2% and 9.0% for the vertical and longitudinal components. The responses described in Section 3 of the Section Model Study are not adjusted for the increased level of turbulence (nor the deficiency in low frequency turbulence). The analysis of the dynamic loads includes an adjustment to consider both of these areas, as well as a mode shape correction. A vertical turbulence intensity of 6.7% was used in the analysis. The ESDU wind parameters given in Table 4.5 provide for a good simulation of open country turbulence characteristics [12, 13].

The equivalent static load analysis was carried out separately for each stage of construction - a selected under construction stage and the completed bridge, with and without the sidewalk. The lowest symmetric and asymmetric deck modes of vibration for these two configurations were selected as the dominant sources of resonant wind excitation of the structure. These modes correspond to loading functions which are pictorially shown in Figure 4.2 for the structure. The fundamental mode shapes which are also used as the load distribution functions are shown in Figure 4.3 for the completed bridge and Figure 4.4 for the construction stage. The same mode shapes and frequencies were used for the deck with sidewalk since the sidewalk is expected to have minimal impact on these parameters. The equivalent static wind loads resulting from the analysis of the bridge deck for the configurations are presented in Figures 4.5 and 4.6. A mean hourly wind speed of 80 mph at deck height is used as a reference wind speed for illustrative purposes and the loads for this speed are reproduced in equation form below. The actual values of $\overline{W}$, $\widetilde{W}_1$ and $\widetilde{W}_2$ shown in the equations are given in Table 4.6 for each configuration.

These loads are summarized for the assumed prototype damping case of 0.5% of critical. Loads for other wind speeds can be interpolated from the plots.

$$W_x(\eta) = \overline{W}_x \alpha(\eta) \pm \gamma_{1x} \widetilde{W}_{1x} \alpha_{1x}(\eta) \pm \gamma_{2x} \widetilde{W}_{2x} \alpha_{2x}(\eta) \qquad (1)$$

$$W_z(\eta) = \overline{W}_z \alpha(\eta) \pm \gamma_{1z} \widetilde{W}_{1z} \alpha_{1z}(\eta) \pm \gamma_{2z} \widetilde{W}_{2z} \alpha_{2z}(\eta) \qquad (2)$$

$$W_\theta(\eta) = \overline{W}_\theta \alpha(\eta) \pm \gamma_{1\theta} \widetilde{W}_{1\theta} \alpha_{1\theta}(\eta) \pm \gamma_{2\theta} \widetilde{W}_{2\theta} \alpha_{2\theta}(\eta) \qquad (3)$$

In the equations, W_x (lb/ft), W_z (lb/ft) and W_θ (lb-ft/ft) are the desired wind loads per unit length resulting from the application of: $\overline{W}$, the mean, distributed according to $\alpha(\eta)$ (normally with a constant value of 1), $\widetilde{W}_1$, the symmetric, according to $\alpha_1(\eta)$ and $\widetilde{W}_2$, the asymmetric, according to $\alpha_2(\eta)$. These distribution functions vary according to the mode shapes presented in Figures 4.3 and 4.4 with a maximum value of 1.0.

To reflect the multitude of combinations with which the fluctuating loads can occur, the load combination factors γ_{1x}, γ_{2x}, γ_{1z}, γ_{2z}, $\gamma_{1\theta}$ and $\gamma_{2\theta}$ should be used in any combination of the modal terms whose values are taken as follows: γ = ±1.0 if only one modal term is included; ±0.8 for two terms; ±0.7 for three terms and ±0.6 for four or more terms. This applies to all modal terms whether they are in X, Z and θ, singly or together.

TABLE 4.1 SUMMARY OF PROTOTYPE PROPERTIES

	BRIDGE COMPLETE	CONSTRUCTION
Deck Height:	154 ft	154 ft
Deck Width:	57.5 ft	57.5 ft
Deck Length:	2118 ft	1034 ft
Mass:	779.5 slug/ft	630.4 slug/ft
Mass Moment of Inertia:	1.895E+05 slug-ft^2/ft	1.574E+05 slug-ft^2/ft
Structural Damping:	0.5% of critical	0.5% of critical

	Frequency (Hz)					
	Symmetric			Anti-symmetric		
Configuration	**drag**	**lift**	**torque**	**drag**	**lift**	**torque**
Completed Bridge (with and without sidewalk)	0.242	0.327	1.104	0.781	0.500	2.198
Construction Stage (without sidewalk)	0.764	0.554	1.287	1.449	0.858	1.961

TABLE 4.2 SUMMARY OF MODEL PROPERTIES, NO SIDEWALK

Test data file:	sma2a001.aer
Frequency:	4.476 Hz (Lift)
	15.197 Hz (Torque)
Mass:	0.157 slug/ft
Mass moment of Inertia:	0.00759 slug-ft^2/ft
Structural Damping:	0.5% of critical
Length:	7 ft
$dC_z / d\alpha$	0.85
C_x **at 0°**	0.261

TABLE 4.3 SUMMARY OF MODEL PROPERTIES, SIDEWALK UPWIND

Test data file:	smb2a001.aer
Frequency:	4.414 Hz (Lift)
	14.816 Hz (Torque)
Mass:	0.159 slug/ft
Mass moment of Inertia:	0.00781 slug-ft^2/ft
Structural Damping:	0.5% of critical
Length:	7 ft
$dC_z / d\alpha$	1.87
C_x **at 0°**	0.249

TABLE 4.4 SUMMARY OF MODEL PROPERTIES, SIDEWALK DOWNWIND

Test data file:	smc2a001.aer
Frequency:	4.414 Hz (Lift)
	14.816 Hz (Torque)
Mass:	0.159 slug/ft
Mass moment of Inertia:	0.00781 slug-ft^2/ft
Structural Damping:	0.5% of critical
Length:	7 ft
$dC_z / d\alpha$	1.11
C_x **at 0°**	0.253

TABLE 4.5 SUMMARY OF WIND CHARACTERISTICS

Wind Characteristics

based on ESDU 82026, ESDU 83045, ESDU 85020

Aerodynamic roughness length:	z_o	0.1 ft
Height of deck:	H	154 ft
Reference hourly mean wind speed at deck height:	V_{ref}	80 mph
Latitude:		44.5°
Longitudinal turbulence intensity:	I_u	0.147
Vertical turbulence intensity:	I_w	0.067
Longitudinal length scale:	L_u	393 ft
Vertical length scale:	L_w	54 ft

TABLE 4.6 VALUES OF $\overline{W}$, $\tilde{W}_1$ AND $\tilde{W}_2$ FOR A WIND SPEED OF 80 MPH

Configuration	**Completed bridge**									**Construction stage**		
Sidewalk	**No sidewalk**			**Sidewalk upwind**			**Sidewalk downwind**			**No sidewalk**		
Load Direction	X	Z	θ	X	Z	θ	X	Z	θ	X	Z	θ
$\overline{W}$ (lb/ft for force and lb-ft/ft for torque)	250	150	6560	238	116	4340	242	128	6930	250	190	6710
$\tilde{W}_1$ (lb/ft for force and lb-ft/ft for torque)	404	1670	14800	387	1730	14400	392	1900	14500	593	2510	13900
$\tilde{W}_2$ (lb/ft for force and lb-ft/ft for torque)	161	1180	9030	154	1130	9490	157	1260	9500	177	1530	11400

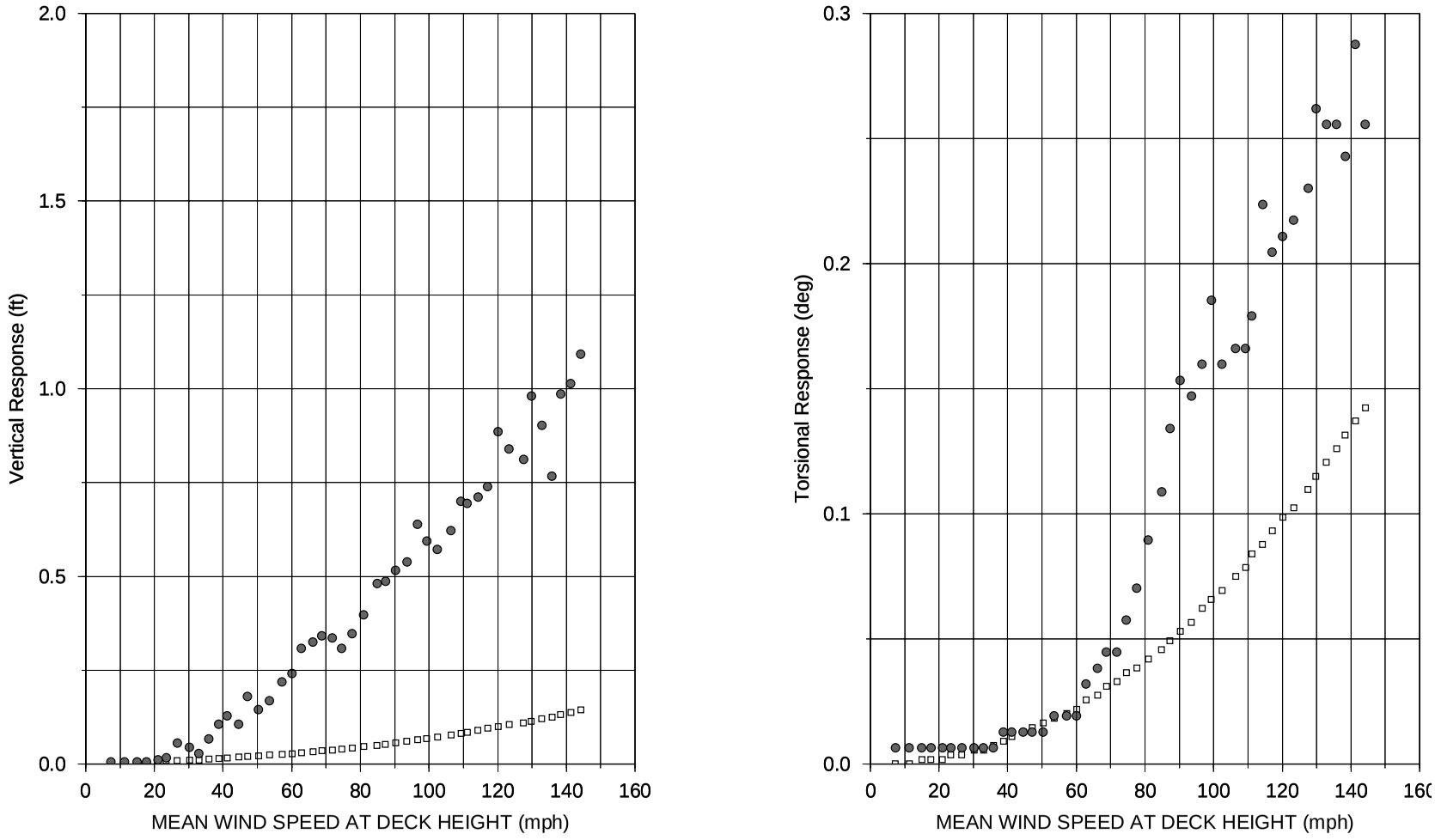

FIGURE 4.1 DYNAMIC TEST RESULT, TURBULENT FLOW AT 0° ANGLE OF ATTACK, NO SIDEWALK

$$W_x(\eta) = \overline{W}_x\,\overline{a}(\eta) + \gamma_{1_x} W_{1_x}\, a_1(\eta) + \gamma_{2_x} W_{2_x}\, a_2(\eta)$$

$$W_z(\eta) = \overline{W}_z\,\overline{a}(\eta) + \gamma_{1_z} W_{1_z}\, a_1(\eta) + \gamma_{2_z} W_{2_z}\, a_2(\eta)$$

$$W_\theta(\theta) = \overline{W}_\theta\,\overline{a}(\eta) + \gamma_{1_\theta} W_{1_\theta}\, a_1(\eta) + \gamma_{2_\theta} W_{2_\theta}\, a_2(\eta)$$

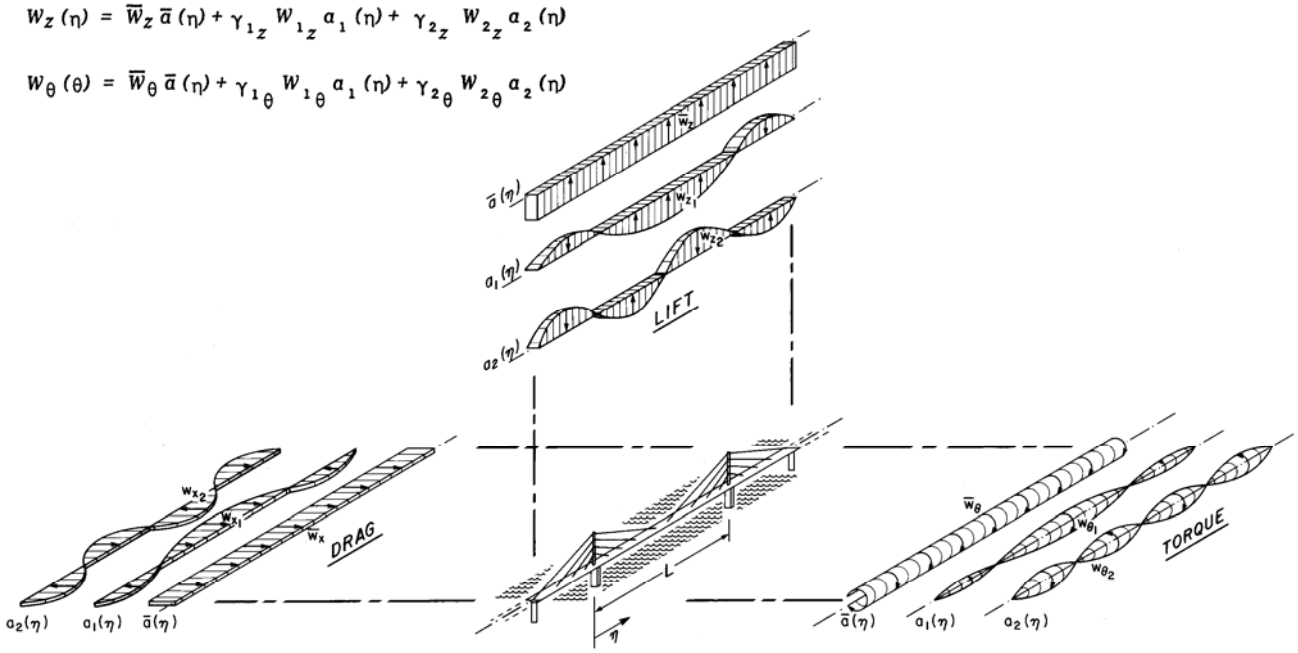

FIGURE 4.2 DISTRIBUTED WIND LOAD COMPONENTS

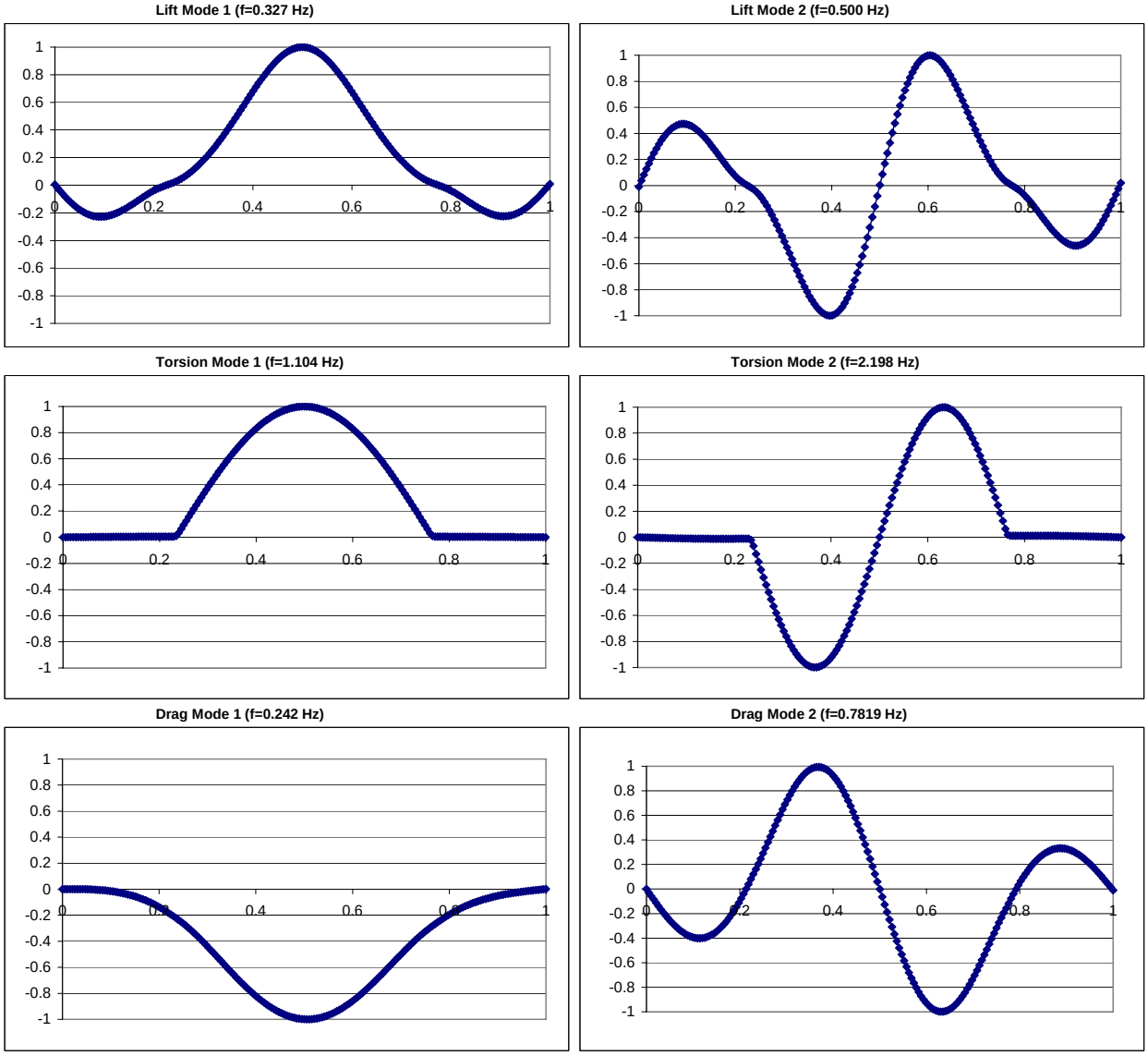

FIGURE 4.3 MODE SHAPE DISTRIBUTION FUNCTIONS FOR COMPLETED BRIDGE (NO SIDEWALK)

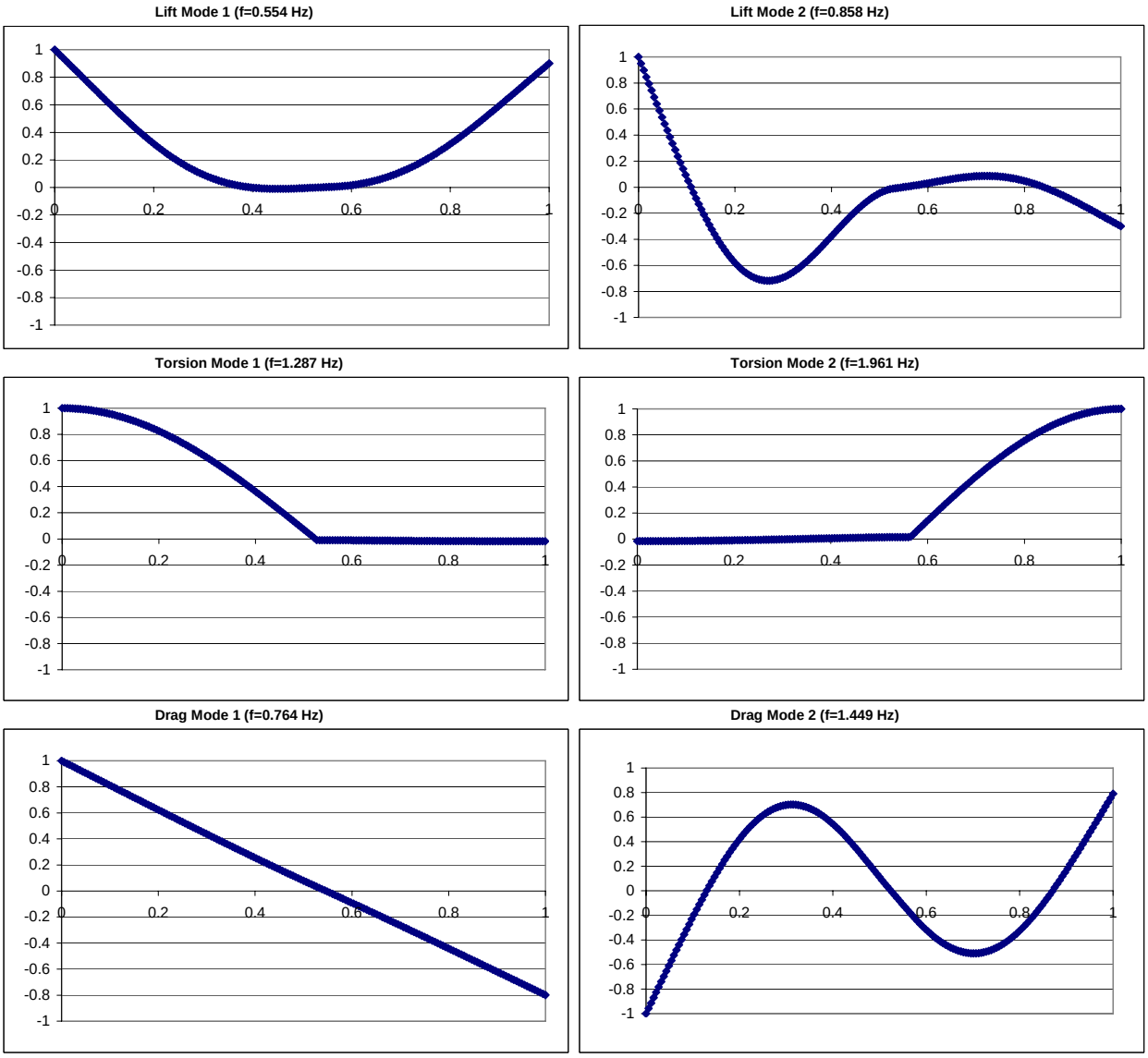

FIGURE 4.4 MODE SHAPE DISTRIBUTION FUNCTIONS FOR CONSTRUCTION STAGE (NO SIDEWALK)

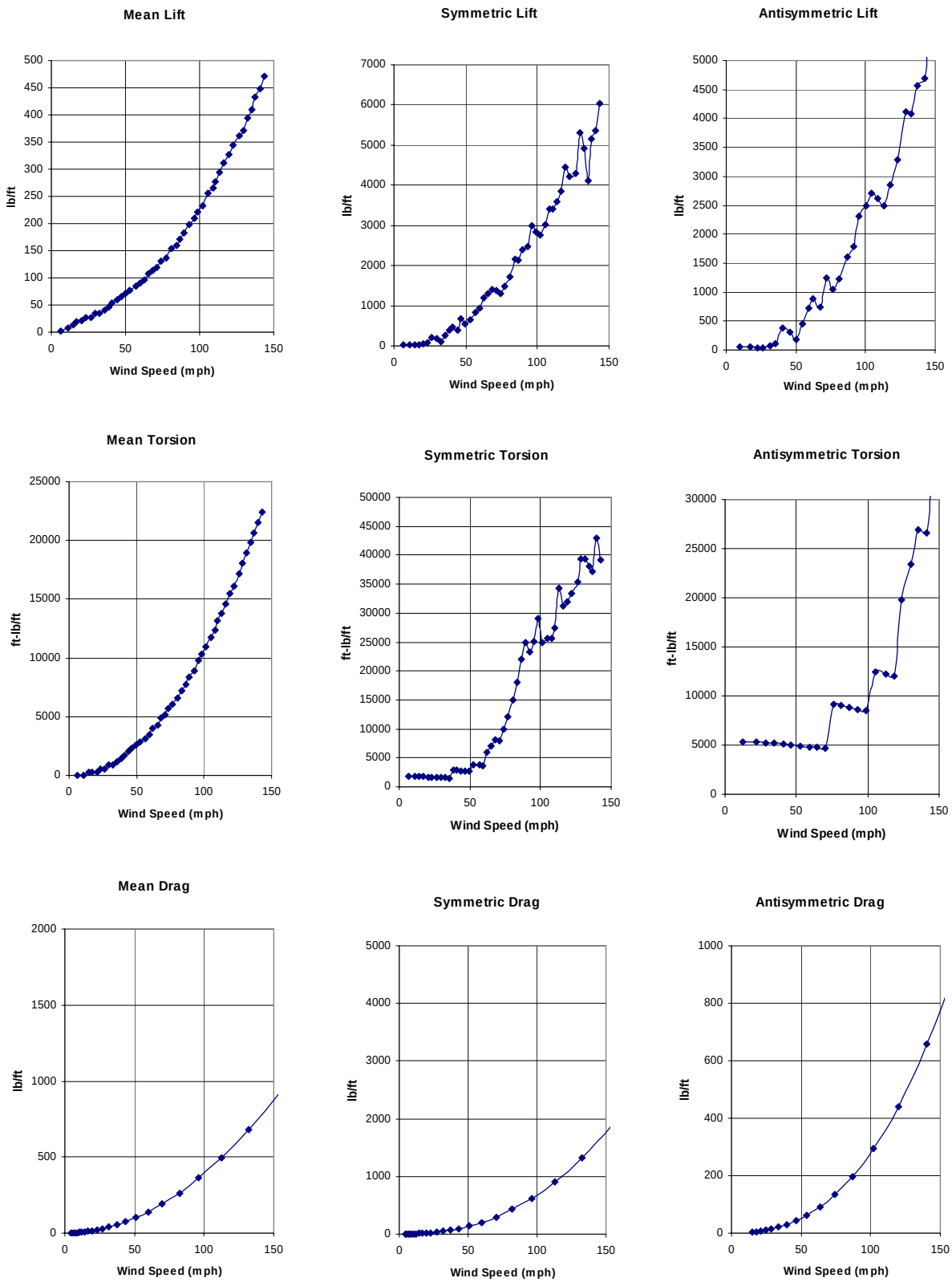

FIGURE 4.5 WIND LOAD COMPONENTS FOR COMPLETED BRIDGE (NO SIDEWALK)

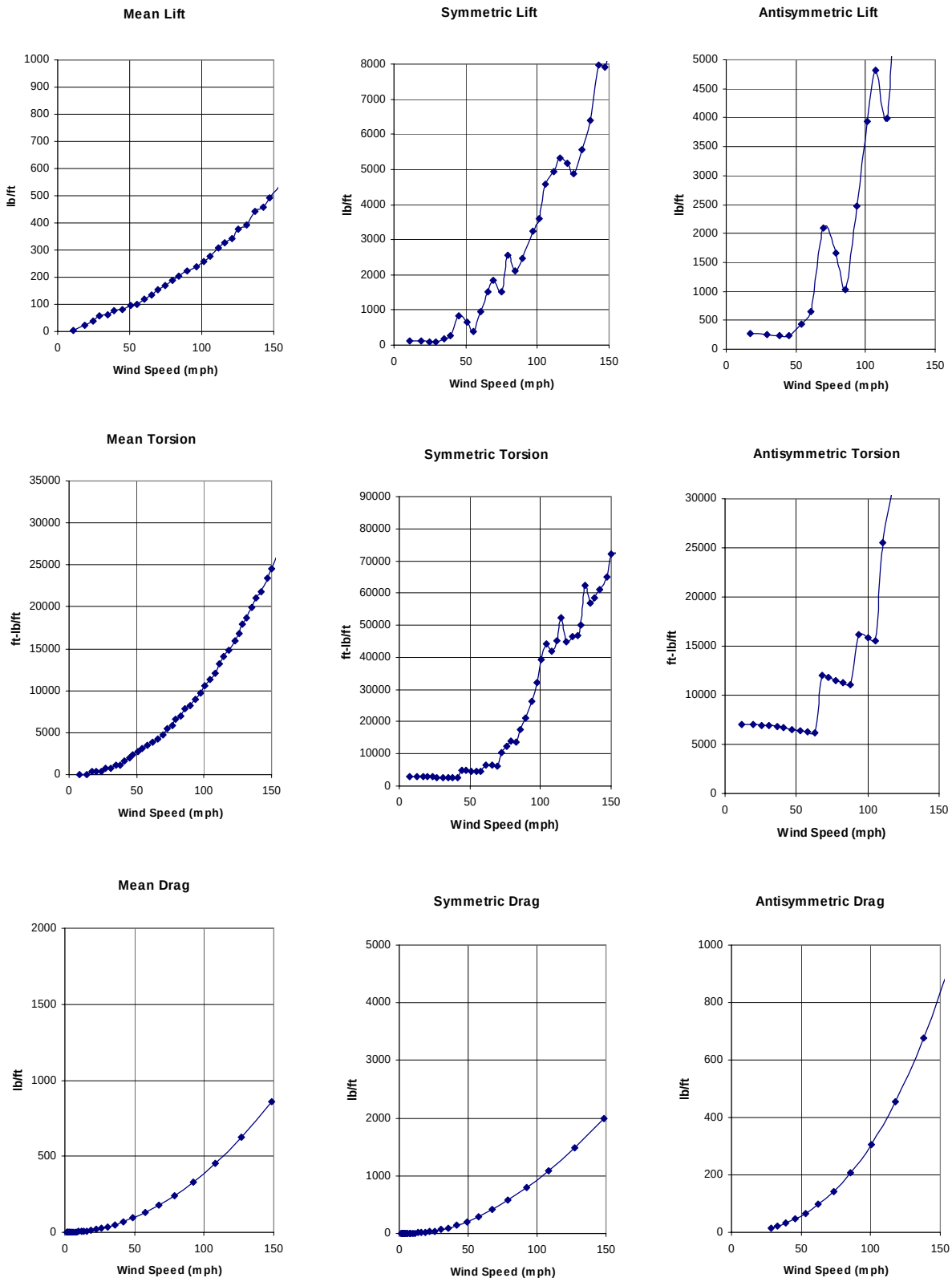

FIGURE 4.6 WIND LOAD COMPONENTS FOR CONSTRUCTION STAGE (NO SIDEWALK)

5 PROSPECT PYLON PRESSURE STUDY

5.1 Overall Approach

The behavior of the Prospect Pylon pressure model was studied in the High-Speed Test Section in the Boundary Layer Wind Tunnel II, where the automated turntable could be utilized. The pylon has an overall height of 430 ft from the base with 292.6 ft above the deck. The Prospect Pylon includes a multi storey observation area with glass curtain walls. This portion of the model was instrumented with pressure taps. The observatory level sits above 372 ft and has a height of about 42 ft.

Detailed measurements were made of wind-induced pressures and suctions on the glass cladding of the exterior surfaces of the Prospect Pylon observation levels, using a rigid model of the pylon constructed at a scale of 1:200. In the test, the upwind terrain was modeled within the 42.6m long wind tunnel test section, which represented approximately 5 miles of upwind fetch. The oncoming flow was conditioned by a set of turbulence generating roughness, including spires, floor roughness and a large scale eddy-generating trip. This methodology has been highly developed and is documented in References 14 and 15. One upstream exposure, simulating the hurricane profile, was used in the test.

Figure 5.1 shows the test set-up with the modeled upstream terrain. A close-up view of the pressure model is shown in Figure 5.2. In the test, a dummy model of a portion of the new bridge was incorporated. The surrounding hills around the bridge site were also not modeled in the pressure test in order to provide upper bound estimates for the surface pressures.

Figure 5.3 presents the vertical profile of the mean speed and of the intensity of the longitudinal component of turbulence. The selected wind profile ensures that the ratio of mean pylon-height-to-reference-height wind speed in the wind tunnel matches expected full-scale values. The normalized mean wind speed $\overline{V}(h)/\overline{V}_{ref}$ is plotted along with the local turbulence intensity $\sigma(h)/\overline{V}(h)$. The wind profile and turbulence intensity in the lower portion of the boundary layer within the pylon height of about 450 ft from mean water level compares very well with the hurricane data discussed in [2, 3, 16], as well as with ESDU 82026 [12, 13], a widely accepted form of defining the variation of wind characteristics with height.

A total of 34 pressure taps were installed on the observation levels of the model, with the numbering and locations given in Figure 5.4. There are 3 regular rings of pressure taps on the glass cladding with 10 taps for each ring, with an additional 4 taps on each face of the cone shaped pylon top.

Measurements were taken at 10° internals for the full 360° azimuth range. Pressures were sampled at 400 samples per second for 60 seconds (equivalent to about 7 samples per second for 1 hour in full scale). In addition to recording the maximum, minimum, mean and RMS pressure from the time histories, all of the samples were retained for future analysis. A detailed description of the procedures followed and definitions used are presented in Reference [1].

The experimental pressure data do not show any unusual sensitivity to the precise angle of the wind, so the measurements at 10° increments in wind azimuth describe the pressure response with good resolution. The largest magnitudes of the measured external pressure coefficients found over all azimuths are tabulated in Table 5.1 for all pressure taps. All external pressure coefficients, including the plot showing the pressure coefficient variation with azimuth, are given in Appendix A. The experimental data indicates that local pressure loads on the project, normalized by the dynamic pressure at gradient height, are quite significant. The largest peak external pressure and suction coefficients (referenced to the gradient-height dynamic pressure) are 1.7 and 3.0 respectively.

Using the methodology described in Reference [1], a range of mean internal pressure coefficients were determined at all wind angles, assuming leakage through many small openings over the pylon's exterior surfaces in the observation levels. This is typical of most nominally-sealed structures. A list of these coefficients is given in Table 5.2. These internal pressure coefficients were then subtracted from the external pressure coefficients to form differential pressure coefficients.

The differential pressure coefficients, as well as the external pressure coefficients, were combined with the passages of the simulated storms of the hurricane wind climate in terms of wind speed and direction in the project area to provide predictions of peak pressures and suctions for a return period of 500 years at each pressure tap location on the pylon. The hurricane wind climate information is provided in Section 2 of this report. Results of the extreme mean hourly wind speeds for various return periods are summarized in Figure 5.2 for the hurricane winds. The design wind speed from the hurricane wind climate, consistent with the definition in ASCE 7-02 (500-year return wind speed divided by $\sqrt{1.5}$), is about 100 mph at upper level (500m). Therefore, the design wind pressures and suctions were calculated by dividing the 500 year return period predictions by 1.5, which is again consistent with the requirements of ASCE 7-02 [Reference 17].

5.2 Pylon Pressure Results

Table 5.3 shows the predicted peak design pressures and suctions. The largest predicted design pressure (inward-acting load) and suction (outward-acting load) are about 54 and 63 psf respectively. The largest pressure occurs on the south side, while the worst suction occurs on the East side near the top corner.

In the process to predict the design differential pressures and suctions on the glass cladding of the pylon, the worst case (i.e., the largest pressures and suctions) from the analysis at each tap location are selected in the final result. This means that in the analysis, where the external pressure prediction is greater than the differential pressure prediction, the external pressure prediction is presented as the peak design pressure. Table 5.4 presents a list of predictions of the external pressures and suctions.

Note that for the use of these wind loads in the design of the curtain wall and exterior cladding, the loads must be multiplied by the appropriate load factor, which has not been included in the Figures. In addition, these results do not include any allowance for stack (thermal) effects or the direct effects of mechanical systems.

TABLE 5.1 SUMMARY OF THE MAXIMUM AND MINIMUM EXTERNAL PRESSURE COEFFICIENTS

Tap No.	Maximum Cp	Azimuth (degree)	Minimum Cp	Azimuth (degree)
1	0.88	10	-2.19	130
2	1.35	50	-2.92	110
3	1.35	20	-2.03	130
4	1.42	350	-2.97	290
5	1.49	40	-2.60	270
6	1.57	20	-2.44	280
7	1.61	350	-2.68	120
8	1.49	60	-2.84	280
9	1.55	20	-2.34	290
10	1.60	350	-2.73	130
11	0.76	290	-2.44	210
12	1.29	310	-2.65	0
13	1.43	260	-2.78	210
14	1.46	310	-2.51	0
15	1.49	270	-2.59	210
16	1.45	310	-2.40	10
17	1.59	280	-2.62	210
18	1.12	210	-2.36	300
19	1.50	230	-2.91	290
20	1.50	210	-2.24	100
21	1.39	160	-2.99	110
22	1.58	230	-2.42	80
23	1.62	210	-2.28	300
24	1.48	170	-2.27	300
25	1.46	240	-2.38	90
26	1.65	210	-2.30	110
27	1.54	160	-2.31	300
28	0.76	110	-2.67	30
29	1.42	130	-2.94	190
30	1.27	80	-2.69	30
31	1.58	140	-2.85	190
32	1.49	90	-2.59	30
33	1.65	130	-2.57	180
34	1.50	90	-2.77	30

Notes: The external pressure coefficients in this table are normalized by the gradient height wind speed. If normalization using the pylon height wind speed is desired, a ratio of $(1/0.88)^2$=1.29 has to be multiplied by these numbers.

TABLE 5.2 SUMMARY OF THE MEAN INTERNAL PRESSURE COEFFICIENTS

Wind Direction (degree)	Upper Bound	Average	Lower Bound
0	-0.036	-0.401	-0.767
10	-0.053	-0.414	-0.776
20	-0.052	-0.414	-0.777
30	-0.065	-0.439	-0.813
40	-0.045	-0.403	-0.761
50	-0.010	-0.337	-0.665
60	0.050	-0.273	-0.597
70	0.062	-0.259	-0.581
80	0.008	-0.328	-0.665
90	-0.053	-0.368	-0.683
100	-0.083	-0.391	-0.699
110	-0.101	-0.423	-0.746
120	-0.090	-0.408	-0.727
130	-0.038	-0.365	-0.691
140	0.035	-0.296	-0.627
150	0.080	-0.261	-0.602
160	0.071	-0.269	-0.608
170	0.001	-0.334	-0.670
180	-0.028	-0.402	-0.775
190	-0.042	-0.427	-0.811
200	-0.034	-0.407	-0.779
210	-0.047	-0.442	-0.836
220	-0.031	-0.417	-0.804
230	0.003	-0.335	-0.673
240	0.070	-0.258	-0.587
250	0.078	-0.266	-0.611
260	0.037	-0.302	-0.642
270	-0.034	-0.352	-0.670
280	-0.080	-0.407	-0.733
290	-0.086	-0.401	-0.716
300	-0.086	-0.402	-0.718
310	-0.044	-0.353	-0.662
320	0.033	-0.283	-0.599
330	0.075	-0.245	-0.564
340	0.069	-0.252	-0.574
350	-0.001	-0.319	-0.637

Notes: Above coefficients are calculated from the mean external pressure coefficients, as detailed in *Reference 5*. Stack effect and the effects of mechanical system are not included.

TABLE 5.3 SUMMARY OF THE PREDICTED PEAK DIFFERENTIAL PRESSURES AND SUCTIONS (PSF)

Tap Location No.	Peak Pressures (PSF)	Peak Suctions (PSF)
1	29.1	50.8
2	40.5	62.4
3	35.9	46.3
4	27.7	48.9
5	45.0	51.2
6	39.2	51.6
7	32.1	57.8
8	44.2	53.4
9	39.2	48.9
10	29.1	58.7
11	24.6	54.5
12	31.1	49.9
13	38.7	59.0
14	31.7	50.1
15	40.5	55.2
16	32.9	48.7
17	41.1	55.1
18	42.0	50.3
19	46.7	44.8
20	50.2	49.9
21	48.3	62.1
22	48.7	55.4
23	53.3	48.7
24	49.8	45.6
25	46.0	55.5
26	53.5	51.2
27	49.7	46.6
28	34.0	54.7
29	48.8	63.2
30	46.5	45.2
31	52.3	59.5
32	50.2	48.8
33	52.6	56.0
34	51.1	51.2

TABLE 5.4 SUMMARY OF THE PREDICTED PEAK EXTERNAL PRESSURES AND SUCTIONS (PSF)

Tap Location No.	Peak Pressures (PSF)	Peak Suctions (PSF)
1	14.9	50.8
2	25.4	62.4
3	21.6	46.3
4	17.4	48.9
5	29.6	51.2
6	25.0	51.6
7	19.6	57.8
8	29.4	53.4
9	24.9	48.9
10	19.4	58.7
11	12.2	54.5
12	19.2	49.8
13	26.0	59.0
14	19.9	50.1
15	28.0	55.2
16	20.8	48.7
17	28.6	55.1
18	23.5	50.3
19	30.1	44.8
20	31.8	49.9
21	31.2	62.1
22	31.7	55.4
23	34.7	48.7
24	33.7	45.6
25	29.7	55.5
26	35.2	51.2
27	33.7	46.6
28	16.7	54.7
29	32.5	63.2
30	29.5	45.2
31	36.2	59.5
32	33.7	48.8
33	36.2	56.0
34	34.2	51.2

FIGURE 5.1 PHOTOGRAPHS OF THE MODEL IN THE WIND TUNNEL SHOWING THE UPSTREAM TERRAIN MODEL (EXPOSURE) USED

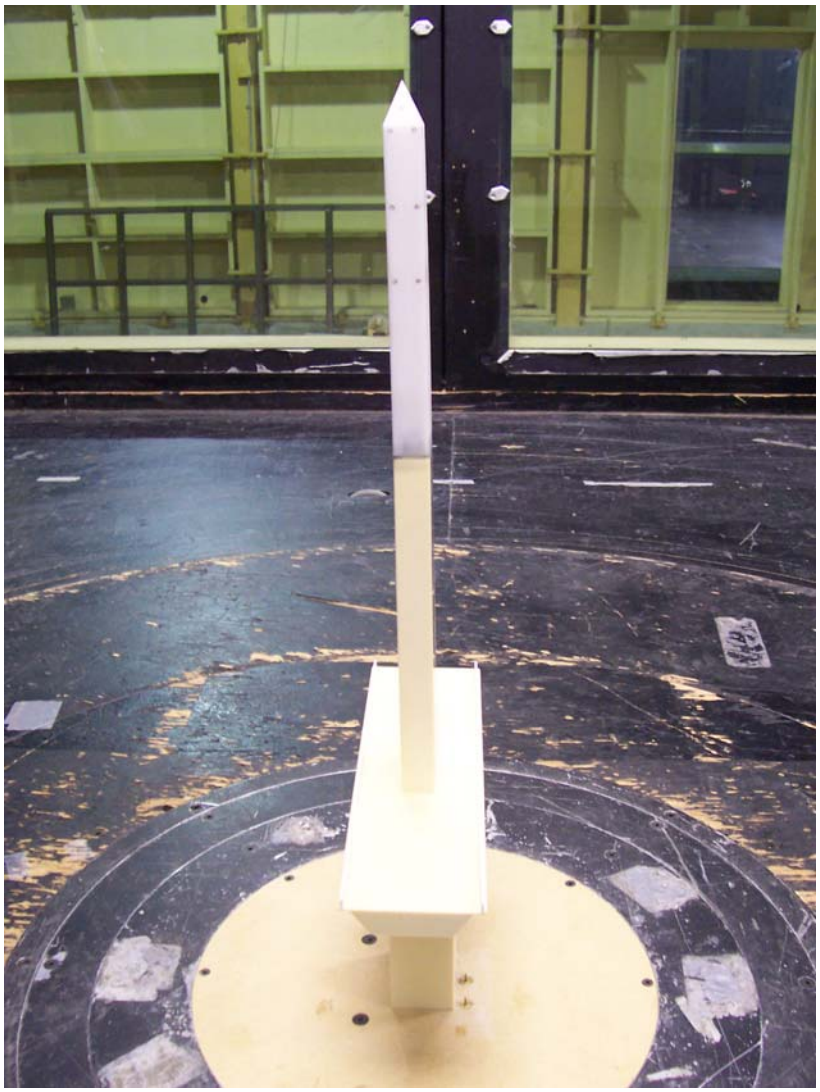

FIGURE 5.2 CLOSE UP VIEWS OF THE PRESSURE MODEL

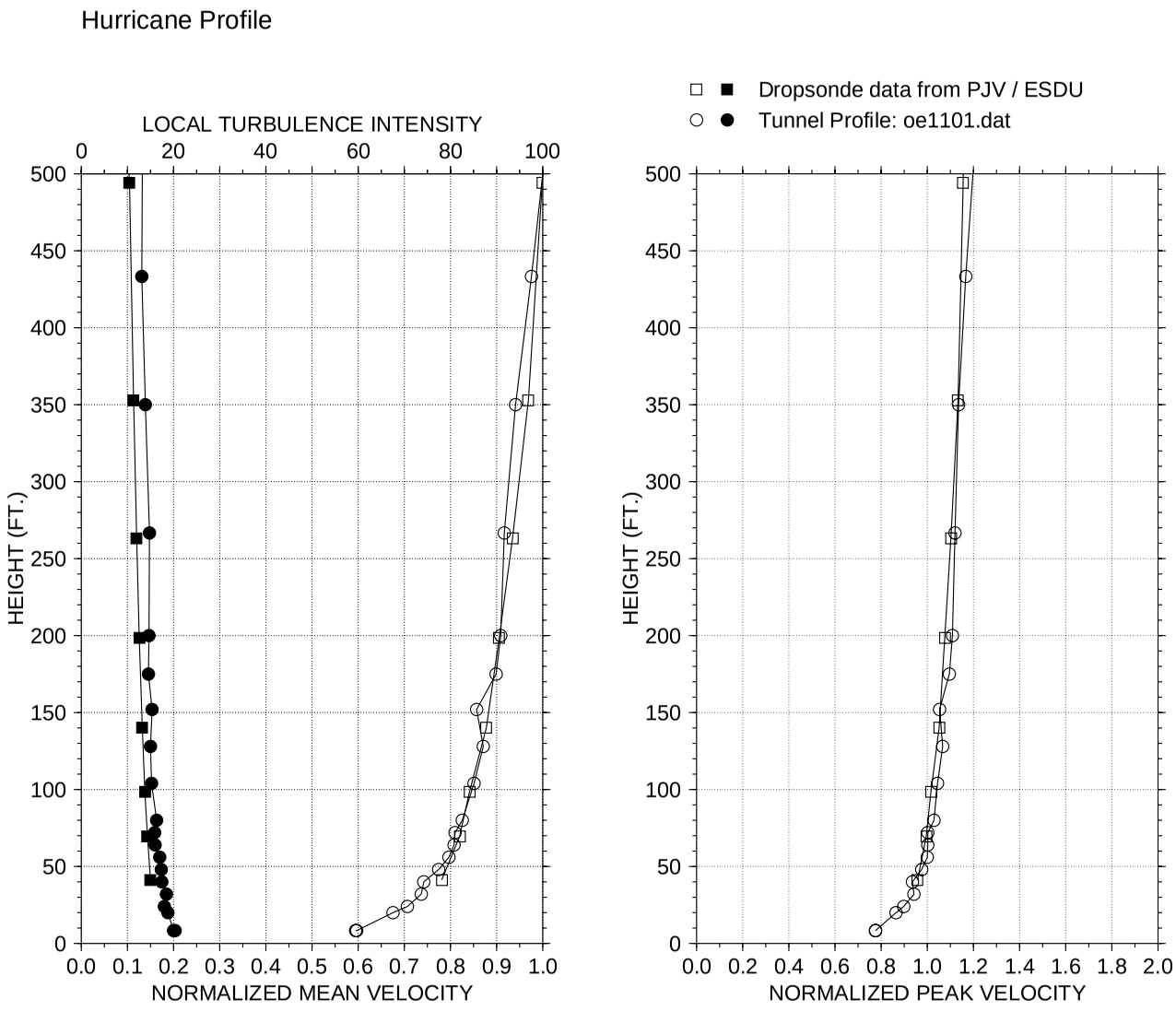

FIGURE 5.3 VERTICAL PROFILE OF MEAN WIND SPEED AND LONGITUDINAL TURBULENCE INTENSITY MEASURED JUST UPSTREAM OF THE PROXIMITY MODEL.

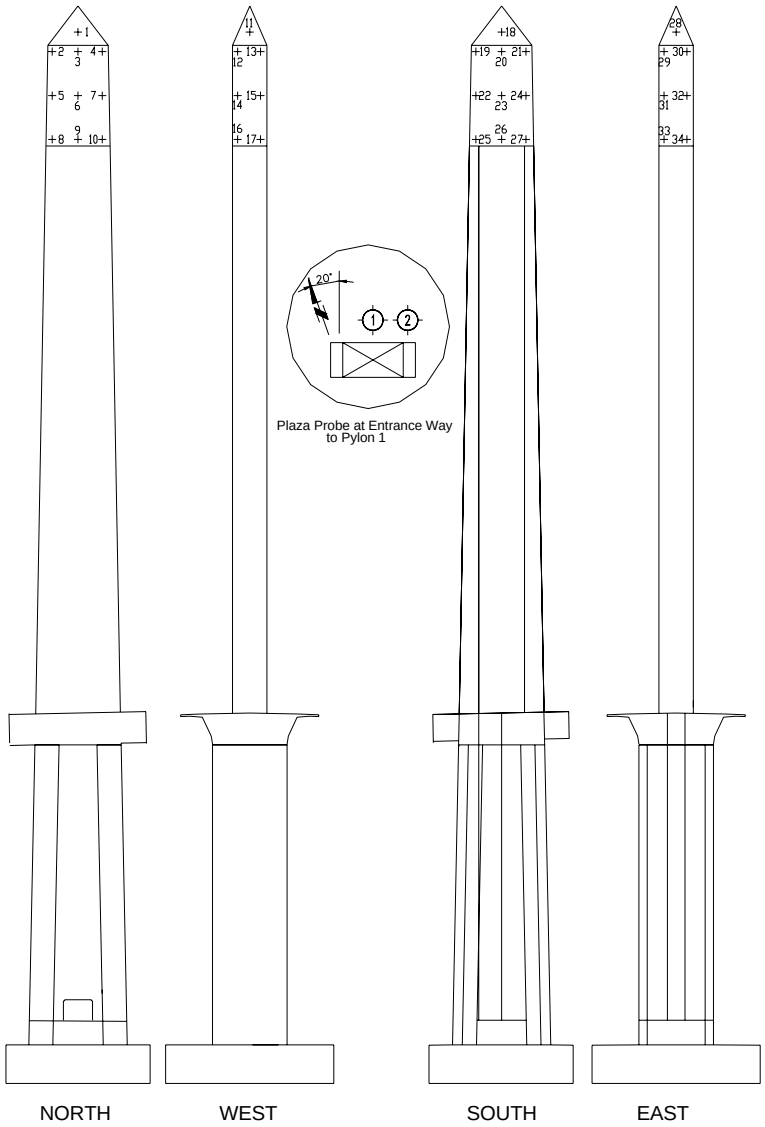

FIGURE 5.4 LOCATIONS OF PRESSURE TAPS AND WIND PROBES

6 DETERMINATION OF PEDESTRIAN LEVEL WIND

6.1 Overall Approach

Measurements were made of pedestrian level wind speeds at two locations around the entrance area of the Prospect Pylon. Experimental results were then combined with the extratropical wind climates developed for the project to provide predictions of the wind speeds expected at the pylon entrance area and are compared directly with acceptance criteria for pedestrian comfort and safety respectively. The two extratropical wind climates used in this analysis were developed on the basis of full scale meteorological records from the nearby weather stations at Bangor and Rockland, Maine. Figure 6.3 shows the location of the bridge and the locations of these two weather stations. Results of the hourly-mean wind speeds predicted for various return periods at these two stations are summarized in Figures 6.1 and 6.2 respectively.

Figure 6.4 shows the 2 locations at which speed measurements were taken around the Prospect Pylon entrance. Since the local topographic features were not modeled in the test, the current estimation of the wind conditions may be conservative. The wind conditions at these two locations were re-evaluated with local topography close to the bridge site during the full aeroelastic tests. The local terrain is expected to have a relatively significant effect on the pedestrian level wind condition.

Measurements were made using omni-directional pressure sensors which measure both mean and fluctuating components of the wind speed parallel to the ground at a height of about 4.5 to 6 feet full scale. Measurements were taken at 10° intervals for the full range of azimuths. Measured coefficients of mean and gust wind speeds at the two locations are presented in Figure 6.5. The gust wind speed, based on considerations of pedestrian comfort described elsewhere [18, 19], is taken as the mean speed plus 1.5 standard deviations of the wind speed. The polar plots in Figure 6.5 show the wind speed at each of the sensors, expressed as a ratio of the mean wind speed at gradient height. The angular coordinate gives the direction of the approach wind, relative to true North.

The radial magnitudes and the shapes of the polar plots in Figure 6.5 provide valuable indications of the relative magnitudes of wind speeds at different locations and their sensitivity to the direction of the approach wind. For example, both locations are clearly sheltered for wind directions where they are downstream of the pylon, while it also shows higher wind speeds for wind directions where the wind is rounding the corner of the pylon.

6.2 Statistical Prediction of Pedestrian Level Winds

The extratropical wind climates described in Section 2 were combined with the aerodynamic data measured in the wind tunnel to provide the following two types of prediction:

1. Wind speeds exceeded during 5% of the time on an annual basis.
2. Wind speeds exceeded once per year.

Criteria for pedestrian comfort and safety, for temperate climates are as follows:

CRITERIA	DESCRIPTION	MEAN WIND SPEED EXCEEDED 5% OF THE TIME
Comfort level 1	Fast Walking	22 mph
Comfort level 2	Leisurely Walking	18 mph
Comfort level 3	Standing, Sitting - short exposure	13 mph
Comfort level 4	Standing, Sitting - long exposure	9 mph
CRITERIA	**DESCRIPTION**	**MEAN WIND SPEED EXCEEDED ONCE PER YEAR**
Safety level 1	Fair-Weather Areas	45 mph
Safety level 2	All-Weather Areas	34 mph

Note: Fair-weather areas refer to areas that are not used in severe weather, such as parks, lookout points, etc. All weather areas are areas that need to be used in all weather conditions, such as building entrances, sidewalks, etc.

These criteria reflect the findings of many pedestrian wind studies at The Boundary Layer Wind Tunnel Laboratory and were first used to evaluate wind conditions at the Canary Wharf Development in London, England [20]. These criteria were first published by Kapoor et al [21].

Figure 6.6 shows the predicted wind speeds at these two locations and the comparison with accepted criteria for both safety and comfort levels. Predictions for typical suburban and open country areas are also shown for comparison,. Table 6.1 lists the actual wind speeds predicted. In general, these two locations meet the criteria for pedestrian comfort conditions for intended activities (short sitting and leisurely walking). However, to assure the safety of pedestrians in public areas, it is an accepted recommendation that the 34 mph threshold of potentially hazardous wind conditions should not be exceeded more than once per year for all weather areas. At location 2, the predicted wind speed exceeded once per year is about 36 mph and above the recommended guideline, however the pylon observation platform will be likely closed to public in severe weather conditions. Figure 6.5 indicates that if the observation pylon is only open in fair weather, the probe 2 location would meet the safety requirement. In addition, since none of the local terrain is modeled in this preliminary study, this test is expected to provide conservative estimates of the wind conditions at the base of the pylon. The estimates of the pedestrian level wind condition are improved in the full aeroelastic test for which the local topography is simulated.

TABLE 6.1 PREDICTED WIND CONDITIONS AT THE TWO LOCATIONS TESTED

Probe Location No.	Hourly Mean Wind Speeds Exceeded During 5% of the Time Annually (mph)	Hourly Mean Wind Speeds Exceeded Once per year (mph)
1	13.7	32.0
2	16.7	35.7

Notes:

1. The mean wind speed which is exceeded 5% of the time is used to check the comfort level of the location in comparison to accepted comfort criteria.

2. The mean wind speed which is exceeded once per year is used to check the pedestrian safety of the location in comparison to accepted pedestrian safety criteria.

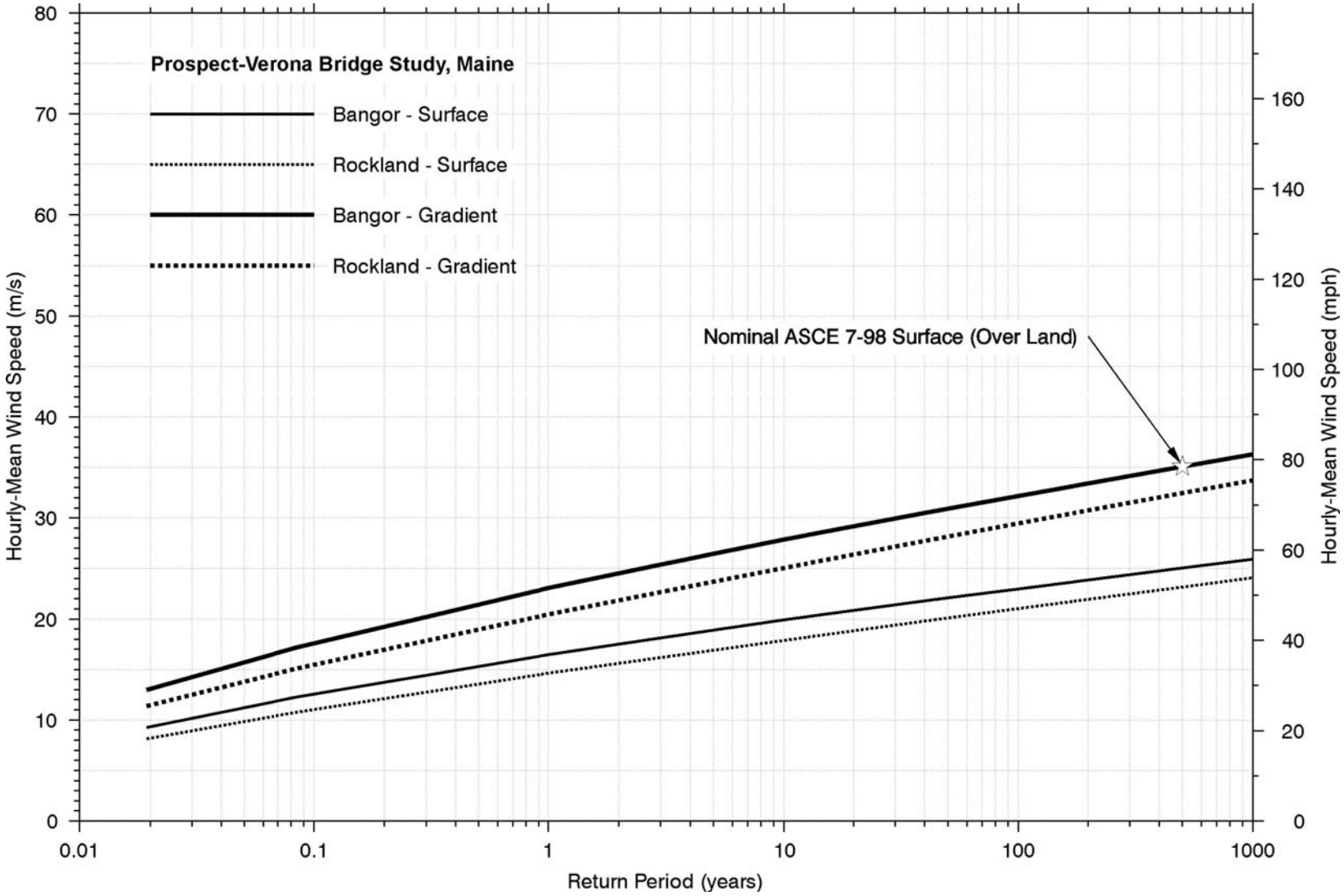

FIGURE 6.1 PREDICTED EXTREME HOURLY MEAN SURFACE WIND SPEEDS FOR VARIOUS RETURN PERIODS, WIND CLIMATE DATA AT BANGOR AND ROCKLAND

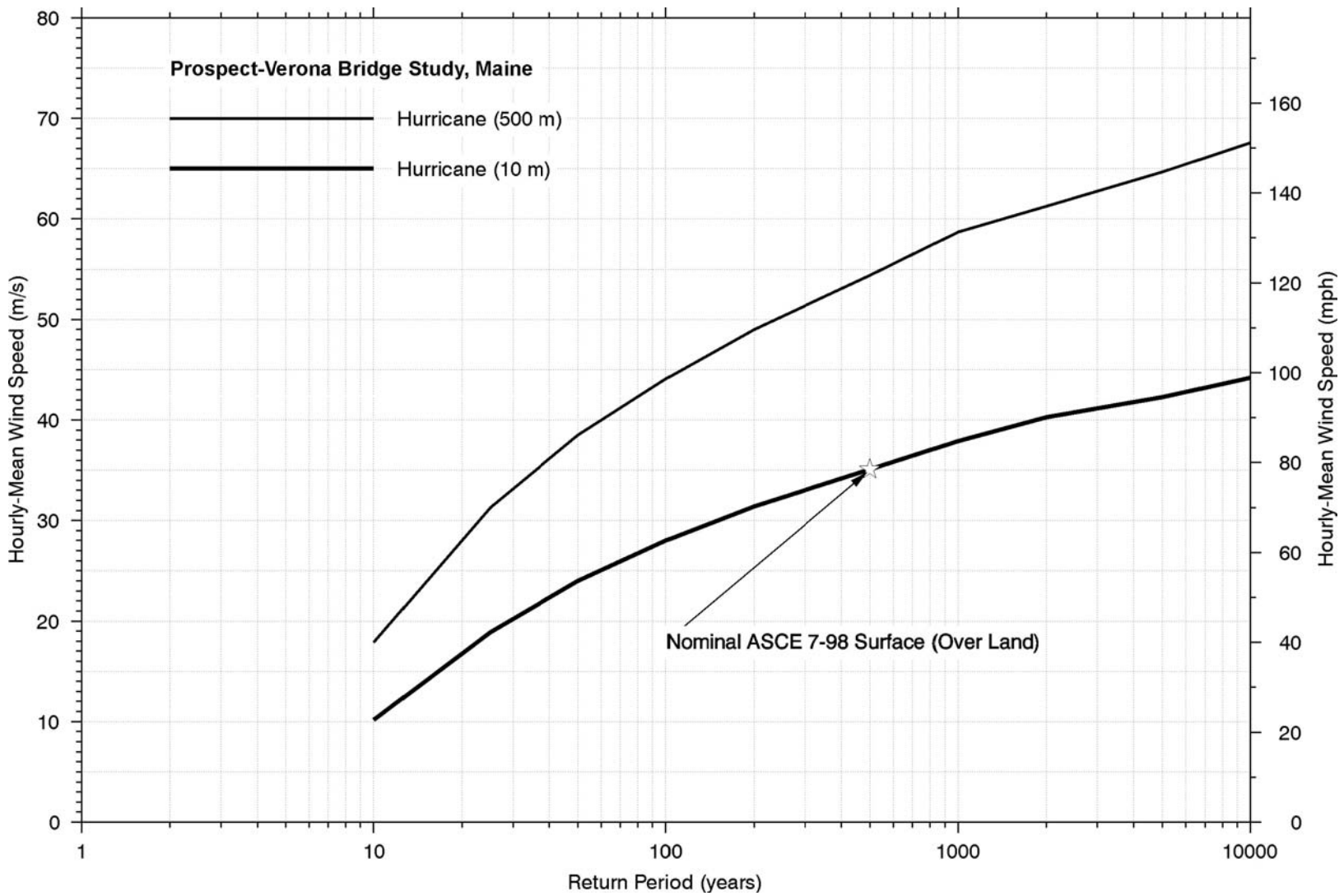

FIGURE 6.2 PREDICTED EXTREME HOURLY MEAN SURFACE WIND SPEEDS FOR VARIOUS RETURN PERIODS, HURRICANE WINDS

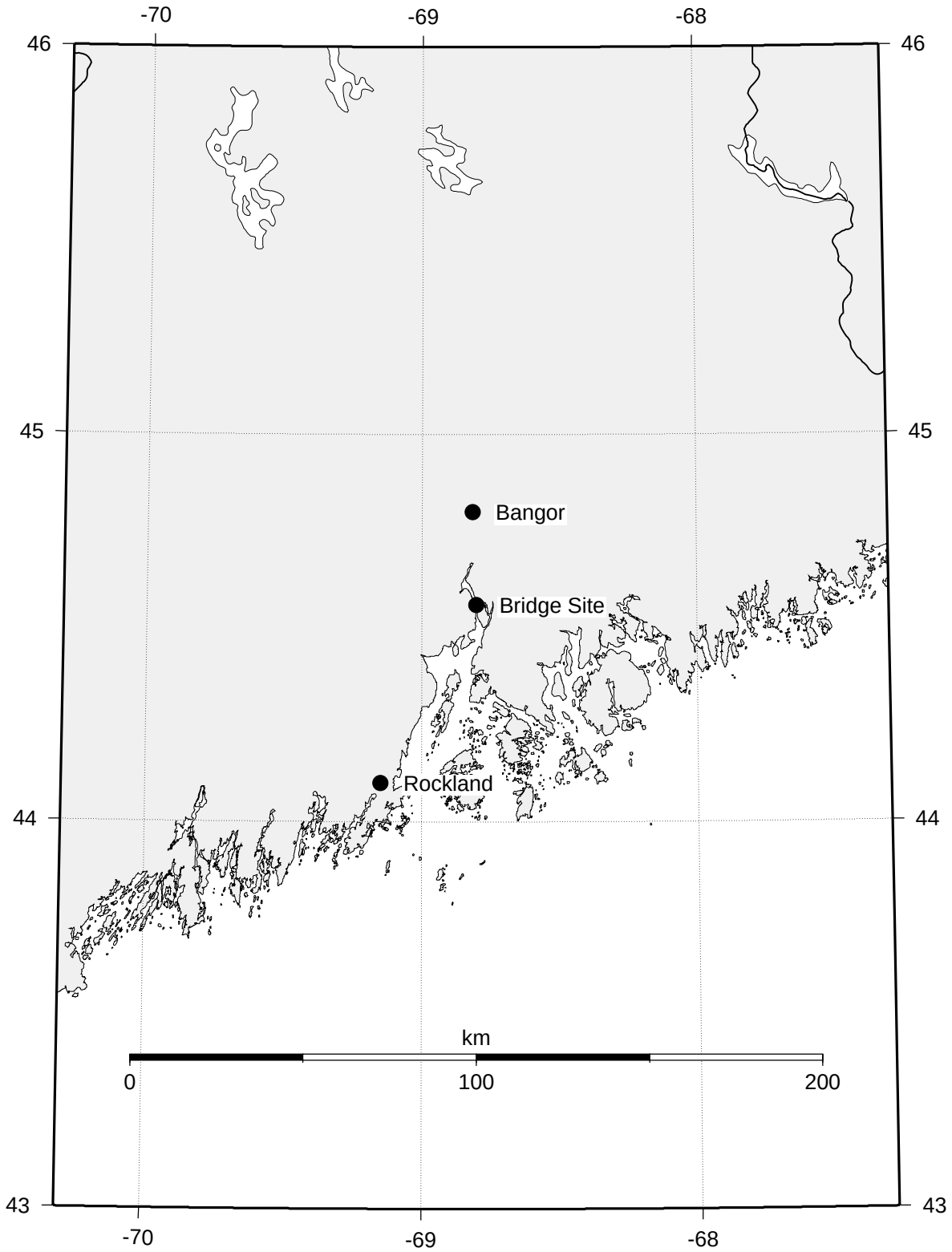

FIGURE 6.3 LOCATION MAP FOR THE PROSPECT-VERONA BRIDGE AND THE PRIMARY WEATHER STATIONS AT ROCKLAND, MAINE AND BANGOR, MAINE

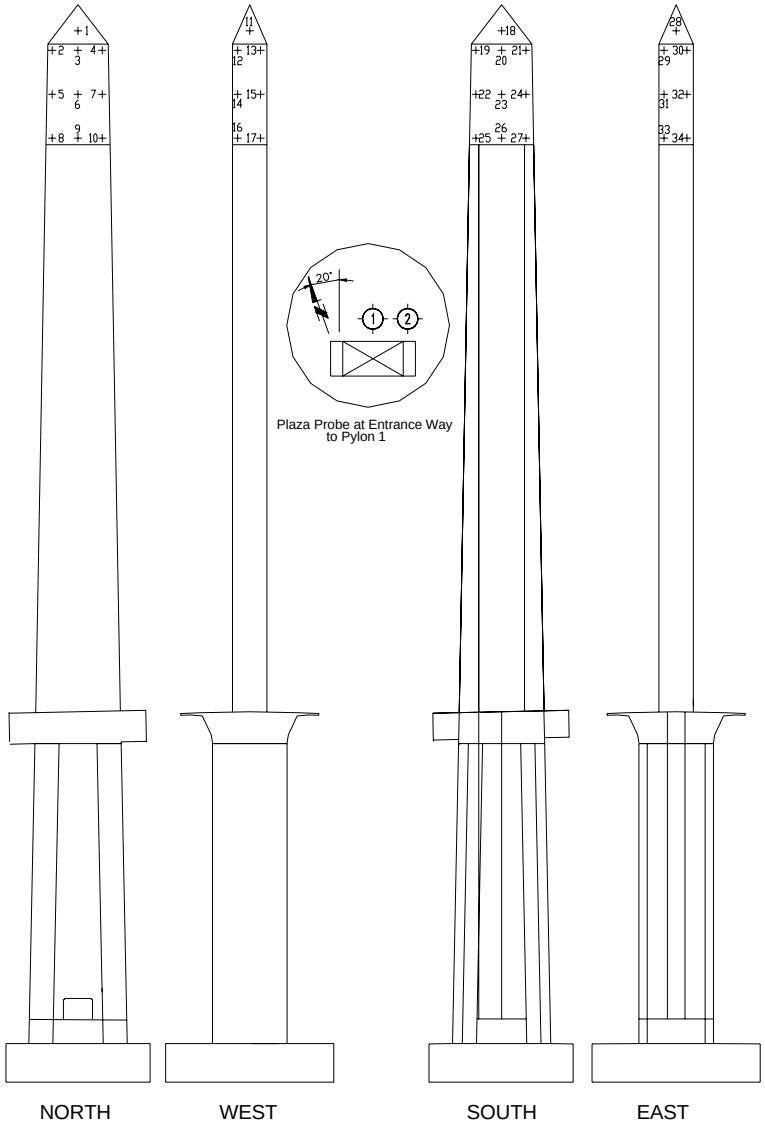

FIGURE 6.4 LOCATIONS OF PRESSURE TAPS AND WIND PROBES

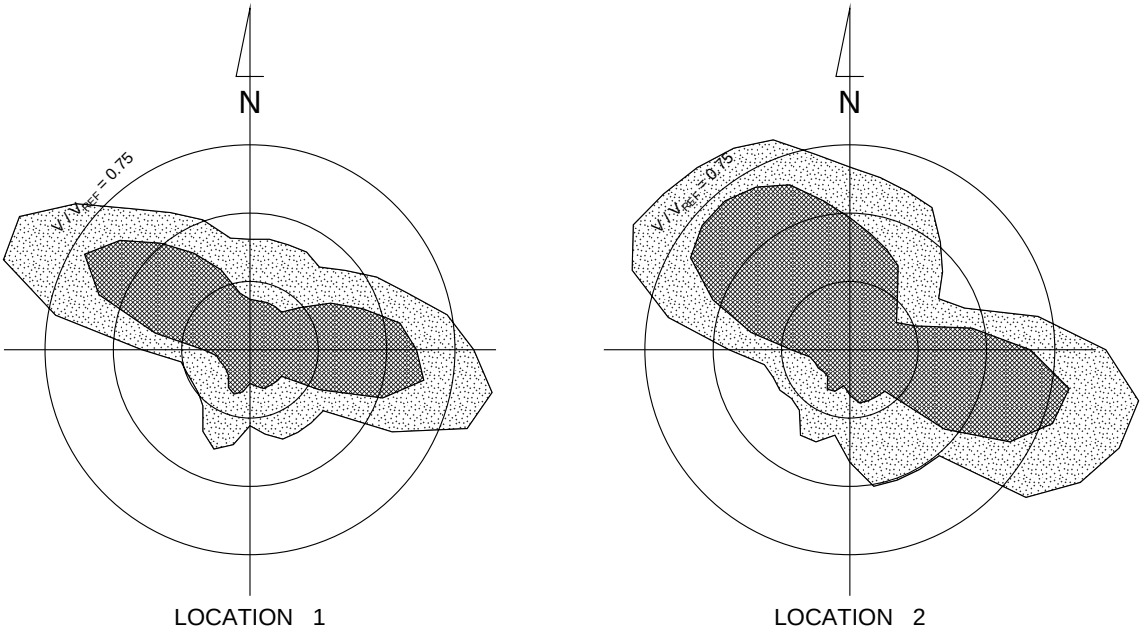

LEGEND: INNER CONTOUR - MEAN
OUTER CONTOUR - FORMED PEAK

Plaza Wind at the Entrance Level to the Prospect Pylon.

File: p025
Dec. 01, 2004

FIGURE 6.5 POLAR PLOTS OF SPEED COEFFICIENTS

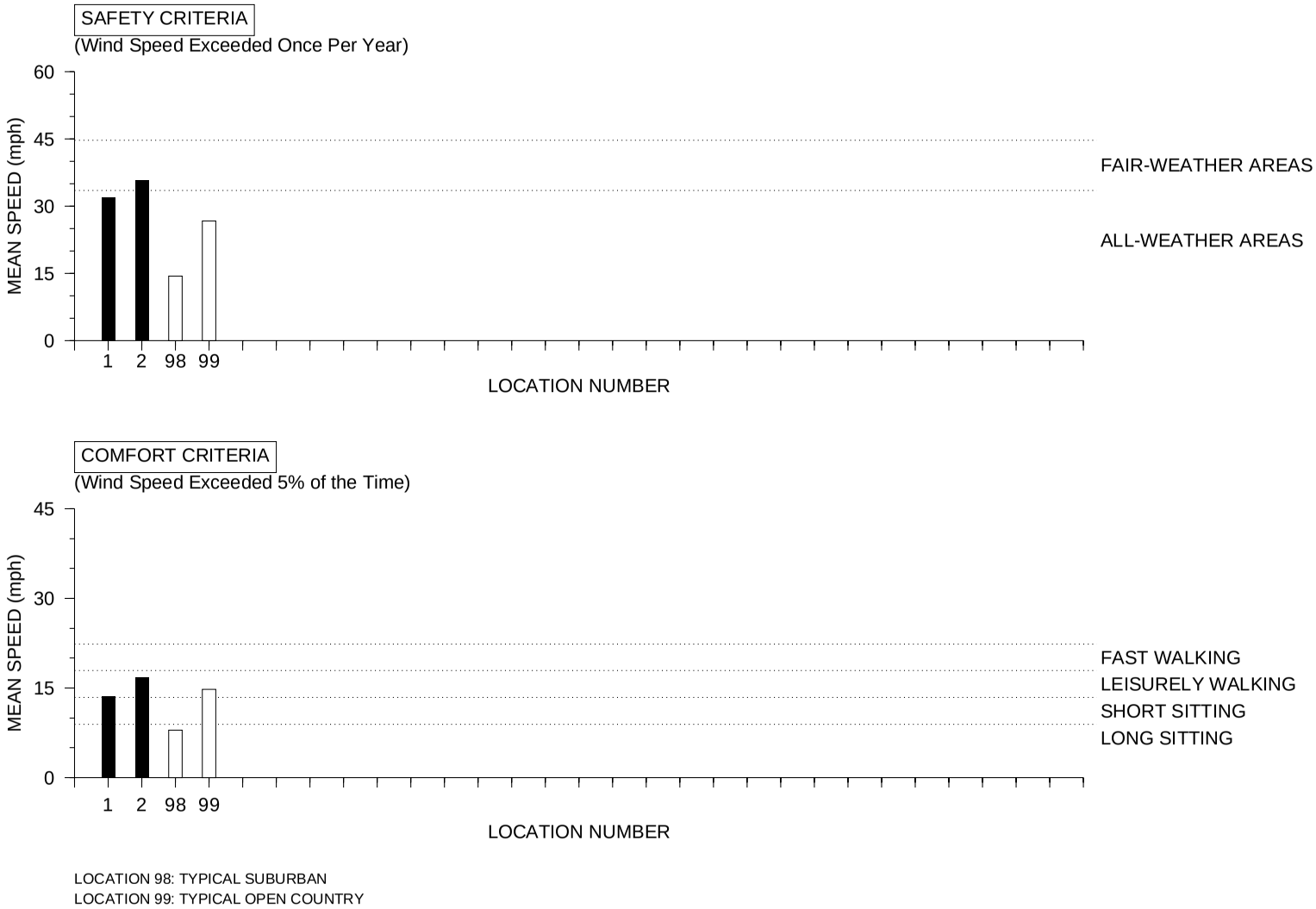

File: p025
Dec. 01, 2004

FIGURE 6.6 PREDICTED MEAN WIND SPEEDS COMPARED WITH CRITERIA FOR PEDESTRIAN COMFORT AND SAFETY

7 FULL AEROELASTIC MODEL STUDY

7.1 General

A full bridge aeroelastic model of the Prospect Verona Bridge was designed and constructed at a geometric scale of 1 to 200 relative to the prototype.. This scale was selected to provide an appropriate simulation of full scale turbulence characteristics, which is important for the development of the aerodynamics of the bridge. The total length of the modeled bridge deck along the bridge span is about 2120 ft in full scale. The approach taken for the full aeroelastic model study has been discussed in [1], and has been used in a variety of long and short span bridge studies.

A detailed topographic model of the local terrain surrounding the project site was constructed for the testing of the aeroelastic model. Stepped elevation contours of 16.6ft (8.3ft close to the pylon entrance) were used in the near-field model for a radius of 1 mile. Additional topography which simulated the general features of the terrain was constructed in order to provide the features important for developing a proper simulation of the flow field upstream of the model. The initial flow was conditioned with appropriate floor roughness to provide either a hurricane exposure or an open country exposure, leading into the topographic model. The wind characteristics generated in the wind tunnel are considered to be a good representation of the wind conditions at the bridge site.

Based on local wind climate information and site terrain condition, four potential critical wind directions were identified and modelled, with wind from the east (along bridge 0°), southeast (30° and 60°), and south (perpendicular to bridge 90°). In addition, a test with wind from the north at 270° was also conducted with the existing bridge upwind to assess its effect on the behavior of the proposed Prospect Verona Bridge.

Tests were performed for the completed bridge and the double cantilever under-construction stage. The behavior of the aeroelastic models was tested under two wind profiles; firstly, a hurricane profile obtained from GPS dropsonde field measurement [22]; secondly, a typical open country exposure. In order to identify any potential vortex shedding induced vibration and flutter instability, an additional “smooth flow” test was carried out with the bridge model elevated above the boundary layer of the wind tunnel floor. The latter tests were only conducted for wind perpendicular to the bridge at 90°. In the test, the bridge model was elevated about 1.5ft off the tunnel floor, resulting in a uniform smooth flow condition with low turbulence intensities of about 1.7% from the deck level to top of the pylon.

Photographs of the bridge model in 90° turbulent boundary layer flow (hurricane profile and open country exposure), as well as in smooth flow are given in Figure 7.1. The existing bridge modeled in the test can be seen upwind of the Prospect Verona Bridge in Figure 7.2. Close-up views of the bridge model are given in Figure 7.3. This figure includes some of the instrumentation set-up and the construction enclosures for the construction stage. Examples of the model in different wind directions tested are shown in Figure 7.4. The location of the proposed bridge and the local terrain surrounding the bridge are shown in Figure 7.5. The definition of the wind directions used in the tests is also sketched in Figure 7.5.

7.2 Dynamic Similarity

A description of the design methodology for full aeroelastic models follows below. The aeroelastic modeling of structures generally requires equality of the following non-dimensional quantities in addition to an overall geometric similarity:

- Froude number (ratio of the gravitational to the inertia forces);
- Cauchy number (ratio of the elastic to inertia forces);
- Density Ratio (ratio of the inertia force of the structure to that of the flow);
- Damping Ratio;

- Reynolds number (based on the dimensions of the structure).

In design of the full bridge aeroelastic model for the Prospect Verona Bridge, it was decided that Froude number scaling ($Fr = gL/V^2$) is preserved. This fact requires tests to be conducted at low wind speeds since the velocity scaling is coupled to the length scale. With the selected length scale of 1:200 for the aeroelastic model, the resulting Froude scaled velocity ratio of 14.14:1 between prototype and model is well suited to the scaling of the turbulent boundary layer in the Low Speed Test Section of BLWTII.

Cauchy number is a non-dimensional parameter which represents the ratio of the elastic forces of the bridge to the inertia forces of the flow ($Ca = E / \rho V^2$). This parameter is preserved in the design of the model.

The density ratio ($\rho_{model} / \rho_{air}$) fixes the mass of the model with respect to the air in the wind tunnel. Since the air density of the prototype is assumed the same as that of the model, the density of the model must be identical to that of the prototype.

The damping ratio ($\delta_{model} / \delta_{prototype}$) is an important quantity to preserve, since it has a direct effect on the resonant motions. In the majority of cases, the damping is approximately that which may be (conservatively) expected to be found in the prototype bridge (i.e. between 0.2 and 1.0% of critical in different modes of vibration). The design of aeroelastic models does not easily allow for the adjustment of the structural damping and in order to identify possible instabilities under the action of wind, the model is designed to have as low a value of structural damping as possible. This also has the effect of providing conservative estimates of the structural responses. The effect of increased damping in the prototype can be estimated through an analytical correction to the test results if required.

Reynolds number similarity ($Re = VL/\nu$) is not practical in most cases and aeroelastic tests are usually carried out at a Reynolds number several orders of magnitude lower than that of full scale. For sharp edged bodies such as bridge decks, the effects of this relaxation of *Re* scaling is not severe for overall wind induced forces and responses. Reynolds number effects can be significant in the modeling of circular objects such as cables. In these instances, the model cable diameter is adjusted to equate to the mean drag wind effects using an equivalent C_dDL approach.

7.3 Description of Model Design

The full aeroelastic model was designed using the scaling parameters listed in Table 7.1. Prototype values of the relevant structural and non-structural elements for the bridge, as provided by the Engineers are given in Table 7.2. The CNC (Computer Numeric Control) and RP-FDM (Rapid Prototyping – Fused Deposition Method) facilities at the University Machine Services were used in the construction of the full aeroelastic model. A complete set of model drawings for the bridge is given in Figure 7.6.

7.3.1 Pylon

The elastic properties of the pylon were modelled by a central "spine" providing the appropriate longitudinal and lateral stiffness of the pylon in the upper part above the deck. The longitudinal, lateral and torsional stiffness in the two pylon legs below the deck were modelled. High strength aluminum sections were machined in a rectangular shape for the upper part of the pylon for the simulation of the two degrees of freedom in the primary bending directions, and in a channel shape for the lower legs to allow for the simulation of the three degrees of freedom; in the two primary bending directions, as well as the torsional direction. A fixed connection was designed to connect the upper rectangular spine and the lower spines. The bases of the pylon legs provided fixed end conditions for the spines.

The pylon modules provide no additional stiffness to the structural spine of the pylon, yet provide the necessary mass and geometric shape for the proper simulation of the aerodynamic forces. The individual pylon modules are separated from each other through a small gap (1/32 inch), which has been shown to be aerodynamically insignificant. The pylon cladding modules were constructed using the RP machine

and ballasted with brass weights to provide the scaled value of mass per unit length of the pylon. The cladding segments were affixed to the spine at the center of each segment.

7.3.2 Deck

The elastic properties of the deck were modeled by a central "spine" providing the appropriate vertical, lateral and torsional stiffness of the deck. A high-strength aluminum structural element was machined in a channel shape to allow for the simulation of the three degrees of freedom in lateral, vertical and torsional directions. The deck spine was fabricated in four sections, with connections at the two pylon locations, as well as a splice plate connection located in the main span at midspan. In this manner, the double cantilever construction stage could be simulated by removal of the splice plate at the midspan, and the leaf springs at both ends of the deck.

The deck cladding modules were fabricated using RP machine technology, reflecting the aerodynamic shape of the deck. The detailed prototype railings were simulated and fabricated in the model using RP machine to provide an equivalent porosity to the prototype. Each module was ballasted with additional brass weights to provide the scaled values of mass and mass moment of inertia per unit length of the structure. The cladding segments were affixed to the spine at the appropriate centre of twist of the deck through the use of a machined aluminium cross beam. The cross beam also provided increased rigidity to the deck and a connection from the cables to the structural spine.

7.3.3 Connections and Bearings

The appropriate bearing conditions at the abutments of the back spans were accomplished in the model by the use of vertically oriented leaf springs allowing longitudinal displacement, however, providing a restraint to vertical motion and deck torsion. Fixed restraints were used between the deck and pylon.

7.3.4 Cables

In consideration of the large number of stay cables in the aeroelastic model, every two neighbouring cables were grouped as one cable in the model. Each pair of stay cables was modeled by 0.017” flexible aircraft cables with additional foam cylindrical cladding to approximate the mean drag force of the prototype cable. The equivalent axial stiffness (AE) of each group of prototype stay cables was provided by extension springs. The drag forces on the cables were well simulated with the combination of the wind drag on the aircraft cable plus that on the foam cladding. The simulation was aimed above an equivalent prototype wind speed at which the prototype cables can be assumed to be in the supercritical Reynolds number region (with an approximate C_d of 0.7). The model cable, if scaled directly via the Length Scale would be in the subcritical region with a C_d of 1.2. The mass per unit length of the cables was not simulated in this approach, as the response of the cables at the extremely small scale of the full aeroelastic model is not representative of full scale behavior.

7.3.5 Construction Enclosure

Temporary construction enclosures at midspan and at both ends of the bridge deck were used in the construction stage. The enclosure was approximately 31 ft high, 77’7” transverse to the bridge and 35’3” in the longitudinal direction. An additional test was performed at 90° wind with a scaled enclosure at each end of the cantilever to give an indication of the effect. The enclosure was simulated as a lightweight rectangular block at the ends of the cantilever – no other construction equipment was modeled.

7.4 Instrumentation

The model deck spine was instrumented with strain gages at four main cross sections. Lift and drag bending moments, as well as deck torque were measured; close to the deck-pylon connection at the mainspan and backspan, at the center of the backspan and near the midspan of the mainspan.

The bridge model was fitted with six non-contacting laser displacement transducers to monitor deck displacements. These transducers were located at the quarter points and at midspan of the mainspan.

Two transducers were oriented in a vertical manner separated by a fixed distance at each cross section. The time history output of these two channels was digitally summed and differenced to provide measures of the deck vertical motion and rotation. A third transducer was placed at each cross section downwind of the model to yield drag displacements. The resolution of the displacement measuring system was 0.002" in model scale (or 0.4" in full scale). This translates into a resolution of the angular motion of approximately 0.06 degrees. All displacements and rotations presented in the plots are well within the resolution of the instrumentation.

Two pair of high sensitivity accelerometers were placed at the middle points of the deck backspan and mainspan (oriented to provide vertical accelerations at the edge of the deck). The time history outputs of these paired accelerometers were summed and differenced to obtain the vertical and rotational accelerations. An additional two accelerometers were located at these locations in the transverse direction to provide a measure of the lateral accelerations.

The pylon model spine was instrumented with strain gages at three sections. The in-plane and out-of-plane bending moments, as well as torque were measured on each leg of the Prospect Pylon near the foundation level. Lateral and longitudinal bending moments were also measured in the pylon spine above the deck level.

A pair of laser transducers was located at the top of the Prospect pylon at the observation deck level. One transducer was mounted in the longitudinal direction and the other in the transverse direction. In addition, two high sensitivity accelerometers were placed at the same level of the pylon to measure the longitudinal and lateral accelerations.

Two hot-film wind probes were installed at the Prospect pylon entrance area to monitor the pedestrian level wind speed in this area.

The wind speed at deck height was monitored throughout the tests and used as the reference wind speed for subsequent analyses of the experimental data. In addition, wind speeds at the pylon height were also recorded during the tests.

In summary, a total number of 43 channels were used in the tests for the Prospect Verona Bridge. An additional 8 channels were formed during the analysis using the recorded time histories. These formed channels included: the vertical displacement and rotation of the deck at midspan and ¼ point of the mainspan, the vertical and rotational accelerations of the deck midspan and the center of the backspan. Details of the instrumentation used and their locations for the completed bridge configuration are summarized in Table 7.3. They are also given schematically in Figure 7.7.

7.5 Wind Simulation

The turbulent boundary layer profile and turbulence characteristics used for the testing of the aeroelastic model were expected to be similar to wind over the terrain approaching the actual bridge site. The 1:200 scale aeroelastic model was tested in two upwind conditions; a hurricane profile for wind from the ocean corresponding to a roughness length, Z_o of about 0.03ft, and an open country exposure from the land with a Z_o of 0.1ft. In addition, the bridge model was also tested in smooth flow with the model elevated about 1.5 ft off the tunnel floor. In the smooth flow set-up, a fairing plate of about 2 ft long was added to the supporting beam of the bridge model in order to ensure smooth wind flow over the model and to inhibit wind-induced vibrations of the model support beam.

Hot-wire measurements of the vertical variation in the mean wind speed and turbulence intensity were made. Figure 7.8 presents the vertical profiles of the mean wind speed and of the intensity of the longitudinal component of turbulence obtained in the tunnel for each of the upstream terrain conditions. The target mean wind speed profiles and turbulence intensities at the bridge site are also plotted for comparison. The mean profile for the open country exposure and the longitudinal turbulence intensities for both exposures are based on ESDU standard profiles [12, 13]. The mean profile for the hurricane exposure an accepted standard and is based on GPS dropsonde field measurements, which is discussed in [22]. Figure 7.8 shows that both the mean profiles and the longitudinal turbulence intensities from the

wind tunnel data compare very well to the target values over the range from the deck height of about 150ft to the pylon height around 450ft.

Five wind angles, 0° (along the deck), 30°, 60°, 90° (perpendicular to deck) and 270° (perpendicular to deck with existing bridge upwind), were selected for the turbulent boundary layer flow tests. The smooth flow test with the bridge model elevated was conducted in 90° wind.

7.6 Wind Speed Measurements

The deck height wind speed used in the analysis and plotting for this project corresponds to a full scale wind speed averaged over a time period of 15 minutes, which is very close to the mean hourly wind speed.

The definition of mean wind speed used in the study is the arithmetic average wind speed over the specified time period and at a specified height above ground level. The international standard (WMO) is at the 10m level for an average time of 10 minutes in an open country terrain condition.

The fastest-mile wind speed is the average wind speed in miles per hour for a 'mile of wind' to pass a particular point. For example, a fastest-mile speed of 60 mph would have an averaging time of 60 seconds (i.e. 3600/60 = 60 seconds), while a 100 mph fastest mile speed would have an averaging time of 36 seconds (i.e. 3600/100 = 36 seconds). The use of the fastest-mile speed was discontinued with the introduction of ASCE 7-95.

The instantaneous gust speed is a wind speed with an averaging time of 1-3 seconds typically. The current ASCE 7-98 [4] uses a 3-second gust.

The relationship between wind speeds with various averaging times, ranging from 1 second and longer is shown in relation to a 1-hour average in the curve by Durst [23] for the open country exposure, as shown in Figure 7.9 from ASCE 7-98. Figure 7.10 also shows this relationship. For other terrain conditions other than the open country exposure, this ratio can be estimated from the following equation,

$$\frac{U_t(Z)}{U_{3600}(Z)} = 1 + c(t) \times I_u$$

where, I_u is the turbulence intensity in the longitudinal direction at the specified height and $C(t)$ takes the values from the following table depending on the time duration.

t	1	10	20	30	50	100	200	300	600	1000	3600
$C(t)$	3.00	2.32	2.00	1.73	1.35	1.02	0.70	0.54	0.36	0.16	0.00

Two exposures were modeled in the test for the Prospect Verona Bridge study; namely, a hurricane and an open country profile. Using the above equation for each exposure (with corresponding turbulence intensities) and height, different factors can be obtained for 3-second gust to mean wind speed ratio.

7.7 Aeroelastic Model Test Procedure

The tests of the full aeroelastic model was comprised of taking measurements and records of time histories of all channels for various responses at each wind speed for a selected range of wind speeds. The responses at approximately 60 to 80 wind speeds were examined in each test. The mean, root-mean-square (RMS), maximum and minimum values of all measured bridge responses were obtained in a subsequent analysis of the time histories. A total of 43 channels, including various bridge deck and pylon responses, wind speeds at deck height and pylon height were recorded for a scaled time period of about 15 minutes at each wind speed.

The responses as presented contain all responses up to 40 Hz in model scale or 2.8 Hz prototype. The peak response was formed from the root-mean-square (RMS) response multiplied by a peak factor. Thus, the total response is equal to the mean, plus or minus the peak. In these plots, the peak response equals to the RMS multiplied by a statistically-based peak factor for random response (i.e. turbulent buffeting) of 3.5. Since the peak factor at the vortex peak location decreases, the use of a constant value of 3.5 for these wind speeds would over-estimate the dynamic response when vortex induced peak occurs. Thus, for the range of wind speeds where the model has shown a large vortex shedding peak, the actual peak factor calculated from the test for the corresponding wind speed was used rather than the random response peak factor of 3.5.

7.8 Response of Completed Bridge and Construction Stage Configurations

7.8.1 General

All tests performed in this study for the completed bridge configuration are summarized in Table 7.4. Table 7.5 lists the tests performed for the double cantilevered construction stage. The test conditions corresponding to each test and the maximum wind speeds tested in each condition are given in the tables. A complete set of response plots for all tests performed for the completed bridge configuration is contained in Appendix G. Results for the under-construction stage are included in Appendix H.

The wind criteria for the proposed Prospect Verona Bridge require that the bridge should not exhibit any flutter instability up to a mean hourly wind speed of 140mph at deck height for the completed bridge configuration, and 100 mph for the construction stage configuration.

7.8.2 Completed Bridge

All tests conducted in this study for the completed bridge configuration reached the target wind speed of 140mph with no flutter instability observed.

Bridge buffeting responses are generally proportional to the turbulence intensity level in the wind. Bridge lateral (drag direction) responses are governed by the longitudinal turbulence intensity, while the vertical (lift direction) and torsional responses are determined by the vertical turbulence intensity. In general, the effect of the upstream exposure alone seems small on some of the bridge deck and pylon responses. This may indicate that the effect of the topographic model (the hills) in the immediate surroundings of the bridge is significant.

The behavior of the completed bridge configuration can be summarized as follows,

- No flutter instability was observed in any of the tests performed up to a full scale wind speed of 140 mph ~ 180 mph at deck height.
- No vortex shedding peaks were observed in the tests of 0° wind for wind along the bridge.
- A wide vortex peak between 40 and 80mph was observed in the response of the backspan mid-point torsional acceleration at 30° wind in the hurricane exposure. Though a similar peak could be also seen in the same response in the test with the open country exposure, the peak became narrower and smaller because of the higher turbulence in the flow.
- Three peaks were observed in the response of the backspan mid-point torsional acceleration at 30mph, 50mph and 90mph at 60° wind. Some of these peaks were observed in other responses in the same test, such as the pylon longitudinal acceleration and the backspan mid-point lift acceleration.
- The smooth flow test at 90° wind showed several very small peaks at various deck responses, however none were of significant magnitude. Two relatively dominant peaks were observed at about 45 and 90mph in the backspan mid-point lift and torsional accelerations in both the hurricane and open country exposures. The peak at 45mph was reduced with higher turbulence in the open country exposure, while the magnitude of the peak at 90mph was

unaffected. It is suspected that the hills upwind on the Prospect Pylon side may have played a significant role in creating these vortex peaks through a funnelling of the wind flow.

- Spectral analysis was performed on the responses for the 90° wind tests in smooth flow and the two upstream exposures. The small, but noticeable peak in smooth flow at about 30mph, corresponds to a single dominant frequency of 46Hz (a full scale frequency of 3.25Hz). In addition, the peak at 45mph in both hurricane and open country exposures relates to a dominant frequency of 15Hz (a full scale frequency of 1.06Hz), while the peak at 90mph corresponds to its harmonics of 30Hz (a full scale frequency of 2.12Hz).

- There were no significant vortex peaks observed in any of the responses with the existing bridge upwind at 270°.

- As shown in the response plots, buffeting responses in the open country exposure are generally higher than the responses in the hurricane profile (smoother and less turbulent).

7.8.3 Bridge Under Construction

All tests conducted with the double cantilever under-construction stage also reached the target wind speed of 100 mph with no occurrence of flutter instability.

The effect of the construction enclosures were studied in some of the tests for the construction stage. Two tests were conducted at 90° wind in the hurricane exposure with and without the construction enclosures. In addition, the tests at 270° wind (with the existing bridge upwind) included the construction enclosures in both hurricane and open country exposures.

The behavior of the bridge while under construction can be summarized as follows,

- No flutter instability was observed in any of the tests performed up to a full scale wind speed of 100 mph at deck height.

- No vortex shedding peaks were observed in the tests of 0° wind (along the bridge).

- No significant vortex peaks were seen in the tests of 30° wind other than a small peak shown at about 25mph in the backspan mid-point torque and the pylon longitudinal acceleration in both exposures.

- The smooth flow test at 90° wind showed two vortex peaks at about 35mph and 45mph in the mainspan lift moment at pylon. Both peaks were still visible in the test with the hurricane exposure at 90° wind. Though the peak at 35mph was still shown in the response in the rougher open country exposure, the peak at 45mph was eliminated. In addition, the vortex peak at 35mph was also observed at the 60° wind in both exposures.

- Spectral analysis was performed for the 90° wind tests in smooth flow and the two upstream exposures. The peak at 35mph corresponds to a dominant frequency of 38Hz (a full scale frequency of 2.69Hz), while the peak at 45mph relates to a dominant frequency of 13Hz (a full scale frequency of 0.92Hz).

- The effect of the presence of the construction enclosures was examined for the 90° wind. The vortex peak at about 35mph was somewhat reduced with the construction enclosures. Otherwise, the effect of the construction enclosures on the various deck and pylon responses is small.

- The effect of the existing bridge upwind of the model at 270° was seen to have a beneficial effect on the bridge responses through the introduction of turbulence, with no vortex peak observed in any of the responses in the test.

7.9 Pylon Accelerations at Observation Level

The pylon lateral and longitudinal accelerations were measured at the top of the observation level in the bridge aeroelastic test. The top of the observatory level sits about 435 ft above the base. The result could be used to assess the occupant comfort. The criterion used here is discussed in [24], which suggests an acceptability of structural motion of 20~25 milli-g.

The lateral and longitudinal pylon accelerations were studied for each individual test. Results showed that the worst case came from wind at 30° to the bridge, in which both the pylon lateral and longitudinal accelerations became larger than 20 milli-g when the mean hourly wind speed ate deck height reached 23 mph. Table 7.6 lists the pylon accelerations at 30° wind as well as the criterion., The table also shows the values of acceleration for wind perpendicular to the bridge at 90° for purposes of comparison.

Pylon responses are directly related to the pylon damping values. In order to estimate the effect of increased damping on the pylon accelerations further analysis was performed. The lateral damping in the pylon was found to be 0.55% and the longitudinal damping was 0.20%. It was considered that these numbers are low compared to the values that may be present in the full scale concrete pylon, which may be of the order of 1.0% of critical. The response of the pylon lateral and longitudinal accelerations were then fit to a V^2 relation and the response spectra was examined to identify the frequencies associated with vortex peaks.

Figures 7.11 and 7.12 show the pylon accelerations at different damping values for the 30° wind and 90° wind respectively. In the plots, the responses from the tests are marked with symbols, while the fitted data are plotted in solid curves. The fitted curves can be regarded as pure turbulent buffeting response with no vortex shedding peaks. A structural damping value of 1.0% of critical was used for the lateral response, while both 0.5% and 1.0% were used for the longitudinal response. The criterion of 20 milli-g is also plotted in the figures. The pylon lateral response is seen to be pure turbulent buffeting response for the 90° wind, thus the fitted curve can be used directly. With a 1% damping, the figure shows that the critical wind speed is over 50mph with the pylon response reaching the 20 milli-g. A small vortex peak was observed between 35mph and 55mph in the longitudinal response in 90° wind. Spectral analysis shows that this peak is associated with a single dominant frequency of 25.9Hz in model scale, corresponding to a full scale frequency of about 1.8Hz, which likely corresponds to the 5th vertical deck mode. Normally, with a single dominant frequency in the spectrum, the vortex peak magnitude will be inversely proportional to the structural damping. In this case, the pylon response peak is significantly reduced and then the response is characteristic of turbulent buffeting. The response then can be approximated in the figure by the red squares for a structural damping of 0.5% and blue triangles for 1.0%. The critical wind speed is also seen to reach over 50 mph with a structural damping of 1%.

The pylon longitudinal response at 30° wind also shows a critical wind speed over 50 mph at 1.0% damping. The pylon lateral response at 30° wind showed a small peak between 30 mph and 40 mph which was not reduced below the 20 milli-g with an increase in the damping to 1%. The critical wind speed is seen to be about 28mph. In order to reach a critical wind speed of 50mph, additional measures, such as the use of a tuned mass damper system, may be required to reduce the pylon response to acceptable levels.

7.10 Pedestrian Level Wind at Prospect Pylon Entrance

Two wind probes were also installed at the same locations as those used in the pylon pressure test, one at the Prospect Pylon entrance and the other at the northeast corner. Figure 7.13 shows the wind probe locations.

The measurement of wind speeds at these two probe locations were carried out for the wind angles examined in the full bridge aeroelastic test. Wind speed ratios were calculated. This parameter was defined as the ratio of the wind speed measured at the probe location to the wind speed measured at an upper level in the wind tunnel where the effect of the tunnel floor and the turbulence generating devices becomes negligible. A linear fit of the test data was performed and the slope of the fitted line is the wind

speed ratio. This practice is similar to the analysis in the pedestrian level wind study in Section 6, thus a direct comparison of the wind speed ratio could be made for each wind angle.

Table 7.7 presents the comparison of the wind speed ratios obtained in the tests performed for the full aeroelastic model (tested in topographic conditions) and the pylon pressure model test (performed in standard boundary layer flow). The observed wind speeds ratios were smaller for the aeroelastic test with the topographic model for location 1 at the Prospect Pylon entrance. This was also true for four of the five angles for location 2 at the pylon northeast corner. However, the 30° wind results in higher ratios in the aeroelastic test with the topographic model. The wind speed ratio (shown in Figure 6.4) varies significantly from a true azimuth of 110° to 140° (corresponding to aeroelastic model wind angles of 0° and 30° respectively) without the topographic model. Therefore, the upstream hills at 30° wind in the aeroelastic test could have an effect of redirecting and funnelling the wind to an angle that is critical to location 2, resulting in a large wind speed ratio. As discussed in Section 6, the pylon will likely be closed to the public in severe weather conditions so the windiness of Location 2 may not be a critical issue. Location 2 meets the safety criteria for fair weather.

TABLE 7.1 AEROELASTIC SCALING PARAMETERS (FROUDE SCALED)

Parameter	Similitude Requirement	Value
Length*	$\lambda_L = L_m / L_P$	5.00E-03
Density	$\lambda_\rho = \rho_m / \rho_P$	1
Velocity**	$\lambda_V = V_m / V_P$	7.07E-02
Mass per Unit Length	$\lambda_m = \lambda_\rho \lambda_L^2$	2.50E-05
Mass	$\lambda_M = \lambda_\rho \lambda_L^3$	1.25E-07
Mass Moment of Inertia per Unit Length	$\lambda_i = \lambda_m \lambda_L^2$	6.25E-10
Mass Moment of Inertia	$\lambda_I = \lambda_M \lambda_L^2$	3.13E-12
Time	$\lambda_T = T_m / T_P = \lambda_L / \lambda_V$	7.07E-02
Damping	$\lambda_\xi = \xi_m / \xi_P$	1
Elastic Stiffness	$\lambda_{EI} = \lambda_{GC} = \lambda_V^2 \lambda_L^4$	3.13E-12
	$\lambda_{EA} = \lambda_V^2 \lambda_L^2$	1.25E-07
Force per Unit Length	$\lambda_f = \lambda_V^2 \lambda_L = \lambda_L^3 / \lambda_T^2$	2.50E-05
Force	$\lambda_F = F_m / F_P = \lambda_V^2 \lambda_L^2$	1.25E-07
Bending and Torsional Moment	$\lambda_{BM} = \lambda_V^2 \lambda_L^3$	6.25E-10
Warping Stiffness	$\lambda_{CwE} = \lambda_V^2 \lambda_L^6$	7.81E-17

*Length Scale = 1:200

**Velocity Scale = 1:14.14

$^{**}\lambda_V = \lambda_T = \sqrt{\lambda_L}$

(Froude Scaling)

TABLE 7.2 PARAMETERS FOR DESIGN OF THE AEROELASTIC MODEL

	Parameter		Prototype Value Used in Model Design	Scaled Target Value for Model
Deck Main Span	Moment of Inertia - Vertical	I_x	2595 ft^4	7.42×10^{-5} in^4
	Moment of Inertia - Lateral	I_y	26232 ft^4	7.51×10^{-4} in^4
	Torsional Constant	C	5760 ft^4	1.78×10^{-4} in^4
	Mass per unit length	m	25.1 kips/ft	0.052 lb/in
	Mass Moment of Inertia per unit length	I_θ	6101 kip-ft²/ft	0.046 lb-in²/in
	Elastic Modulus	E_d	Concrete: 4.42×10^6 lb/in²	Aluminum: 1.00×10^7 lb/in²
	Shear Modulus	E_d	Concrete: 1.84×10^6 lb/in²	Aluminum: 3.85×10^6 lb/in²
Deck Back Span	Moment of Inertia - Vertical	I_x	3960 ft^4	1.13×10^{-4} in^4
	Moment of Inertia - Lateral	I_y	34328 ft^4	9.82×10^{-4} in^4
	Torsional Constant	C	9425 ft^4	2.92×10^{-4} in^4
	Mass per unit length	m	37.5 kips/ft	0.078 lb/in
	Mass Moment of Inertia per unit length	I_θ	7991 kip-ft²/ft	0.06 lb-in²/in
Lower Pylon Leg (values per leg)	Moment of Inertia – Lateral	I_x	420 ft^4	1.20×10^{-5} in^4
	Moment of Inertia - Longitudinal	I_y	7108 ft^4	2.03×10^{-4} in^4
	Torsional Constant	C	739 ft^4	2.29×10^{-5} in^4
	Mass per unit length	m	28.2 ~ 29.2 kips/ft	0.06 lb/in
	Mass Moment of Inertia per unit length	I_θ	1272 ~ 1319 kip-ft²/ft	
Upper Pylon	Moment of Inertia – Lateral	I_x	5326 ~ 8021 ft^4	3.66×10^{-4} ~ 1.37×10^{-3} in^4
	Moment of Inertia - Longitudinal	I_y	12802 ~ 48028 ft^4	1.52×10^{-4} ~ 2.29×10^{-4} in^4
	Torsional Constant	C	9606 ~ 26816 ft^4	
	Mass per unit length	m	31.2 ~ 55.0 kips/ft	0.064 ~ 0.109 lb/in
	Mass Moment of Inertia per unit length	I_θ	2719 ~ 8438 kip-ft²/ft	
Cables	Area	A	11.3 ~ 20.1 in²	a spring with a stiffness 11.34 to 4.07 lb/in
	Length	L	118.4 ~ 587.2 ft	
	Elastic Modulus – cable	E_c	2.8×10^7 lb/in^2	
	Stiffness – cable	K_c	2.05×10^5 to 9.11×10^4 lb/in per cable	

TABLE 7.3 INSTRUMENTATION LOCATIONS, PROSPECT VERONA BRIDGE

Instrumentation **x – longitudinal, y – lateral (Drag), z – vertical (Lift)**	**Instrumentation Locations**
Strain Gages:	
M_x, M_y and M_z at Prospect Pylon Leg A (marked A)	Lateral and Longitudinal Bending Moments, as well as Torque at 25ft from Pylon Footing
M_x, M_y and M_z at Prospect Pylon Leg B (marked B)	Lateral and Longitudinal Bending Moments, as well as Torque at 25ft from Pylon Footing
M_x, M_y and M_z at Back Span Mid-Point (marked C)	Lift and Drag Moments, as well as Torque at 230ft from Pylon Centerline
M_x, M_y and M_z at Back Span Deck close to Pylon (marked D)	Lift and Drag Moments, as well as Torque at 28ft from Pylon Centerline
M_x, M_y and M_z at Main Span Deck close to Pylon (marked E)	Lift and Drag Moments, as well as Torque at 25ft from Pylon Centerline
M_x and M_y at Prospect Pylon above Deck (marked F)	Lateral and Longitudinal bending Moments at 23ft above Deck Surface
M_x, M_y and M_z at Main Span Mid-Point (marked H)	Lift and Drag Moments, as well as Torque at 23ft from Midspan
Accelerometers:	
y, z and θ accel. at Main Span Mid-Point (marked H)	Lift, Drag and Torsional Accelerations at 25ft from Main Span Mid-Point to the Prospect Side
y, z and θ accel. at Back Span Mid-Point (marked C)	Lift, Drag and Torsional Accelerations at 255ft from Abutment 1
y and z accel. at Top of Prospect Pylon (marked I)	Lateral and Longitudinal Accelerations at the observation deck level (435ft from Pylon footing)
Displacements:	
y, z and θ displacements at Main Span Mid-Point (marked H)	Lift and Drag Displacements, as well as Deck Rotation at 25ft from Midspan to the Prospect Side
y, z and θ displacements at Main Span 1/4 point (marked G)	Lift and Drag Displacements, as well as Deck Rotation at 310ft from Midspan to the Prospect Side
y and z displacements at Top of Prospect Pylon (marked I)	Lateral and Longitudinal Displacements at the observation deck level (435ft from Pylon footing)
Wind Speeds:	
Plaza Probes at Prospect Pylon Entrance Way (marked 1 & 2)	Pedestrian Level
Deck Level	Deck Height
Pylon Top	Pylon Height

Note: Instrumentation used in the tests of the completed bridge and the construction stage are identical.

TABLE 7.4 SUMMARY OF FULL BRIDGE AEROELASTIC MODEL TESTS, COMPLETED BRIDGE CONFIGURATION

Test File	Test No.	Flow condition	Existing bridge	Wind direction (Test angle)	V_{deck} (mph) Maximum wind speed at deck height
VS9201	1	Hurricane profile	No	Perpendicular to bridge (90°)	158
VS0201	2	Hurricane profile	No	Along the Bridge (0°)	143
VS3201	3	Hurricane profile	No	30° to the bridge	140
VS6201	4	Hurricane profile	No	60° to the bridge	142
VS2201	5	Hurricane profile	Yes	Perpendicular to bridge (270°)	150
VS6301	6	Open Country profile	No	60° to the bridge	163
VS3301	7	Open Country profile	No	30° to the bridge	155
VS0301	8	Open Country profile	No	Along the Bridge (0°)	161
VS9301	9	Open Country profile	No	Perpendicular to bridge (90°)	169
VS2301	10	Open Country profile	Yes	Perpendicular to bridge (270°)	183
VS9101	11	Smooth Flow	No	Perpendicular to bridge (90°)	147

TABLE 7.5 SUMMARY OF FULL BRIDGE AEROELASTIC MODEL TESTS, CONSTRUCTION STGE

Test File	Test No.	Flow condition	Existing bridge	Construction Box at Cantilever Ends	Wind direction (Test angle)	V_{deck} (mph) Maximum wind speed at deck height
VC9201	1	Hurricane profile	No	Yes	Perpendicular to bridge (90°)	103
VC9202	2	Hurricane profile	No	No	Perpendicular to bridge (90°)	103
VC0201	3	Hurricane profile	No	No	Along the Bridge (0°)	99
VC3201	4	Hurricane profile	No	No	30° to the bridge	100
VC6201	5	Hurricane profile	No	No	60° to the bridge	99
VC2201	6	Hurricane profile	Yes	Yes	Perpendicular to bridge (270°)	99
VC6301	7	Open Country profile	No	No	60° to the bridge	101
VC3301	8	Open Country profile	No	No	30° to the bridge	106
VC0301	9	Open Country profile	No	No	Along the Bridge (0°)	111
VC9301	10	Open Country profile	No	No	Perpendicular to bridge (90°)	105
VC2301	11	Open Country profile	Yes	Yes	Perpendicular to bridge (270°)	127
VC9101	12	Smooth Flow	No	No	Perpendicular to bridge (90°)	122

TABLE 7.6 SUMMARY OF WIND SPEED (mph) FOR PYLON ACCELERATIONS WITHIN 20 milli-g, AND COMPARISON TO CRITERIA

Test File	Flow condition	Existing bridge	Wind direction (Test angle)	Wind Speed (mph) for Pylon Lateral Motion below 20 milli-g	Wind Speed (mph) for Pylon Longitudinal Motion below 20 milli-g
VS9201	Hurricane profile	No	90° (Perpendicular to bridge)	41	33 (due to vortex shedding)
VS9301	Open Country profile			37	31 (due to vortex shedding)
VS3201	Hurricane profile		30°	24	24
VS3301	Open Country profile			23	23

Criteria for acceptability of building motions (Isyumov, N. “Motion Perception, Tolerance and Mitigation”, 5th World Congress of the Council on Tall Buildings and Urban Habitat, Amsterdam, The Netherlands, May 1995):

	Criteria for acceptability of structure motions
Office building, observation towers	20-25 milli-g

* Note: Building accelerations generally become perceivable at about 3~5 milli-g by 10% of the population. However at this level the building motion may not cause discomfort.

TABLE 7.7 COMPARISON OF WIND SPEED RATIOS IN PYLON PRESSURE TEST AND FULL BRIDGE AEROELASTIC TEST FOR THE TWO WIND PROBES MEASURED AT THE PROSPECT PYLON ENTRANCE FOR FIVE WIND ANGLES

True Azimuth	Wind Angles Defined in Aeroelastic Test	Speed Ratio in Pressure Test		Speed Ratio in Aeroelastic Test	
		Probe at Entrance	Probe at Corner	Probe at Entrance	Probe at Corner
degree	degree	V / Vg	V / Vg	V / Vg	V / Vg
20	270 (perpendicular to bridge, with existing bridge upwind)	0.183	0.391	0.124	0.328
110	0 (along bridge)	0.518	0.789	0.293	0.409
140	30	0.151	0.198	0.110	0.514
170	60	0.137	0.198	0.114	0.163
200	90 (perpendicular to bridge)	0.173	0.162	0.163	0.143

(A) HURRICANE EXPOSURE

(B) OPEN COUNTRY EXPOSURE

FIGURE 7.1 PHOTOGRAPHS OF THE AEROELASTIC MODEL IN THE WIND TUNNEL SHOWING THE UPSTREAM TERRAIN MODELS (EXPOSURES) USED

(C) SMOOTH FLOW WITH BRIDGE MODEL ELEVATED

FIGURE 7.1 (CONT.) PHOTOGRAPHS OF THE AEROELASTIC MODEL IN THE WIND TUNNEL SHOWING THE UPSTREAM TERRAIN MODELS (EXPOSURES) USED

(A) WITH EXISTING BRIDGE, 270° WIND

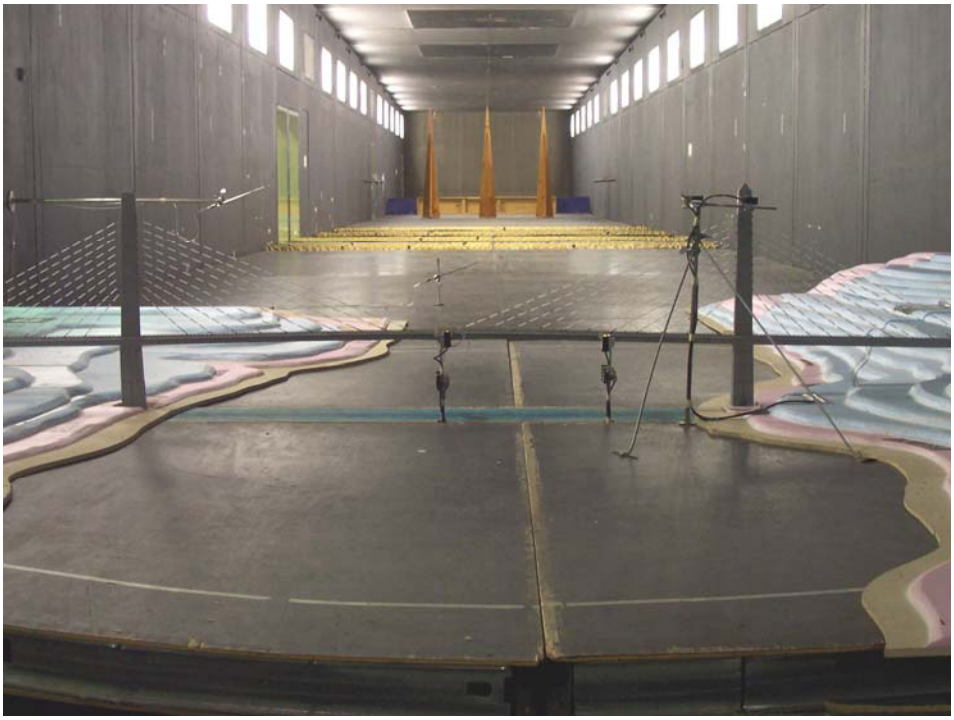

(B) WITHOUT EXISTING BRIDGE, 90° WIND

FIGURE 7.2 PHOTOGRAPHS OF THE AEROELASTIC MODEL IN THE WIND TUNNEL, WITH AND WITHOUT THE EXISTING BRIDGE

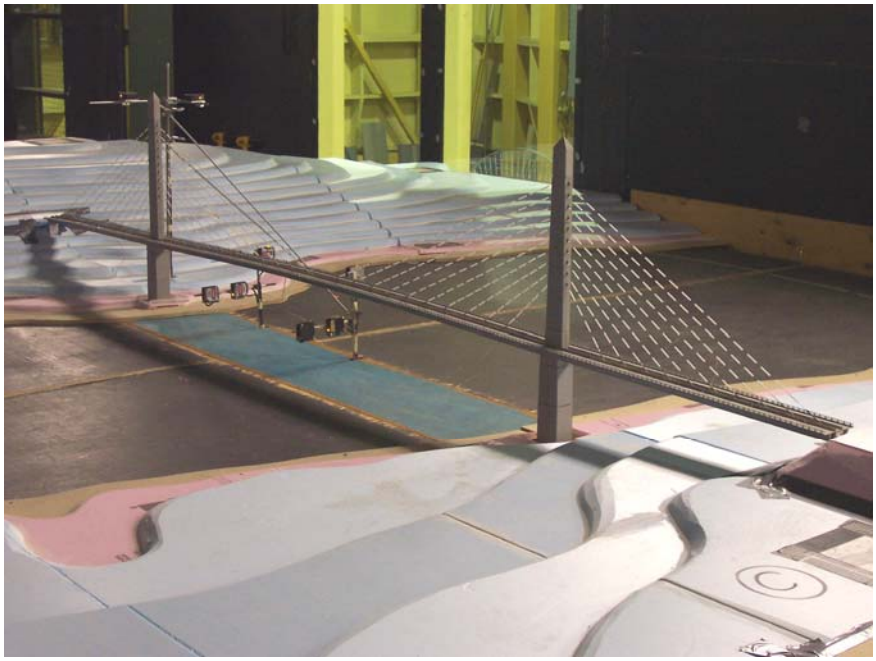

FIGURE 7.3 CLOSE-UP VIEWS OF THE AEROELASTIC MODEL, PROXIMITY MODEL AND INSTRUMENTATION

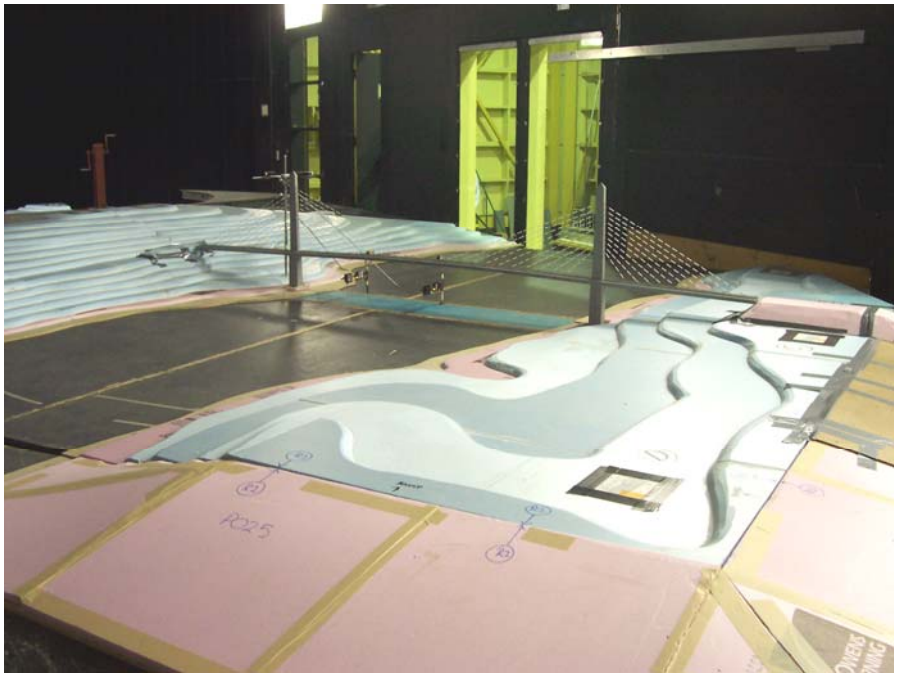

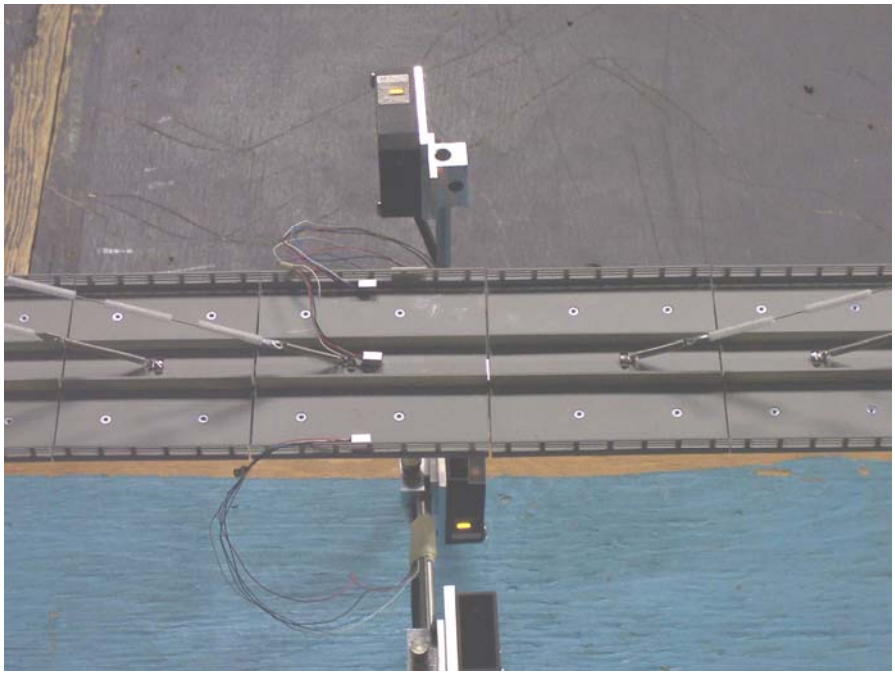

FIGURE 7.3 (CONT.) CLOSE-UP VIEWS OF THE AEROELASTIC MODEL, PROXIMITY MODEL AND INSTRUMENTATION

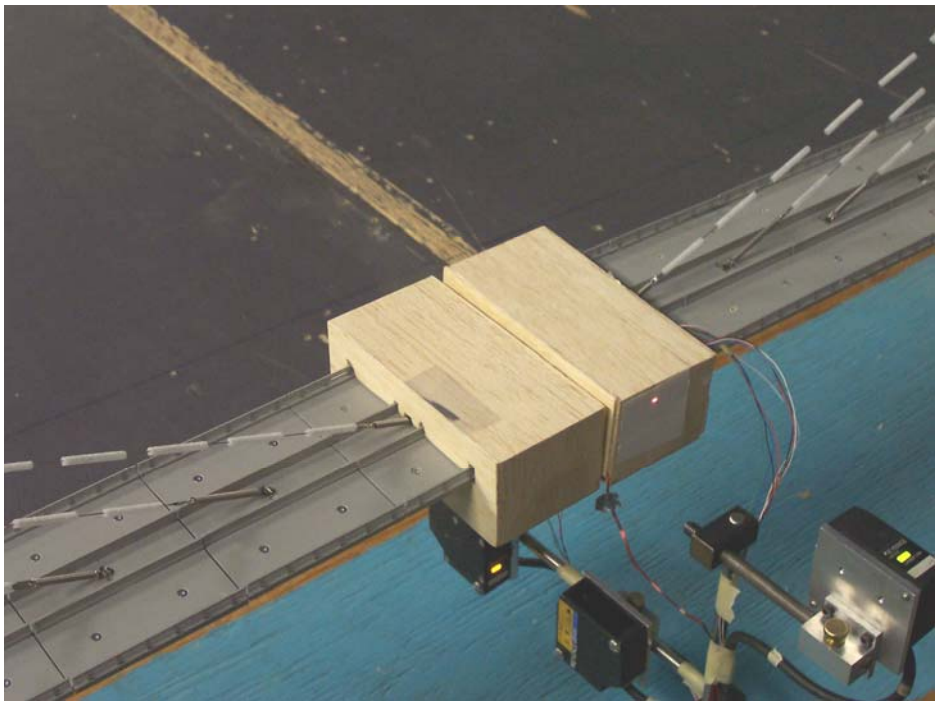

(A) CONSTRUCTION ENCLOSURE AT DECK MIDSPAN

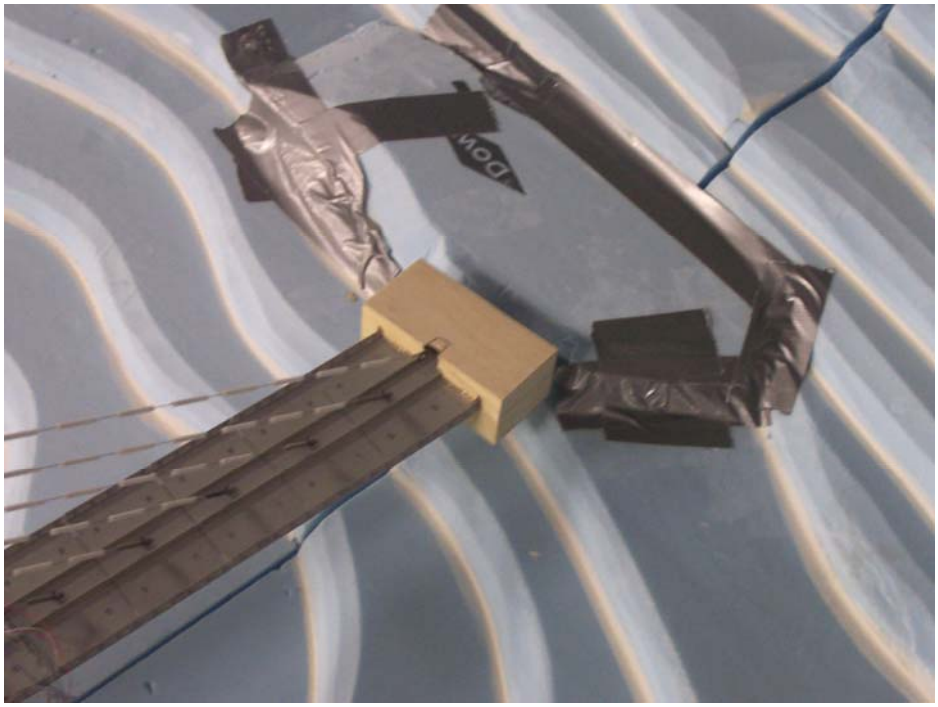

(B) CONSTRUCTION ENCLOSURE AT END OF DECK

FIGURE 7.3 (CONT.) CLOSE-UP VIEWS OF THE AEROELASTIC MODEL, PROXIMITY MODEL AND INSTRUMENTATION

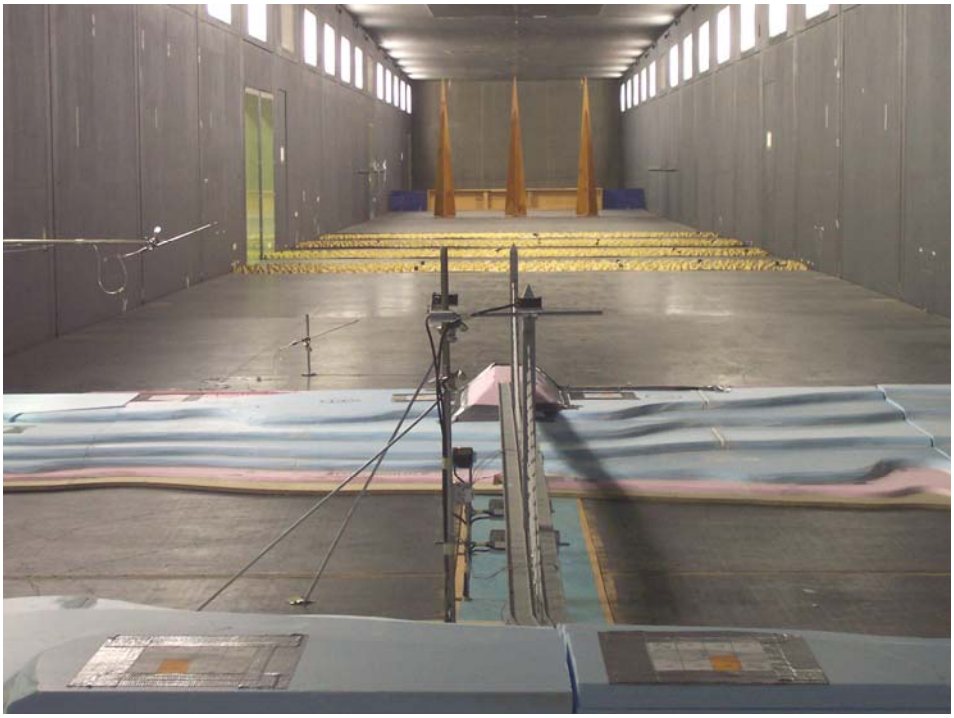

(A) 0° WIND

(B) 30° WIND

FIGURE 7.4 PHOTOGRAPHS OF THE AEROELASTIC MODEL AT DIFFERENT WIND ANGLES

(C) 60° WIND

(D) 90° WIND

FIGURE 7.4 (CONT.) PHOTOGRAPHS THE AEROELASTIC MODEL AT DIFFERENT WIND ANGLES

(C) 270° WIND

(D) 90° WIND, CONSTRUCTION STAGE WITH ENCLOSURES

FIGURE 7.4 (CONT.) PHOTOGRAPHS THE AEROELASTIC MODEL AT DIFFERENT WIND ANGLES

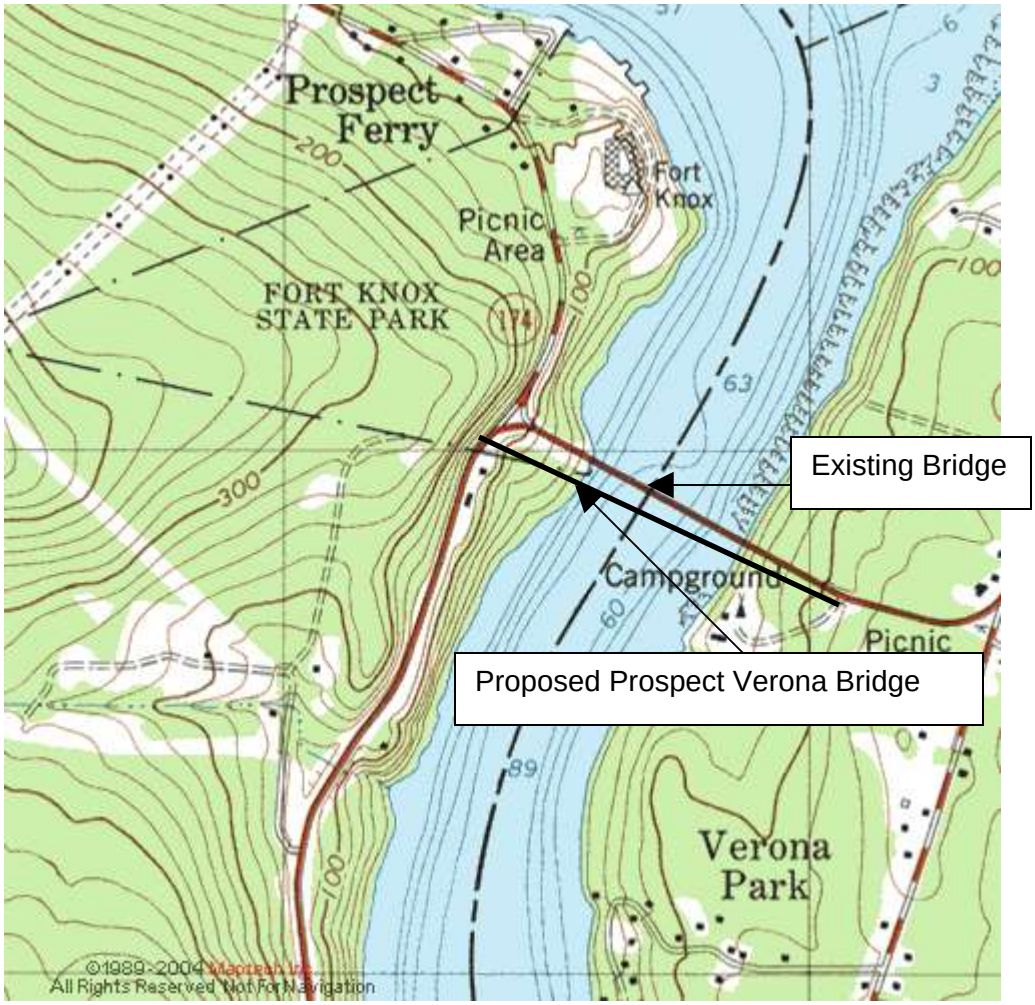

FIGURE 7.5 (A) LOCATION OF THE PROPOSED PROSPECT VERONA BRIDGE AND THE SURROUNDING TERRAIN

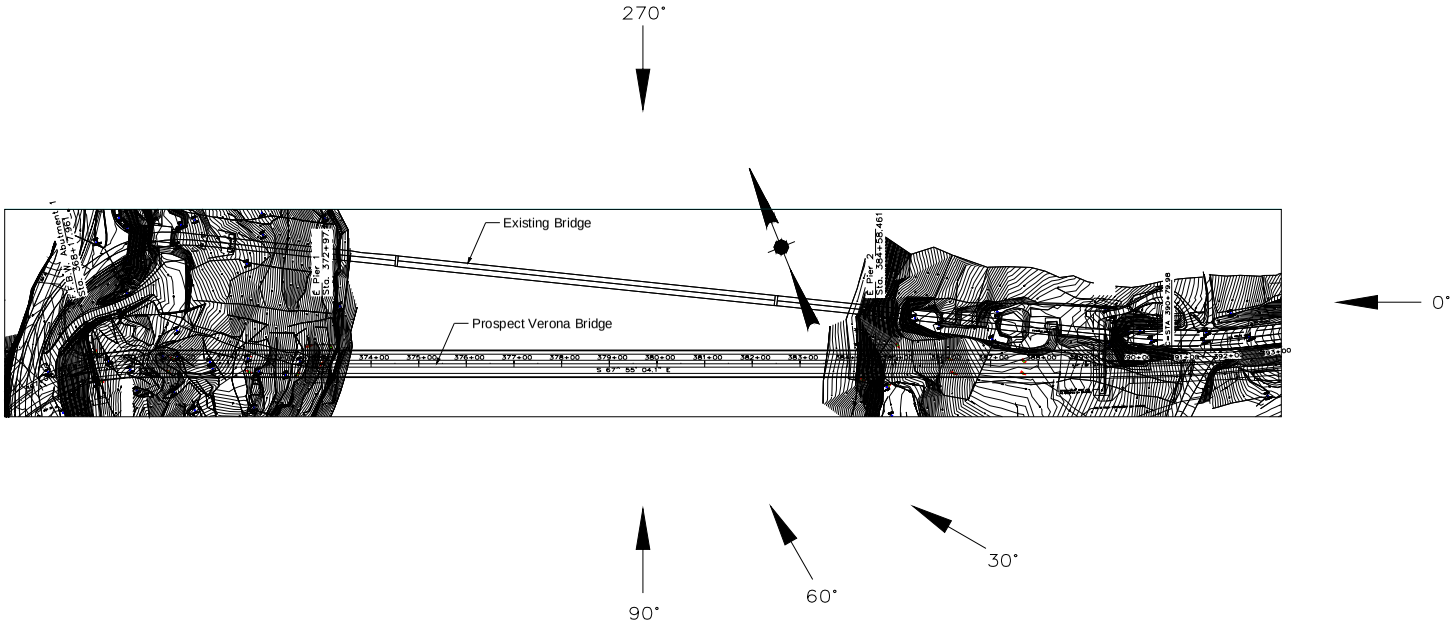

WIND DIRECTION DEFINITION

FIGURE 7.5 (B) LOCATION OF EXISTING BRIDGE AND WIND DIRECTIONS TESTED

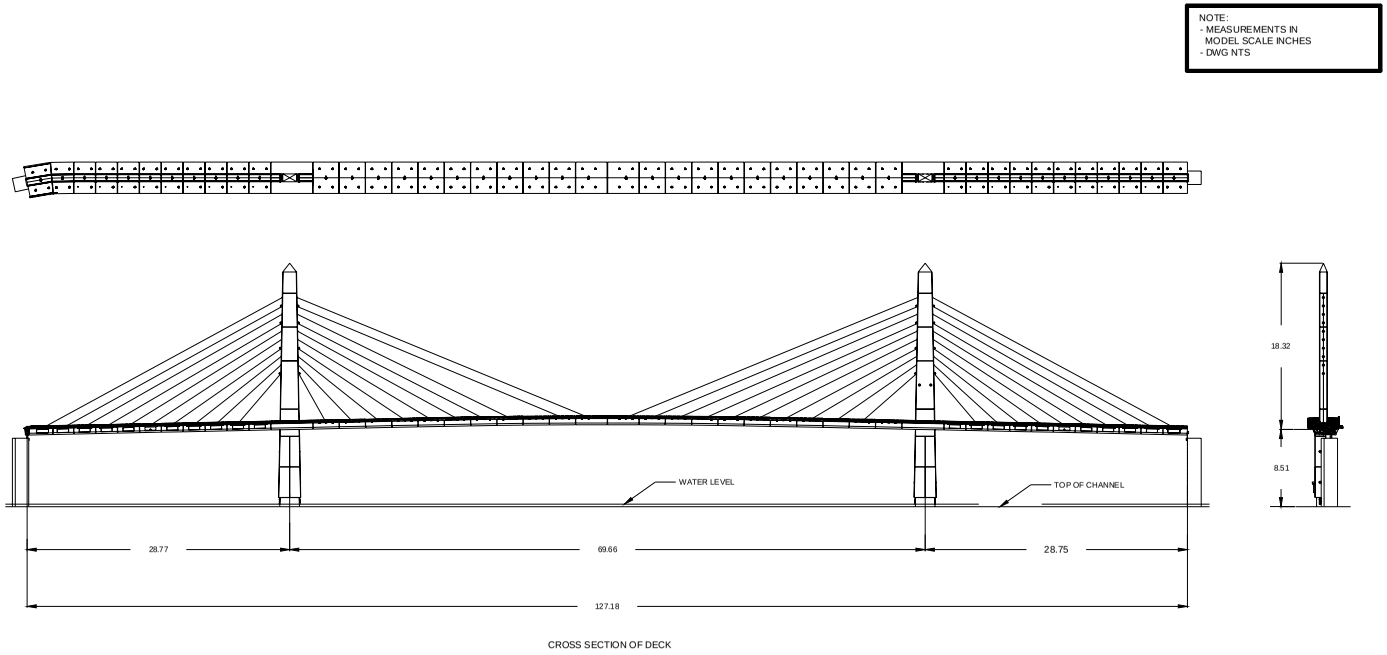

FIGURE 7.6 THE 1:200 SCALE AEROELASTIC MODEL

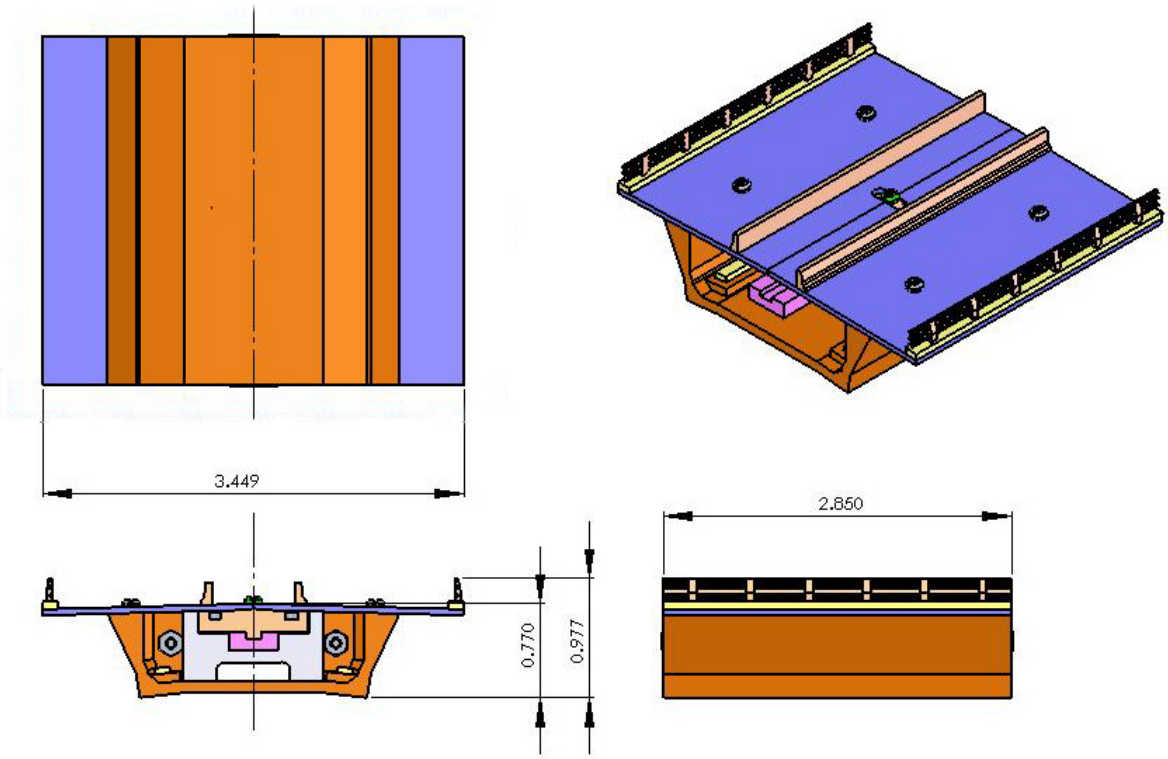

FIGURE 7.6 (CONT.) THE 1:200 SCALE AEROELASTIC MODEL

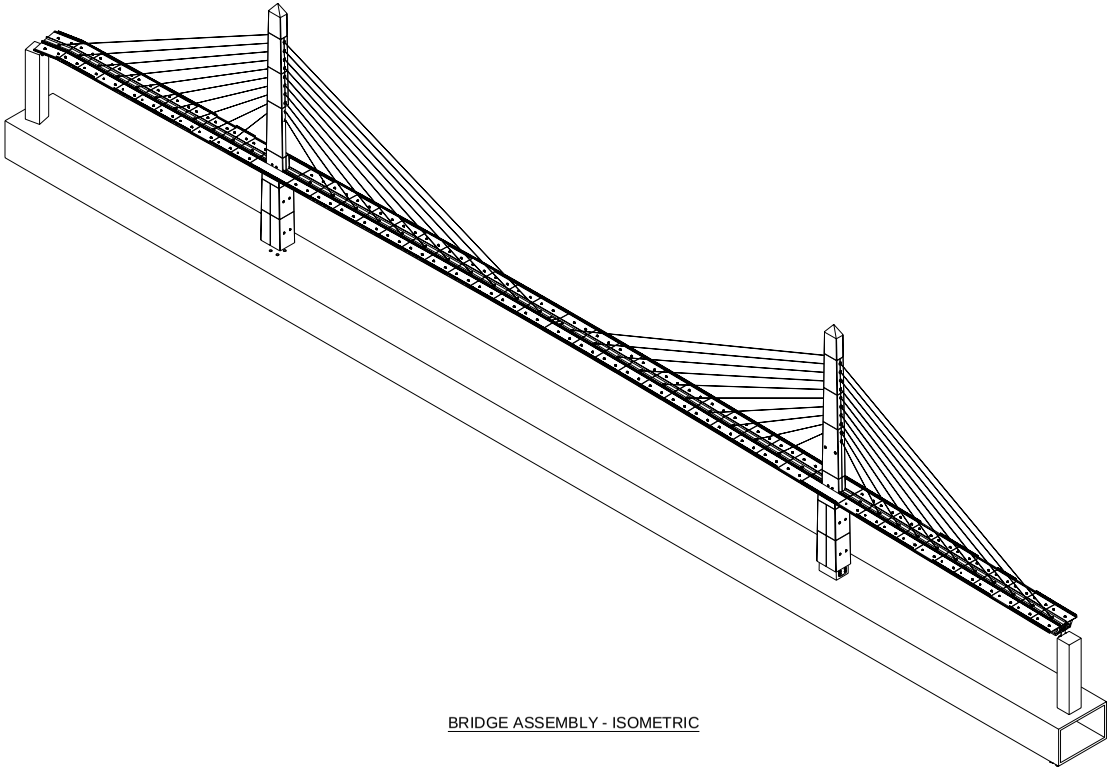

FIGURE 7.6 (Cont.) THE 1:200 SCALE AEROELASTIC MODEL

NOTE:
- MEASUREMENTS IN MODEL SCALE INCHES
- DWG NTS

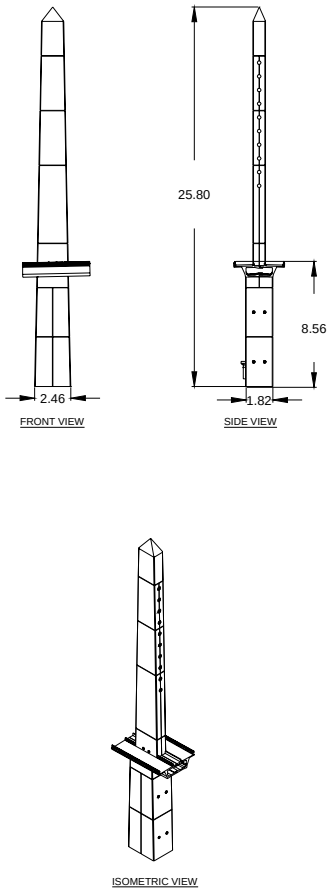

FIGURE 7.6 (CONT.) THE 1:200 SCALE AEROELASTIC MODEL

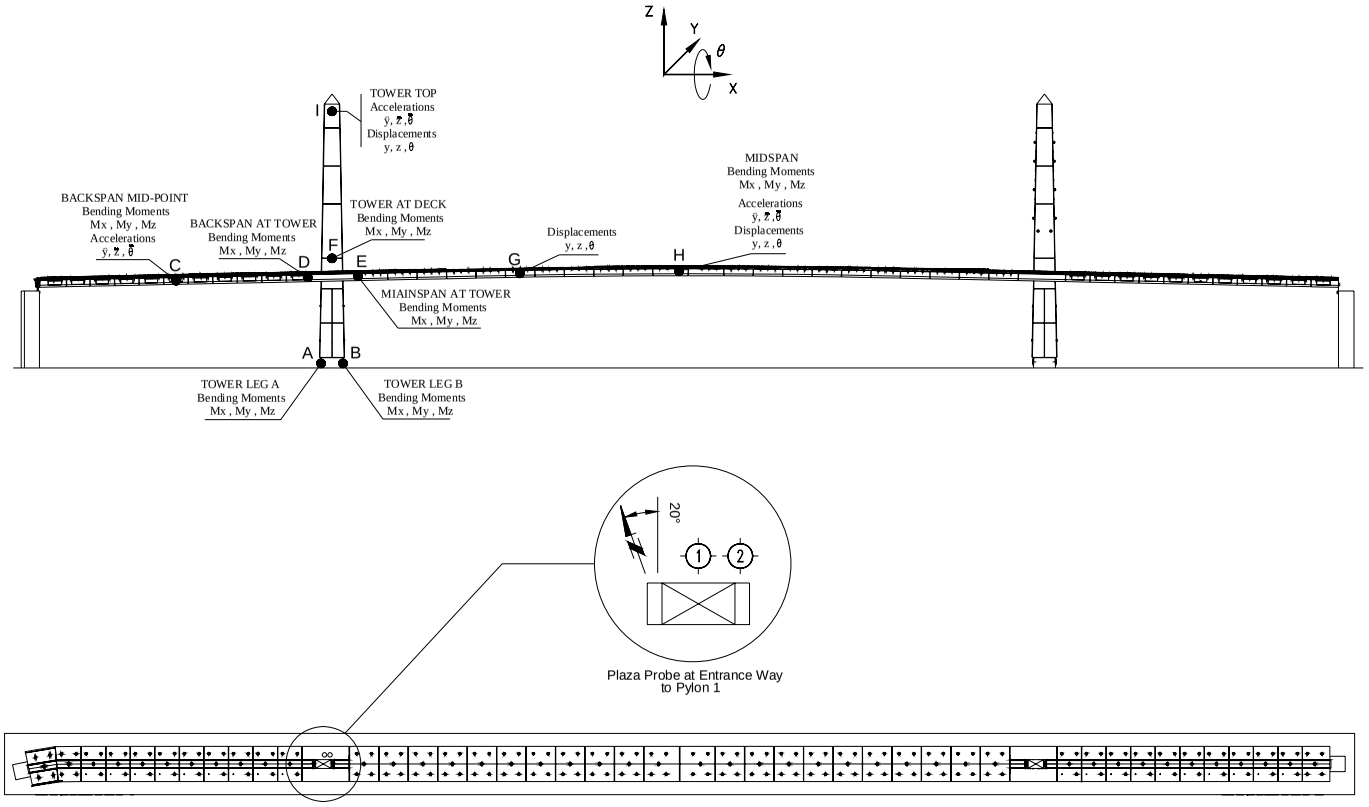

(Cables removed in drawing)

FIGURE 7.7 INSTRUMENTATION LOCATIONS AND SIGN CONVENTION, COMPLETED BRIDGE (CABLES REMOVED IN THIS FIGURE)

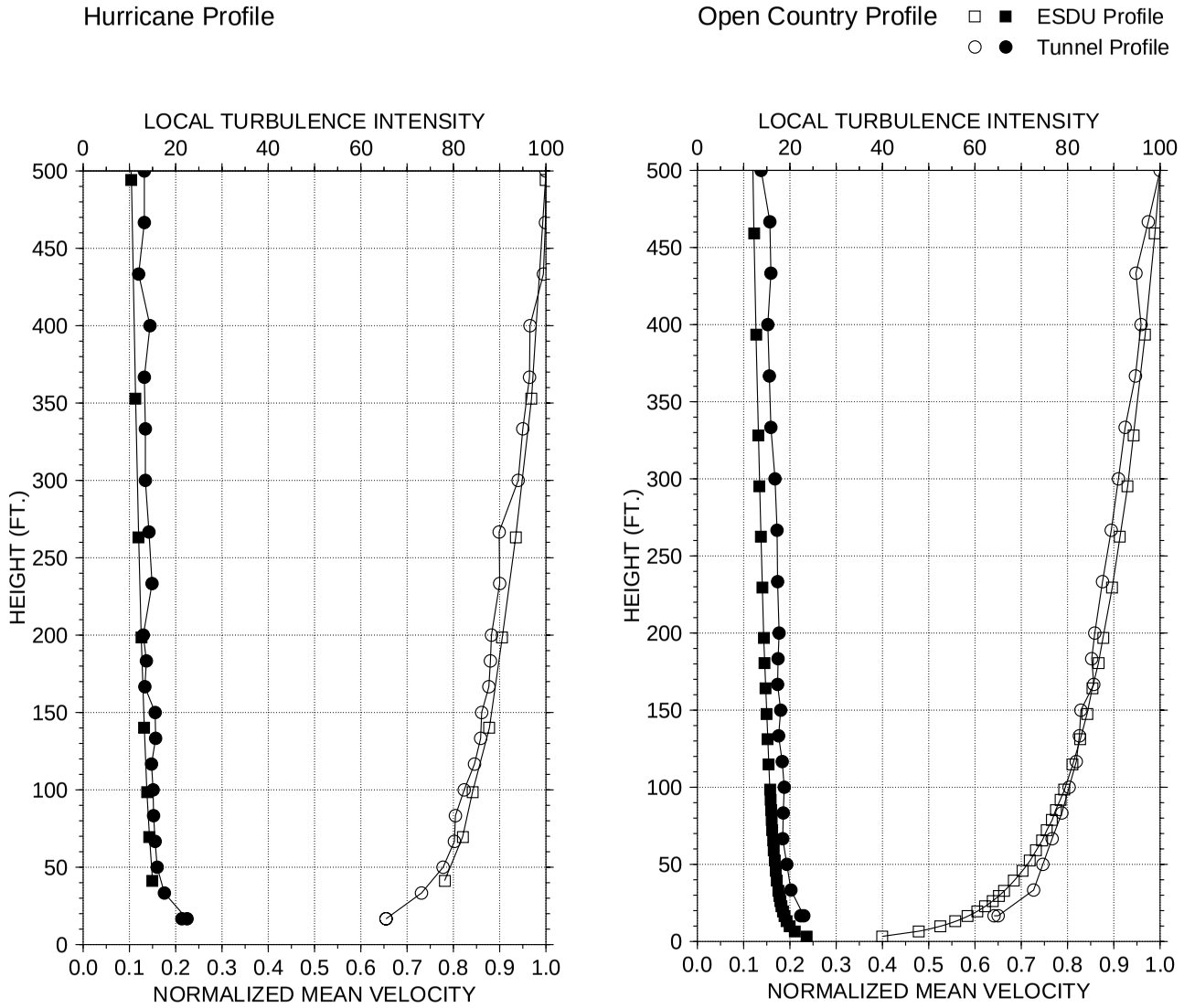

FIGURE 7.8 WIND PROFILES USED IN THE FULL BRIDGE MODEL TESTS, HURRICANE AND OPEN COUNTRY EXPOSURES

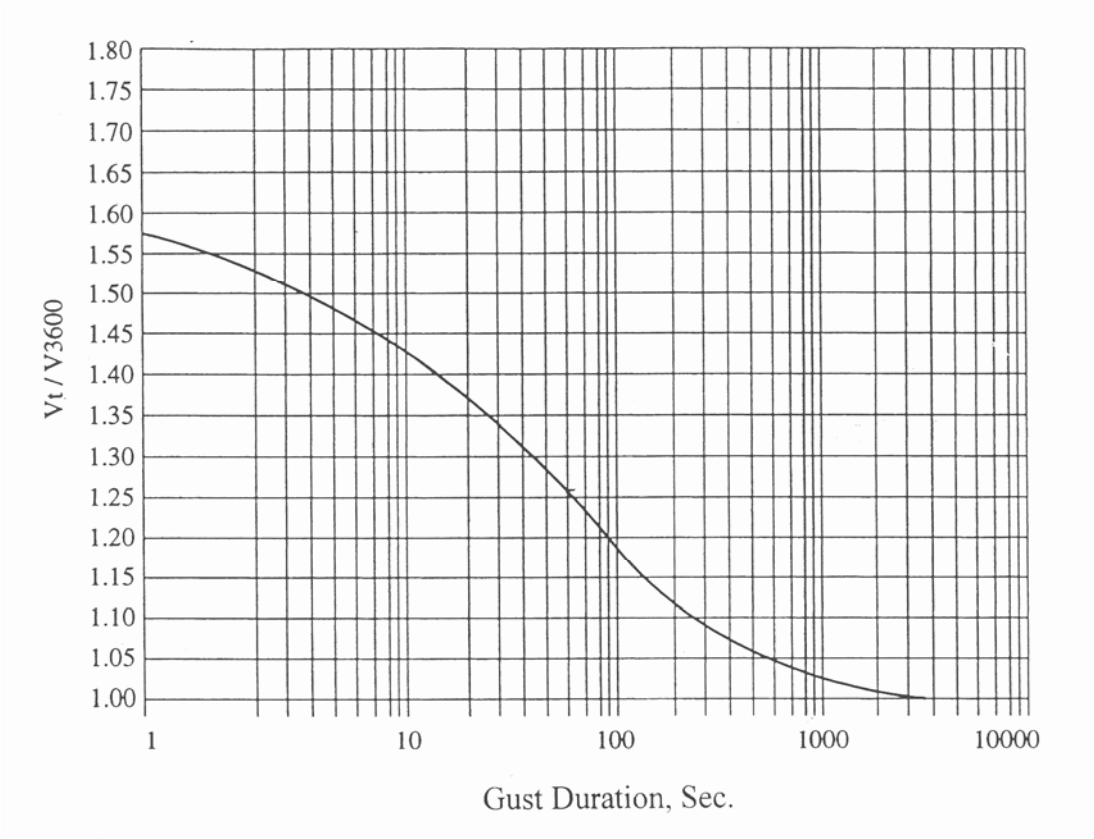

FIGURE 7.9 RATIO OF PROBABLE MAXIMUM SPEED AVERAGED OVER t SECONDS TO HOURLY MEAN SPEED

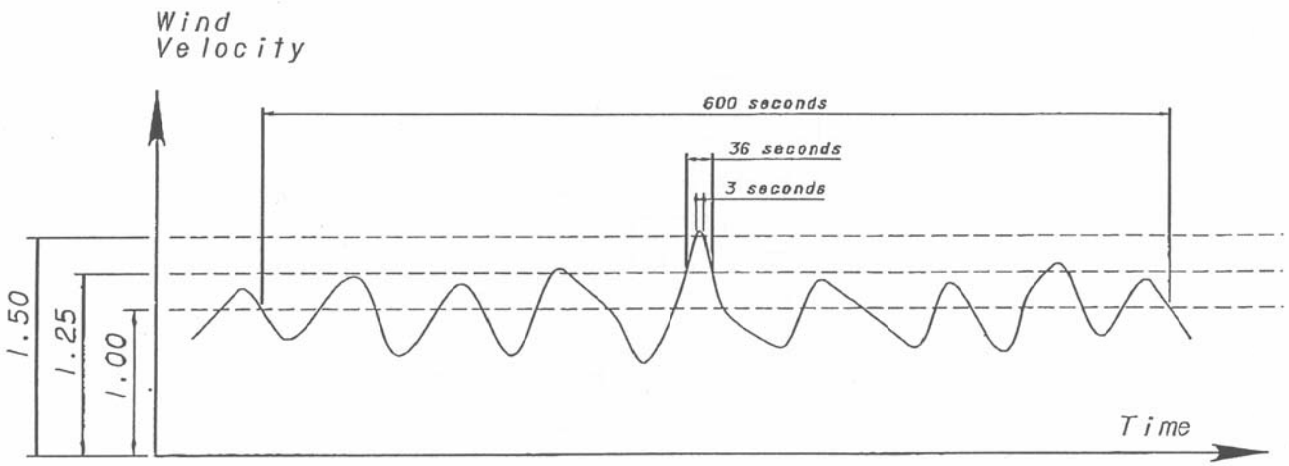

Mean Wind Speed = 10 minute (600 seconds) average

Fastest Mile = 36 seconds (AASHTO 100 mph definition)

Instantaneous Speed = peak 3 second speed

FIGURE 7.10 DEFINITION OF WIND SPEEDS FOR VARIOUS AVERAGING TIME

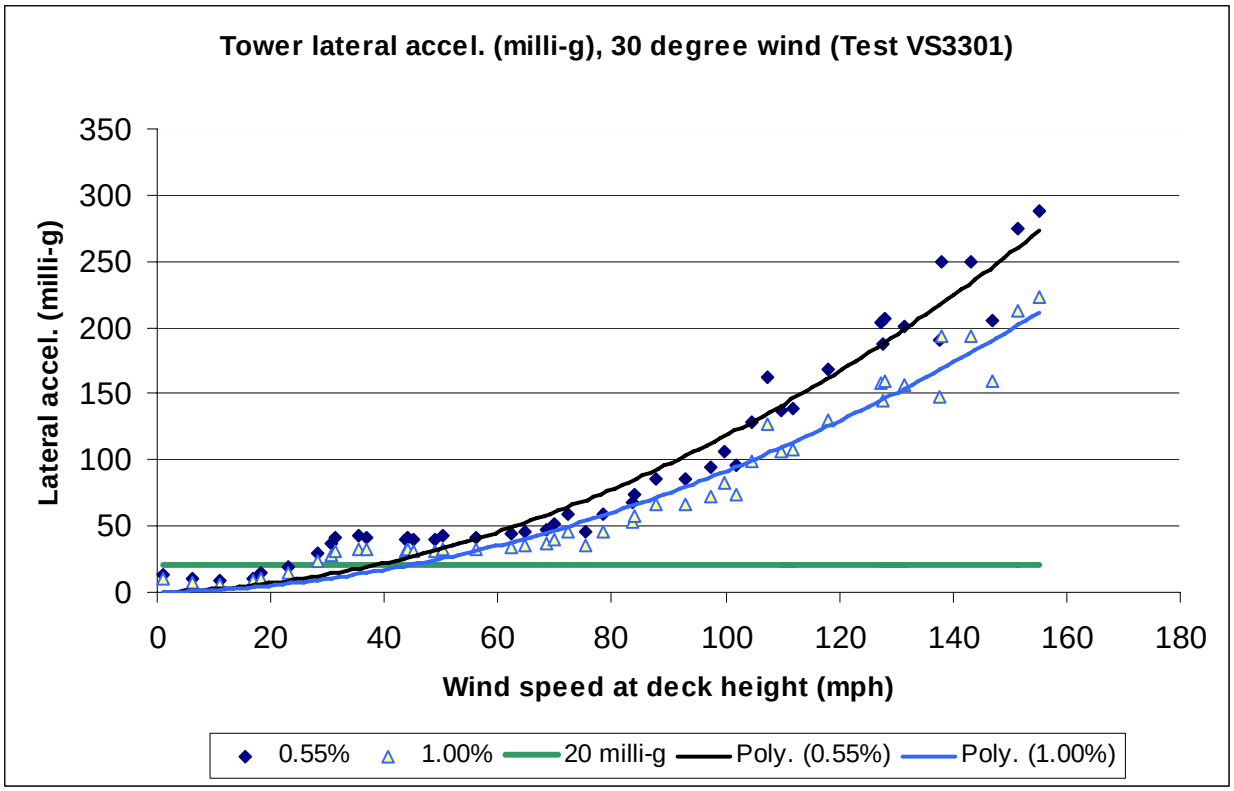

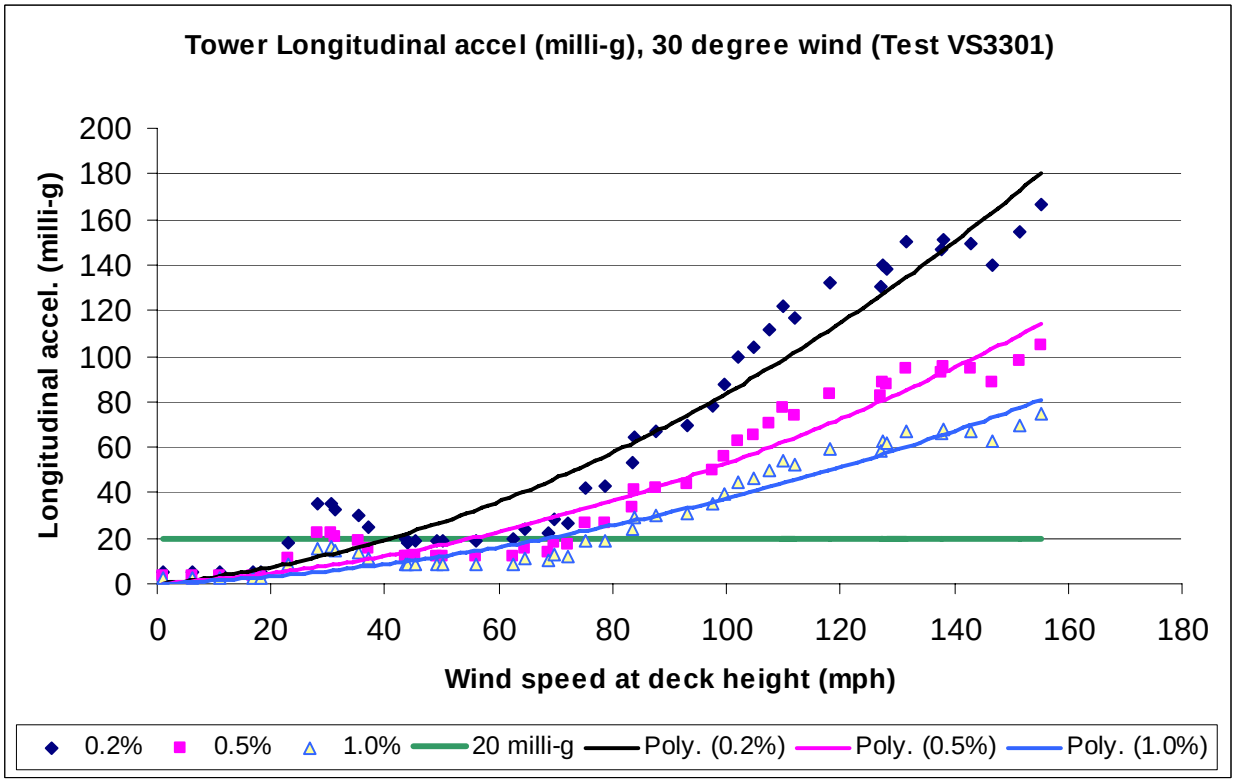

FIGURE 7.11 PYLON ACCELERATIONS AT 30° WIND

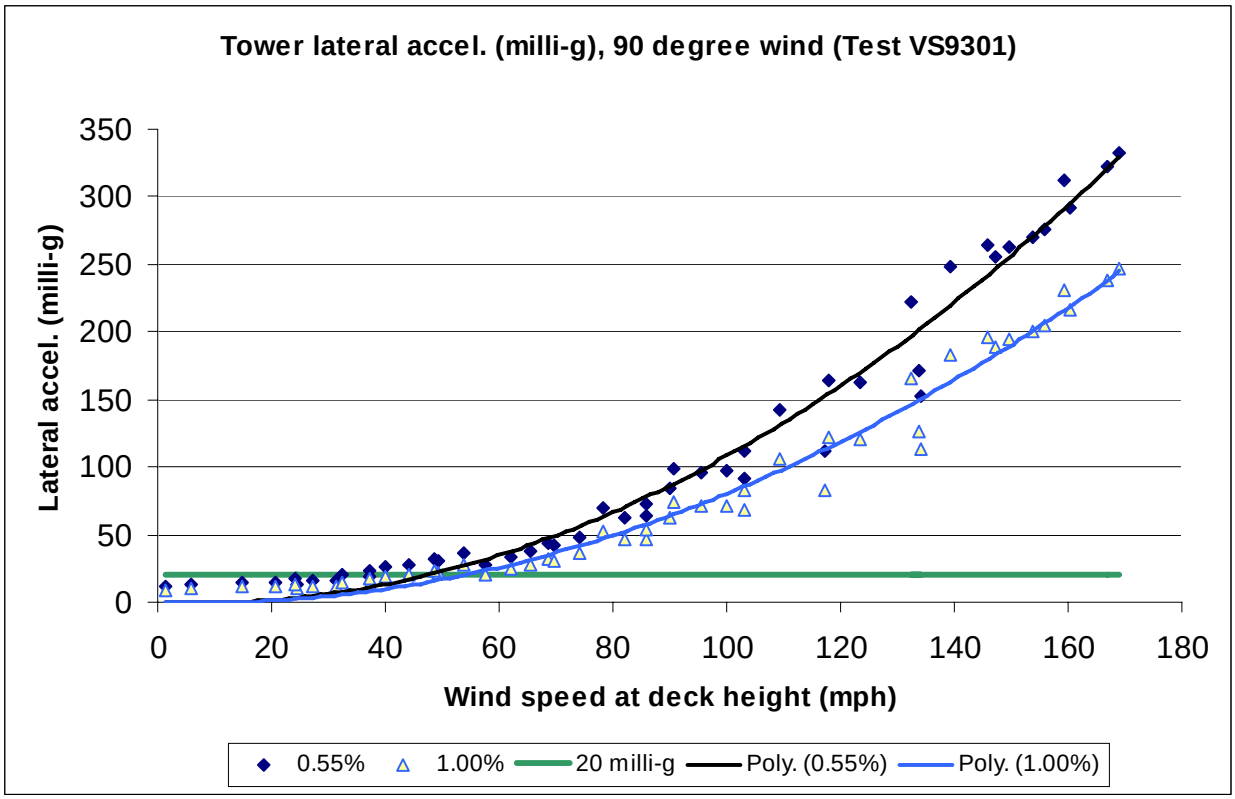

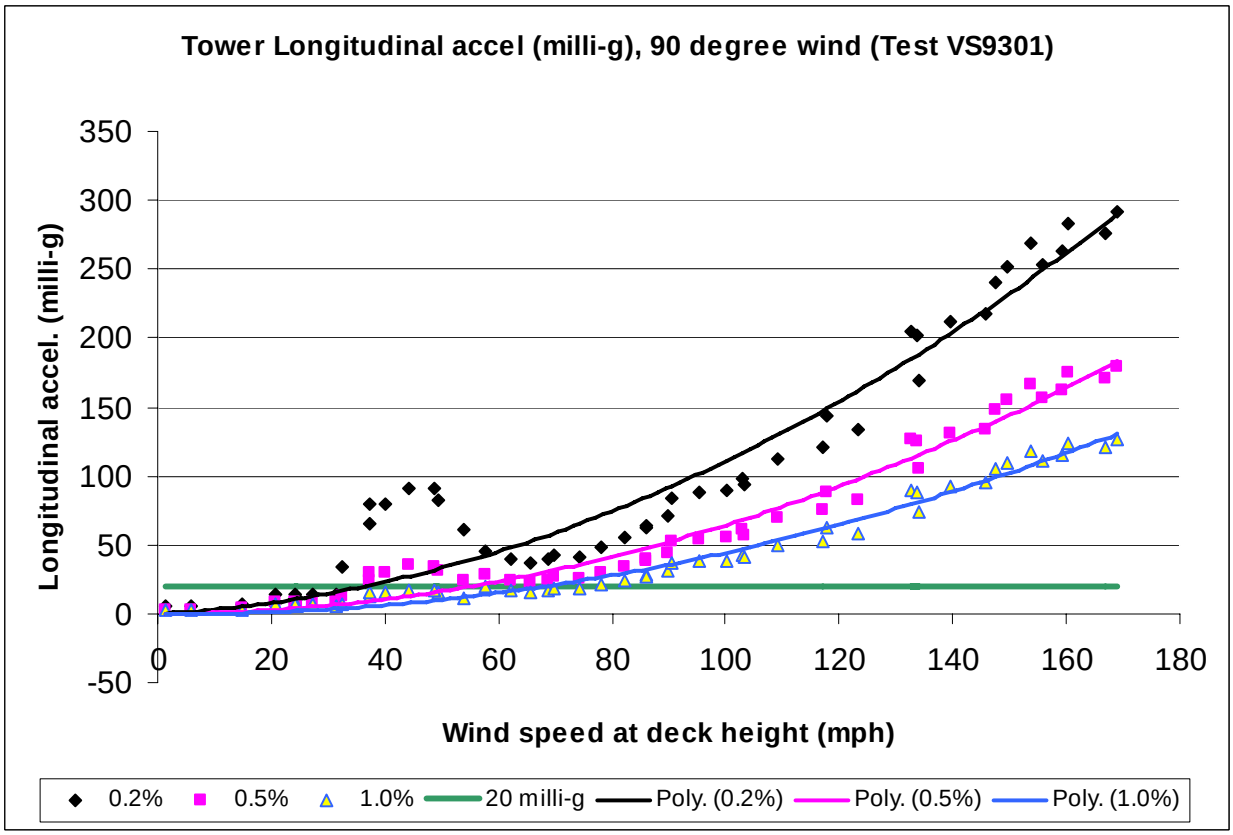

FIGURE 7.12 PYLON ACCELERATIONS AT 90° WIND (PERPENDICULAR TO BRIDGE)

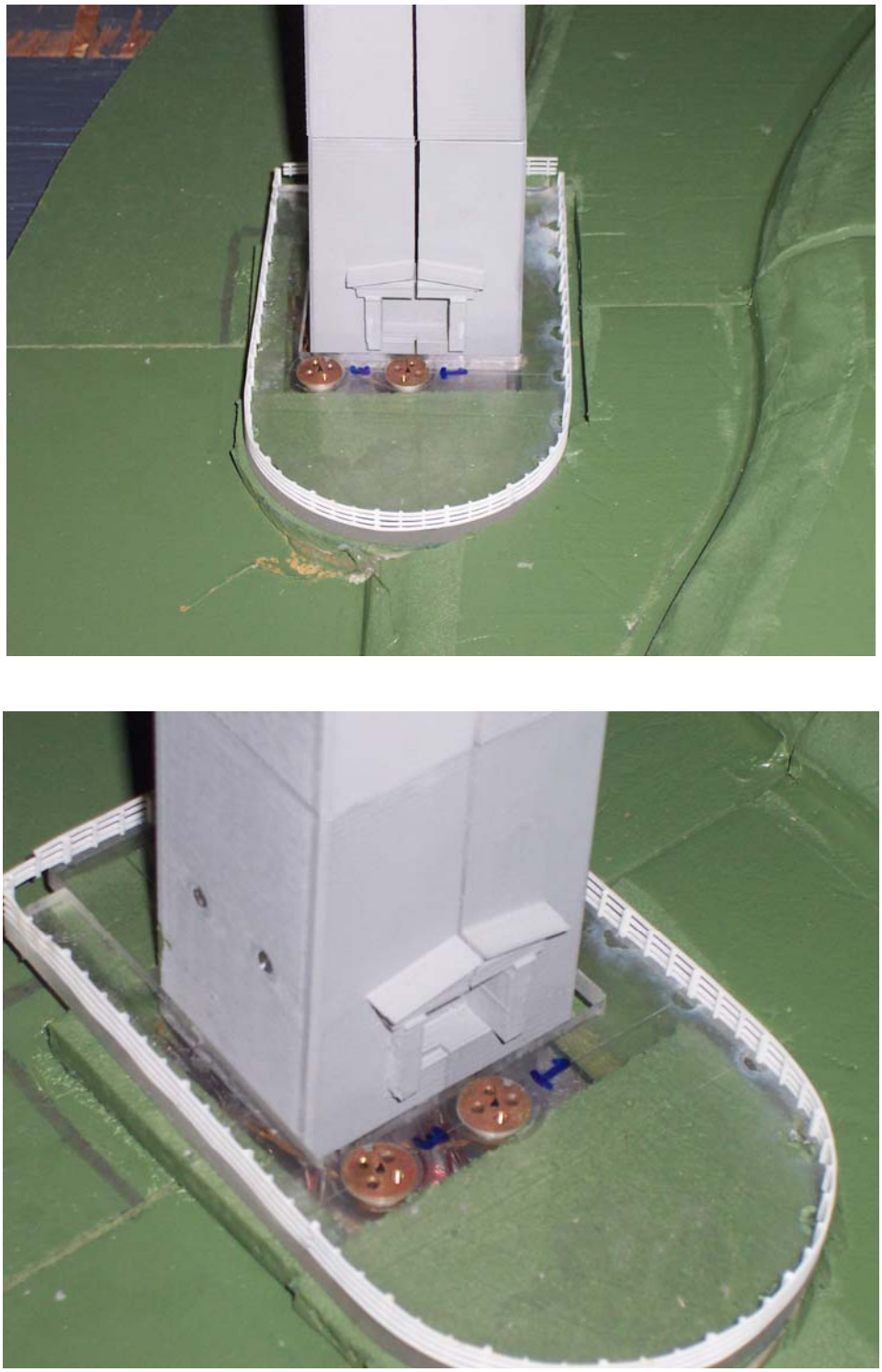

FIGURE 7.13 CLOSE-UP VIEWS OF THE WIND PROBE LOCATIONS AT PROSPECT PYLON ENTRANCE AREA

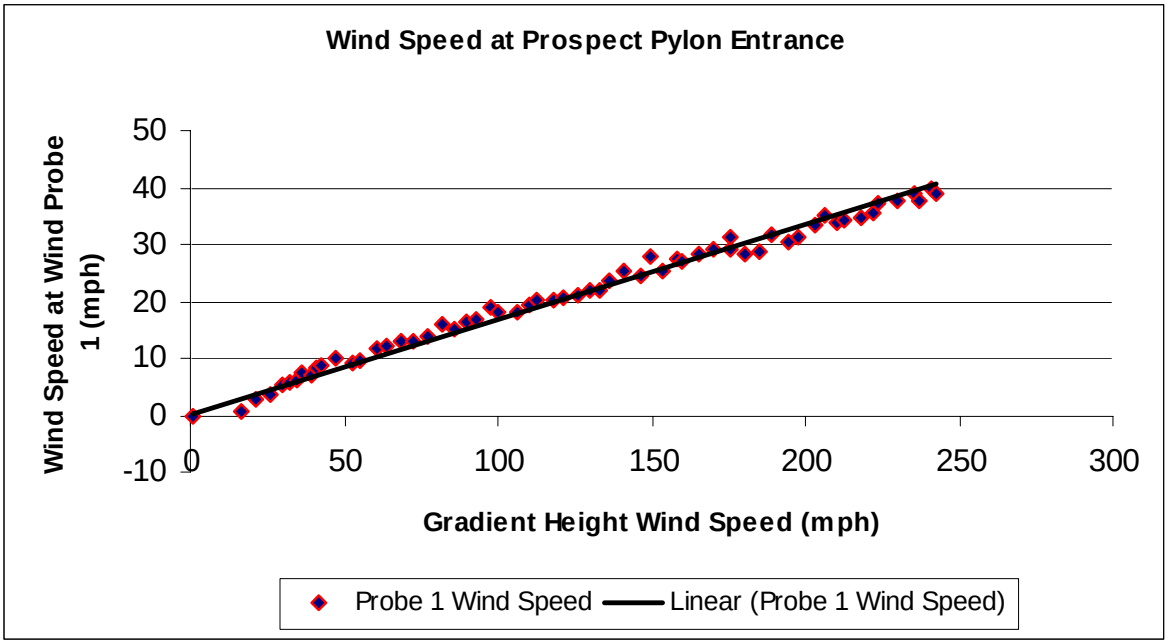

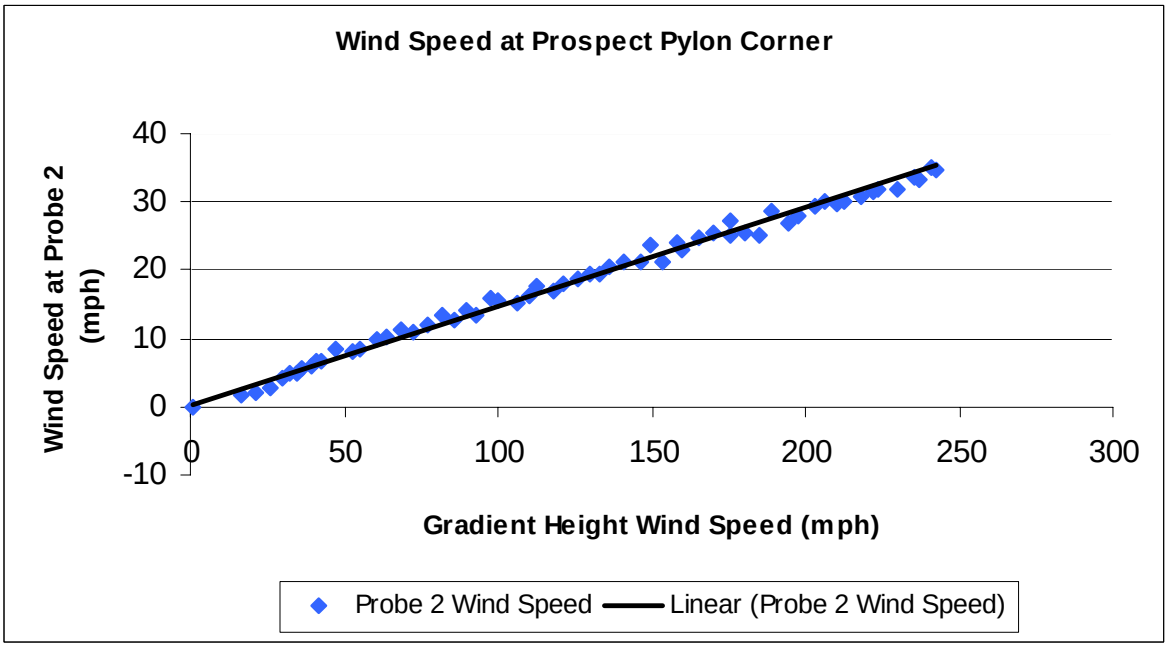

FIGURE 7.14 SAMPLE PLOT OF WIND SPEEDS MEASURED IN FULL BRIDGE AEROELASTIC TEST, AT 90 DEGREE WIND

REFERENCES

1) “Wind Tunnel Testing: A General Outline”, The University of Western Ontario, Boundary Layer Wind Tunnel Laboratory General Outline Report, May 1999.

2) Vickery, P.J., Skerlj, P.F., Steckley, A.C. and Twisdale, L.A., “Hurricane Wind-Field Model for use in Hurricane Simulation”, Journal of Structural Engineering, ASCE, 126(10), pp. 1203-1222, 2000.

3) Vickery, P.J., Skerlj, P.F. and Twisdale, L.A., “Simulation of Hurricane Risk in the US using Empirical Track Model”, Journal of Structural Engineering, ASCE, 126(10), pp. 1222-1237, 2000.

4) ASCE, “Minimum Design Loads for Buildings and Other Structures – ASCE 7-98”, American Society of Civil Engineers, New York, N.Y., January, 2000.

5) King, J.P.C., Ho, E. and Davenport, A.G., "A Study of Wind Effects for the Helgelands Bridge, Norway, Cable Stayed Alternate", The University of Western Ontario, Faculty of Engineering Science Research Report, BLWT-SS17-1988, The University of Western Ontario, London, Ontario, Canada, 1988.

6) King, J.P.C., Larose, G.L. and Davenport, A.G., "A Study of Wind Effects for the New Bridge Over Johnston's Bay, Sydney, Australia", The University of Western Ontario, Faculty of Engineering Science Research Report, BLWT-SS11-1990, The University of Western Ontario, London, Ontario, Canada, 1990.

7) King, J.P.C. and Davenport, A.G., "A Study of Wind Effects for the Seo Hae Grand Bridge, Korea”, The University of Western Ontario, Faculty of Engineering Science Research Report, BLWT-SS25-1992, The University of Western Ontario, London, Ontario, Canada, 1992.

8) Davenport, A.G. and King, J.P.C., "A Study of Wind Effects for the Sunshine Skyway Bridge, Tampa, Florida - Concrete Alternate", The University of Western Ontario, Faculty of Engineering Science Research Report, BLWT-SS24-1982, London, Ontario, Canada, 1982.

9) Davenport, A.G. and King, J.P.C., "A Study of Wind Effects for the Sunshine Skyway Bridge, Tampa, Florida - Steel Alternate", The University of Western Ontario, Faculty of Engineering Science Research Report, BLWT-SS25-1982, The University of Western Ontario, London, Ontario, Canada, 1982.

10) Davenport, A.G. and King, J.P.C., "The Incorporation of Dynamic Wind Loads into the Design Specifications for Long Span Bridges", ASCE Fall Convention: Structures Congress, New Orleans, La., October 1982.

11) Davenport, A.G. and King, J.P.C., "Dynamic Wind Forces on Long Span Bridges", 12th IABSE Congress, Vancouver, Canada, September 1984.

12) Engineering Sciences Data Unit, “Strong Winds in the Atmospheric Boundary Layer”, Data Items 82026, 83045, London, 1982, 1983.

13) Engineering Sciences Data Unit, “Characteristics of Atmospheric Turbulence Near the Ground”, Data Item 74031, October, 1974.

14) Davenport, A.G. and Isyumov, N. "The Application of the Boundary Layer Wind Tunnel to the Prediction of Wind Loading", International Research Seminar on Wind Effects on Buildings and Structures, Ottawa, Canada, September 1967, University of Toronto Press, 1968.

15) Surry, D. and Isyumov, N. "Model Studies of Wind Effects - A Perspective on the Problems of Experimental Technique and Instrumentation", Int. Congress on Instrumentation in Aerospace Simulation Facilities, 1975 Record, pp. 76-90.

16) Twisdale, L. A. and P. J Vickery, 1992. “Predictive Methods for Hurricane Winds in the United States,” Final Report, Small Business Innovation Research Grant ISI 916035, National Science Foundation, Washington, DC, September.

17) American Society of Civil Engineers. “Minimum Design Loads for Buildings and other Structures.” ASCE, Reston Virginia, 2002.

18) Isyumov, N. and Davenport, A.G., “The Ground Level Wind Environment in Built-up Areas”, Proc. of 4th Int. Conf. on Wind Effects on Buildings and Structures, London, England, Sept. 1975, Cambridge University Press, 1977.

19) Isyumov, N., “Studies of the Pedestrian Level Wind Environment at the Boundary Layer Wind Tunnel Laboratory of the University of Western Ontario”, Jour. Industrial Aerodynamics, Vol. 3, 187-200, 1978.

20) Isyumov, N., Amos, K., Mikitiuk, M., Heagy, W. and Davenport, A.G., “A Study of the Pedestrian Level Wind Environment for Canary Wharf, London, England”, The University of Western Ontario, Engineering Science Research Report, BLWT-SS16-1986.

21) Kapoor, V., Page, C., Stepfanowicz, P., Livesey, F., Isyumov, N., “Pedestrian Level Wind Studies to Aid in the Planning of a Major Development”, Structures Congress Abstracts, American Society of Civil Engineers, 1990.

22) Powell, M.D., Reinhold T.A. and Vickery P.J., “Engineering Implications of New Information on Boundary Layer Profiles in Hurricanes”, Americas Conference on Wind Engineering 2001.

23) Durst, C.S., “Wind Speeds over Short Periods of Time”, Meteor. Mag. 89, 181-187, 1960.

24) Isyumov, N. “Motion Perception, Tolerance and Mitigation”, 5th World Congress of the Council on Tall Buildings and Urban Habitat, Amsterdam, The Netherlands, May 1995.

APPENDIX A

THE SECTION MODEL APPROACH FOR THE STUDY OF WIND ACTION ON LONG SPAN BRIDGES

A1 DESIGN OF THE SECTION MODEL

The most elementary of the tools available to the wind engineer for the study of the aerodynamics of long span bridges is the section model. It is also, perhaps the most productive and economical of these tools [A1,A2].

The section model consists of a typical rigid section of the deck, geometrically and aerodynamically similar to the prototype, mounted in the wind tunnel in such a way as to measure the wind produced static and dynamic lift, drag and moment. The model is usually located within the parallel walls of the wind tunnel, or equipped with end plates in order to channel the wind over the deck in a two-dimensional manner.

In a fixed position, the section model can be instrumented to measure lift, drag and torsion either through the mounting of the model on a three component force balance, or on stiff springs to reduce the dynamic motions. The bridge deck is rotated with respect to the oncoming flow to measure the variation in the forces with angle of attack, usually between +15° and -15°. The force coefficients are typically specified as follows:

Lift force per unit length: $$L = \frac{1}{2}\rho V^2 B C_L \quad \text{(A1)}$$

Drag force per unit length: $$D = \frac{1}{2}\rho V^2 B C_D \quad \text{(A2)}$$

Torsional force per unit length: $$T = \frac{1}{2}\rho V^2 B^2 C_T \quad \text{(A3)}$$

Where ρ is the air density, B is the model deck width and C_L, C_D, C_T are dimensionless lift, drag and torsional force coefficients, respectively.

As first used in early applications, the section model was conceived as a substitute for the prototype bridge. Since its dynamics and aerodynamics cannot fully duplicate those of the full scale bridge, interpretation of the results of any section model test is required. Research in recent years has better defined the limited but important role of the section model.

Mounted on springs, with scaled mass per unit length, mass moment of inertia per unit length, structural damping and natural frequencies, the section model is commonly used to investigate the following:

- the dynamic response to vortex shedding
- to ensure that the section is aerodynamically stable to an acceptably high wind speed, given the meteorology of the bridge site
- to determine the response to turbulence

Usually, the effect of turbulence is to reduce the response of the bridge deck to vortex shedding. Consequently, tests are conducted in flow conditions with low turbulence intensity (or, so-called “smooth flow”) in order to conservatively estimate the amplitudes of motion. Various edge treatments can be

investigated to improve the response to vortex shedding. The model is also tested with the same low turbulence flow to provide conservative estimates of flutter behaviour of the section. The response is often investigated with several structural damping ratios.

A uniform grid or spires are used to provide simulations of the scaled atmospheric turbulence. Measured response to turbulent buffeting can be interpreted using an appropriate theory to provide estimates of the prototype wind loading that can be used in the design of the bridge.

The section model can also be used to measure the motion-related forces. Mounted on springs, or driven through sinusoidal motions, the section model experiences aerodynamic forces proportional to the bridge motion and the time derivatives of the motion. These so-called "flutter" forces can be measured and used in a dynamic theoretical model of the bridge in order to predict its performance and aerodynamic stability.

A2 DESIGN OF THE SECTION MODEL

Aeroelastic modeling of structures generally requires equality of the following non-dimensional quantities, in addition to an overall geometric similarity [A3, A4, A5]:

- Froude Number (ratio of the gravitational to the inertia forces);
- Cauchy Number (ratio of the elastic to inertia forces);
- Density Ratio (ratio of the inertia force of the structure to that of the flow);
- Damping Ratio
- Reynolds Number (based on the dimensions of the structure)

Froude Number scaling ($F_r = gL/V^2$) is not necessary in section model studies, since the stiffness is supplied by external springing and not due to gravitational effects. L is a characteristic dimension, V is the wind speed and g is the acceleration due to gravity. Cauchy Number is rewritten in terms of $V/(fB)$ and provides the link in the wind speeds between model and prototype. f is a natural frequency and B is the bridge deck width. Density scaling (ρ_s/ρ_α) is important, where the subscripts s and a refer to the structure and air respectively. This ensures that the mass is scaled correctly, in relation to the added mass of air due to the moving bridge. Equal modal damping (ζ_s in a ratio to critical or δ_s in logarithmic decrement) between model and prototype is required, but exploratory tests are often performed with lower model damping in order to ensure that any instability can readily be identified.

Reynolds Number similarity ($R_e=VL/\nu$, where ν is the kinematic viscosity of the air) is not practical in most cases and section model tests are usually carried out at a Reynolds Number several orders of magnitude lower than that of full scale. For sharp edged bodies such as bridge decks, the effects of this relaxation of R_e scaling is not severe for overall wind induced forces and responses. In the case of the geometric modeling of circular objects such as the cables and handrails, however, R_e effects can be significant and an "equivalent force effect" approach should be taken.

The full scale data that is needed to design the model and springing system consists of:

- a constant mass ($m_v = \rho_s B^2$) per unit length of span, or a calculated value, giving the correct modal mass in the case of a non-uniform span-wise distribution
- a mass moment of inertia ($I_T = \rho_s B^4$) per unit length of span, or a calculated value, as for the mass, in the case of a non-uniform span-wise distribution, or a radius of gyration, r, of the mass, m_v
- target values of modal damping for the modes of vibration to be examined (nominally the fundamental vertical and torsional modes)

- natural frequencies of the modes to be examined
- location of the rotation centre of the deck cross section which determines the torsional mode

Most section model rigs have two dominant modes of vibration, namely, vertical and torsional motion. It is through the selection of the springs and the spring spacing that the above scaling is applied. Firstly, the geometric scale factor is selected, along with the model length. Typical geometric scales are in the order of 1:40 to 1:80, in order that deck details are well simulated. The length of the model should be of the order of 4-5 times the deck width in order that correlation effects of the wind on the structure are correct.

The target mass and mass moment of inertia are determined through the expressions above. Before selecting the model support stiffness a target value for the velocity scale factor, $V_{prototype}/V_{model} = (fB)_{prototype}/(fB)_{model}$, is set such that the range of wind speed available in the wind tunnel corresponds to a satisfactory range of wind speeds in the prototype.

It is important to include the model support mass as part of the moving mass of the model as well as providing sufficient model stiffness such that internal flexing or twisting of the model does not occur.

A typical arrangement of springs for the section model rig in use at the Boundary Layer Wind Tunnel Laboratory at the University of Western Ontario is as shown in Figure A1. The arrangement of the model mounting system incorporates radial bearings at the ends of the model at the K_3 support, which allow the locking of vertical or torsional motion to perform single degree of freedom tests.

The following spring stiffnesses are considered:

- k_1 is four main springs above the model, at a spacing X
- k_2 is four main springs below the model
- k_3 is four leaf springs in pairs on each end of the model which provide a drag restraint and allows only vertical motion (in other section model rigs, this spring system has often been modelled using a very long drag-wire fore and aft of the model)
- k_{lc} is four load cell transducers

The simplified equation for the natural frequencies of vertical and torsional modes of vibration is:

$$f_V = \frac{1}{2\pi}\sqrt{\frac{k_V}{m}} \qquad \text{(A4)}$$

and:

$$k_V \approx 4k_1 + 2k_3 + 4\frac{1}{\frac{1}{k_2} + \frac{1}{k_k}} \qquad \text{(A5)}$$

also: $f_T = f_V\left(\frac{X}{2r}\right)$ (where r is the radius of gyration and X is the spring spacing)

Dashpots are installed at appropriate locations on the main arms of the rig to provide the desired structural damping in the vertical and torsional modes of vibration. Although with this arrangement of spring supports it is not possible to prevent the model from undesirable rocking modes of vibration, by summing and differencing the load cell outputs, the electrical output from this type of mode can be eliminated.

The spring system is mounted on a frame structure which is independent of the wind tunnel and can accommodate virtually any length of model. The section model test set-up is shown in the wind tunnel in Figure A2 with the turbulence generating grid at the inlet to the test section. The frame structure is enclosed in an aerodynamic fairing system which minimizes the wall boundary layers and helps to ensure homogeneous flow conditions across the span of the model. The springing and dashpot system are shown in Figure A3. With this design, the model can be installed on the rig and calibrated outside of the wind tunnel, providing clear efficiencies in the test procedure. Both static and dynamic calibrations are performed on the model, ensuring that the modal mass and mass moment of inertia are as desired. A relationship between the dynamic deflection and the load cell output is obtained through this calibration, as well as a confirmation of the stiffness of the springing system.

A3 THE SECTION MODEL TEST AND ANALYSIS

The dynamic section model tests are usually comprised of a manual and automatic run. The manual run allows the wind tunnel operator to gradually increase the wind speed, while carefully noting any visual signs of instabilities and establishing a safe upper bound wind speed for the test. A set of wind speeds (~50) are selected and the test repeated under automatic control. Measurements include the time history of the vertical and torsional motions of the model as well as the wind speed. The time history is analyzed on-line and the instantaneous maximum, minimum, root-mean-square (RMS) and mean value is recorded. A Leiblein analysis of the peaks is also performed. This is repeated for each of the desired wind speeds. Additional wind speeds are set in the vicinity of any vortex shedding peaks in order to establish the response peak.

The presence of a vortex shedding peak or flutter instability is obvious from an examination of the response data. This type of instability is marked as a change in the response from a random motion to a sinusoidal motion. An examination of the “peak factor” (or the ratio of the peak to RMS value) clearly indicates this change. The peak factor for random motion is of the order of 3-4 while that for a pure sinusoid is $\sqrt{2}$.

The tests are performed both for uniform flow and for grid-generated turbulent flow conditions. The results in turbulent flow are often used in an analysis of Equivalent Static Loads, which effectively translate the results from the section model tests into effective loads which can be used for design [A6].

REFERENCES - APPENDIX A

A1. “Manual of Practice for Wind Tunnel Tests of Buildings and Structures”, American Society of Civil Engineers - Aerospace Division, New York, NY, June 1997.

A2. Hjorth-Hansen, E., "Section Model Tests", Proc. Aerodynamics of Large Bridges, Balkema, Rotterdam, 1992.

A3. Davenport, A.G. and Isyumov, N., "The Application of the Boundary Layer Wind Tunnel to the Prediction of Wind Loading", Proceedings of the Int. Res. Sem., N.R.C., Ottawa, Canada, September 1967, Vol. 1, Univ. of Toronto Press.

A4. Davenport, A.G. and King, J.P.C., "A Study of Wind Effects for the Sunshine Skyway Bridge, Tampa, Florida - Concrete Alternate", The University of Western Ontario, Faculty of Engineering Science Research Report, BLWT-SS24-1982, London, Ontario, Canada, 1982.

A5. Davenport, A.G. and King, J.P.C., "A Study of Wind Effects for the Sunshine Skyway Bridge, Tampa, Florida - Steel Alternate", The University of Western Ontario, Faculty of Engineering Science Research Report, BLWT-SS25-1982, The University of Western Ontario, London, Ontario, Canada, 1982.

A6. Davenport, A.G. and King, J.P.C., "Dynamic Wind Forces on Long Span Bridges", 12th IABSE Congress, Vancouver, Canada, September 1984.

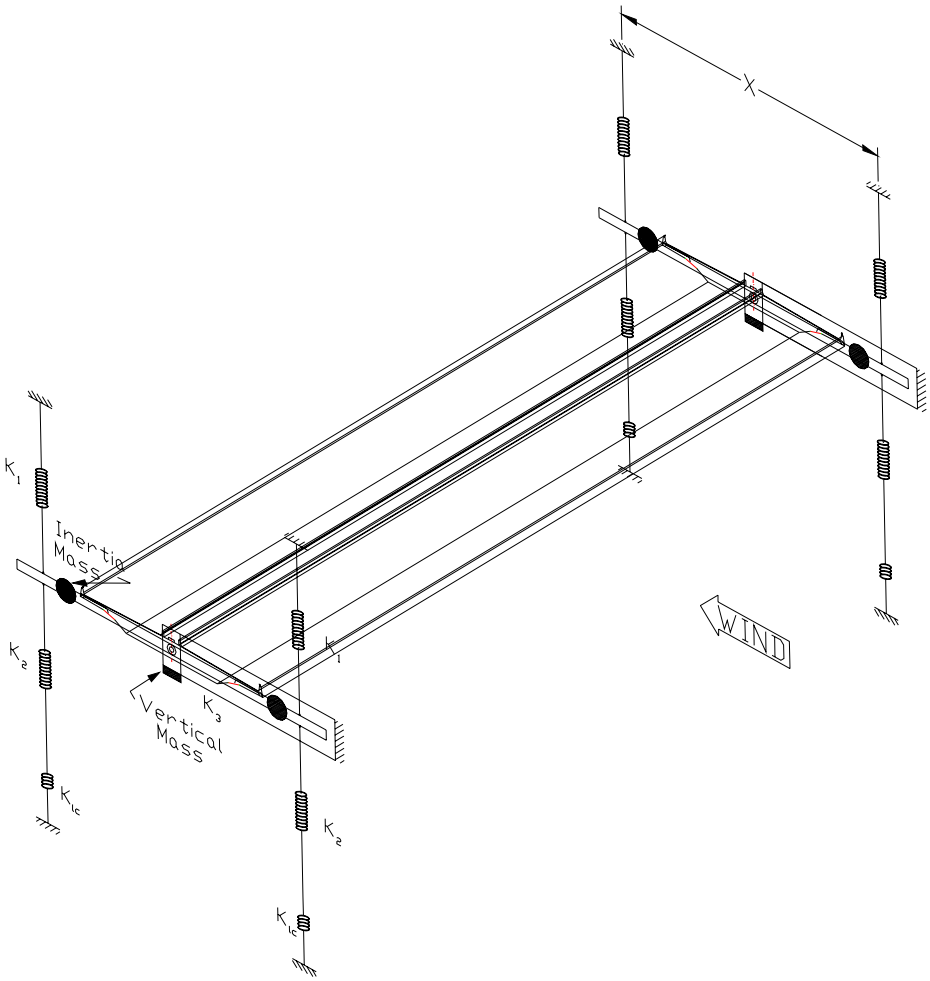

FIGURE A1 DYNAMIC SECTION MODEL RIG

FIGURE A2 2.13m LONG DYNAMIC SECTION MODEL

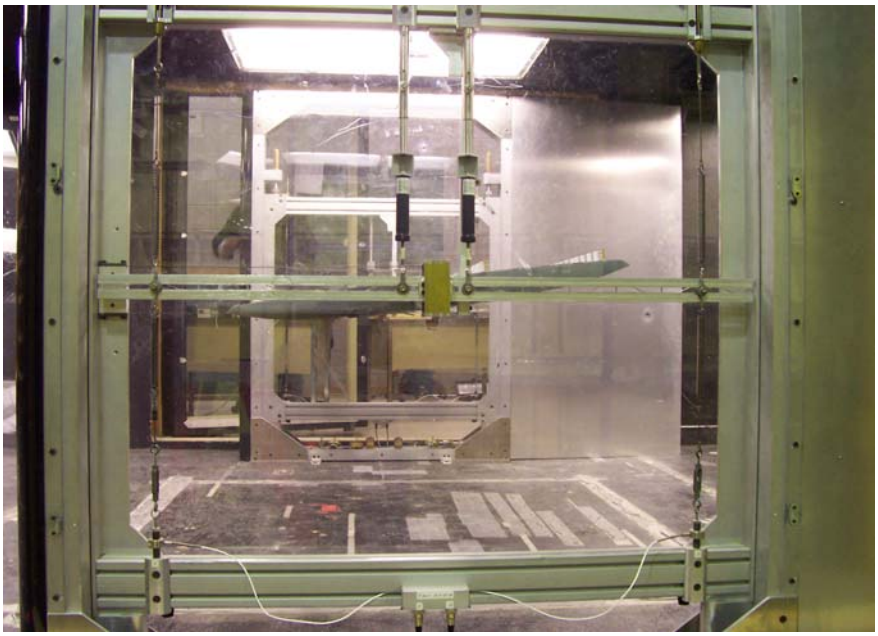

FIGURE A3 DETAILS OF DYNAMIC TEST RIG

APPENDIX B

RESULTS OF DYNAMIC SECTION MODEL TESTS

TABLE B1 SUMMARY OF DYNAMIC TEST RESULTS

FOR 0° ANGLE OF ATTACK

No.	Label	Flow	Sidewalk	Damping (nominal)	f_v (Hz)	f_t (Hz)	Vmax (mph)	Flutter	Vortex-Induced Vibrations
1	sma101	smooth	none	0.5%	4.476	15.197	145	not observed	Vertical: 21 mph, 0.55 ft Torsional: 81 mph, 0.15^{o}
2	sma201	turbulent	none	0.5%	4.476	15.197	145	not observed	not observed
3	sha101	smooth	none	1.0%	4.476	15.197	147	not observed	Torsional: 82 mph, 0.16^{o}
4	smb101	smooth	upstr.	0.5%	4.414	14.816	146	not observed	Vertical: 22 mph, 0.84 ft Torsional: 79 mph, 0.12^{o}
5	smb201	turbulent	upstr.	0.5%	4.414	14.816	148	not observed	not observed
6	shb101	smooth	upstr.	1.0%	4.414	14.816	145	not observed	Vertical: 21 mph, 0.38 ft Torsional: 78 mph, 0.10^{o}
7	smc101	smooth	downstr.	0.5%	4.414	14.816	147	not observed	Vertical: 22 mph, 0.58 ft Torsional: 76 mph, 0.16^{o}
8	smc201	turbulent	downstr.	0.5%	4.414	14.816	148	not observed	not observed

PART 1 PLOTS OF DYNAMIC TEST RESULTS

NO SIDEWALK

units = imperial
Data File = sma10x.mst
Information File = sma101.inf
Aug. 06, 2004

MEAN
PEAK (RMS * 3.5)

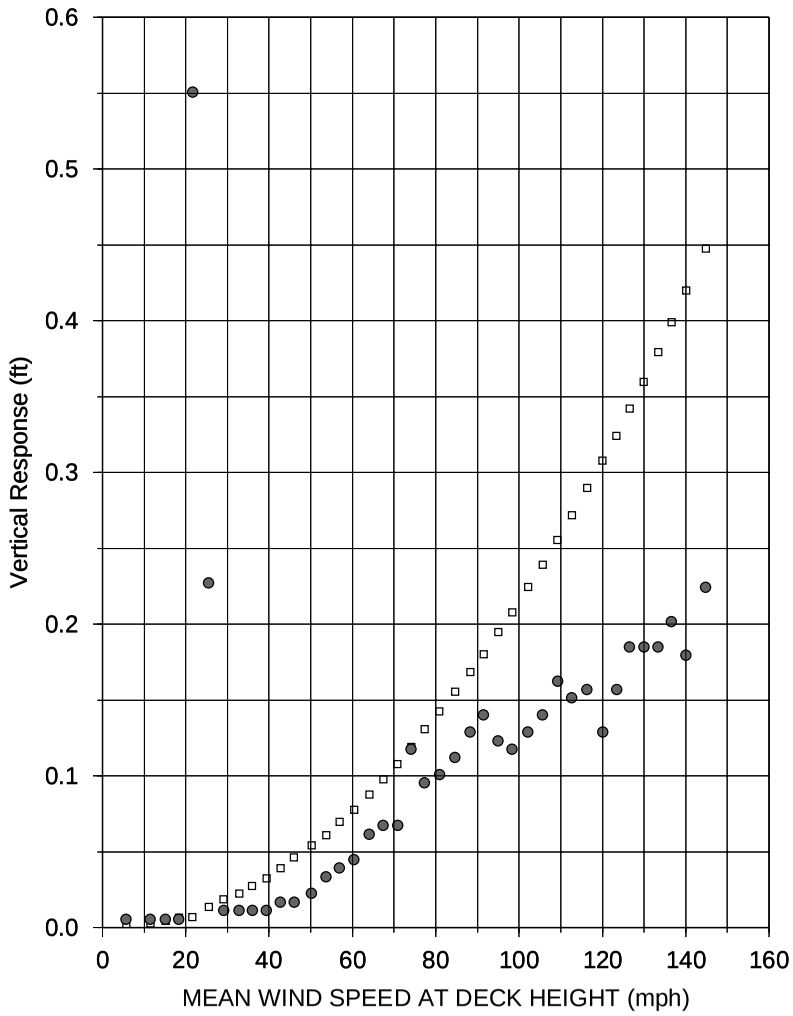

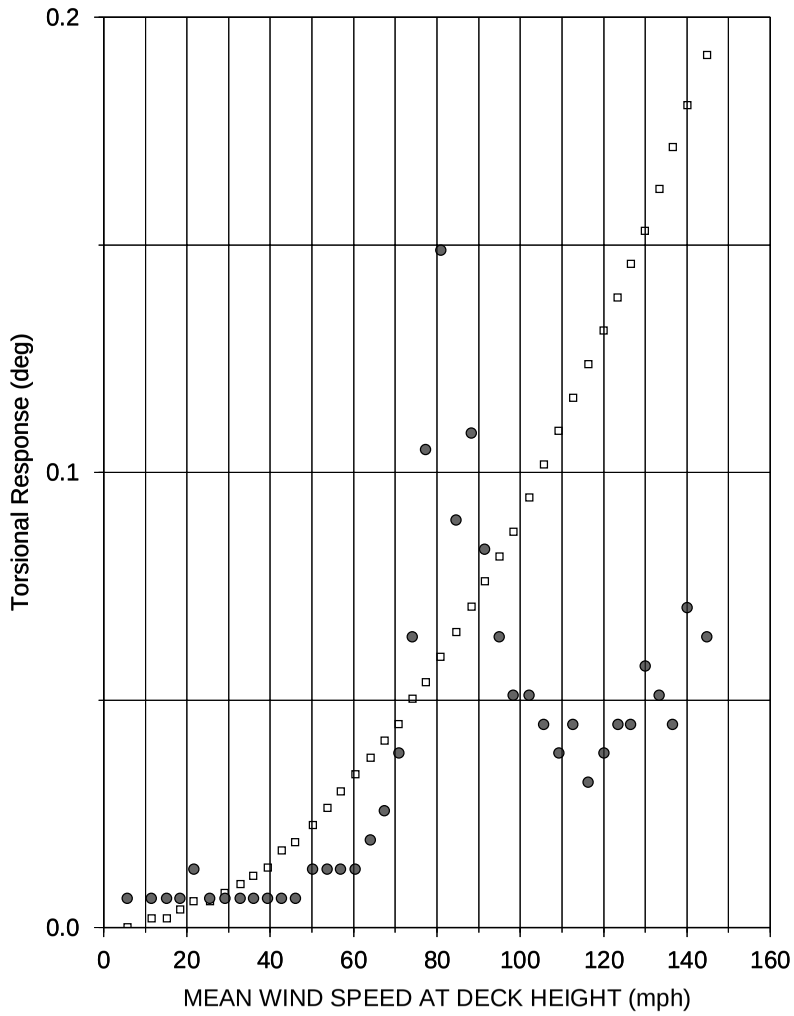

Prospect Verona, no sidewalk, smooth flow, 0.5% damping, 0 degrees

units = imperial
Data File = sma10x.mst
Information File = sma101.inf
Aug. 06, 2004

PEAK FACTOR

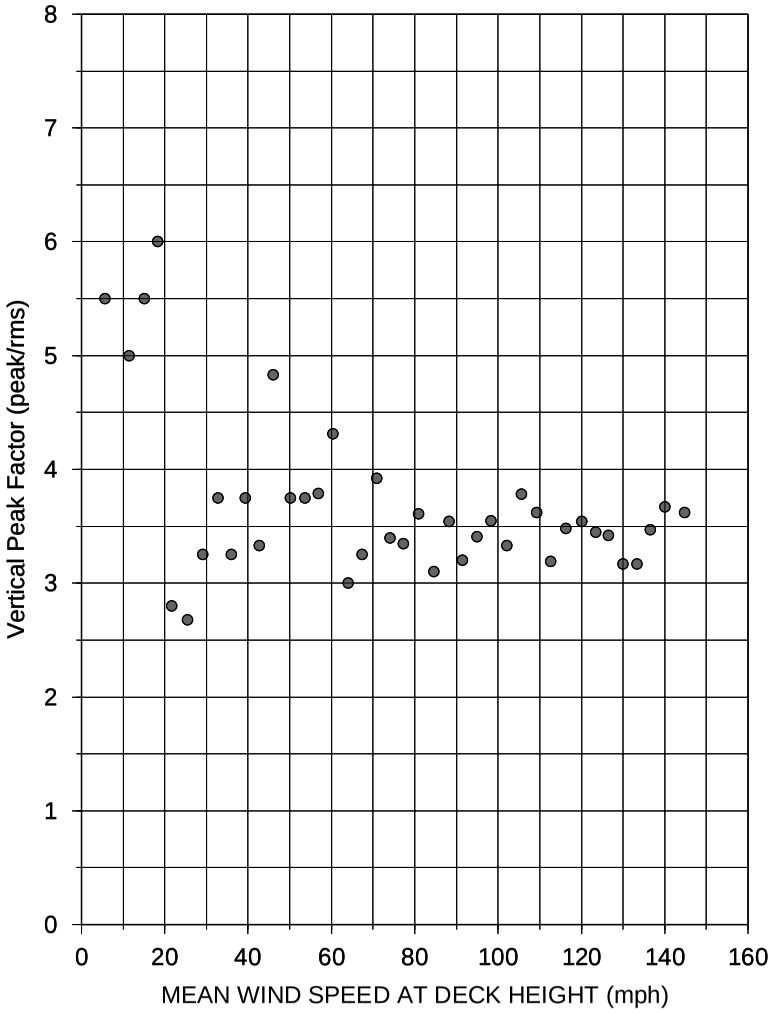

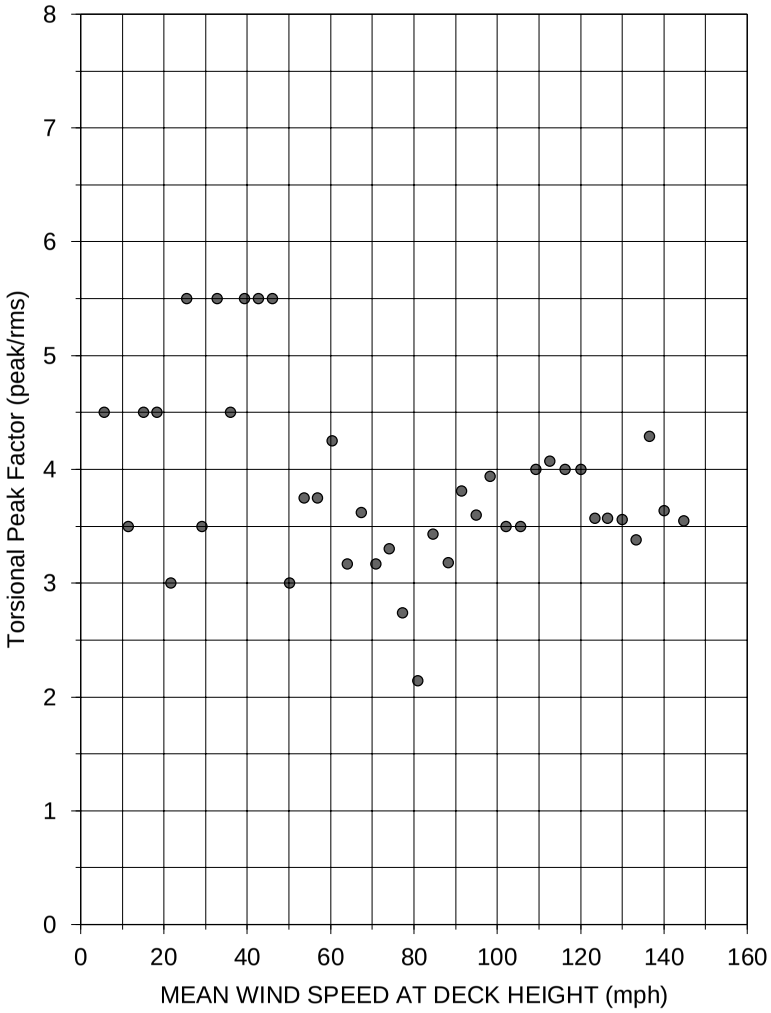

Prospect Verona, no sidewalk, smooth flow, 0.5% damping, 0 degrees

units = imperial
Data File = sma201.mst
Information File = sma201.inf
Aug. 06, 2004

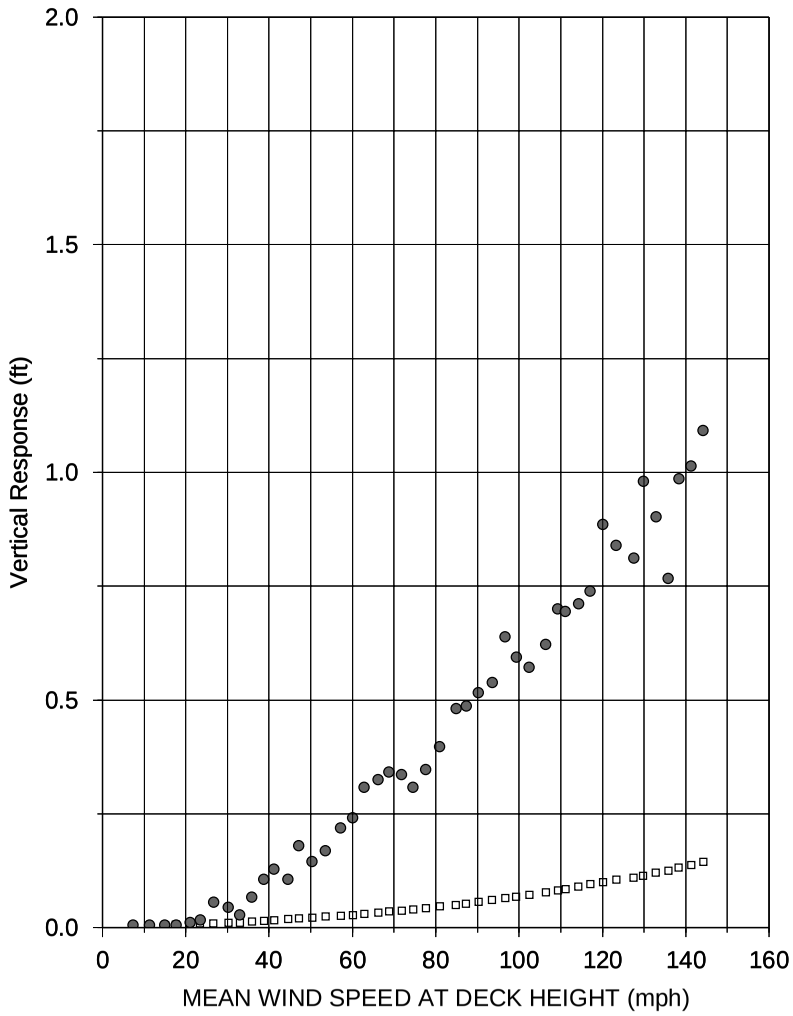

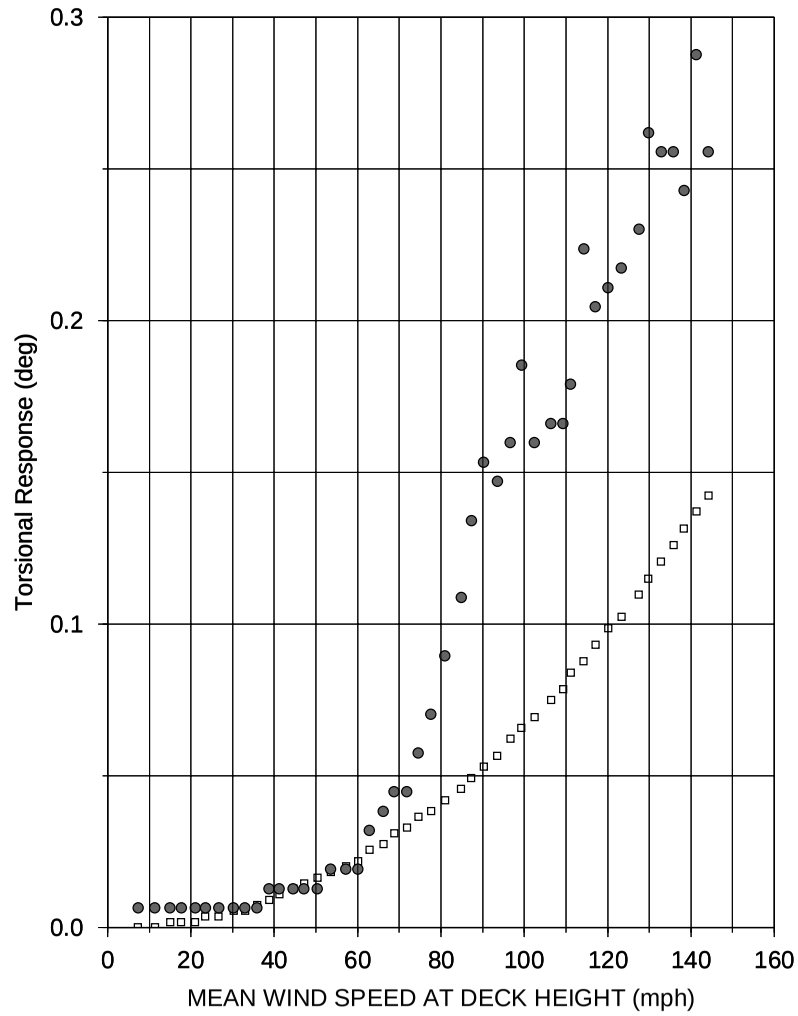

Prospect Verona, no sidewalk, turbulent flow, 0.5% damping, 0 degrees

units = imperial
Data File = sma201.mst
Information File = sma201.inf
Aug. 06, 2004

PEAK FACTOR

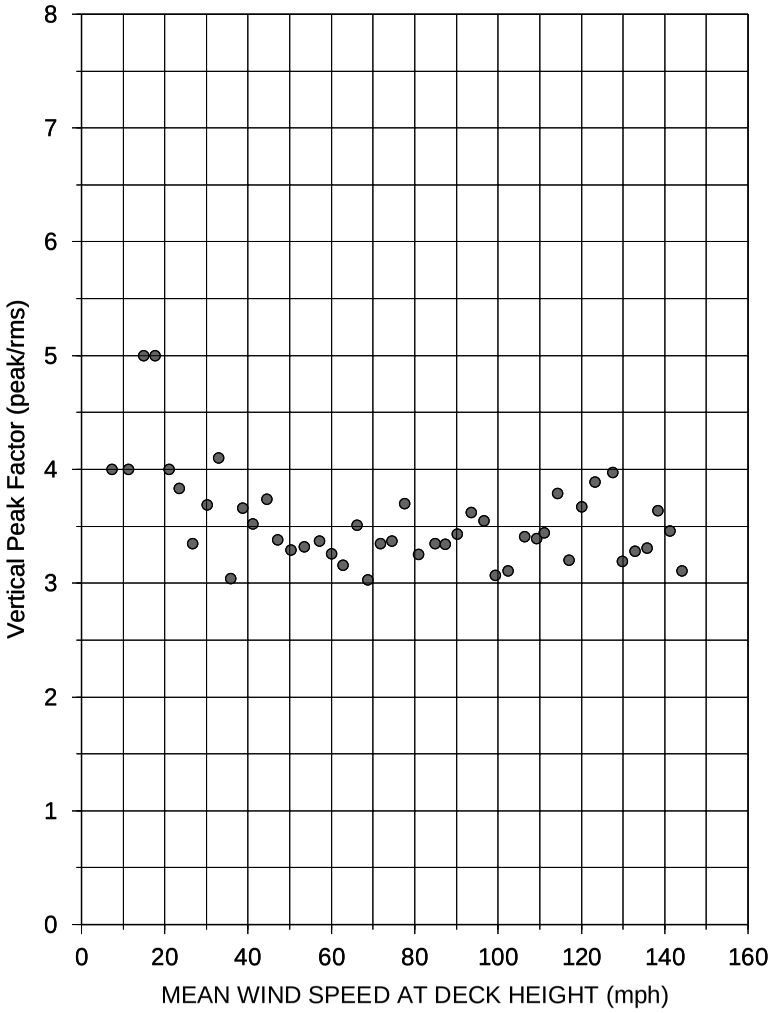

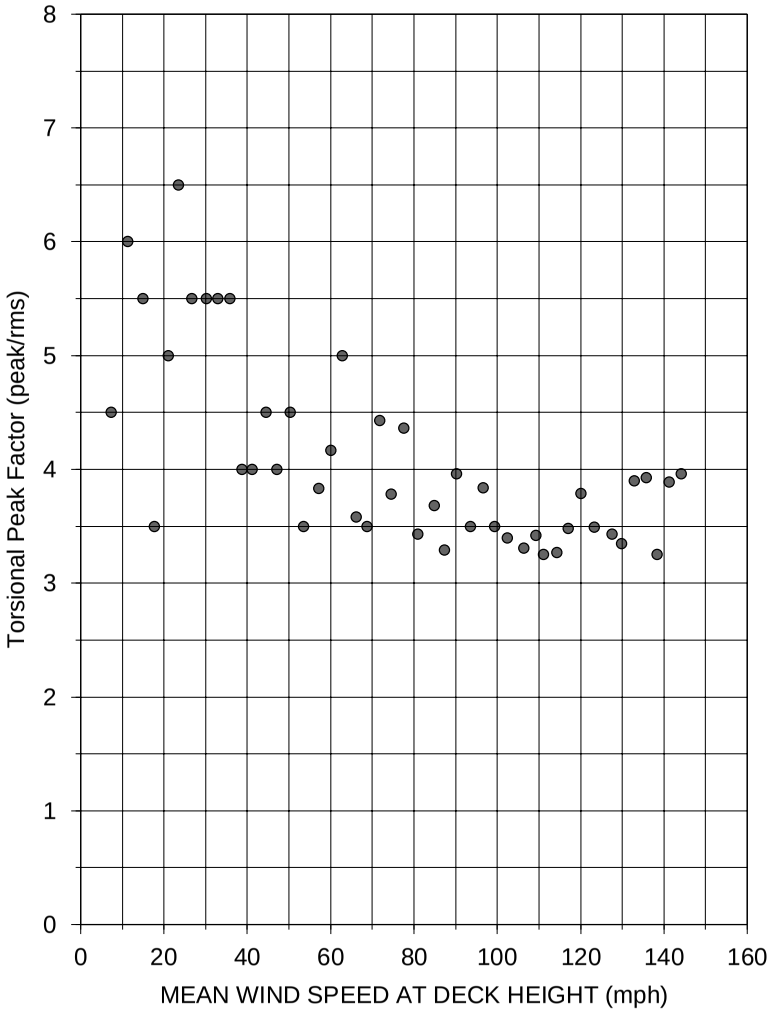

Prospect Verona, no sidewalk, turbulent flow, 0.5% damping, 0 degrees

units = imperial
Data File = sha101.mst
Information File = sha101.inf
Aug. 06, 2004

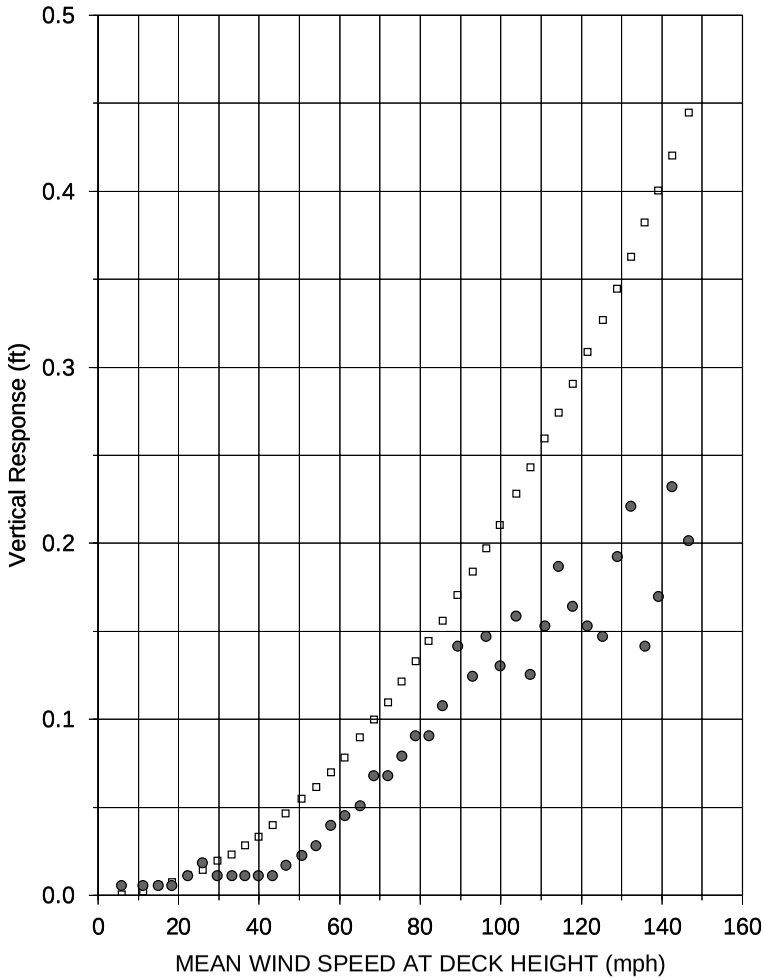

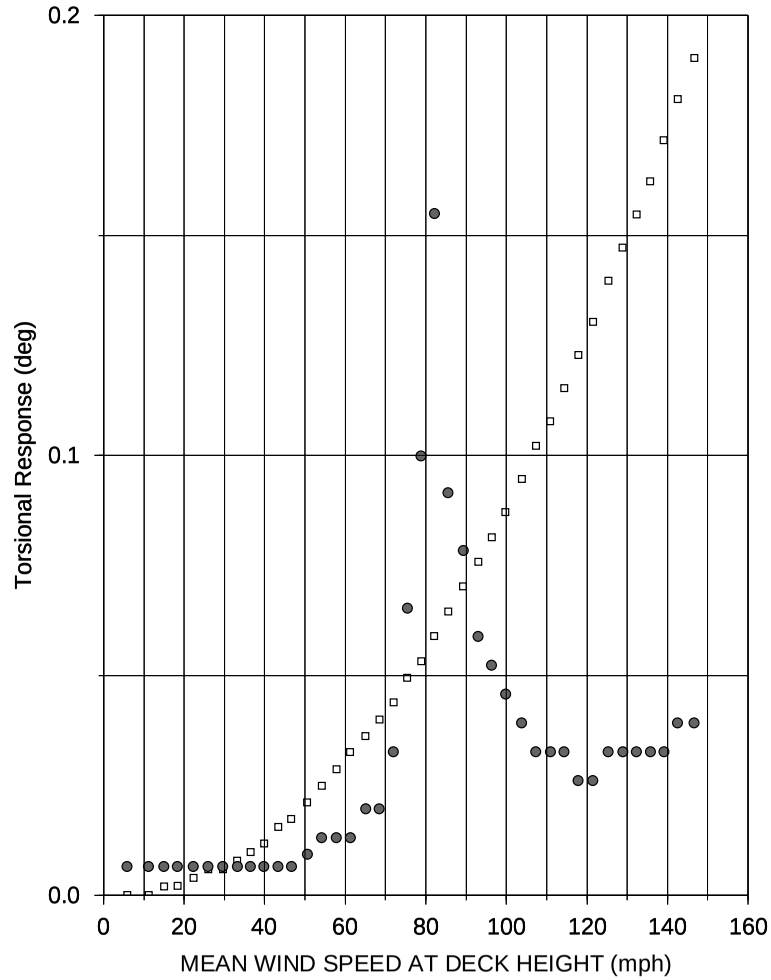

Prospect Verona, no sidewalk, smooth flow, 1% damping, 0 degrees

PART 2 PLOTS OF DYNAMIC TEST RESULTS

SIDEWALK on WINDWARD (UPSTREAM) SIDE

units = imperial
Data File = smb101.mst
Information File = smb101.inf
Aug. 06, 2004

MEAN
PEAK (RMS * 3.5)

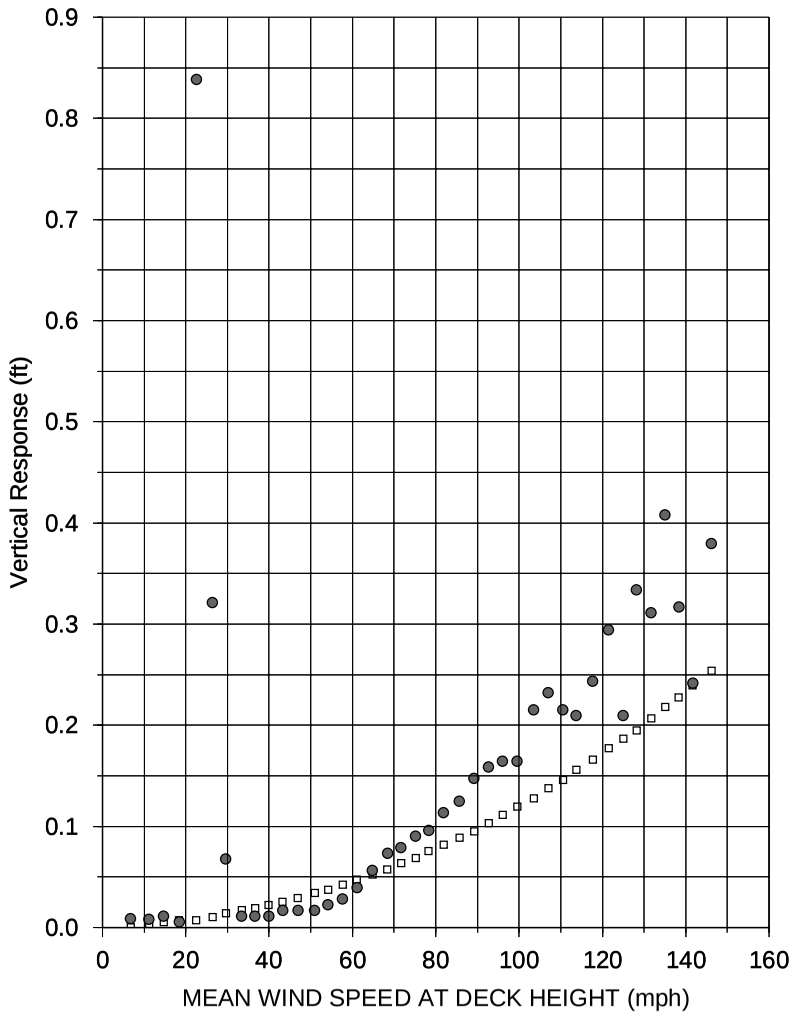

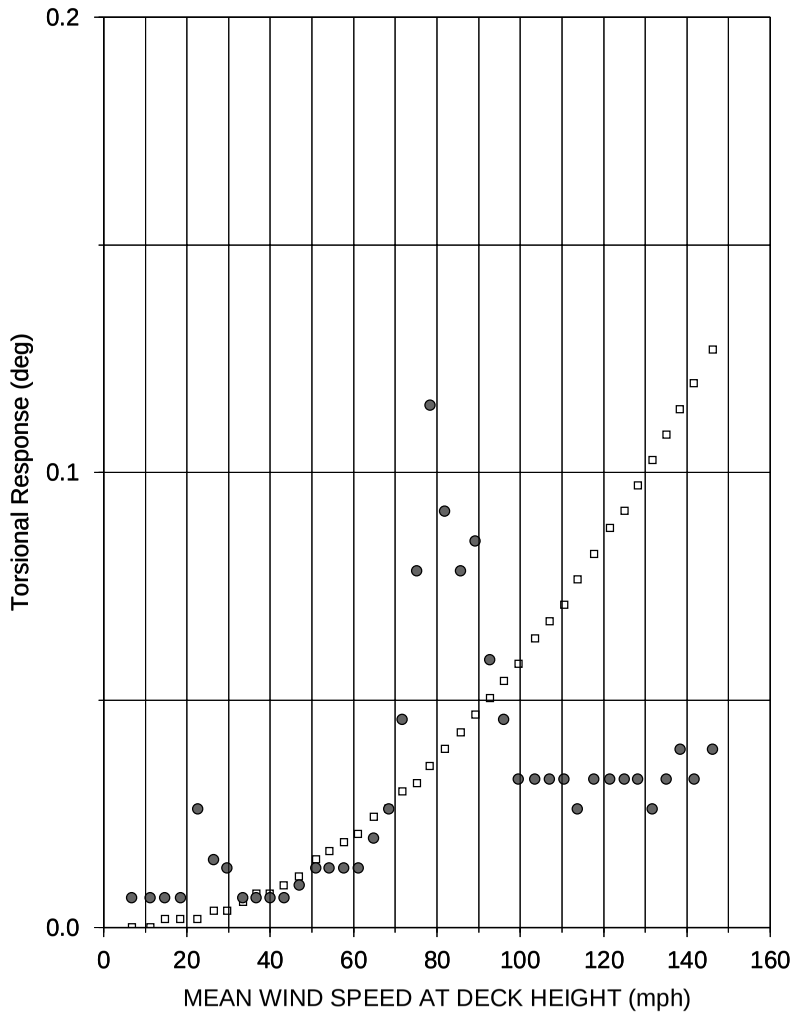

Prospect Verona, sidewalk upstream, smooth flow, 0.5% damping, 0 degrees

units = imperial
Data File = smb201.mst
Information File = smb201.inf
Aug. 06, 2004

MEAN
PEAK (RMS * 3.5)

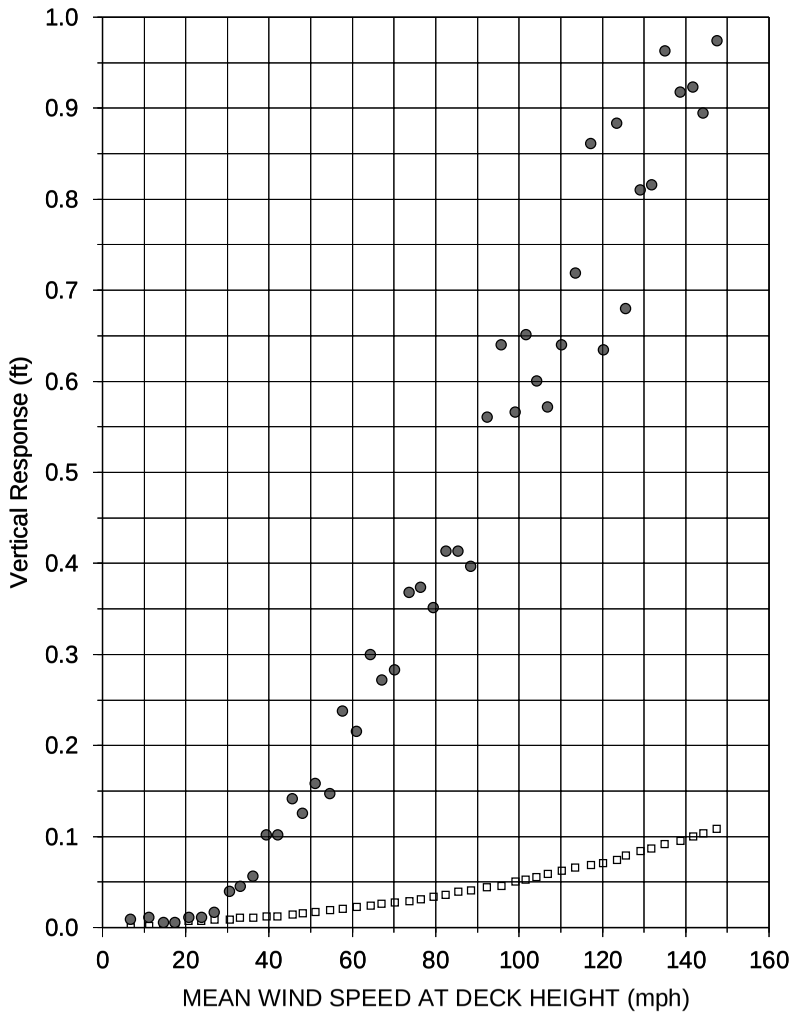

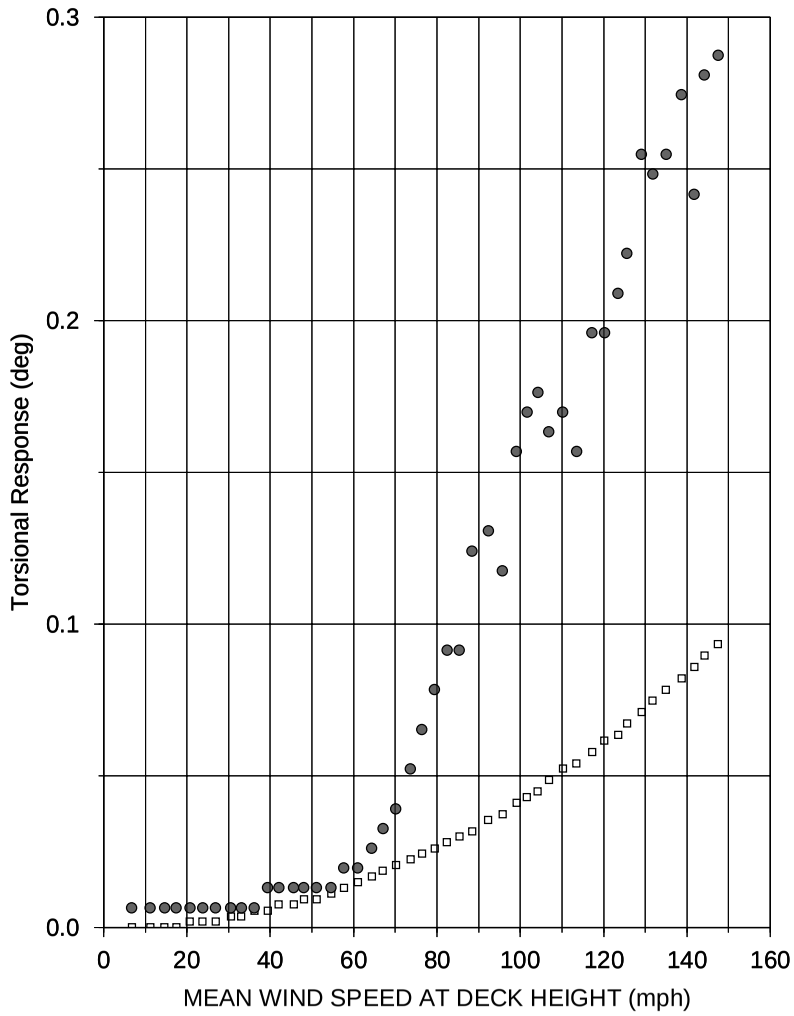

Prospect Verona, sidewalk upstream, turbulent flow, 0.5% damping, 0 degrees

units = imperial
Data File = shb101.mst
Information File = shb101.inf
Aug. 06, 2004

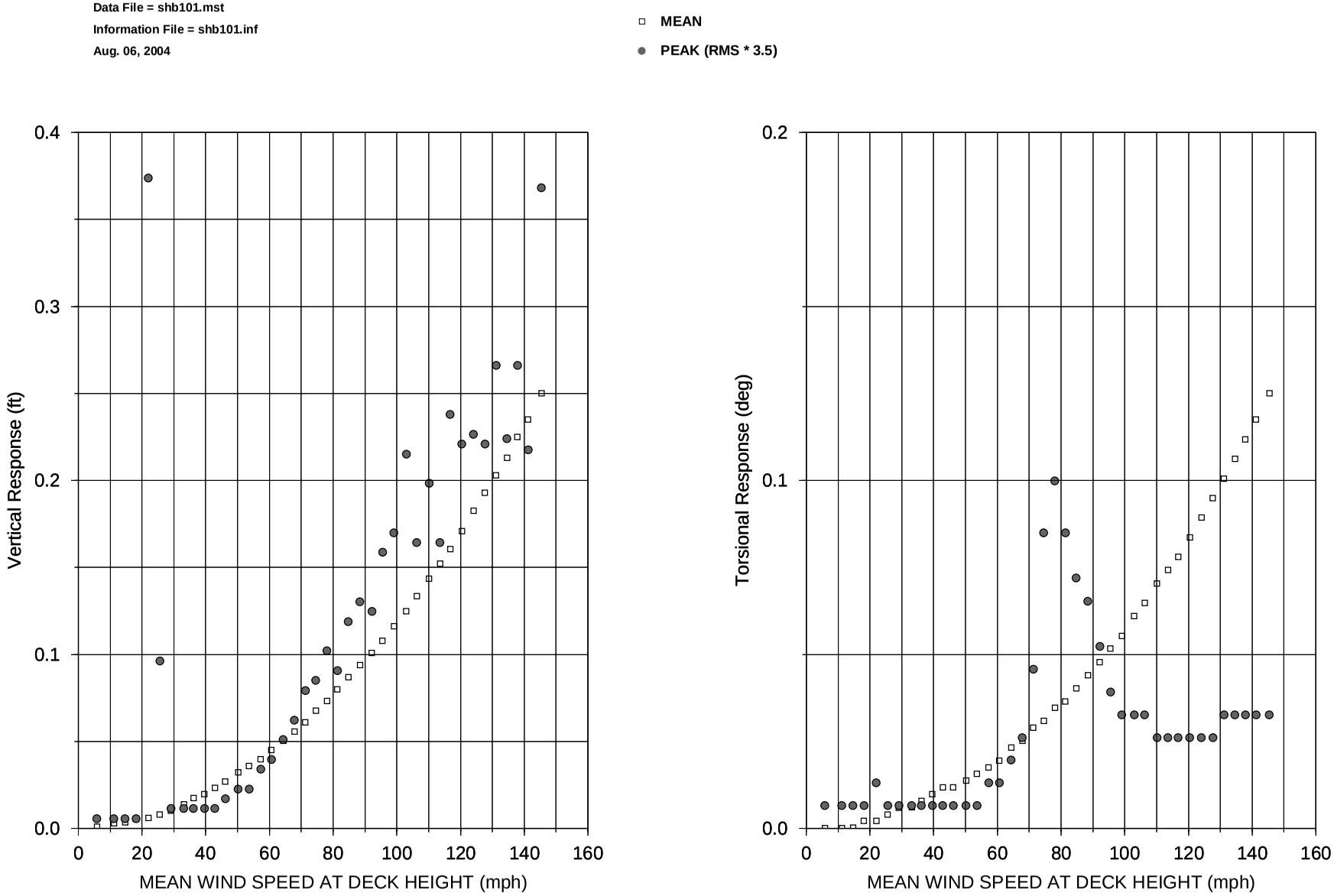

Prospect Verona, sidewalk upstream, smooth flow, 1% damping, 0 degrees

PART 3 PLOTS OF DYNAMIC TEST RESULTS

SIDEWALK on LEEWARD (DOWNSTREAM) SIDE

units = imperial
Data File = smc101.mst
Information File = smc101.inf
Aug. 06, 2004

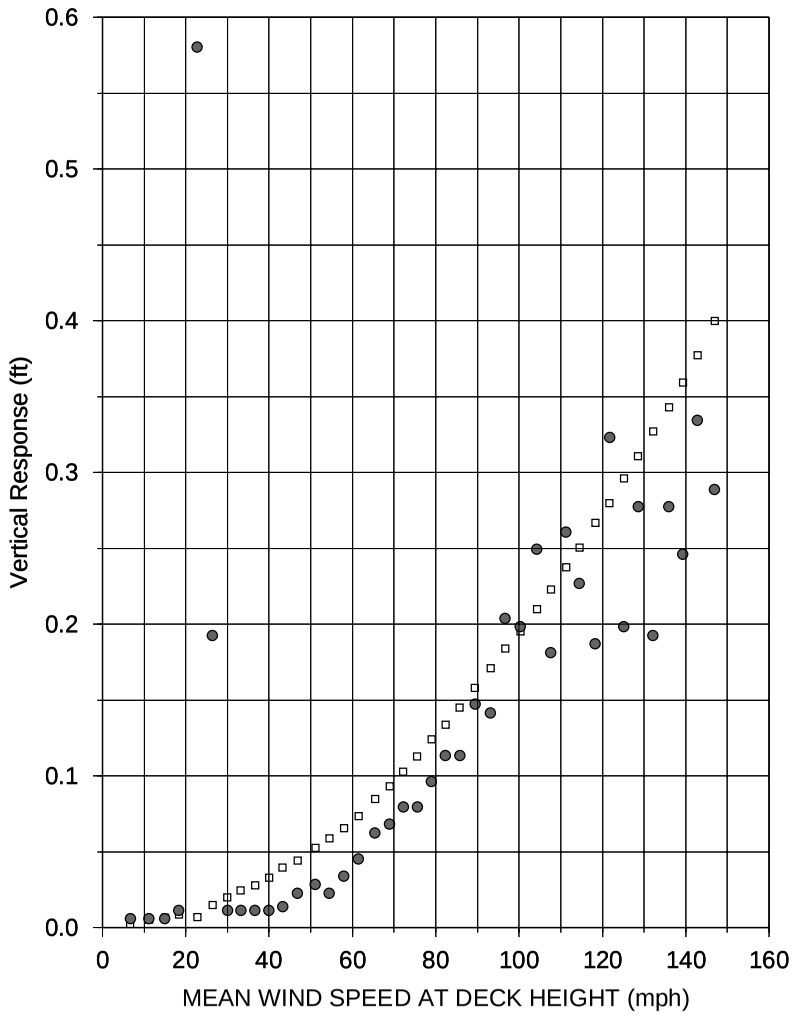

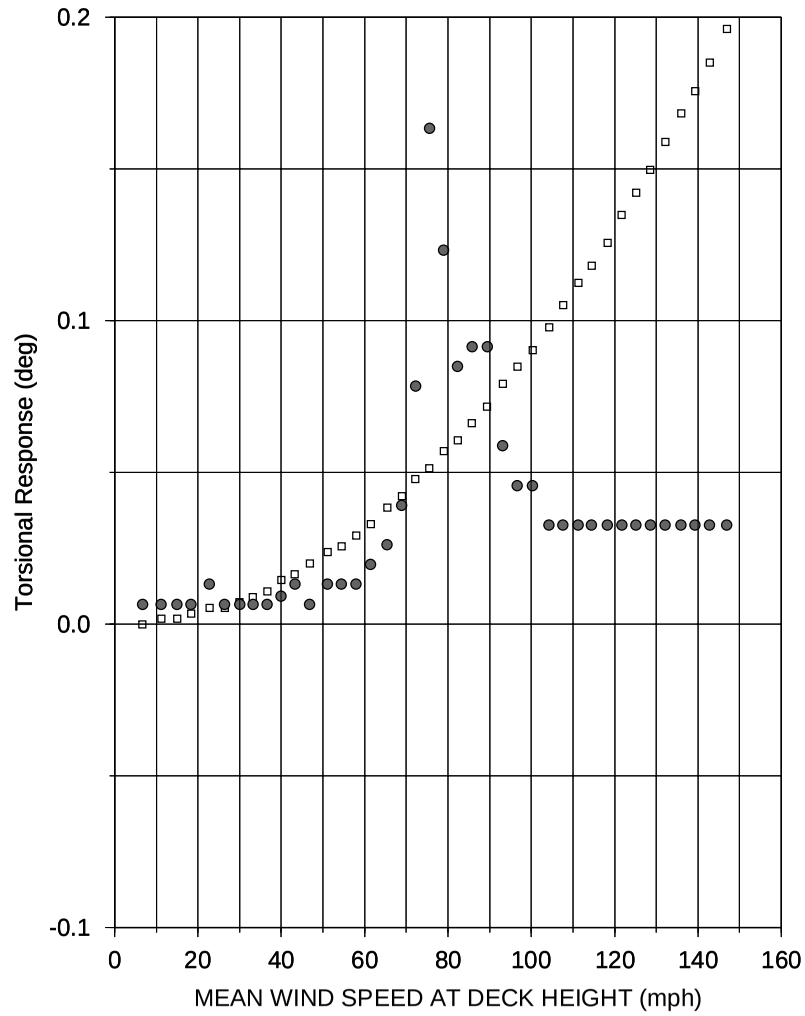

Prospect Verona, sidewalk downstream, smooth flow, 0.5% damping, 0 degrees

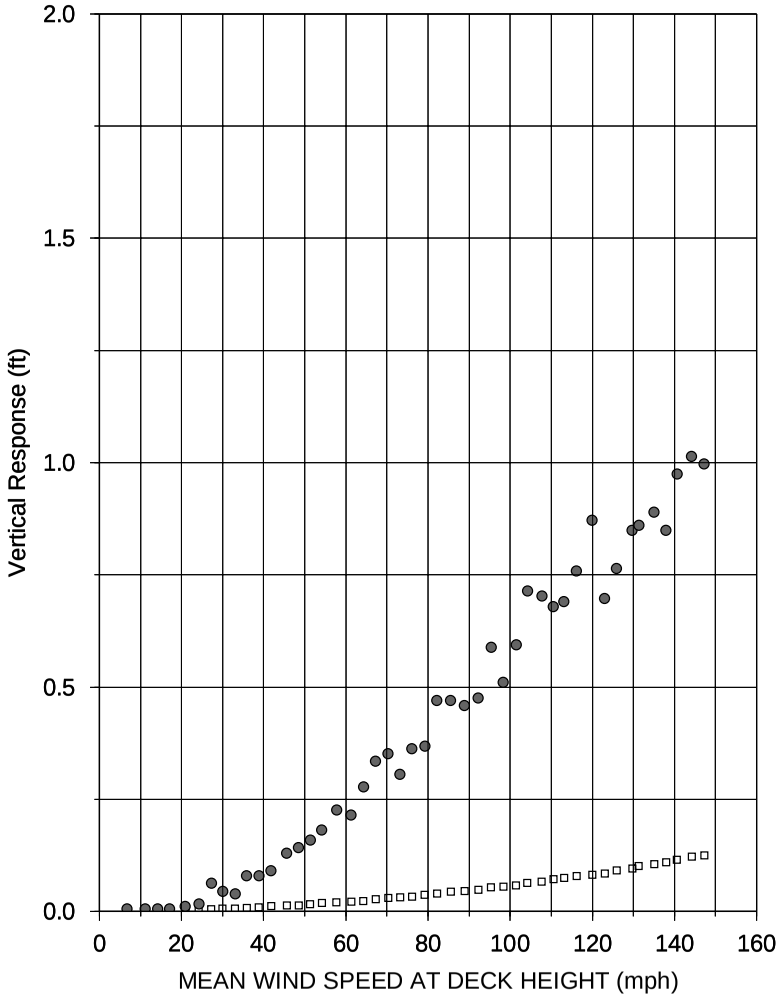

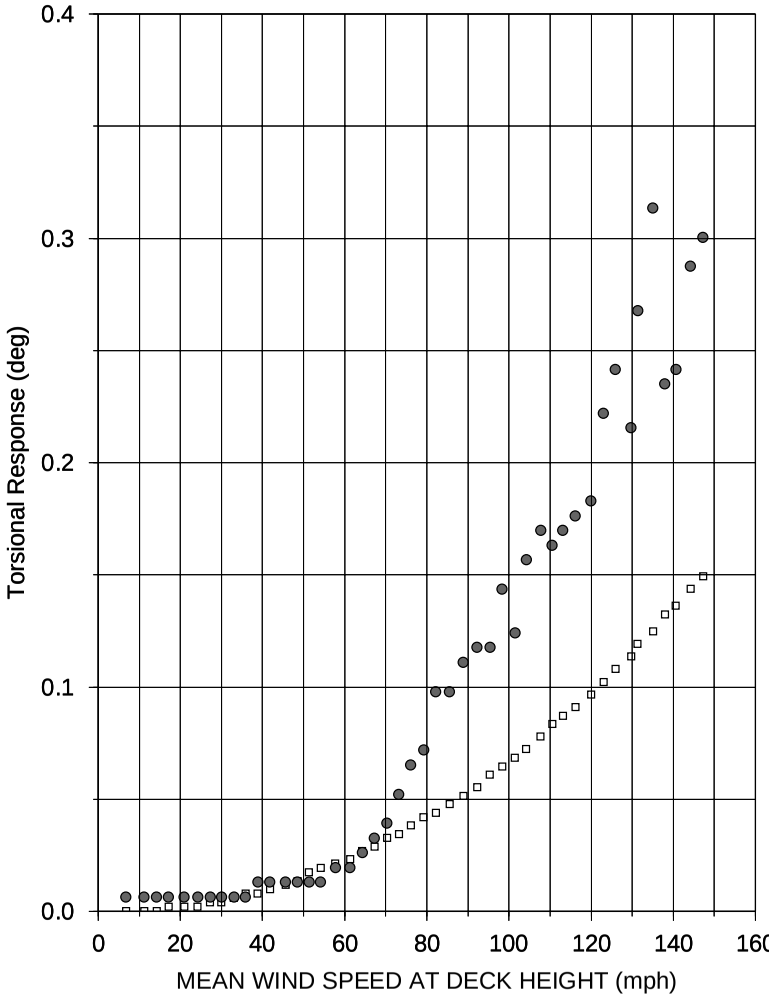

Prospect Verona, sidewalk downstream, turbulent flow, 0.5% damping, 0 degrees

APPENDIX C

RESULTS OF STATIC SECTION MODEL TESTS

TABLE C1 STATIC FORCE COEFFICIENTS (NO SIDEWALK), SMOOTH FLOW

Angle of Attack	Cx	Cz	Cm
-10	0.39455	-0.21665	0.089258
-9	0.396079	-0.13002	0.102209
-8	0.394058	-0.03931	0.115827
-7	0.388132	0.050262	0.128527
-6	0.37932	0.140506	0.139508
-5	0.366372	0.23054	0.150851
-4	0.360798	0.295682	0.16204
-3	0.346472	0.374409	0.168402
-2	0.338713	0.426248	0.172505
-1	0.329796	0.467381	0.17136
0	0.323554	0.483535	0.167679
1	0.322412	0.483305	0.164508
2	0.322356	0.47112	0.161926
3	0.32274	0.448058	0.159904
4	0.324364	0.418435	0.158329
5	0.325596	0.382916	0.15699
6	0.325218	0.333956	0.154164
7	0.322934	0.278366	0.149613
8	0.320972	0.230341	0.143574
9	0.321257	0.210818	0.137885
10	0.324964	0.214826	0.13486

Slope of Cz Curve =	0.61
Slope of Cm Curve =	-0.16
Cz at 0° =	0.484
Cx at 0° =	0.324
Cm at 0° =	0.168

TABLE C2 STATIC FORCE COEFFICIENTS (NO SIDEWALK), TURBULENT FLOW

Angle of Attack	Cx	Cz	Cm
-10	0.296552	-0.19145	0.065211
-9	0.299308	-0.14174	0.074398
-8	0.300704	-0.09074	0.084058
-7	0.30018	-0.04479	0.092938
-6	0.29651	0.000299	0.101507
-5	0.294937	0.038811	0.109747
-4	0.288432	0.074414	0.116267
-3	0.281805	0.104511	0.121909
-2	0.275181	0.128083	0.125873
-1	0.269276	0.144769	0.12863
0	0.260501	0.160723	0.128766
1	0.255931	0.175032	0.129085
2	0.248568	0.186701	0.12669
3	0.244568	0.201493	0.12462
4	0.237998	0.213927	0.119437
5	0.238078	0.239384	0.11784
6	0.235189	0.257437	0.113603
7	0.2363	0.279994	0.110892
8	0.239533	0.301592	0.108932
9	0.24192	0.319516	0.106268
10	0.24482	0.334105	0.10417

Slope of Cz Curve =	0.85
Slope of Cm Curve =	0.01
Cz at 0° =	0.161
Cx at 0° =	0.261
Cm at 0° =	0.129

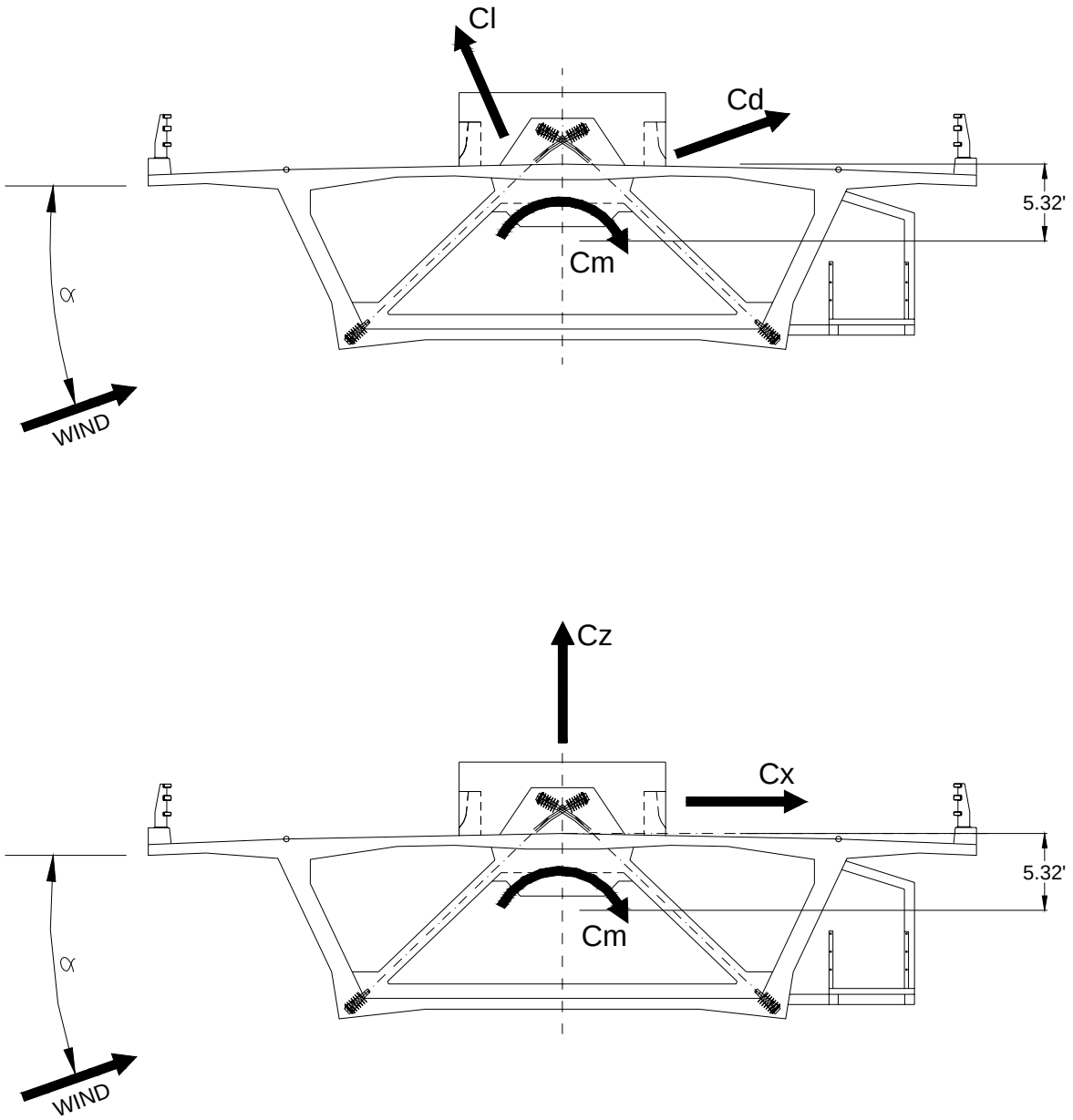

FIGURE C1 SKETCH SHOWING SIGN CONVENTION OF FORCES

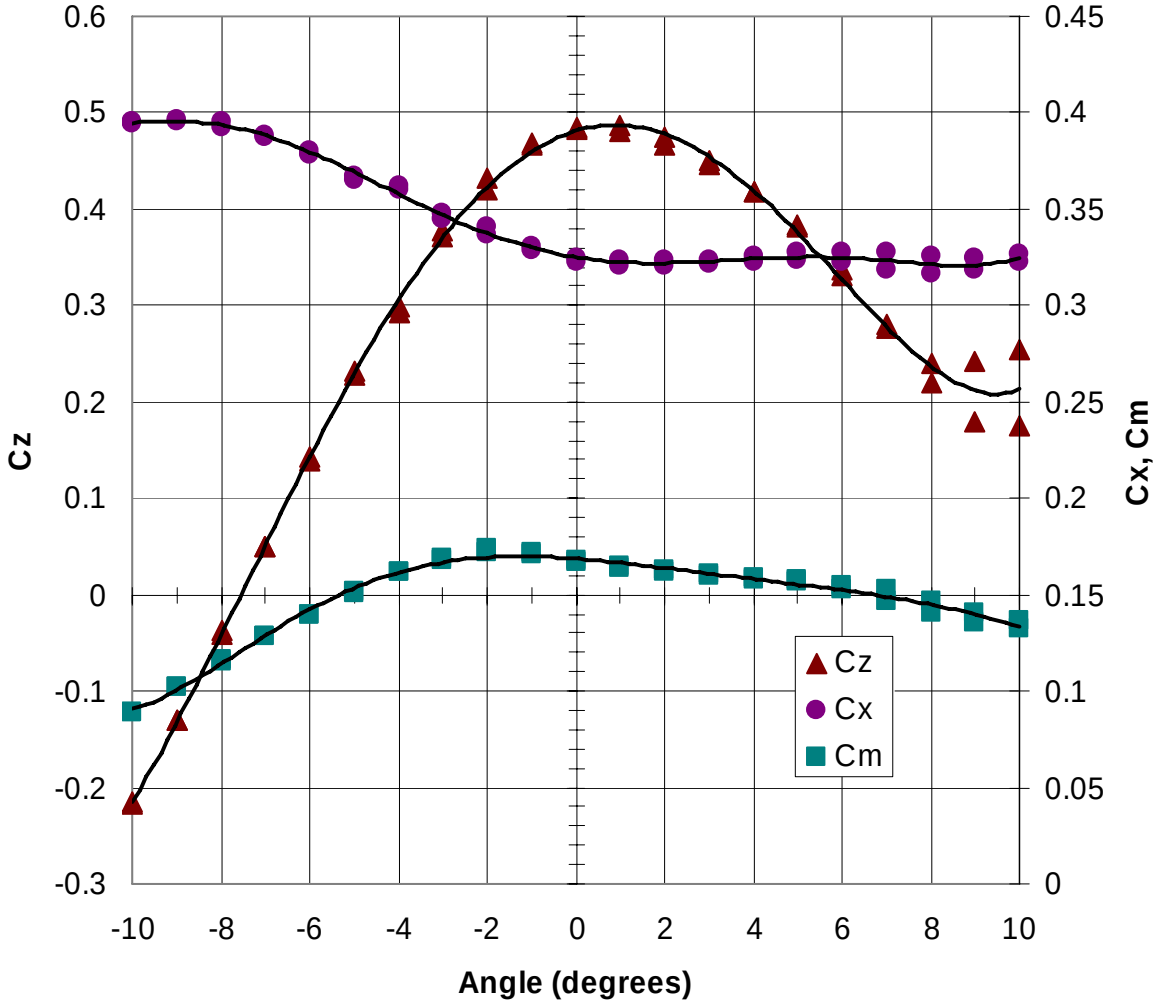

FIGURE C2 STATIC LOAD COEFFICIENTS (NO SIDEWALK) - SMOOTH FLOW

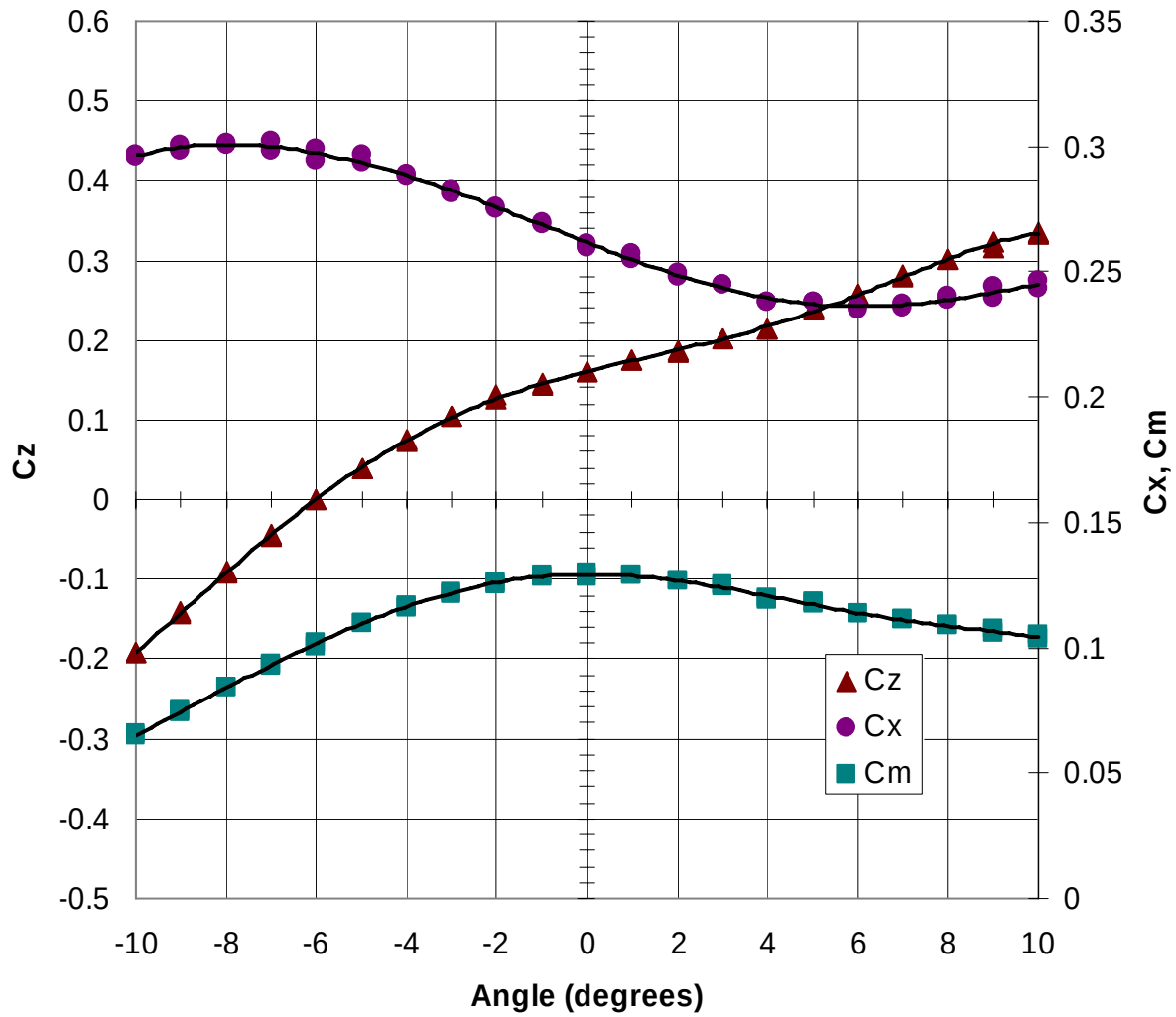

FIGURE C3 STATIC LOAD COEFFICIENTS (NO SIDEWALK) - TURBULENT FLOW

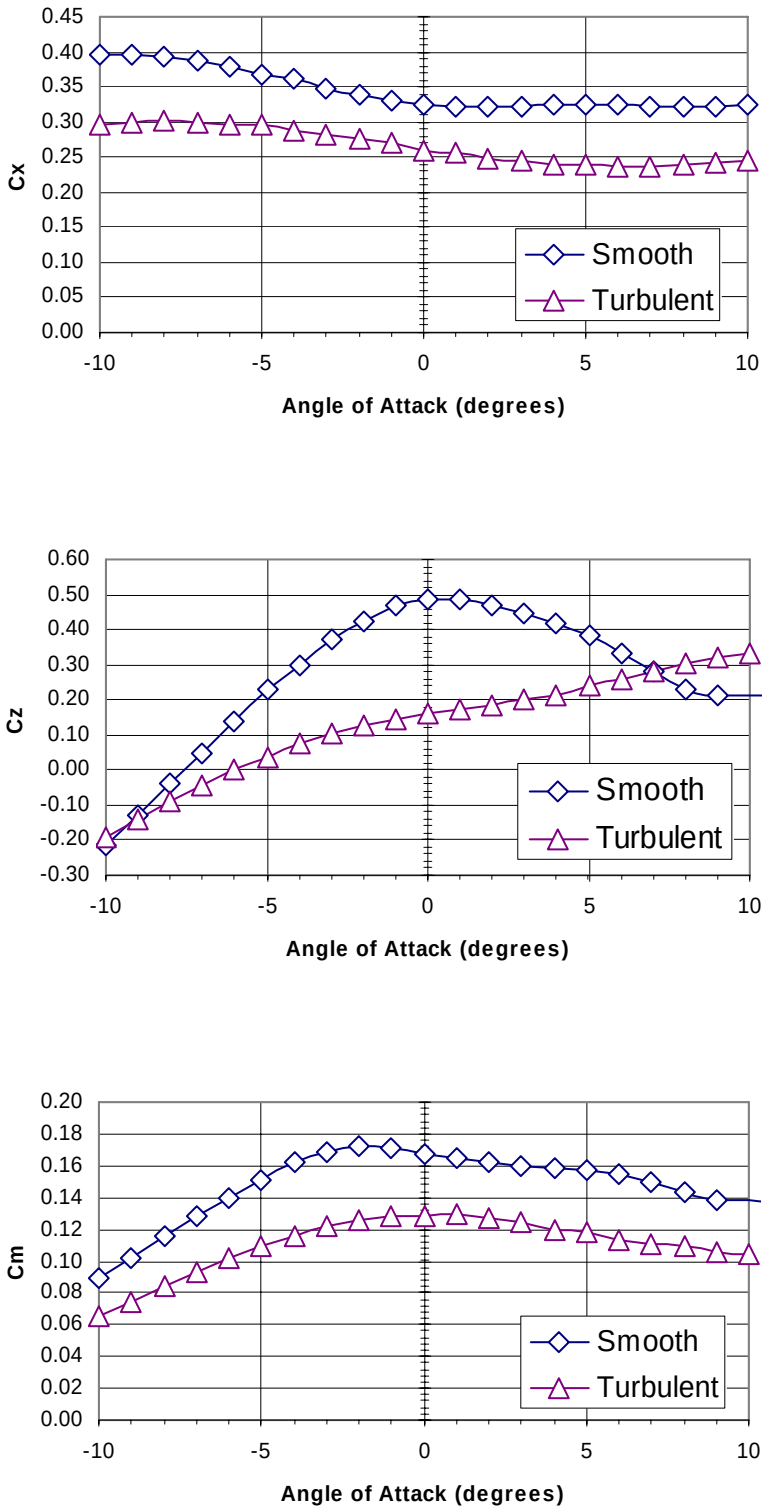

FIGURE C4 STATIC LOAD COEFFICIENTS (NO SIDEWALK)

TABLE C3 STATIC FORCE COEFFICIENTS (SIDEWALK UPSTREAM), SMOOTH FLOW

Angle of Attack	Cx	Cz	Cm
-10	0.383994	-0.22814	0.052889
-9	0.382287	-0.16552	0.063548
-8	0.376903	-0.09036	0.075382
-7	0.373273	-0.01639	0.087027
-6	0.366016	0.054704	0.099406
-5	0.359968	0.117569	0.111062
-4	0.347756	0.179561	0.118139
-3	0.336734	0.231531	0.121469
-2	0.325079	0.267846	0.120364
-1	0.317036	0.277684	0.116249
0	0.311976	0.266291	0.110324
1	0.30728	0.239733	0.102825
2	0.30632	0.209024	0.096837
3	0.304642	0.182244	0.090081
4	0.30477	0.17612	0.084902
5	0.307731	0.194891	0.082582
6	0.311406	0.215378	0.081225
7	0.318523	0.247876	0.082027
8	0.325235	0.276746	0.083157
9	0.332242	0.280649	0.08467
10	0.338547	0.301117	0.086556

Slope of Cz Curve =	-0.89
Slope of Cm Curve =	-0.35
Cz at 0° =	0.266
Cx at 0° =	0.312
Cm at 0° =	0.110

TABLE C4 STATIC FORCE COEFFICIENTS (SIDEWALK UPSTREAM), TURBULENT FLOW

Angle of Attack	Cx	Cz	Cm
-10	0.305689	-0.20837	0.04058
-9	0.302633	-0.16646	0.047429
-8	0.302369	-0.12573	0.055942
-7	0.294551	-0.08711	0.06159
-6	0.291263	-0.05181	0.068027
-5	0.281989	-0.01922	0.072125
-4	0.275869	0.010221	0.076465
-3	0.268029	0.037634	0.07895
-2	0.261926	0.069558	0.081379
-1	0.253713	0.096858	0.081851
0	0.249122	0.130732	0.08227
1	0.242009	0.164095	0.080843
2	0.238248	0.199132	0.080403
3	0.23445	0.233858	0.078554
4	0.233975	0.266873	0.077288
5	0.234804	0.298326	0.076563
6	0.234155	0.320151	0.074367
7	0.239637	0.344495	0.07501
8	0.240715	0.357647	0.073805
9	0.247416	0.378332	0.07494
10	0.249381	0.38603	0.074595

Slope of Cz Curve =	1.87
Slope of Cm Curve =	-0.02
Cz at 0° =	0.131
Cx at 0° =	0.249
Cm at 0° =	0.082

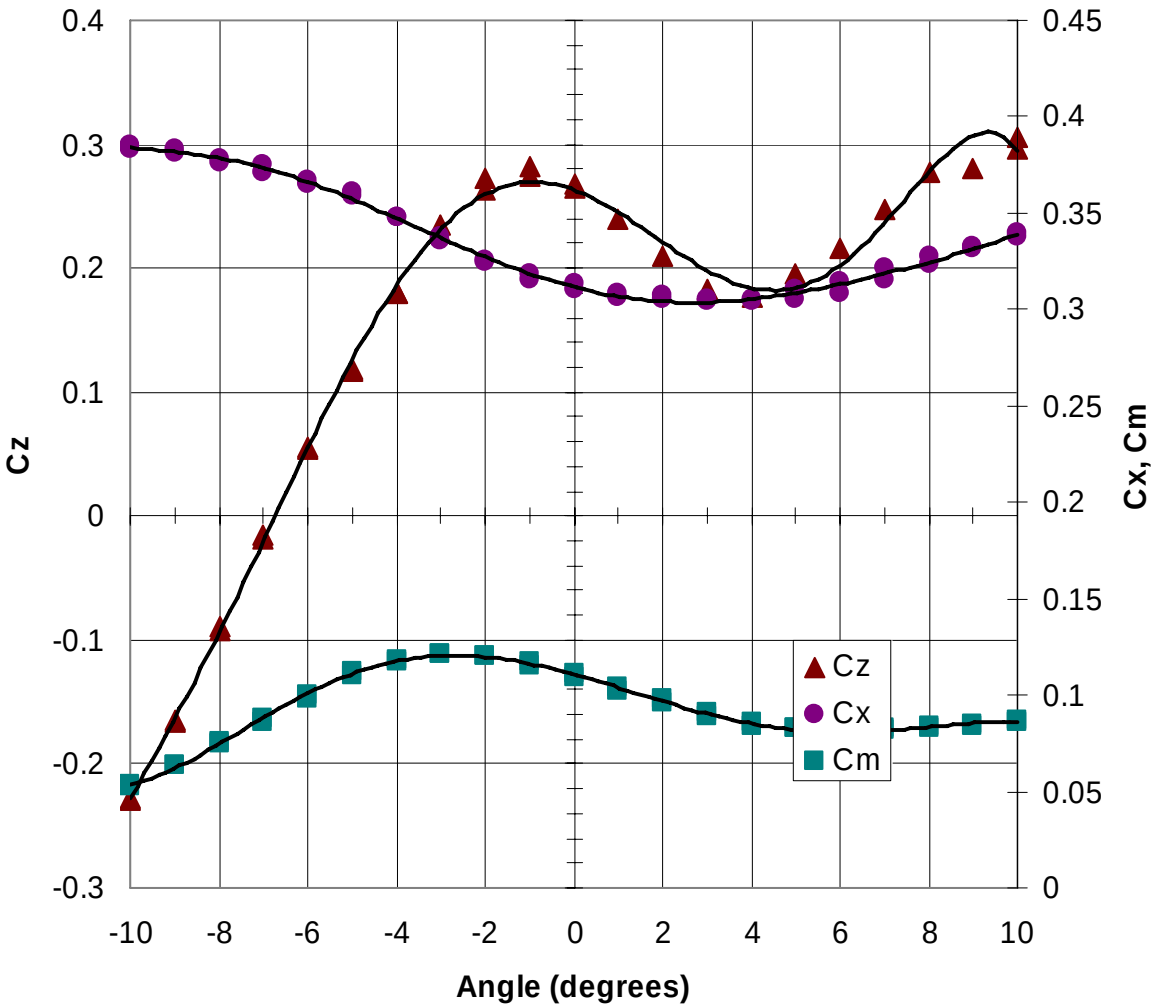

FIGURE C5 STATIC LOAD COEFFICIENTS (SIDEWALK UPSTREAM) - SMOOTH FLOW

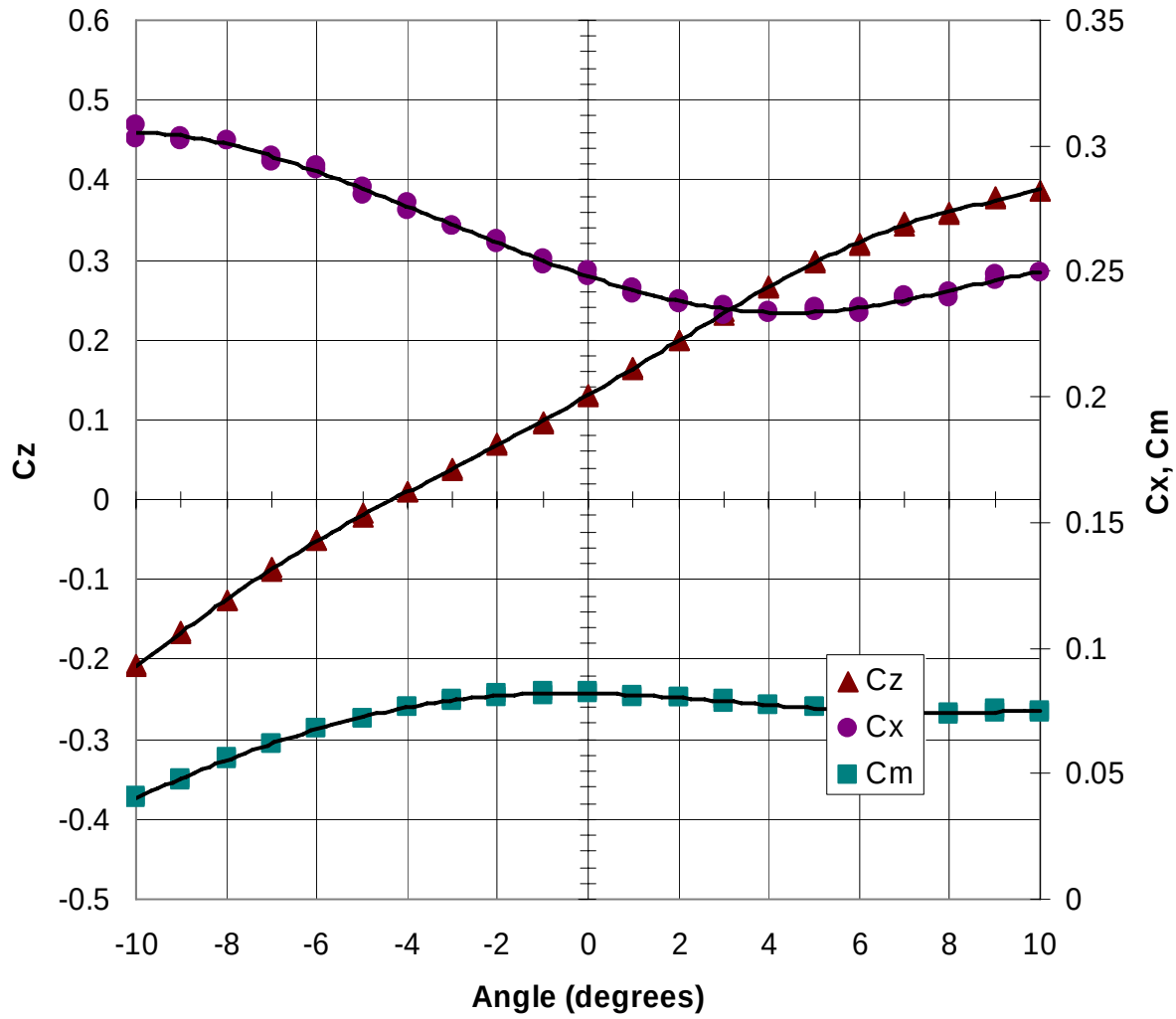

FIGURE C6 STATIC LOAD COEFFICIENTS (SIDEWALK UPSTREAM) - TURBULENT FLOW

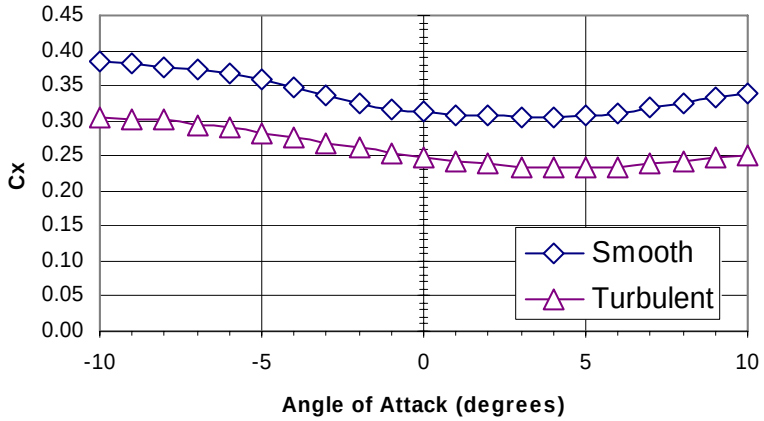

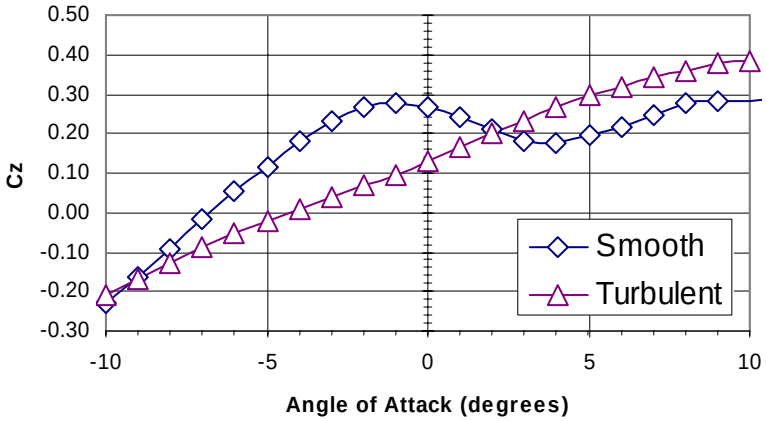

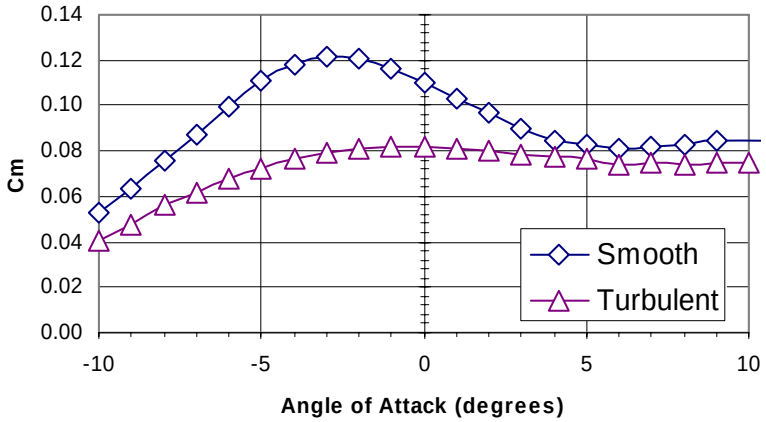

FIGURE C7 STATIC LOAD COEFFICIENTS (SIDEWALK UPSTREAM)

TABLE C5 STATIC FORCE COEFFICIENTS (SIDEWALK DOWNSTREAM), SMOOTH FLOW

Angle of Attack	Cx	Cz	Cm
-10	0.388497	-0.18456	0.092237
-9	0.38903	-0.10076	0.105245
-8	0.386763	-0.0152	0.118861
-7	0.382384	0.069026	0.130903
-6	0.373009	0.155649	0.14224
-5	0.361941	0.23638	0.153442
-4	0.356781	0.295904	0.164279
-3	0.344806	0.36524	0.171069
-2	0.335335	0.402175	0.174876
-1	0.327283	0.4202	0.173836
0	0.322495	0.4341	0.17081
1	0.319138	0.424707	0.165407
2	0.318722	0.41122	0.163658
3	0.318302	0.386513	0.161314
4	0.318322	0.358146	0.158925
5	0.320292	0.32592	0.157419
6	0.320551	0.285334	0.154732
7	0.321712	0.246683	0.148798
8	0.319737	0.210697	0.141994
9	0.319979	0.207995	0.131549
10	0.325722	0.251267	0.122393

Slope of Cz Curve =	0.13
Slope of Cm Curve =	-0.18
Cz at 0° =	0.434
Cx at 0° =	0.322
Cm at 0° =	0.171

TABLE C6 STATIC FORCE COEFFICIENTS (SIDEWALK DOWNSTREAM), TURBULENT FLOW

Angle of Attack	Cx	Cz	Cm
-10	0.290994	-0.20433	0.06669
-9	0.291698	-0.16214	0.074729
-8	0.293514	-0.1189	0.084571
-7	0.288812	-0.07704	0.091915
-6	0.289467	-0.04012	0.101341
-5	0.284386	-0.00455	0.107962
-4	0.281499	0.028283	0.115237
-3	0.274567	0.0557	0.119982
-2	0.26795	0.082512	0.124255
-1	0.262612	0.106009	0.127052
0	0.252551	0.126985	0.125692
1	0.249138	0.153735	0.126551
2	0.227699	0.155892	0.124304
3	0.190331	0.162541	0.125771
4	0.179423	0.222614	0.129178
5	0.170926	0.287198	0.132544
6	0.164581	0.35668	0.136291
7	0.160555	0.418101	0.136229
8	0.156745	0.484795	0.136534
9	0.154472	0.536493	0.133447
10	0.154984	0.575914	0.134015

Slope of Cz Curve =	1.11
Slope of Cm Curve =	0.00
Cz at 0° =	0.127
Cx at 0° =	0.253
Cm at 0° =	0.126

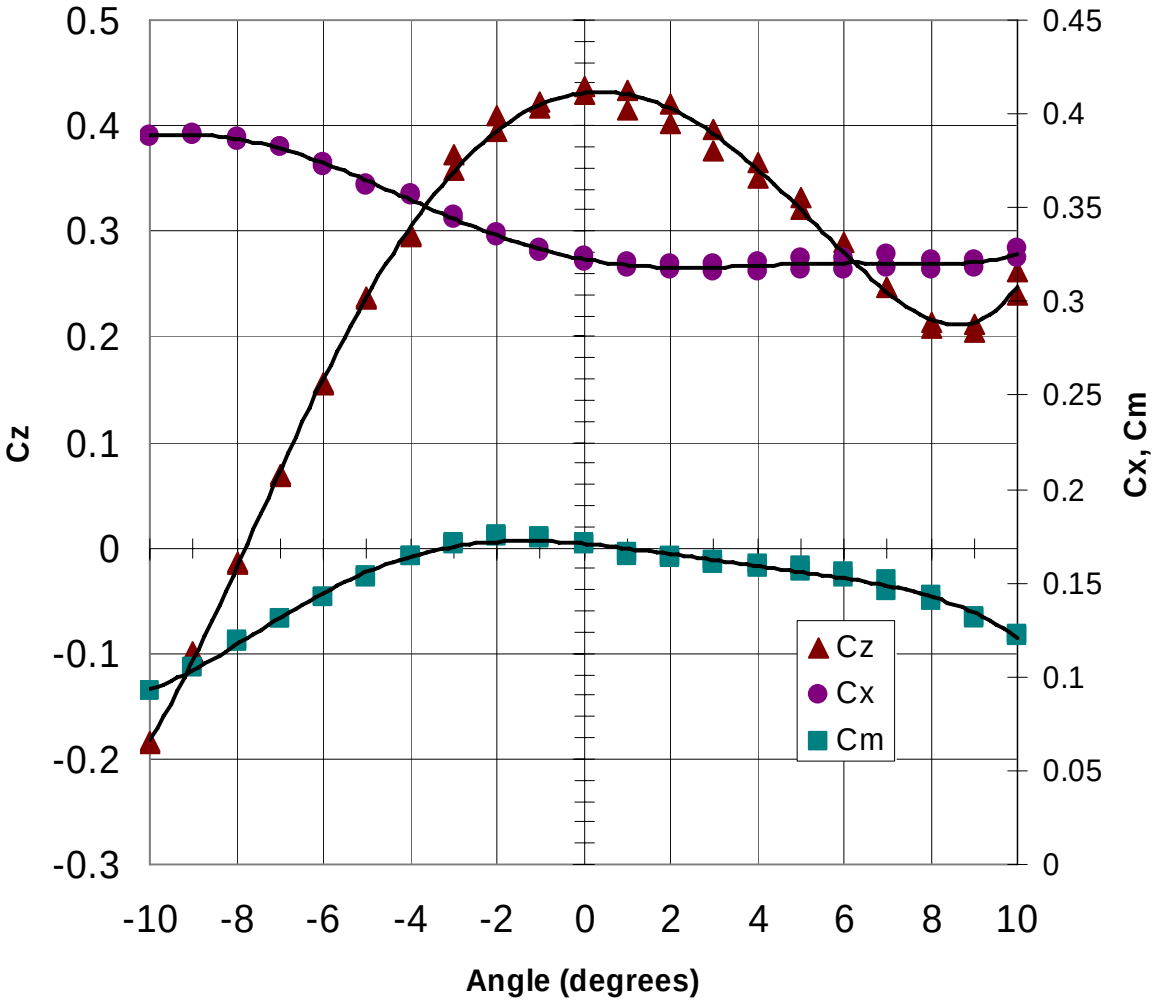

FIGURE C8 STATIC LOAD COEFFICIENTS (SIDEWALK UPSTREAM) - SMOOTH FLOW

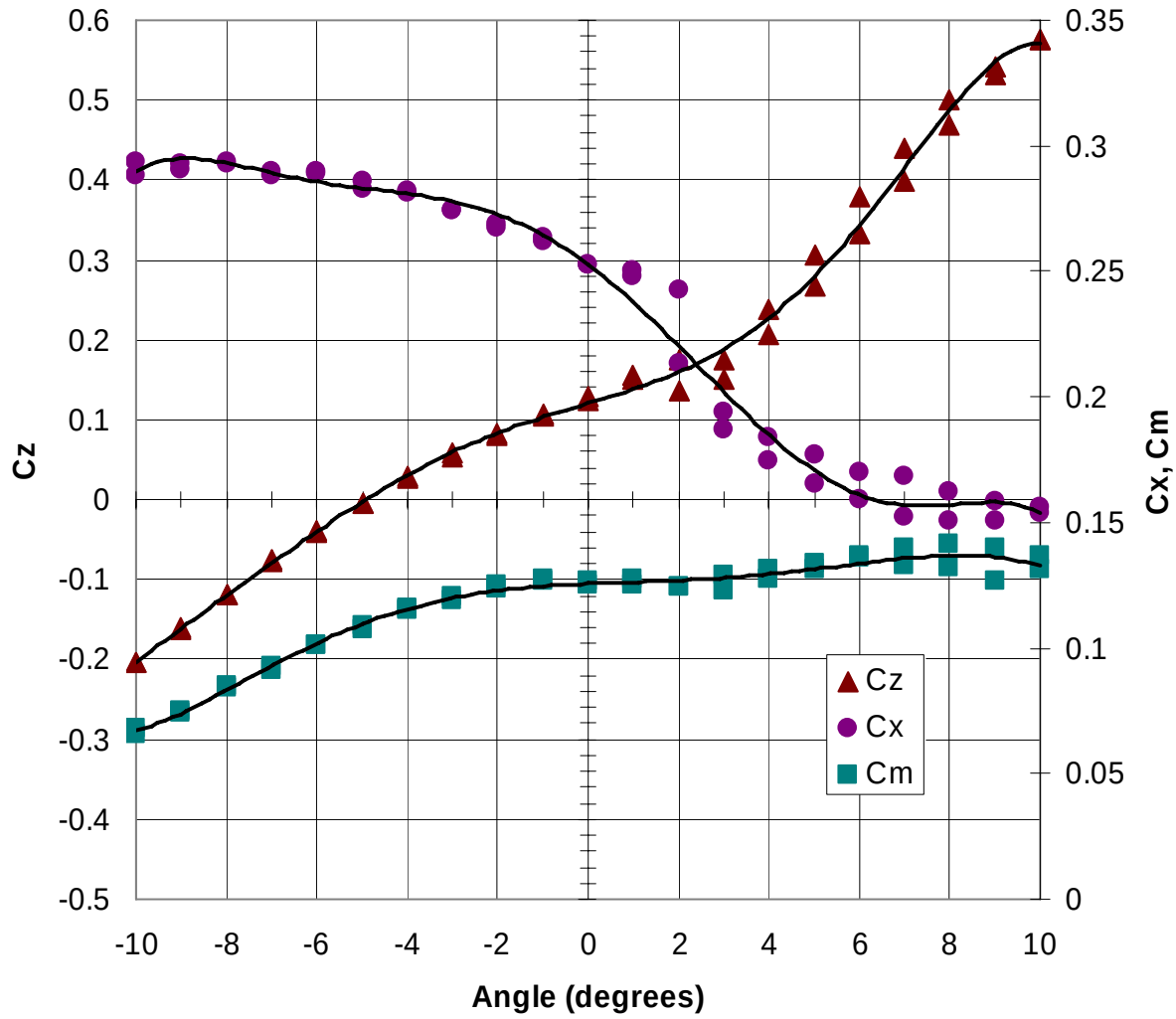

FIGURE C9 STATIC LOAD COEFFICIENTS (SIDEWALK UPSTREAM) - TURBULENT FLOW

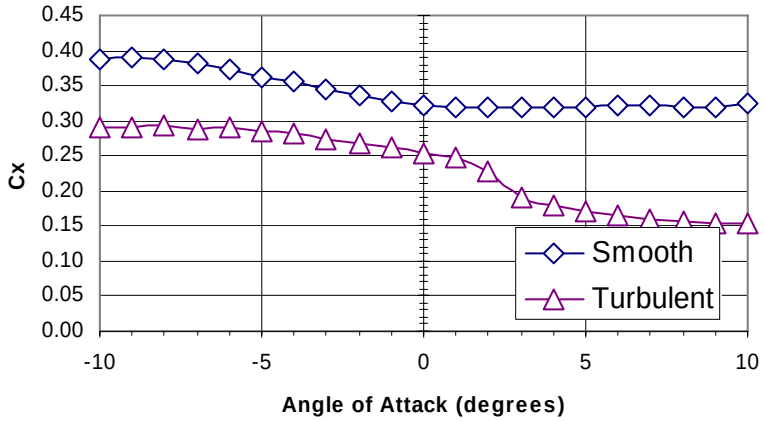

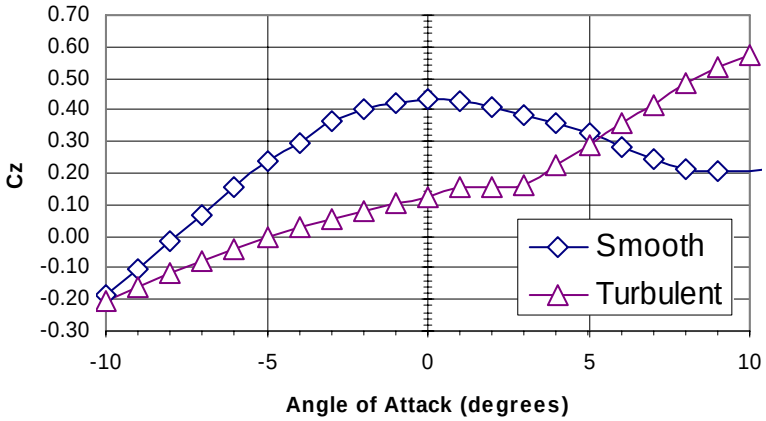

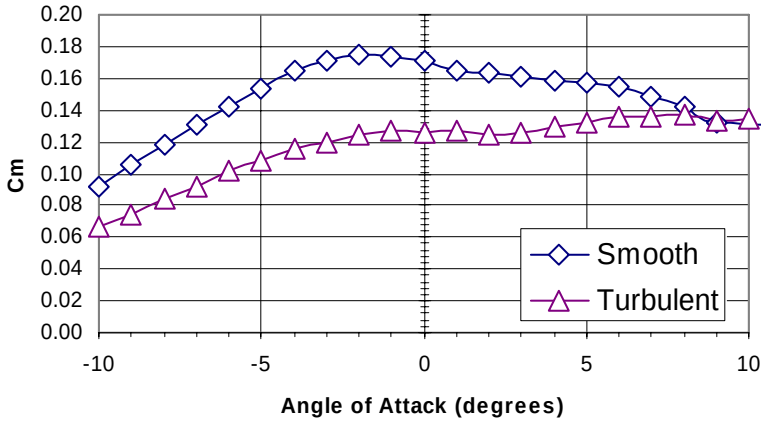

FIGURE C10 STATIC LOAD COEFFICIENTS (SIDEWALK UPSTREAM)

APPENDIX D

FLUTTER INSTABILITY CRITERIA

The definition of “flutter” used in this report is related to the “peak factor”, which is defined as the ratio of the largest observed reading during the sample period to the Root Mean Square (RMS) of the sample. Each of the data points on the response plots result from the measurements of real, stable, limited amplitude motion as opposed to a negative total damping case where the amplitude continues to grow in magnitude for the same wind speed. The peak factor can be used to see whether the motion is in a “locked-in” state of sinusoidal motion or only a random type motion.

The onset of a “flutter instability” is defined as when the character of the response changes from a random type motion to that of a regular, sinusoidal motion, involving either pure torsional or a coupled vertical-torsional vibration. This can be clearly identified through an examination of the peak factor. A random signal has peak factors in the 3-4 range, while a sinusoid has a peak factor of $\sqrt{2}$ or 1.41. For the purposes of this investigation, a peak factor of less than 2 was selected as the governing criteria.

There are other definitions of flutter that have been used by this Laboratory and other researchers. One could determine a limiting amplitude beyond which the response is unacceptable. This criterion was used for the Tsing Ma Bridge [D1] and Ting Kau Bridge [D2] studies with a limiting RMS torsional amplitude of 0.5^0 (or a peak amplitude of 3.5^0 on the response plots).

Another method, has been also used, is based on the steepness of the response curves with wind speed to determine flutter instability. This has some logic associated with it since there is a very definite chance in the character of the response from a uniform, steady growth with wind speed to that which is becoming alarmingly violent. However, the steepness of the curves is highly dependent on the total damping of the structure (structure plus aerodynamic damping). In the low wind speed areas, the structural term dominates (or the aerodynamic term is positive). In the high wind speed range, the aerodynamic term dominates and is negative, but does not yet exceed the structural term in magnitude. Infinite amplitudes occur when the total damping becomes equal to zero or negative, since response is inversely proportional to the total damping.

REFERENCES - APPENDIX D

D1. King, J.P.C. and Davenport, A.G., "Lantau Fixed Crossing - Tsing Ma Bridge, Full Aeroelastic Model Tests of Completed Bridge", The University of Western Ontario, Faculty of Engineering Science Research Report, BLWT-SS11-1997, London, Ontario, Canada, 1997.

D2. King, J.P.C. and Davenport, A.G., "Ting Kau Bridge - Wind Tunnel Report", The University of Western Ontario, Faculty of Engineering Science Research Report, BLWT-SS29-1995, London, Ontario, Canada, 1995.

APPENDIX E

DYNAMIC WIND FORCES ON LONG SPAN BRIDGES USING EQUIVALENT STATIC LOADS

E1: INTRODUCTION

The conventional treatment of wind loading on long span bridges has tended to consider the static design wind loading used in normal strength design, and the aerodynamic stability as two separate and distinct aspects. The procedure described in this appendix takes a more unified approach. It depends on the measurement of the dynamic response of section models to grid turbulence rather than smooth flow. The response is corrected for discrepancies in the intensity and spectrum of turbulence, the damping, and the Joint Acceptance Function for the mode shape. A small correction is also added for the deficiency in low frequency excitation from grid turbulence. The design loads are found from the estimates of dynamic motion in the lowest symmetric and asymmetric modes as well as the mean load. This approach is an outgrowth of earlier studies in turbulent flow on the Murray MacKay Bridge(E1), the Bronx-Whitestone Bridge(E2), and Sunshine Skyway Bridge(E3).

E2: THE DESCRIPTION OF DESIGN LOADS

The persistent movements of any long span bridge (E4, E5) in strong wind are organized through its various mode shapes - horizontal, vertical, and torsional. They cover a range of frequencies but take place mostly at or near the individual modes and have a random character due to the continual shifts in phase and amplitude. To summarize the variety of load actions which the dynamic movements will produce in a severe wind storm, a wind load description for design has been proposed as in Figure E1. In this, *x, z* and θ denote the horizontal (downwind), vertical (upward) and torsional (nose-up) components; (see Figure E2); $\overline{W}$, W_1 and W_2 are the mean, symmetric and antisymmetric components per unit length of deck; $\overline{\alpha}, \alpha_1(\eta)$ and $\alpha_2(\eta)$ are the mean and modal load distribution functions; γ_1 and γ_2 are statistical load combination factors and take on ± 1.0 if only one modal term is included; ± 0.8 for two terms; ± 0.7 for three terms and ± 0.6 for four or more terms.

The description of the mean time average wind load components produced by the mean wind is straightforward. They are defined through the force coefficients $C_x(\alpha), C_z(\alpha)$ and $C_\theta(\alpha)$ which may be measured for a range of angles of attack α, the deck width *B*, and the mean reference velocity pressure at deck height *H*, $q_H = \frac{1}{2}\rho U_H^2$. The three mean forces per unit length are then:

$$\overline{W}_x = q_H B C_x(0^0), \overline{W}_z = q_H B C_z(0^0), \overline{W}_\theta = q_H B^2 C_\theta(0^0) \qquad \text{(E1)}$$

Two points should be made. First the coefficients in turbulent flow may differ from those in smooth flow. Second, normally only horizontal mean winds need to be considered. Only in steep mountainous valleys is there likely to be any appreciable inclination to the mean flow.

E3: EVALUATION OF THE MODAL LOAD COMPONENTS W_1 AND W_2

Although the response of a suspension bridge has been represented by coupled vertical and torsional equations of motion (E6, E7), in fact the aerodynamic coupling terms are usually negligible, and the aerodynamic stiffness terms are usually small in comparison to the stiffness of the bridge itself. This leaves the aerodynamic damping as the most significant aerodynamic force induced by motion. If this is negative and numerically greater than the structural damping, large motion will result. The response of each uncoupled mode of vibration to the turbulent wind can be studied separately and superimposed at the end; usually, only the lowest modes are significant.

We can represent the peak modal load amplitude by the following:

$$W = g\sqrt{\sigma_{wb}^2 + \sigma_{wr}^2} \qquad \text{(E2)}$$

where g is a statistical peak factor, σ_{wb}^2 is the mean square background excitation acting quasi-statically, and σ_{wr}^2 is the mean square excitation at or near the resonant frequency.

The two components of the excitation can be identified in the typical power spectrum shown in Figure E3. The background excitation covers a broad frequency band below the natural frequency; the resonant excitation is concentrated in a peak at the natural frequency, the height of which is controlled by the damping. The two components can be estimated from the following expressions:

$$\sigma_{wbx,z,\theta}^2 = \int_0^\infty f^* S_{Fx,z,\theta}\left(f^*\right) \bullet \left|J_{x,z,\theta}\left(f^*\right)\right|^2 \bullet d\left(\ln f^*\right) \qquad \text{(E3a)}$$

$$\sigma_{wrx,z,\theta}^2 = \frac{(\pi/4)}{\left(\zeta_s + \zeta_a\left(f_o^*\right)\right)} \bullet f_o^* S_{Fx,z,\theta}\left(f_o^*\right) \bullet \left|J_{x,z,\theta}\left(f_o^*\right)\right|^2 \qquad \text{(E3b)}$$

In the above, the subscripts x,z,θ imply the equations are written for each variable in turn; f* and f_o^* are the reduced frequencies fB/U_H and f_0B/U_H ; ζ_s and $\zeta_s(f^*)$ are the structural damping and aerodynamic damping at frequency f*; $f^* S_{Fx,z,\theta}$ (f*) is the power spectral density of the externally induced x, z, θ components on a cross-section of the bridge deck at the reduced frequency f*; $\left|J_{x,z,\theta}\left(f^*\right)\right|$ is the "Joint Acceptance Function", relating the generalized modal force component with the mode shape and the force components at frequency f* at cross-sections of the bridge and involves the spanwise correlation of the forces.

The external forces on a bridge cross-section arise from either the direct action of turbulence in the wind or through the action of flow fluctuations in the wake. The latter are commonly described as vortex shedding. We can write:

$$f^* S_F\left(f^*\right) = \left(f^* S_F\left(f^*\right)\right)_{turb} + \left(f^* S_F\left(f^*\right)\right)_{wake} \qquad \text{(E4)}$$

The turbulent term can be written:

$$\left(f^* S_F\left(f^*\right)\right)_{turb} = (q_H B)^2 \bullet \left(C_{x.z.\theta}^2 \left|A\left(f^*\right)\right|^2\right) \bullet \left(f^* S_{u,v,w}\left(f^*\right)\right) \qquad \text{(E5)}$$

where:

$f^* S_{u,v,w}\left(f^*\right)$ = the power spectra of the turbulent velocity fluctuations *u,v,w*

$A\left(f^*\right)$ = the "Aerodynamic Admittance" which translates the turbulent velocity fluctuations into forces on a cross section;

$C_{x,z,\theta}$ = a reference aerodynamic coefficient.

The contributions of the turbulence to the expressions for σ_{wb}^2 and σ_{wr}^2 can be written as follows. To simplify the notation we will consider the lift *(z)* force and only include the vertical *(w)* component of turbulence, which normally will dominate.

$$\left(\sigma^2_{wbz}\right) = \left(q_H B C'_z\right) \bullet \left(\frac{\sigma_w}{\overline{U}_H}\right)^2 \bullet \int_0^\infty \frac{f^* S_w\left(f^*\right)}{\sigma_w^2} \bullet \left|A\left(f^*\right)\right|^2 \bullet \left|J_z\left(f^*\right)\right|^2 d\left(\ln f^*\right) \qquad \text{(E6)}$$

$$\left(\sigma^2_{wrz}\right) = \left(q_H B C'_z\right) \bullet \left(\frac{\sigma_w}{\overline{U}_H}\right)^2 \bullet \frac{f_0^* S_w\left(f_0^*\right)}{\sigma_w^2} \bullet \left|A\left(f_0^*\right)\right|^2 \bullet \left|J_z\left(f_0^*\right)\right|^2 \frac{(\pi/4)}{\left(\zeta_s + \zeta_s\left(f_0^*\right)\right)} \qquad \text{(E7)}$$

The coefficient C'_z denotes ($aC_z/a\alpha$). Similar expressions for the torsion can be written with θ replacing z and introducing an additional factor B^2. For the drag direction, $2C_x$ replaces C'_z and u replaces w.

If the left hand terms are normalized by the $\left(q_H B C'_z\right)^2$ term, the response is a function primarily of the reduced frequency f* and the intensity of turbulence $\left(\sigma_{w'}\overline{U}_h\right)$, two homologous quantities which link the full-scale bridge behavior with any dynamically scaled model. Otherwise, the turbulence controlled response is bound up in the functional form of the turbulence spectrum, S_w, the aerodynamic admittance, A_z, the Joint Acceptance Function, J_z, and the aerodynamic damping .

The Aerodynamic Admittance reflects the efficiency of the bridge deck as a lift generator, as well as the correlation of the flow in the vicinity of the deck. The theoretical and observed form of this function is shown in Figure E8. The Joint Acceptance Function can be written:

$$\left|J_z\left(f^*\right)\right|^2 = \int_0^L \int_0^L R_{F_1F_2}\left(\eta_1, \eta_2; f^*\right) \mu(\eta_1) \mu(\eta_2) d\eta_1 d\eta_2 \qquad \text{(E8)}$$

where $\mu(\eta) =$ the mode shape with unit mean square amplitude; and

$$R_{F_1F_2}\left(\eta_1, \eta_2; f^*\right) = exp\left(-cf^* \frac{L}{B} \frac{|\eta_1 - \eta 2|}{L}\right) \qquad \text{(E9)}$$

In which c is a constant which defines the effective width of the correlation. A similar expression can be written for the spanwise cross-correlation of the velocity component in which case c=8 is representative. It is reasonable to assume the same value holds for the forces F_1 and F_2 on the basis of the "strip assumption".

Equations (E6) and (E7) apply to both the full scale bridge and a model in a turbulent wind tunnel flow. Ideally the latter should be an exact scaling of the former. This ideal, however, is difficult to satisfy in the wind tunnel and some compromises may have to be made. There are significant advantages to using an elongated section model in a turbulent flow generated behind a coarse grid. Although the turbulence scale and intensity cannot be made to exactly correspond to full scale, the values can be made sufficiently close.

To adapt the results of the dynamic section model testing to full scale, corrections need to be applied as follows: (a) Corrections of the low frequency quasi-static, "background" response, σ^2_{wb}, largely omitted from the section model due to the deficit in the vertical velocity spectrum generated by the grid. This can be estimated with reasonable accuracy from equation (E6) using either theoretical or experimental data as outlined below. (b) Correction of the terms in the resonant response σ^2_{wr} for the discrepancies in the turbulence intensity, vertical velocity spectrum, Joint Acceptance Function and damping. No correction is needed in the Aerodynamic Admittance. The following formula encompasses these corrections:

$$\left(\sigma^2_{wr}\right)_{full\ scale} = \left(\sigma^2_{wr}\right)_{mod\ el} \bullet \phi_{\sigma w} \bullet \phi_{sw} \bullet \phi_J \bullet \phi_\zeta \qquad \text{(E10)}$$

Where the terms $\phi_{\sigma w}, \phi_{Sw}, \phi_J$ *and* ϕ_ζ reflect corrections to the terms in the response due to the discrepancies between the section model and the full scale. These correction factors are found from the ratios of the quantities involved for model and full-scale. Through the appropriate selection of turbulence characteristics in the section model test and the model length, these corrections are relatively small. This last fact should lead to satisfactory reliability.

E4: EXPERIMENTAL DETERMINATION OF DESIGN LOAD COMPONENTS

The wind tunnel testing of the section models of the two Sunshine Skyway Bridge alternates provided an opportunity to apply the proposed method. The proposed structure, over Tampa Bay in Tampa, Florida is a cable-stayed design with a 366m main span. The concrete alternate used a precast, segmental box girder 29.03m wide and 4.27m deep. Two single strut pylons carry a system of radiating stays located on the longitudinal axis of the bridge (Figure E4).

The model of the 1 in 80 scale bridge section shown in Figure E5 is 7 ft. (~2m) in length corresponding to a 170m section of the full scale structure. The model was tested with spring mounting giving the correct frequency ratio in lift and torque and 0.5% damping. Measurements of mean and peak dynamic motion are plotted in Figure E6, and show marked differences between smooth and turbulent flow. With smooth flow there is evidence of some coupling between static lift and torque (i.e. the twisting of the deck due to torque modifies the lift). Although not essential to the method, aerodynamic damping and admittance functions were also measured in the experiments.

The large mesh size and bar spacing of the turbulence grid were selected to give a close representation of the natural wind. The measured vertical turbulence intensity behind this grid is found to be 0.05 compared to the expected full scale value of 0.06 over open water. The grid turbulence spectrum and the target full scale spectrum are drawn together in Figure E10 on a double logarithmic scale. Both have similar form, although the full scale has slightly more energy than does the grid turbulence at lower frequency.

E5: DETERMINATION OF DESIGN WIND LOADS

Following equation (E6), the wind load from the background turbulence excitation is found through the integration with reduced frequency of the product of the vertical wind spectrum (Figure E7), Aerodynamic Admittance Function (Figure E8) (assuming the Sears function), and the Joint Acceptance Function for the particular mode (Figure E9). The form of these functions is such that the bulk of the energy is in the range of reduced frequency f^* between 0.01 and 0.1 and any uncertainty of the functional values at these low frequencies generally introduce little error. Added to this is the resonant component following equation (E7). The resonant modal response, measured in terms of deflection has been converted to an equivalent static load through the modal stiffness:

$$\sigma_{w_{rz}} = m(2\pi f_o)^2 \sigma_z; \qquad \sigma_{w_{r\theta}} = I_o(2\pi f_o)^2 \sigma_\theta \qquad \text{(E11)}$$

The correction terms are determined from the ratios of the quantities involved between full scale and model scale. The correction factor for the turbulence intensity, $\phi_{\sigma w}$ is a constant equal to $(.06/.05)^2 = 1.44$ (i.e. this is the ratio of target full scale to model values). Similarly, the correction factor for the vertical velocity spectrum ϕ_{Sw} is shown in Figure E7, the Joint Acceptance Function, ϕ_J, in Figure E9, and the damping, ϕ_ζ, in Figure E10. The addition of the background and resonant components as in equation (E2), results in the loading shown in Figures E11a and b. The final wind speed scaling will depend upon the final design frequencies of the structure. Thus the example wind loads have been determined for a nominal wind speed at deck height based on the estimates of vertical and torsional frequencies noted in the figures. Verification of this procedure, using 1:350 scale aeroelastic models of both the steel and concrete bridges tested in a turbulent boundary layer were excellent (E3).

E6: CONCLUSIONS

A method has been presented whereby wind tunnel section model test results can be incorporated directly into a load format suitable for the definition of the design wind loads of long span structures. The procedure has

been verified experimentally with the satisfactory prediction of the response of two full bridge aeroelastic models to boundary layer shear flow.

REFERENCES - APPENDIX E

E1. Davenport, A.G., Isyumov, N., Fader, D.J. and Bowen, C.F.P., "A Study of Wind Action on a Suspension Bridge During Erection and Completion", University of Western Ontario, Faculty of Engineering Science, Research Report BLWT-3-1969, London, Ontario, Canada, May 1969 and March 1970.

E2. Davenport, A.G., Isyumov, N., Rothman, H. and Tanaka, H., "Wind Induced Response of Suspension Bridges, Wind Tunnel Model and Full Scale Observations", Proc. 5th Int. Conf. Wind Engineering, Ft. Collins, Colorado, 1979, pp. 807-824.

E3. Davenport, A.G. and King, J.P.C., "The Incorporation of Dynamic Wind Loads into the Design Specifications For Long Span Bridges", ASCE Fall Convention, New Orleans, La., 1982.

E4. Tanaka, H. and Davenport, A.G., "Wind Induced Response of Golden Gate Bridge", University of Western Ontario, Faculty of Engineering Science Research Report, BLWT-1-1982, Paper accepted for publication by JSD, ASCE, June 1982.

E5. Melbourne, W.H., "Model and Full Scale Response to Wind Action of the Cable Stayed Box Girder West Gate Bridge", Practical Experience With Flow Induced Vibrations, Symposium Karlsruhe, Germany, 1979, pp. 625-652.

E6. Ukeguchi, N., Sakata, H. and Nishitani, H., "An Investigation of Aeroelastic Instability of Suspension Bridges", Proc. International Symposium on Suspension Bridges, Lisbon, 1966, pp. 273-284.

E7. Scanlan, R.H., "An Examination of Aerodynamic Response Theories and Model Testing Relative to Suspension Bridges", Proc. Wind Effects on Buildings and Structures, Tokyo, 1971, pp. 941-951.

$$W_x(\eta) = \overline{W}_x\,\overline{a}(\eta) + \gamma_{1_x} W_{1_x}\, a_1(\eta) + \gamma_{2_x} W_{2_x}\, a_2(\eta)$$

$$W_z(\eta) = \overline{W}_z\,\overline{a}(\eta) + \gamma_{1_z} W_{1_z}\, a_1(\eta) + \gamma_{2_z} W_{2_z}\, a_2(\eta)$$

$$W_\theta(\theta) = \overline{W}_\theta\,\overline{a}(\eta) + \gamma_{1_\theta} W_{1_\theta}\, a_1(\eta) + \gamma_{2_\theta} W_{2_\theta}\, a_2(\eta)$$

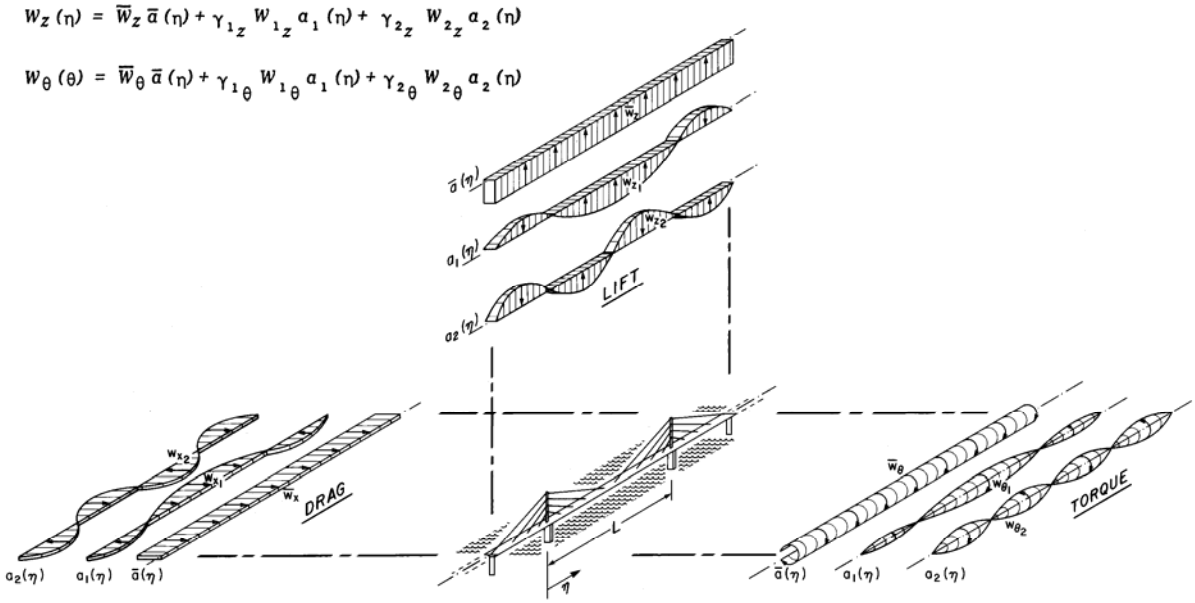

FIGURE E1 DISTRIBUTED WIND LOAD COMPONENTS

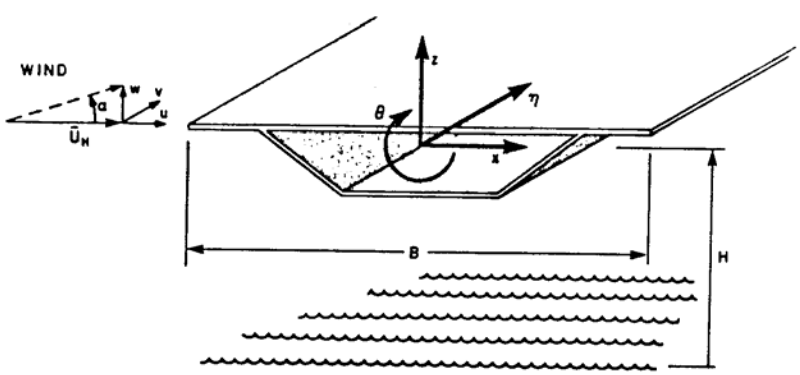

FIGURE E2 NOTATION

$$W_r = g\sqrt{\sigma^2_{W_B} + \sigma^2_{W_R}}$$

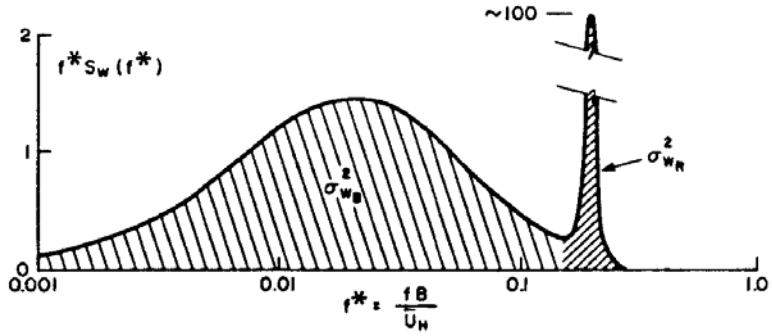

FIGURE E3 SPECTRUM OF MODAL LOAD AMPLITUDE

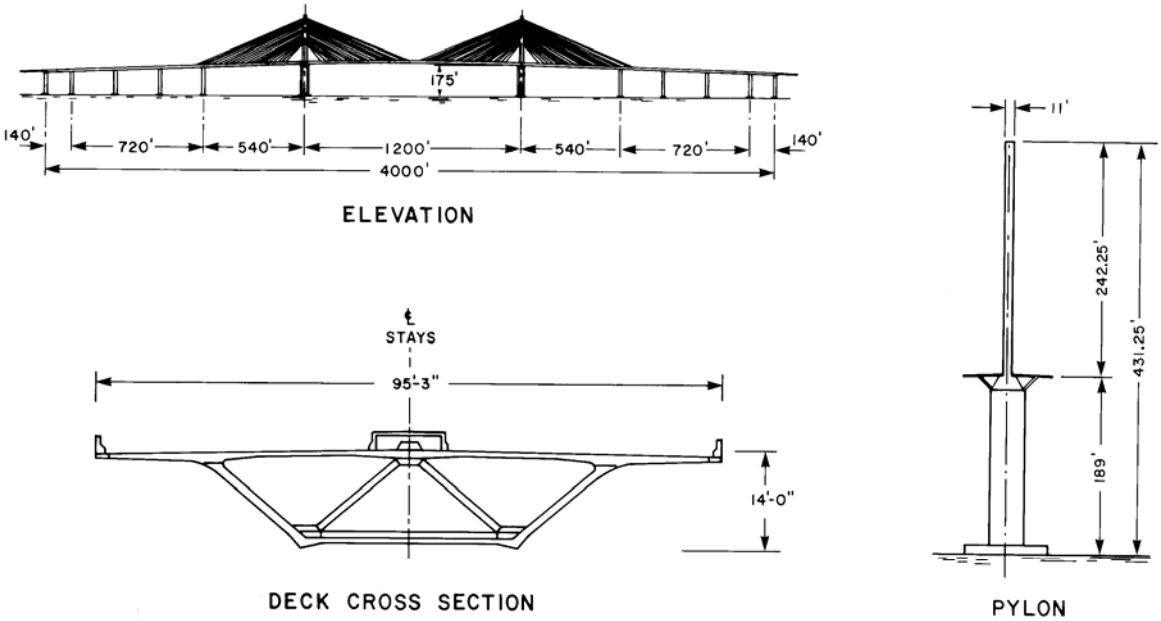

FIGURE E4 THE SUNSHINE SKYWAY BRIDGE

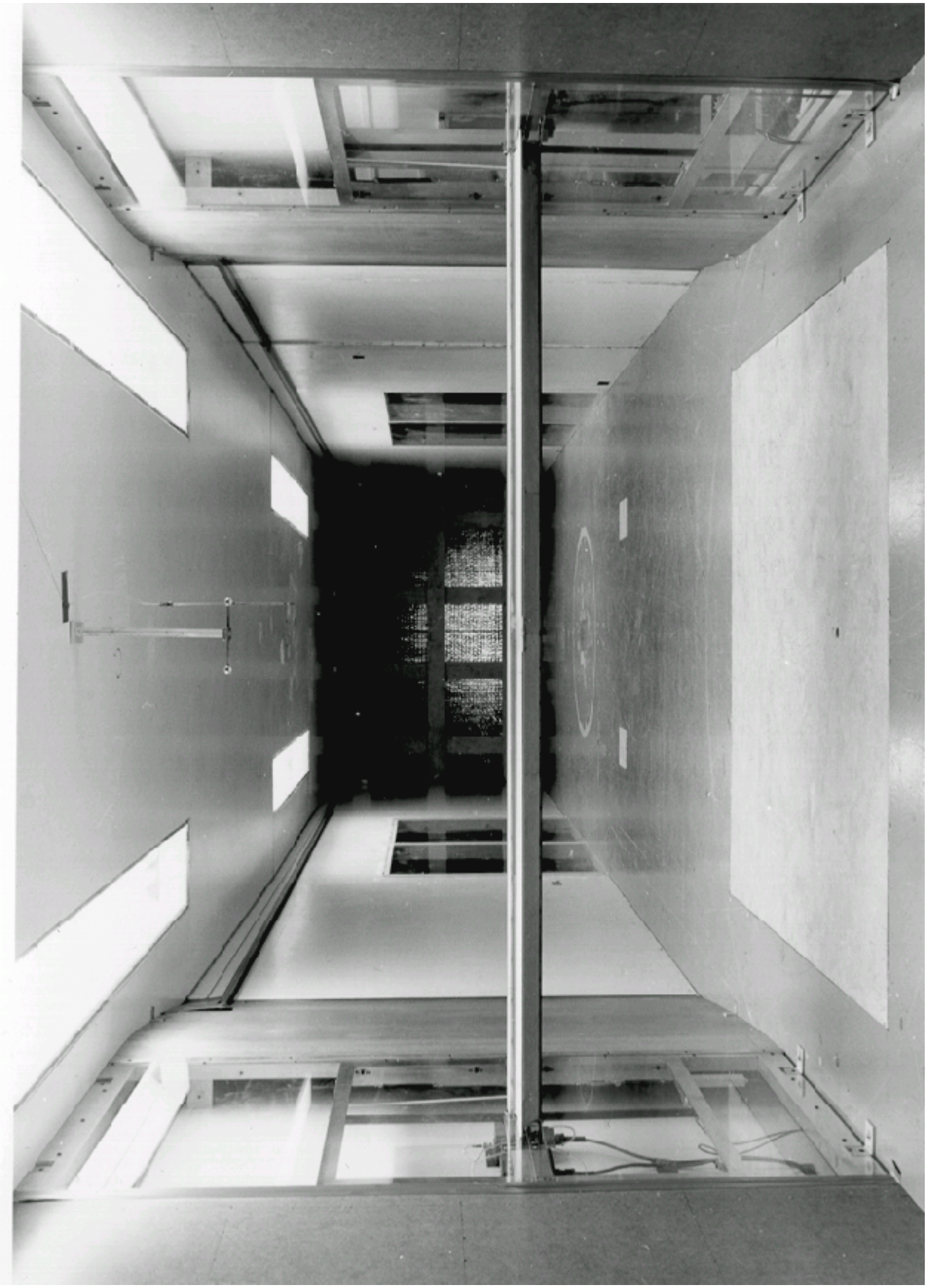

FIGURE E5 SECTION MODEL IN WIND TUNNEL WITH TURBULENCE GRID AT INLET

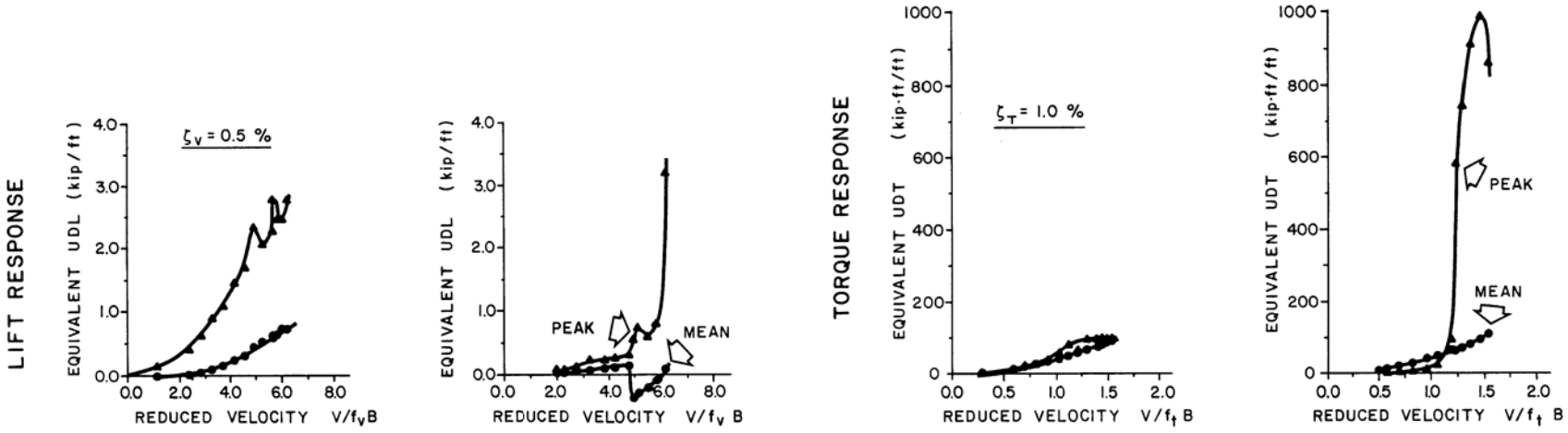

FIGURE E6 SECTION MODEL RESPONSE (UNCORRECTED)

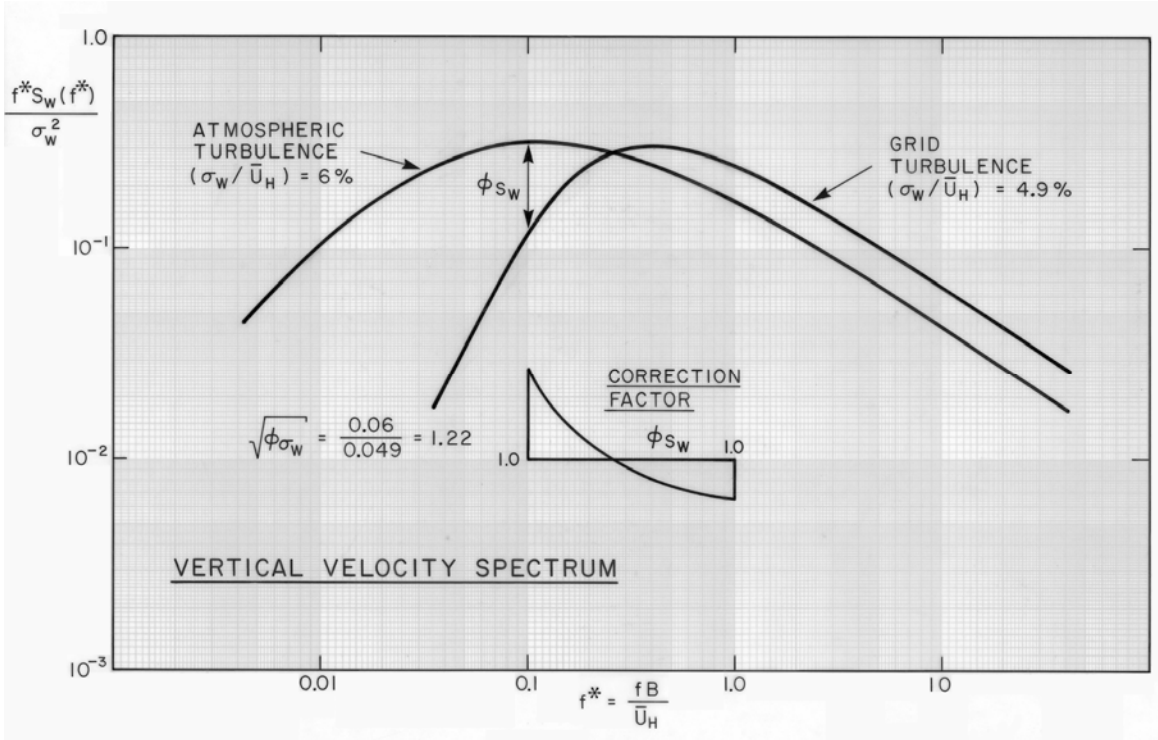

FIGURE E7 SPECTRUM OF VERTICAL COMPONENT OF TURBULENCE

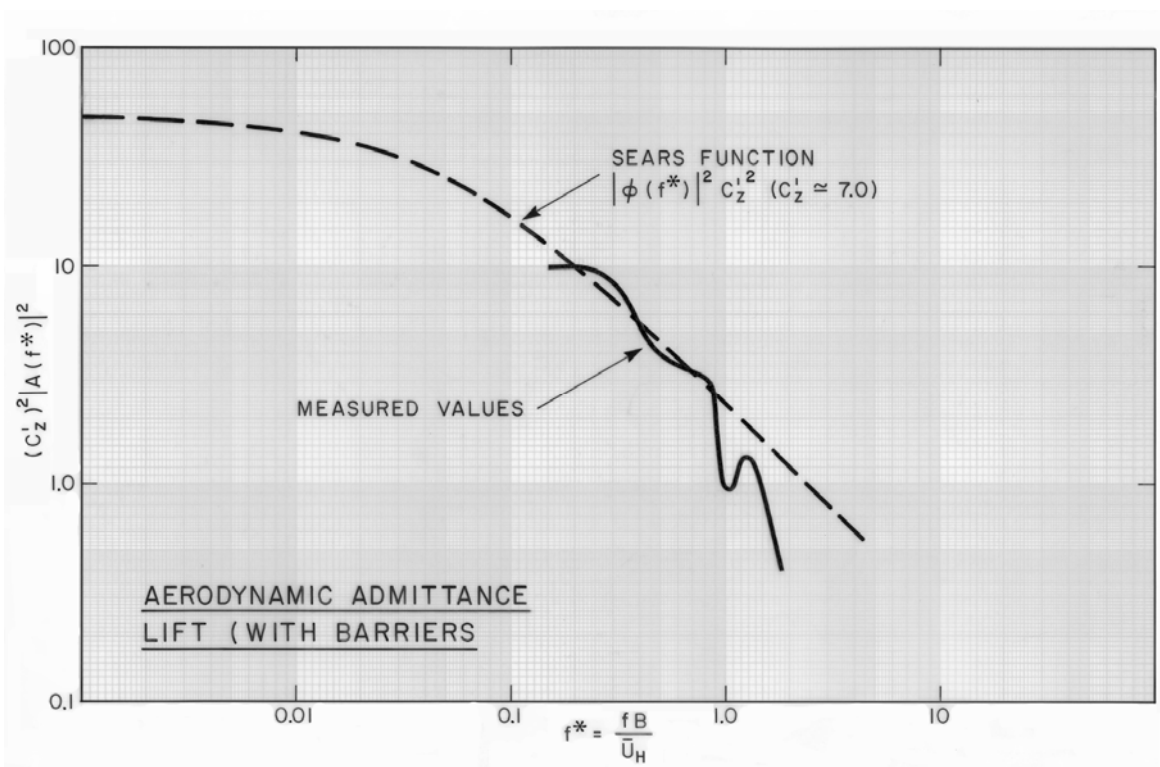

FIGURE E8 AERODYNAMIC ADMITTANCE

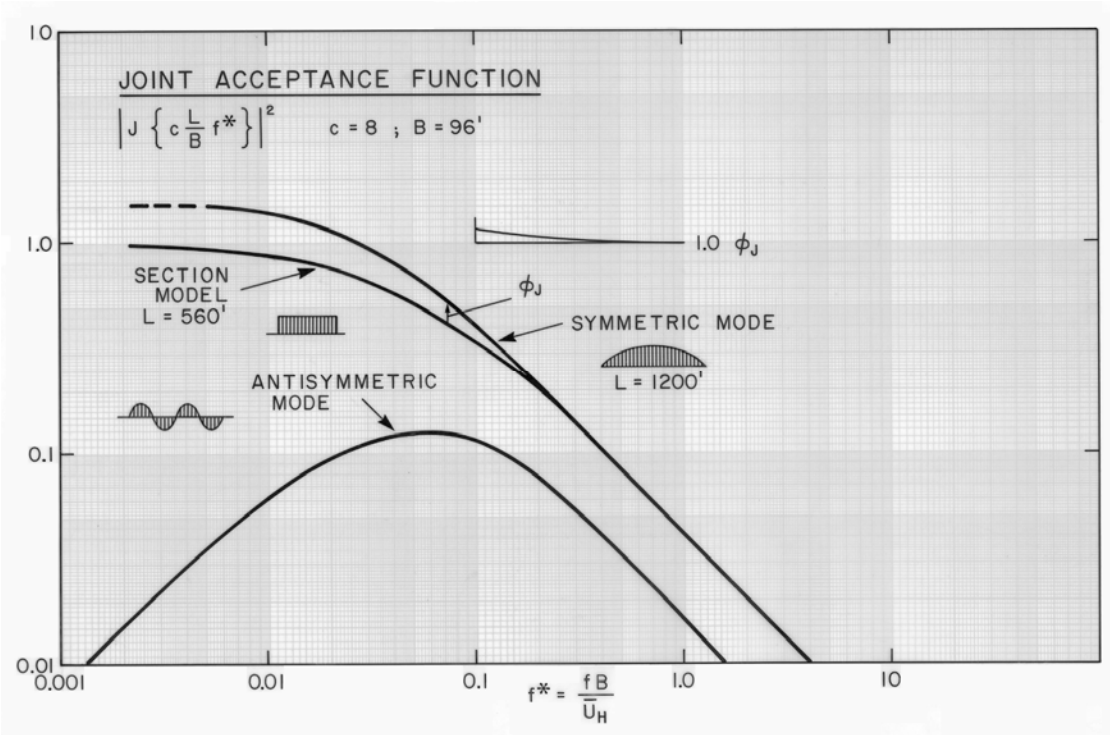

FIGURE E9 JOINT ACCEPTANCE FUNCTION

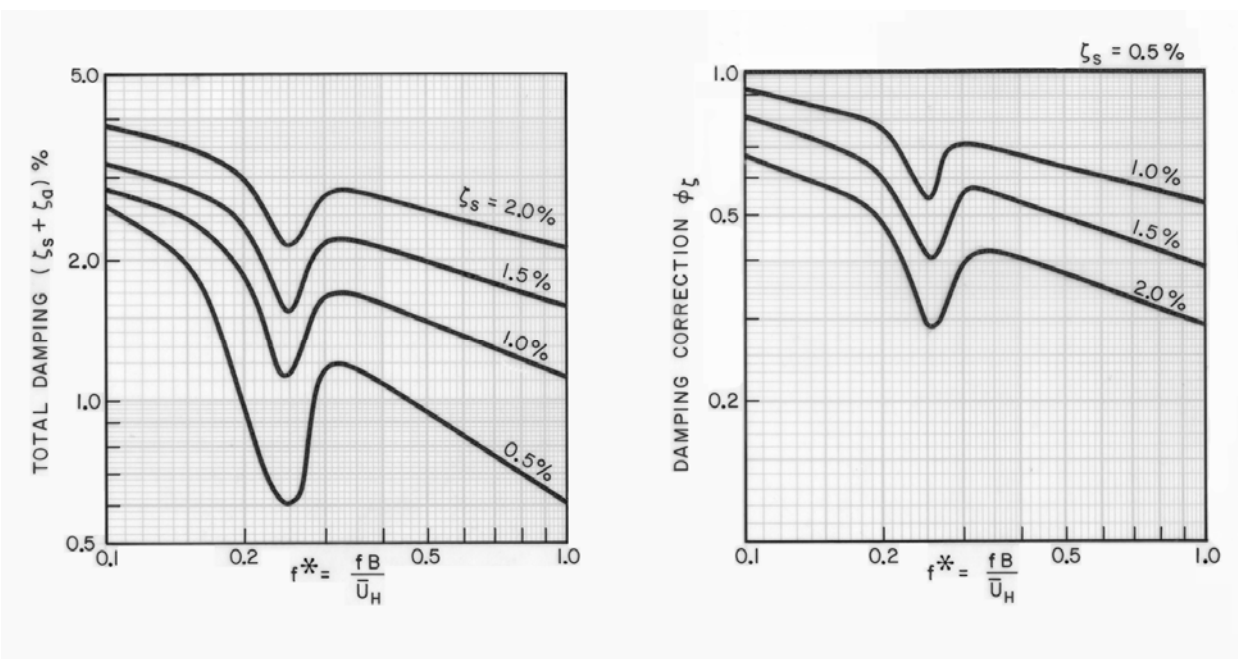

FIGURE E10 DAMPING FUNCTIONS

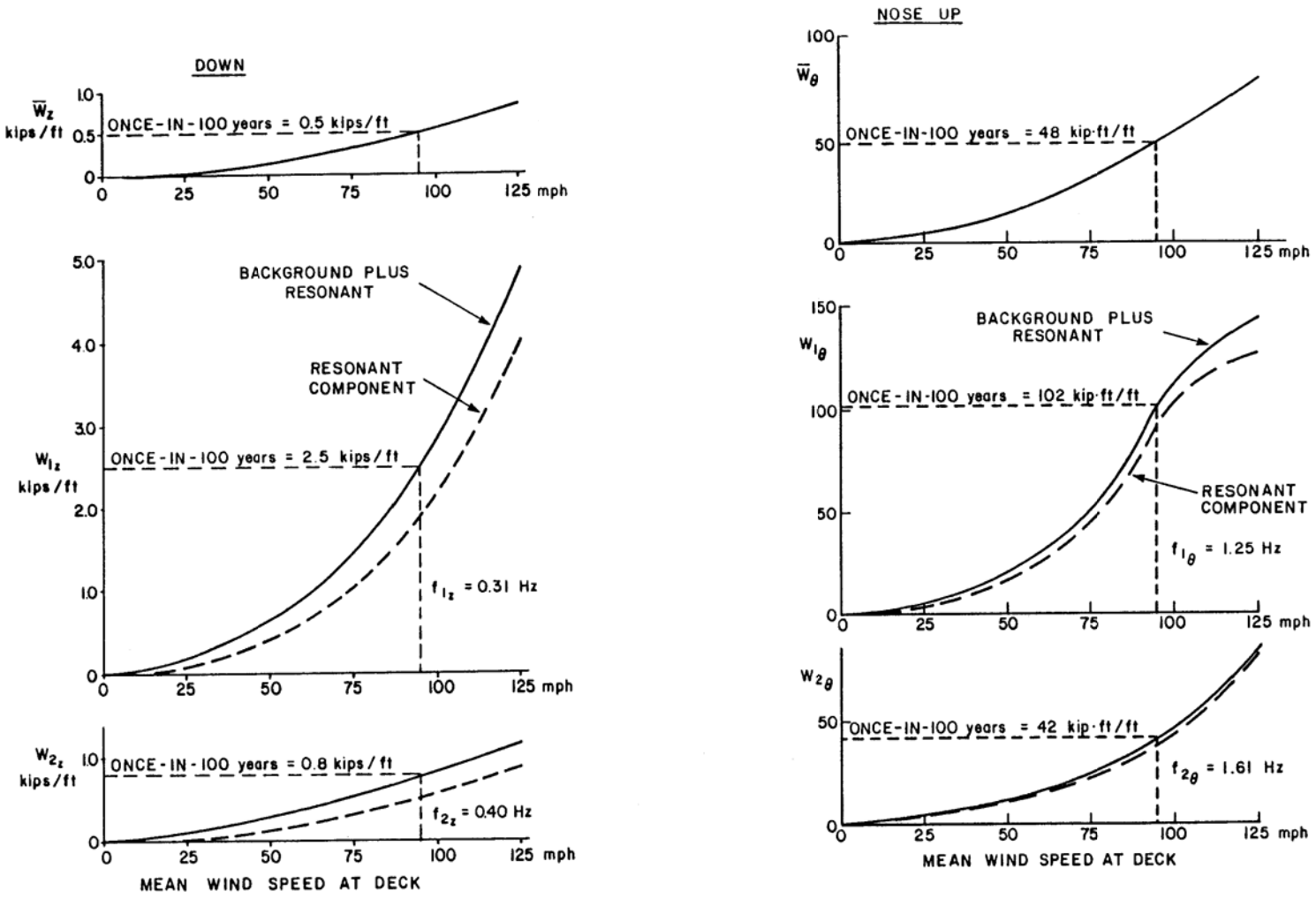

FIGURE E11 WIND LOAD COMPONENTS ON COMPLETED BRIDGE

APPENDIX F

PLOT OF EXTERNAL PRESSURE COEFFICIENTS

In the plot:

Azimuths are measured from true north and are such that:

0° = North	180° = South
90° = East	270° = West

- Pressure coefficients are referenced to the gradient height dynamic pressure $q_g = \frac{1}{2}\rho V_g^2$, where $\rho =$ air density and V_g is the mean hourly wind speed at gradient height. Thus the pressure coefficients are defined as $C_P = \frac{\text{pressure}}{q_g}$, where the pressure is the pressure at the tap relative to the undisturbed gradient static pressure.

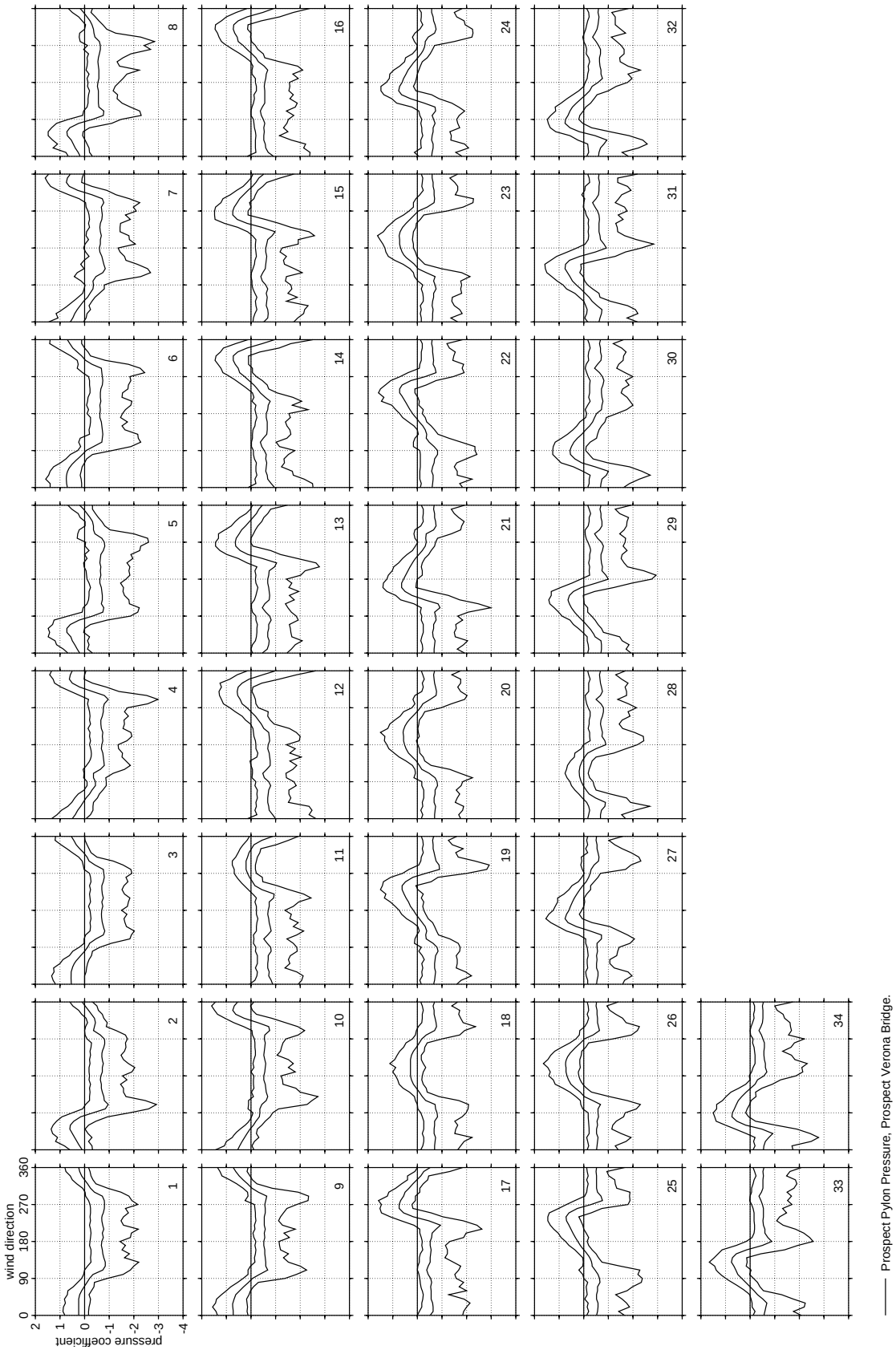
wind direction
0
90
180
270
360
pressure coefficient
2
1
0
-1
-2
-3
-4
1
2
3
4
5
6
7
8
9
10
11
12
13
14
15
16
17
18
19
20
21
22
23
24
25
26
27
28
29
30
31
32
33
34
Prospect Pylon Pressure, Prospect Verona Bridge.

Dec. 01, 2004

APPENDIX G

RESULTS OF FULL BRIDGE AEROELASTIC TESTS, COMPLETED BRIDGE

Notes:

1. The bending moments given in the plots have the units of kip-ft. The numbers read directly from the plots should be multiplied by 10^5 to obtain the actual bending moments in kip-ft. For example on page G8 of the Tower at Deck Lateral Moment (the lower right figure on that page), both the mean and peak moments at about 100mph are approximately 1.0×10^5 kip-ft (not 1.0 kip-ft).

2. The total response is equal to the mean, plus or minus the peak.

3. X is along the longitudinal direction, Y is the lateral direction (drag direction), and Z is the vertical direction (lift direction). Thus M_x is the torque, M_y is the lift moment (generated by the lift) and M_z is the drag moment (generated by the drag).

TABLE G1 INSTRUMENTATION LOCATIONS FOR THE FULL BRIDGE AEROELASTIC MODEL, COMPLETED BRIDGE

Instrumentation **x – longitudinal, y – lateral (Drag), z – vertical (Lift)**	**Instrumentation Locations**
Strain Gages:	
M_x, M_y and M_z at Prospect Pylon Leg A (marked A)	Lateral and Longitudinal Bending Moments, as well as Torque at 25ft from Pylon Footing
M_x, M_y and M_z at Prospect Pylon Leg B (marked B)	Lateral and Longitudinal Bending Moments, as well as Torque at 25ft from Pylon Footing
M_x, M_y and M_z at Back Span Mid-Point (marked C)	Lift and Drag Moments, as well as Torque at 230ft from Pylon Centerline
M_x, M_y and M_z at Back Span Deck close to Pylon (marked D)	Lift and Drag Moments, as well as Torque at 28ft from Pylon Centerline
M_x, M_y and M_z at Main Span Deck close to Pylon (marked E)	Lift and Drag Moments, as well as Torque at 25ft from Pylon Centerline
M_x and M_y at Prospect Pylon above Deck (marked F)	Lateral and Longitudinal bending Moments at 23ft above Deck Surface
M_x, M_y and M_z at Main Span Mid-Point (marked H)	Lift and Drag Moments, as well as Torque at 23ft from Midspan
Accelerometers:	
y, z and θ accel. at Main Span Mid-Point (marked H)	Lift, Drag and Torsional Accelerations at 25ft from Main Span Mid-Point to the Prospect Side
y, z and θ accel. at Back Span Mid-Point (marked C)	Lift, Drag and Torsional Accelerations at 255ft from Abutment 1
y and z accel. at Top of Prospect Pylon (marked I)	Lateral and Longitudinal Accelerations at the observation deck level (435ft from Pylon footing)
Displacements:	
y, z and θ displacements at Main Span Mid-Point (marked H)	Lift and Drag Displacements, as well as Deck Rotation at 25ft from Midspan to the Prospect Side
y, z and θ displacements at Main Span 1/4 point (marked G)	Lift and Drag Displacements, as well as Deck Rotation at 310ft from Midspan to the Prospect Side
y and z displacements at Top of Prospect Pylon (marked I)	Lateral and Longitudinal Displacements at the observation deck level (435ft from Pylon footing)
Wind Speeds:	
Plaza Probes at Prospect Pylon Entrance Way (marked 1 & 2)	Pedestrian Level
Deck Level	Deck Height
Pylon Top	Pylon Height

TABLE G2 SUMMARY OF TESTS FOR FULL BRIDGE AEROELASTIC MODEL, COMPLETED BRIDGE CONFIGURATION

Test File	Test No.	Flow condition	Existing bridge	Wind direction (Test angle)	V_{deck} (mph) Maximum wind speed at deck height
VS9201	1	Hurricane profile	No	Perpendicular to bridge (90°)	158
VS0201	2	Hurricane profile	No	Along the Bridge (0°)	143
VS3201	3	Hurricane profile	No	30° to the bridge	140
VS6201	4	Hurricane profile	No	60° to the bridge	142
VS2201	5	Hurricane profile	Yes	Perpendicular to bridge (270°)	150
VS6301	6	Open Country profile	No	60° to the bridge	163
VS3301	7	Open Country profile	No	30° to the bridge	155
VS0301	8	Open Country profile	No	Along the Bridge (0°)	161
VS9301	9	Open Country profile	No	Perpendicular to bridge (90°)	169
VS2301	10	Open Country profile	Yes	Perpendicular to bridge (270°)	183
VS9101	11	Smooth Flow	No	Perpendicular to bridge (90°)	147

TABLE G3 SUMMARY OF FULL BRIDGE MODEL PROPERTIES, COMPLETED BRIDGE CONFIGURATION

	Deck Lateral		**Deck Vertical**		**Deck Torsional**			
	symmetric	**asymmetric**	**symmetric**	**asymmetric**	**symmetric**	**asymmetric**	**Pylon Long.**	**Pylon Lateral**
Model Frequency (Hz)	4.6	10.7	5.6	8.4	17.4	34.4	5.4	3.7
Model Damping (% of critical)	-		0.16%	-	-		0.20%	0.55%

TABLE G4 SUMMARY OF LONGITUDINAL TURBULENCE INTENSITIES IN TEST

	Hurricane Exposure (Zo=0.03ft)	Open Country Exposure (Zo=0.1ft)	Smooth Flow
Height	**Longitudinal Turbulence**	**Longitudinal Turbulence**	**Longitudinal Turbulence**
Deck Height (154 ft)	15.5%	19.1%	1.7%
Top of Pylon (430ft)	12.2%	15.2%	1.7%

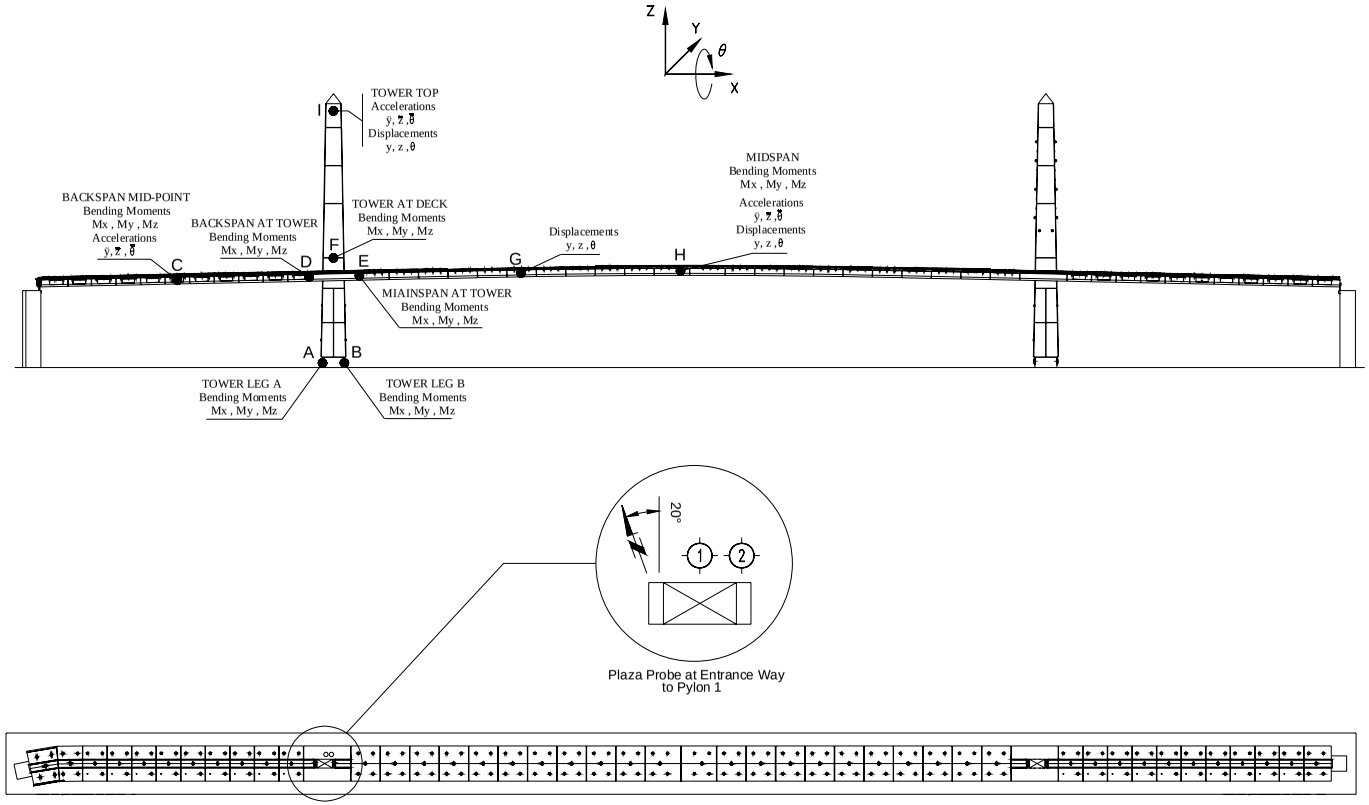

(Cables removed in drawing)

FIGURE G1 INSTRUMENTATION LOCATIONS AND SIGN CONVENTION, COMPLETED BRIDGE (CABLES REMOVED IN THIS FIGURE)

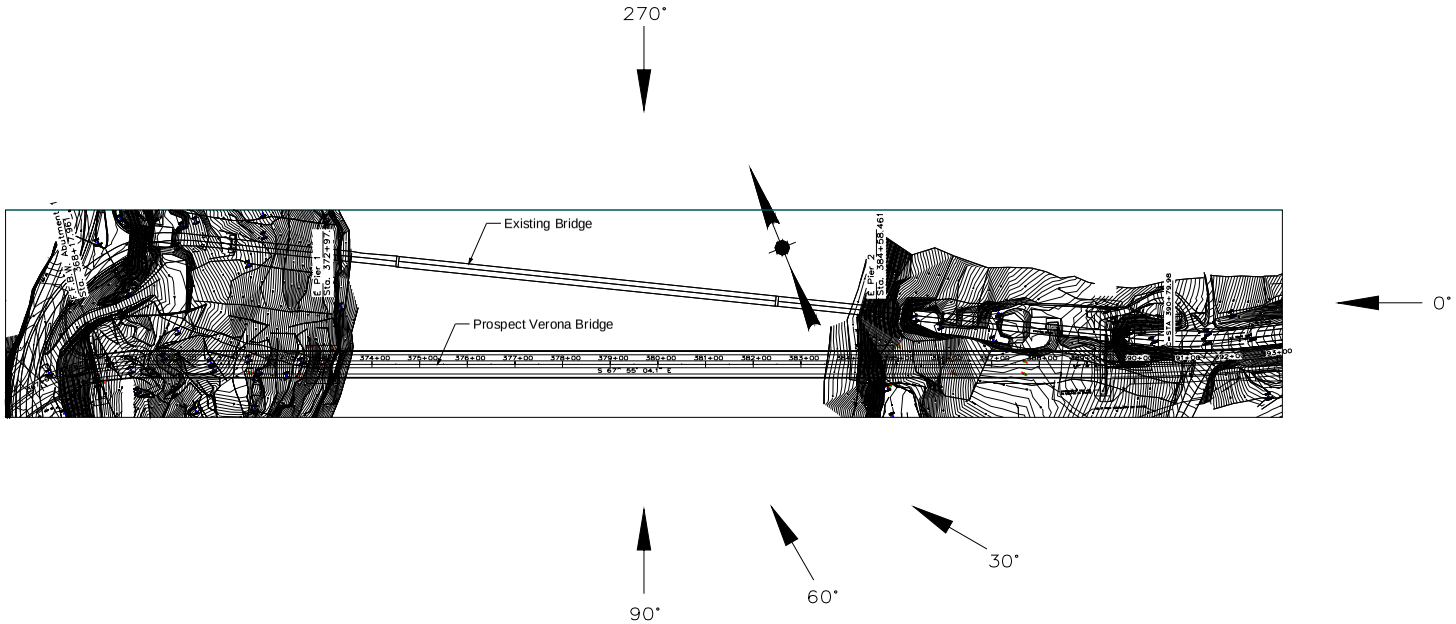

WIND DIRECTION DEFINITION

FIGURE G2 LOCATION OF EXISTING BRIDGE AND WIND DIRECTIONS TESTED

Nov. 30, 2004
Data File =vs9201.mst
Information File =vs9201.inf

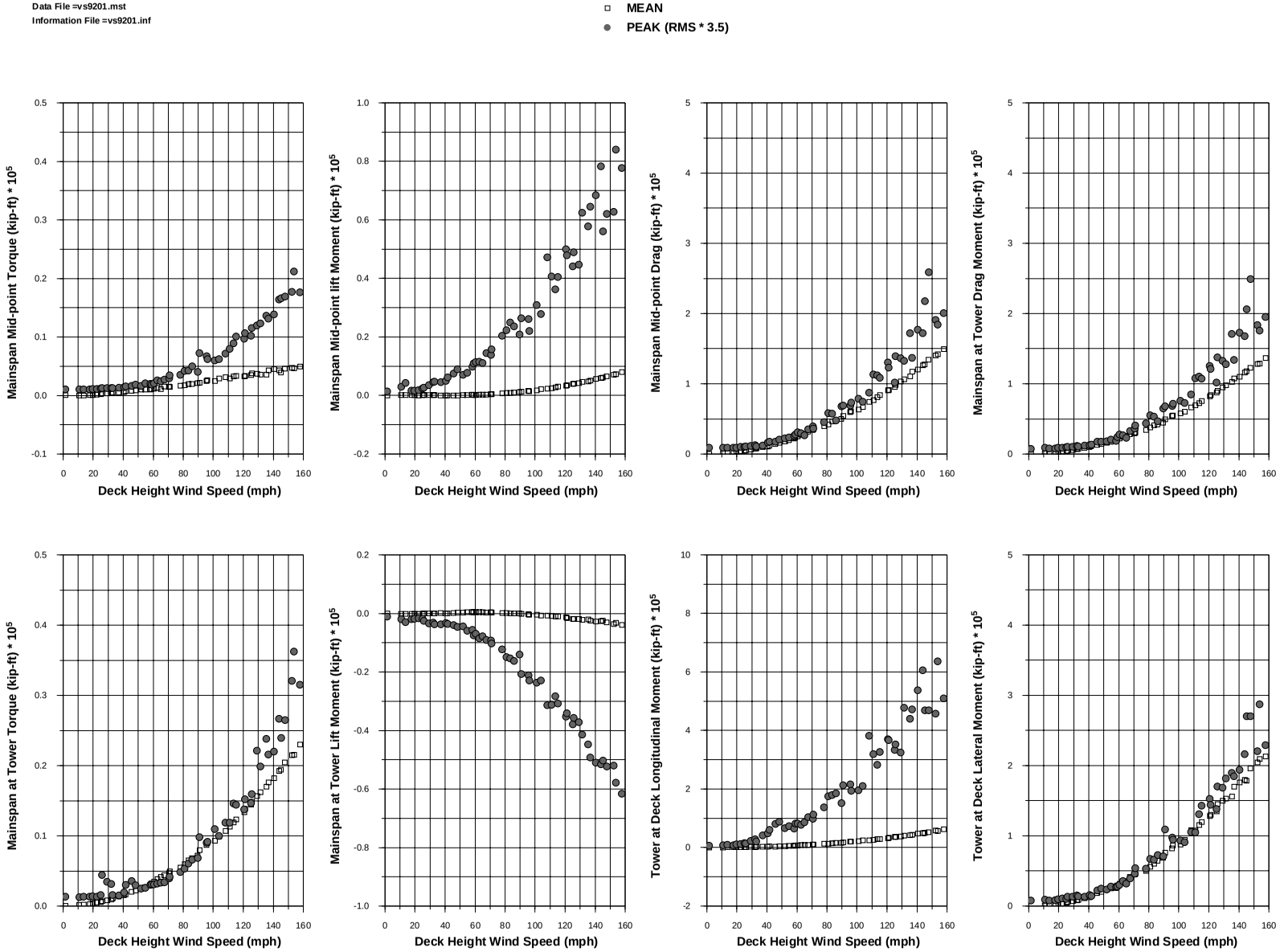

Prospect Verona bridge, Hurricane Profile, 90 degrees (perpendicular to deck)

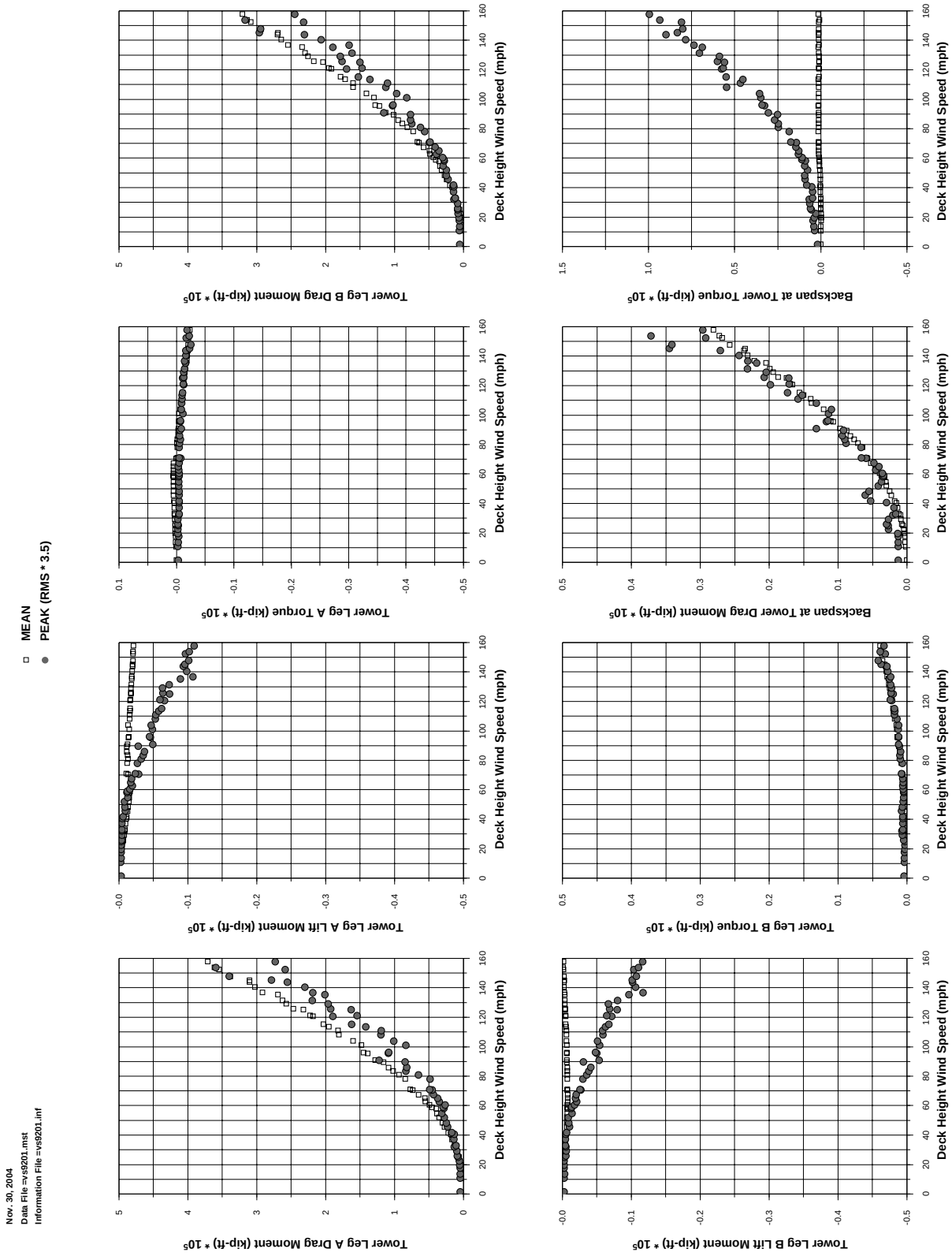

Prospect Verona bridge, Hurricane Profile, 90 degrees (perpendicular to deck)

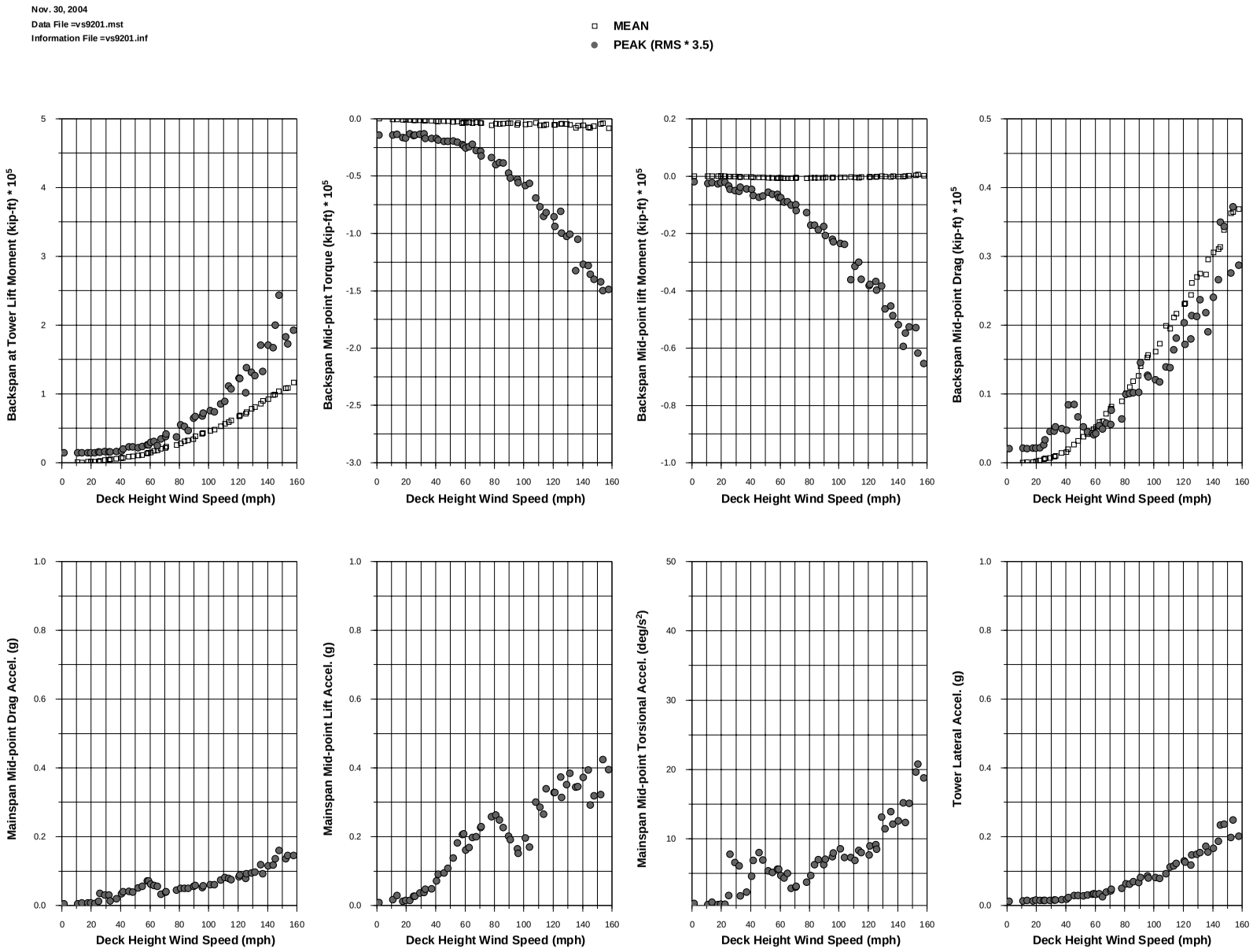

Prospect Verona bridge, Hurricane Profile, 90 degrees (perpendicular to deck)

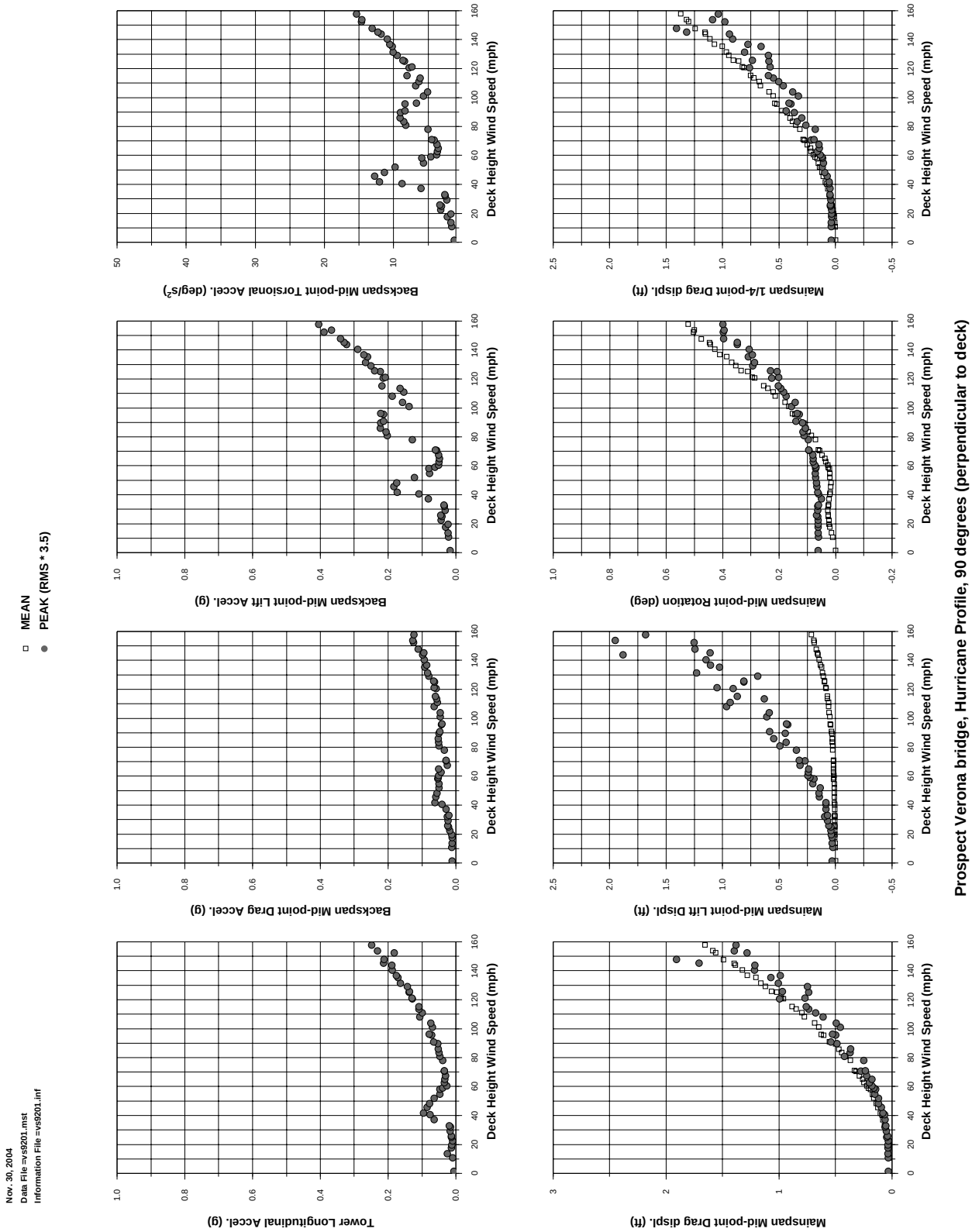

Prospect Verona bridge, Hurricane Profile, 90 degrees (perpendicular to deck)

Nov. 30, 2004
Data File =vs9201.mst
Information File =vs9201.inf

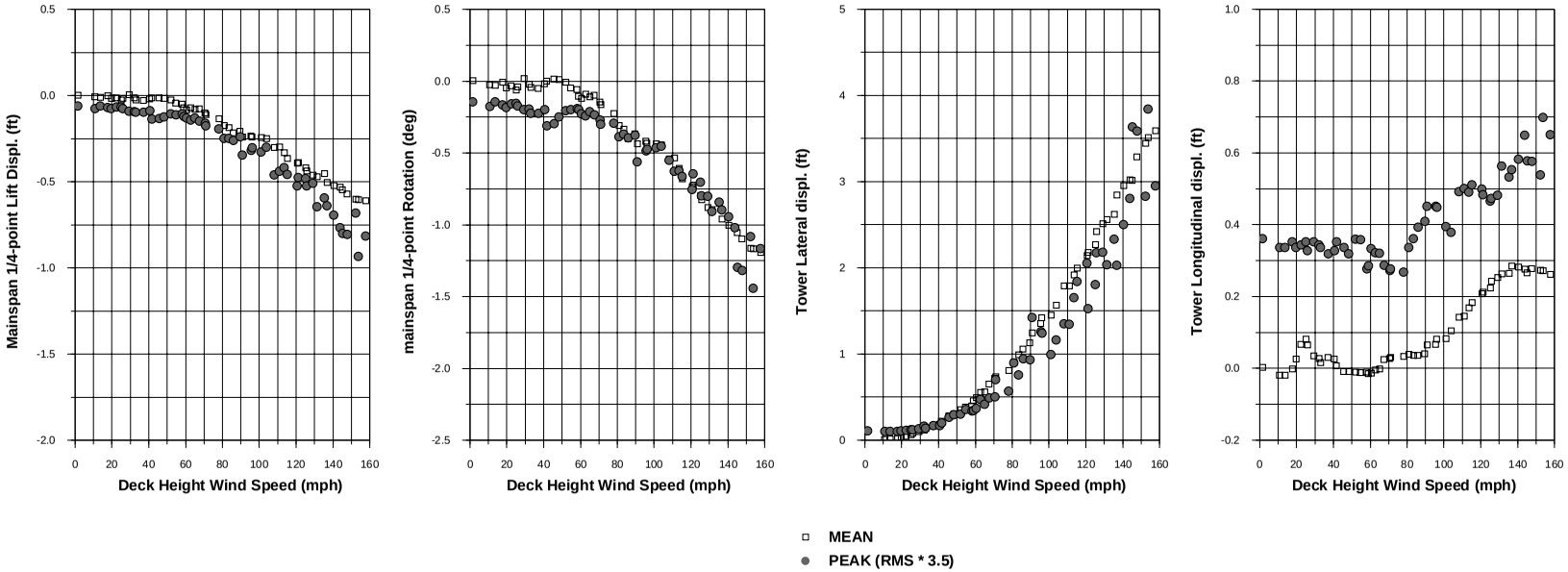

Prospect Verona bridge, Hurricane Profile, 90 degrees (perpendicular to deck)

Nov. 30, 2004
Data File =vs0201.mst
Information File =vs0201.inf

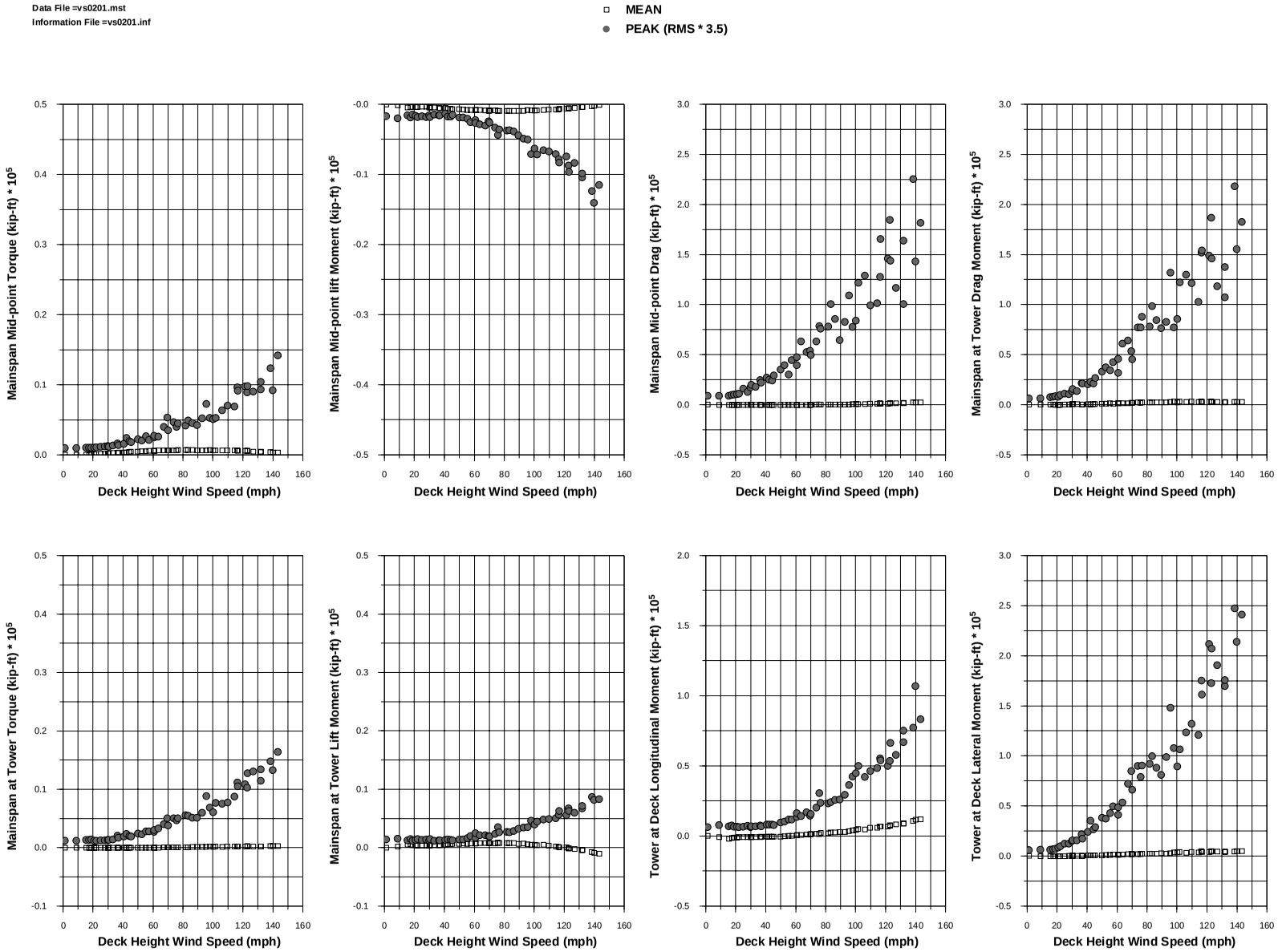

Prospect Verona Bridge, Hurricane profile, 0 degrees (along bridge)

Nov. 30, 2004
Data File =vs0201.mst
Information File =vs0201.inf

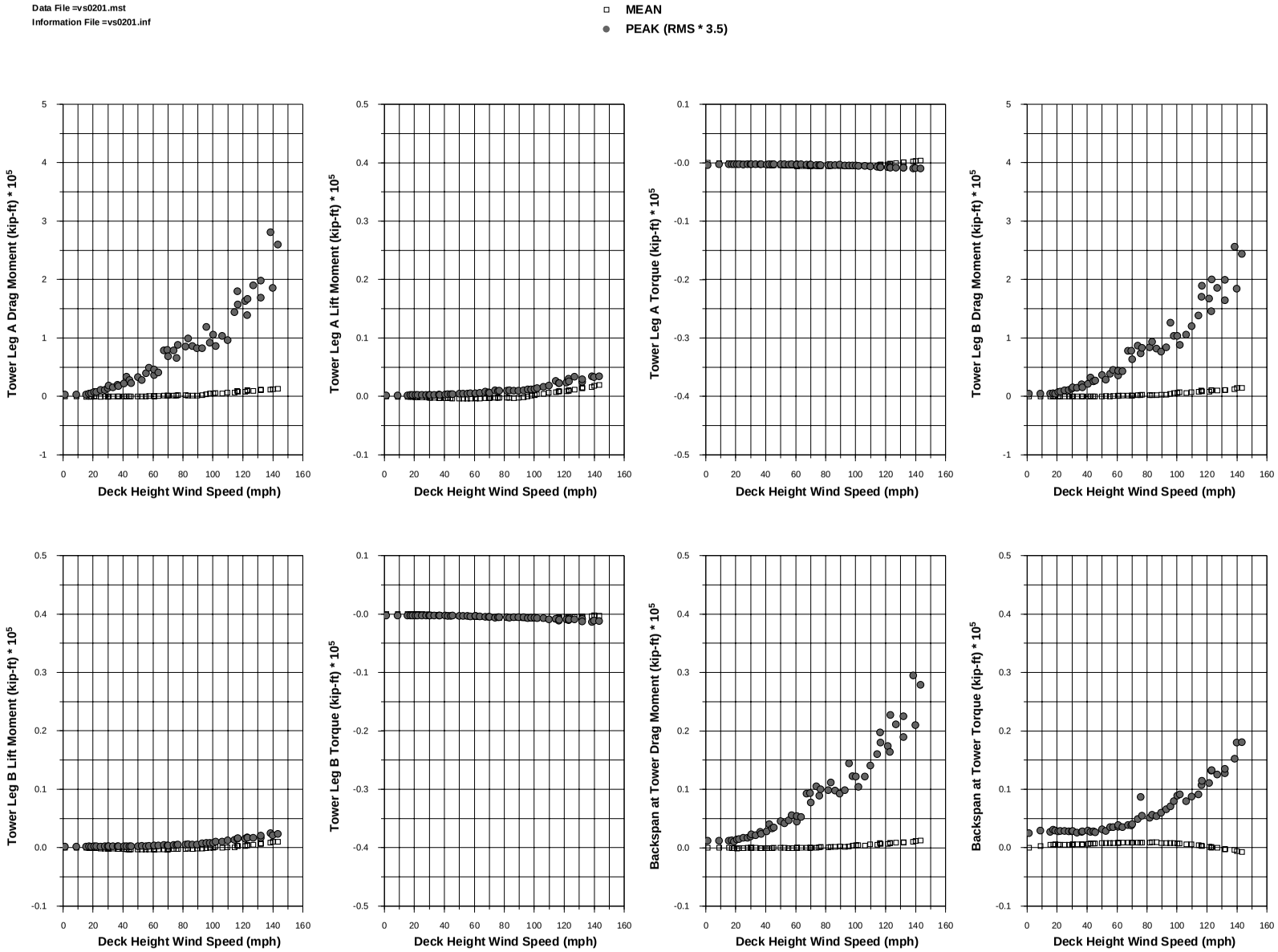

Prospect Verona Bridge, Hurricane profile, 0 degrees (along bridge)

Nov. 30, 2004
Data File =vs0201.mst
Information File =vs0201.inf

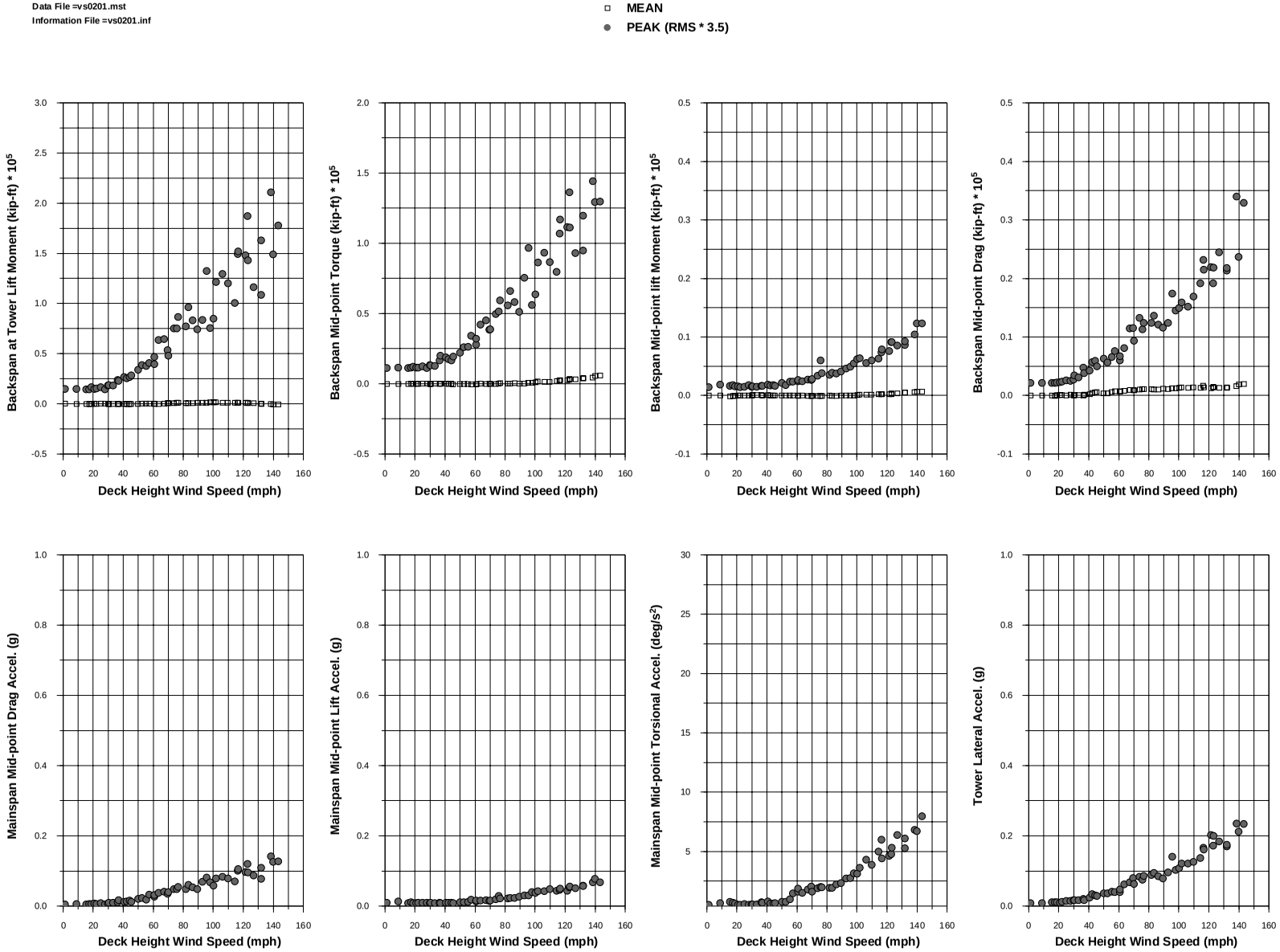

Prospect Verona Bridge, Hurricane profile, 0 degrees (along bridge)

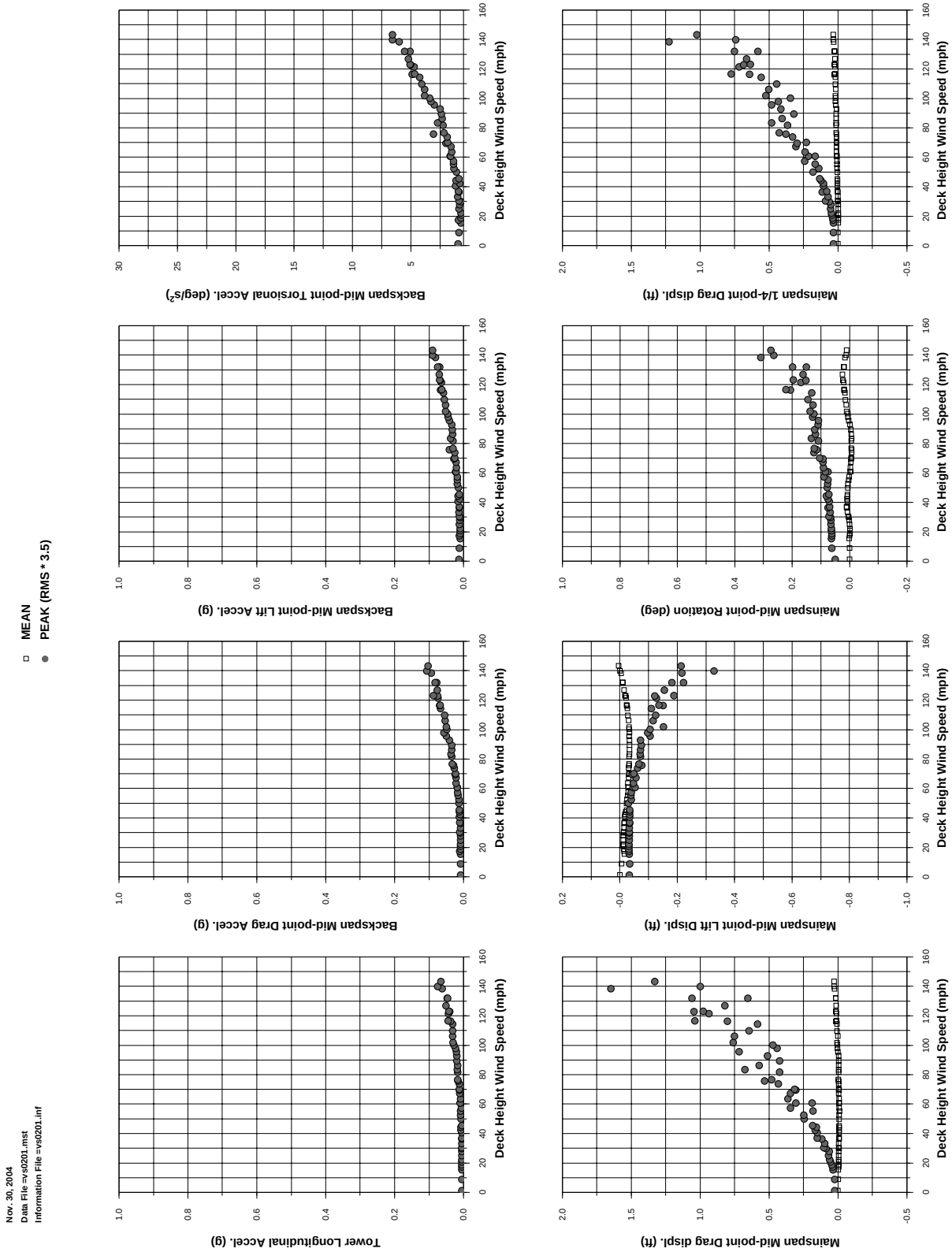

Prospect Verona Bridge, Hurricane profile, 0 degrees (along bridge)

Nov. 30, 2004
Data File =vs0201.mst
Information File =vs0201.inf

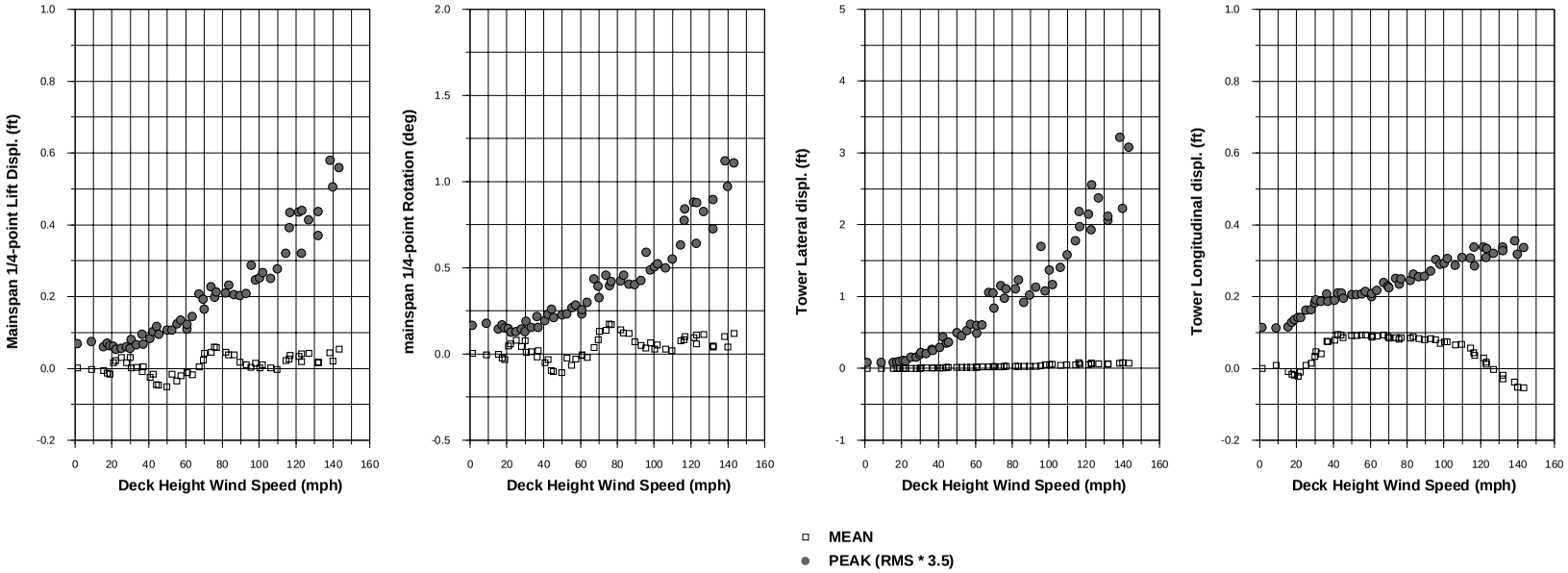

Prospect Verona Bridge, Hurricane profile, 0 degrees (along bridge)

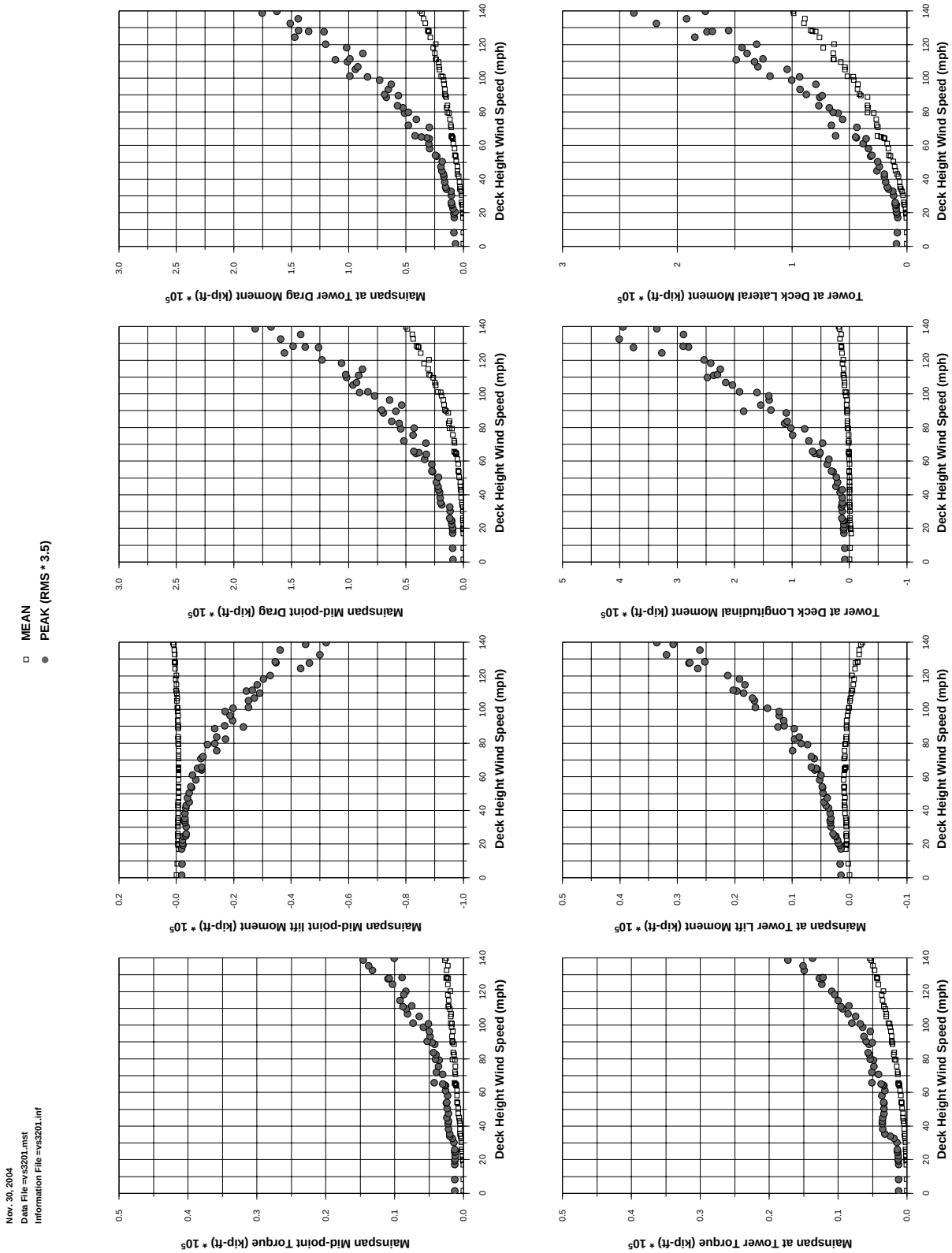

Prospect Verona Bridge, hurricane profile, 30 degrees

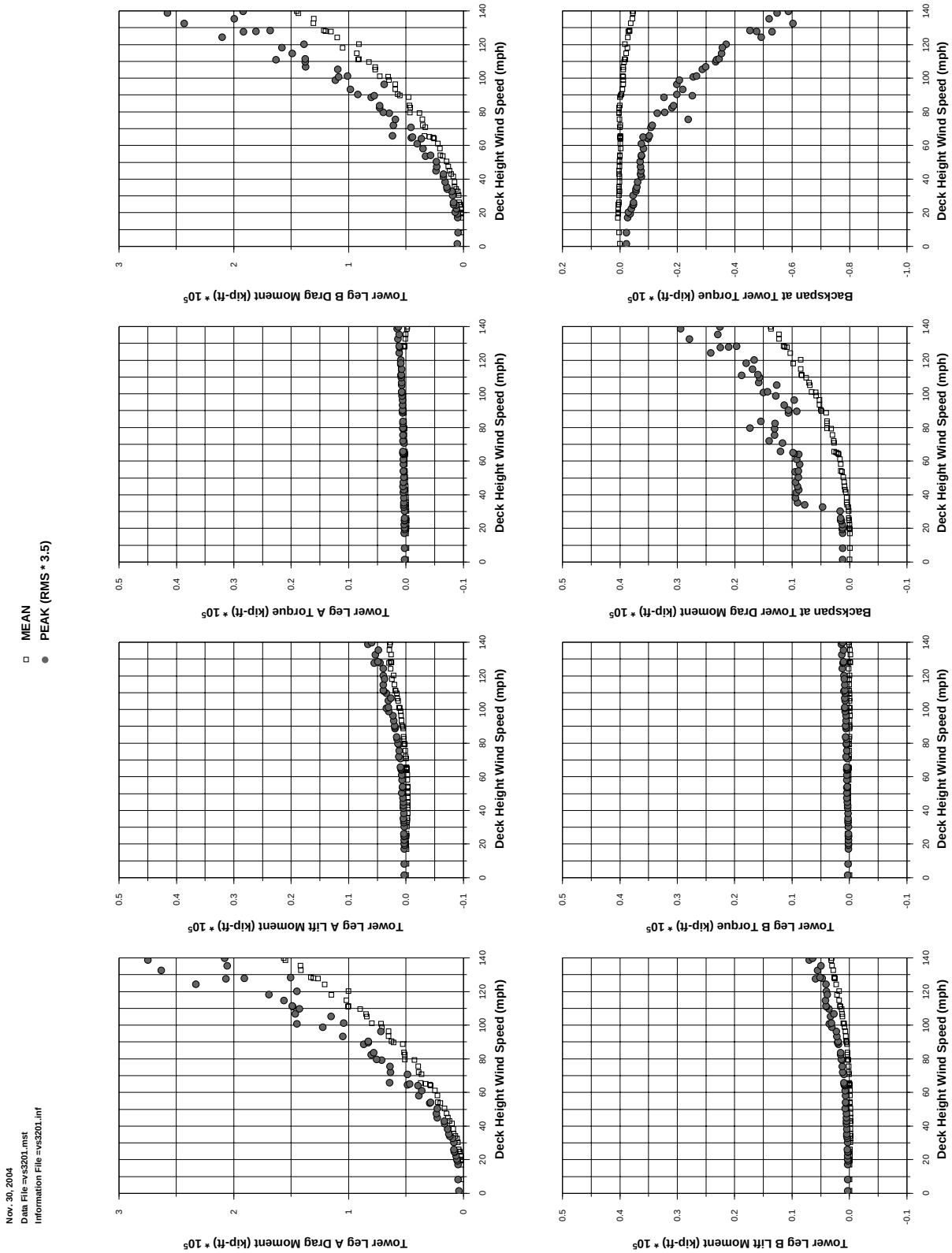

Prospect Verona Bridge, hurricane profile, 30 degrees

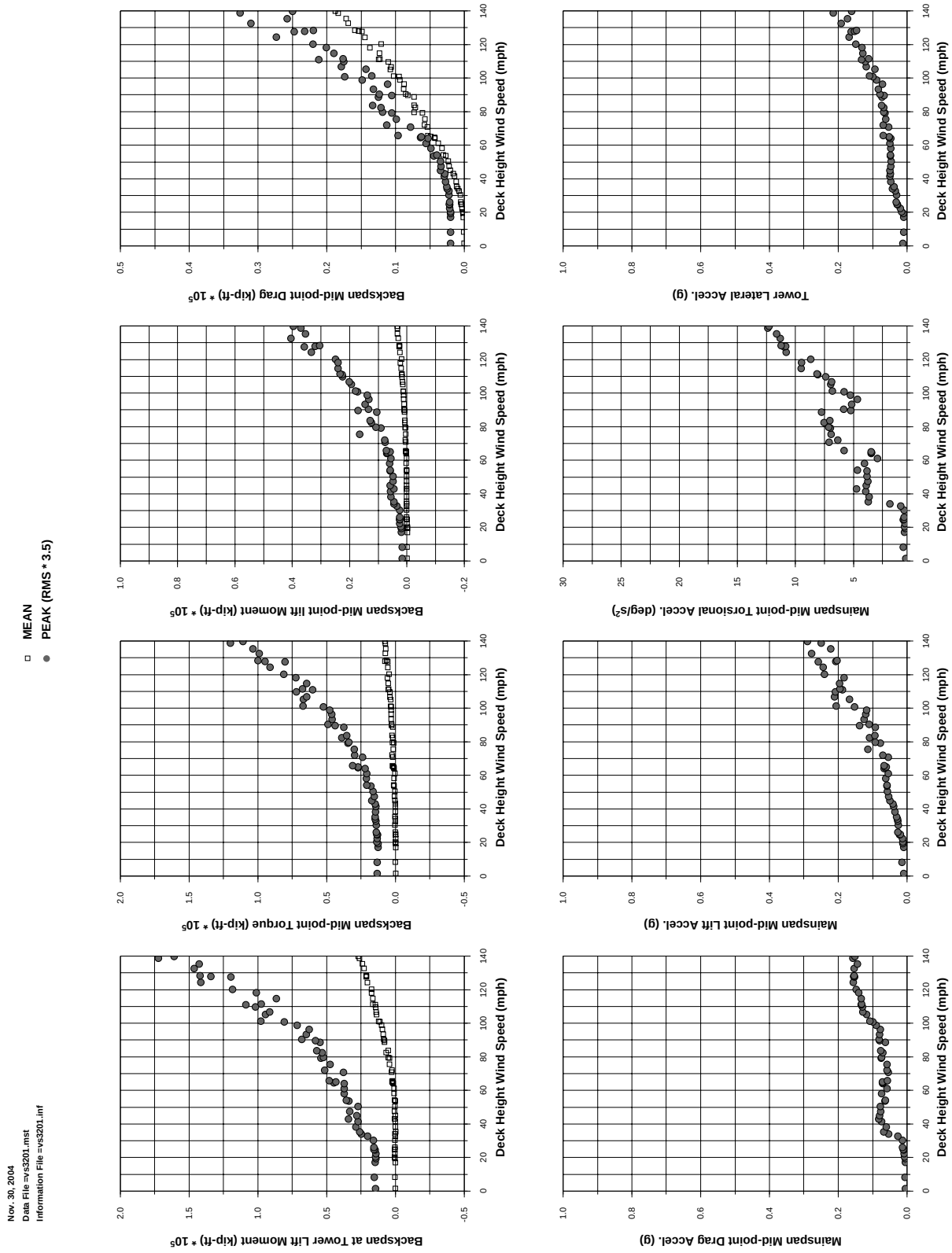

Prospect Verona Bridge, hurricane profile, 30 degrees

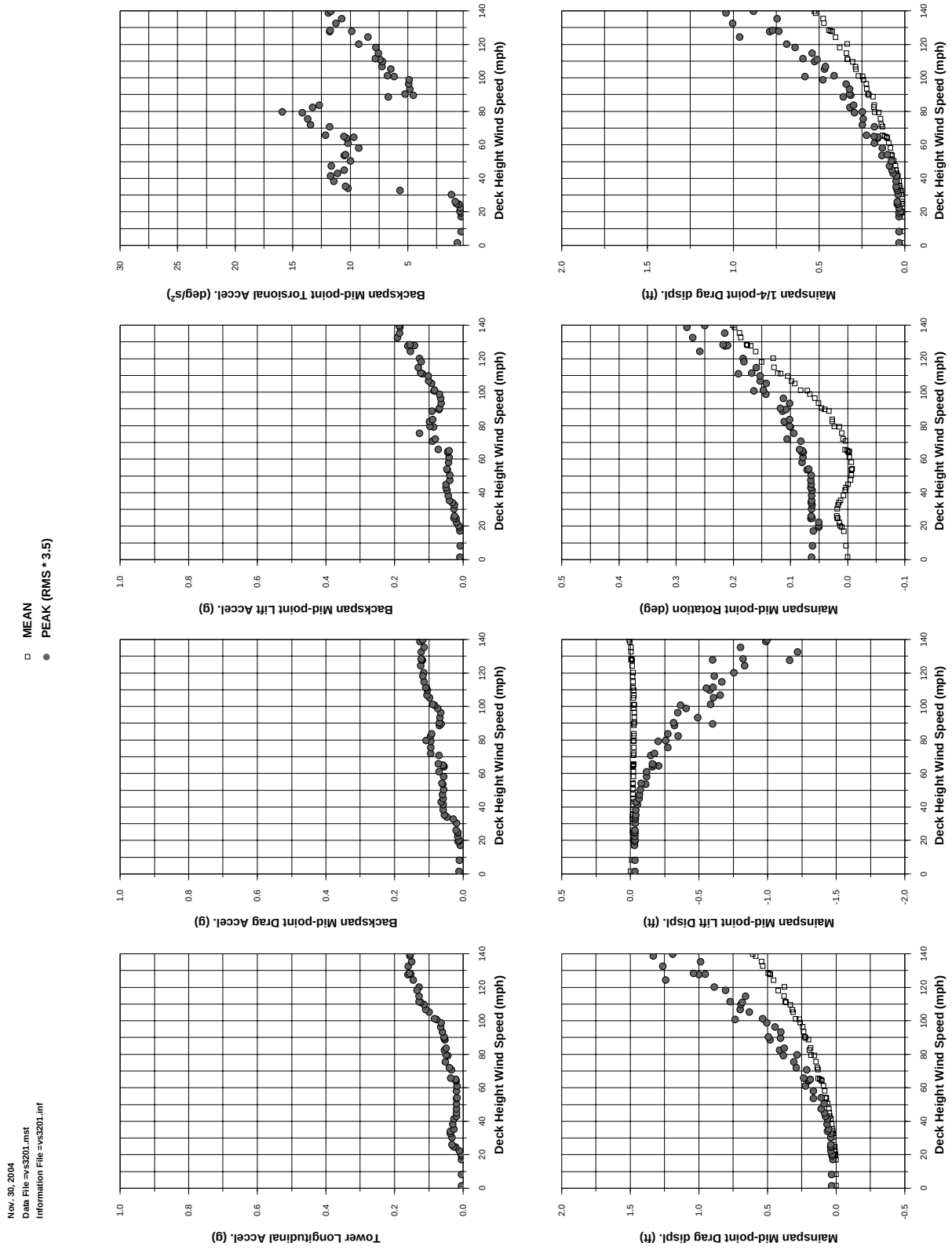

Prospect Verona Bridge, hurricane profile, 30 degrees

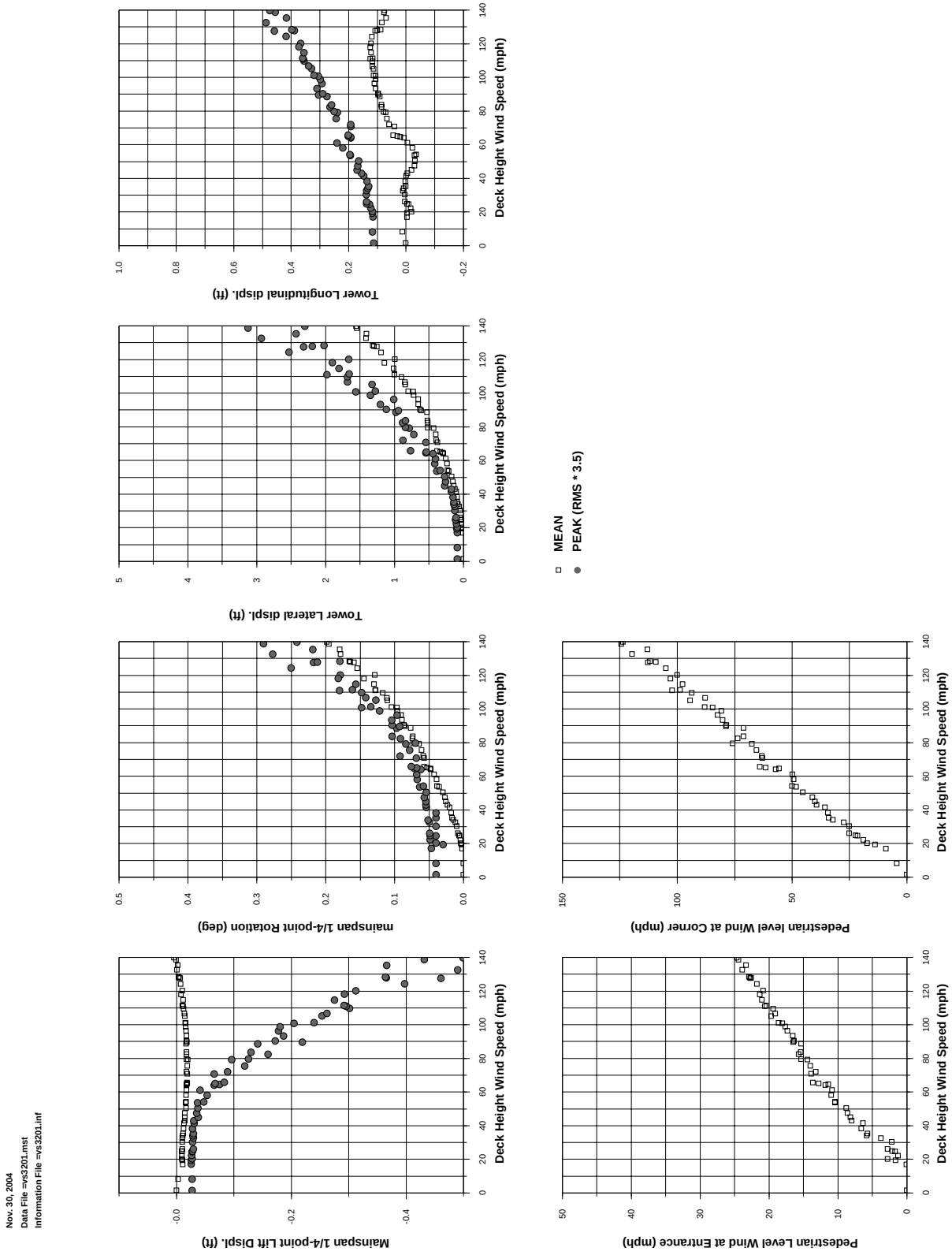

Prospect Verona Bridge, hurricane profile, 30 degrees

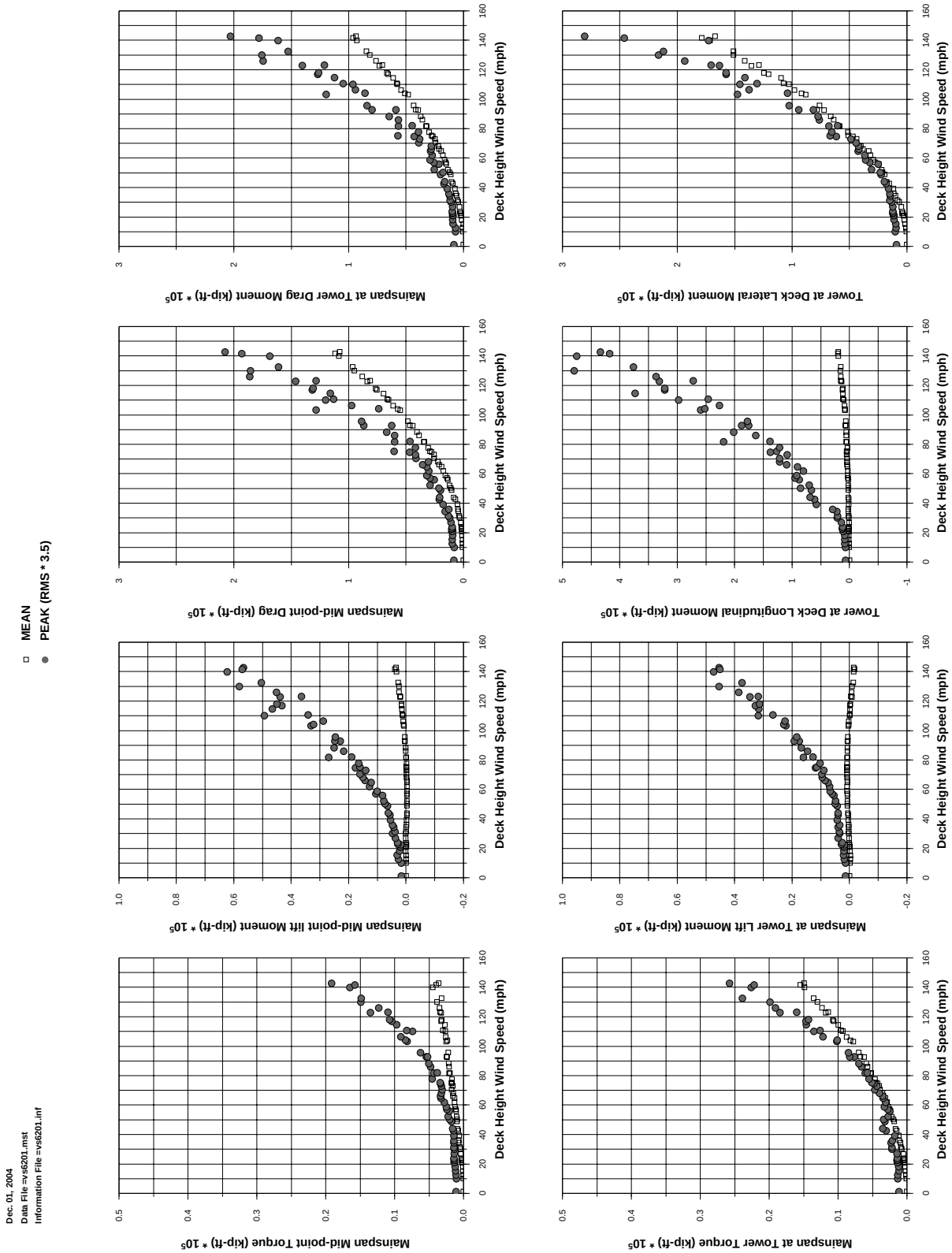

Prospect Verona Bridge, hurricane profile, 60 degrees

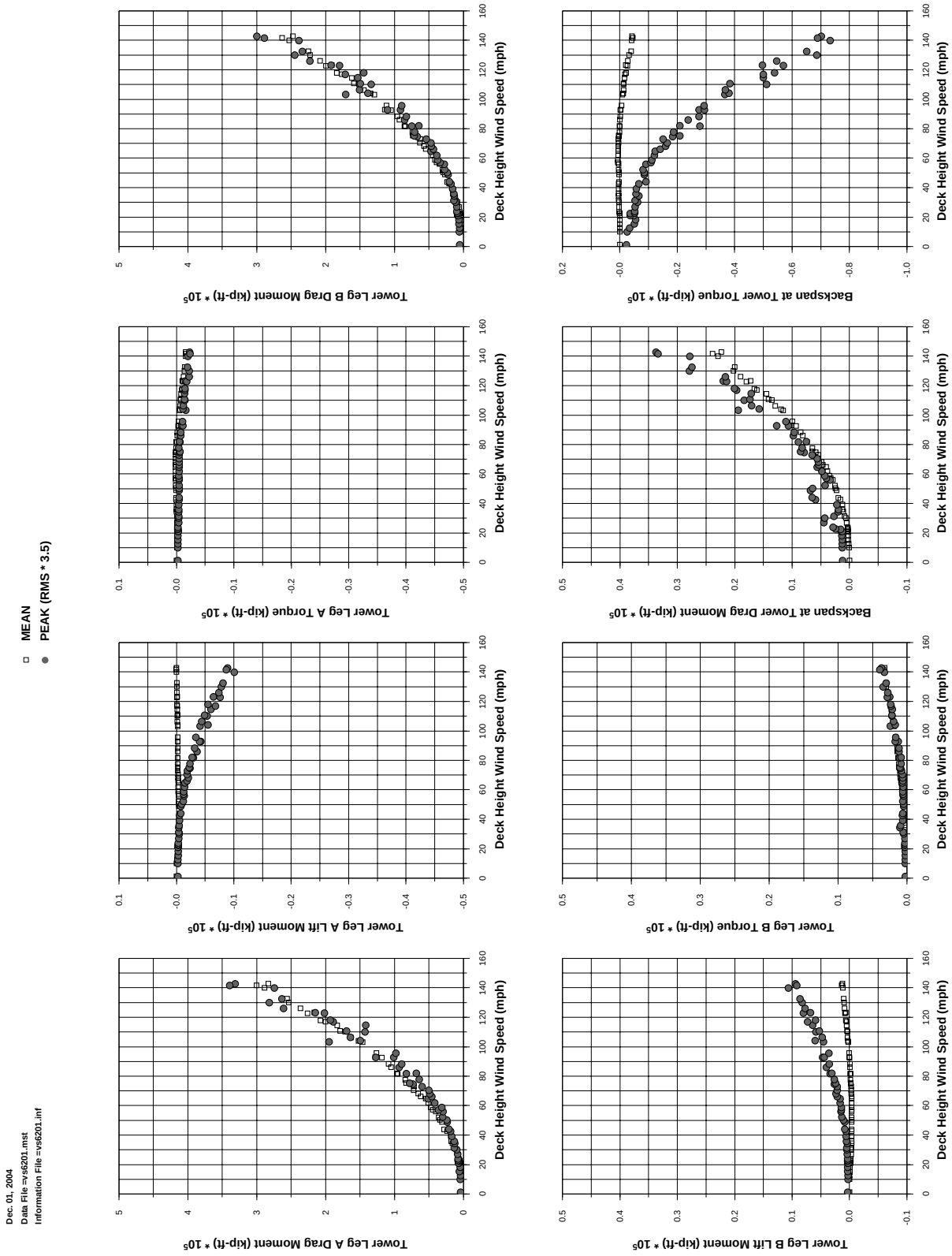

Prospect Verona Bridge, hurricane profile, 60 degrees

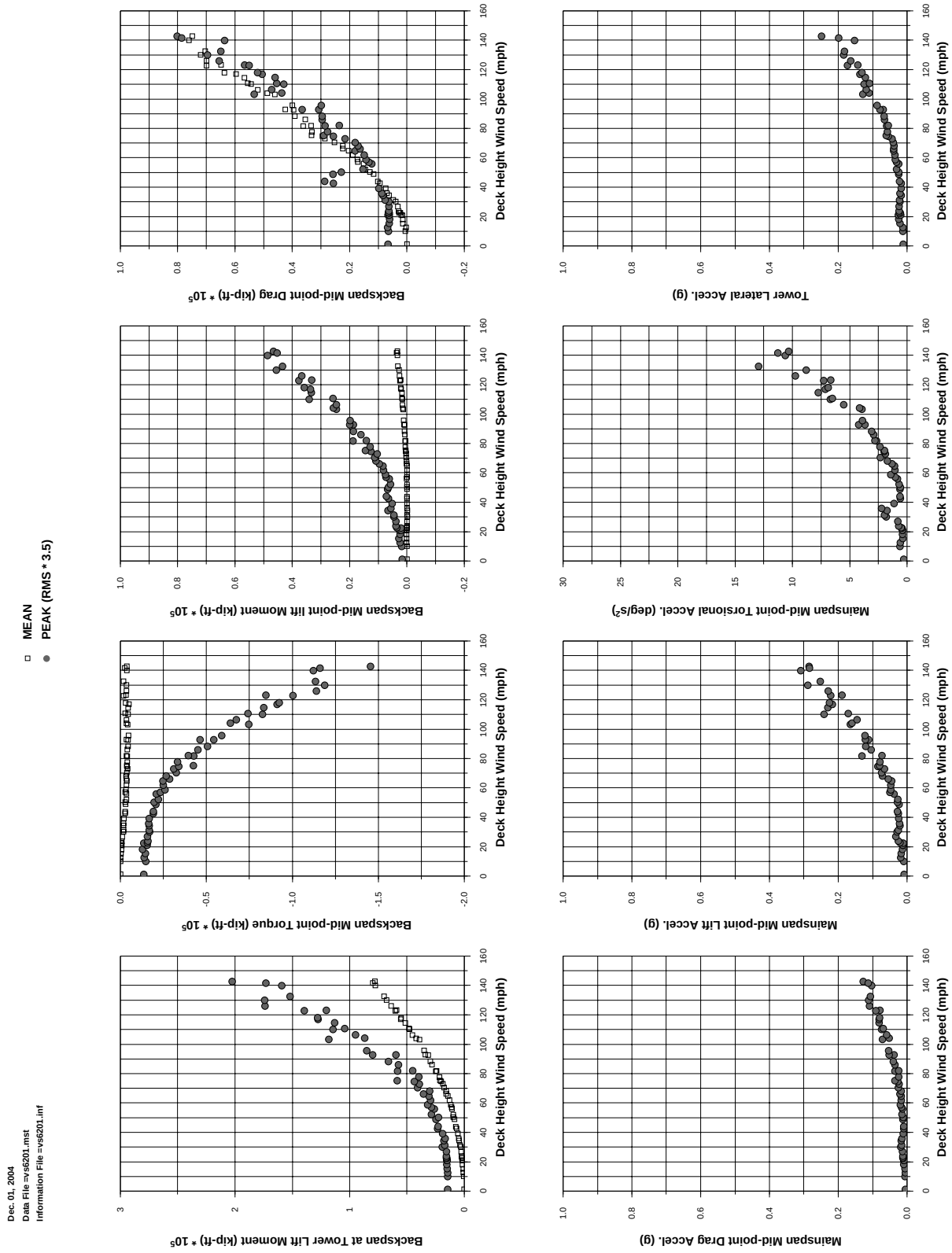

Prospect Verona Bridge, hurricane profile, 60 degrees

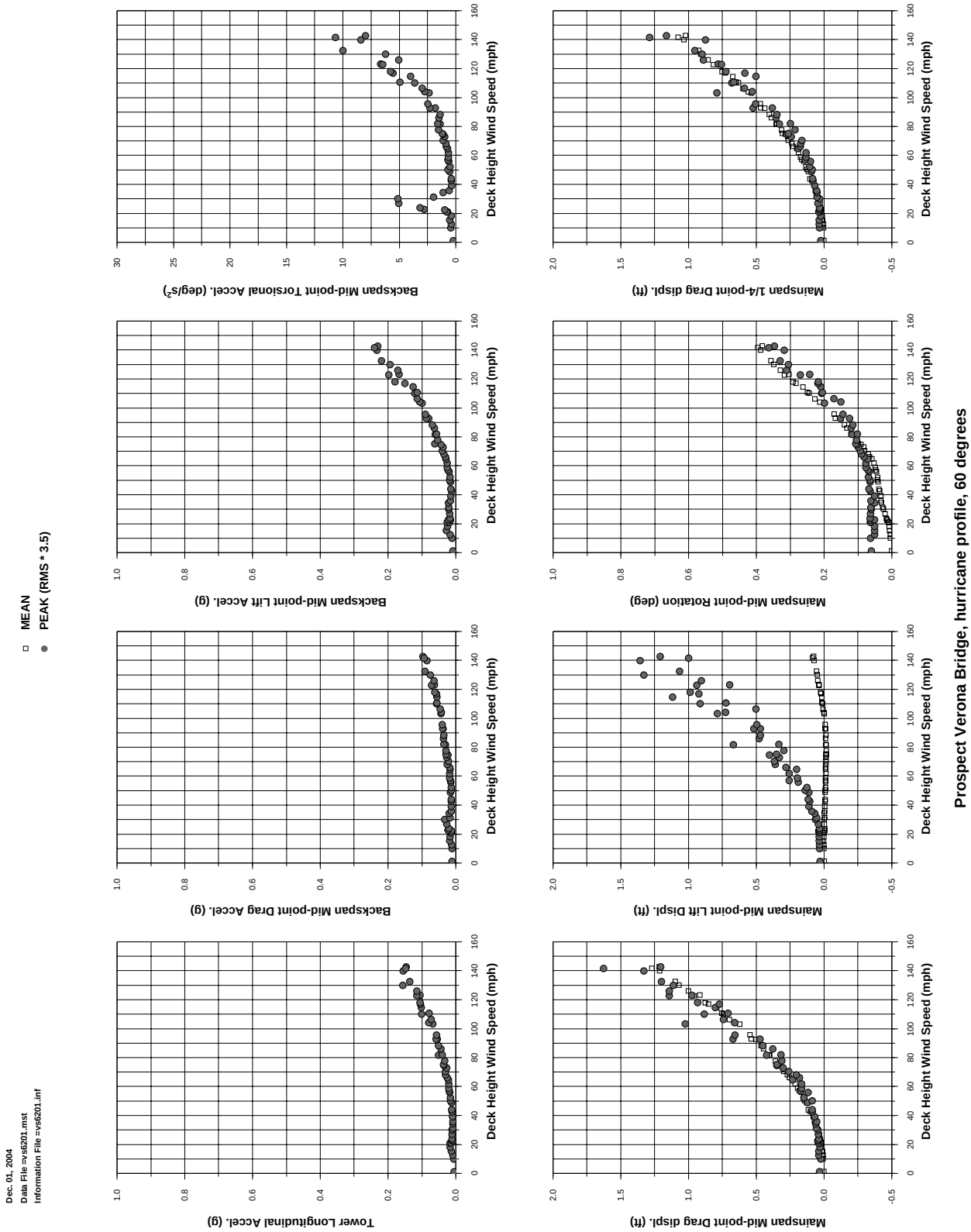

Prospect Verona Bridge, hurricane profile, 60 degrees

Dec. 01, 2004
Data File =vs6201.mst
Information File =vs6201.inf

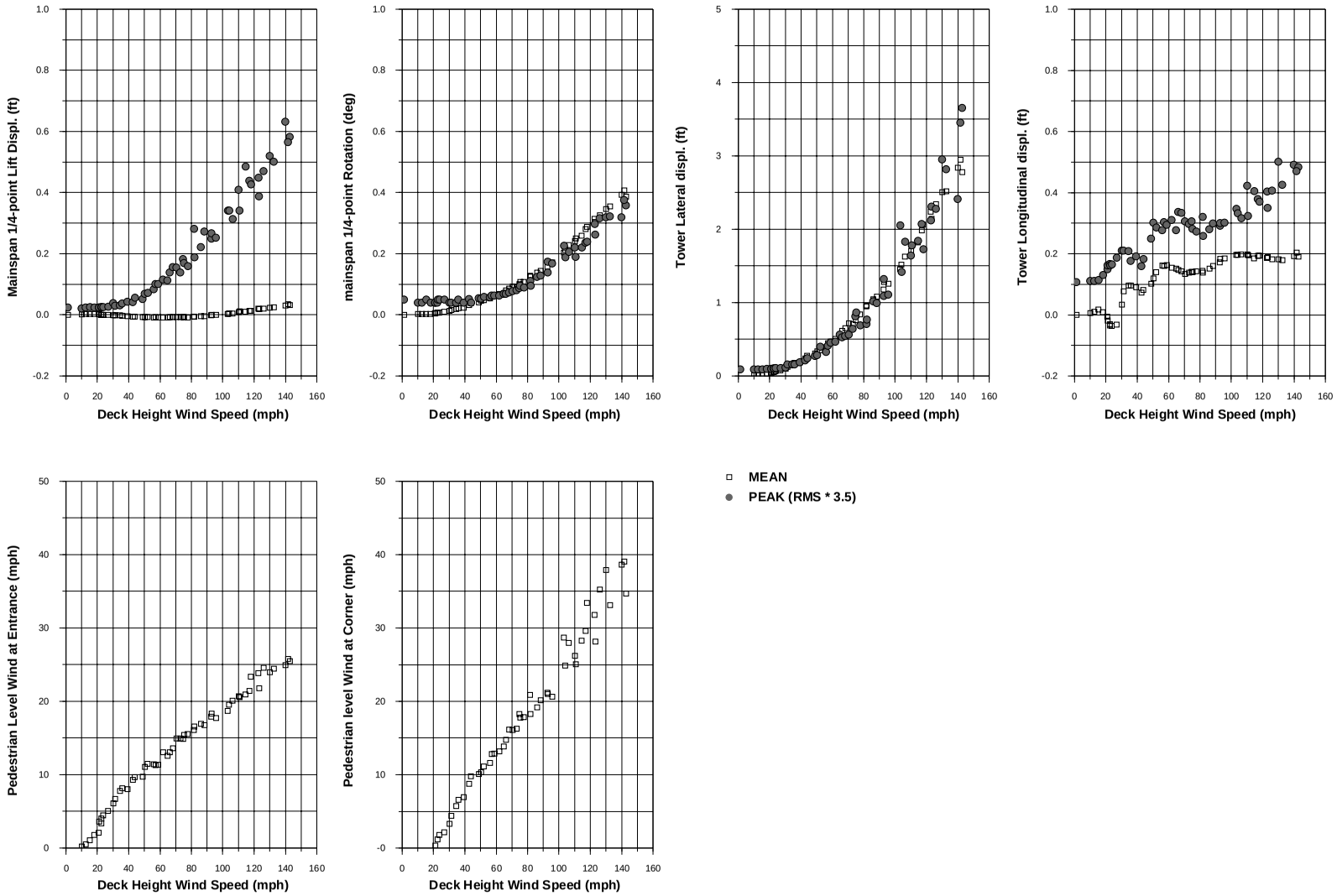

Prospect Verona Bridge, hurricane profile, 60 degrees

Dec. 01, 2004
Data File =vs2201.mst
Information File =vs2201.inf

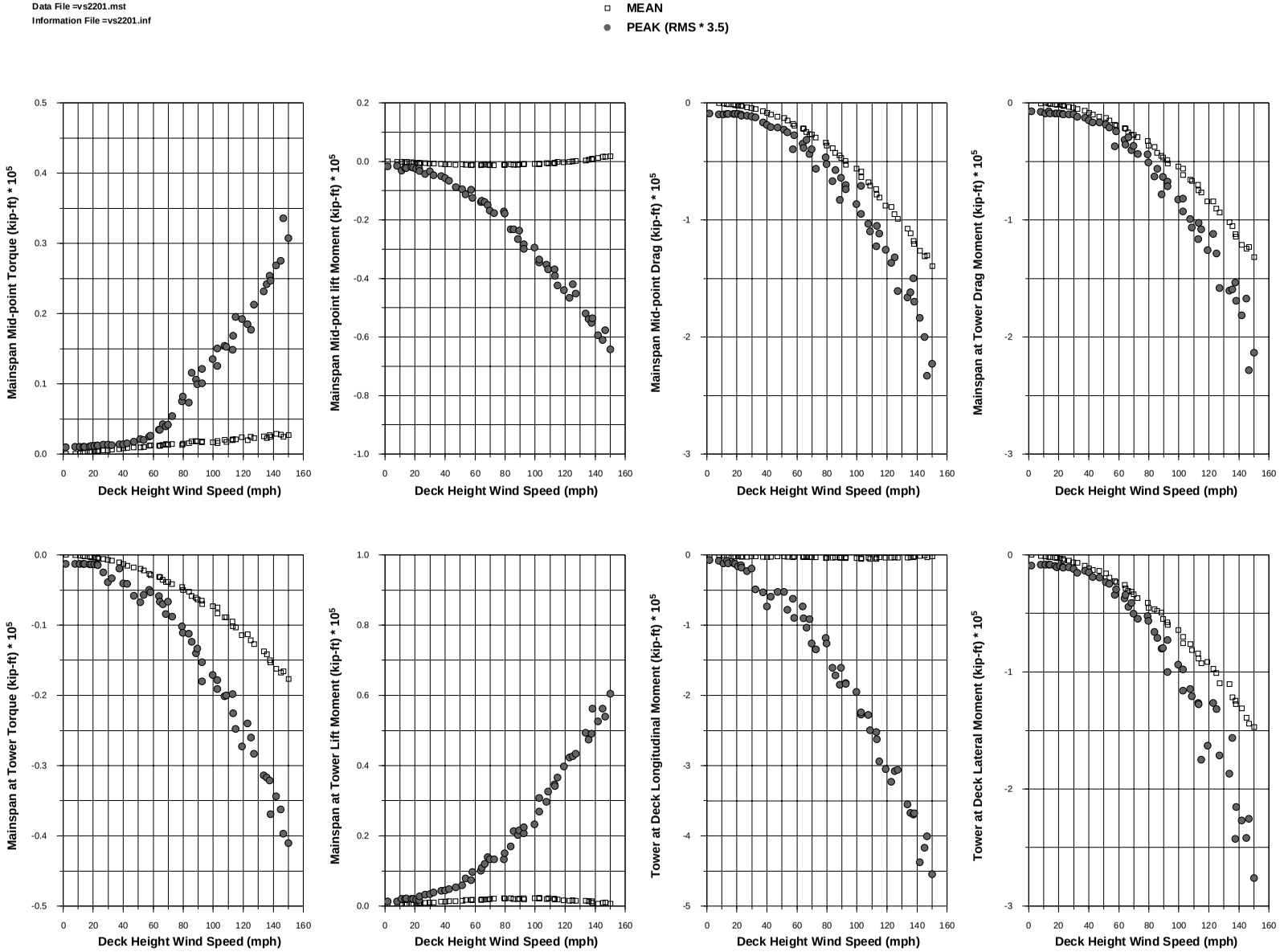

Prospect Verona Bridge, Hurricane Profile, 270 degrees, with existing bridge

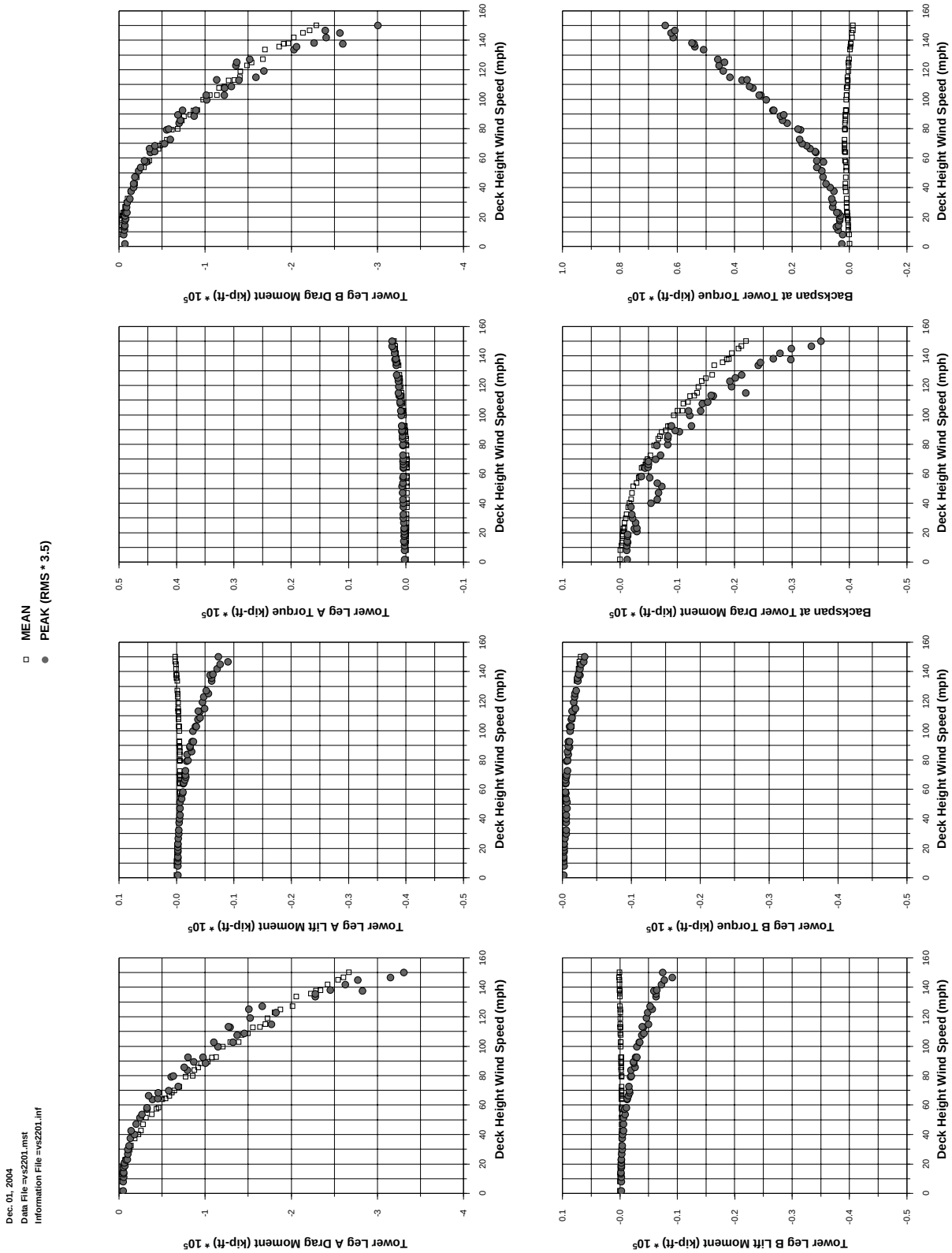

Prospect Verona Bridge, Hurricane Profile, 270 degrees, with existing bridge

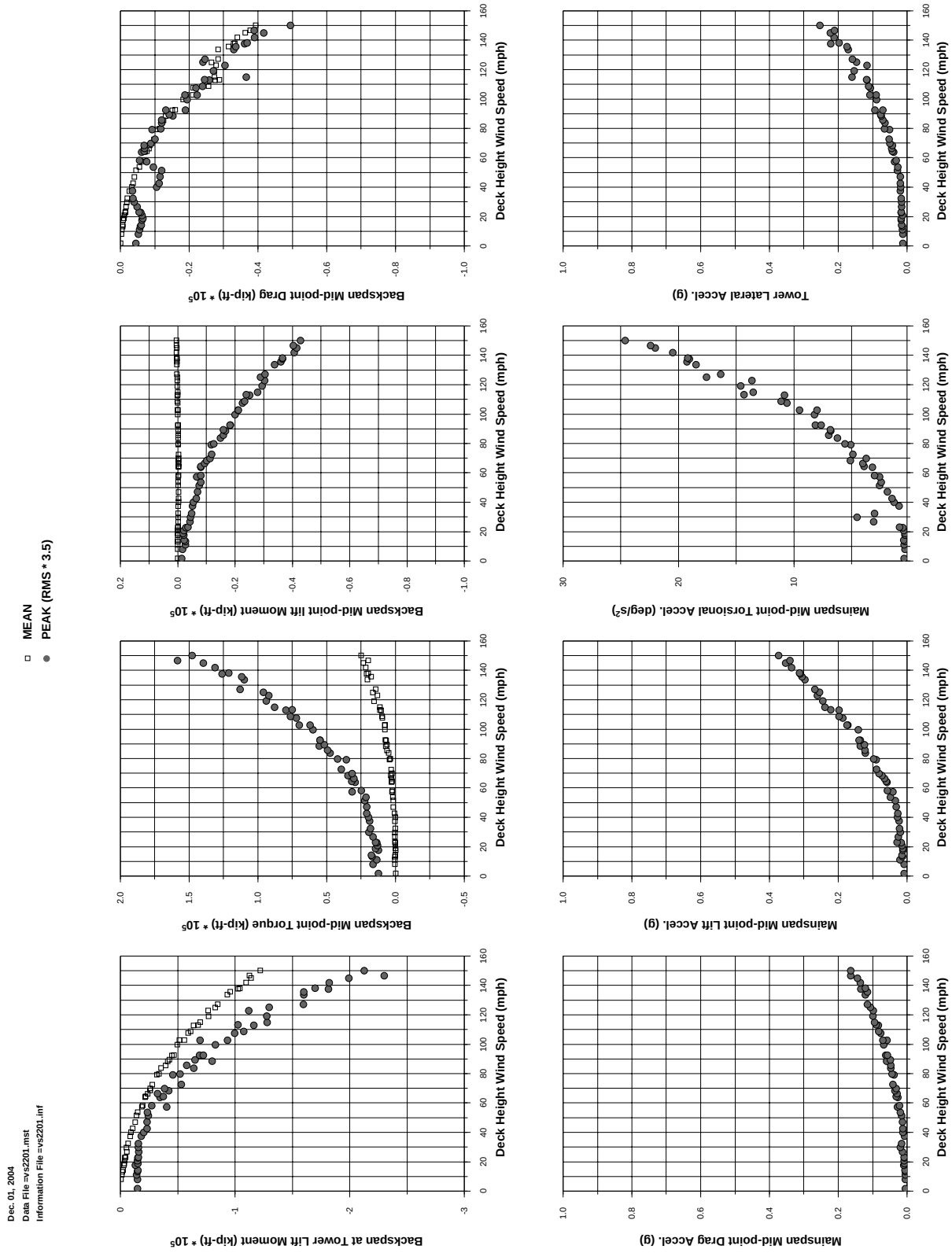

Prospect Verona Bridge, Hurricane Profile, 270 degrees, with existing bridge

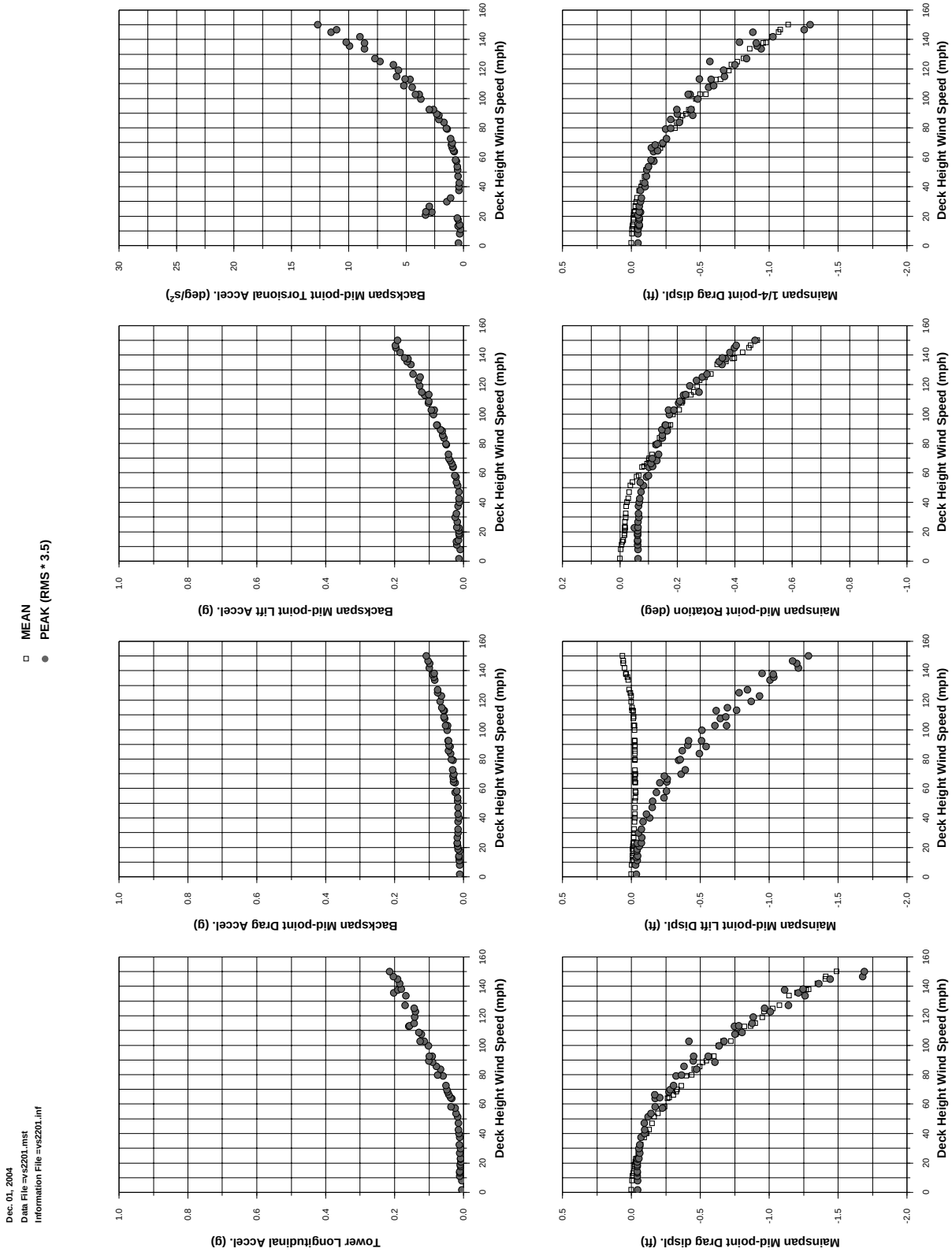

Prospect Verona Bridge, Hurricane Profile, 270 degrees, with existing bridge

Dec. 01, 2004
Data File =vs2201.mst
Information File =vs2201.inf

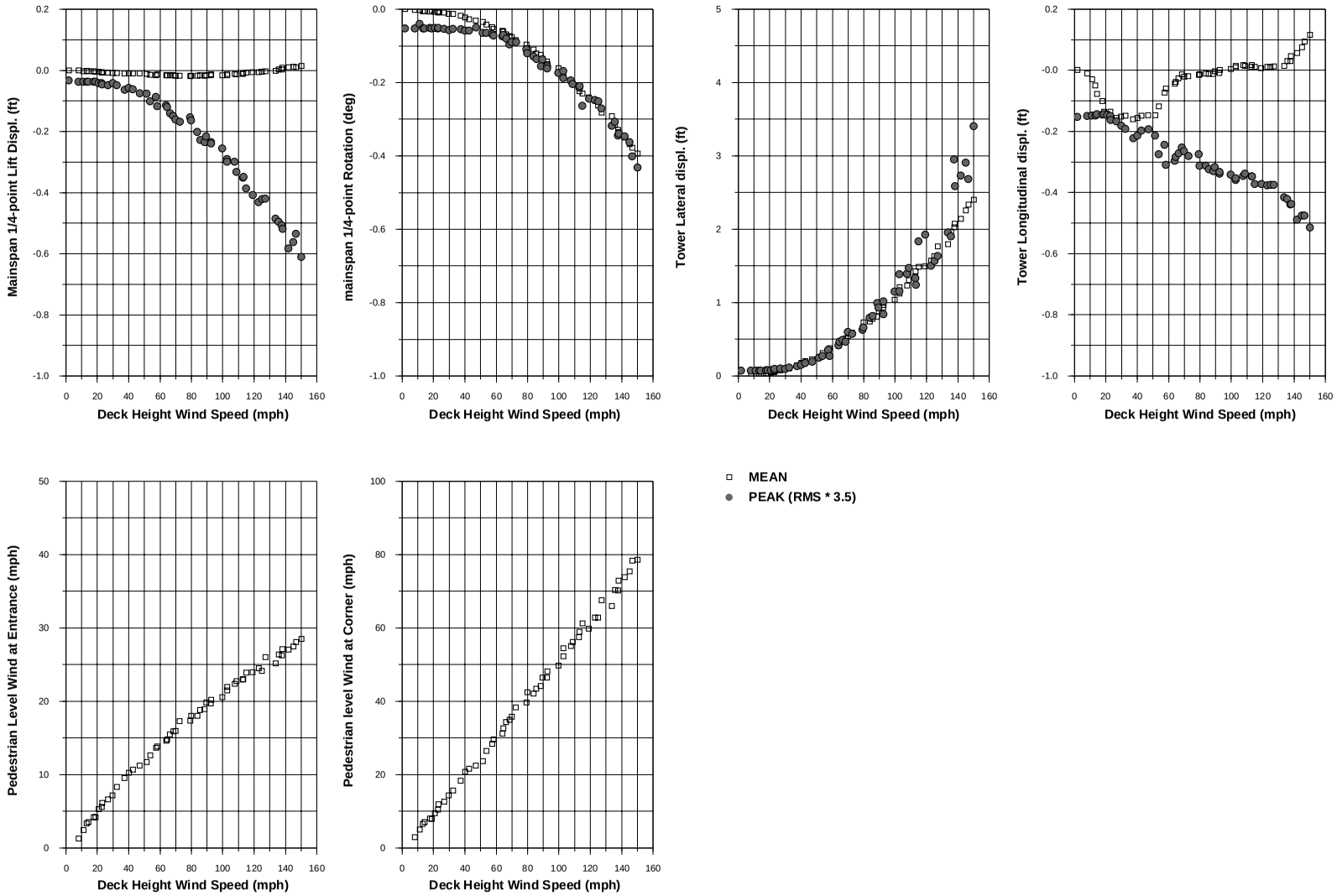

Prospect Verona Bridge, Hurricane Profile, 270 degrees, with existing bridge

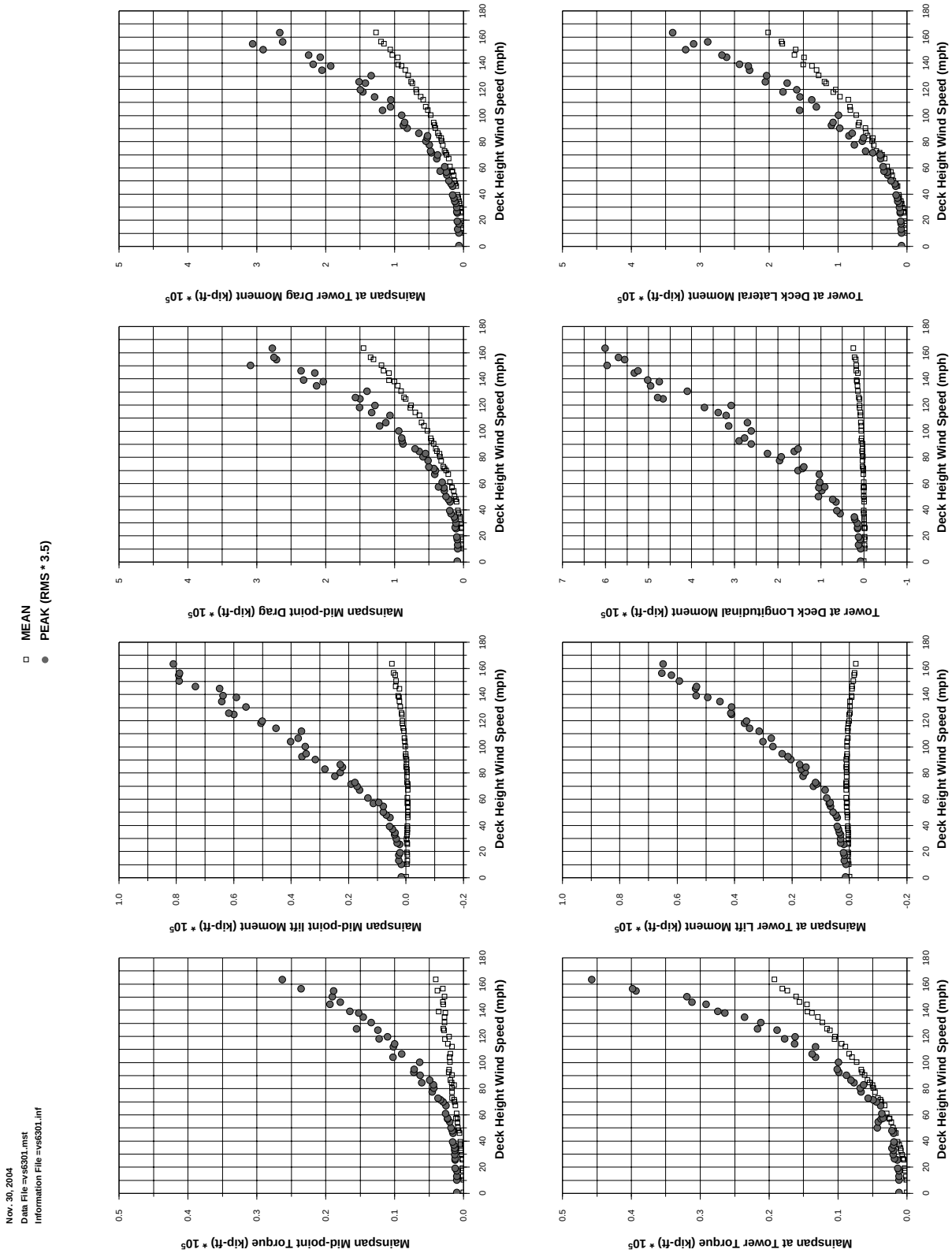

Prospect Verona Bridge, open country profile, 60 degrees

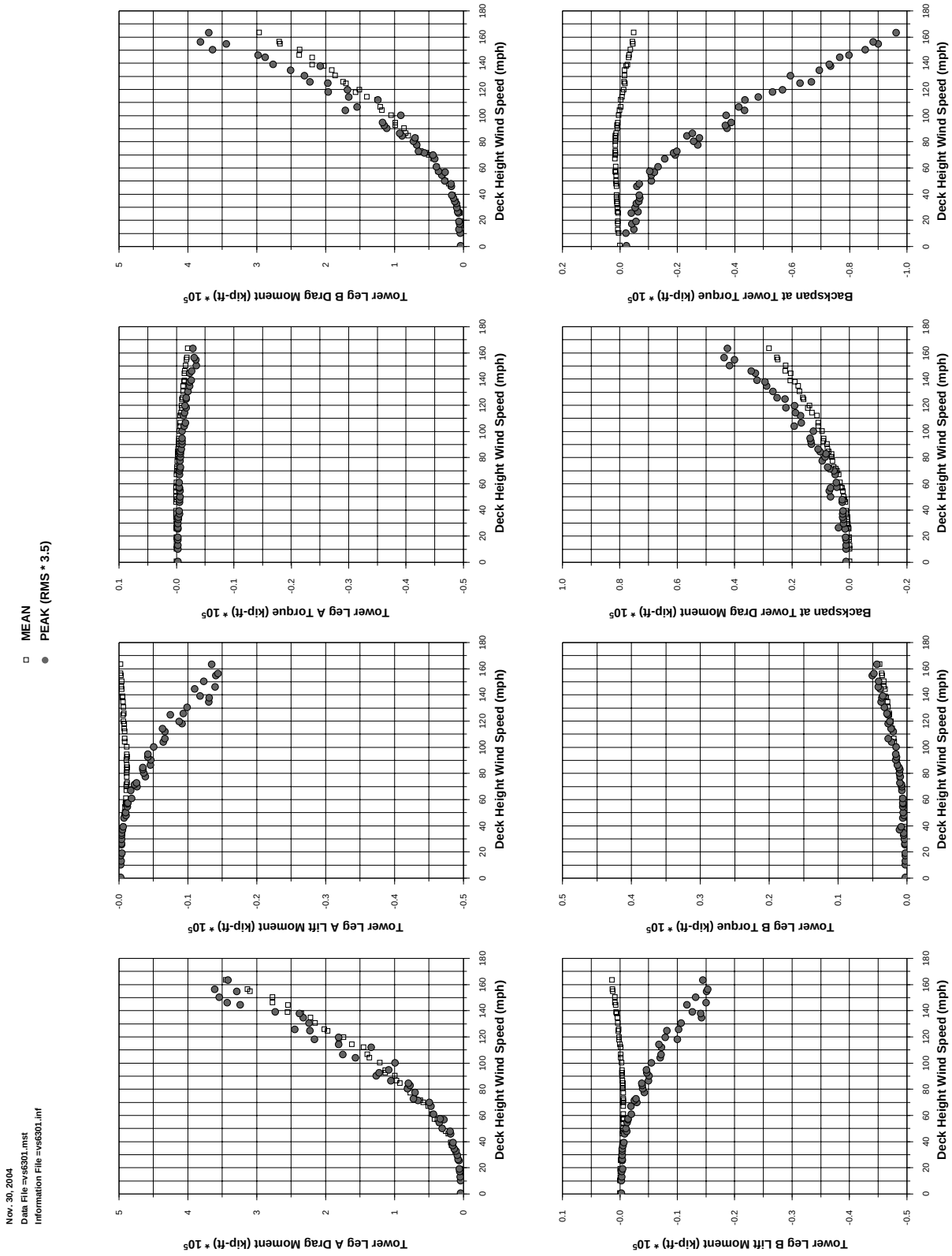

Prospect Verona Bridge, open country profile, 60 degrees

Nov. 30, 2004
Data File =vs6301.mst
Information File =vs6301.inf

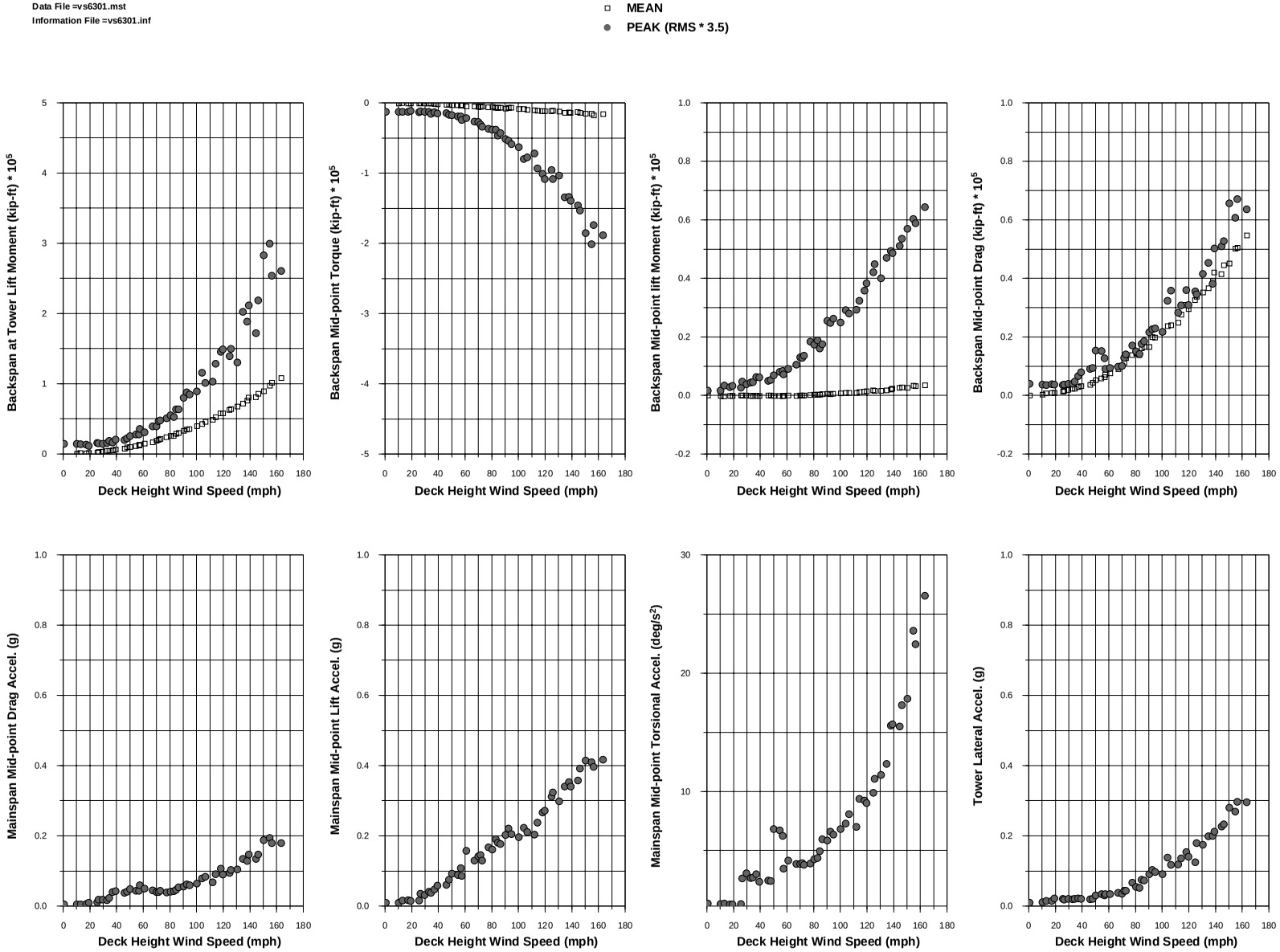

Prospect Verona Bridge, open country profile, 60 degrees

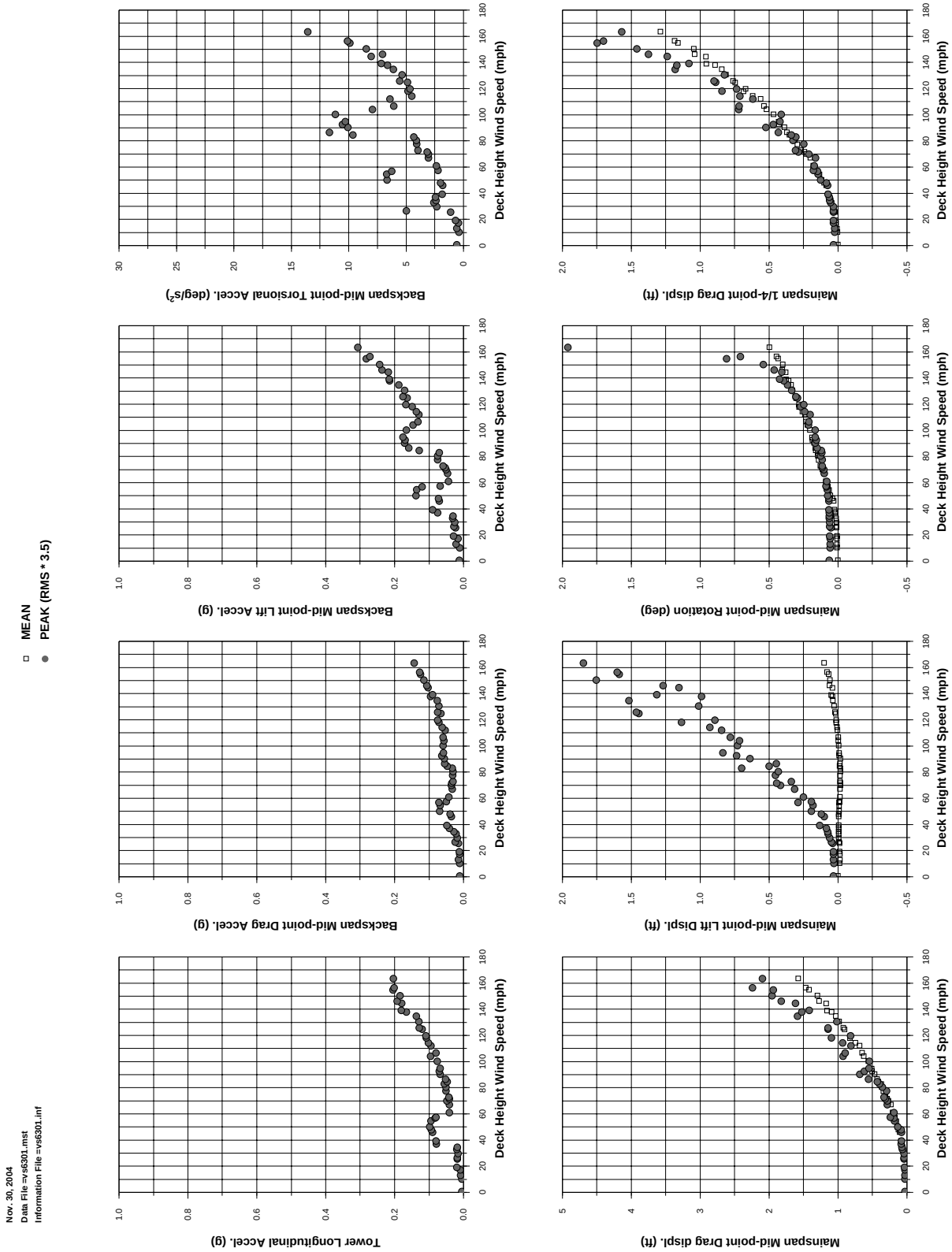

Prospect Verona Bridge, open country profile, 60 degrees

Nov. 30, 2004
Data File =vs6301.mst
Information File =vs6301.inf

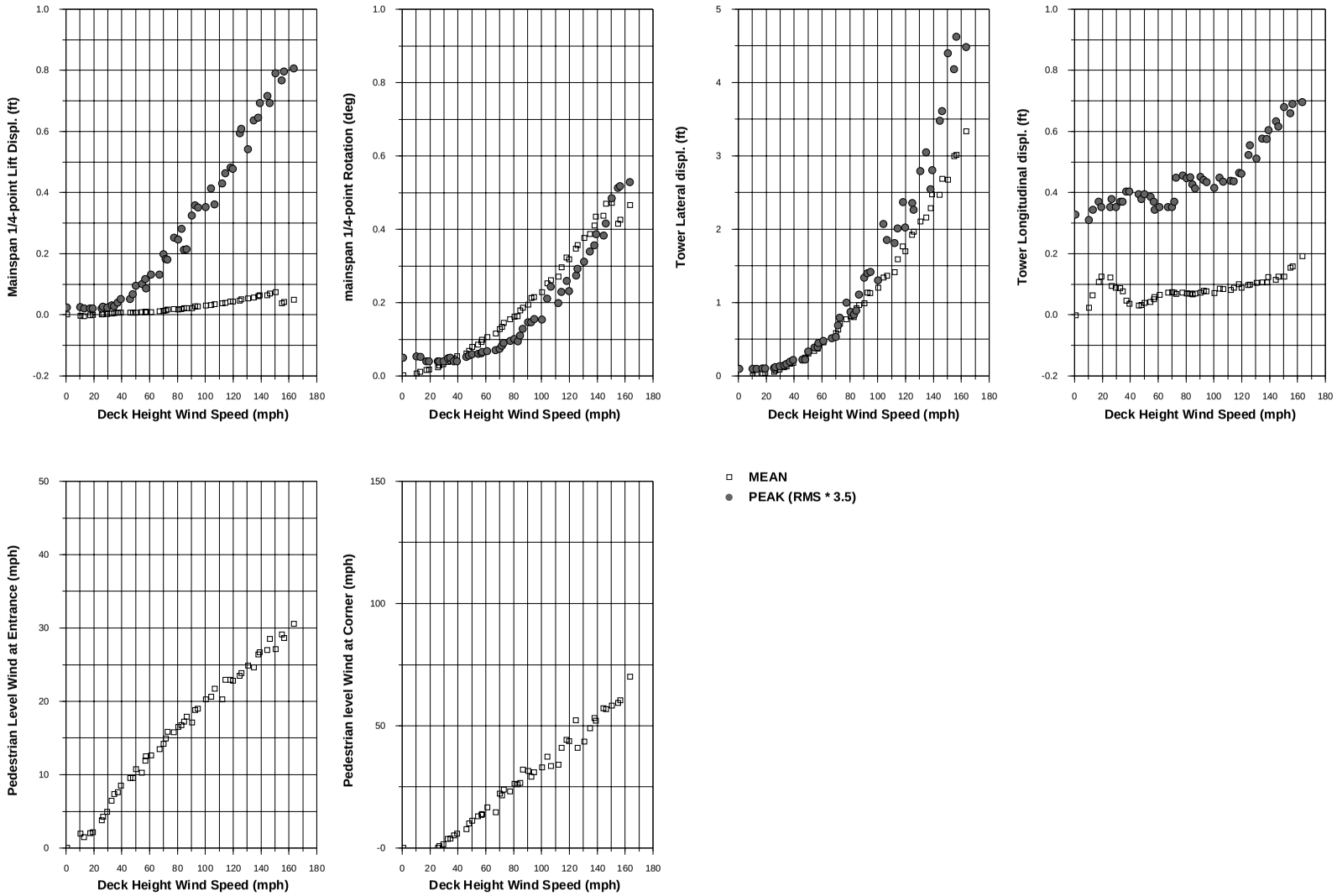

Prospect Verona Bridge, open country profile, 60 degrees

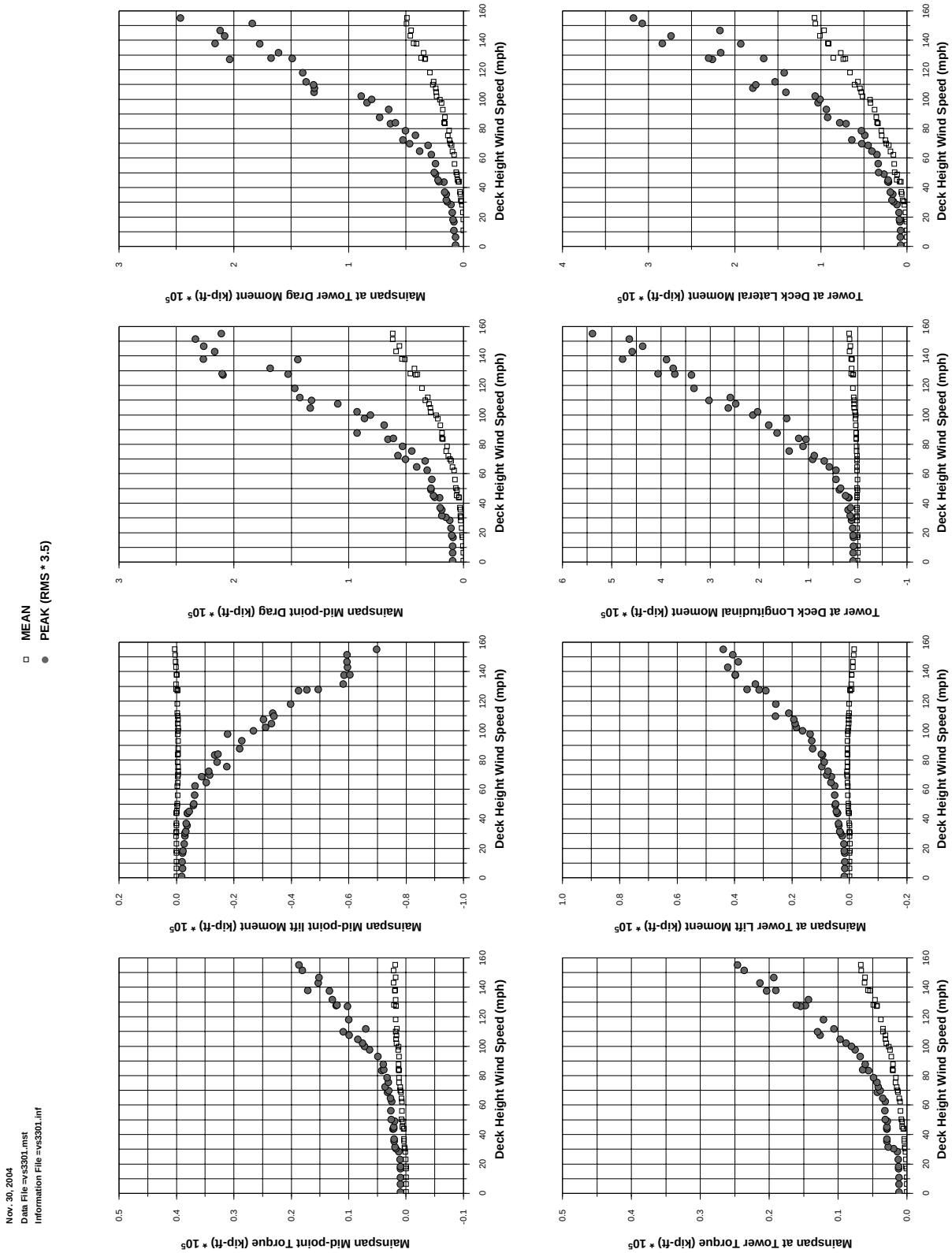

Prospect Verona Bridge, open country profile, 30 degrees

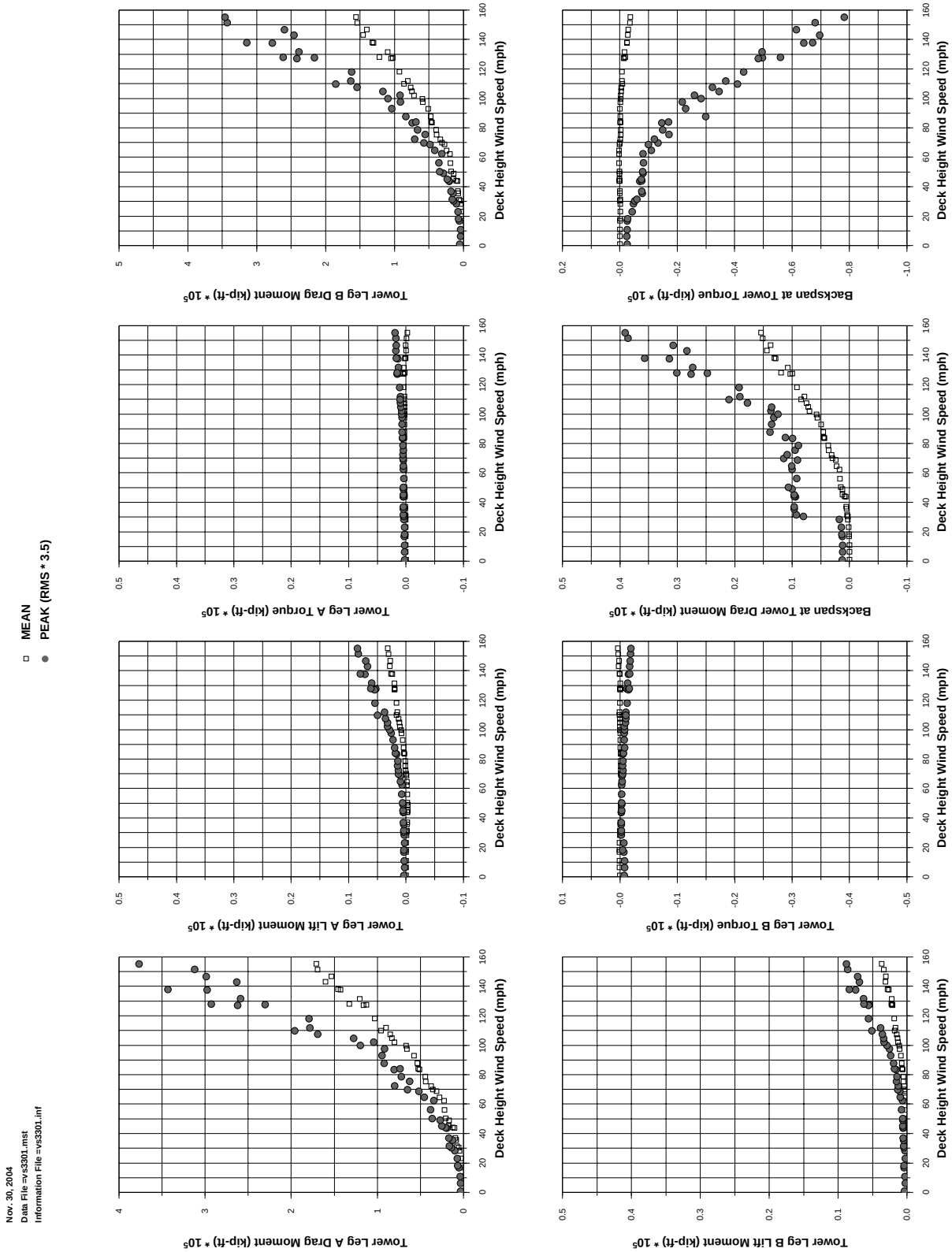

Prospect Verona Bridge, open country profile, 30 degrees

Nov. 30, 2004
Data File =vs3301.mst
Information File =vs3301.inf

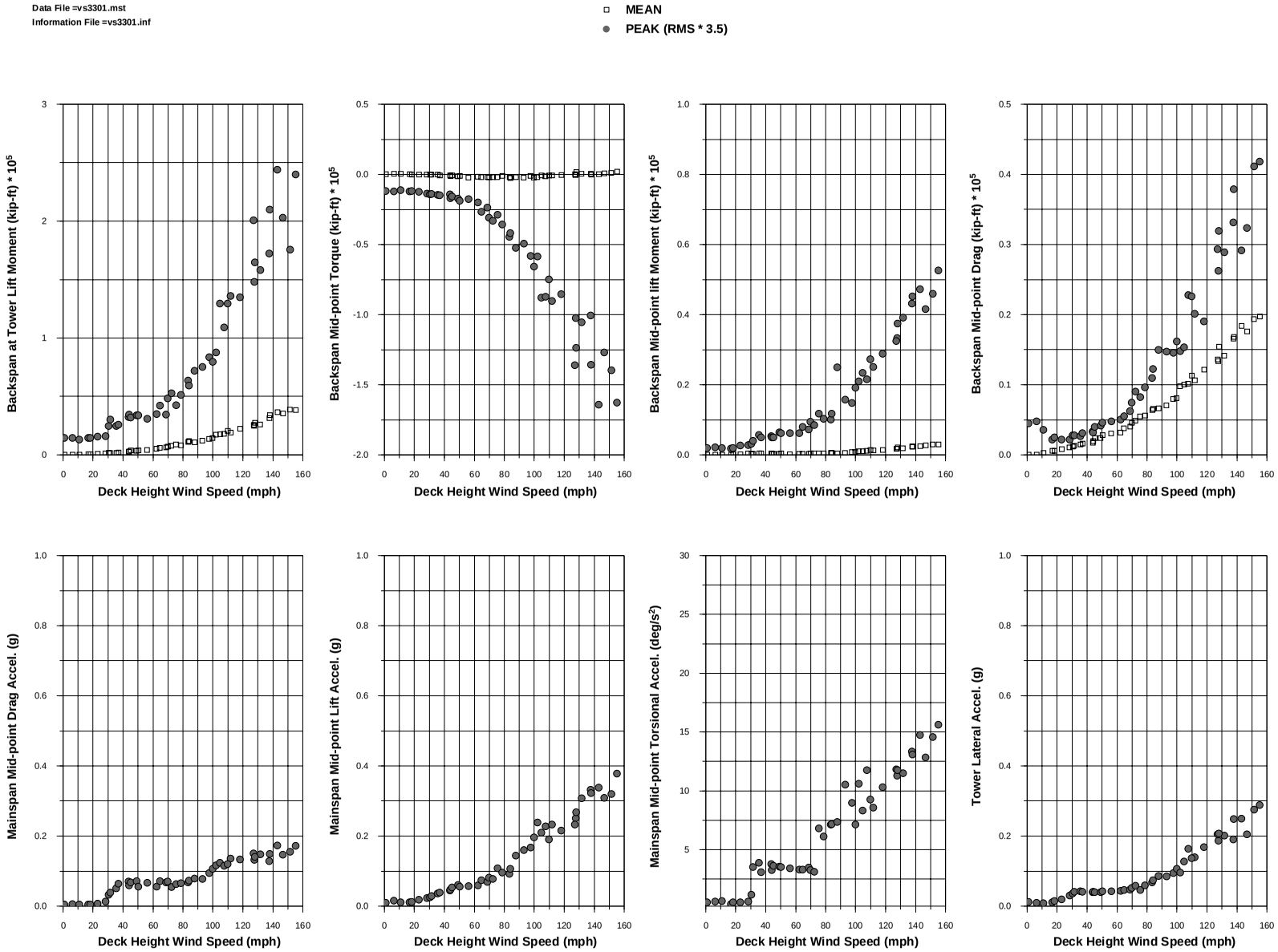

Prospect Verona Bridge, open country profile, 30 degrees

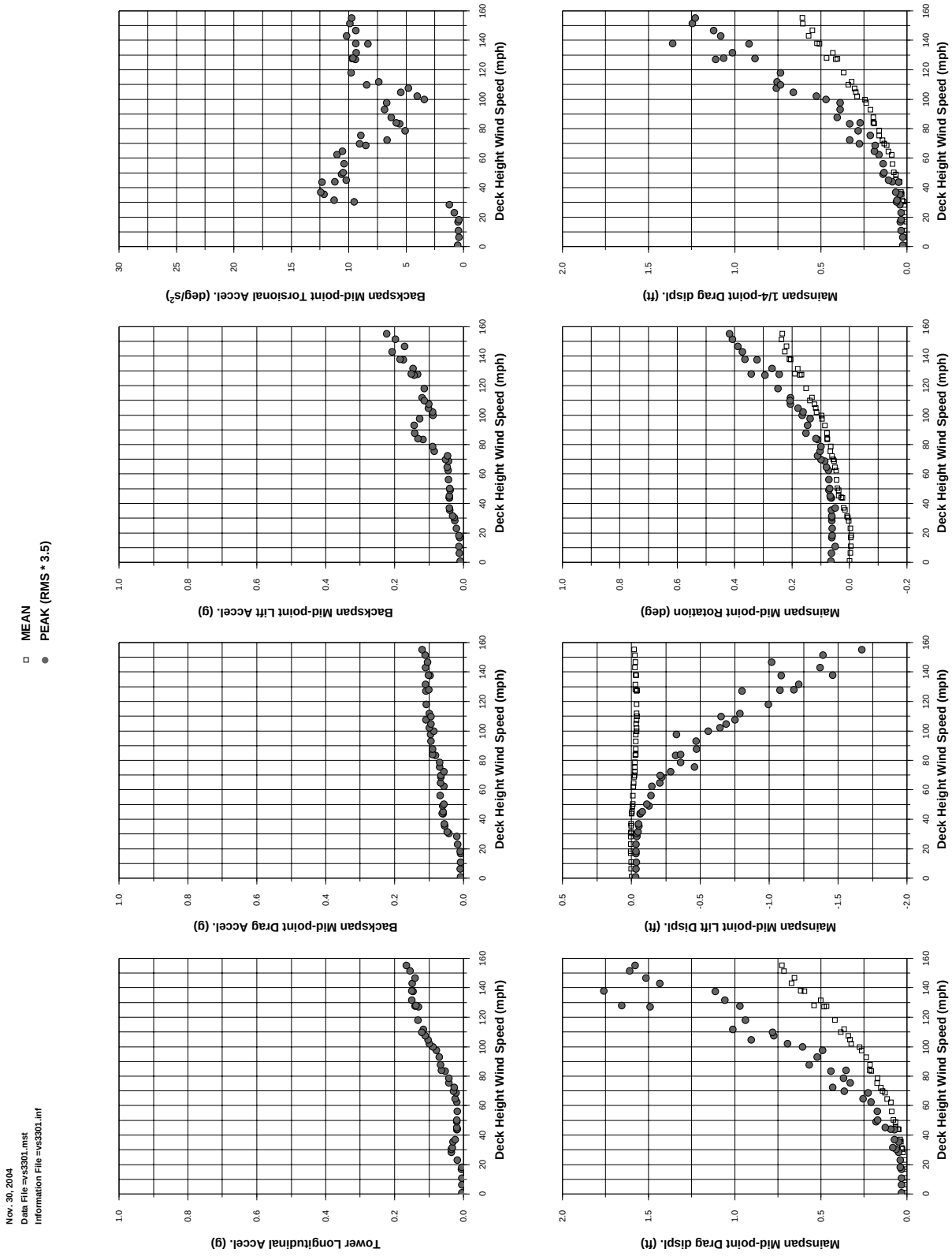

Prospect Verona Bridge, open country profile, 30 degrees

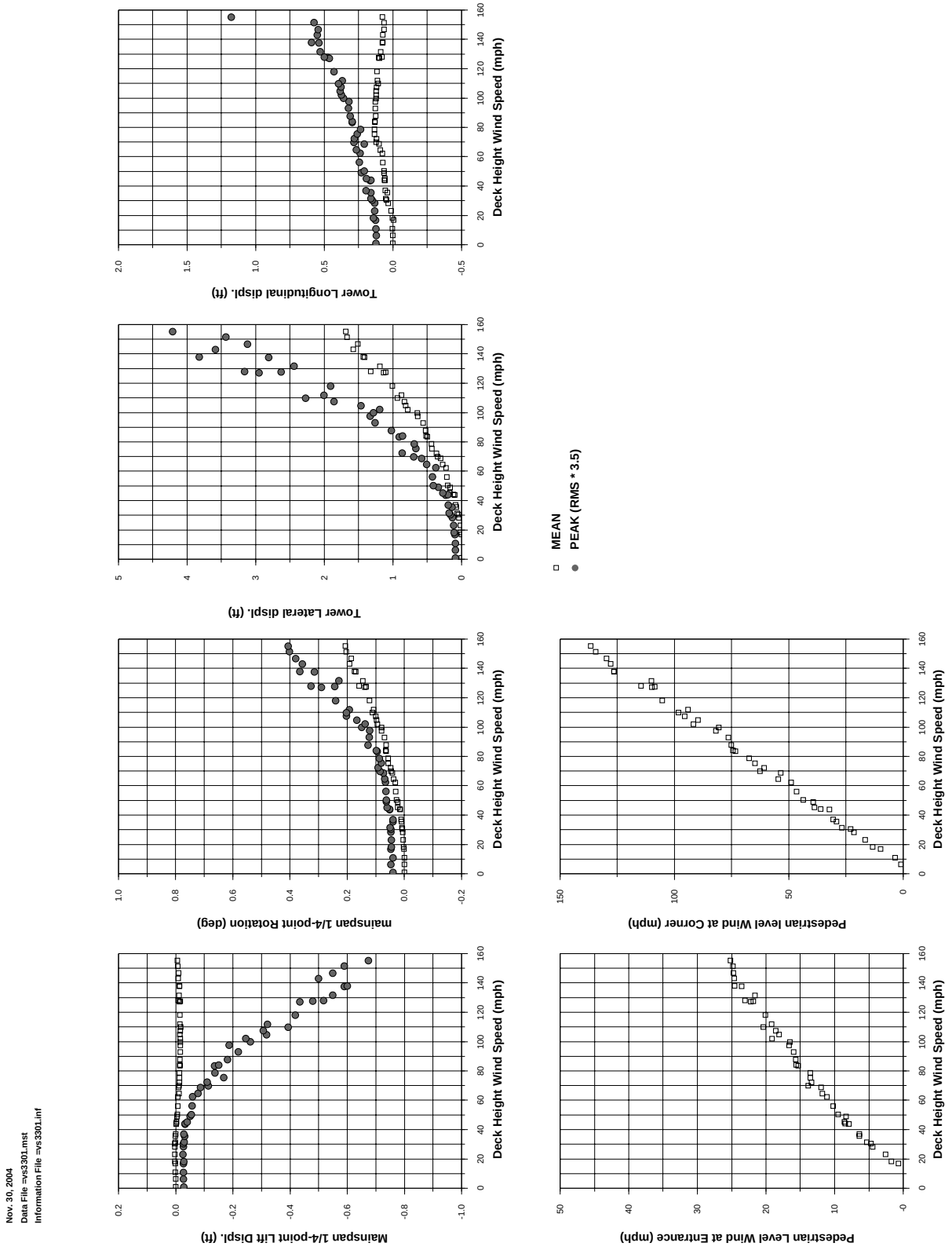

Prospect Verona Bridge, open country profile, 30 degrees

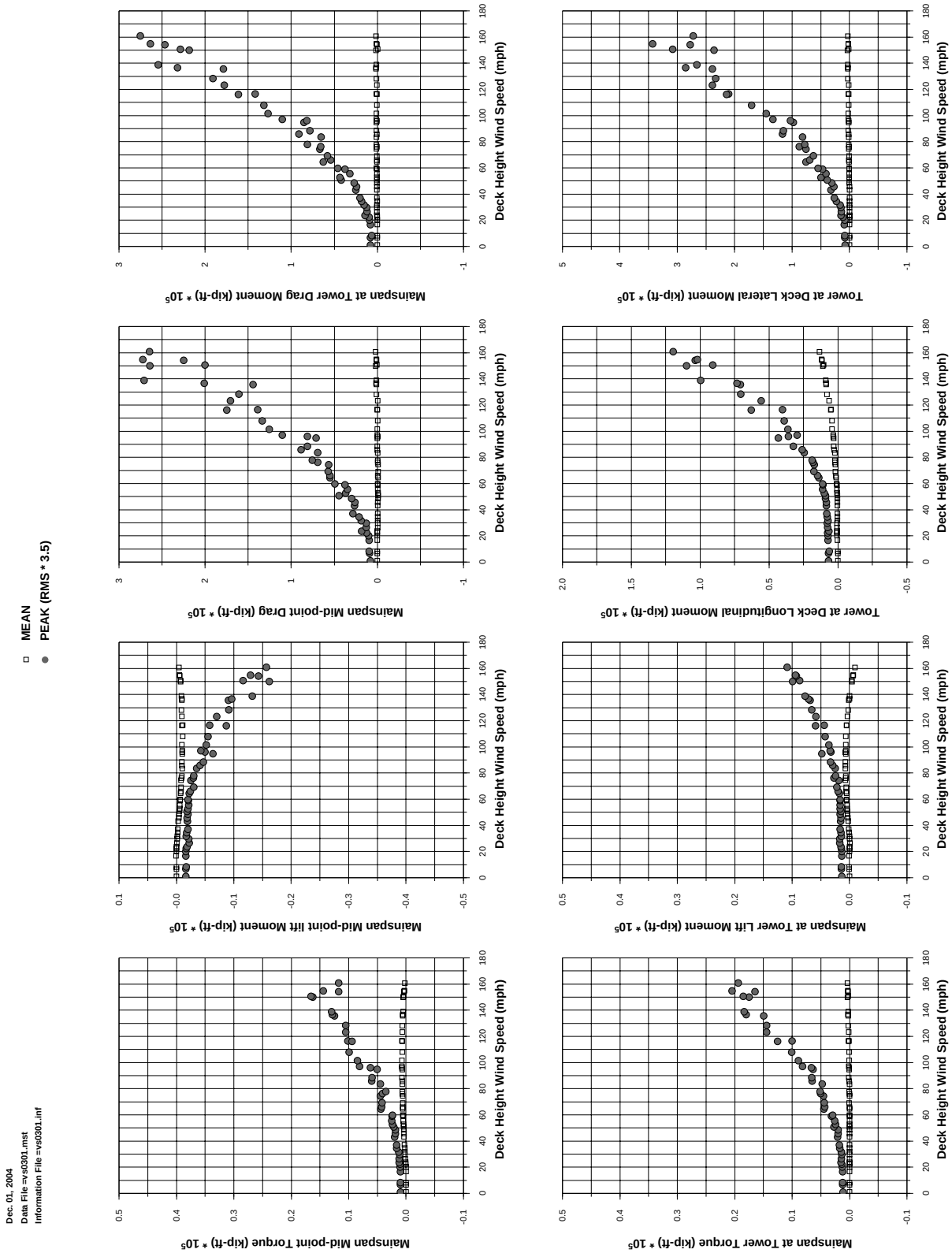

Prospect Verona Bridge, open country profile, 0 degrees (along bridge)

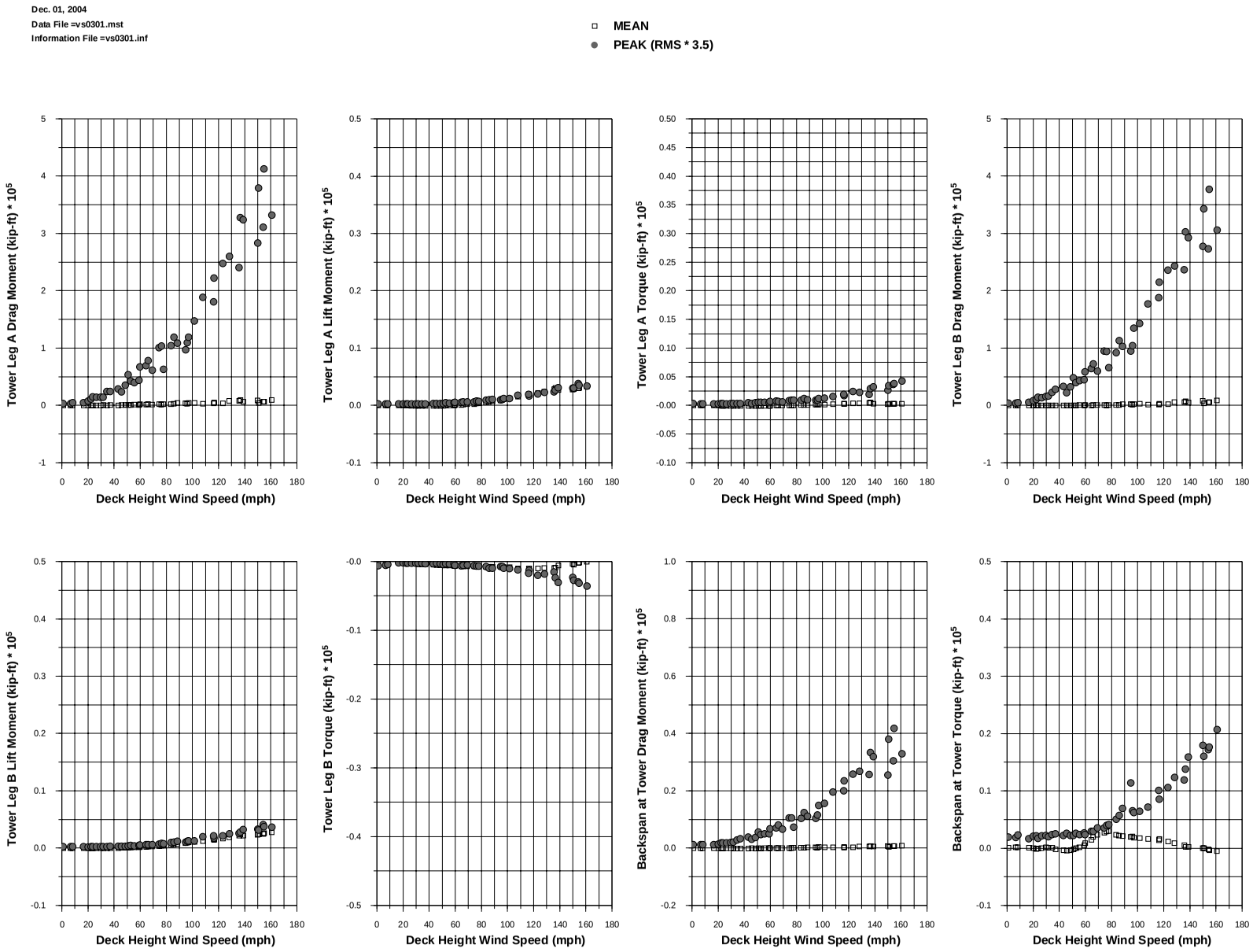

Prospect Verona Bridge, open country profile, 0 degrees (along bridge)

Dec. 01, 2004
Data File =vs0301.mst
Information File =vs0301.inf

MEAN
PEAK (RMS * 3.5)

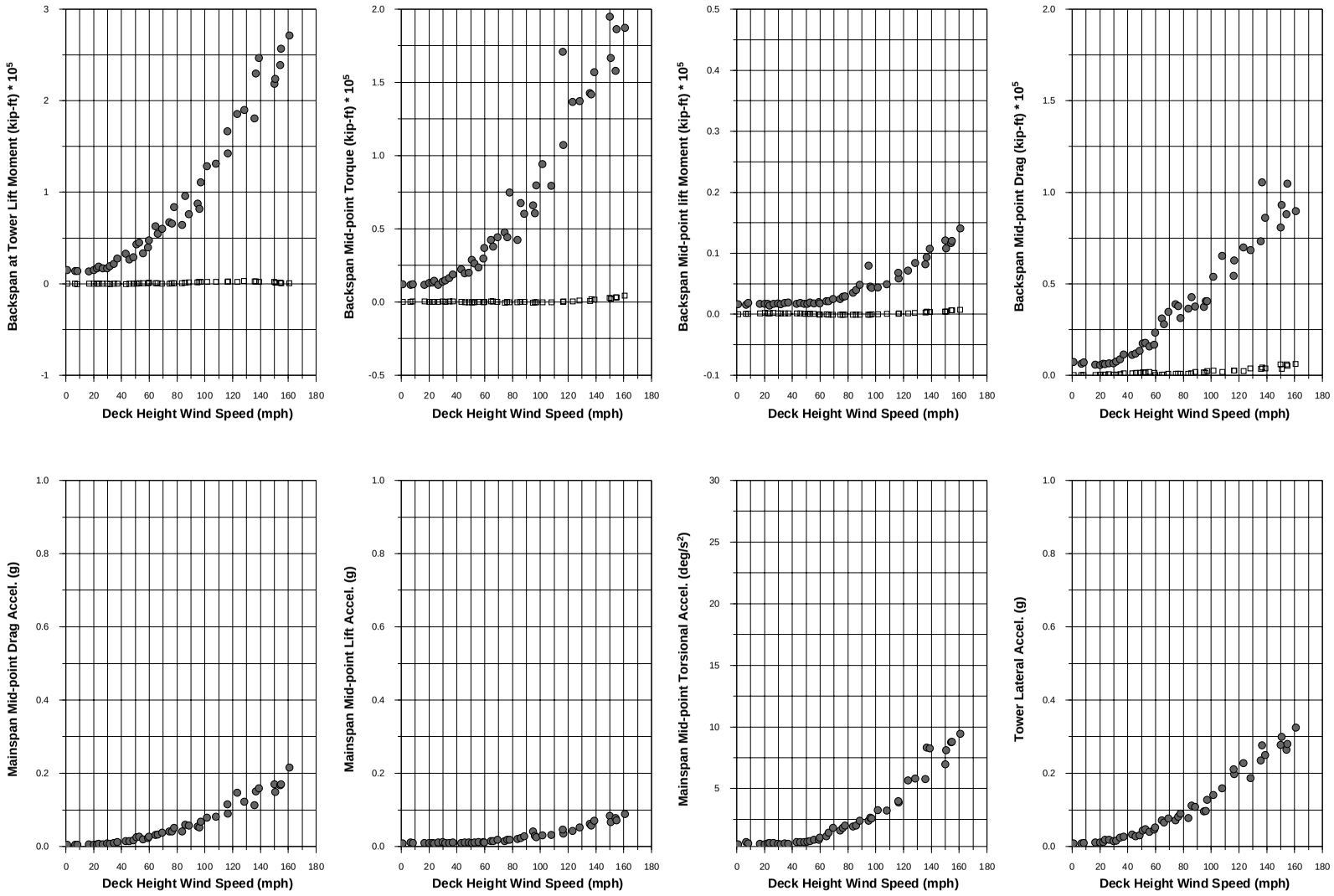

Prospect Verona Bridge, open country profile, 0 degrees (along bridge)

Dec. 01, 2004
Data File =vs0301.mst
Information File =vs0301.inf

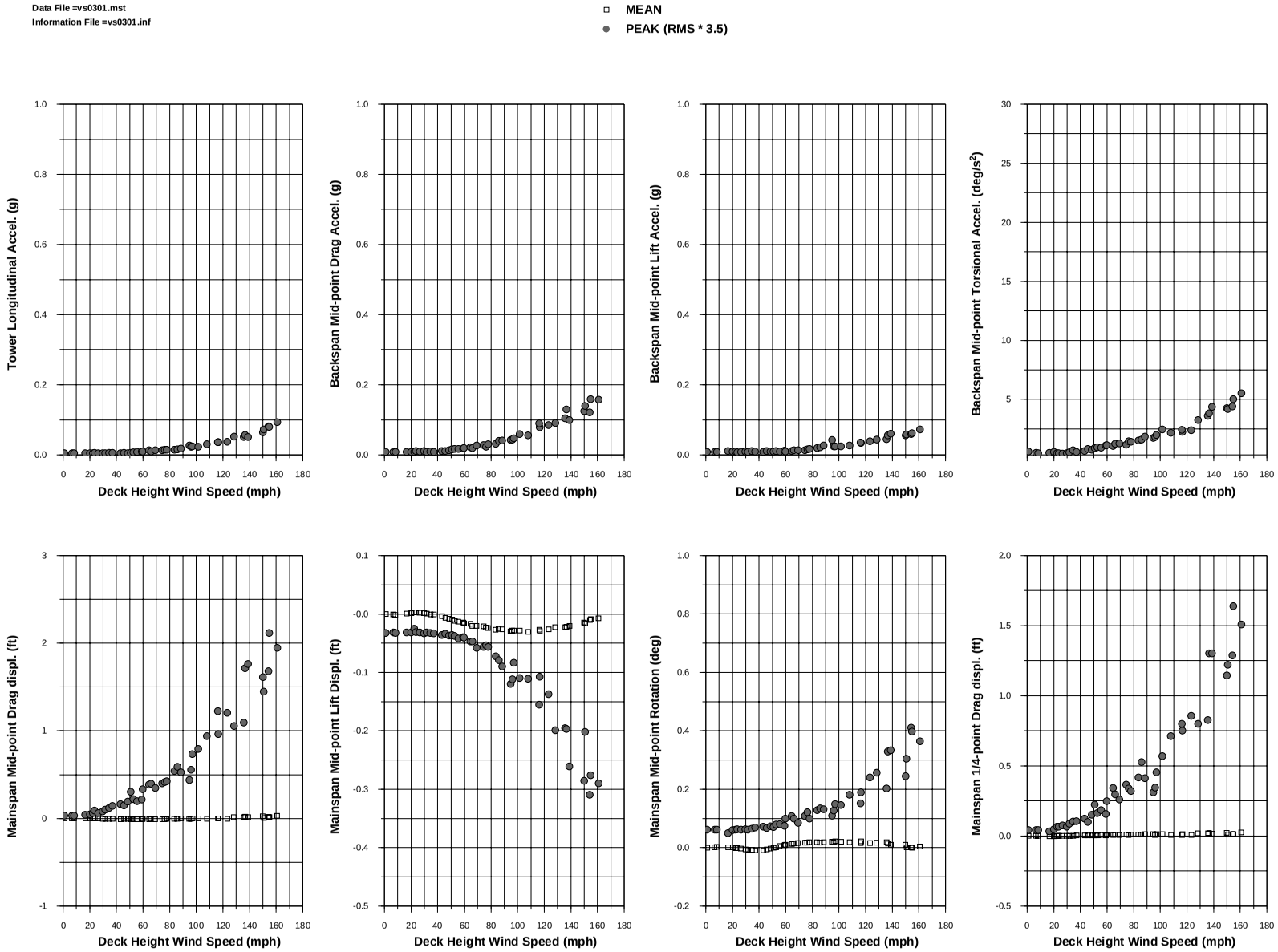

Prospect Verona Bridge, open country profile, 0 degrees (along bridge)

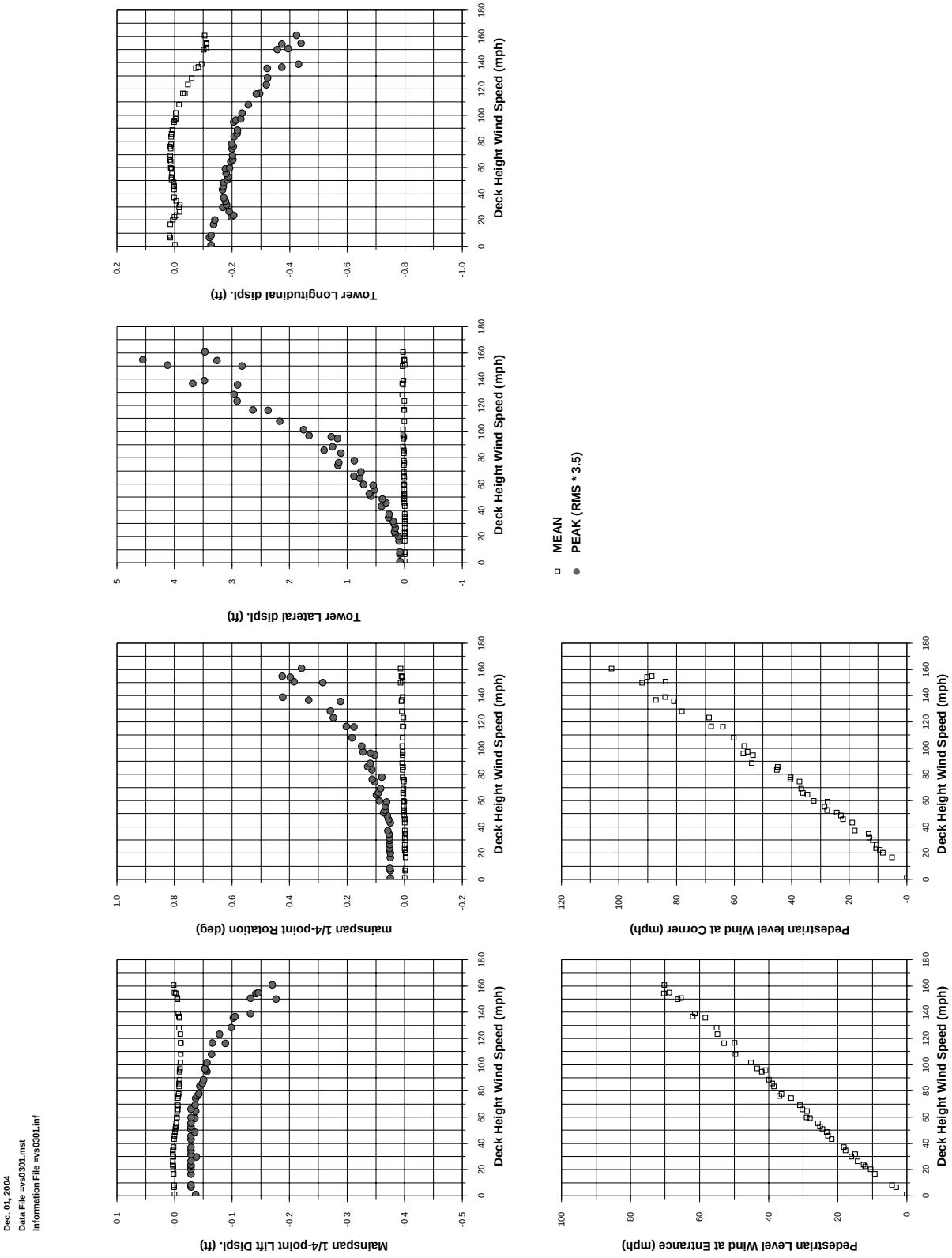

Prospect Verona Bridge, open country profile, 0 degrees (along bridge)

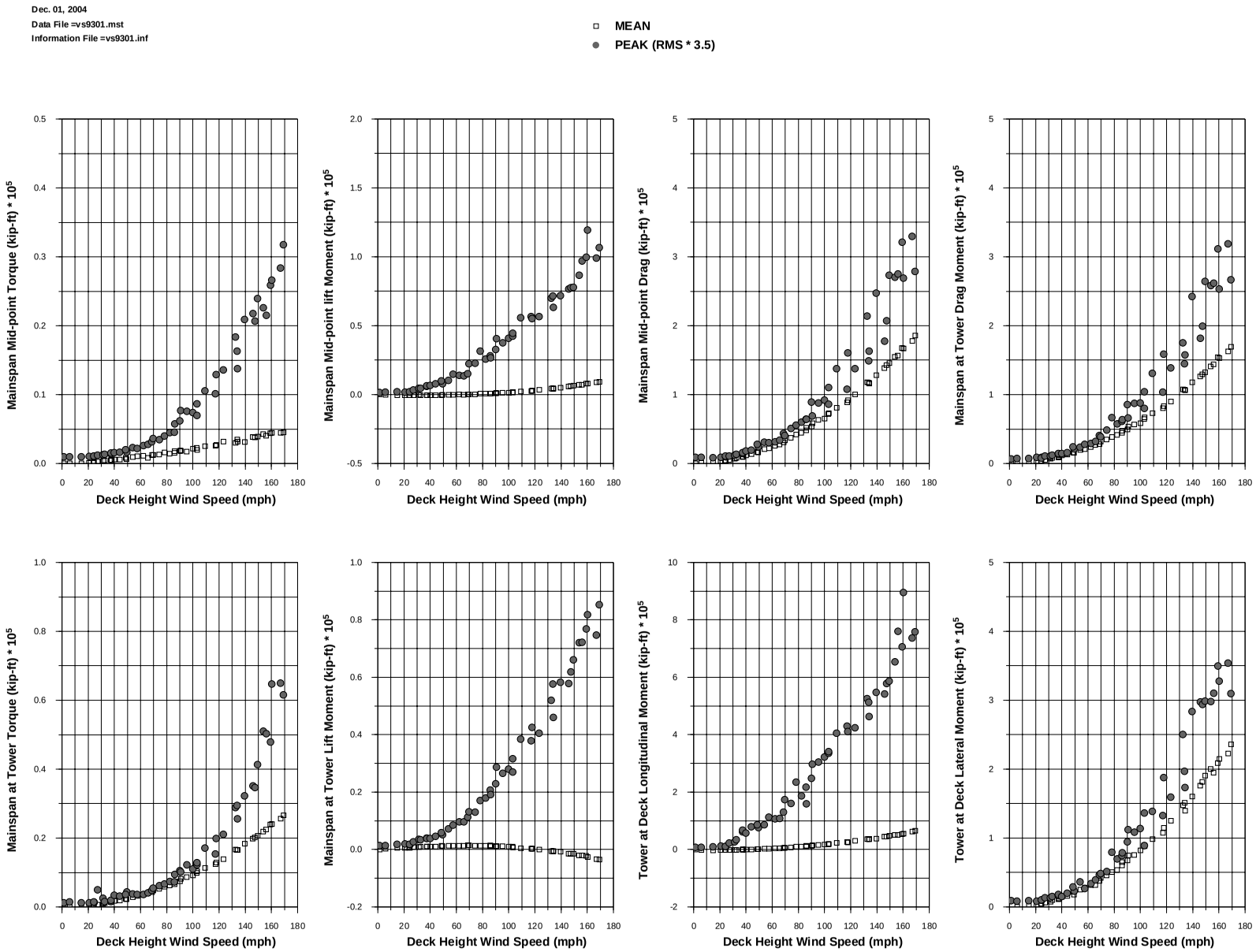

Prospect Verona Bridge, open country profile, 90 degrees (perpendicular to deck)

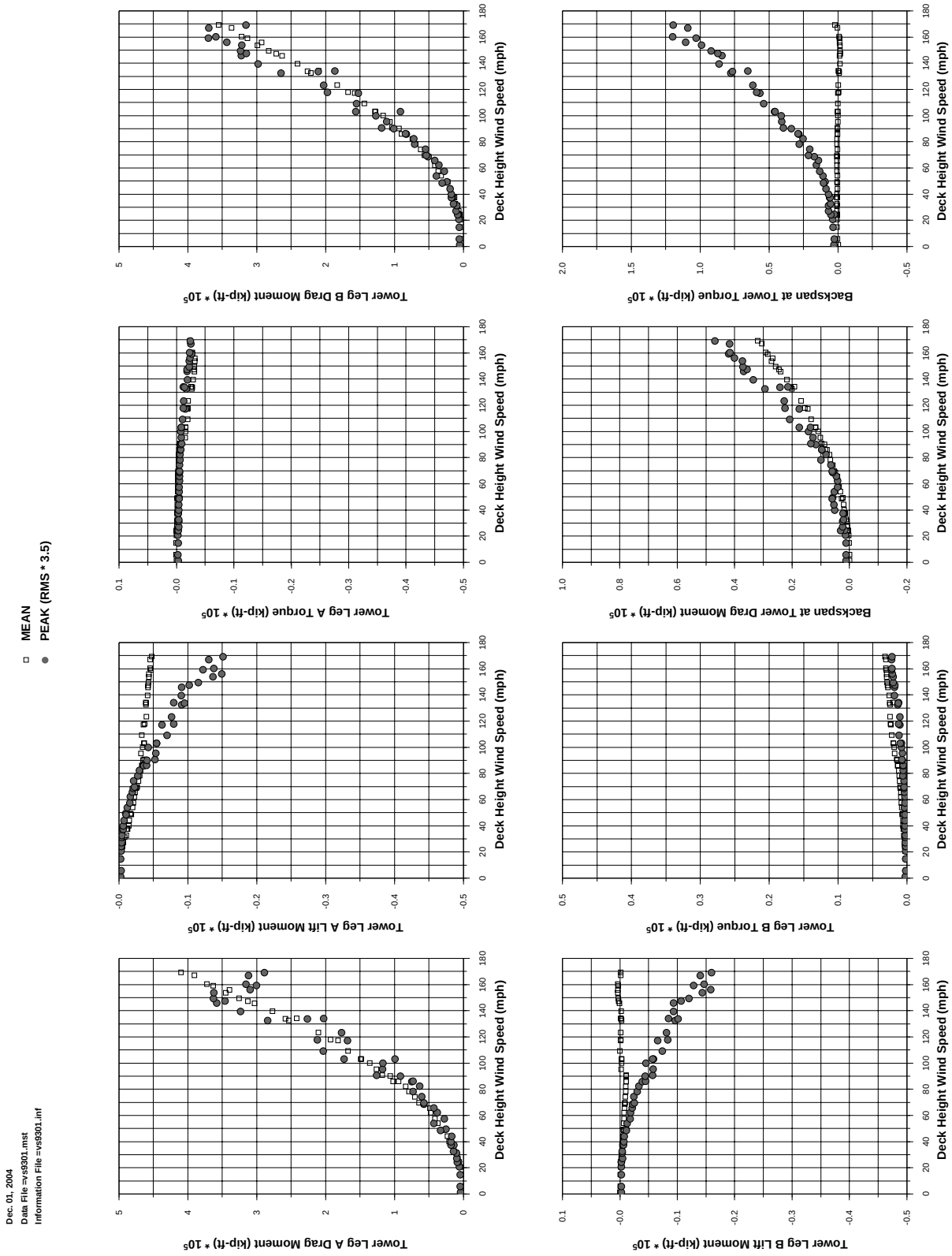

Prospect Verona Bridge, open country profile, 90 degrees (perpendicular to deck)

Dec. 01, 2004
Data File =vs9301.mst
Information File =vs9301.inf

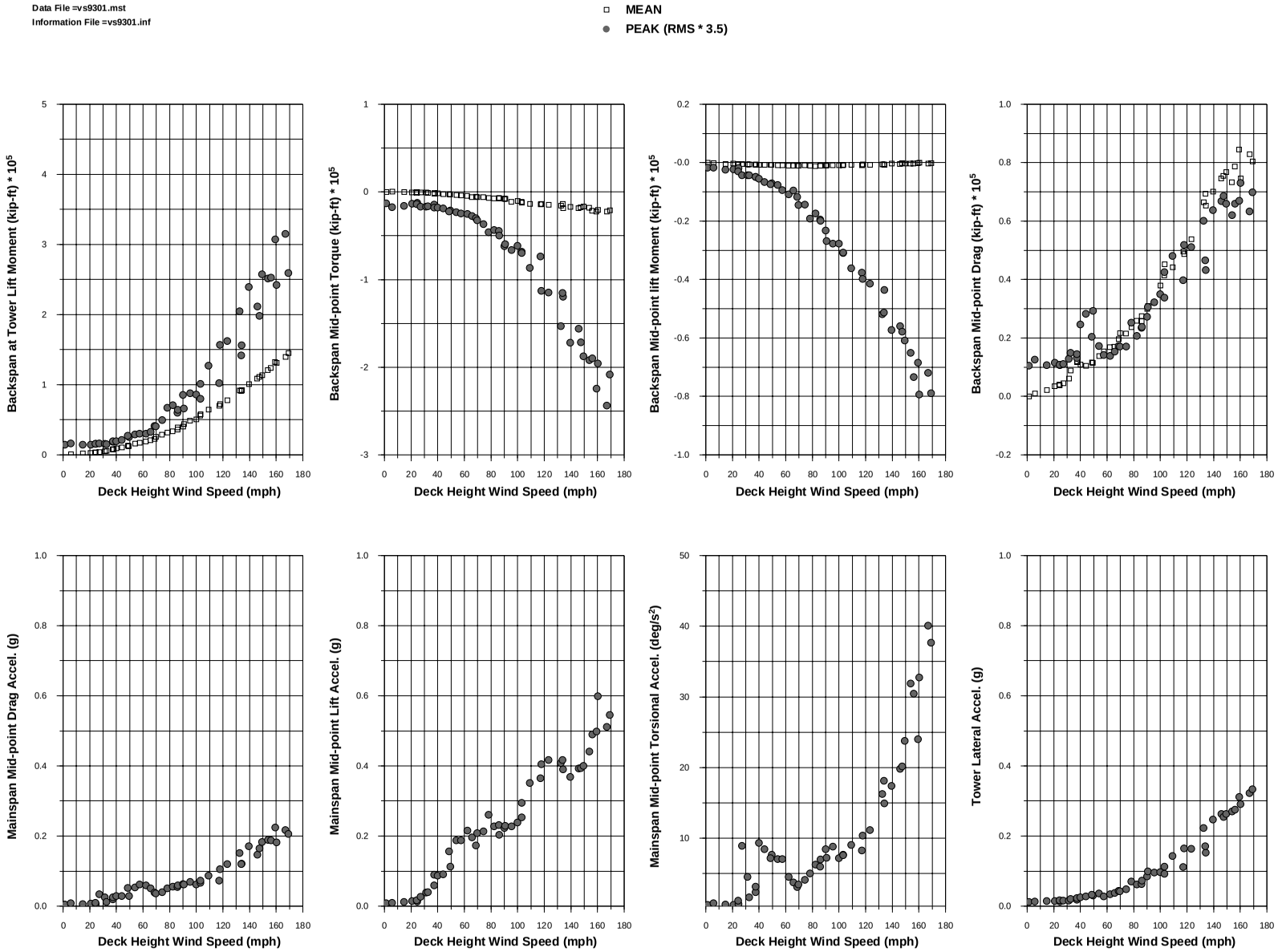

Prospect Verona Bridge, open country profile, 90 degrees (perpendicular to deck)

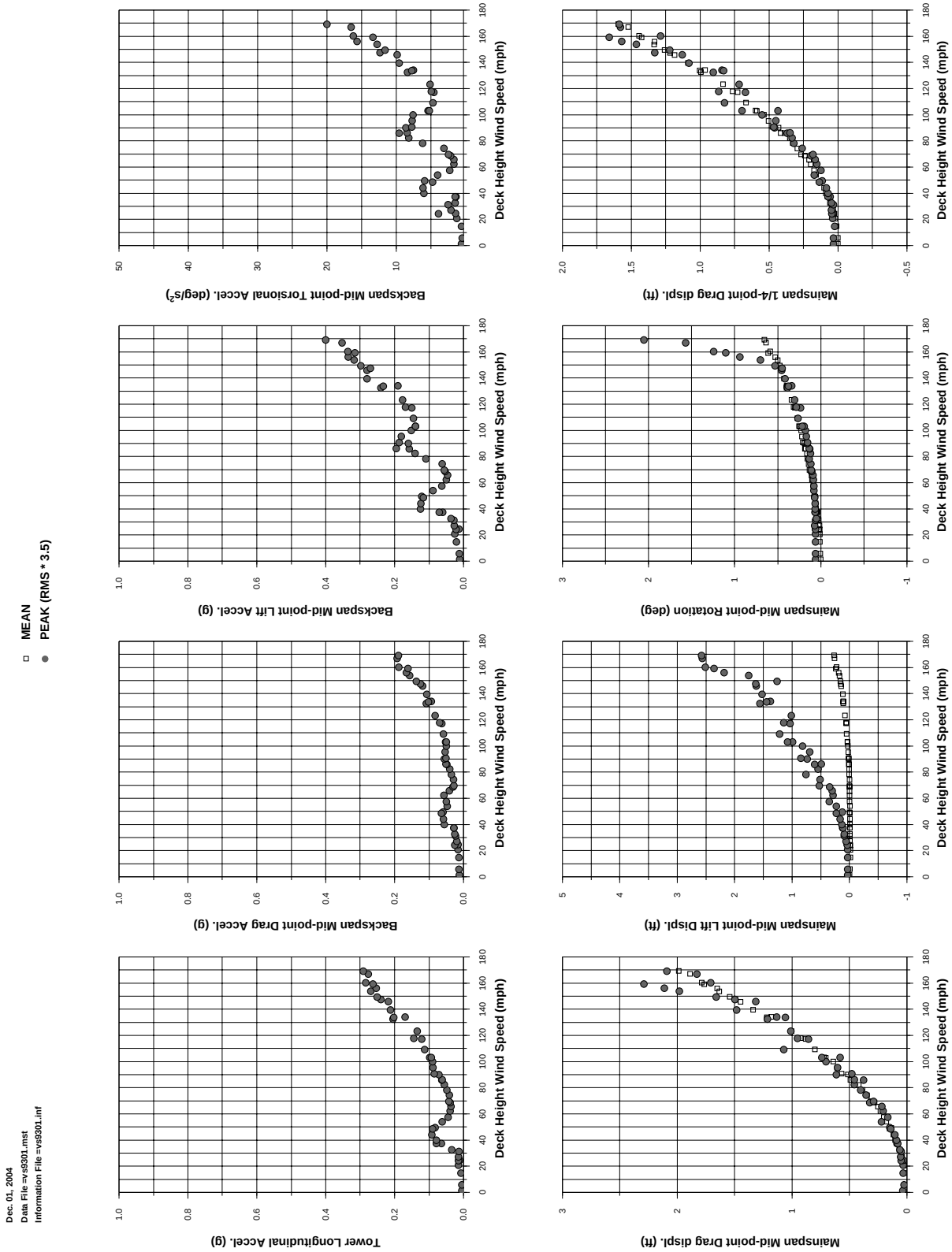

Prospect Verona Bridge, open country profile, 90 degrees (perpendicular to deck)

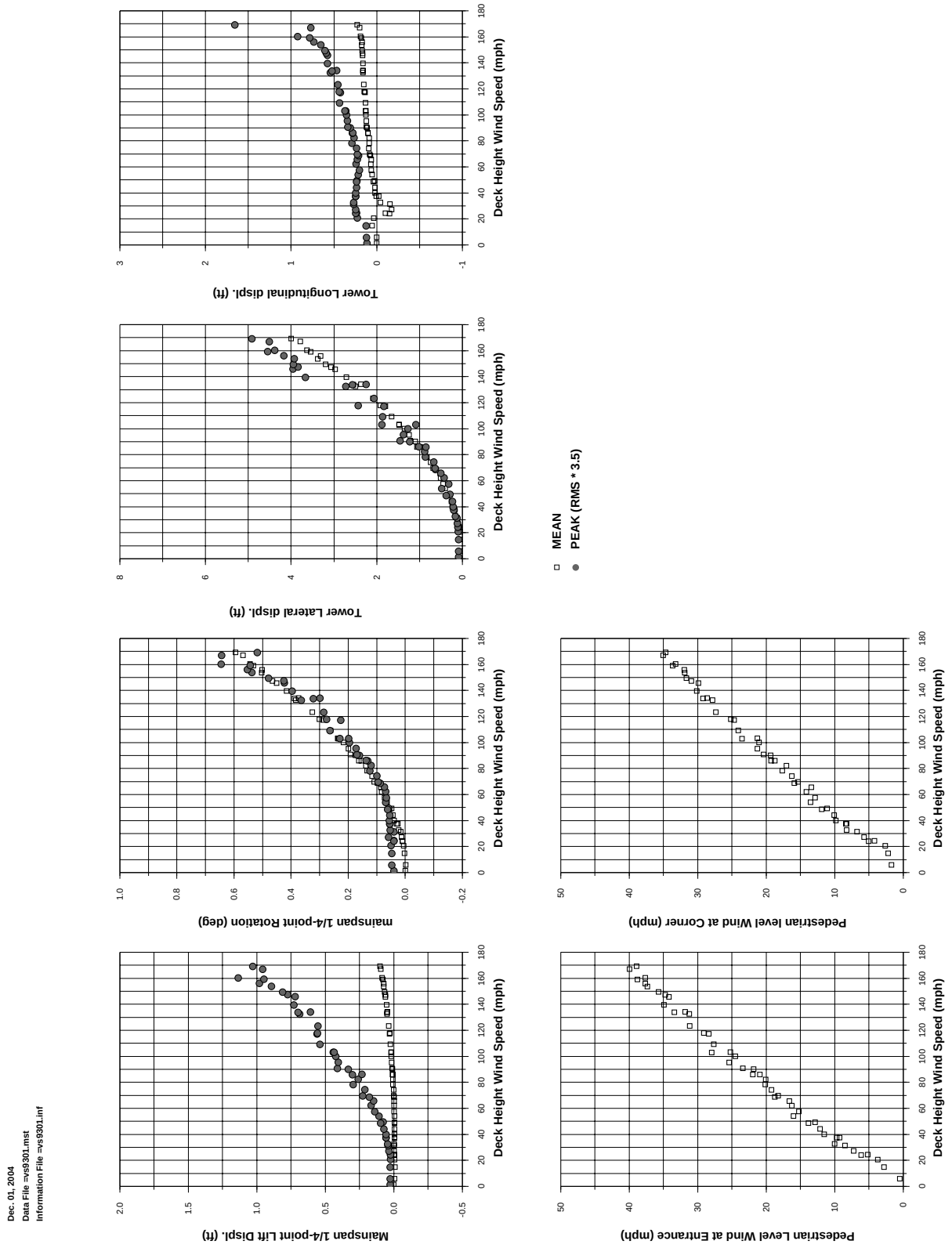

Prospect Verona Bridge, open country profile, 90 degrees (perpendicular to deck)

Dec. 02, 2004
Data File =vs2301.mst
Information File =vs2301.inf

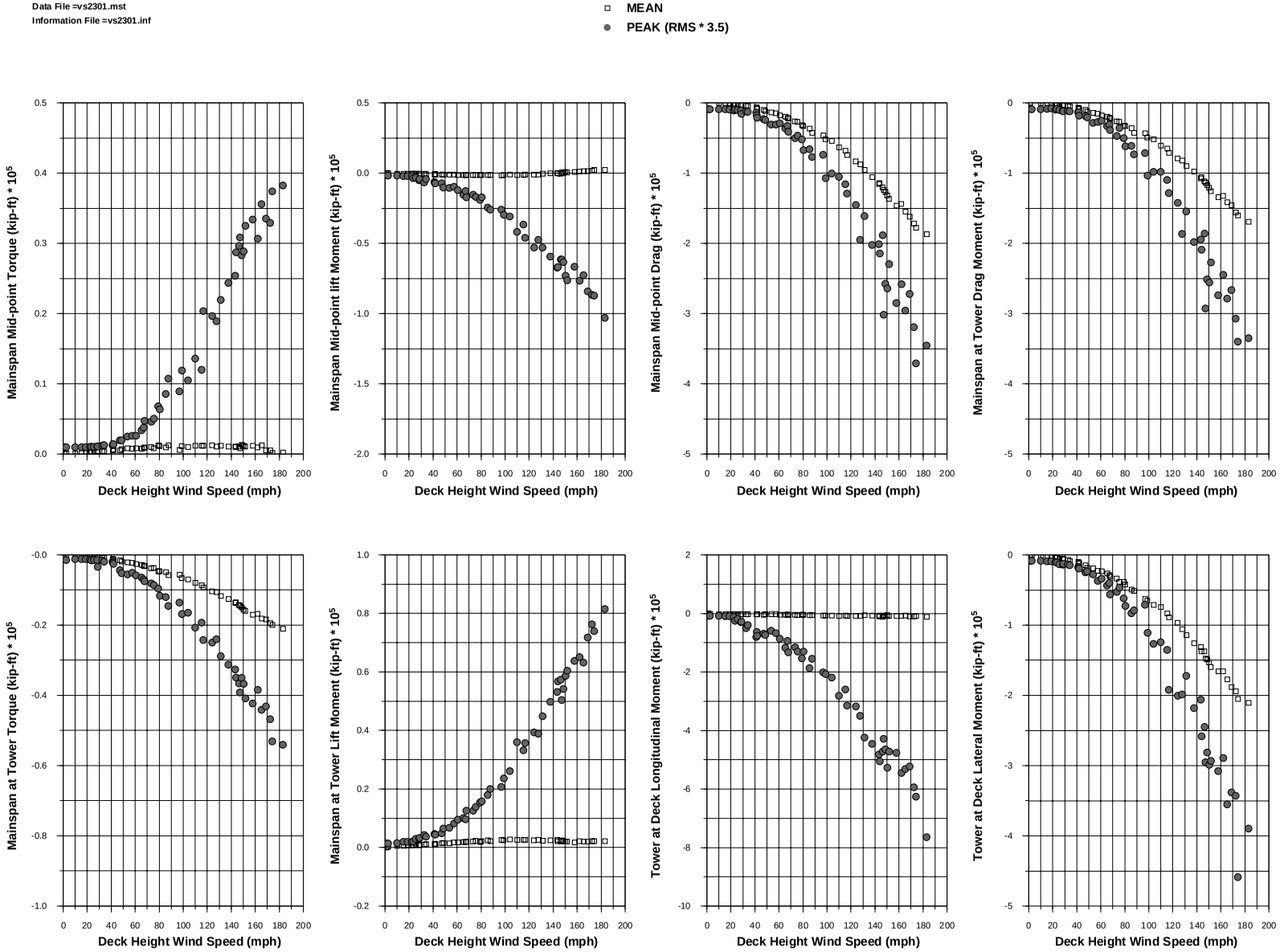

Prospect Verona Bridge, open country profile, 270 degrees, with existing bridge

Dec. 02, 2004
Data File =vs2301.mst
Information File =vs2301.inf

MEAN
PEAK (RMS * 3.5)

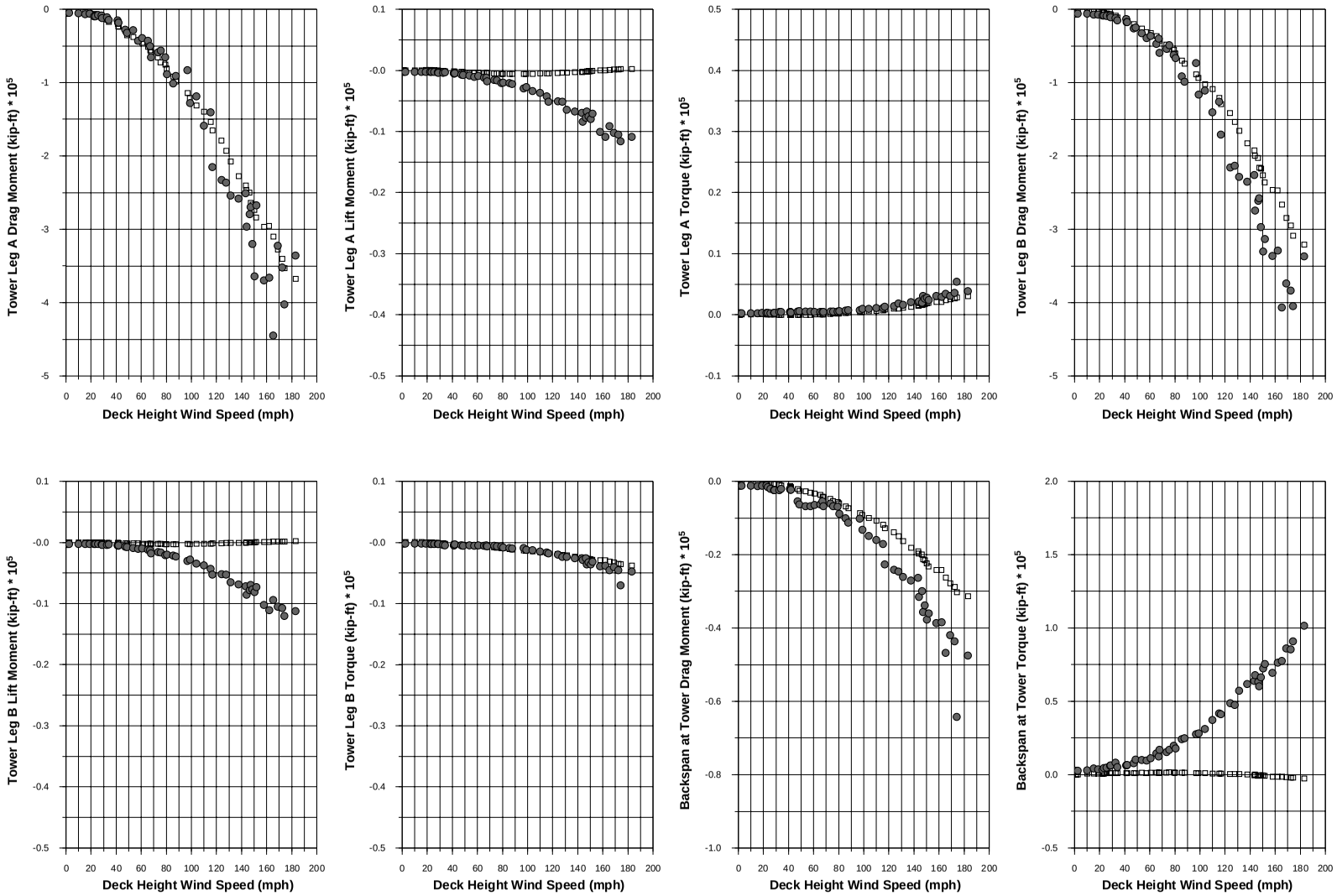

Prospect Verona Bridge, open country profile, 270 degrees, with existing bridge

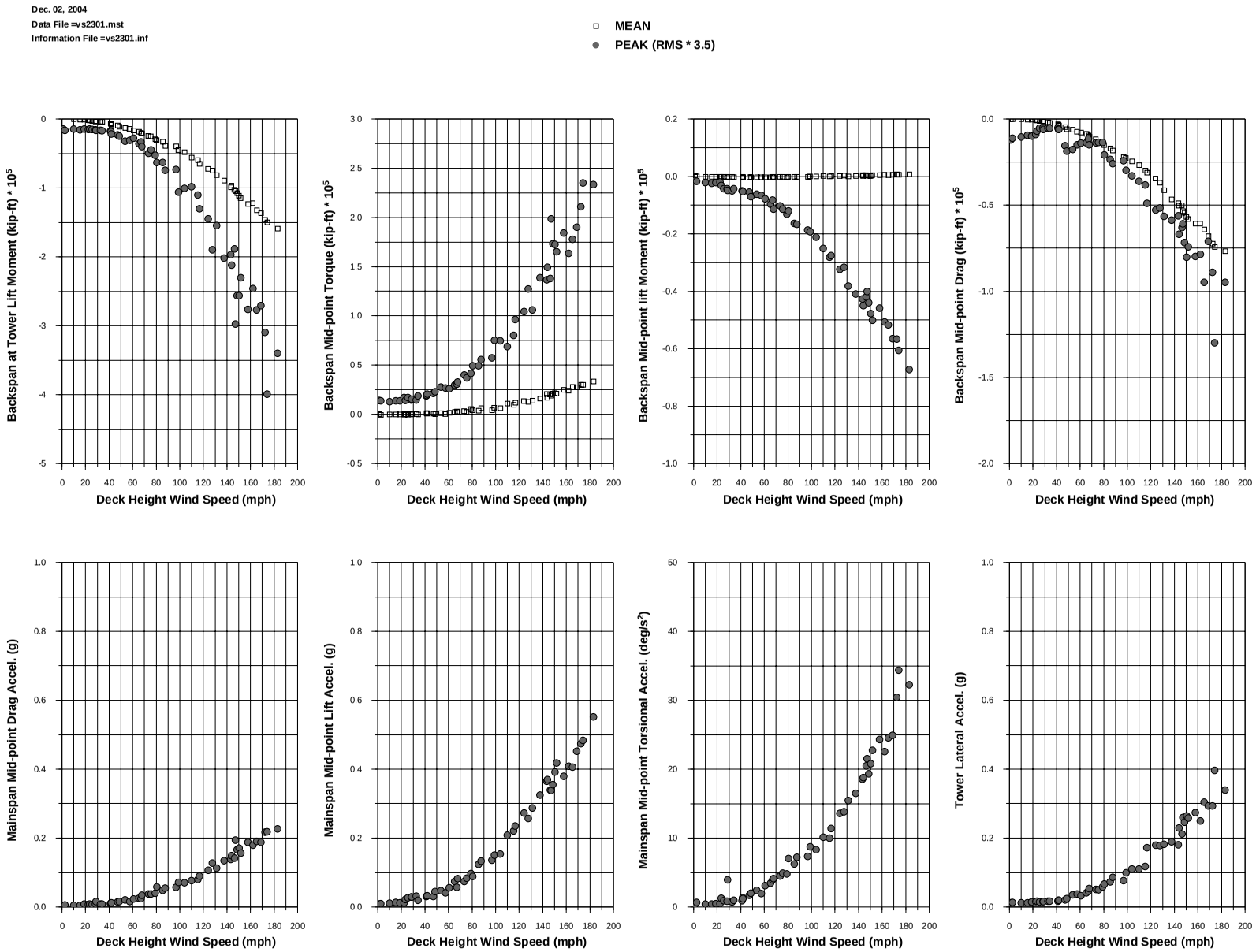

Prospect Verona Bridge, open country profile, 270 degrees, with existing bridge

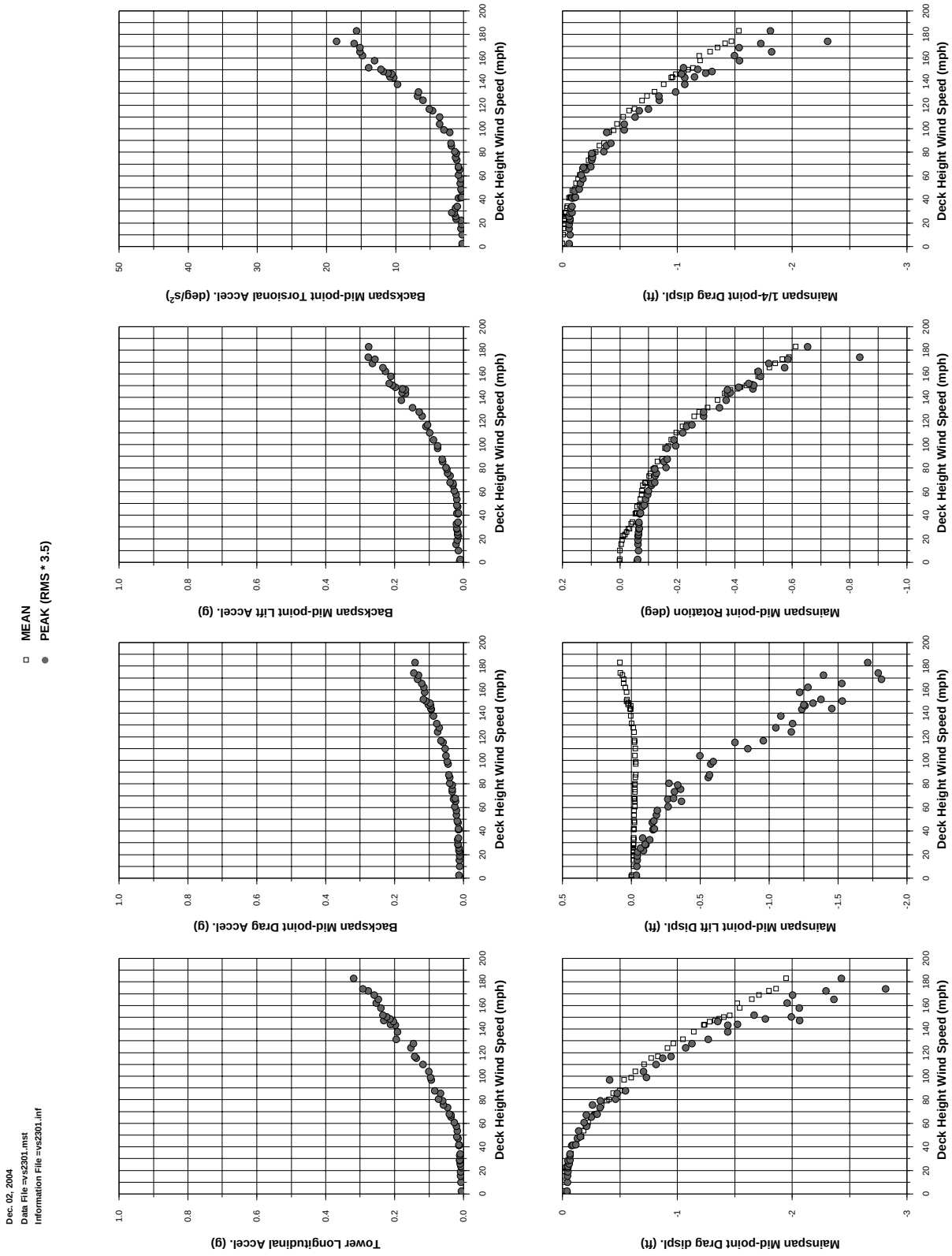

Prospect Verona Bridge, open country profile, 270 degrees, with existing bridge

Dec. 02, 2004
Data File =vs2301.mst
Information File =vs2301.inf

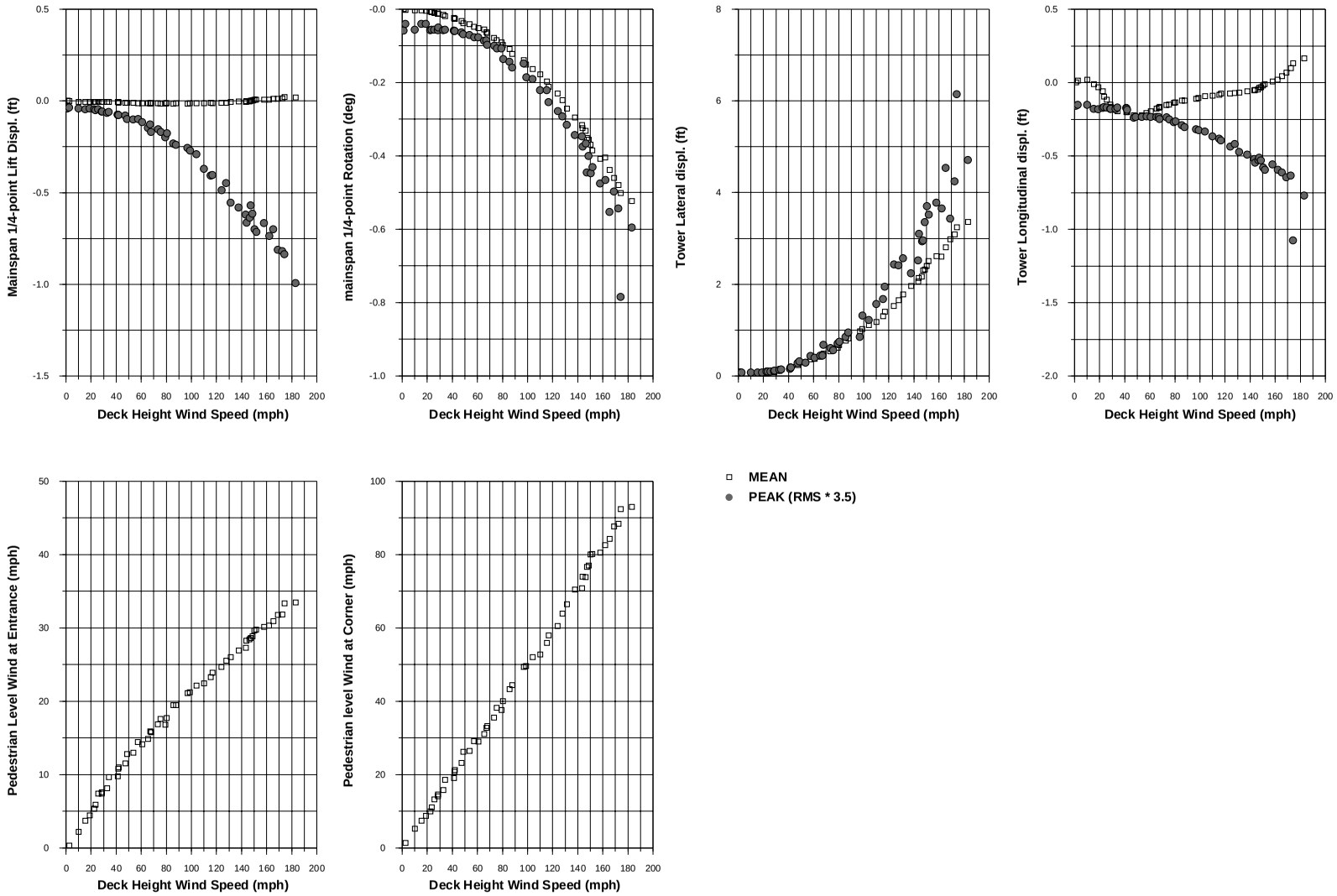

Prospect Verona Bridge, open country profile, 270 degrees, with existing bridge

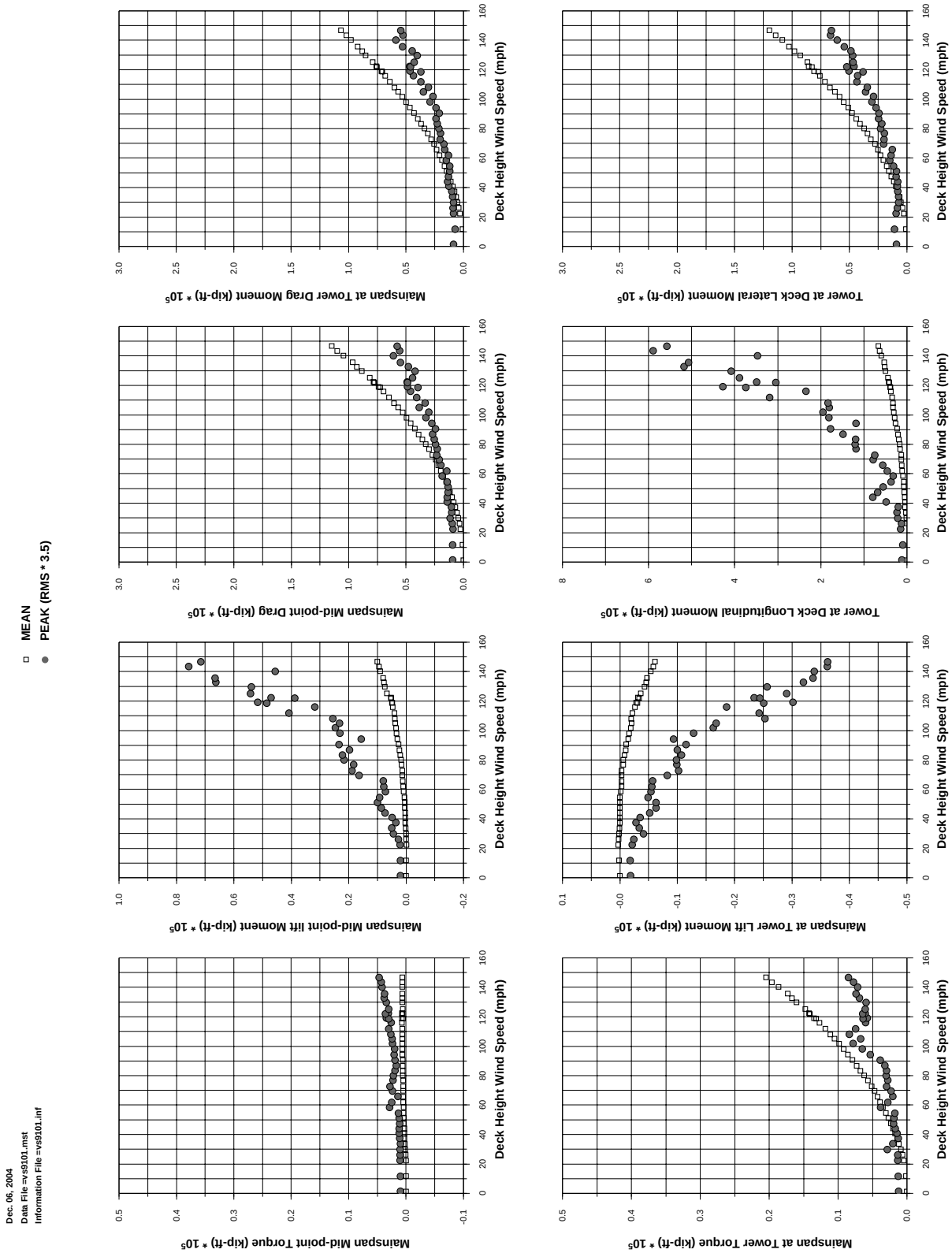

Prospect Verona Bridge, completed bridge, smooth flow, 90 degrees

Dec. 06, 2004
Data File =vs9101.mst
Information File =vs9101.inf

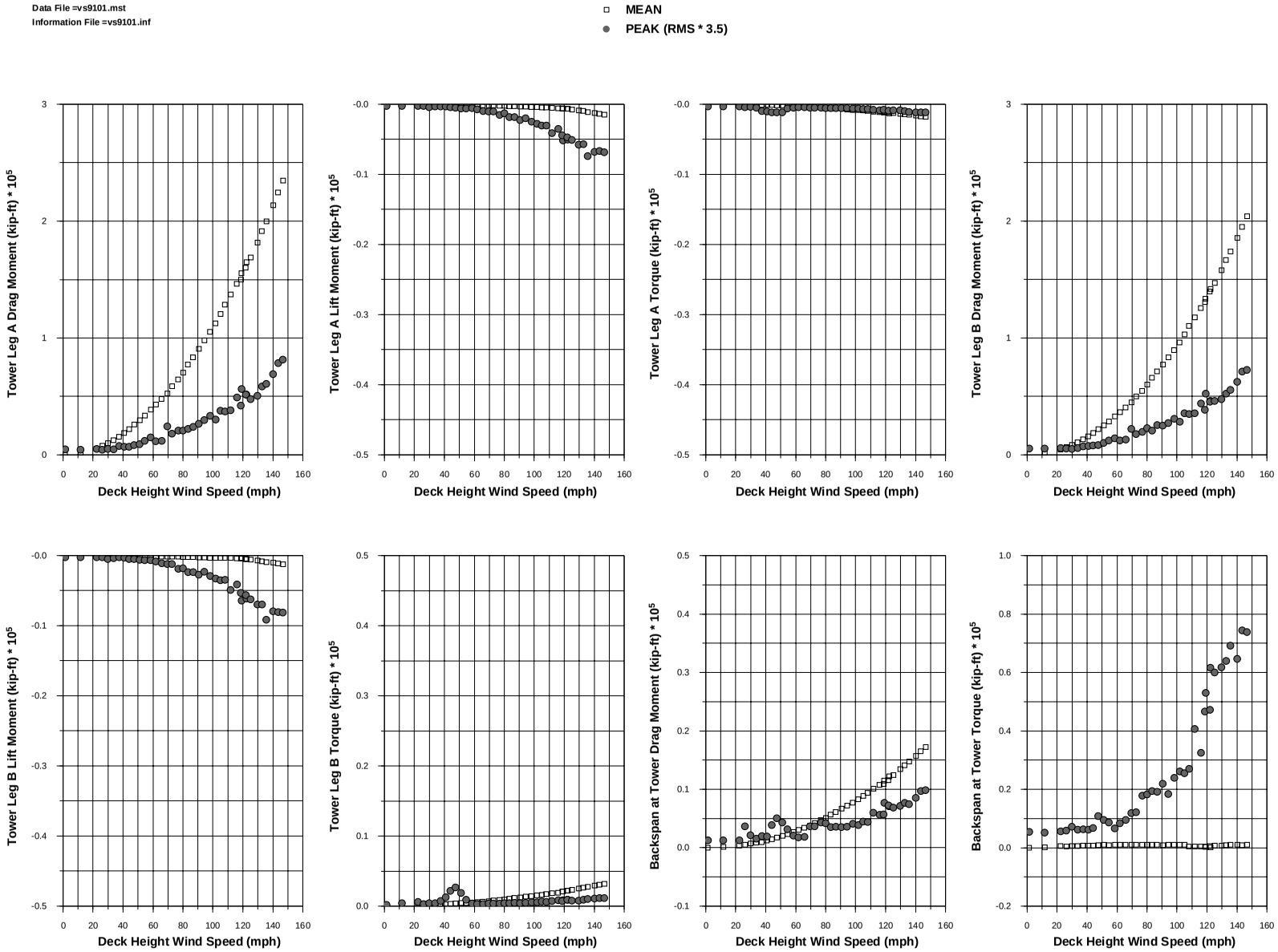

Prospect Verona Bridge, completed bridge, smooth flow, 90 degrees

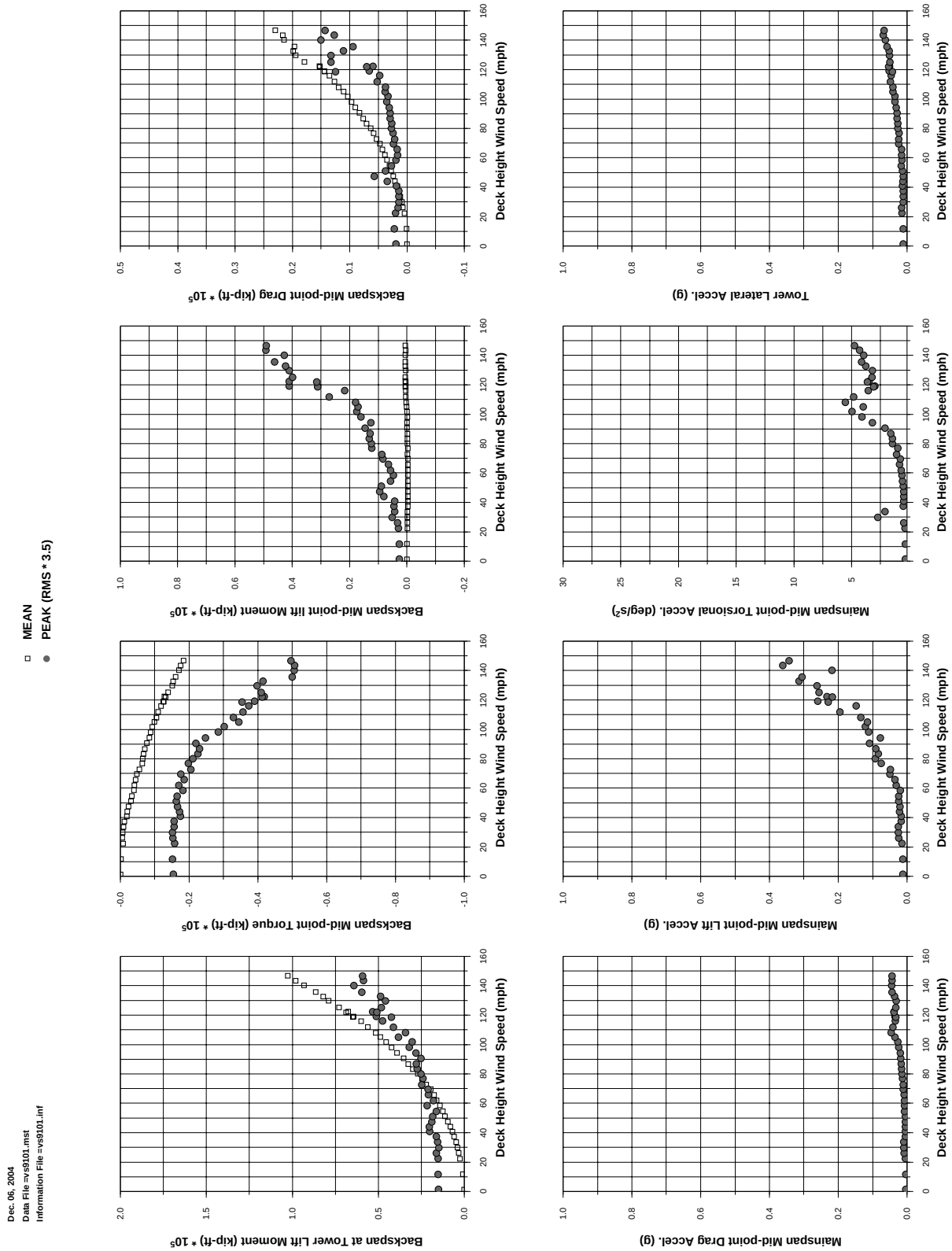

Prospect Verona Bridge, completed bridge, smooth flow, 90 degrees

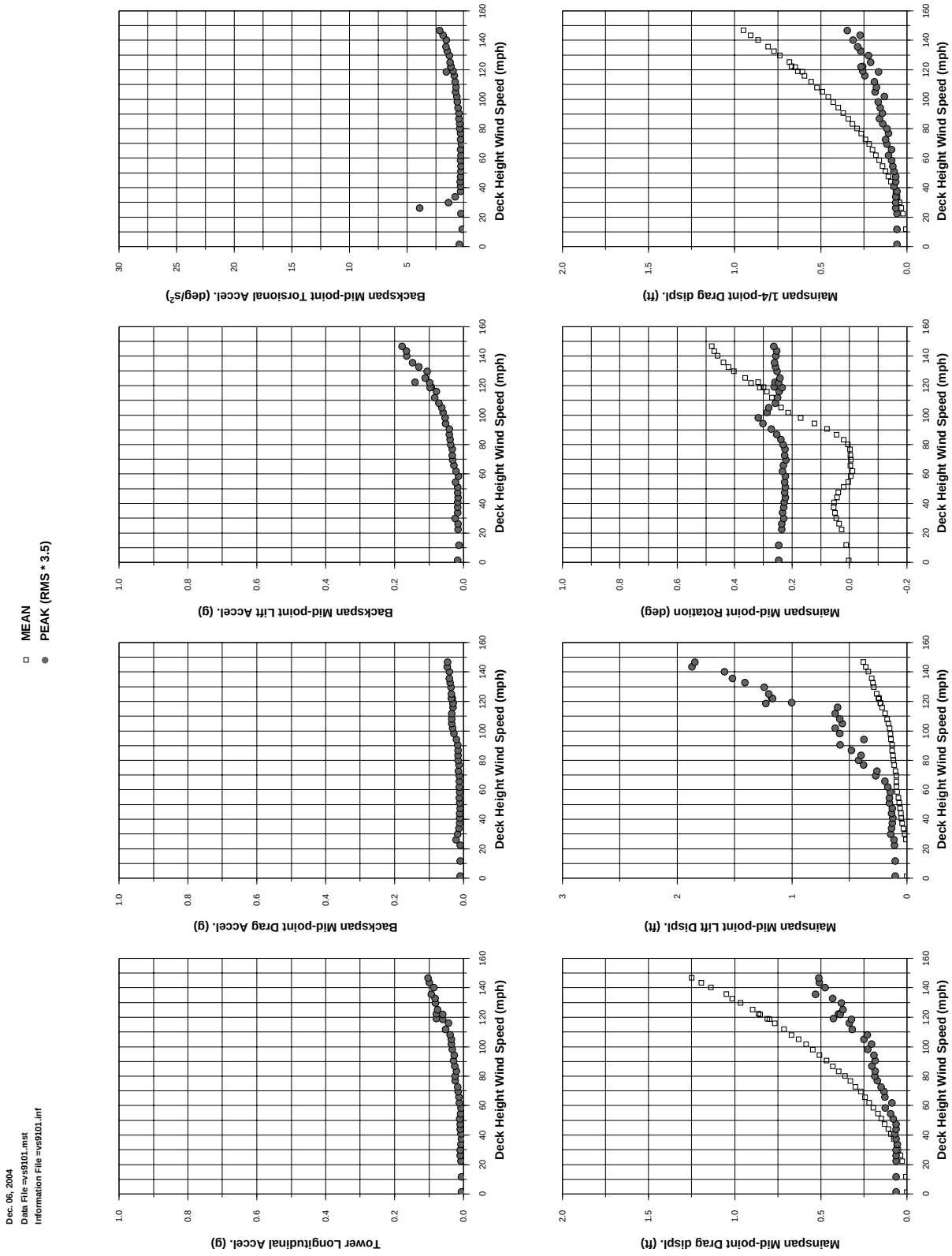

Prospect Verona Bridge, completed bridge, smooth flow, 90 degrees

Dec. 06, 2004
Data File =vs9101.mst
Information File =vs9101.inf

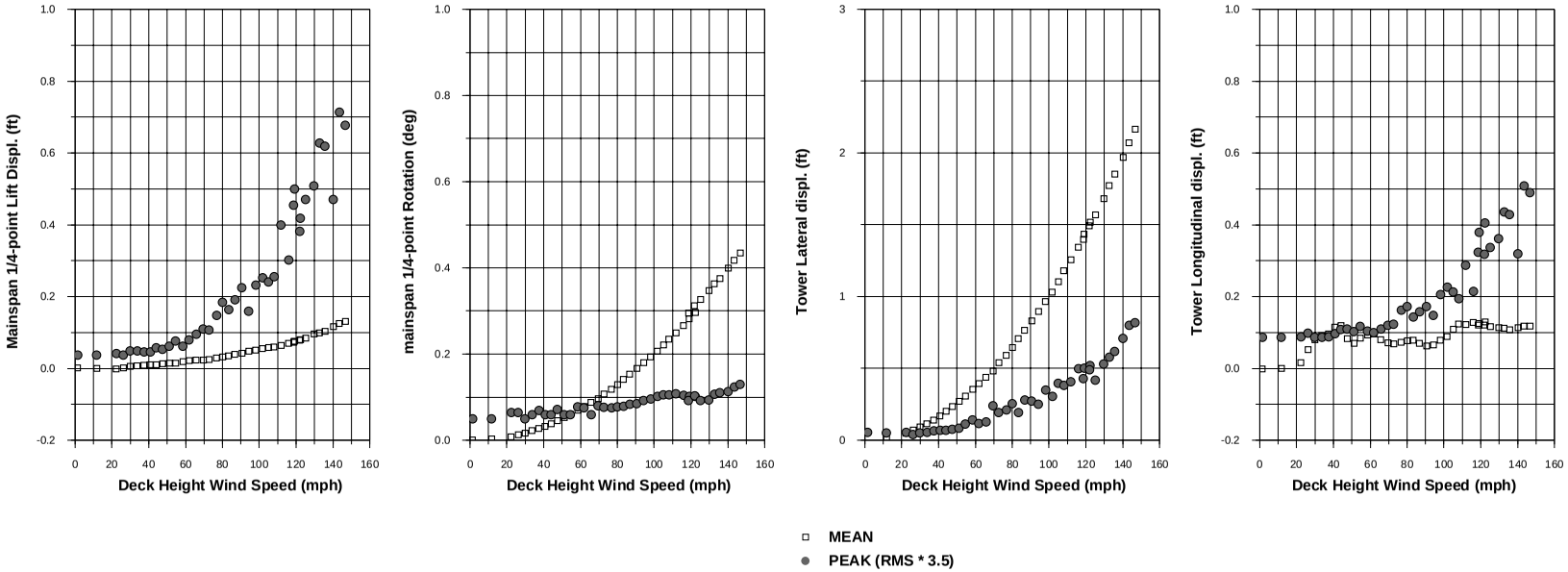

Prospect Verona Bridge, completed bridge, smooth flow, 90 degrees

RESULTS OF FULL BRIDGE AEROELASTIC TESTS, DOUBLE CANTILEVERED CONSTRUCTION STAGE

Notes:

1. The bending moments given in the plots have the units of kip-ft. The numbers read directly from the plots should be multiplied by 10^5 to obtain the actual bending moments in kip-ft. For example on page H6 of the Tower at Deck Lateral Moment (the lower right figure on that page), both the mean and peak moments at about 70mph are approximately 0.5×10^5 kip-ft (not 0.5 kip-ft).

2. The total response is equal to the mean, plus or minus the peak.

3. X is along the longitudinal direction, Y is the lateral direction (drag direction), and Z is the vertical direction (lift direction). Thus M_x is the torque, M_y is the lift moment (generated by the lift) and M_z is the drag moment (generated by the drag).

TABLE H1 INSTRUMENTATION LOCATIONS, CONSTRUCTION STAGE

Instrumentation **x – longitudinal, y – lateral (Drag), z – vertical (Lift)**	**Instrumentation Locations**
Strain Gages:	
M_x, M_y and M_z at Prospect Pylon Leg A (marked A)	Lateral and Longitudinal Bending Moments, as well as Torque at 25ft from Pylon Footing
M_x, M_y and M_z at Prospect Pylon Leg B (marked B)	Lateral and Longitudinal Bending Moments, as well as Torque at 25ft from Pylon Footing
M_x, M_y and M_z at Back Span Mid-Point (marked C)	Lift and Drag Moments, as well as Torque at 230ft from Pylon Centerline
M_x, M_y and M_z at Back Span Deck close to Pylon (marked D)	Lift and Drag Moments, as well as Torque at 28ft from Pylon Centerline
M_x, M_y and M_z at Main Span Deck close to Pylon (marked E)	Lift and Drag Moments, as well as Torque at 25ft from Pylon Centerline
M_x and M_y at Prospect Pylon above Deck (marked F)	Lateral and Longitudinal bending Moments at 23ft above Deck Surface
M_x, M_y and M_z at Main Span Mid-Point (marked H)	Lift and Drag Moments, as well as Torque at 23ft from Midspan
Accelerometers:	
y, z and θ accel. at Main Span Mid-Point (marked H)	Lift, Drag and Torsional Accelerations at 25ft from Main Span Mid-Point to the Prospect Side
y, z and θ accel. at Back Span Mid-Point (marked C)	Lift, Drag and Torsional Accelerations at 255ft from Abutment 1
y and z accel. at Top of Prospect Pylon (marked I)	Lateral and Longitudinal Accelerations at the observation deck level (435ft from Pylon footing)
Displacements:	
y, z and θ displacements at Main Span Mid-Point (marked H)	Lift and Drag Displacements, as well as Deck Rotation at 25ft from Midspan to the Prospect Side
y, z and θ displacements at Main Span 1/4 point (marked G)	Lift and Drag Displacements, as well as Deck Rotation at 310ft from Midspan to the Prospect Side
y and z displacements at Top of Prospect Pylon (marked I)	Lateral and Longitudinal Displacements at the observation deck level (435ft from Pylon footing)
Wind Speeds:	
Plaza Probes at Prospect Pylon Entrance Way (marked 1 & 2)	Pedestrian Level
Deck Level	Deck Height
Pylon Top	Pylon Height

TABLE H2 SUMMARY OF TESTS, CONSTRUCTION STAGE – CONSTRUCTION STAGE

Test File	Test No.	Flow condition	Existing bridge	Construction Box at Cantilever Ends	Wind direction (Test angle)	V_{deck} (mph) Maximum wind speed at deck height
VC9201	1	Hurricane profile	No	Yes	Perpendicular to bridge (90°)	103
VC9202	2	Hurricane profile	No	No	Perpendicular to bridge (90°)	103
VC0201	3	Hurricane profile	No	No	Along the Bridge (0°)	99
VC3201	4	Hurricane profile	No	No	30° to the bridge	100
VC6201	5	Hurricane profile	No	No	60° to the bridge	99
VC2201	6	Hurricane profile	Yes	Yes	Perpendicular to bridge (270°)	99
VC6301	7	Open Country profile	No	No	60° to the bridge	101
VC3301	8	Open Country profile	No	No	30° to the bridge	106
VC0301	9	Open Country profile	No	No	Along the Bridge (0°)	111
VC9301	10	Open Country profile	No	No	Perpendicular to bridge (90°)	105
VC2301	11	Open Country profile	Yes	Yes	Perpendicular to bridge (270°)	127
VC9101	12	Smooth Flow	No	No	Perpendicular to bridge (90°)	122

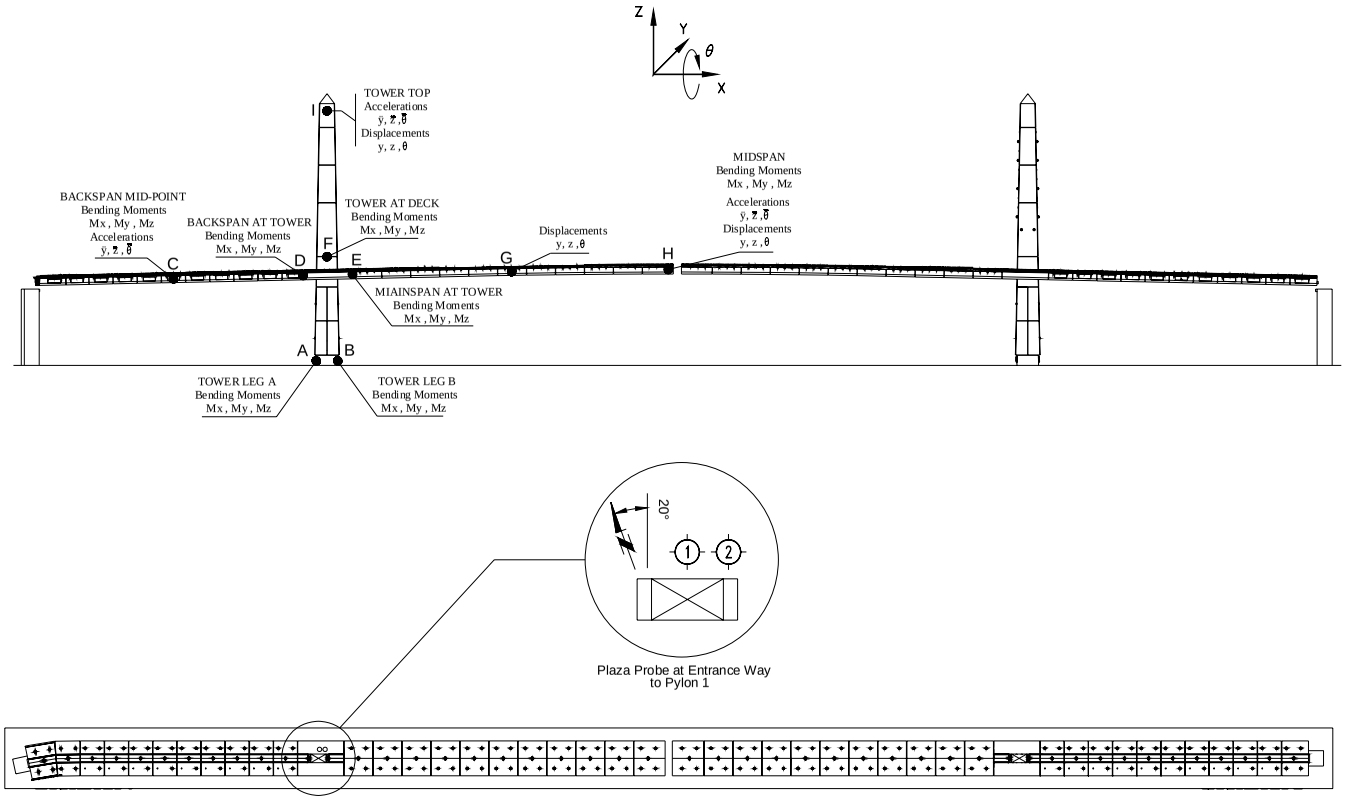

(Cables removed in drawing)

FIGURE H1 INSTRUMENTATION LOCATIONS AND SIGN CONVENTION, CONSTRUCTION STAGE (CABLES REMOVED IN THIS FIGURE)

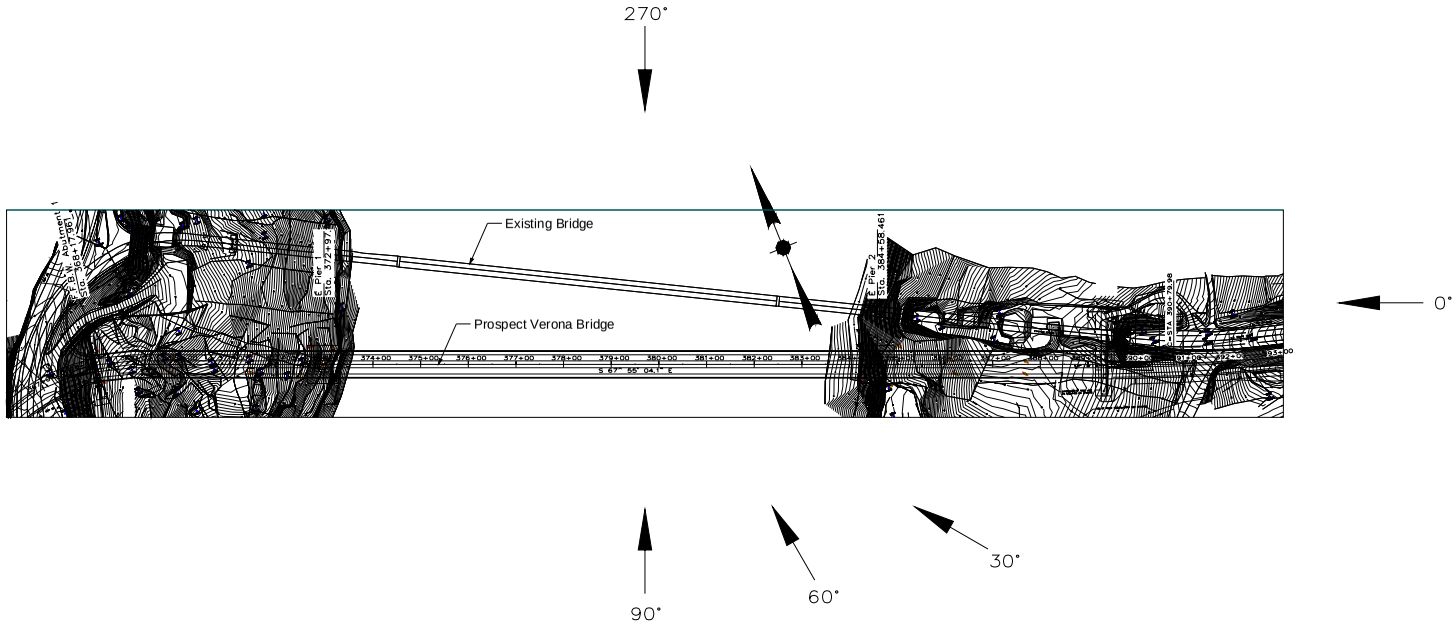

WIND DIRECTION DEFINITION

FIGURE G2 LOCATION OF EXISTING BRIDGE AND WIND DIRECTIONS TESTED

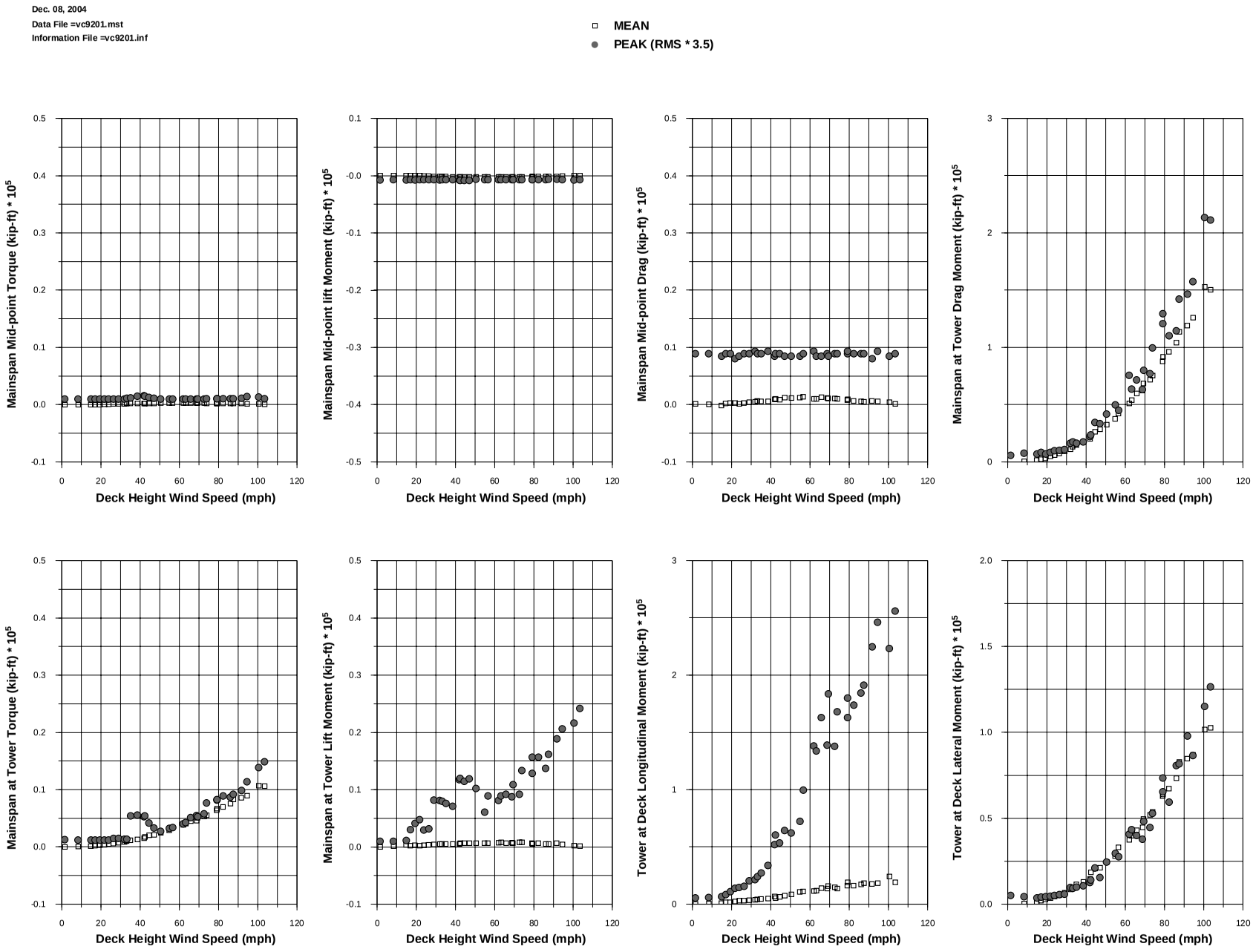

Prospect Verona Bridge, construction stage, hurricane profile, 90 degrees, without existing bridge, with box

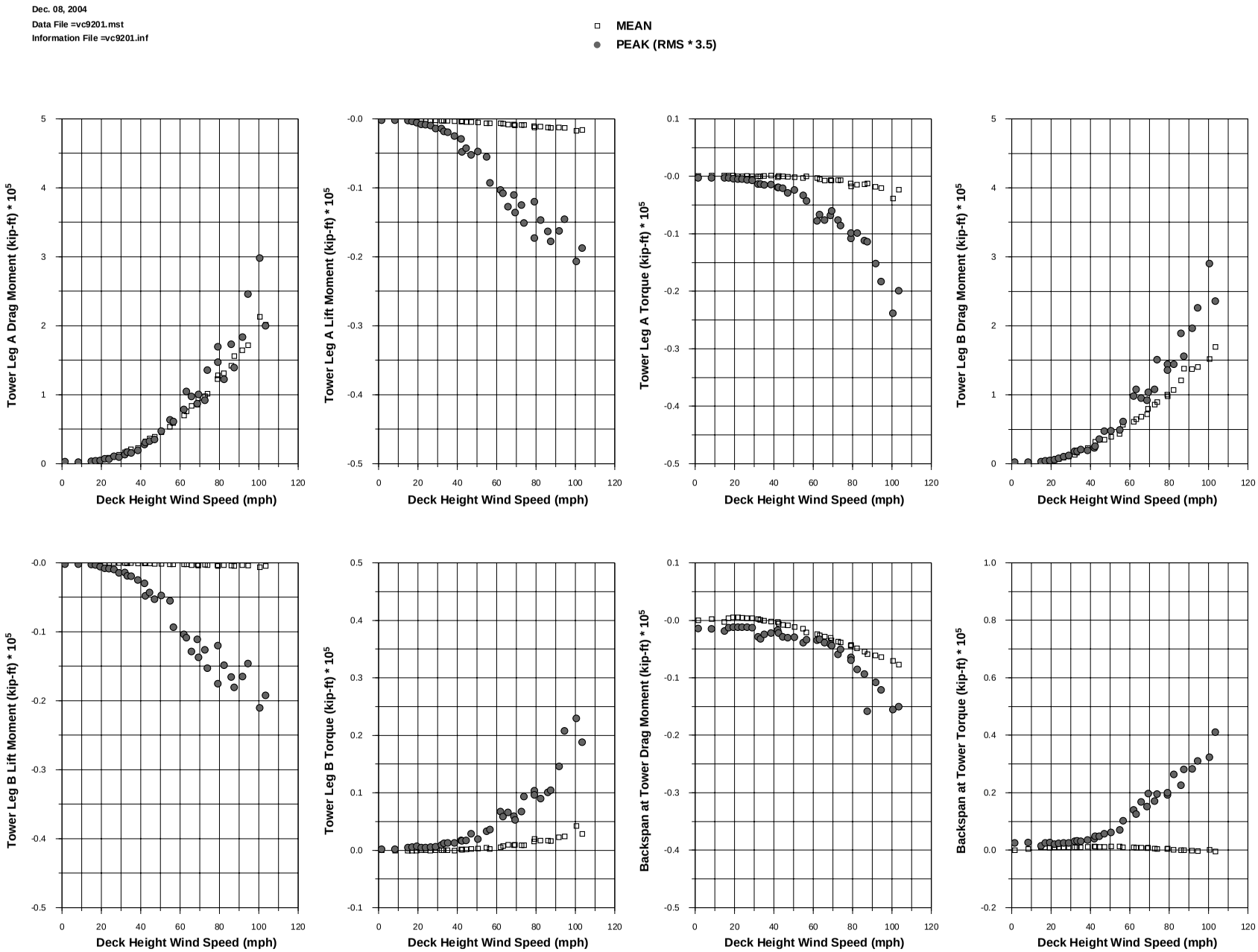

Prospect Verona Bridge, construction stage, hurricane profile, 90 degrees, without existing bridge, with box

Dec. 08, 2004
Data File =vc9201.mst
Information File =vc9201.inf

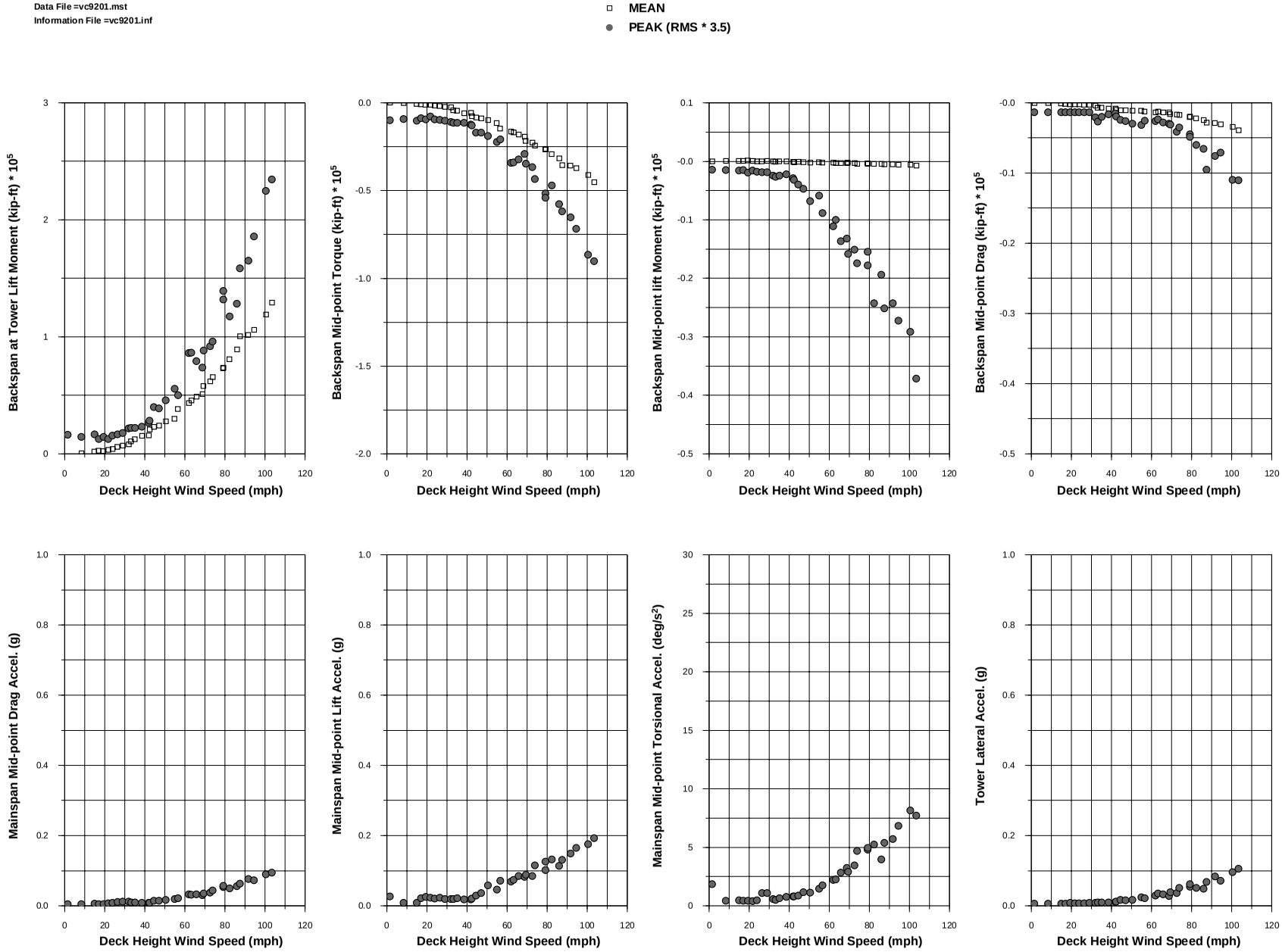

Prospect Verona Bridge, construction stage, hurricane profile, 90 degrees, without existing bridge, with box

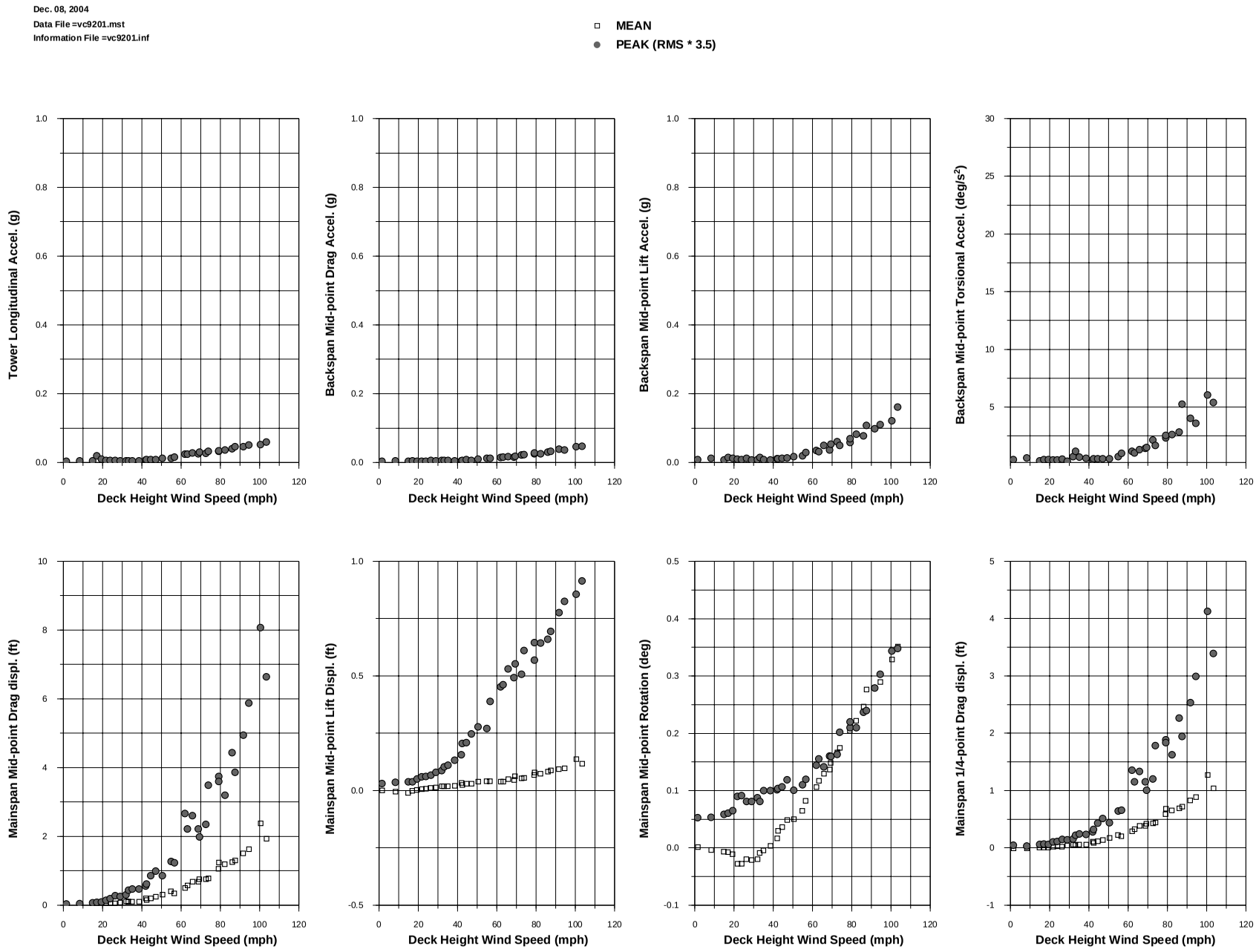

Prospect Verona Bridge, construction stage, hurricane profile, 90 degrees, without existing bridge, with box

Dec. 08, 2004
Data File =vc9201.mst
Information File =vc9201.inf

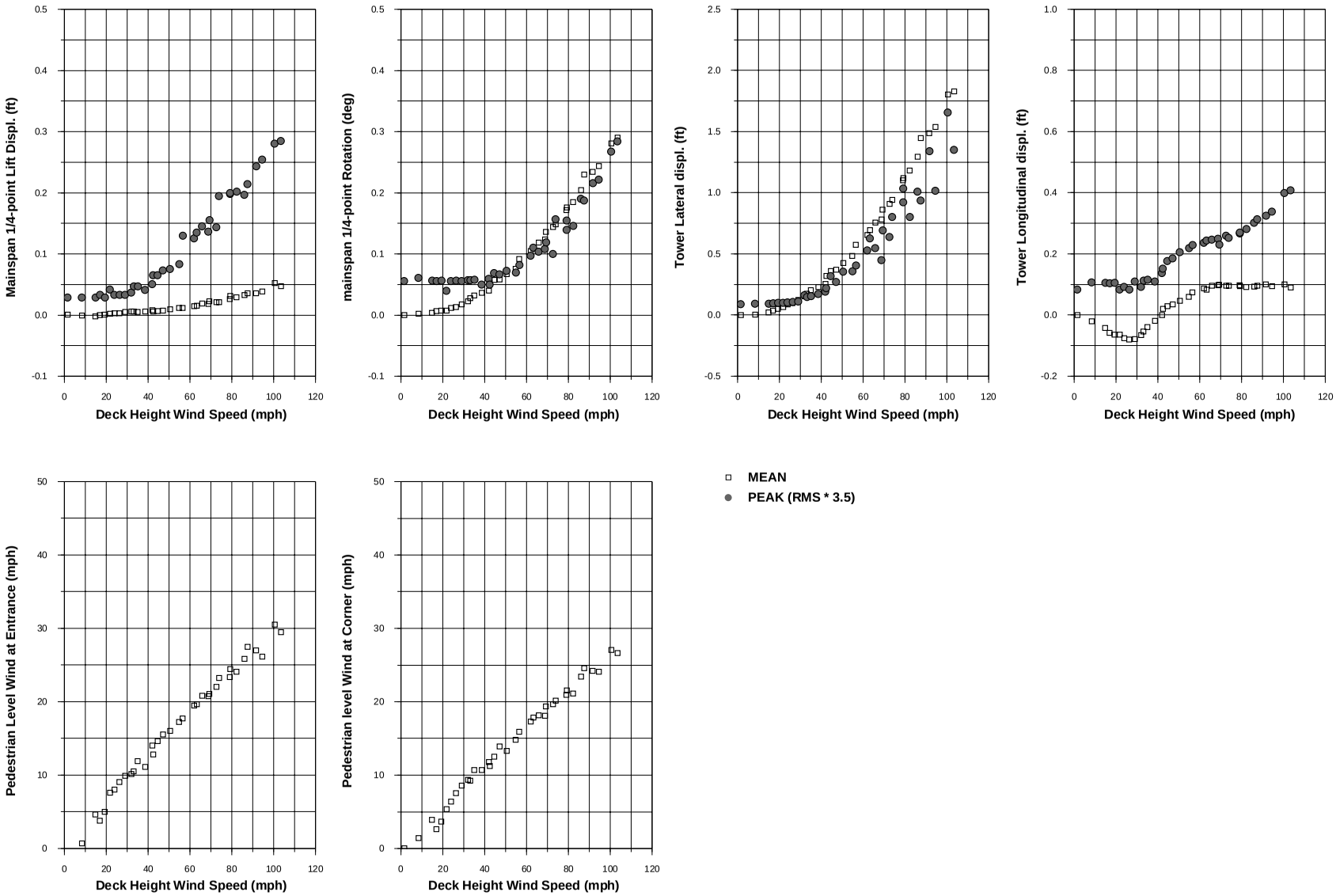

Prospect Verona Bridge, construction stage, hurricane profile, 90 degrees, without existing bridge, with box

Dec. 08, 2004
Data File =vc9202.mst
Information File =vc9202.inf

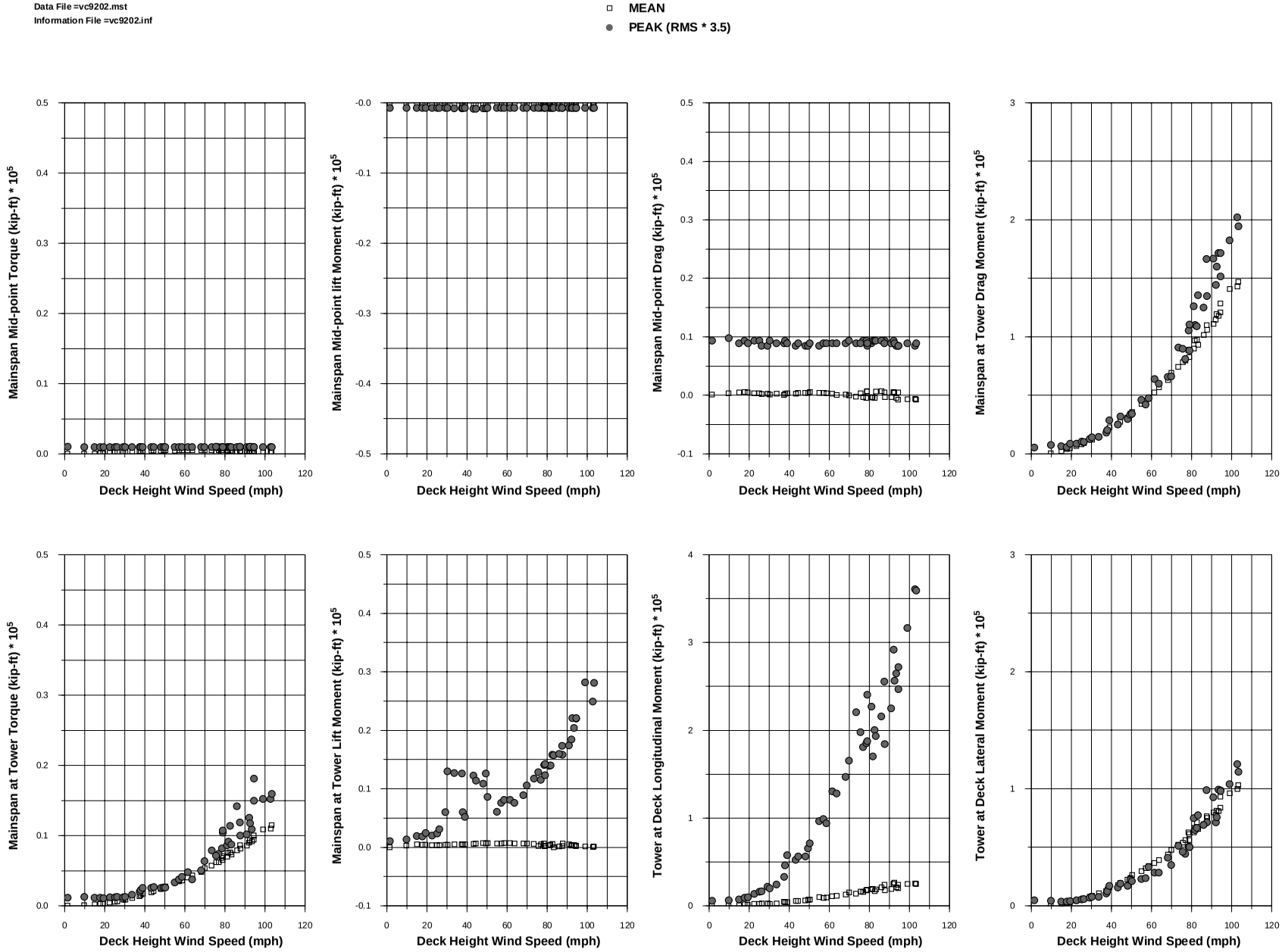

Prospect Verona Bridge, construction stage, hurricane profile, 90 degrees, without existing bridge & box

Dec. 08, 2004
Data File =vc9202.mst
Information File =vc9202.inf

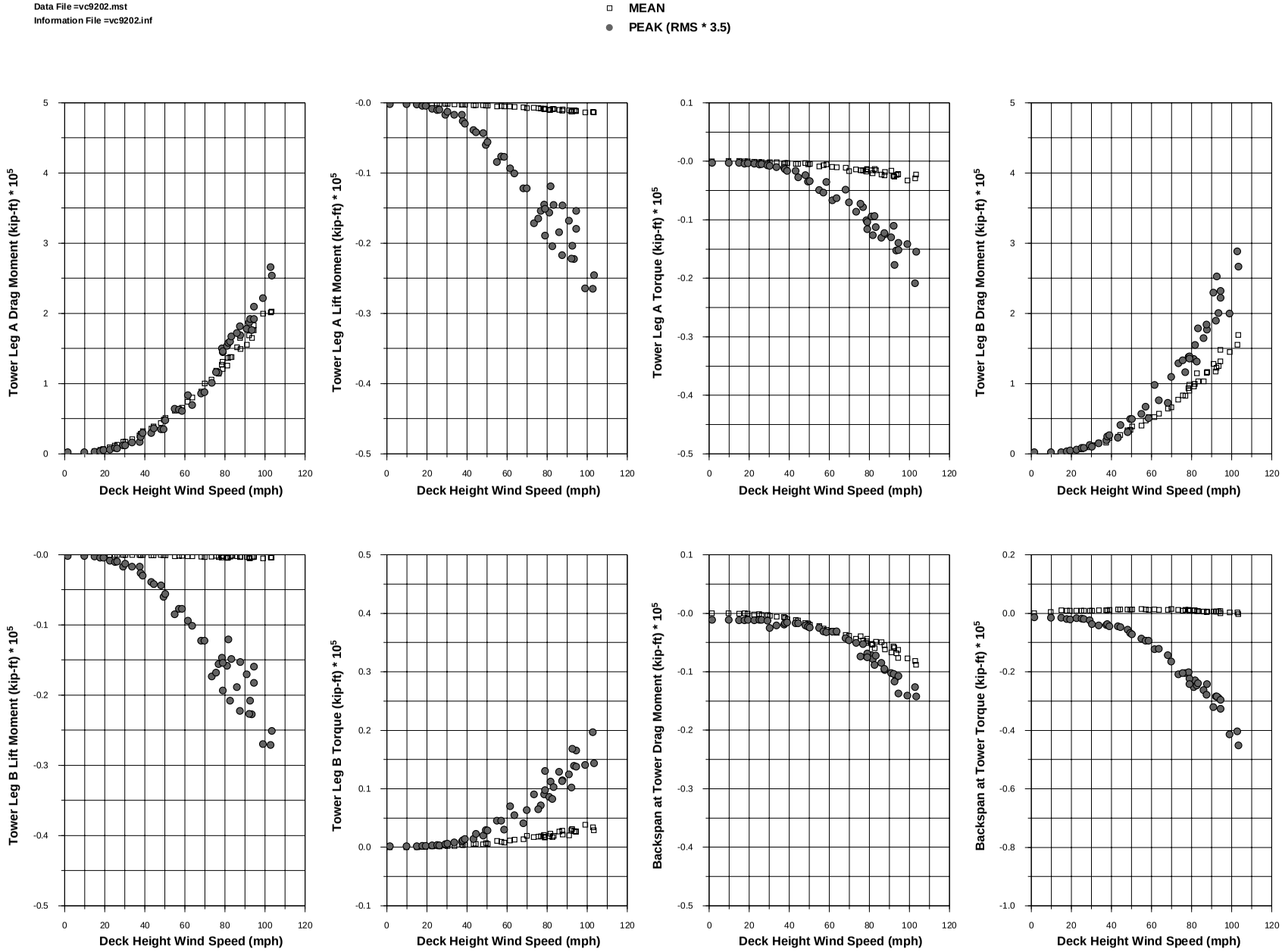

Prospect Verona Bridge, construction stage, hurricane profile, 90 degrees, without existing bridge & box

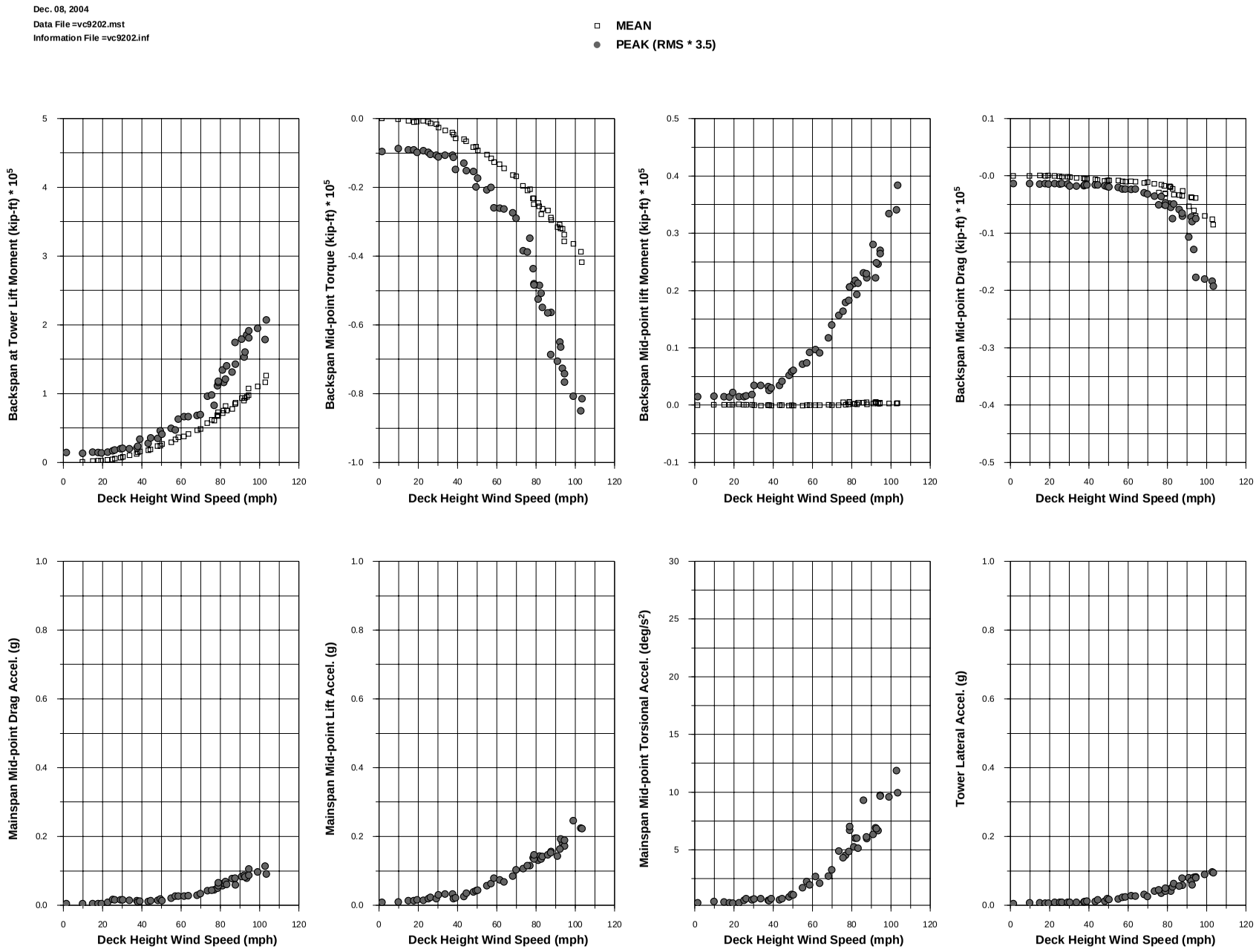

Prospect Verona Bridge, construction stage, hurricane profile, 90 degrees, without existing bridge & box

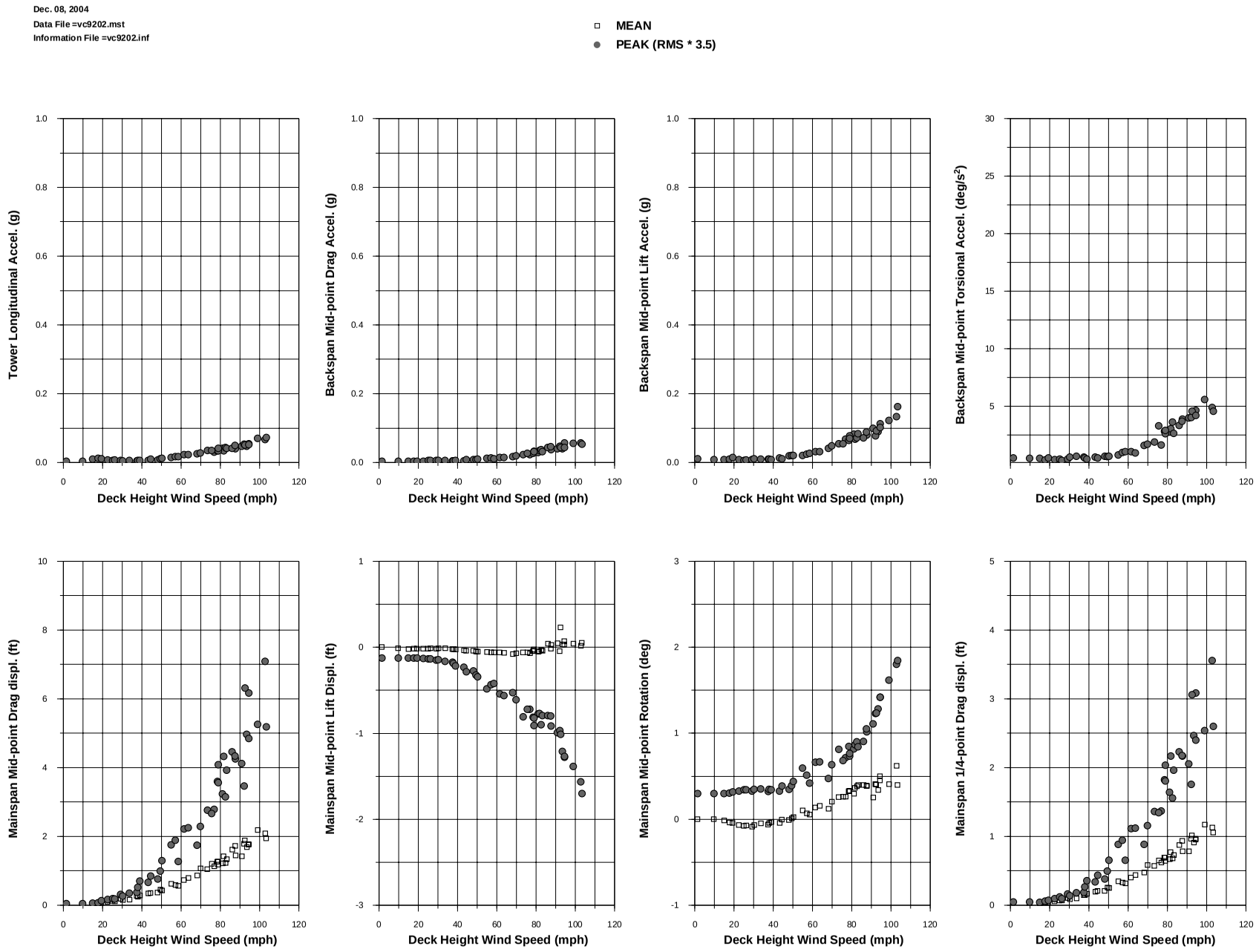

Prospect Verona Bridge, construction stage, hurricane profile, 90 degrees, without existing bridge & box

Dec. 08, 2004
Data File =vc9202.mst
Information File =vc9202.inf

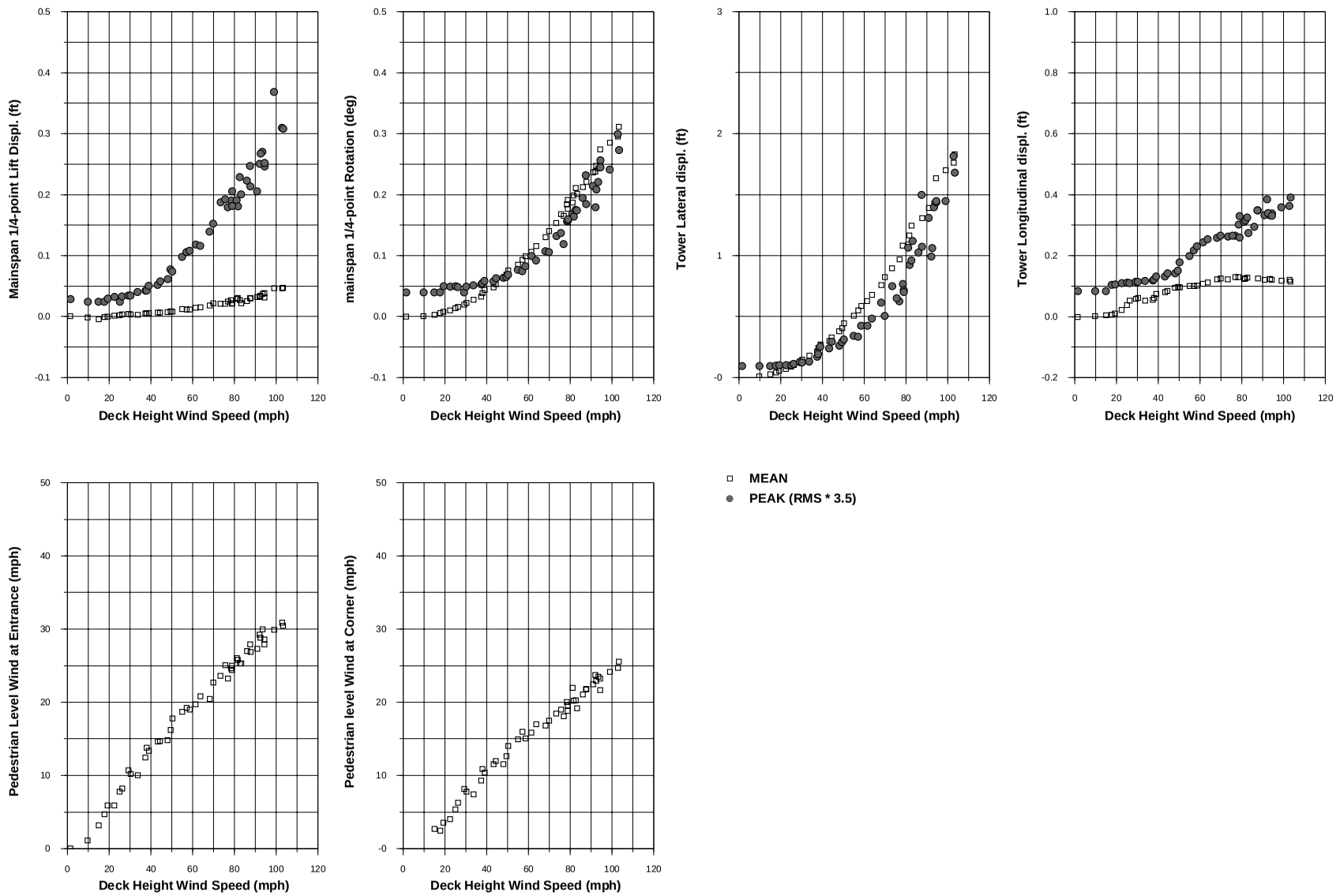

Prospect Verona Bridge, construction stage, hurricane profile, 90 degrees, without existing bridge & box

Dec. 08, 2004
Data File =vc0201.mst
Information File =vc0201.inf

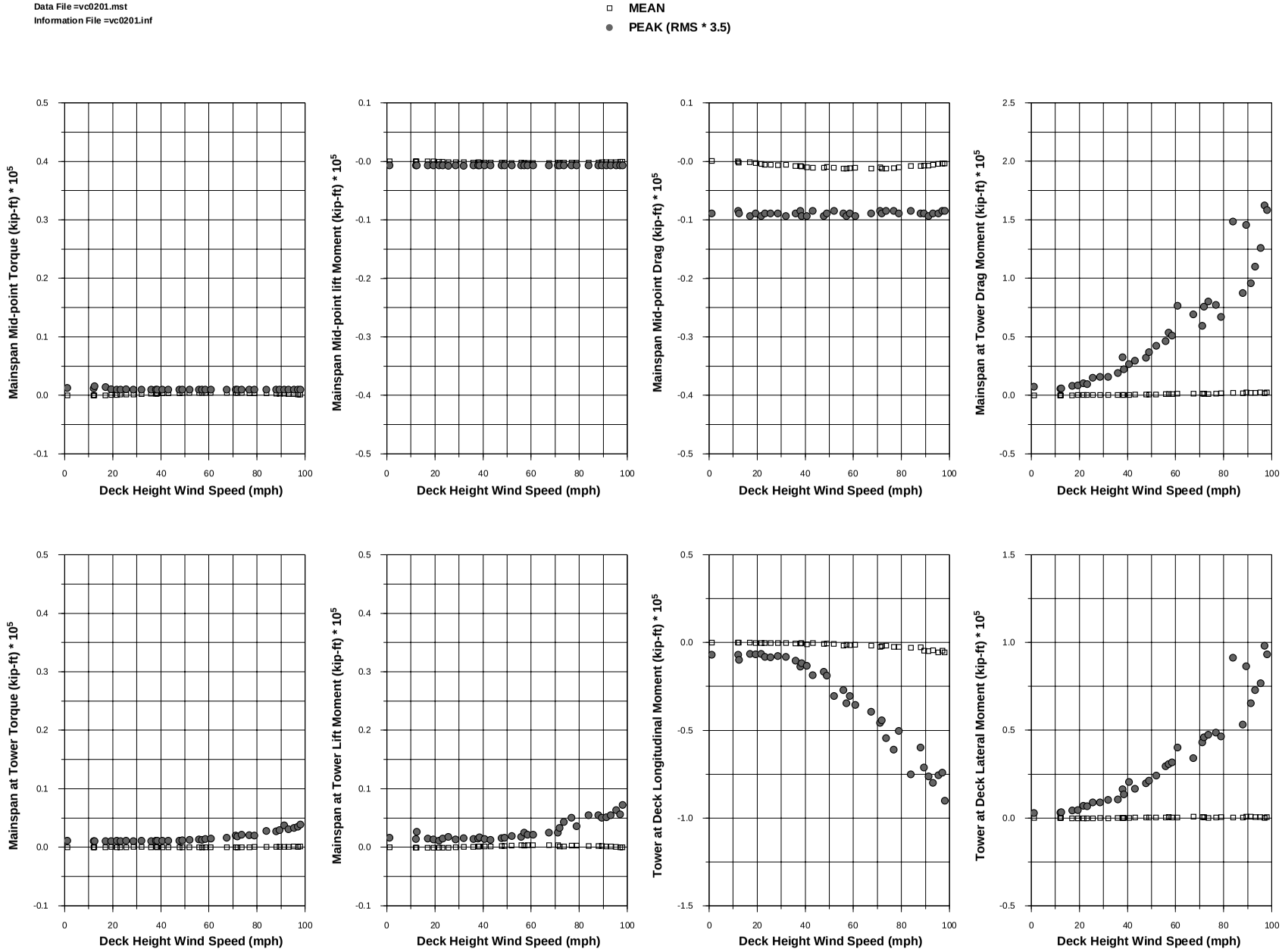

Prospect Verona Bridge, construction stage, hurricane profile, 0 degrees (along bridge)

Dec. 08, 2004
Data File =vc0201.mst
Information File =vc0201.inf

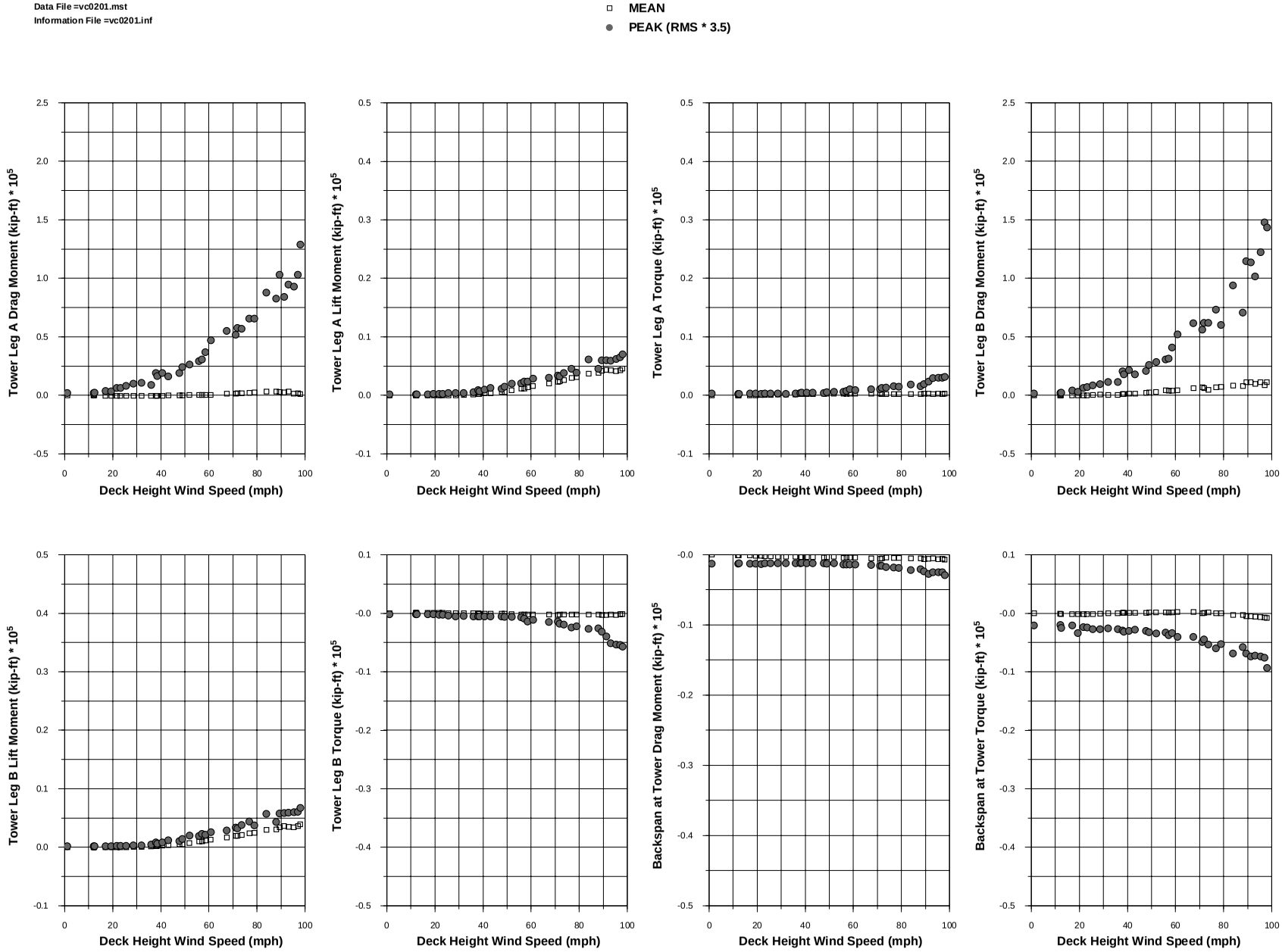

Prospect Verona Bridge, construction stage, hurricane profile, 0 degrees (along bridge)

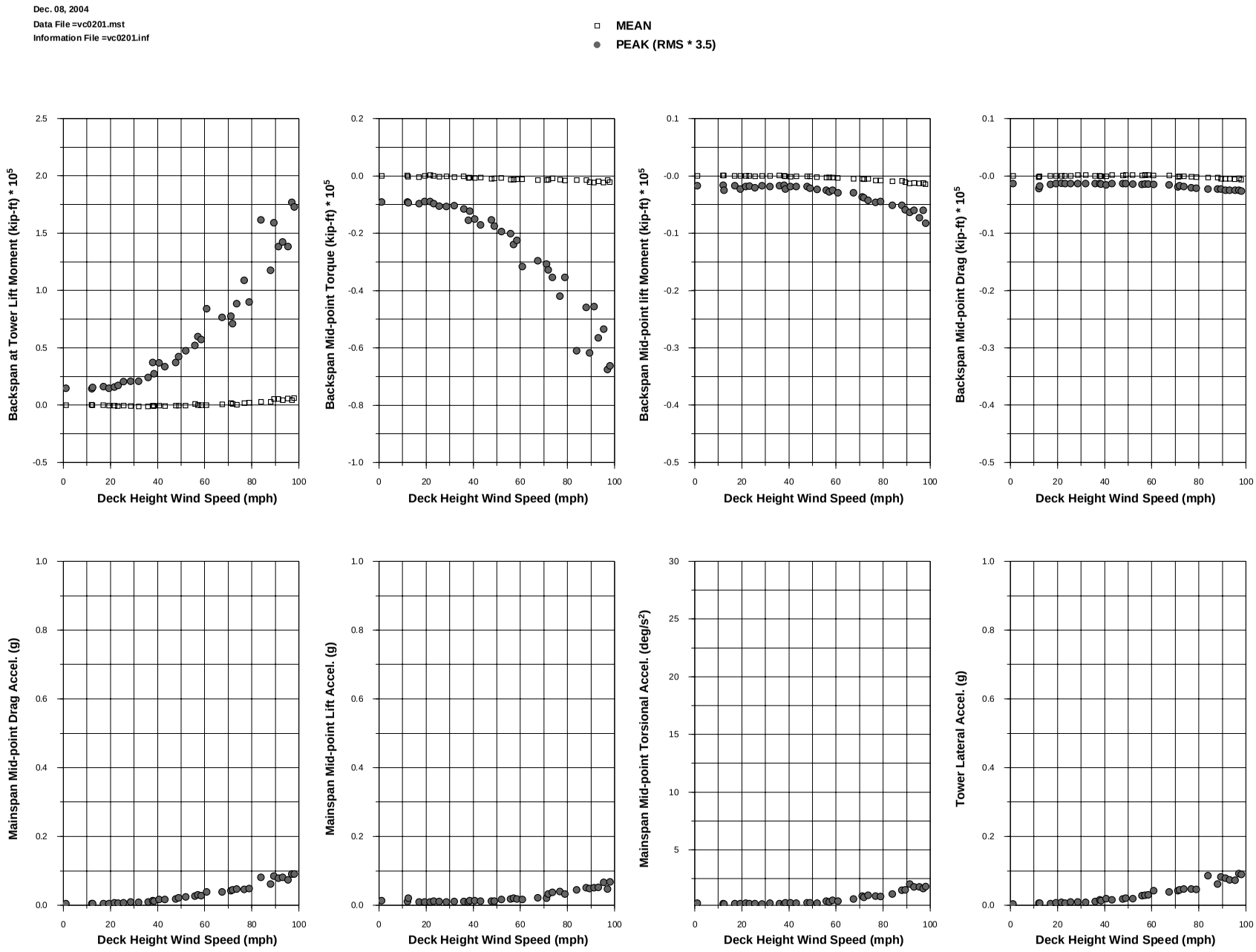

Prospect Verona Bridge, construction stage, hurricane profile, 0 degrees (along bridge)

Dec. 08, 2004
Data File =vc0201.mst
Information File =vc0201.inf

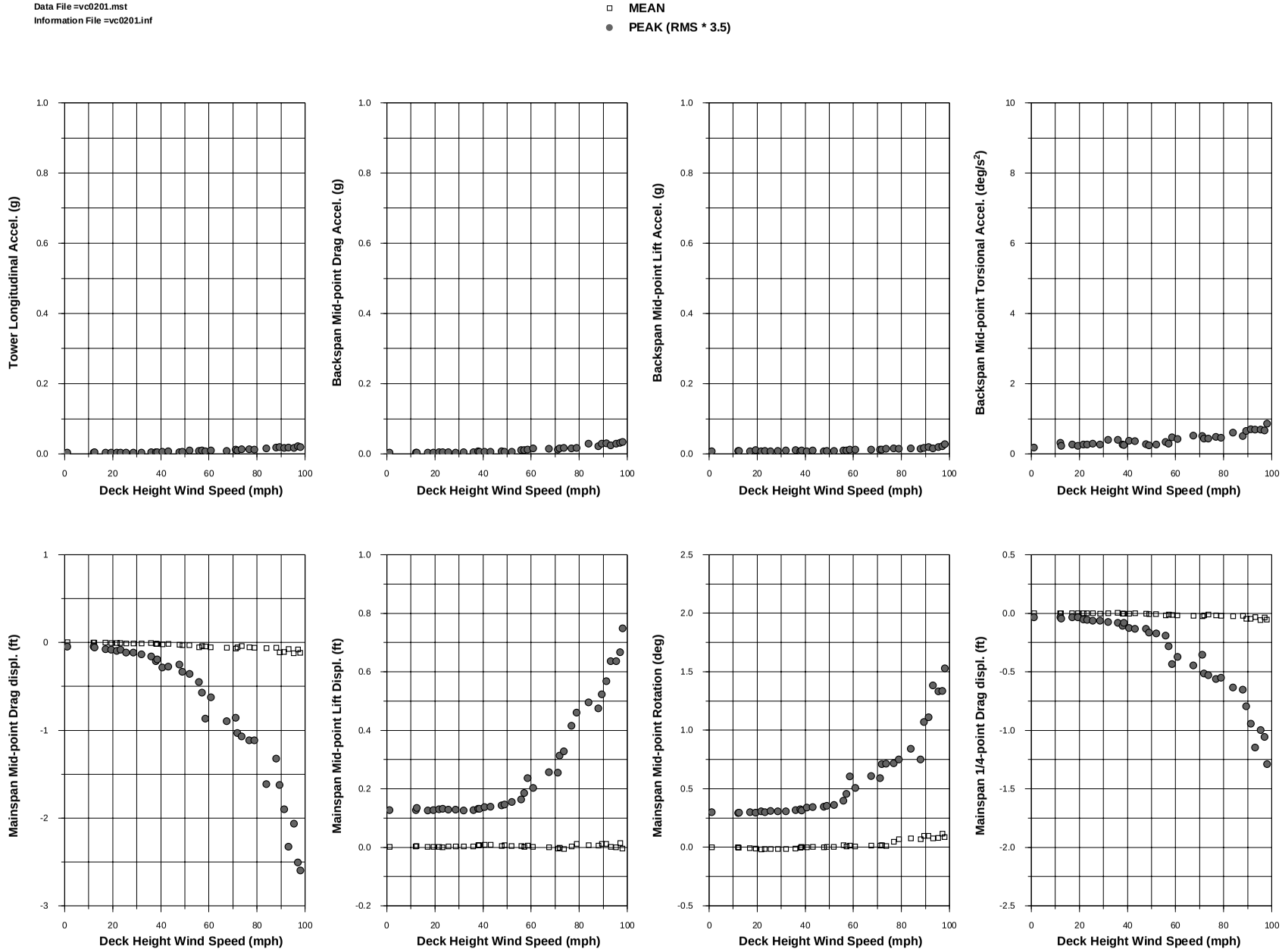

Prospect Verona Bridge, construction stage, hurricane profile, 0 degrees (along bridge)

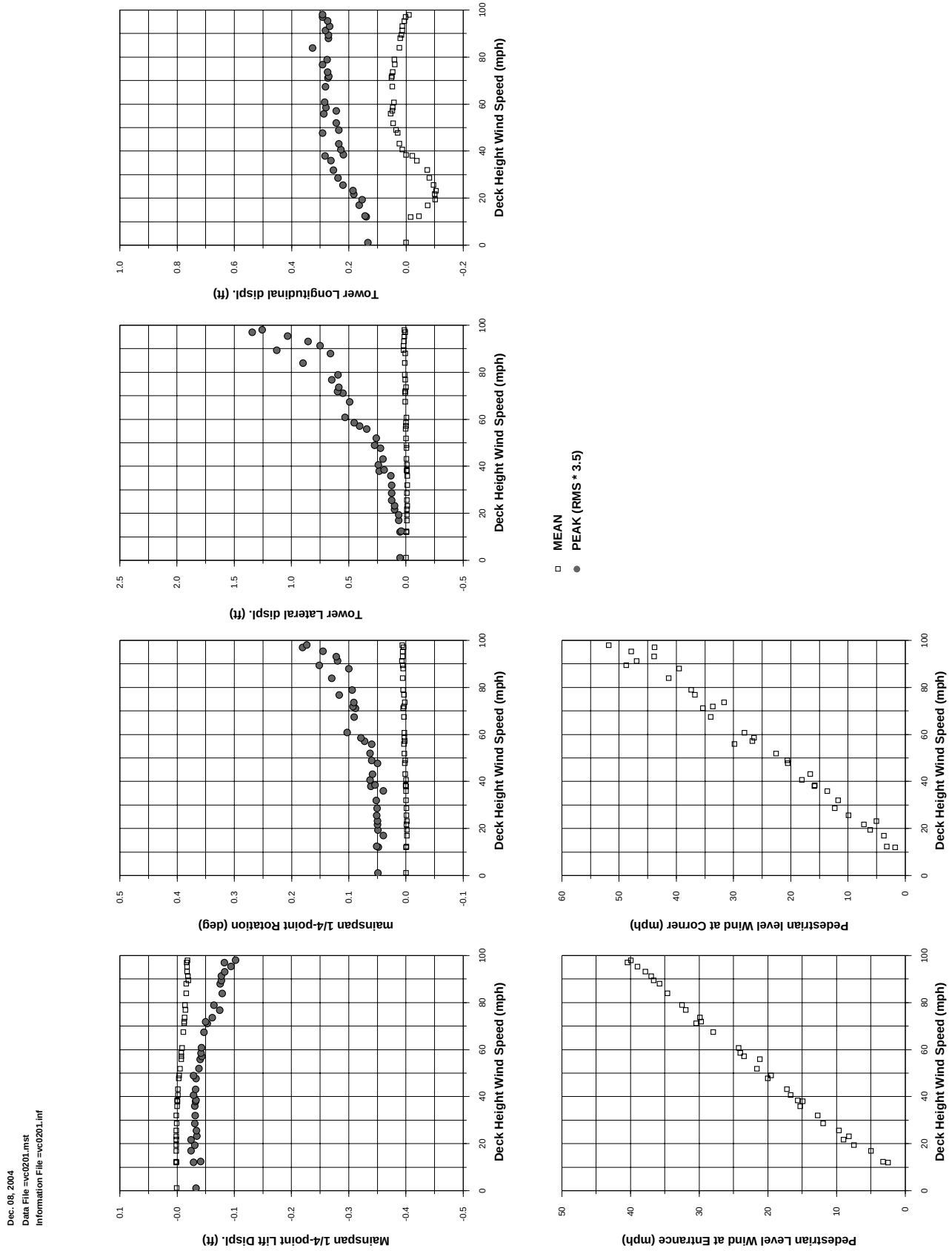

Prospect Verona Bridge, construction stage, hurricane profile, 0 degrees (along bridge)

Dec. 08, 2004
Data File =vc3201.mst
Information File =vc3201.inf

MEAN
PEAK (RMS * 3.5)

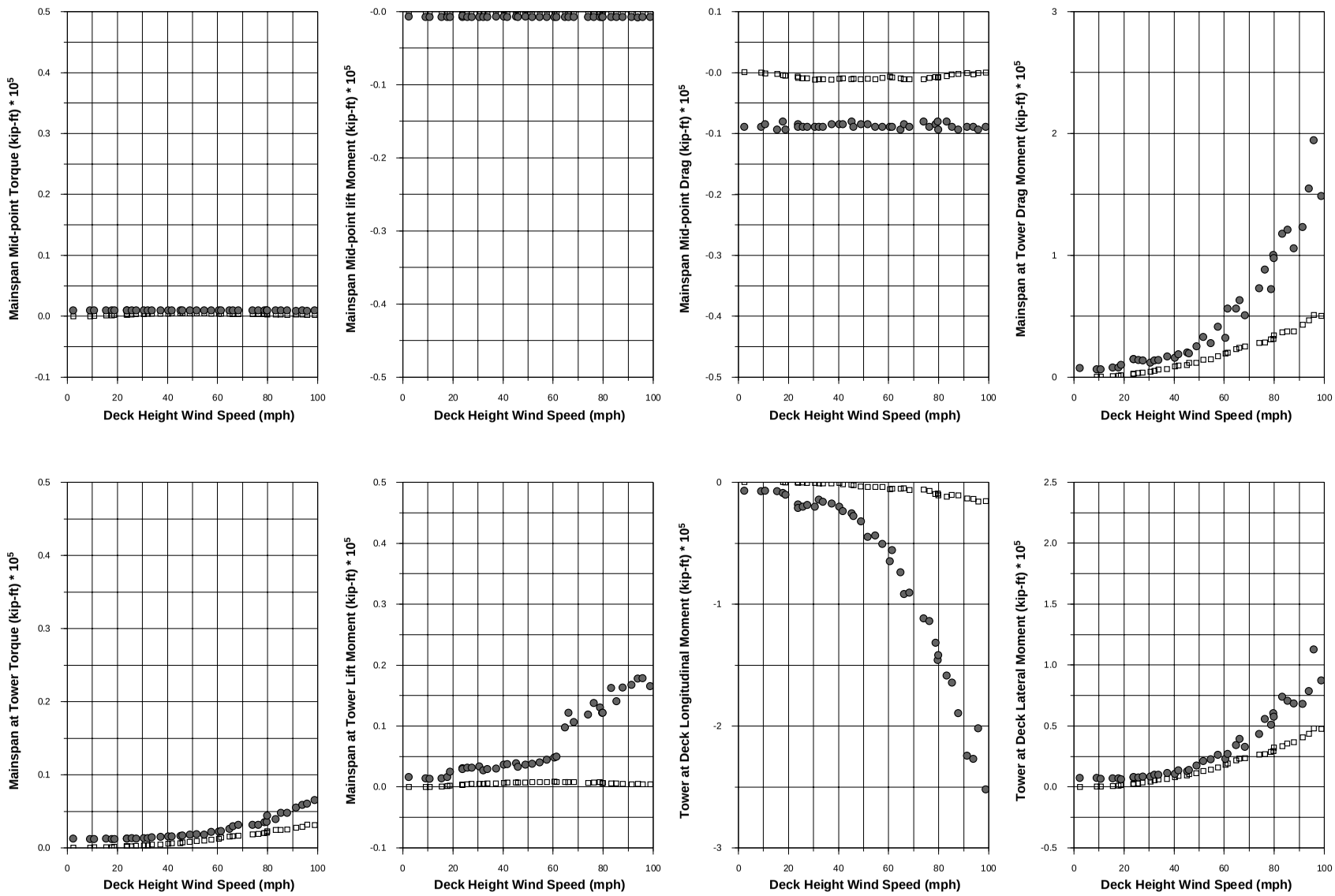

Prospect Verona Bridge, construction stage, hurricane profile, 30 degrees

Dec. 08, 2004
Data File =vc3201.mst
Information File =vc3201.inf

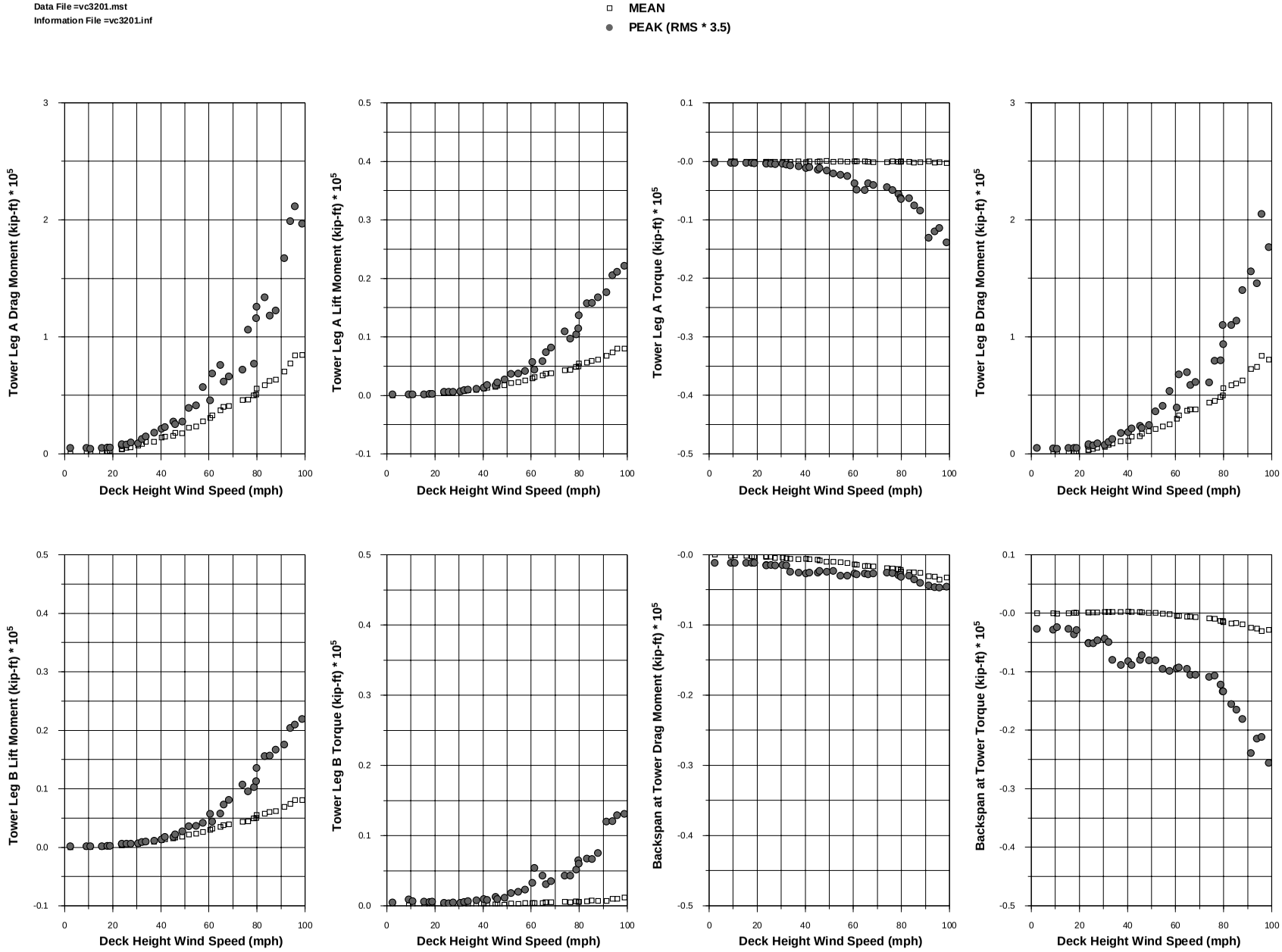

Prospect Verona Bridge, construction stage, hurricane profile, 30 degrees

Dec. 08, 2004
Data File =vc3201.mst
Information File =vc3201.inf

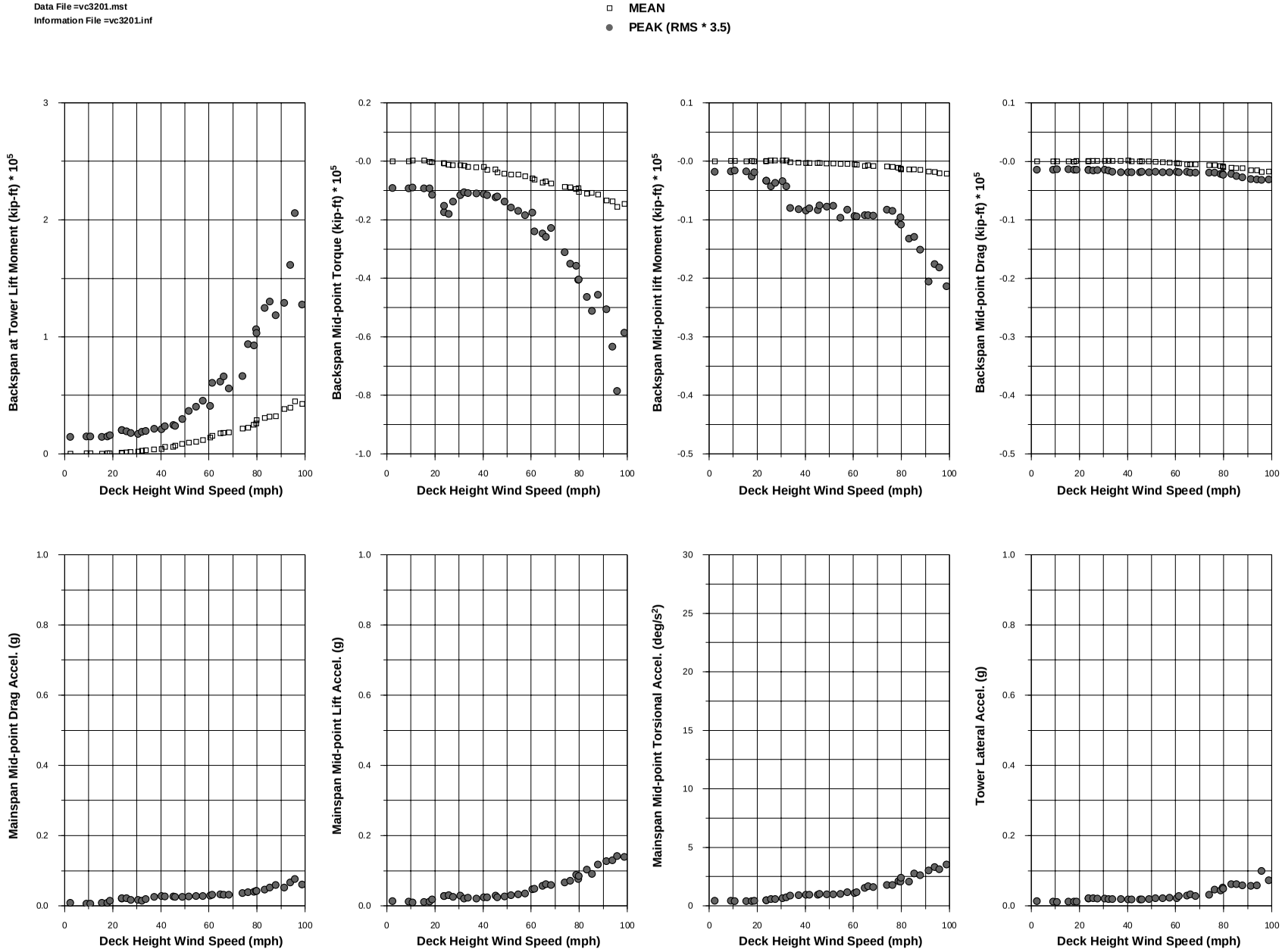

Prospect Verona Bridge, construction stage, hurricane profile, 30 degrees

Dec. 08, 2004
Data File =vc3201.mst
Information File =vc3201.inf

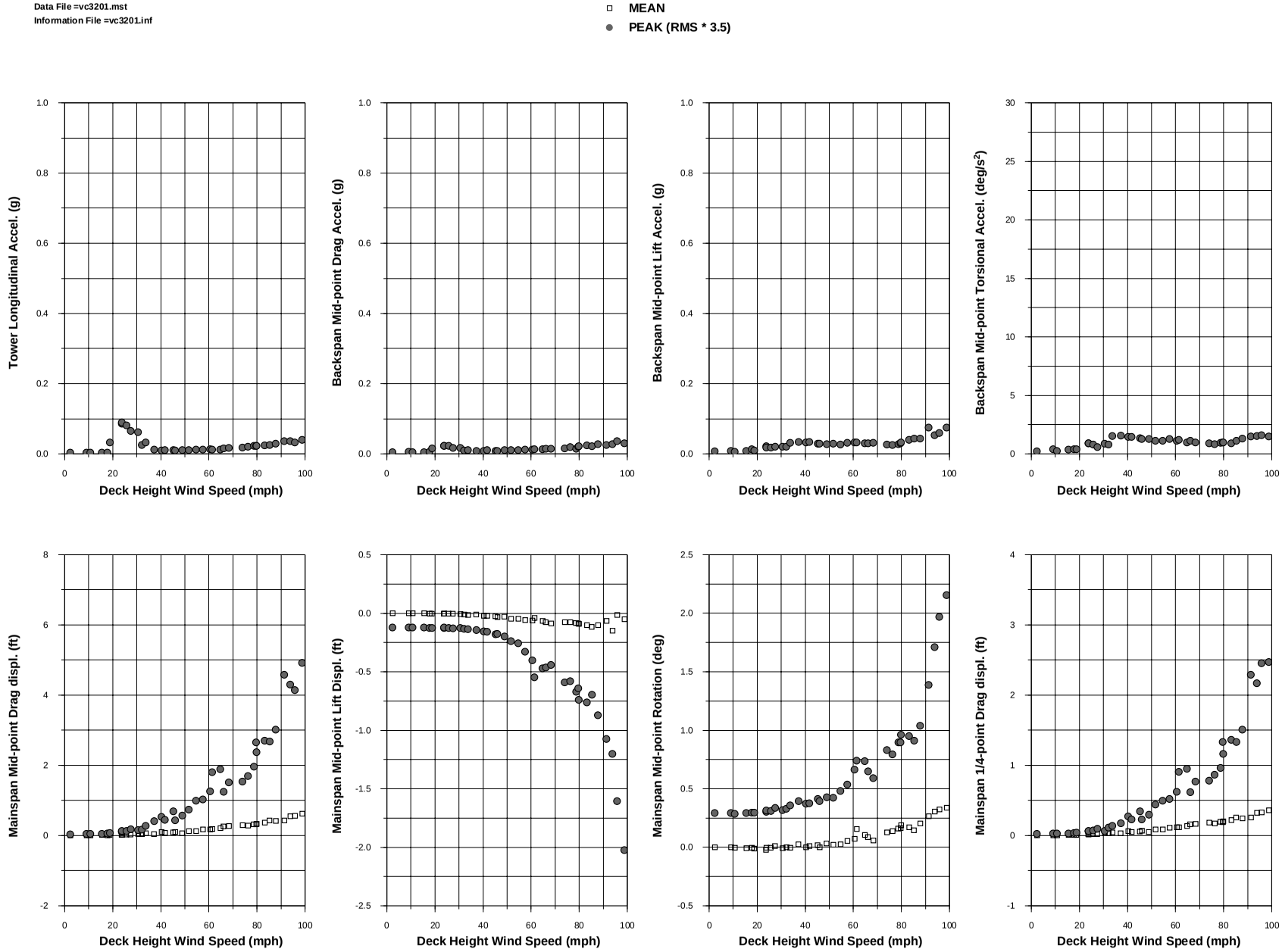

Prospect Verona Bridge, construction stage, hurricane profile, 30 degrees

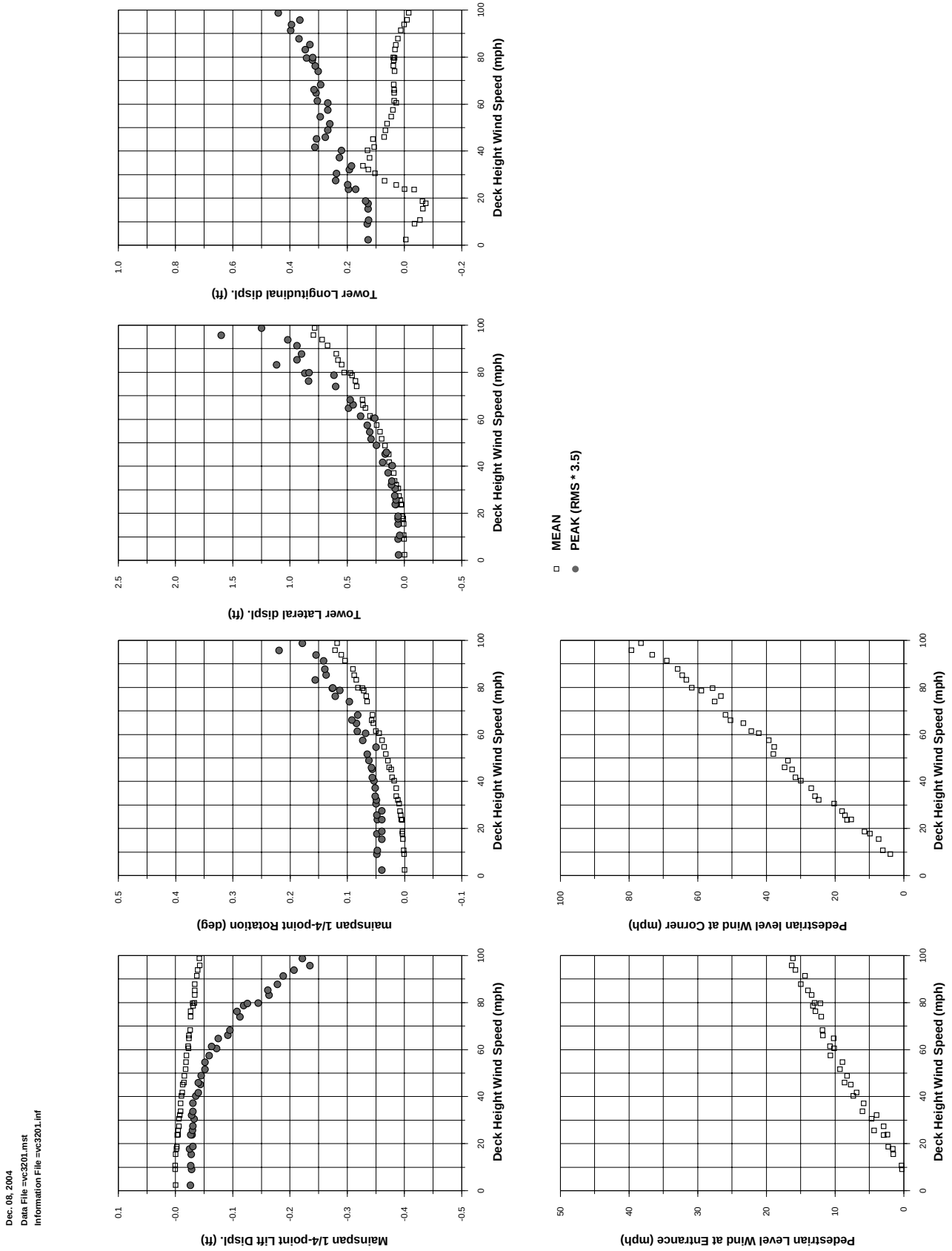

Prospect Verona Bridge, construction stage, hurricane profile, 30 degrees

Dec. 08, 2004
Data File =vc6201.mst
Information File =vc6201.inf

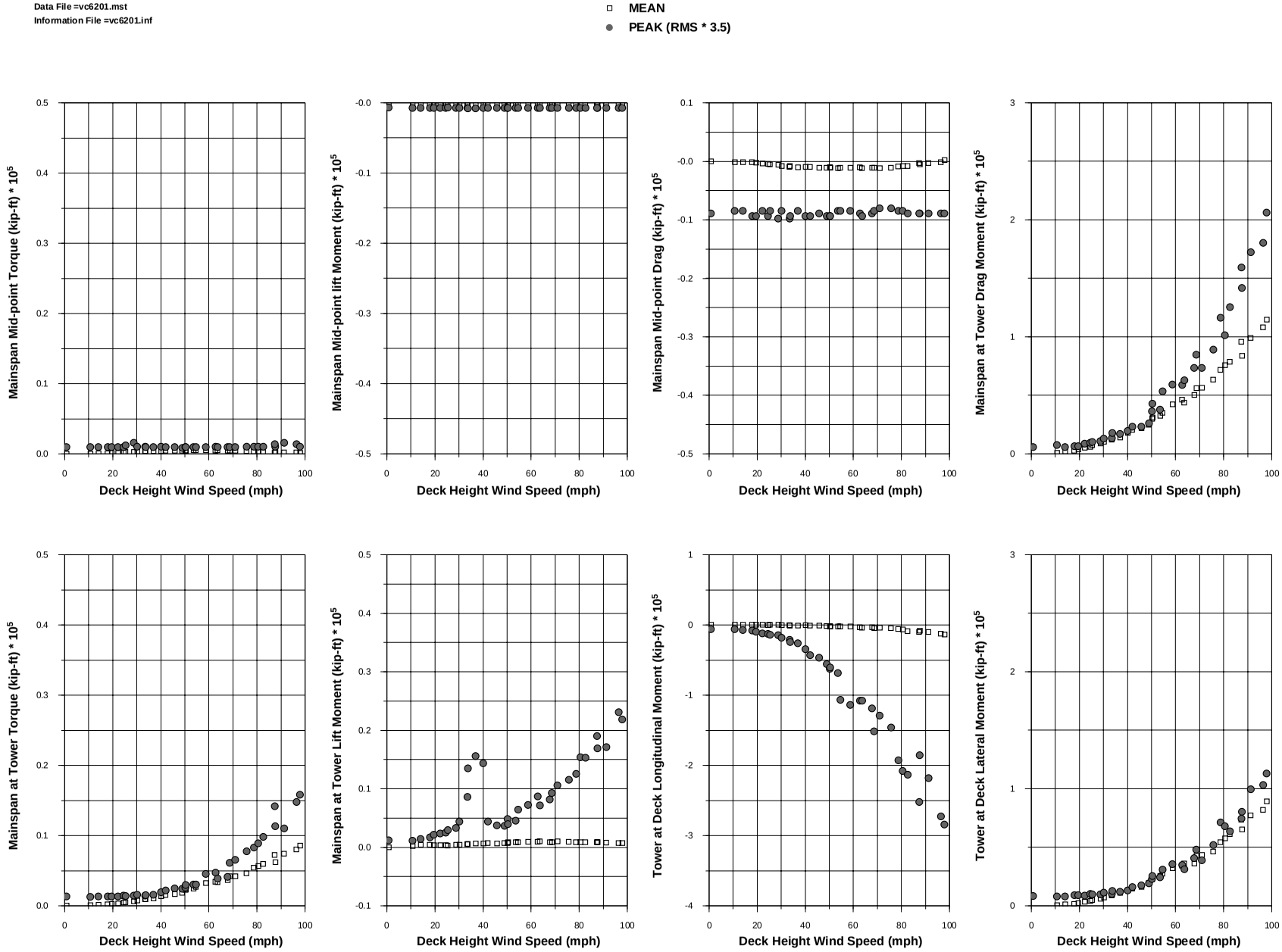

Prospect Verona bridge, construction stage, hurricane profile, 60 degrees

Dec. 08, 2004
Data File =vc6201.mst
Information File =vc6201.inf

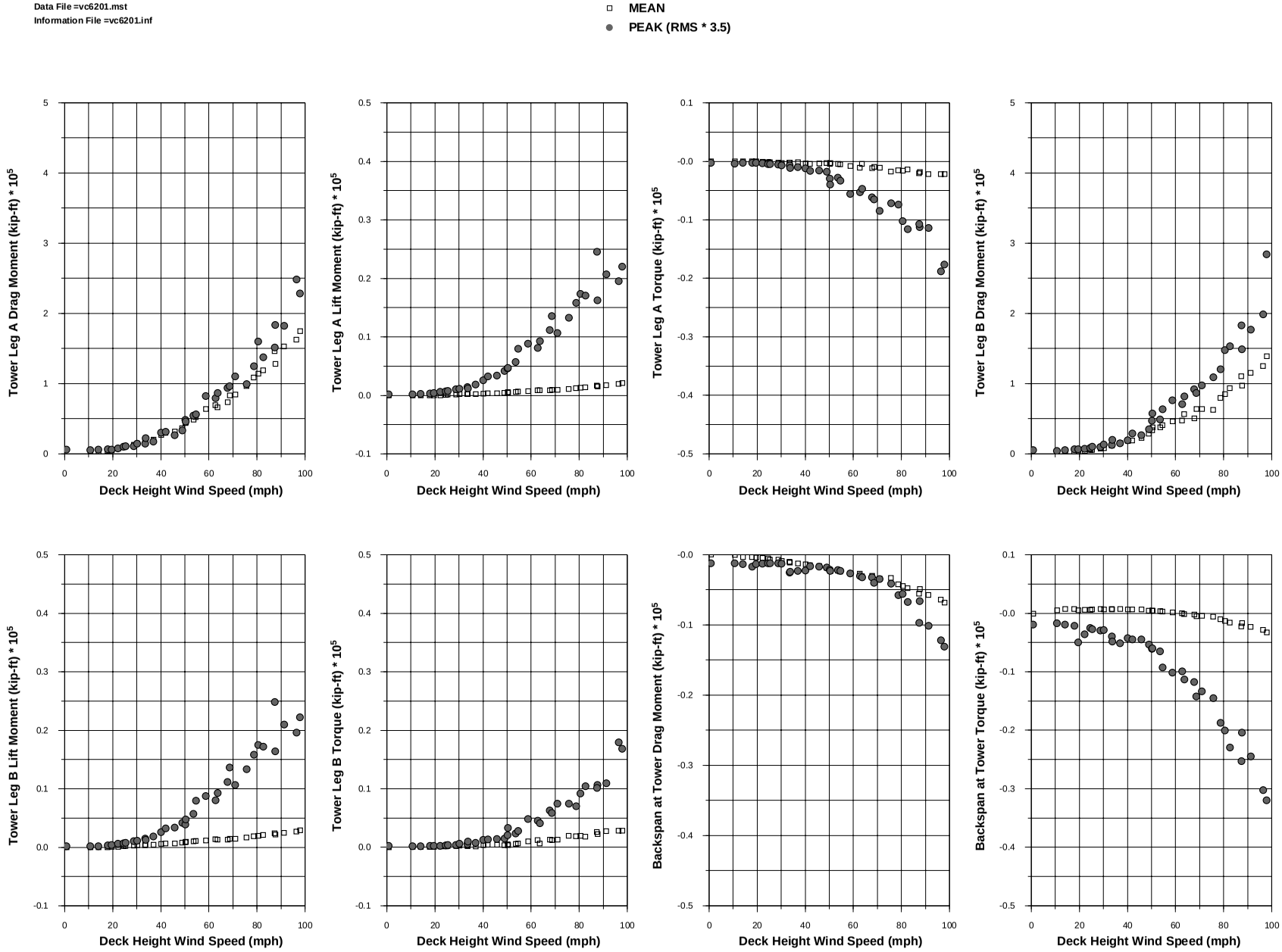

Prospect Verona bridge, construction stage, hurricane profile, 60 degrees

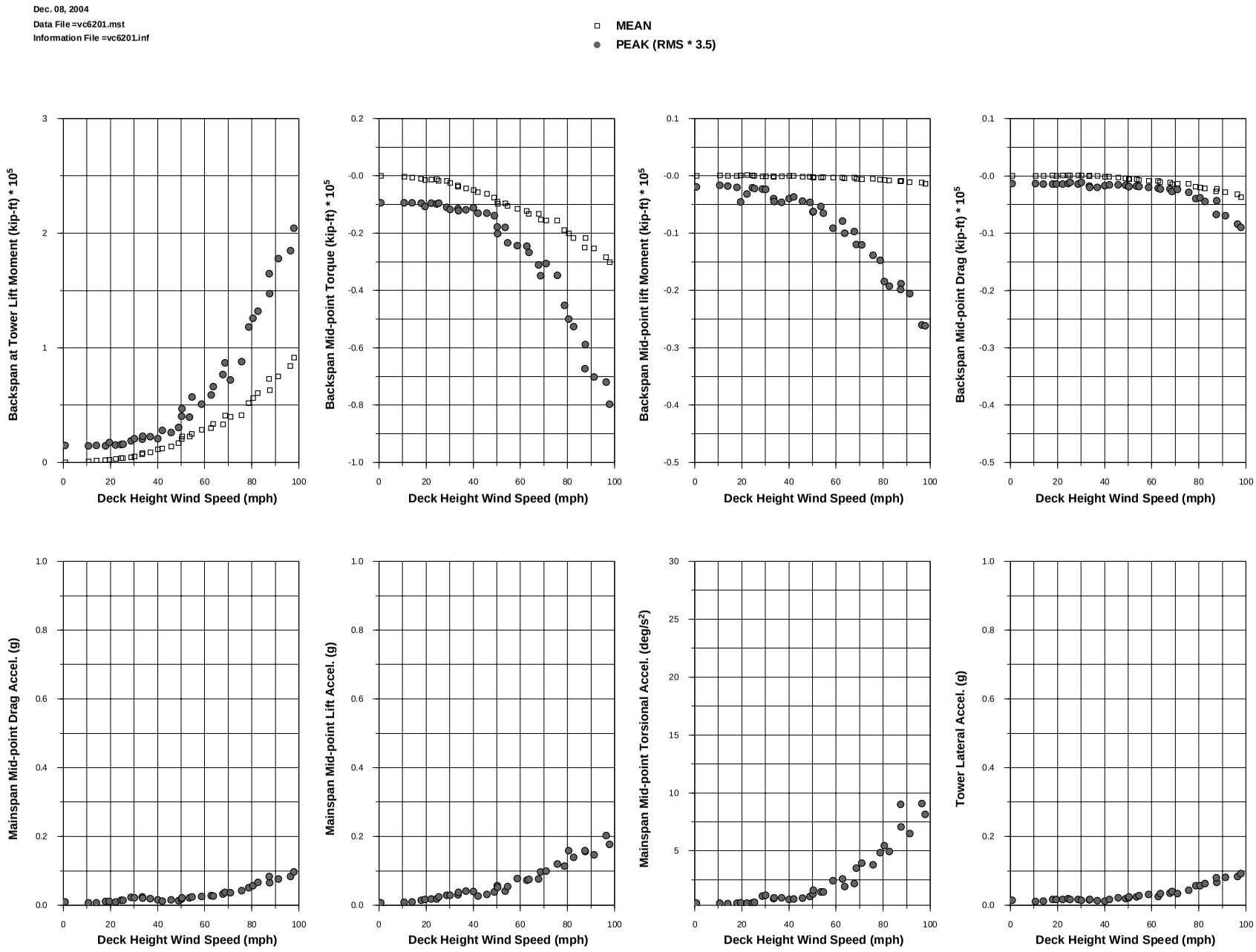

Prospect Verona bridge, construction stage, hurricane profile, 60 degrees

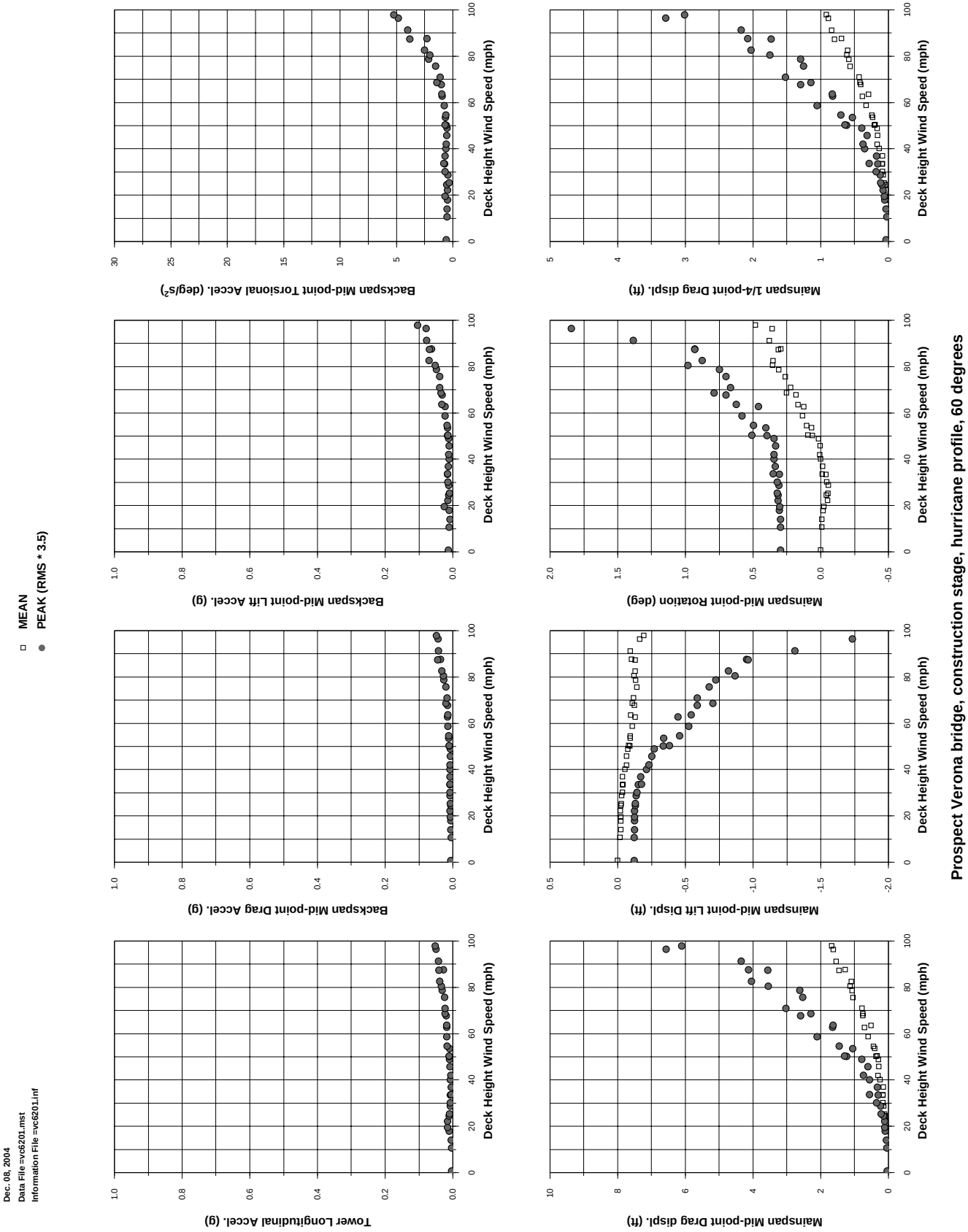

Prospect Verona bridge, construction stage, hurricane profile, 60 degrees

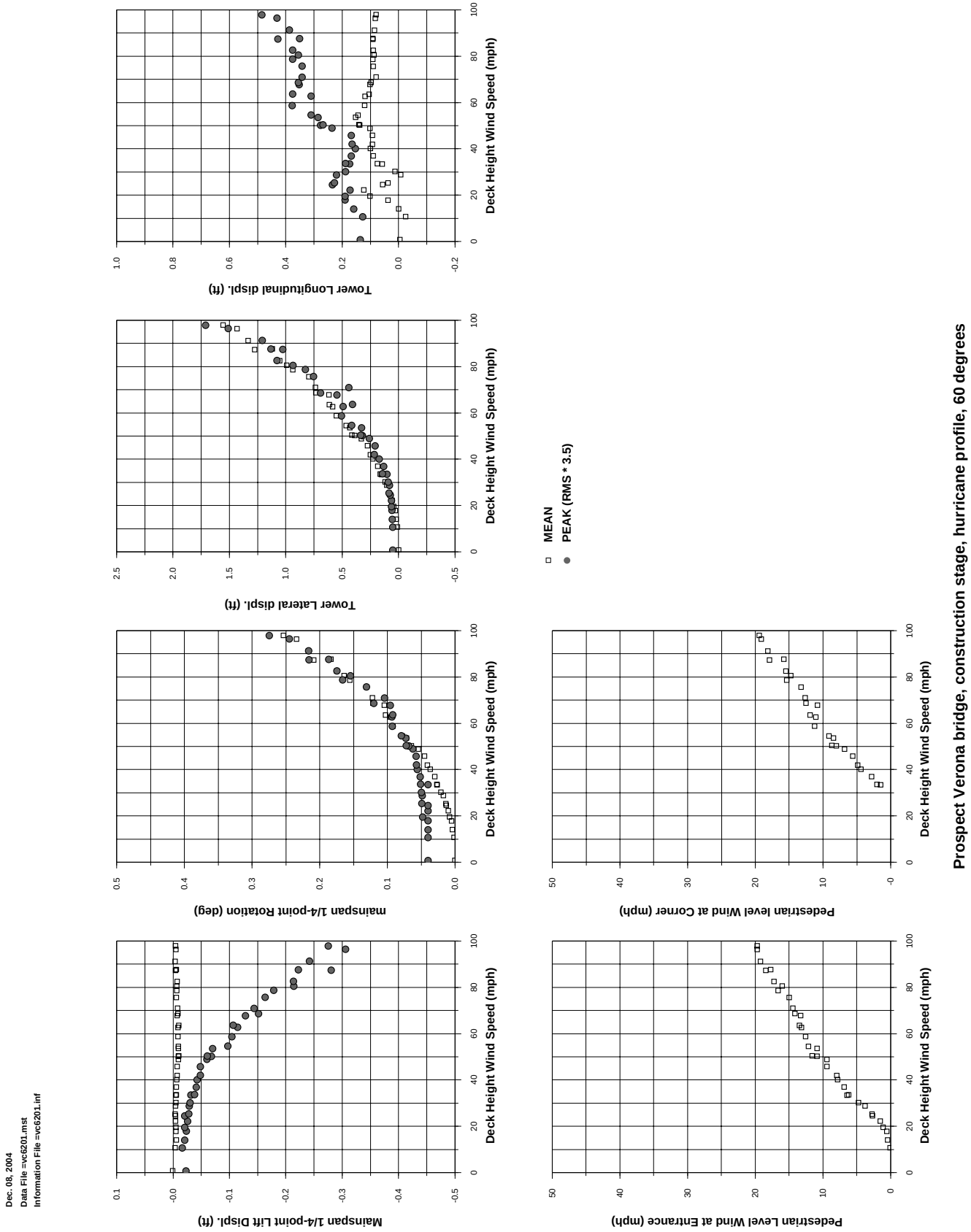

Prospect Verona bridge, construction stage, hurricane profile, 60 degrees

Dec. 07, 2004
Data File =vc2201.mst
Information File =vc2201.inf

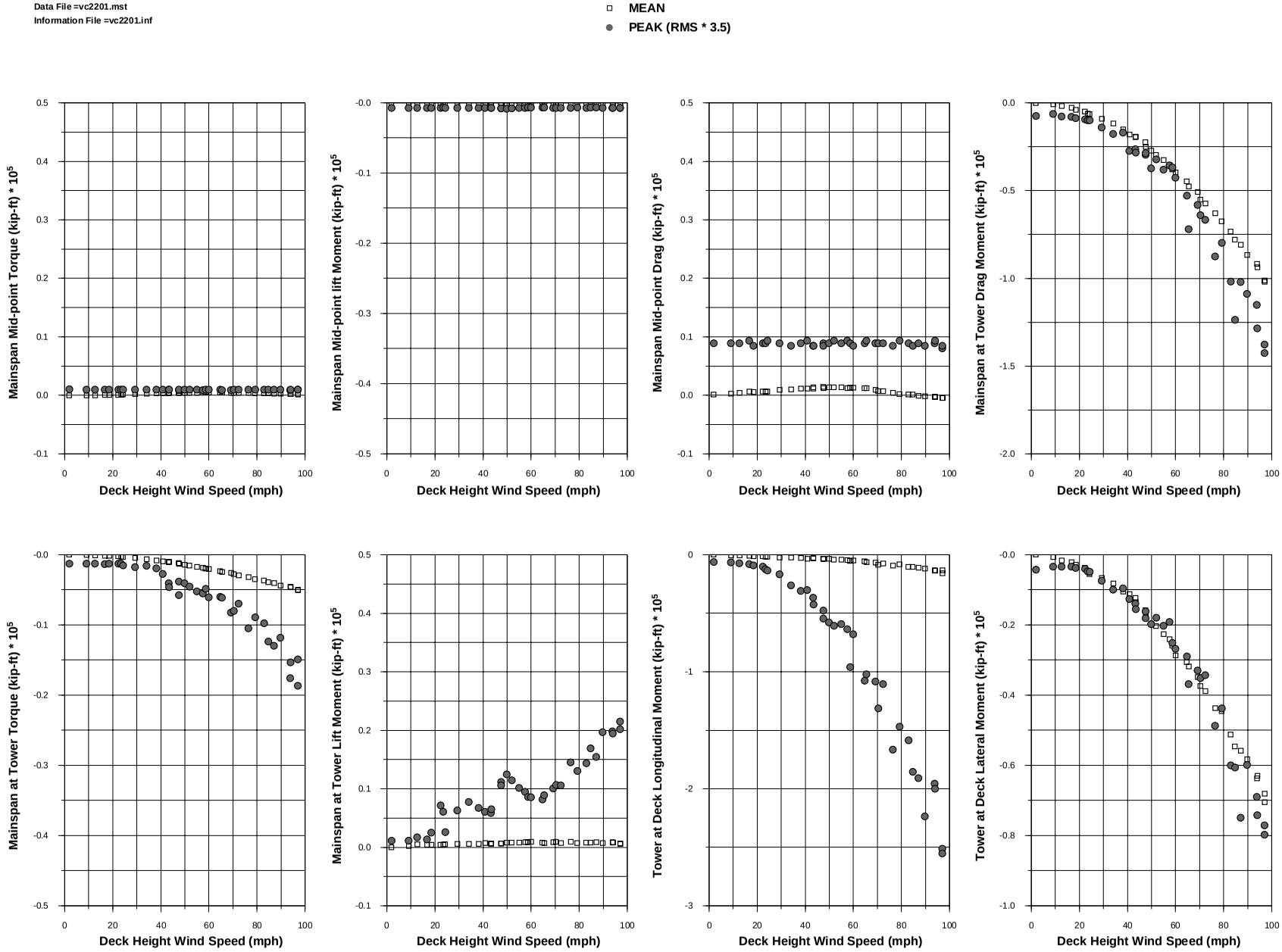

Prospect Verona Bridge, construction stage, hurricane profile, 270 degrees, with existing bridge and box

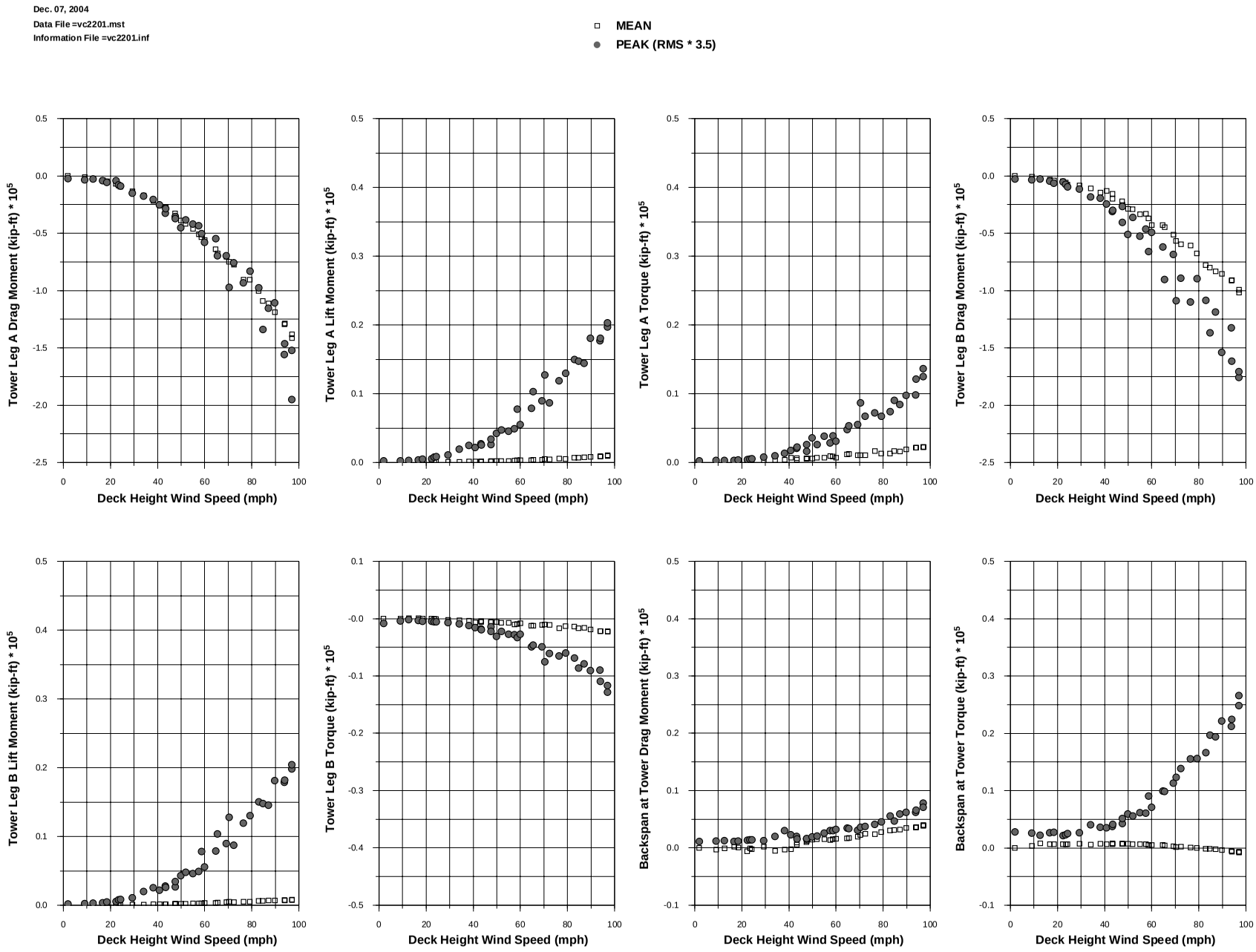

Prospect Verona Bridge, construction stage, hurricane profile, 270 degrees, with existing bridge and box

Dec. 07, 2004
Data File =vc2201.mst
Information File =vc2201.inf

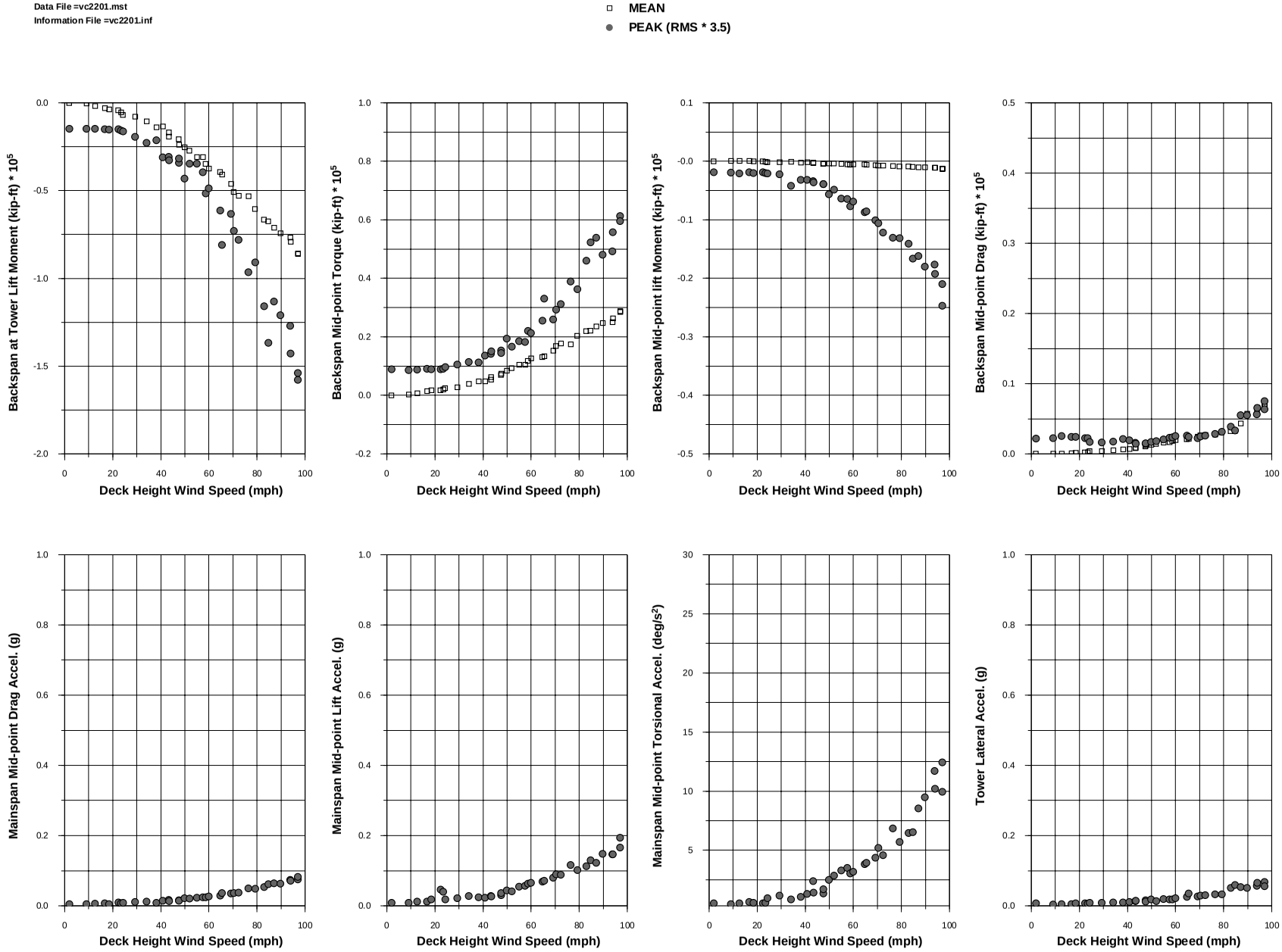

Prospect Verona Bridge, construction stage, hurricane profile, 270 degrees, with existing bridge and box

Dec. 07, 2004
Data File =vc2201.mst
Information File =vc2201.inf

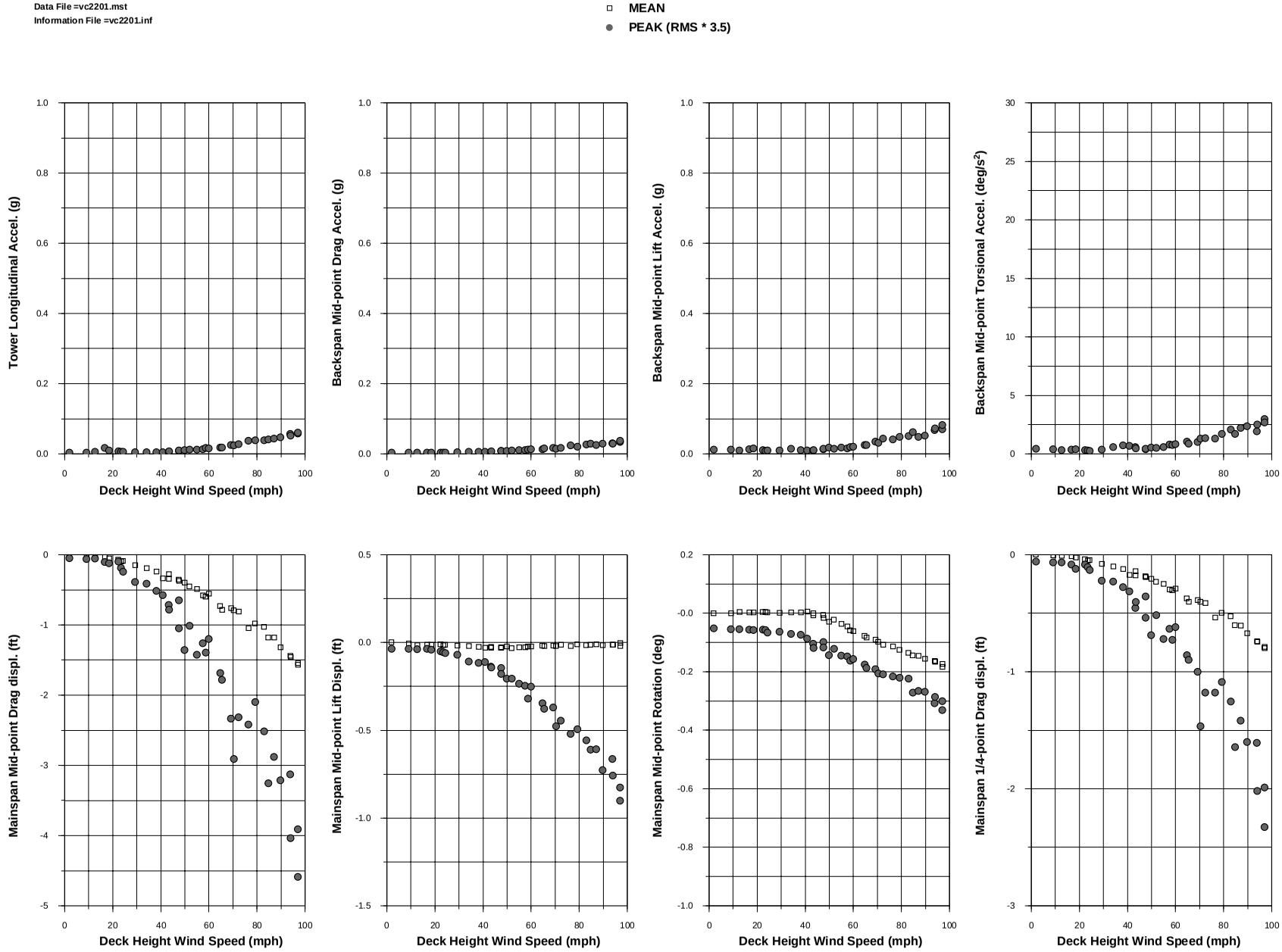

Prospect Verona Bridge, construction stage, hurricane profile, 270 degrees, with existing bridge and box

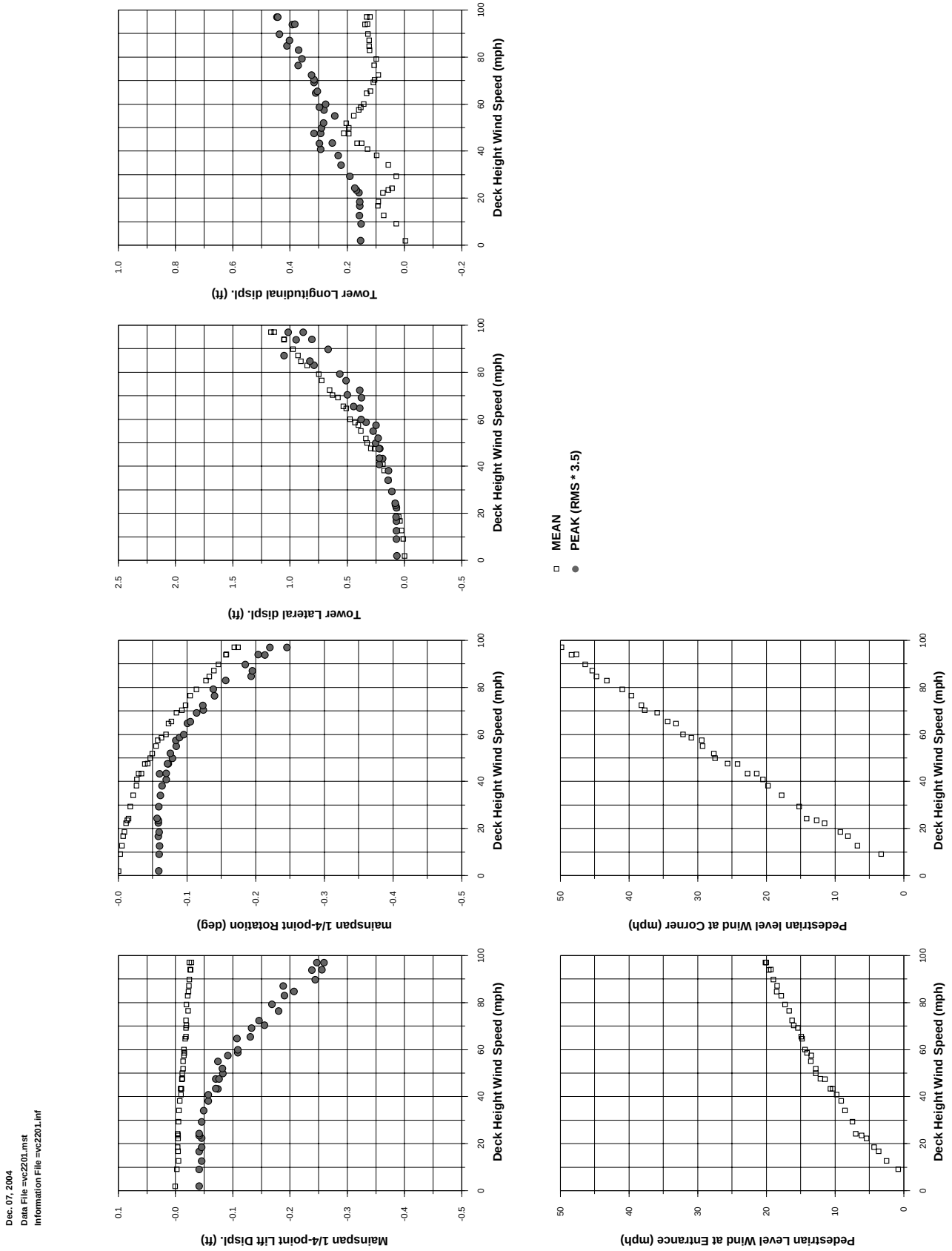

Prospect Verona Bridge, construction stage, hurricane profile, 270 degrees, with existing bridge and box

Dec. 08, 2004
Data File =vc6301.mst
Information File =vc6301.inf

MEAN
PEAK (RMS * 3.5)

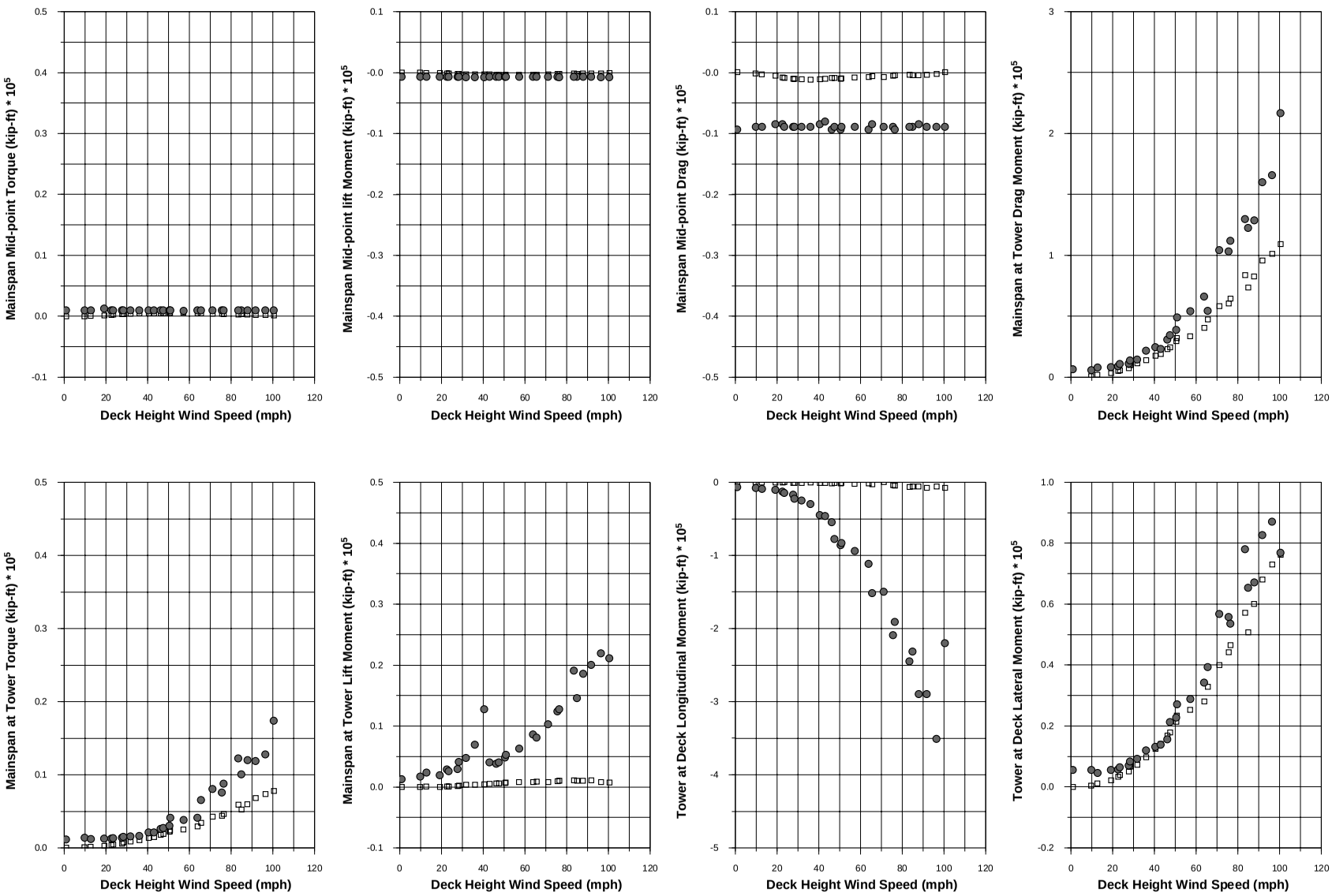

Prospect Verona Bridge, construction stage, open country profile, 60 degrees

Dec. 08, 2004
Data File =vc6301.mst
Information File =vc6301.inf

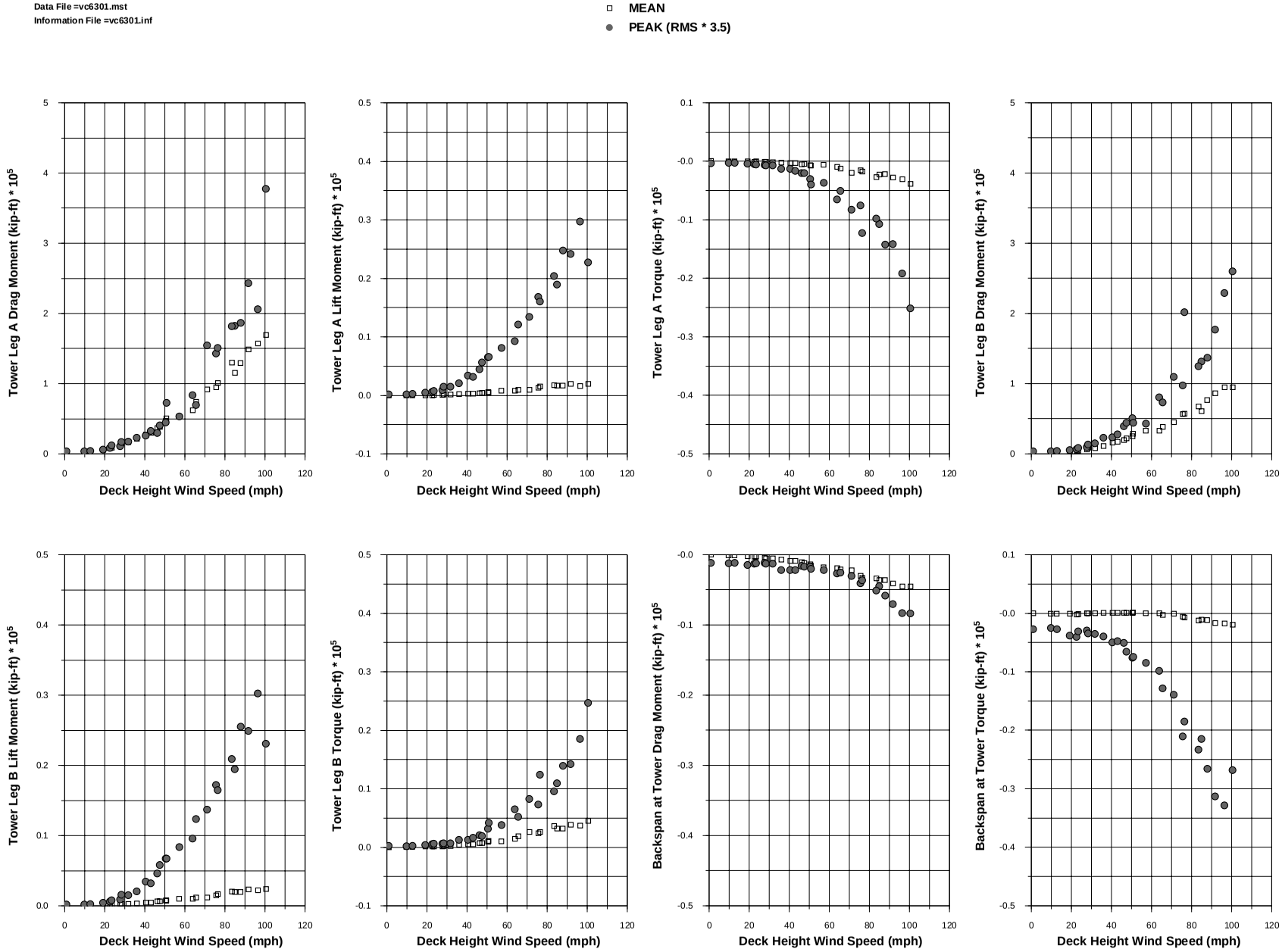

Prospect Verona Bridge, construction stage, open country profile, 60 degrees

Dec. 08, 2004
Data File =vc6301.mst
Information File =vc6301.inf

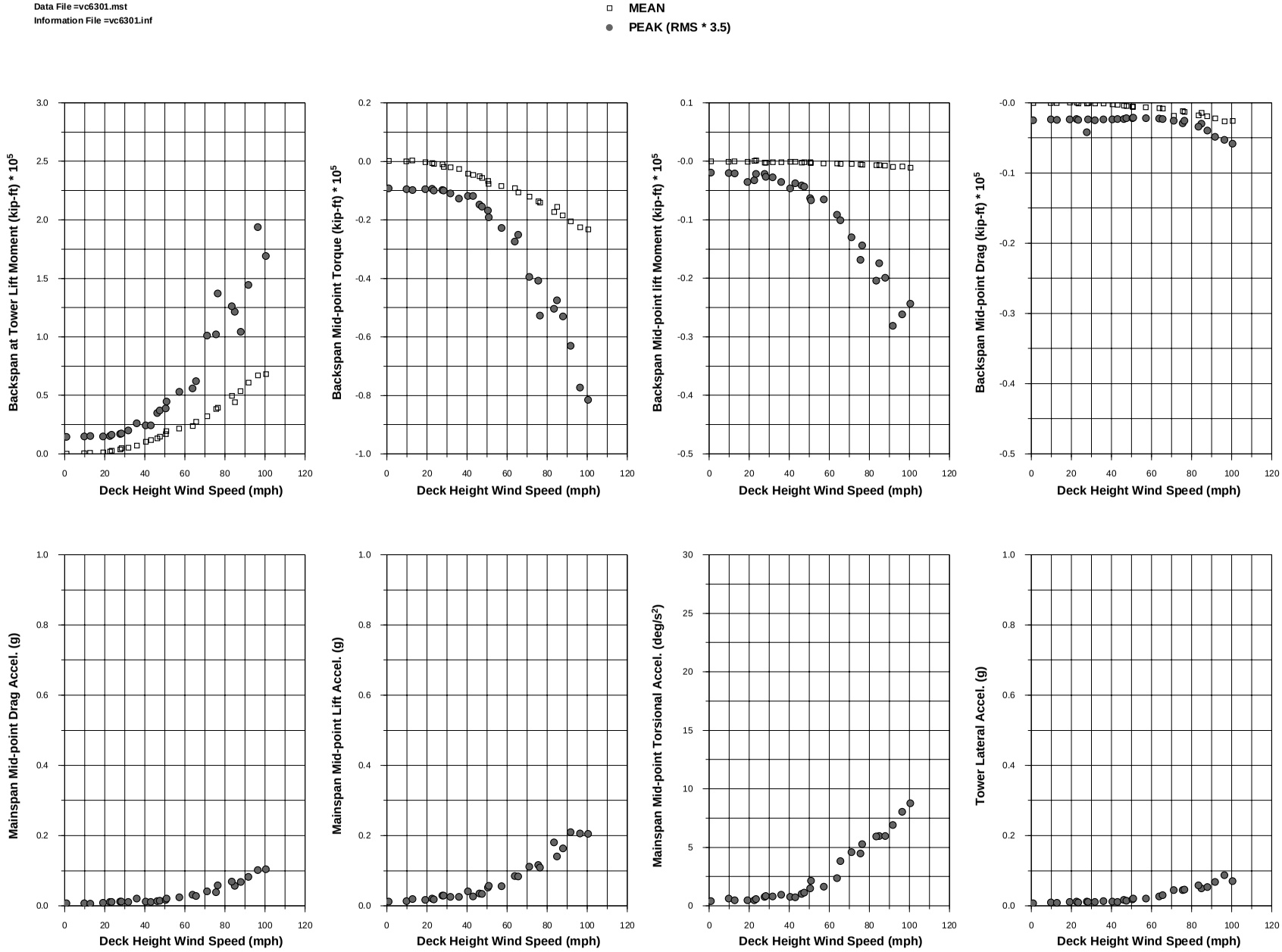

Prospect Verona Bridge, construction stage, open country profile, 60 degrees

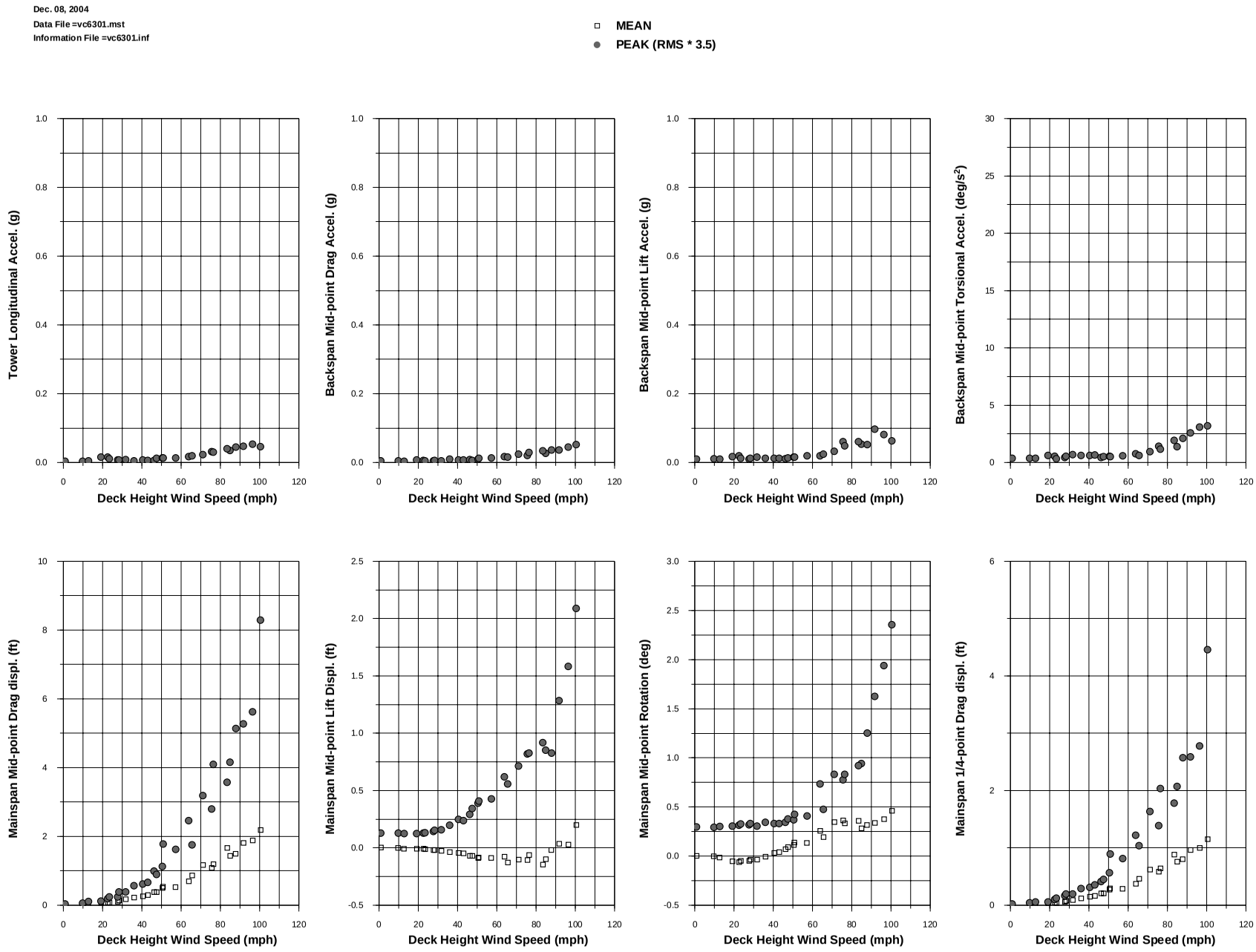

Prospect Verona Bridge, construction stage, open country profile, 60 degrees

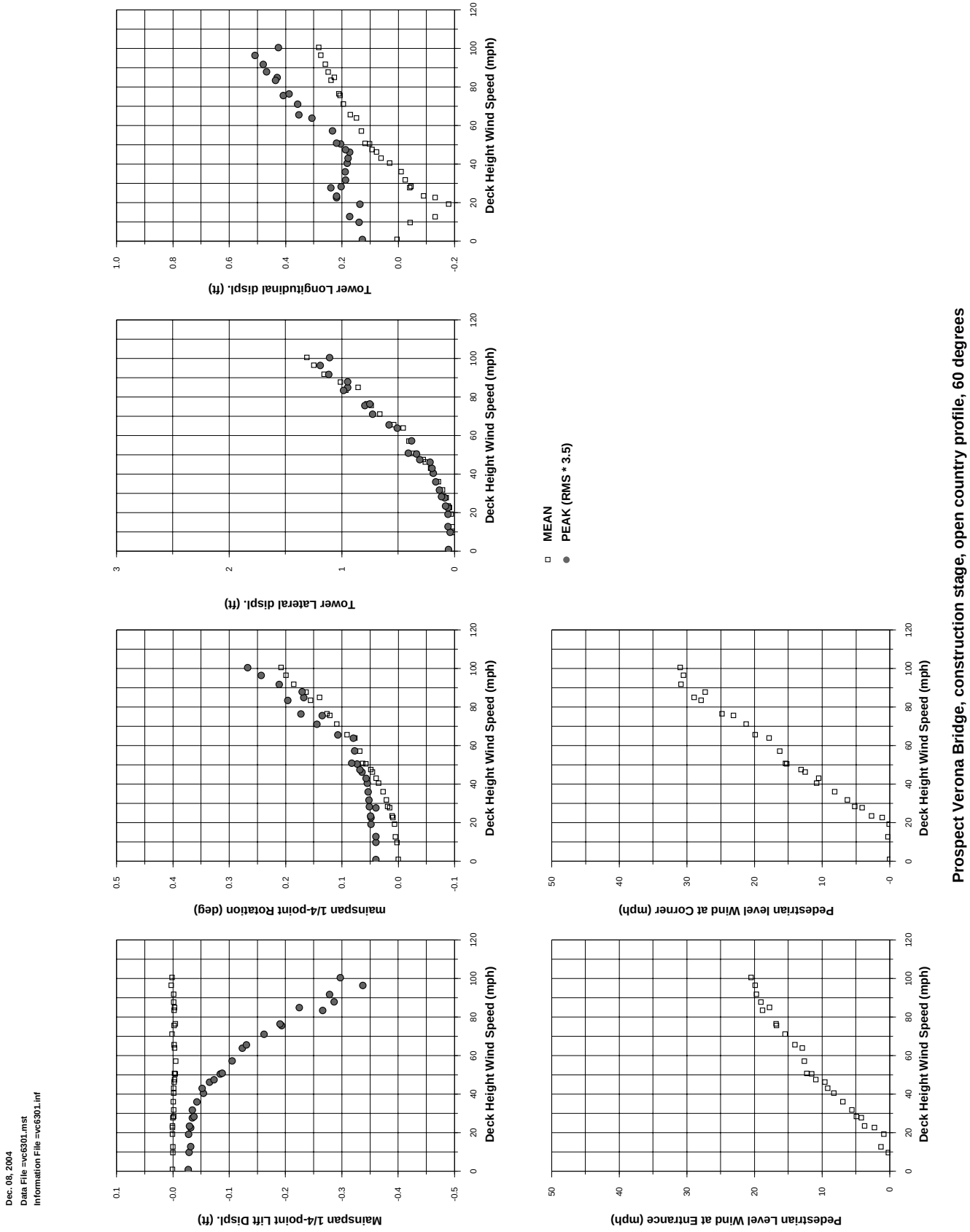

Prospect Verona Bridge, construction stage, open country profile, 60 degrees

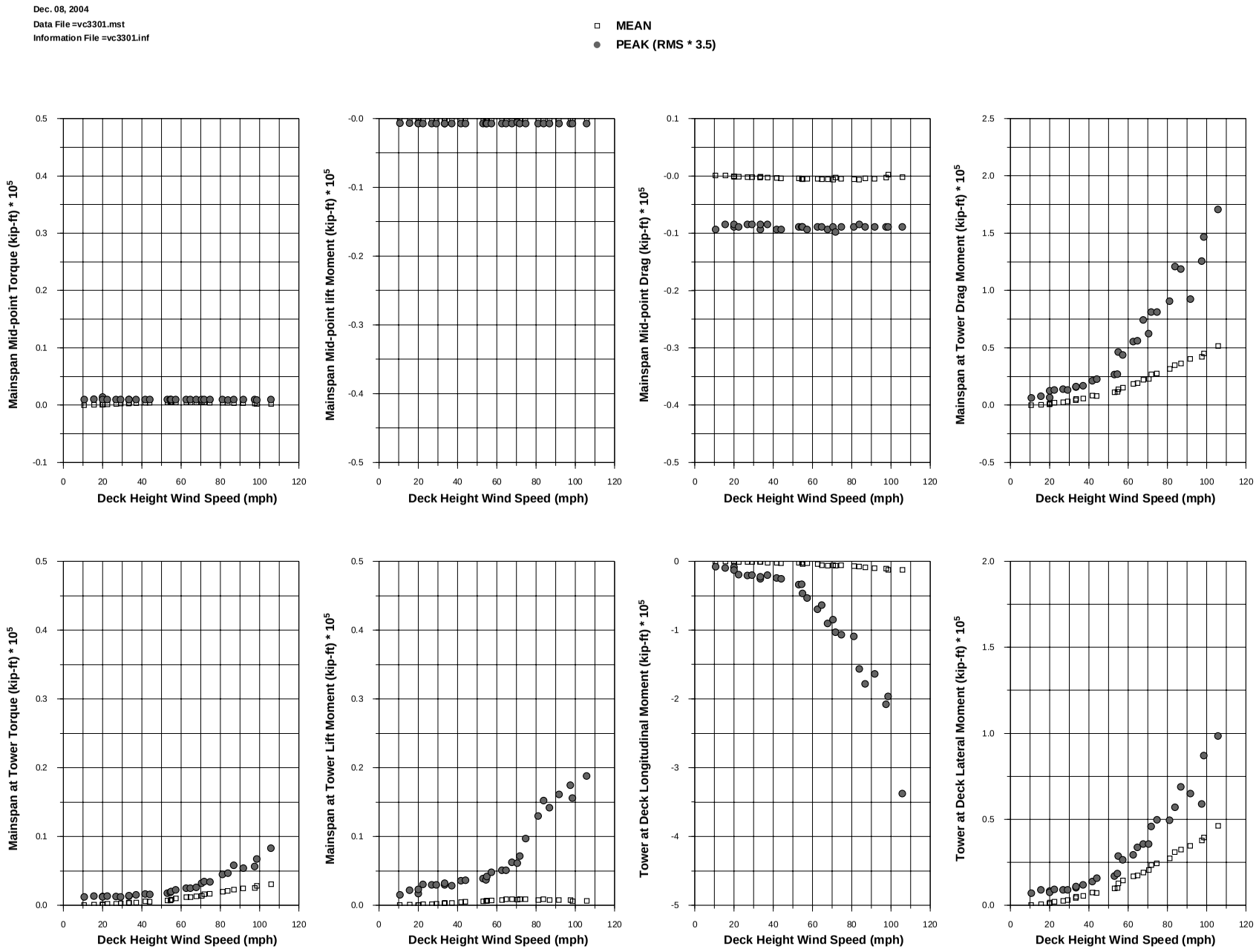

Prospect Verona Bridge, construction stage, open country profile, 30 degrees

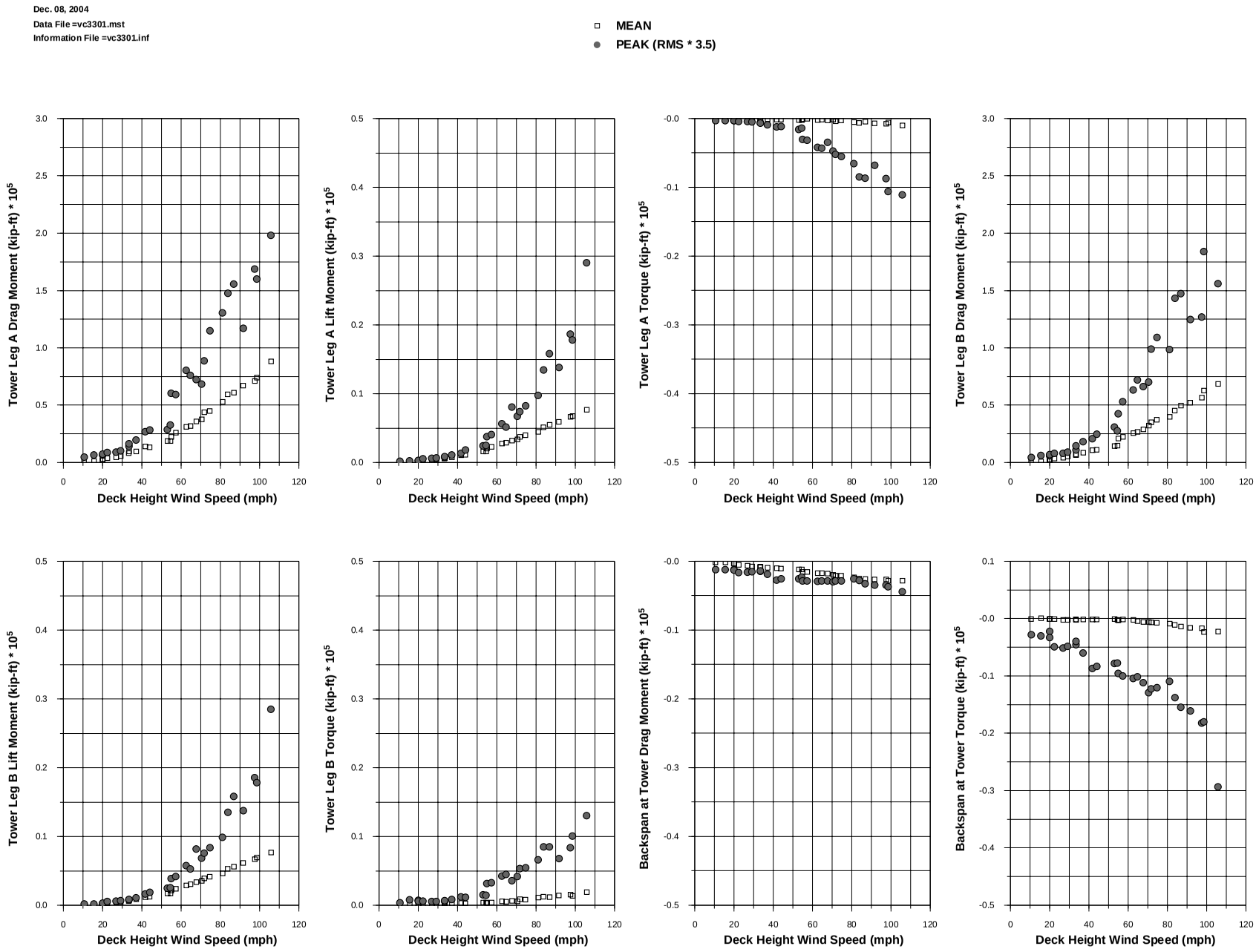

Prospect Verona Bridge, construction stage, open country profile, 30 degrees

Dec. 08, 2004
Data File =vc3301.mst
Information File =vc3301.inf

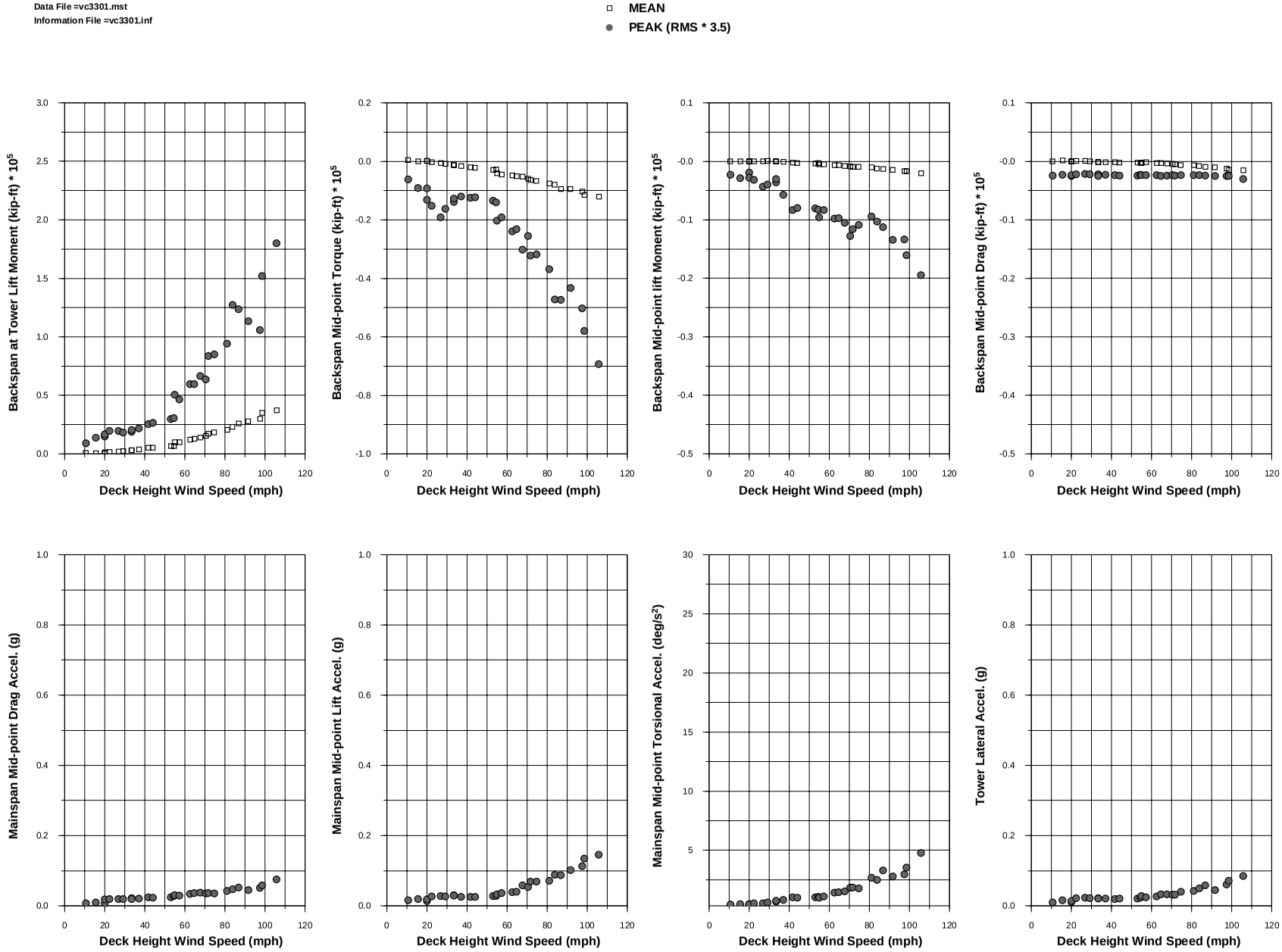

Prospect Verona Bridge, construction stage, open country profile, 30 degrees

Dec. 08, 2004
Data File =vc3301.mst
Information File =vc3301.inf

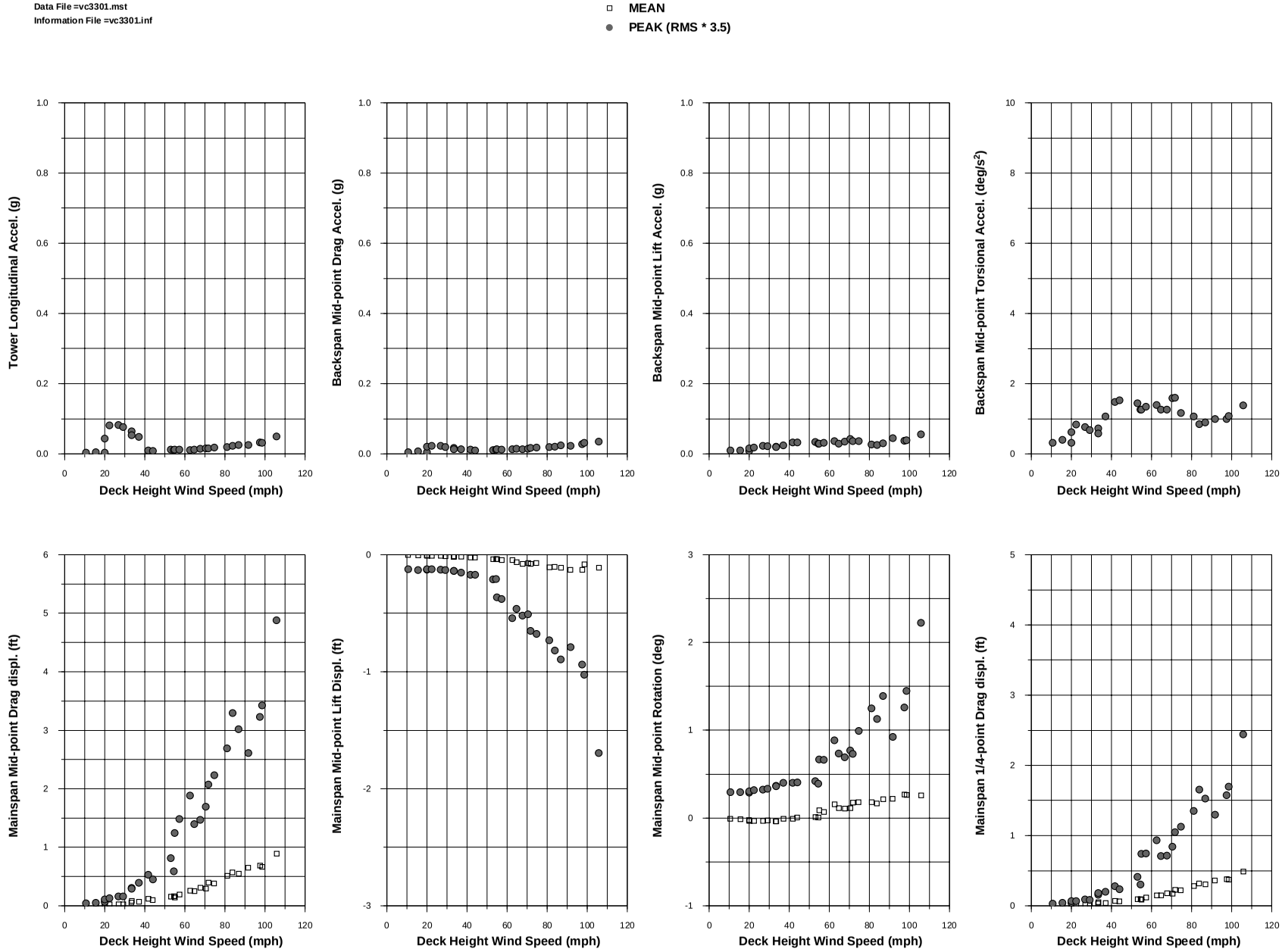

Prospect Verona Bridge, construction stage, open country profile, 30 degrees

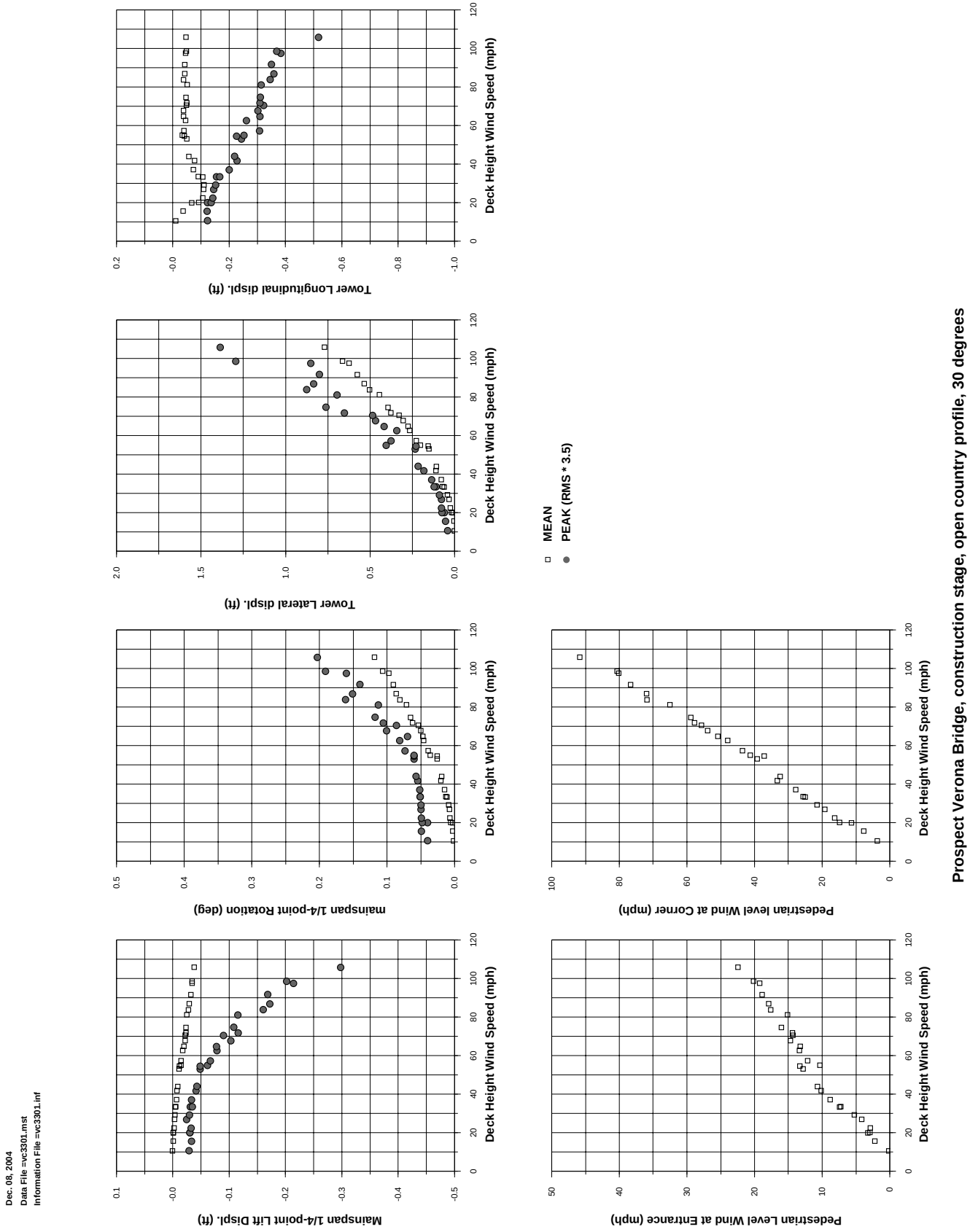

Prospect Verona Bridge, construction stage, open country profile, 30 degrees

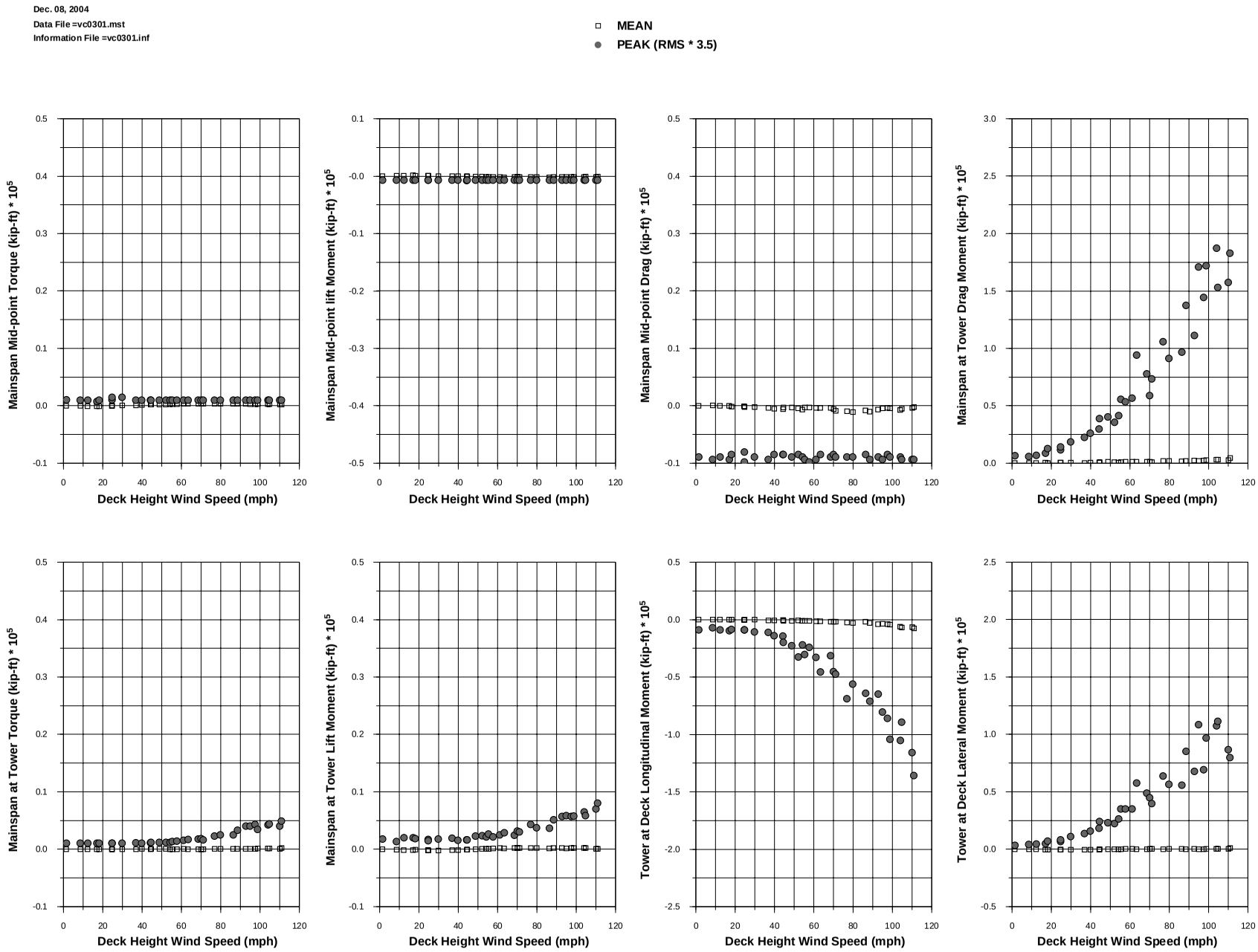

Prospect Verona Bridge, construction stage, open country profile, 0 degrees (along bridge)

Dec. 08, 2004
Data File =vc0301.mst
Information File =vc0301.inf

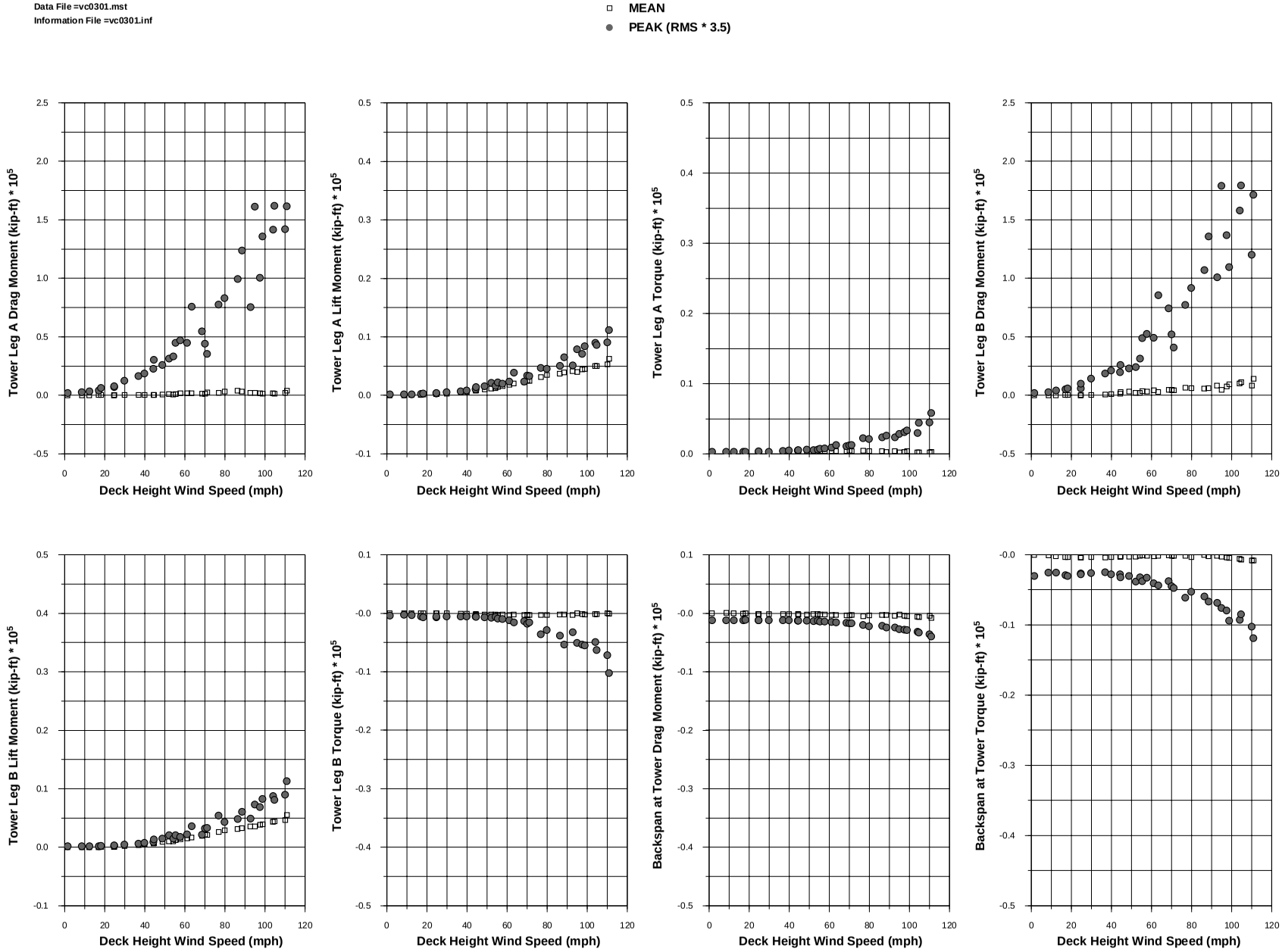

Prospect Verona Bridge, construction stage, open country profile, 0 degrees (along bridge)

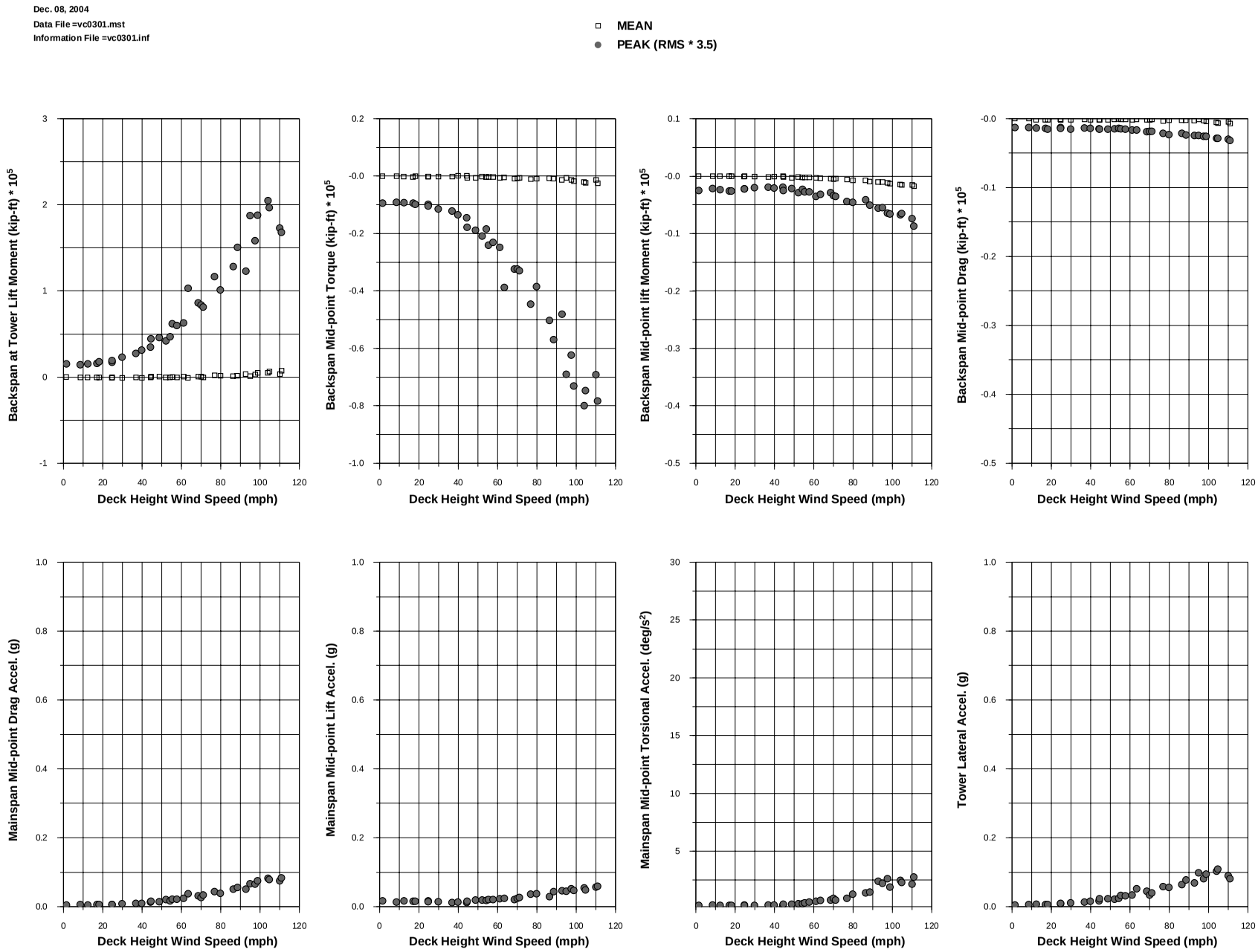

Prospect Verona Bridge, construction stage, open country profile, 0 degrees (along bridge)

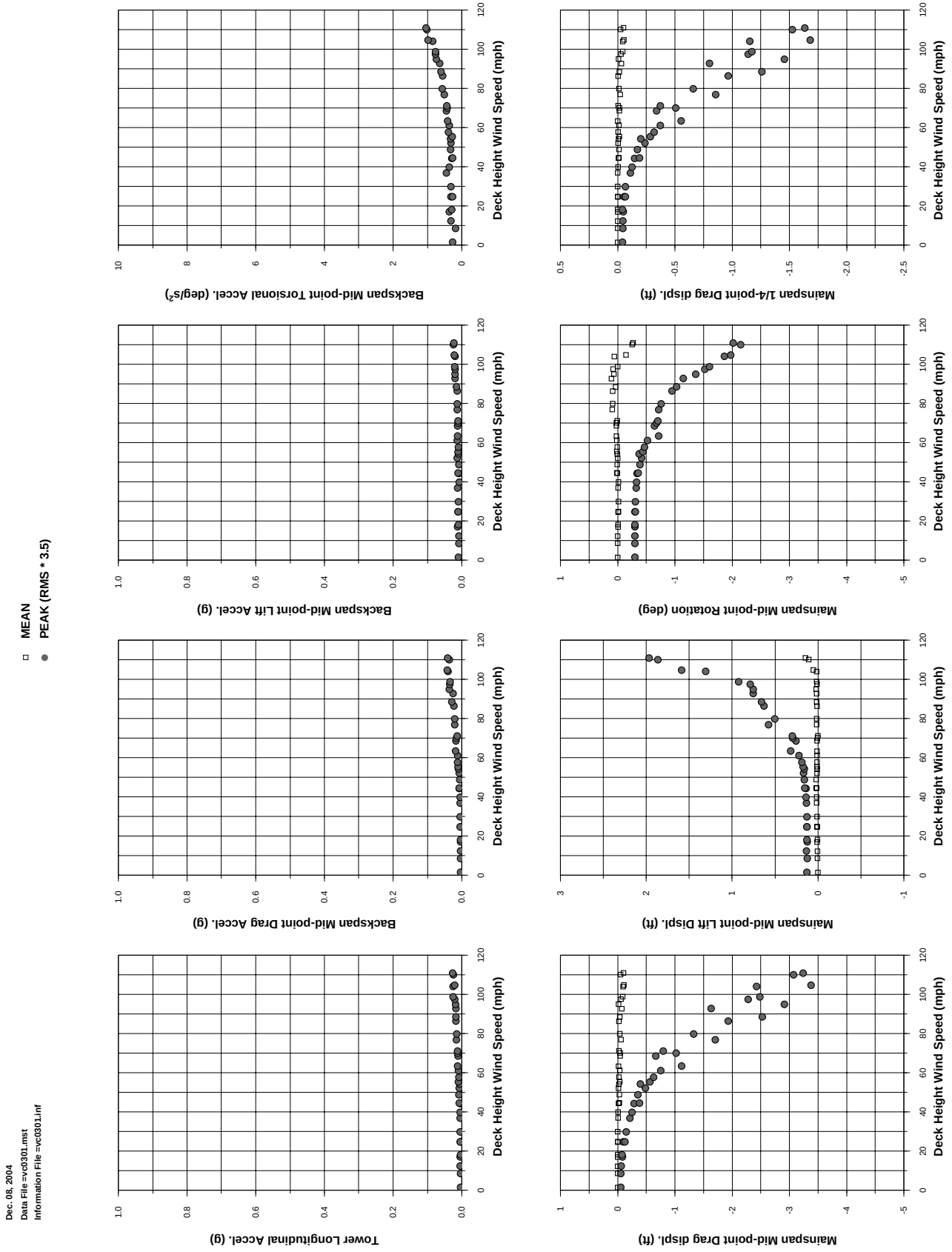

Prospect Verona Bridge, construction stage, open country profile, 0 degrees (along bridge)

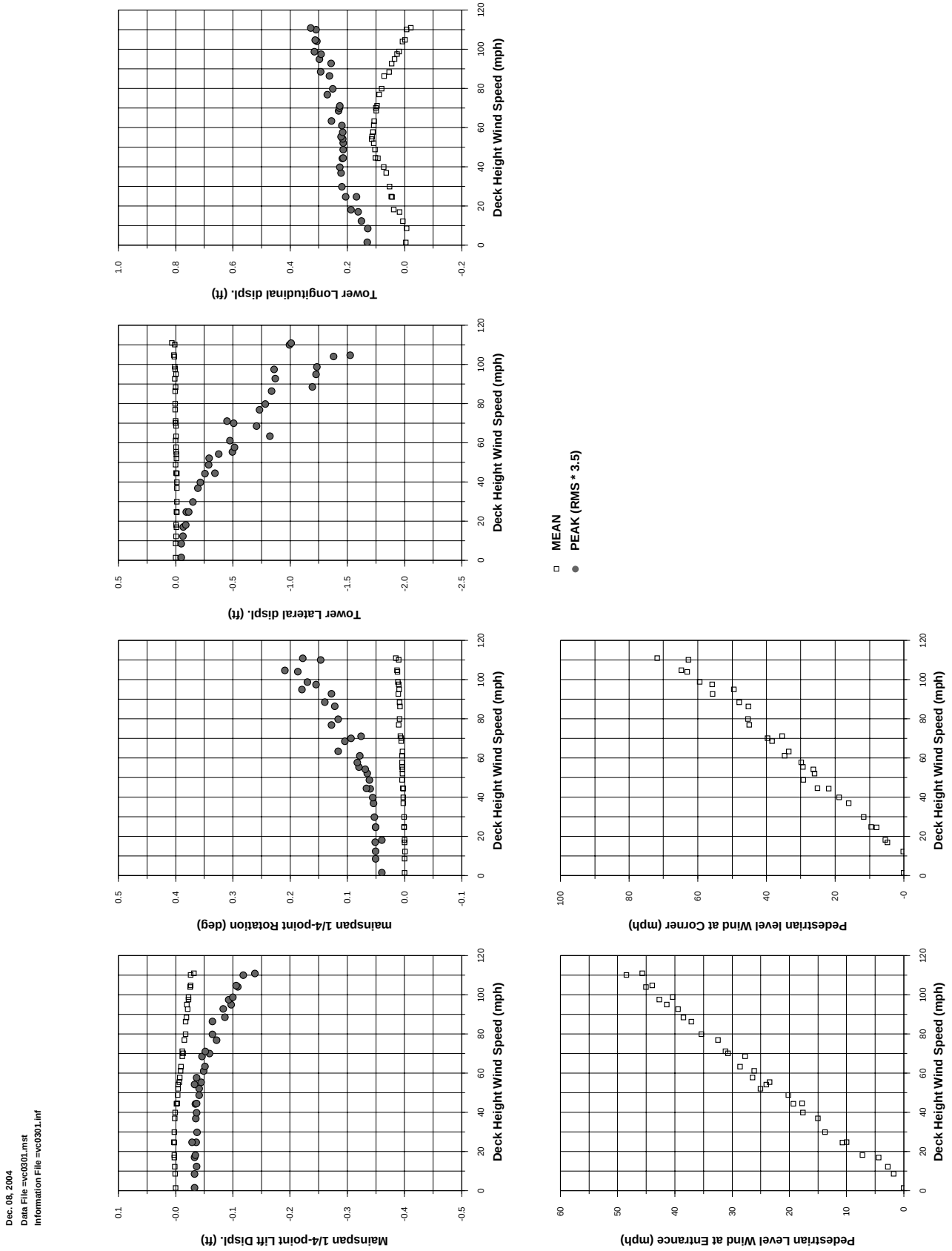

Prospect Verona Bridge, construction stage, open country profile, 0 degrees (along bridge)

Dec. 08, 2004
Data File =vc9301.mst
Information File =vc9301.inf

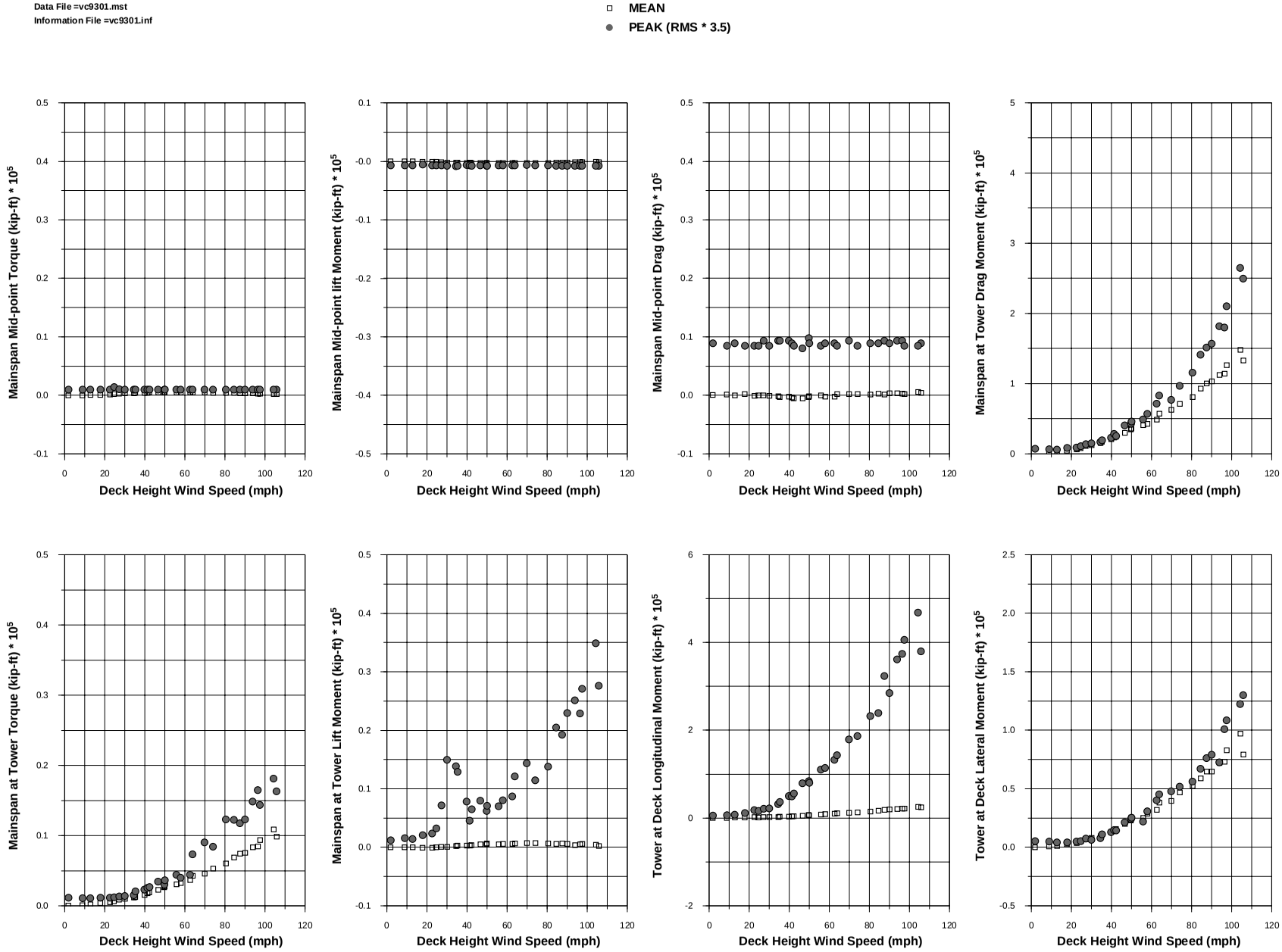

Prospect Verona Bridge, construction stage, open country profile, 90 degrees, without existing bridge & box

Dec. 08, 2004
Data File =vc9301.mst
Information File =vc9301.inf

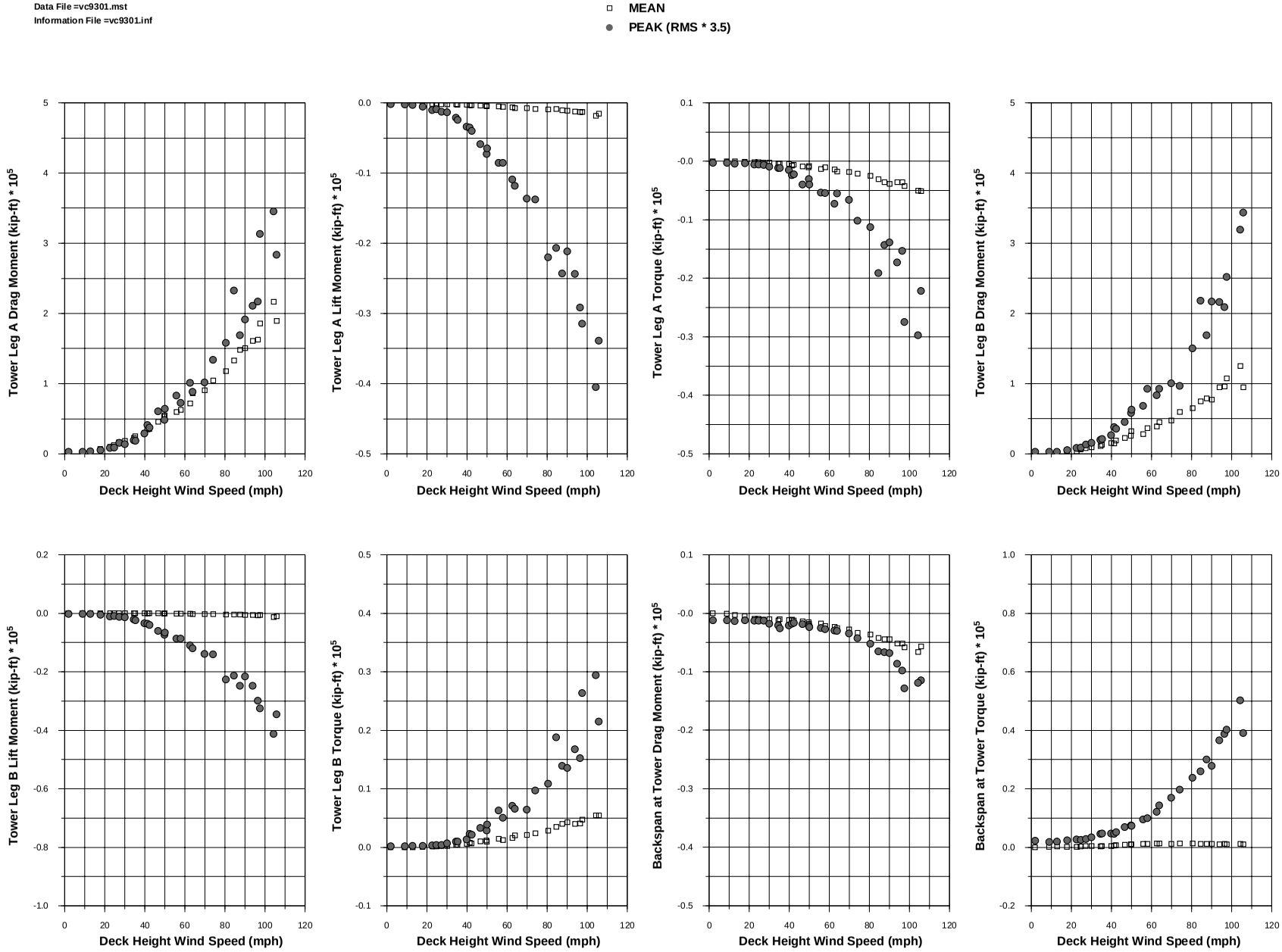

Prospect Verona Bridge, construction stage, open country profile, 90 degrees, without existing bridge & box

Dec. 08, 2004
Data File =vc9301.mst
Information File =vc9301.inf

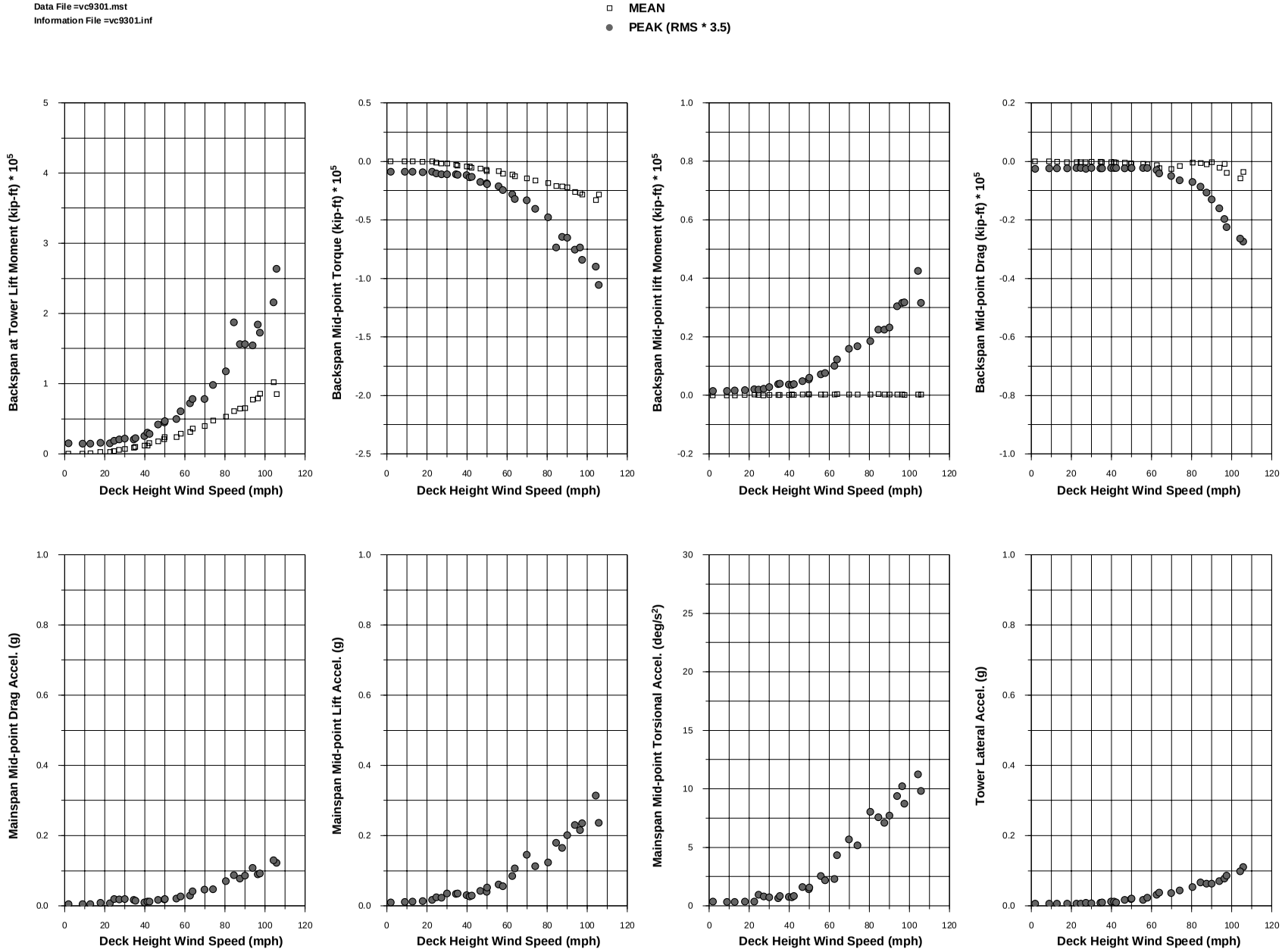

Prospect Verona Bridge, construction stage, open country profile, 90 degrees, without existing bridge & box

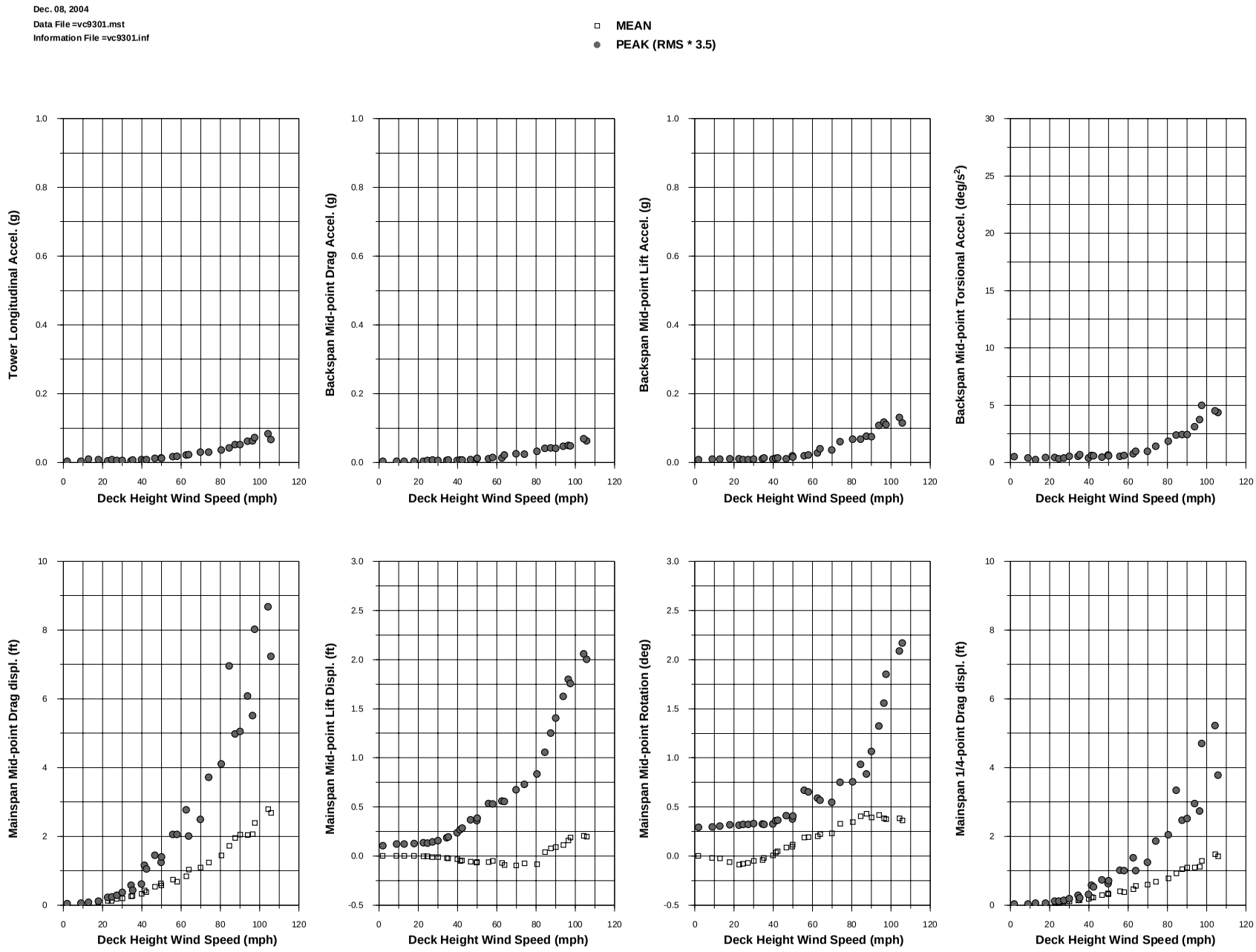

Prospect Verona Bridge, construction stage, open country profile, 90 degrees, without existing bridge & box

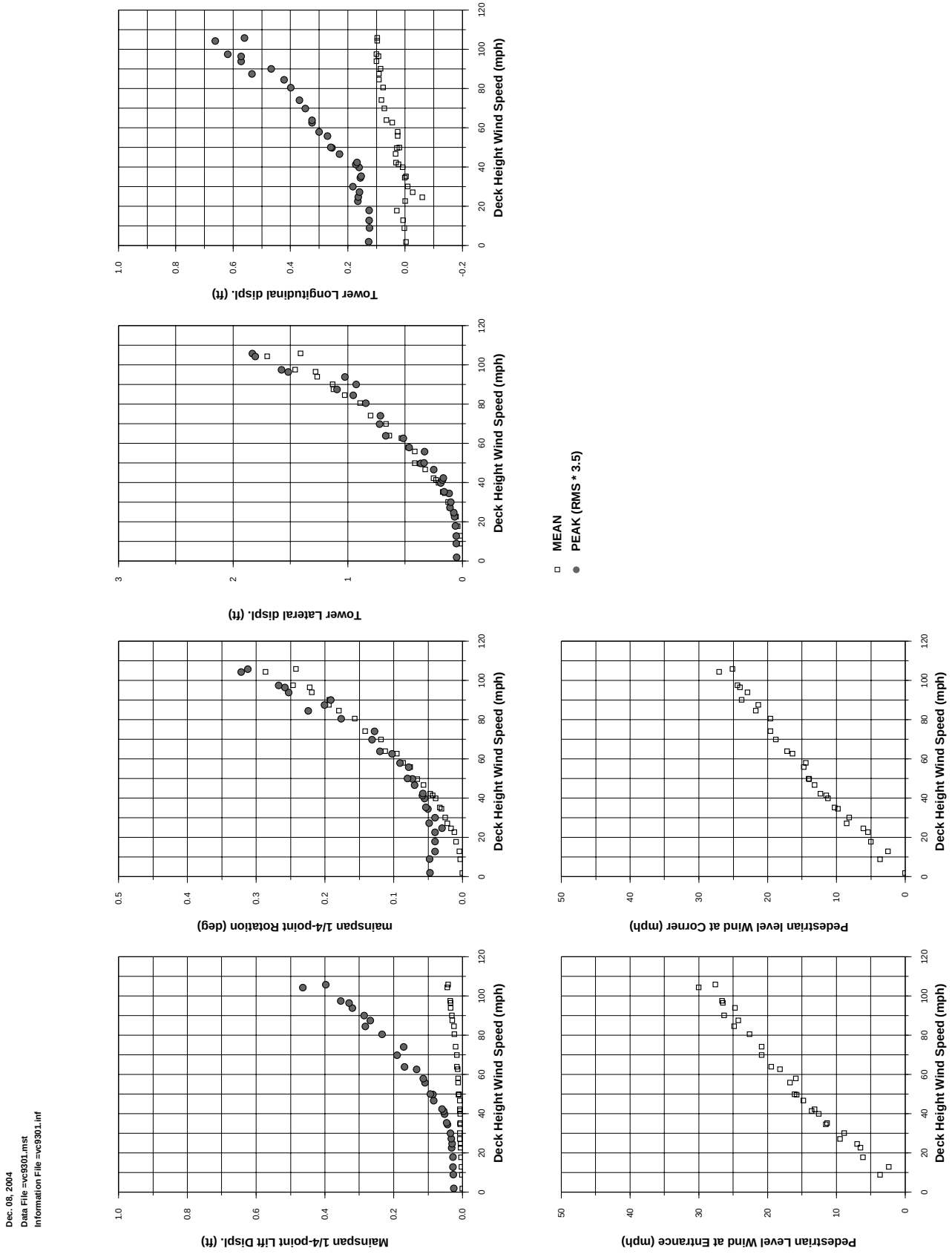

Prospect Verona Bridge, construction stage, open country profile, 90 degrees, without existing bridge & box

Dec. 02, 2004
Data File =vc2301.mst
Information File =vc2301.inf

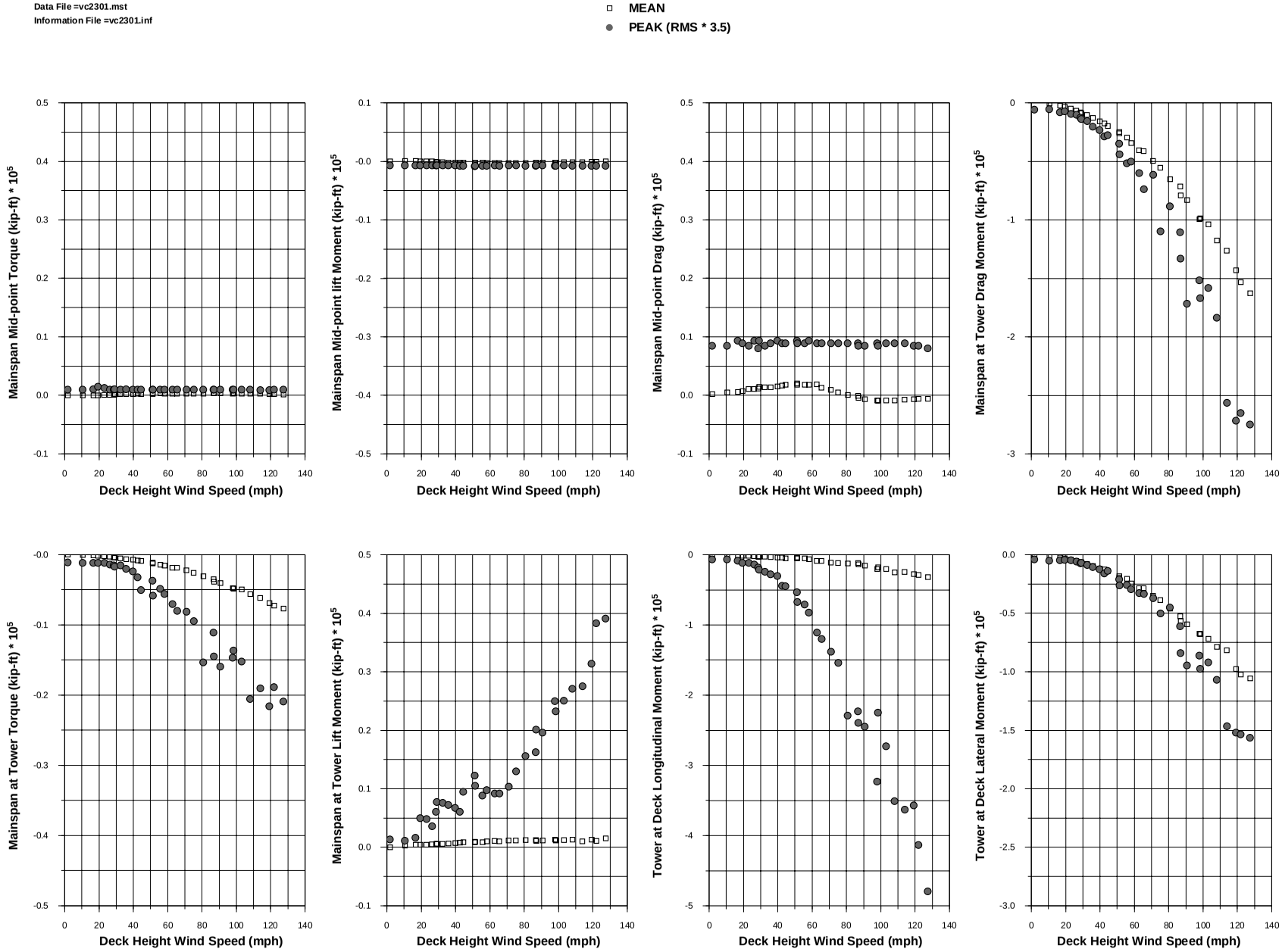

Prospect Verona Bridge, construction stage, open country profile, 270 degrees, with existing bridge & box

Dec. 02, 2004
Data File =vc2301.mst
Information File =vc2301.inf

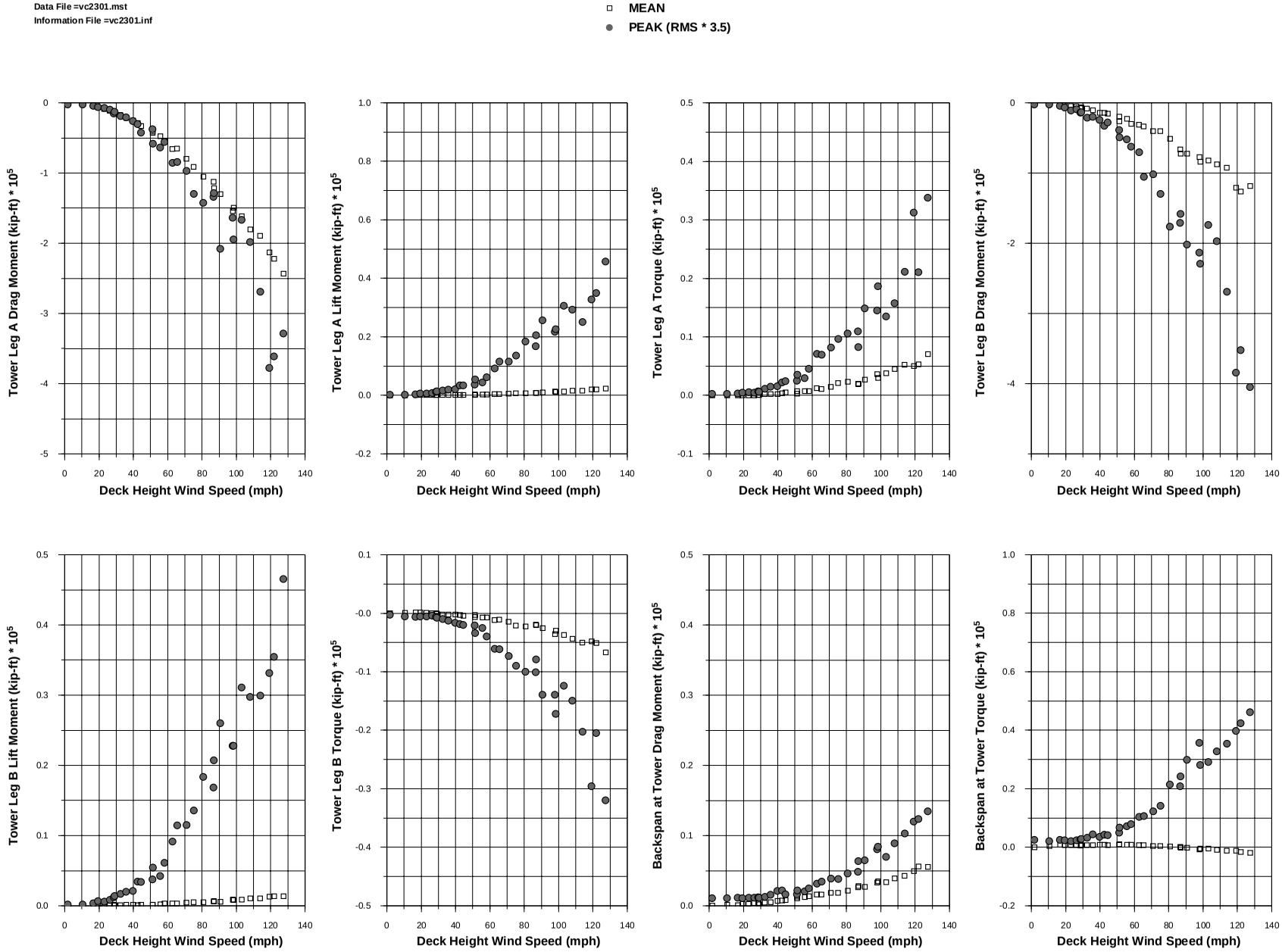

Prospect Verona Bridge, construction stage, open country profile, 270 degrees, with existing bridge & box

Dec. 02, 2004
Data File =vc2301.mst
Information File =vc2301.inf

MEAN
PEAK (RMS * 3.5)

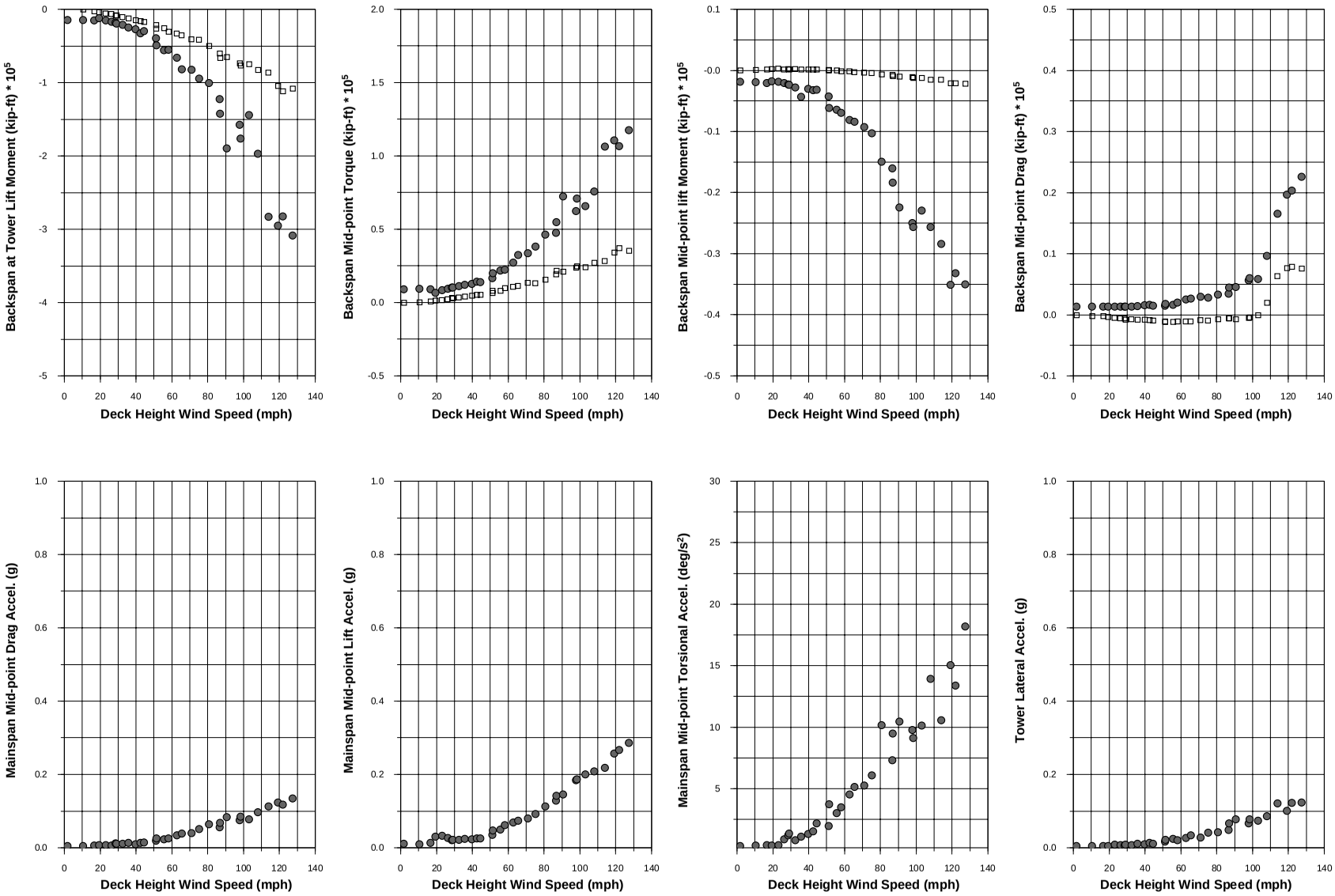

Prospect Verona Bridge, construction stage, open country profile, 270 degrees, with existing bridge & box

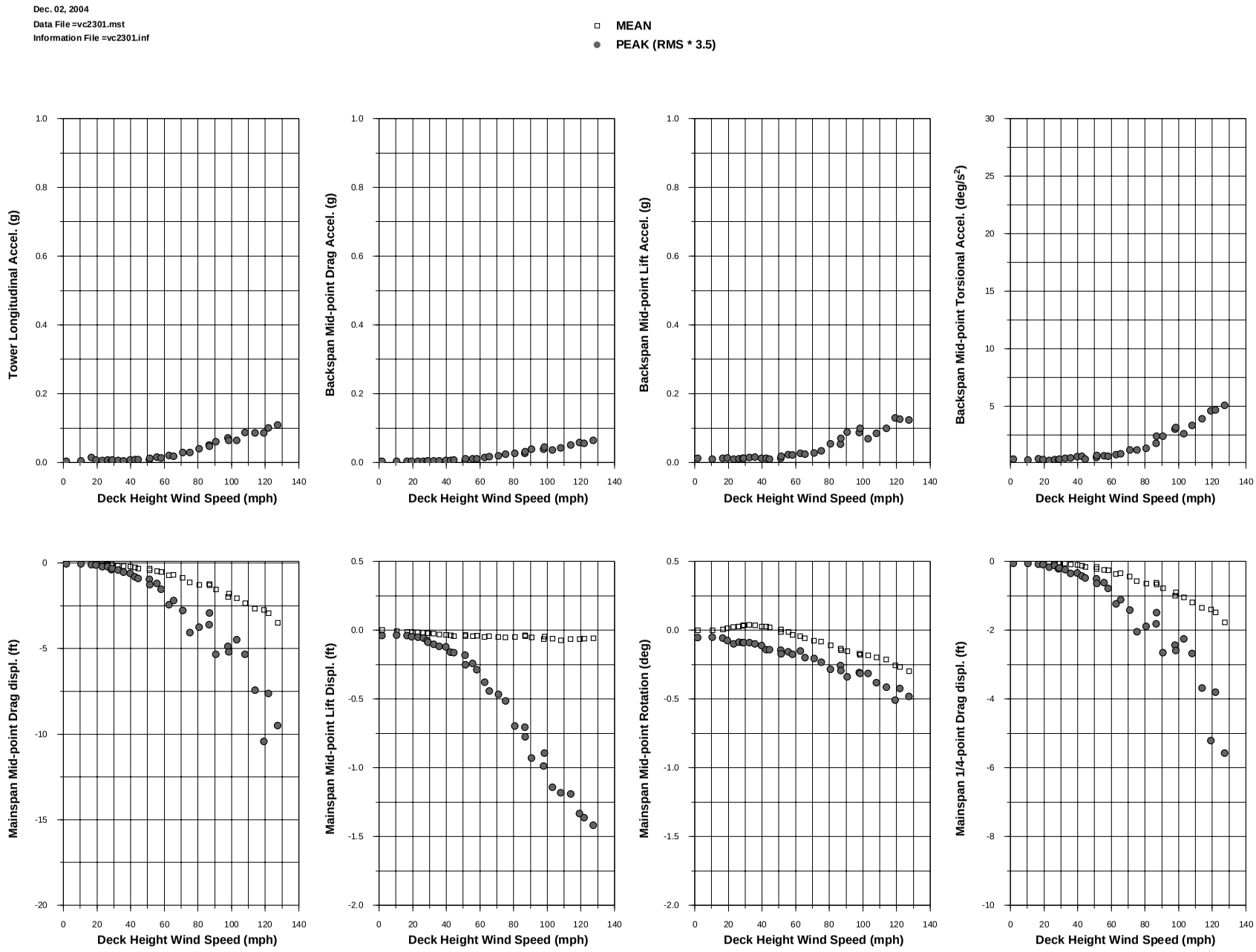

Prospect Verona Bridge, construction stage, open country profile, 270 degrees, with existing bridge & box

Dec. 02, 2004
Data File =vc2301.mst
Information File =vc2301.inf

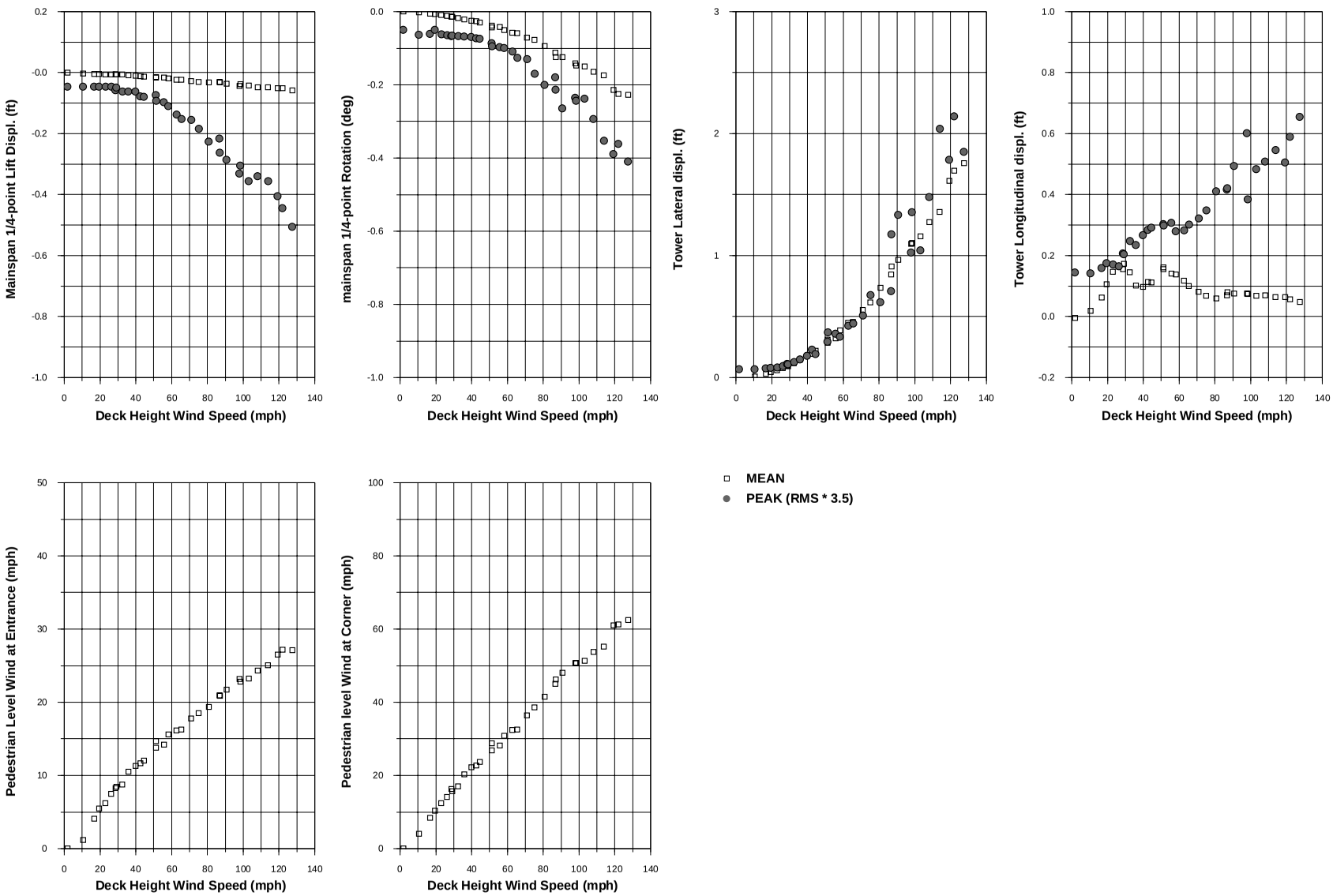

Prospect Verona Bridge, construction stage, open country profile, 270 degrees, with existing bridge & box

Dec. 08, 2004
Data File =vc9101.mst
Information File =vc9101.inf

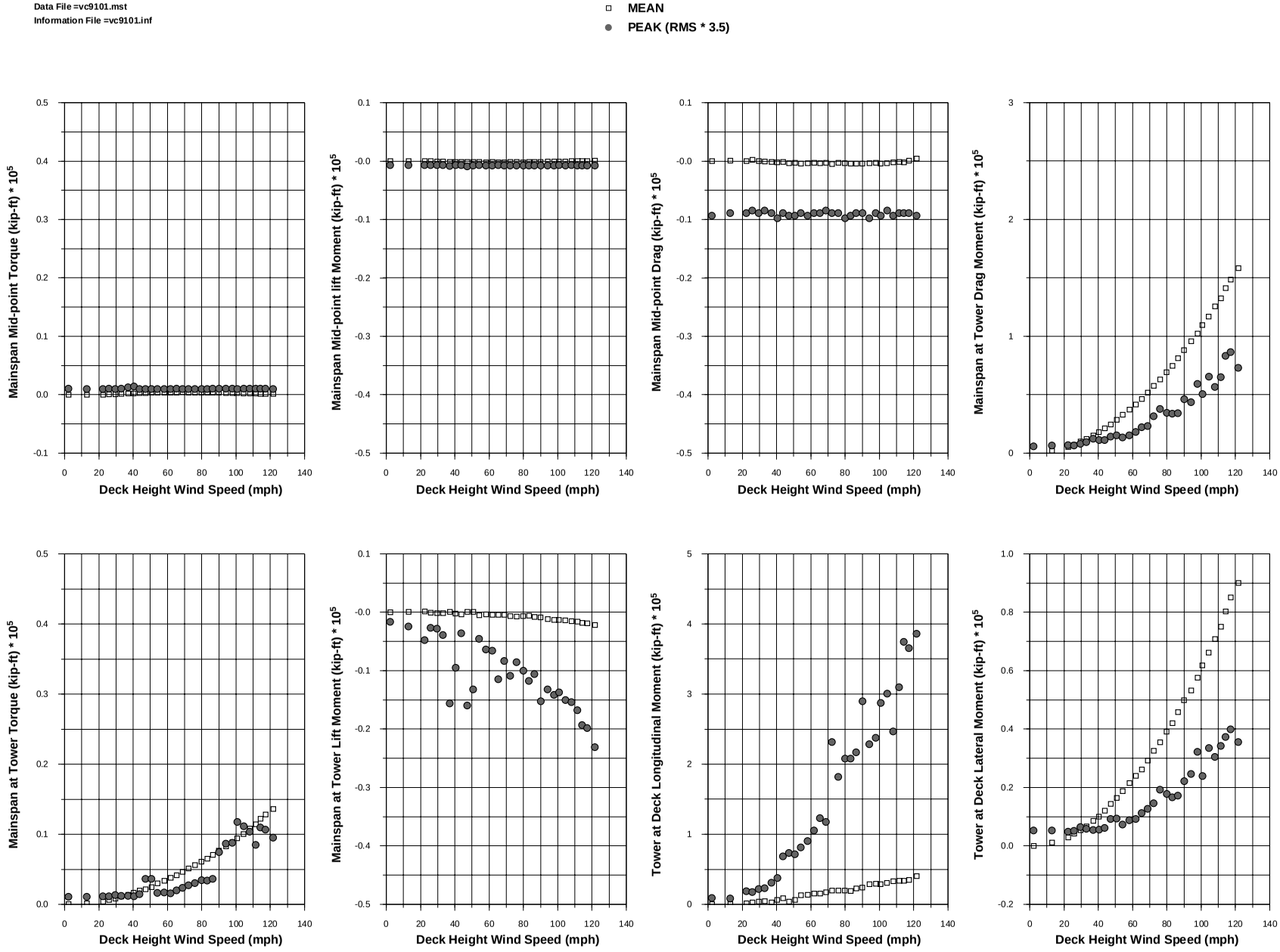

Prospect Verona Bridge, construction stage, smooth flow, 90 degrees

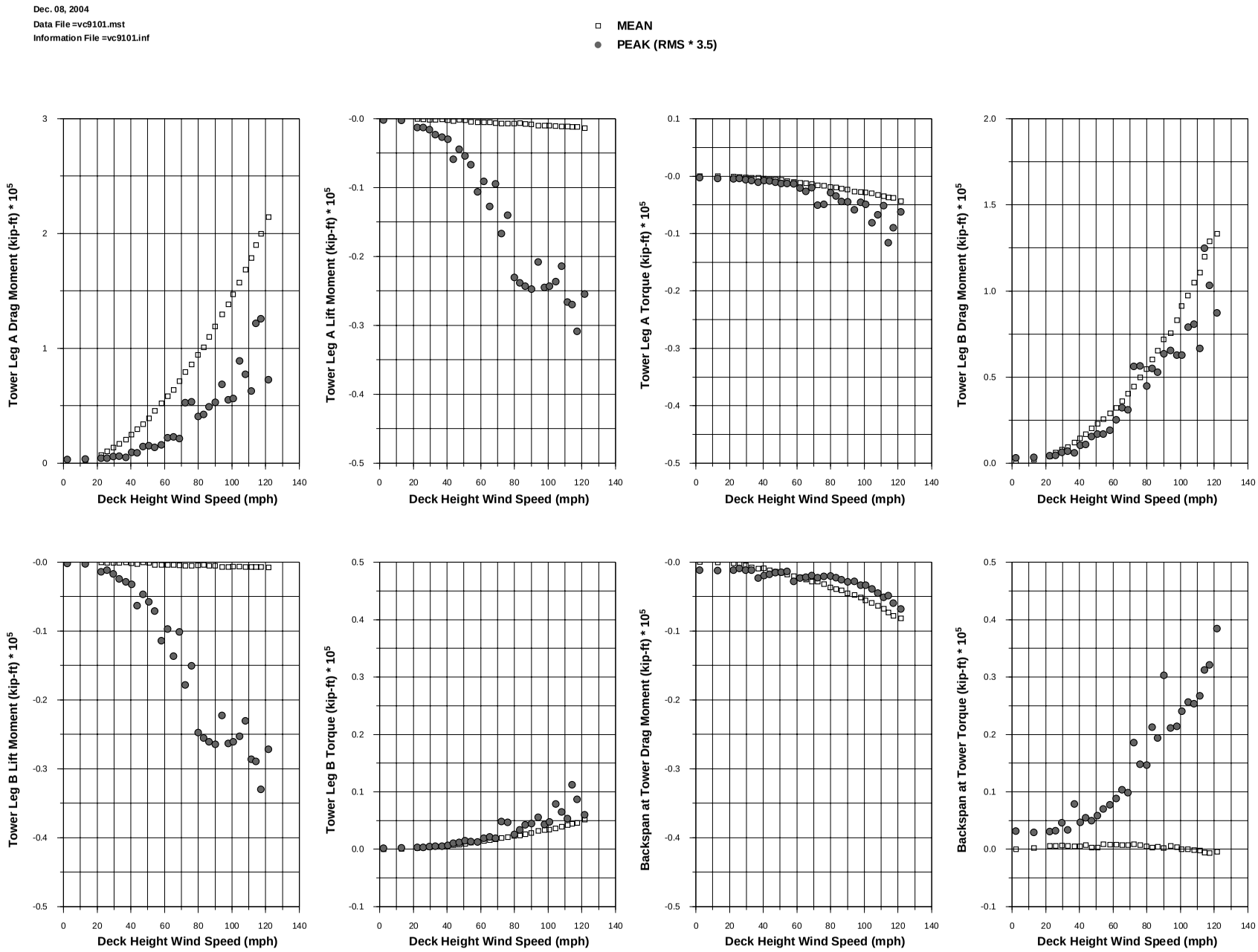

Prospect Verona Bridge, construction stage, smooth flow, 90 degrees

Dec. 08, 2004
Data File =vc9101.mst
Information File =vc9101.inf

MEAN
PEAK (RMS * 3.5)

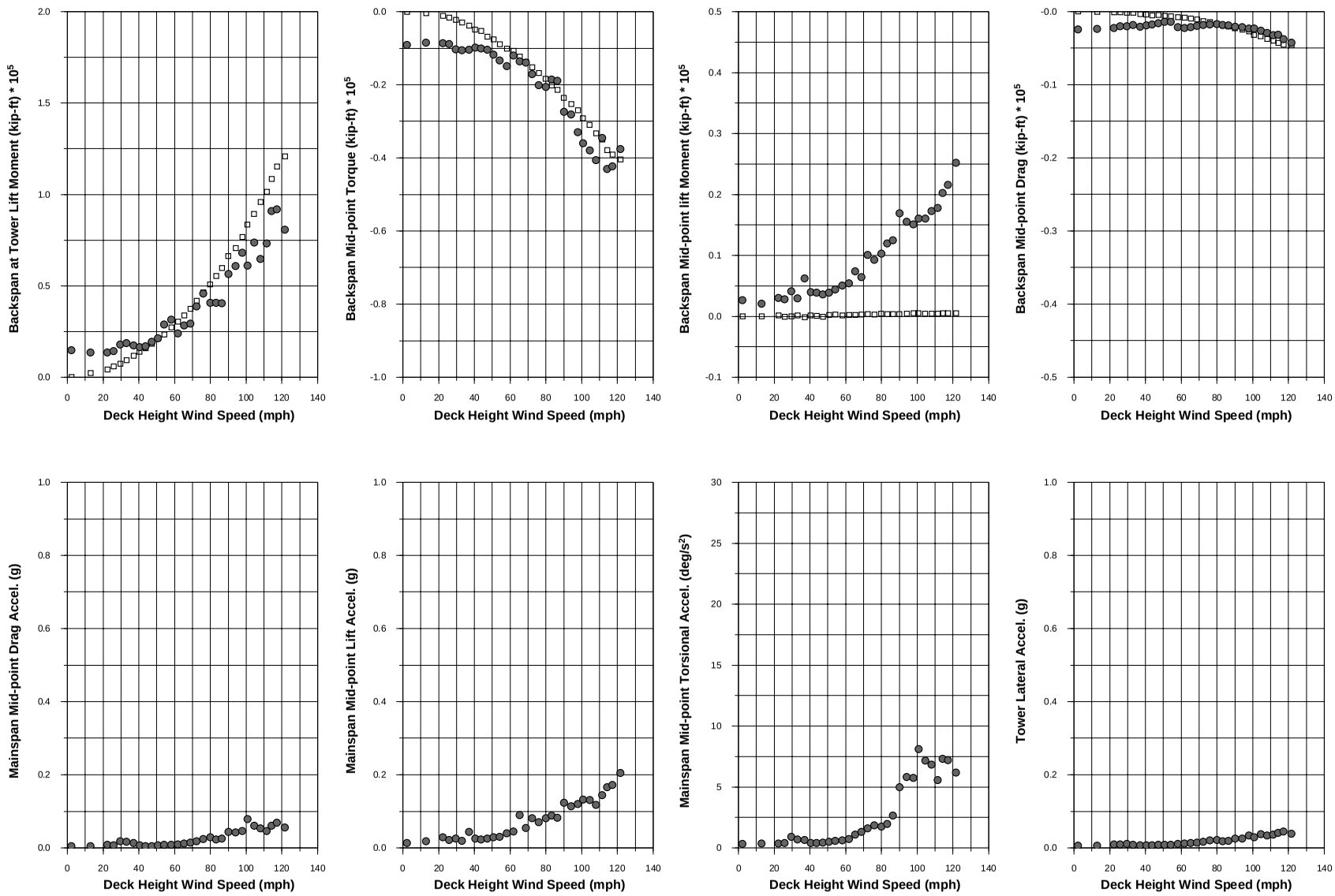

Prospect Verona Bridge, construction stage, smooth flow, 90 degrees

Dec. 08, 2004
Data File =vc9101.mst
Information File =vc9101.inf

MEAN
PEAK (RMS * 3.5)

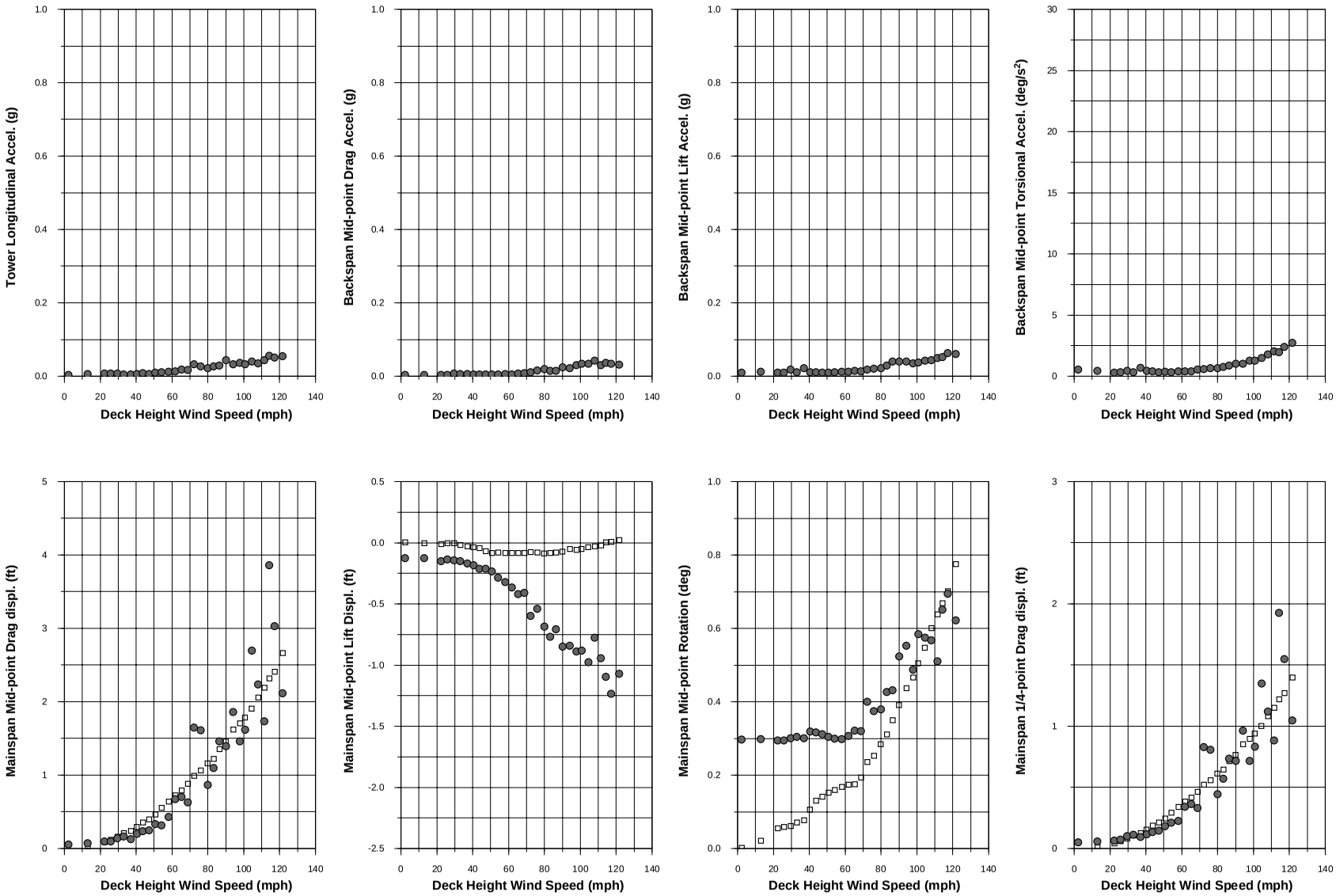

Prospect Verona Bridge, construction stage, smooth flow, 90 degrees

Dec. 08, 2004
Data File =vc9101.mst
Information File =vc9101.inf

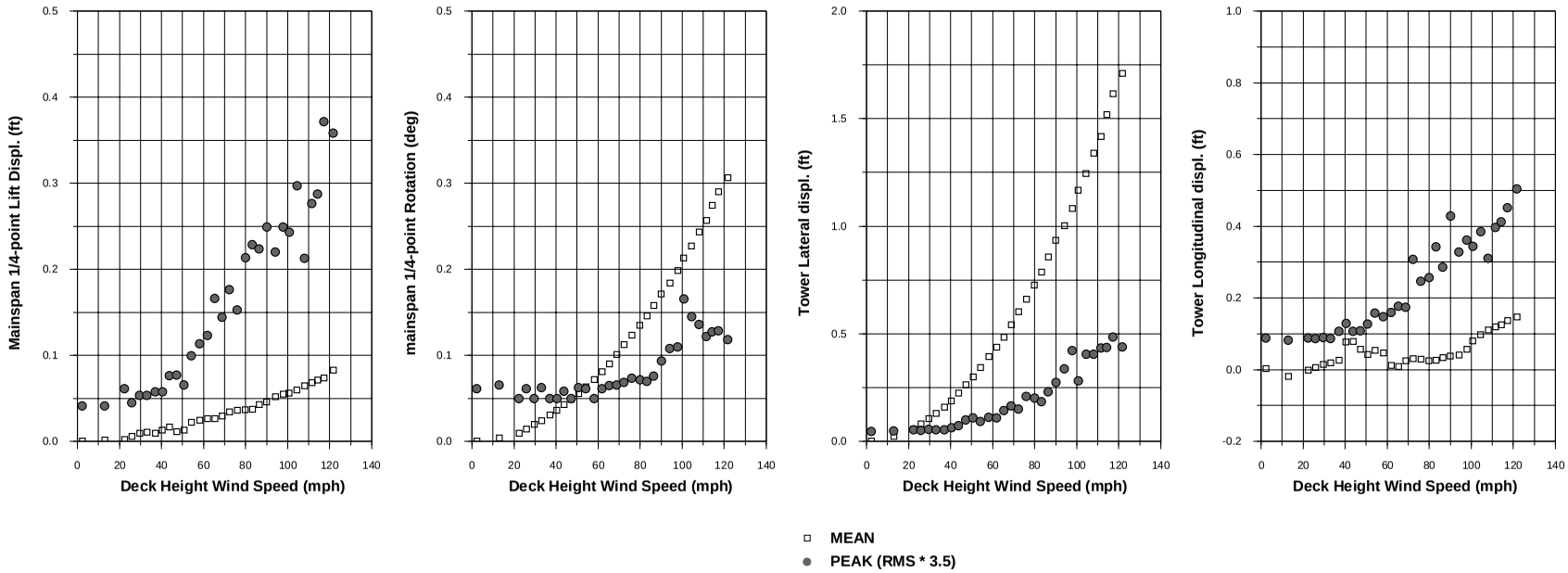

Prospect Verona Bridge, construction stage, smooth flow, 90 degrees